

The
University
Of
Sheffield.

Pyridyl-based Zn(II) complexes as efficient catalysts for the cleavage of phosphodiester

Valerio Viali

Submitted to the University of Sheffield in partial fulfilment of the
requirements for the award of Doctor of Philosophy

March 2022

Author's Declaration

The work described in thesis was carried out between November 2017 and December 2021 in the department of chemistry at the University of Sheffield. It is the individual work of the Author. Any views expressed in this thesis are those of the author, and in no way represent those of University of Sheffield. This thesis has not previously been submitted, in part or whole, for any other degree in this University or any other institution.

March 2022

Valerio Viali

Acknowledgements

I would like to start by acknowledging Professor Nicholas H. Williams for offering me the opportunity of joining his group and working on this project for the MMBio network. His help and support have made me a better scientist, more responsible and accurate, curious and independent.

During the last four years, E75 has been the coolest laboratory in the Department, not only for the temperature jumps but also thanks to the people who have livened it up.

First of all, I would like to thank Søren, who has been the most supportive person during this long and challenging time. Our laughs, despairs and endless chats (especially on squirrels) have been essential for me. I would never get tired of learning from each other, sharing information and speculating on science (and more). Although it was not love at first sight, I am so happy that I know you and glad to call you friend.

I also want to remember the warmest welcome that Fatma's smile gave me in freezing England. Thanks to your positivity and sincere friendship, my days have never been too dark, my hope never too little.

Among all present and past members of NHW's group, I cannot forget Matt, Rebecca and Xiaodong. I will always remember the fun, the discussions and sometimes the cultural crashes that have filled our days in the office. Layla, you are unique. Fatma Ab., I will never forget our laughs and I will always be thankful for the trust you have given me.

Charles, you are the best Post-doc ever.

Special thanks go to the past and present people of E74: Sally, Esther, Jim, Reuben, Mark and Fourat; You are the best, and I have had so much fun with you all.

I want to thank now all the people close to me but far from the Department.

Melissa, “my quokka”, the best editor ever, through challenging times, I look at you, and I find happiness and serenity. I feel loved and lucky as never before, I am ready to challenge together what life will bring us. The team is stronger than ever.

I want to thank my family, my mum and dad (Puff, Puzzetta and Arturo) for cheering up my, sometimes disheartened, mood in our evening video calls, my sister for her super positive attitude in our too early *good morning* calls, my brother-in-law and nephew for the fun and laughs, my Texan uncle and aunt for our endless Sunday call, and my gramma for reminding that whatever could have happened to me, she was definitely feeling worse. The joy and chaos brought by the Talientos and Bellavita-Marks are the best things of our family reunion. The love expressed with great food from the Ligorio-Bortone family is a sure thing.

Thanks to Vincenzo, Cesare and Daisy for getting lost in the peak district, for laughs and food, never enough; you are like family to me.

I want finally to remember the constant support from Paula, Cecilia, Francesco, Elisa and Valerio, and the fun from my amazing “aspettando i 40” friends.

Abstract

Although natural systems demonstrate that simple organic features and metal ion cofactors can combine extremely effectively to lead to efficient catalysis of RNA and DNA cleavage, achieving similar activity with artificial systems has yet to be achieved. One motivation for attempting this would be to create artificial nucleases, which could offer a generic therapeutic approach to controlling gene expression, but require more reactive catalytic sites than have been created to date. This thesis describes studies to develop more effective catalysts for phosphate diester cleavage through the design of small Zn(II) complexes.

Initially, a series of mononuclear Zn(II) catalysts designed to hydrolyse simple phosphate diesters were studied. A comparison between the effect of positioning a sulfonamide or a primary amine in the second coordination sphere was carried out, but the stronger hydrogen bond donor did not lead to an effective catalyst. This was rationalised in terms of the unfavourable ionisation state of the complex at neutral pH.

The amine functional group was then combined with a range of nucleophilic chains to explore how effectively these two activating strategies can be combined. Detailed mechanistic studies were carried out, revealing the mechanistic pathways and the response to inhibition by phosphate diesters and monoesters. The accelerating effects were significant, with the cleavage of bis-4-nitrophenyl phosphate (BNPP) 625 fold faster when an oxime was present as a nucleophile instead of an alcohol group. The effect of exchanging a methyl group for a secondary amine in the secondary sphere was smaller, with a 19 fold increase in activity. Compared to the methyl substituted analogue, the

sensitivity to the leaving group of the substrate is reduced. This increase was accompanied by a strong tendency for the complex to dimerise, reducing the observed activity, but provided the most reactive mononuclear complex for BNPP reported to date.

Based on the observation that strongly acidic groups do not enhance the activity of these complexes, the properties of the amino groups were modified by substitution with aromatic rings. The hypothesis was that this would increase the hydrogen bonding capacity, without creating an acidic site. This strategy was effective, and anisidine lead to a rate enhancement of 10 fold over the parent amino substituted complex for cleaving 2-hydroxypropyl 4-nitrophenyl phosphate (HPNPP). Examining the effect of different substituents on activity revealed that electron donating substituents led to greater activity, in contrast to the expected increase with electron withdrawing groups as observed in related complexes.

This substitution pattern was then incorporated into a dinucleating ligand, and the Zn(II) complex exhibited remarkable activity towards HPNPP cleavage, reducing its half life to a few seconds at neutral pH. This represents an increase in activity of about 1000 fold over the parent amino substituted complex at 0.6 mM. The activity towards a nucleotide dimer was also enhanced, but only about 3 fold. Despite the absence of a nucleophilic functionality in the ligand, this complex also showed high activity towards BNPP. Detailed studies on each of these activities revealed complex behaviour when pH and concentration were varied.

Overall, the modifications introduced have led to enhanced activities for three different types of Zn(II) complexes, with remarkable activity for HPNPP cleavage; however, the

combination of these modifications has also revealed complex behaviour which has been partly but not completely resolved.

Abbreviations

μL	microlitres	NMR	nuclear magnetic
mM	millimolar		resonance
ACN	acetonitrile	NNP	4-nitrophenol
BNPP	bis(4-nitrophenyl)		monophosphate
	phosphate	NP	4-nitrophenol
CHCl₃	chloroform	Nuc	nucleophile
d	doublet	§pH	pH measured in methanol
DCM	dichloromethane	RNA	ribonucleic acid
DMF	dimethyl formamide	s	singlet
DMSO	dimethyl sufoxide	t	triplet
DNA	deoxyribonucleic acid	TFA	trifluoroacetic acid
ES	electrospray	THF	tetrahydrofuran
Et₃N	triethylamine	TIC	Total Ion Chromatogram
EtOAc	ethyl acetate	UpG	Uridyl-(3-5)guanosine
HCl	hydrochloric acid	UpU	Uridyl-(3-5)uridine
HPLC	high performance liquid chromatography	UV-vis	Ultraviolet-visible
HRMS	high resolution mass Spectrometry		
K_a	dissociation constant		
K_D	dimerisation constant		
KOH	potassium hydroxide		
m	multiplet		
MeOH	methanol		
MS	mass spectrometry		
Mg₂SO₄	magnesium sulphate		
NaOH	sodium hydroxide		

Table of Contents

Abbreviations.....	8
Chapter 1 Studies and advances on natural and artificial nucleases	13
1.1 Introduction	14
1.2 How do enzymes catalyse the phosphate diester cleavage?.....	23
1.3 Artificial endonucleases	27
1.3.1 The development of artificial restriction enzymes in molecular biology	28
1.3.2 Chemistry Approach.....	35
1.3.3 Models	40
1.3.4 Design of the catalytic head group	42
1.4 Aims	54
Chapter 2 Optimisation of Zn(II) complexes for the hydrolysis of a phosphate diester model for DNA	58
2.1 Introduction	59
2.2 Result and discussion	66
2.3 Sulfonamide: Hydrogen bond donor or acidic group?	67
2.3.1 Synthesis.....	69
2.3.2 Analysis	72
2.4 Methylamine based Zn(II) complexes.....	75

2.4.1 Synthesis.....	76
2.4.2 Kinetic studies	78
2.5 Conclusions	120
2.6 Experimental	125
2.6.1 Synthesis.....	125
L ₂₋₁	125
L ₂₋₂	131
Methyl amine building block	138
Methyl amine based ligands.....	145
2.6.2 UV - Kinetic experiment	152
2.6.3 HPLC – Kinetic experiment	152
2.6.4 Data.....	155
2.6.5 Potentiometric titration	161
Chapter 3 Mononuclear Zn (II) complexes for the cleavage of phosphate diester models for RNA	166
3.1 Introduction	167
3.2 Results and discussion.....	171
3.2.1 Synthesis.....	172
3.2.2 Kinetic studies	174
Reaction conditions.....	174

3.3 Conclusion.....	208
3.4 Experimental	212
3.4.1 Synthesis.....	212
3.4.2 UV- Kinetic experiment	229
3.4.3 HPLC- Kinetic experiment.....	230
3.4.4 Data.....	231
3.4.5 Zinc binding - Graph of Absorbance at 350 nm against the equivalent of ZnCl ₂	242
3.4.6 UV - Titration	246
3.4.7 Potentiometric Titration.....	252
Chapter 4 Investigations of the activity of a dinuclear Zn(II) complex towards phosphate diester models for RNA and DNA.....	254
4.1 Introduction	255
4.2 Result and discussion	264
4.2.1 Synthesis.....	265
4.2.2 Kinetic studies	266
Transesterification of HPNPP.....	266
Hydrolysis of BNPP.....	291
Transesterification of UpG	300
4.3 Conclusion.....	304

4.4 Experimental	309
4.4.1 Synthesis	309
4.4.2 UV-kinetic experiment	313
4.4.3 HPLC – kinetic experiment	318
4.4.4 Data.....	319
4.4.5 UV titration.....	326
Chapter 5 Conclusions and Future Work.....	328
References.....	332

Chapter 1

Studies and advances on natural and artificial nucleases

1.1 Introduction

DNA and RNA play an essential and central role in the biological world, preserving and regulating the expression of genetic information.¹ Consistent with these roles, both nucleic acids possess high stability in physiological conditions. A key factor in this resistance to hydrolysis is the stability of the phosphate ester functional groups that connect the nucleoside units. At neutral pH and 25 °C, the half-life of RNA is estimated to be approximately 100 years,² but due to the absence of the 2'-hydroxyl group on the ribose ring, the stability of the DNA is much greater and estimated as 30 000 000 years.³ Phosphates have several major biological roles which are crucial for the life of an organism. For example, they are part of the cell membrane as phospholipids and are in the skeletal structure as calcium salts. The energy-rich phosphate anhydrides ATP and ADP are essential to store and dispense energy in living cells. Often proteins regulate their activity by becoming phosphorylated and cAMP and cGMP, working as second messengers, have a role in cell signalling.¹ The wide variety of linking groups present in chemistry has raised the question regarding Nature's widespread use of phosphates.⁴ Westheimer highlighted how conserving the nucleosides' highly elaborate structures is vital for the organism economy. The best chemistry to take it apart and reestablish the connection needs to be an ester group that can readily go through hydrolysis and esterification. In addition, the linking group needs to be a strong tribasic acid capable of forming anhydrides, connecting two molecules but still having a labile acid functionality. As theorised by Davis in 1958,⁵ ionisation has played a fundamental role in the conservation of living organisms' metabolites, which would otherwise diffuse through the cellular membranes and be lost by dilution. The high stability of nucleic acid is due to the ability of the phosphate group to

connect two nucleosides and maintain a negative charge. Hence, ionisation, which is responsible for retaining the nucleic acids within the cell membrane, also reduces the chances of nucleophilic attack by hydroxide or alkoxide due to electrostatic repulsion, preserving the genomic material. Although other groups, like citric acid, might have those characteristics, the stability of a phosphate diester is far higher.

While selecting the kinetically stable phosphate group to protect the genomic information, evolution has also had to create natural catalysts to accelerate its cleavage. Nucleases are a class of enzymes that catalyse the cleavage of phosphodiester bonds and, for example, are used by the organism when exogenous DNA strands must be destroyed or when mutations need to be repaired. For example, staphylococcal nuclease accelerates P–O cleavage by approximately 10^{16} - 10^{21} fold compared to the spontaneous hydrolysis in solution.⁶ Once the messenger RNA has completed its function, ribonucleases catalyse the hydrolysis of the nucleic acid to avoid further encoding and consequent excessive production of proteins.¹

Understanding the mechanisms of the phosphate diester hydrolysis is crucial to explain the huge rate accelerations involved and try to propose artificial system able to compete with the natural catalysts.

Phosphate ester hydrolysis in solution can proceed via two limiting stepwise mechanisms: dissociative ($D_N + A_N$) or associative ($A_N + D_N$).⁷ The difference between the two pathways depends on the timing of the nucleophilic attack; if the leaving group departs before the nucleophile's attack on the phosphorus, generating a metaphosphate-like intermediate, the reaction progresses via a dissociative mechanism. On the other hand, a pentavalent phosphorane is formed when the attack precedes the P–O bond cleavage, typical of an

associative mechanism. Between these two limiting cases, the reaction's mechanism can also be concerted (A_ND_N) with a single transition state due to synchronous formation and break of the two P–O bonds. The A_ND_N pathway is still an associative mechanism, but the character of the transition state varies and, for example, can be described as more or less dissociative according to a smaller or higher degree of bonding to the nucleophile and leaving group, respectively. The pK_a of the leaving group can strongly influence the transition state of the mechanism, and the cleavage of phosphate esters with good leaving groups (lower pK_a) has been shown to proceed by a more dissociative pathway.

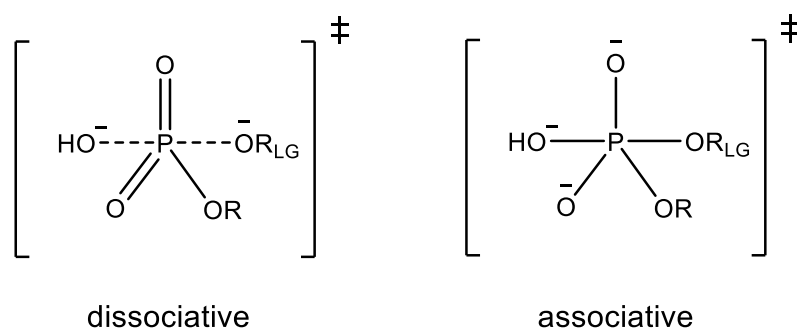
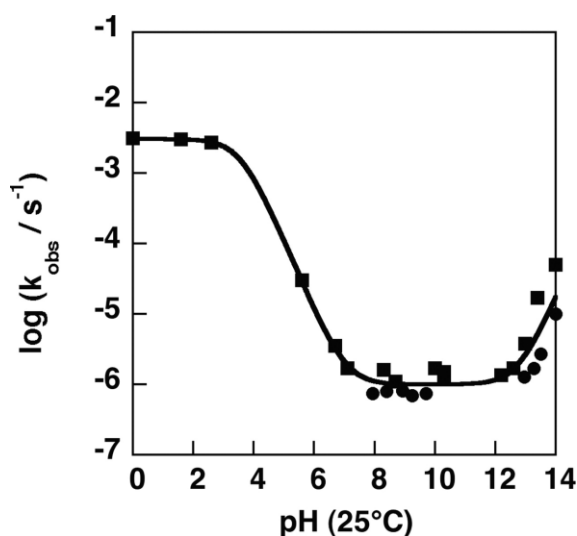


Figure 1.1 Structure of the possible transition state for the phosphoryl transfer reaction of phosphate diesters

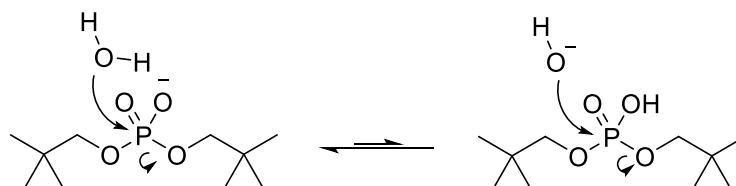
Experimental and computational studies carried out by Kamerlin, Williams and Warshel on dineopentyl phosphate offered an in-depth description of the mechanistic nature of the cleavage reaction across the whole pH scale.^{6,3} Given the high pK_a of its leaving group, dineopentyl phosphate was chosen as a model for DNA. The pH dependence of the observed rate constant measured at 250 °C for hydrolysis (Graph 1.1) shows three distinctive regions. Below pH 6, the acid catalysed reaction proceeds via water attacking the neutral phosphate, and either a stepwise associative or concerted mechanism is

plausible. The phosphorane intermediate of the $A_N + D_N$ pathway is compact, with P–O distances of 1.7 and 2.0 Å for the leaving group and nucleophile, respectively.



Graph 1.1 pH profile of rate for the hydrolysis of dineopentyl phosphate at 250 °C (pH measured at 25 °C)³

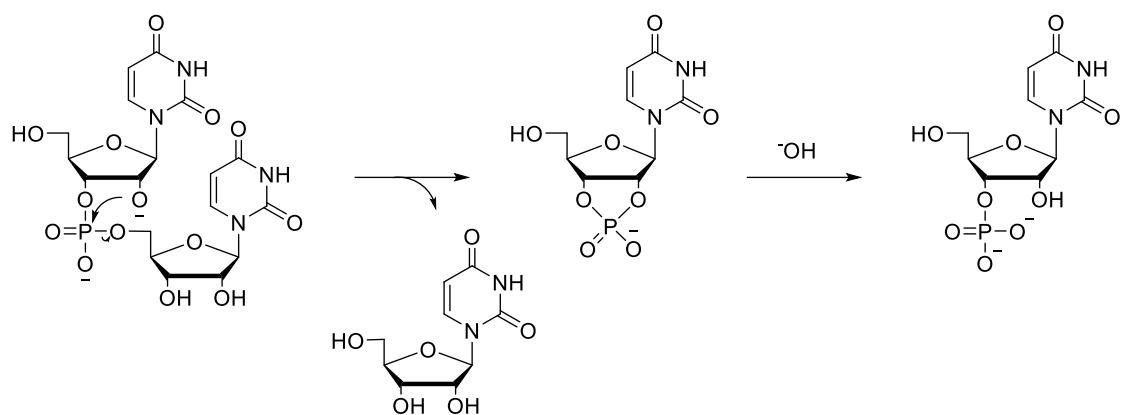
The first transfer of a proton from the attacking water to the phosphorane is followed by its migration to the leaving group, which departs via a second step. The $A_N D_N$ pathway is more expanded than the associative one and is rather dissociative with the bond cleavage advanced over bond formation. In the pH-independent region between pH 6 and 13, the reaction might progress through an attack of the water molecule on the ionised phosphate or via a first pre-equilibrium proton transfer from the water to the phosphate, followed by hydroxide attack (Scheme 1.1).



Scheme 1.1 Proton transfer equilibrium

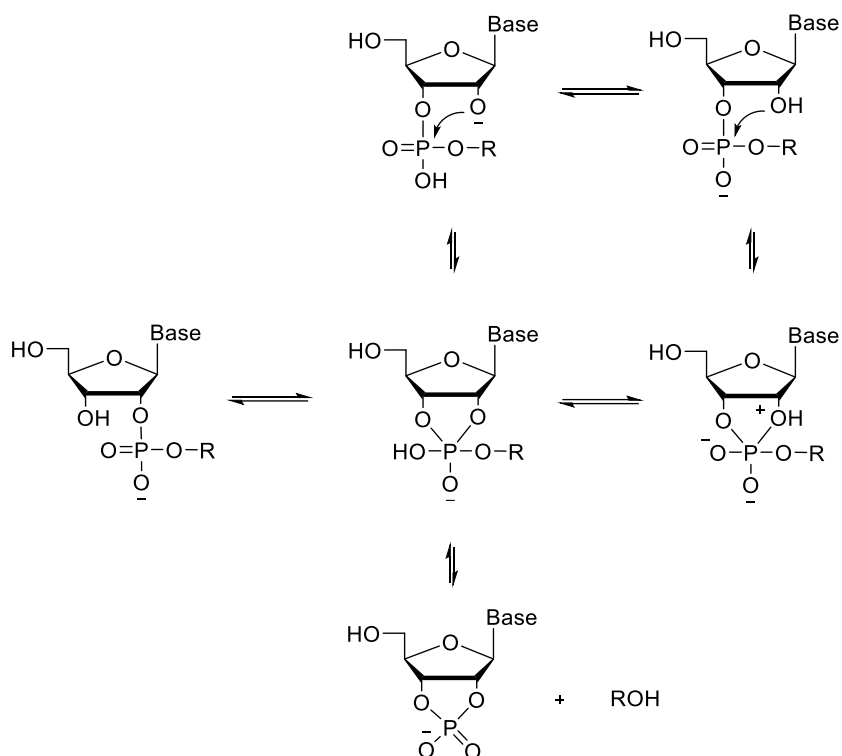
For water attacking the ionised phosphate, the reaction follows an $A_N + D_N$ pathway through a first compact transition state with an energetic barrier of 50 kcal/mol. The P–O bond is formed simultaneously with the proton transfer from water to a phosphate oxygen. Similarly to the acid catalysed reaction, the transferred proton migrates to the departing leaving group in the second step, yielding alcohol and mono-ionised phosphate as the products. It is experimentally impossible to prove if the proton transfer happens concomitantly with the attack by the water molecule or proceeds stepwise. However, by mapping the free energy surface of hydroxide and water attack on the respective neutral and ionised phosphate, the authors observed lower free energy and a more viable mechanism for the system involving the attacking hydroxide. The reaction is base catalysed above pH 13, involving the hydroxide attacking the ionised phosphate. No proton transfer is involved in the mechanism, and both the nucleophile and the leaving group are ionised with the reaction proposed to happen through a synchronous $A_N D_N$ mechanism.

Regarding the hydrolysis of RNA, as schematically represented in Scheme 1.2 for UpU, the mechanism consists of first intramolecular transesterification, which results from the nucleophilic attack 2'OH on the phosphate group, and the following hydrolysis of the cyclic phosphate. Studies by Lönnberg and coworkers ⁸, investigating RNA hydrolysis by using dinucleotides, revealed that the reaction depends on the solution pH and is subject to general acid/base catalysis.



Scheme 1.2 General mechanism for the hydrolysis of RNA

In addition to the hydrolysis of the phosphate, the experimental conditions ($\text{pH} < 7$) can bring about isomerisation from 3'-5'- to 2'-5'- dinucleotide. It has been proposed that both the reactions might happen when the pentacoordinate phosphorane is formed, and the particular condition determines the advance of one or the other pathway. This is supported by the similar pH profile at $\text{pH} < 3$ of the two acid-catalysed reactions, which suggests that the product of hydrolysis and isomerisation are formed from the same intermediate. While the isomerisation is pH independent above pH 3, the hydrolysis is still acid catalysed and, due to this difference, the former dominates the latter. In this region, similar to what was reported for DNA, two indistinguishable mechanisms were proposed to form the phosphorane: the attack of the hydroxyl group on a monoanionic phosphate followed by proton transfer or the attack of the alkoxy to a neutral phosphate diester. The overall process described in Scheme 1.3 refers to the pH independent isomerisation and the acid catalysed and pH independent hydrolysis of the dinucleotide.



Scheme 1.3 Mechanism of the pH independent isomerisation and hydrolysis of UpU

In the pH range from 4 to 7, the phosphorane intermediate is stable enough to allow pseudo rotation and enhance phosphate migration. Above pH 7, where the base catalysed hydrolysis takes over, cyclisation happens by an alkoxide attack on the phosphorous with the consequent departure of the ionised leaving group. In alkaline conditions, isomerisation does not happen. The lack of isomerisation was proposed to be due to the transient nature of the dianionic phosphorane, formed in alkaline conditions, being too unstable to allow phosphate migration. At higher pH, both the negatively charged oxygen atoms of the unstable phosphorane occupy equatorial positions, which might explain the absence of pseudo rotation that leads to the isomerisation. However, more recent studies have demonstrated that the mechanism of alkaline cleavage involves two steps with the

formation of the dianionic intermediate.⁹ In particular, Williams and coworkers, reporting the rate of the hydroxide catalysed reaction over the pK_a of the leaving group, observed a convex break at pK_a of 12.58, indicating a change in the rate limiting step of the reaction. Although this confirmed the presence of an intermediate, the absence of isomerisation might be caused by the low stability of the latter. The two slopes of the Brønsted plot reveal two β_{LG} for the aryl and alkyl leaving groups of -0.52 and -1.34, respectively. Therefore, with leaving groups pK_a higher than 12.58, as is the case for RNA, the rate limiting step is the departure of the leaving group.

Regarding the catalysis delivered by natural or artificial enzymes, interest is focused on phosphate hydrolysis at neutral or mild alkaline pH. The reported analysis on DNA and RNA hydrolysis shows that the mechanism is more associative than dissociative at physiological conditions. Both the RNA and DNA hydrolysis have been proposed to proceed by a stepwise process, with phosphorane formation being a rate limiting step that would benefit from nucleophile activation. In addition, with deactivated substrates as the nucleic acids, the stabilisation of the leaving group is essential. This is key information to explain the behaviour of enzymes and propose artificial systems design to satisfy the requirement of the catalysed reaction. Modulating the local interactions around the phosphate by introducing functional groups and metal ion cofactors can accelerate its hydrolysis, as observed in natural systems.

Detailed aspects of the nature of the phosphoryl-transfer displacement step in enzymes were summarised by Krebs *et al.*¹⁰ As shown in Figure 1.1, there is a difference in the negative charge distribution between the two possible intermediates of an associative or

dissociative mechanism. An increase relative to the ground state is observed for the equatorial oxygen atoms in the pentacoordinate phosphorane, and a reduction in the corresponding positions in the metaphosphate intermediate. The provision of positively charged amino acids and metal ions in the active site stabilises the negative charge on the oxygen atoms, and this electrostatic interaction may be more effective when an associative mechanism is involved. On the other hand, for a dissociative mechanism, the enzyme's microenvironment would stabilise the phosphoryl oxygen of the substrate in the ground state more than those of the metaphosphate intermediate. However, it cannot be excluded that those elements might enhance the reaction by stabilising the metaphosphate-like intermediate. For example, in the active site, the positive charge of metal ions is often reduced by coordination with carboxylate groups, and their ability to stabilise a pentacoordinate phosphorane might be reduced.

Whether Mg(II) or Zn(II) ions have a functional and structural role or are directly involved in catalysis, it is now well known that many enzymes and ribozymes' activity depends on their presence. Figure 1.2 summarises how metal ions coordinating to the substrate and nucleophile can favour the formation of the phosphorane intermediate and the departure of the leaving group.

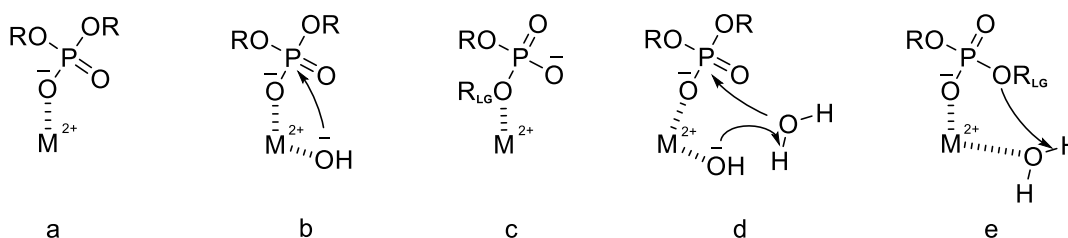


Figure 1.2 Possible direct and indirect activation mode provided by the metal ion

As summarised by Williams *et al.*,¹¹ metal ions can provide three direct (a, b and c) and three indirect activation modes (d, e and electrostatic stabilisation). The metal ions can enhance the electrophilicity of the phosphate group by Lewis acid activation (a), can prepare the aqueous or alcoholic nucleophile for attack by deprotonation (b) and stabilise the leaving group (c). In addition, the interaction of the ions with the outer sphere participants might also facilitate the reaction. Intramolecular general base catalysis can be favoured by the coordinated hydroxide, while the binding of a water molecule to the metal ion might provide a proton donor and lead to general acid catalysis. The presence of positively charged ions can also influence the mechanism by electrostatic effects, favouring deprotonation and proton transfer. When enzymes use two or three ions, the speculation about their mode of action is elaborate, and more than one interaction influences the catalysis. Figure 1.3 shows examples of the synchronous activation provided by two metal ions on the substrate, nucleophile and leaving group.

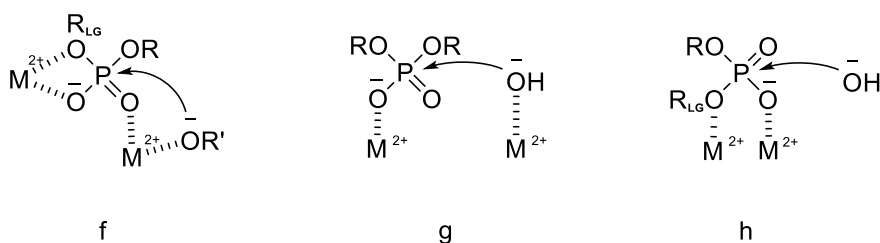


Figure 1.3 Possible synchronous activation modes provided by two metal ion.

1.2 How do enzymes catalyse the phosphate diester cleavage?

Regarding phosphoryl-transfer reactions, the functional groups directly involved in ligating metal ions are limited to sulfide, imidazole and carboxylate, which the enzymes provide

through cysteine, histidine, and aspartic or glutamic acids residues, respectively (Figure 1.4).¹² In particular, the imidazole and carboxylate ligands have a predisposition of the oxygen and nitrogen atoms groups that are not protonated at physiological conditions and free to coordinate the metal ions. As proposed by Sigel *et al.*,¹³ the abundance in proteins of these two ligands is due to their synergistic effect; the π -accepting properties of pyridine-like ligands would increase the metal ion charge, favouring the binding of negatively charged oxygens. The coordinating amino acid ligands play a significant part in modulating the Lewis acidity of divalent ions to generate a reactive metal-bond hydroxide without further decreasing its nucleophilicity. The heterocycle nitrogen site might also enhance the substrate and nucleophiles' oxygen binding to the metal ions, positively influencing the catalysis.¹⁴

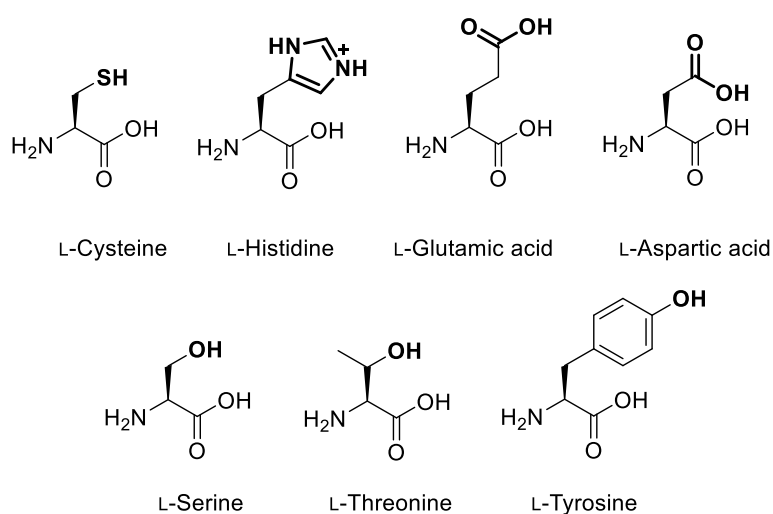


Figure 1.4 L-Amino acids involved in the catalysis

Cysteine and histidine, together with serine, threonine and tyrosine, can also be involved in the catalytic process, acting as nucleophiles and leading to a phosphoenzyme intermediate (Figure 1.4).¹⁰

A relevant example is the 3'-5' exonuclease activity site of the DNA polymerase I.¹⁵ To correct errors occurring during DNA replication, the enzyme, which mainly catalyses the transfer of nucleotides to the 3' end of template primer DNA, has hydrolytic activity in a different domain. These different portions of the enzyme function independently and have separate binding sites for DNA, which allow the separate study of each unit. The 3'-5' exonuclease portion requires the presence of divalent metal ion and proceeds via a single step, proved by inversion of stereochemistry. The cleavage of a single-stranded substrate yields a deoxynucleoside 5'-monophosphate and 3' hydroxyl DNA segments. The high-resolution X-ray crystal structure of a complex of the Klenow fragment of *E. coli* (the portion of the enzyme which consists of both the polymerase and 3'-5'-exonuclease activity) with dTMP and a complex of the Klenow fragment variant (D424A) with a single-stranded DNA sequence provided detailed information regarding the enzyme's interaction with both the product (E·P) and the substrate in the active site (E^{*}·S).¹⁶ The study reveals that the two metal ions largely engage in aspartic and glutamic acid ligation.

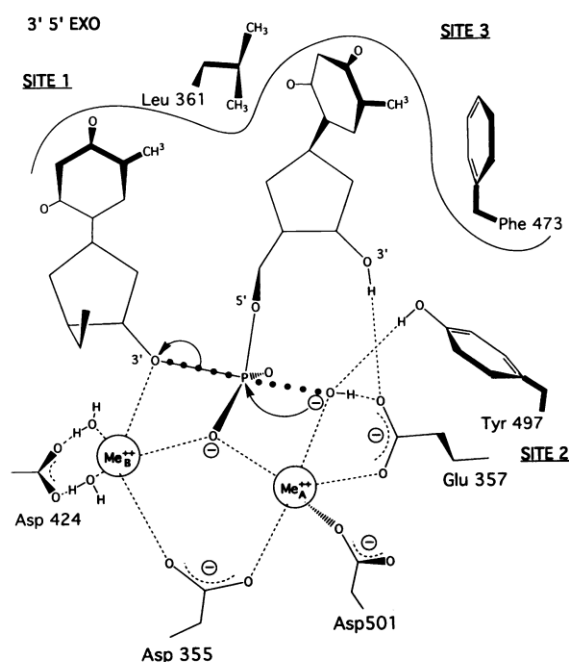


Figure 1.5 Proposed coordination site of the metal ions of the 3'-5' exonuclease, from reference¹⁶

As reported in the proposed mechanism by Beese and Steitz (Figure 1.5), while metal ion A coordinates with Asp355, Glu357, Asp 501, one phosphate oxygen and a hydroxide molecule, metal ion B is involved in the coordination with the bridging carboxylate of Asp 355, two of the phosphate oxygen and other three water molecules. Interestingly, even though the phosphorous group is still well-positioned and activated by metal ion A (which seems to have a more structural function), the absence of metal ion B results in a five order of magnitude activity loss. Although there is scepticism regarding the binding and catalytic relevance of one of the two metal ions, from the X-ray crystallography and the enzyme kinetic data, it has been suggested that their presence might stabilise the trigonal-bipyramidal phosphorous intermediate while enhancing solvent nucleophilicity and assisting the removal of the 3'-hydroxyl of the shortened DNA fragment (effect summarised in Figure 1.3 f).

1.3 Artificial endonucleases

Since the discovery of the first restriction enzyme in 1970,¹⁷ substantial efforts have been put into studying natural systems and developing artificial enzymes that could enhance efficiently and selectively the cleavage of nucleic acids.¹⁸ This interest is pushed by the wide potential applications such studies might provide in genome editing. For example, in molecular biology laboratories, employing artificial restriction enzymes could help sequence genomes, introduce specific nucleotidic patterns into a target double-strand filament, and modulate gene expression.¹⁹ All these operations, which involve cutting the DNA at sites not recognised by currently identified natural enzymes, might also be useful in medicine for gene therapy to replace a defective gene with a normal allele at the correct chromosomal location.²⁰

In addition, synthetic hydrolases could be useful to determine the three-dimensional structure of DNA, such as Z-DNA, supercoiled circles or three and four-stranded DNA molecules. Such information is usually gained from NMR and X-ray crystallography. However, laborious analysis of NMR spectra are required and obtaining X-ray-quality crystals is often hard to achieve. Instead, a catalyst could be designed to recognise specific conformations sequences, such as single-stranded regions or left-handed helices, cleave them, and produce an equivalent result.²¹

Moreover, studying artificial enzymes expands and improves our knowledge about how biological systems work. For example, by understanding the catalytic mechanisms of smaller and easier systems, it has been possible to discover more about the enzymes' mode of action and the role played by metal ions.²²

1.3.1 The development of artificial restriction enzymes in molecular biology

As reviewed by Adli,²³ the first breakthrough in gene editing was understanding the advantages of the inducement of a double-strand break (DSB) into a DNA target site. Causing the break would determine an increase in the frequency of the gene integration of several orders of magnitude. Meganucleases, a subclass of endonucleases that recognise sequences of 14-40 base pairs (bp) of DNA, were first used to introduce a DSB.²⁴ However, one of the limits of this approach is related to the high selectivity of the enzymes. Each of them would target only a specific DNA fragment, and applying this strategy to different loci would have been hard to achieve. In addition, meganucleases repair most of the induced DSBs through an error-prone mechanism called non-homologous end joining (NHEJ), which could create defects and randomly introduce or delete small DNA pieces. These problems were overcome with the discovery and engineering of zinc fingers. Zinc fingers are small protein motifs that bind selectively small DNA and RNA units and mediate protein-protein interaction.²⁵ The most common Cys₂ His₂ zinc finger unit, first identified in the Transcription factor IIIA, consists of a sequence of approximately 30 amino acids, which fold in the presence of Zn(II) to form a two-stranded antiparallel β -sheets and the α -helix domain (Figure 1.6).

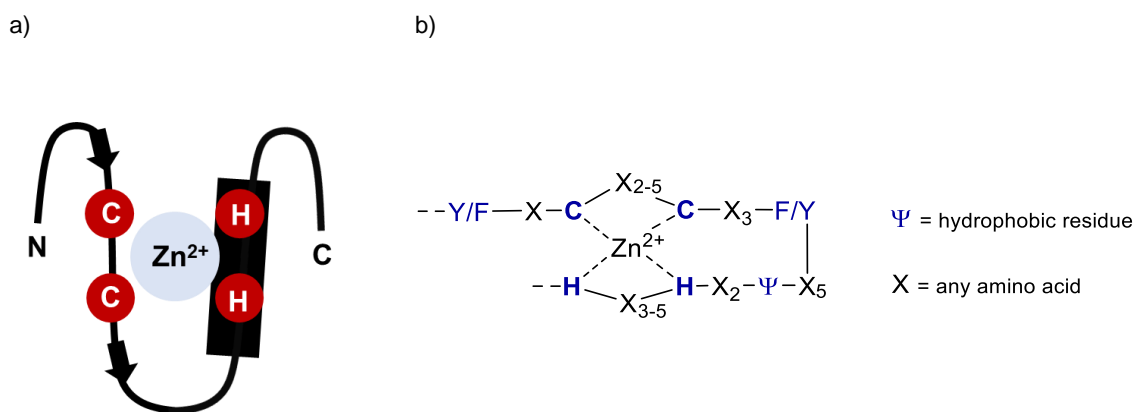


Figure 1.6 a) schematic representation of the coordination site of the Cys₂His₂ Zinc fingers; b) generic amino acids sequence of one Cys₂His₂ Zinc finger domain; in blue the conserved residues. In bold are the cysteine and histidine residues involved in the Zn(II) complexation

Despite the huge number of binding motifs discovered (over 15 000) and the few conserved residues in them,²⁶ the Zn(II) ion always coordinates to Cys and His residues, and the lack of the metal ion leads to unfolding; on the other hand, the substitution of cysteine or histidine leads to the loss of function. These proteins, interacting with DNA by inserting an α -helix into the major groove of the double helix, recognise specific triplet of base pairs and can be fused to create a highly engineered and programmable DNA-binding protein. Chandrasegaran and coworkers, conjugating a multiple fingers complex with the DNA cleavage domain of the restriction endonuclease Fok I, showed an interesting example of a hybrid enzyme.²⁷ Endonuclease Fok I is a member of bipartite restriction enzymes, which have two linked distinct domains: the C-terminal stored the non-specific DNA-cleavage activity and the N-terminal the DNA-binding.²⁸ Through its recognition domain positioned in the major groove of the DNA B-form, the protein strongly interacts with the nucleotides by multiple hydrogen bonds. The cleavage domain is not specific, and even though it exists as a monomer, it breaks both the substrate strands. Its activity strongly depends on two aspartic acids and a lysine residue,²⁹ and its position seems to be regulated by Mg(II) ions.

As reported in Aggarwal and coworkers' study on the X-ray structures of Fok I,³⁰ the domain stands next to the recognition portion, which prevents unnecessary breaks caused by the interaction of the unspecific cleavage site with the nucleic acid.

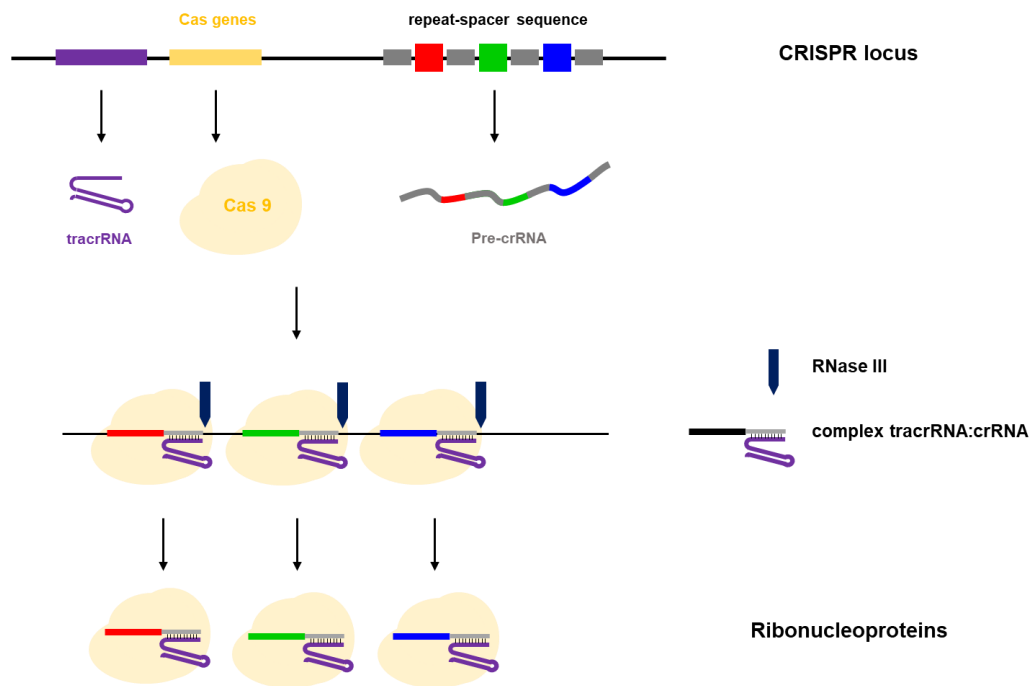
Interestingly, the metal ions have an important structural role, and their presence might be responsible for the enzyme activation, facilitating rotation around the linker and positioning the active domain in the major groove. Removing the recognition site and delegating the substrate binding to the zinc fingers complex allowed the creation of a highly efficient chimeric restriction enzyme. The test of the novel protein with 48.5-kb λ DNA yielded a specific and complete cleavage of the substrate producing primary two fragments (5.5-kb and 43-kb).²⁷ In contrast with the previous example, after the cleavage of double-strand DNA, Fok I leads to so-called homology-directed repair (HDR), determining the incorporation without defects of specific sequences provided by the donor template.²³ The conjugation of Fok I with transcription activator-like (TAL) effectors was a similar successful approach. TAL effectors are key virulence factors of *Xanthomonas*, a genus of proteobacteria that causes severe disease in plants.³¹ By mimicking the eukaryotic transcription factors, these effectors, binding the double strand, mediate gene induction and lead to changes in the development of the plant. In each of them, the domain which controls the recognition consists of a variable number of 33-35 highly conserved amino acids repeats, each capable of binding a single nucleotide.

Similarly to zinc fingers, the combination of the more versatile TAL effectors was used to design the recognition portion of the artificial endonucleases family called TALENs. Although highly efficient, zinc fingers and TAL nucleases required substantial work in

developing and engineering an artificial enzyme exclusively for a specific substrate sequence.^{32,33}

A completely different and revolutionary strategy was instead achieved by using CRISPR. The Cluster Regulatory Interspaced Short Palindromic Repeats is an adaptive immune system that bacteria and archaea use to defend themselves against viral and plasmid cellular invaders.²³ In prokaryotes, CRISPR immunity can be divided into two distinct phases, as summarised in Figure 1.7.³⁴ When the bacteria or archaea first enter in contact with the exogenous DNA, short portions of the latter are incorporated inside the CRISPR locus in the so called spacers, each separated by repeat sequences. The pre CRISPR RNA (pre-crRNA), a long RNA molecule with sequences homologous to the past invaders, is then transcribed by the cell from the spacers/repeats locus. At the same time, the trans-activating CRISPR RNA (tracrRNA), a second RNA fragment complementary to the repetitive regions, is also created from the CRISPR locus. When pre-crRNA is loaded into the Cas protein, it forms a double-stranded RNA with tracrRNA fragments on the repeat sequences. At this stage, the RNaseIII, a restriction enzyme that cuts double-stranded RNA, cleaves the long pre-crRNA filament at the end of each RNA complex determining the formation of multiple ribonucleoproteins (end of Phase I in Figure 1.7).

Phase I :



Phase II :

Exogenous DNA of past invader

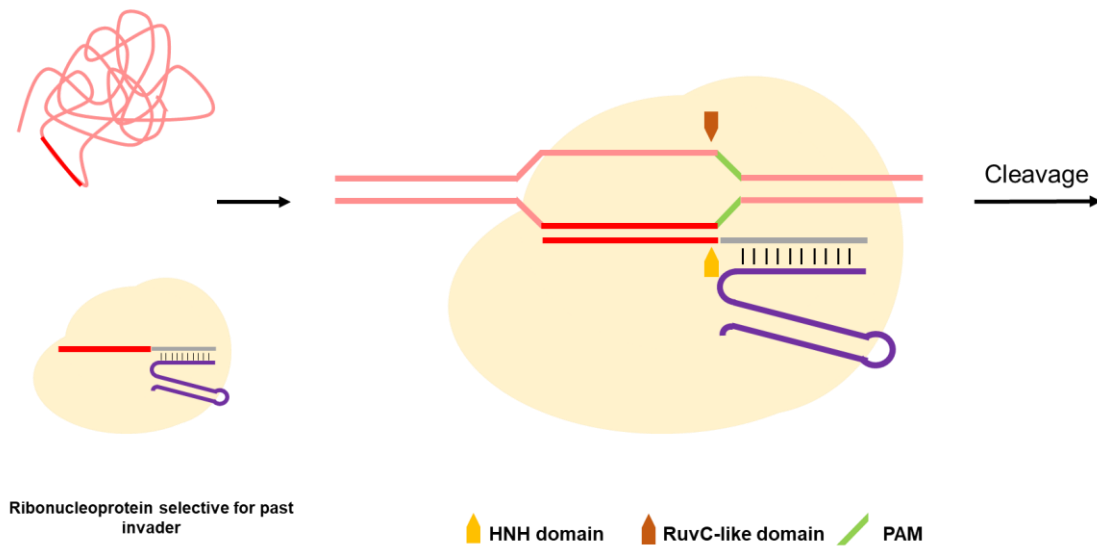


Figure 1.7 Schemes of the two phases of the CRISPR-Cas9 immunity in bacteria and archaea based on reference³⁴

The following phase concerns the organism's defence against the second invasion. Once the invading nucleic acid re-enters the cell, it is cleaved by the ribonucleoprotein due to the interaction with the complementary RNA. However, the formation of the DNA:crRNA hybrid (R loop) is mediated by Cas9, which recognise a specific sequence of the exogenous genome called *Proto-spacer adjacent motif* (PAMs – coloured in green in Figure 1.7). This unit can vary from protein to protein, and the most used *S. pyogenes* Cas9 binds to a 5'-NGG-3' PAM (with N being a generic nucleotide). The interaction of two arginine residues of *S. pyogenes* Cas9 with the guanine nucleobases is critical to facilitate the DNA strand unwinding and the formation of the R loop.³⁵ Eventually, the cut happens by the action of either one or two cleaving domains of Cas9 that nick the complementary (HNH domain) and not complementary (RuvC-like domain) DNA strand of the crRNA. Although Cas9 can repair the DSB by a non-homologous end-joining process, in the presence of a nearby DNA template with homology to the region of the DSB, the integration of a fragment can also be achieved by a homology-directed mechanism.

The process described above shows how CRISPR-Cas9 is an extremely flexible tool that can potentially generate any specific mutations as long as the target gene is known and its sequence has the specific PAM recognised by the protein. The first step of gene editing in eukaryotic cells is the design of the RNA strand corresponding to the target genomic region. Although off-target modification can often be reduced by choosing a 20-nucleotides region adjacent to the PAM site, unselective mutations can happen and cannot completely be avoided.³⁶ Cas9 and both the tracrRNA and crRNA, often combined in a longer sequence called signRNA, are introduced either expressed as DNA, RNA or RNA/protein complex together with a single or double-stranded DNA sequence used as a template for the editing.

CRISPR's high performance, recognised with the 2020 Nobel prize in Chemistry, has made these systems excellent tools for even more elaborate genome editing applications and has renewed the scientific community's attention on artificial and natural endonucleases.²³ However, off-target modifications that alter the experimental result are not completely understood and are still under investigation.³⁶ Aiming to define the mechanism of non-target DNA cleavage, substantial effort has been dedicated to studying the catalytic nature of the Cas protein, particularly the role of the metal ions and the other participants in the RuvC and NHN domains.³⁷ For example, as Wang and coworkers reported,³⁸ the activity of the Cas12i2's RuvC domain (the only DNase catalytic portion of the protein) strictly depends on the presence of two metal ions and specific amino acid residues. As proposed in their work, the two Mg(II) ions, while ligated by two aspartic acids (Asp 599 and Asp 1019) and one glutamic acid (Glu 833), coordinate to the scissile phosphate group's oxygens. Figure 1.8 shows a magnified view of the Mg (II) ions site and highlight the coordination of one of the two ions (A) to a water molecule positioned at 3.9 Å from the phosphate (evidence that suggests potential activation for nucleophilic attack).

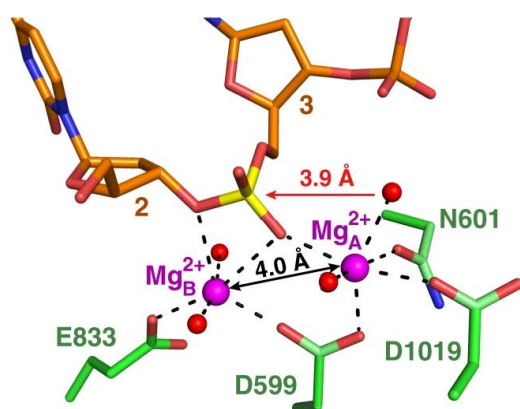


Figure 1.8 Active coordination site of RuvC domain of Cas12i2^{wt} in a ternary complex with crRNA and DNA³⁸

Mechanistic insights can also be achieved by employing smaller systems that mimic the protein activity. Since the discovery of hydrolases, metal ion complexes have been used as promising models to elucidate the mechanism of phosphate hydrolysis, trying to offer a complete picture of enzymatic catalysis.¹¹ In addition, fully synthetic catalysts, able to cleave phosphodiester bonds, could potentially compete with the current molecular biology tools and offer a valuable alternative. Although metal ions complexes have not accomplished comparable accelerations to those of natural systems, their activity can potentially be improved by providing appropriate functional groups. Furthermore, given their rather smaller dimensions than engineered enzymes, the design, development and optimisation of synthetic catalysts can be achieved more rapidly and efficiently.

1.3.2 Chemistry Approach

Following a similar approach to Zn fingers and TALE nucleases, chemists have developed artificial hydrolases in which the recognition and catalytic functionalities are conferred to two different moieties. Zuckermann and Schultz were the first to apply this strategy in their hybrid RNase.^{39,40} Delegating the recognition activity to a single-stranded DNA sequence and the cleavage functionality to the staphylococcal RNase A (unable to cleave the deoxyribonucleic acid) (Figure 1.9), they showed the potential to control and deliver enzymatic activity selectively.

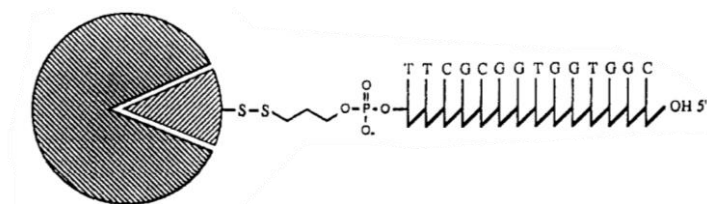


Figure 1.9; Hybrid oligonucleotide-RNase A from reference ³⁹

The separation of the two domains represents a huge advantage that has opened the possibility of designing and optimising fully artificial systems in which the activity is delegated to metal ions complexes.

The first example of synthetic nucleases, published in 1994 by Sampath and coworkers, consists of a 17-mer DNA oligonucleotide attached to a terpyridine ligand at C-5 of an internal uracil residue (*Figure 1.10*).⁴¹

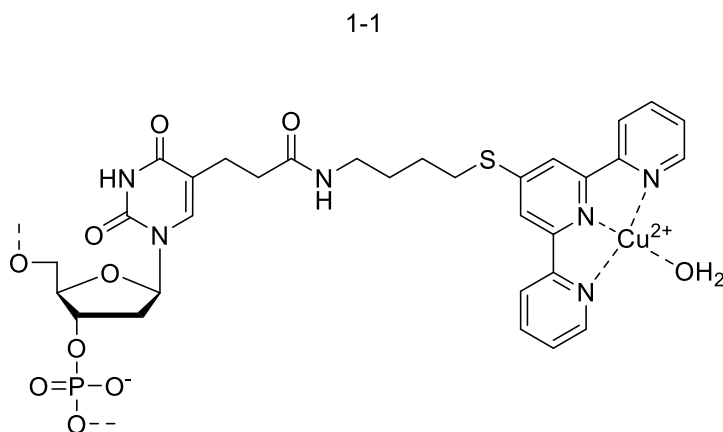
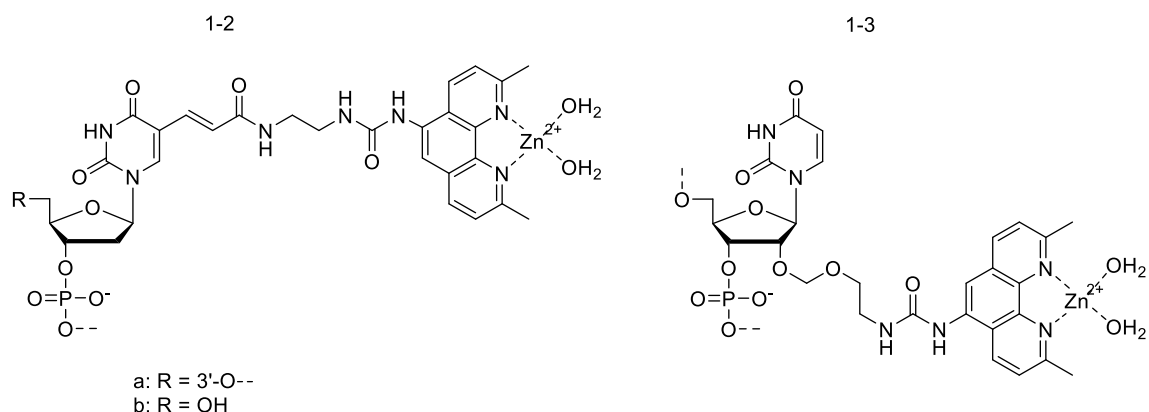


Figure 1.10; The first synthetic functional mimic of a nuclease used to cleave the target RNA⁴¹

The target, 159-mer RNA sequence derived from the gag-mRNA of HIV, is sequence-specifically cleaved at pH 7.5. As this work suggests, the position of the conjugation site in the oligonucleotide sequence could have an important effect on the activity of the catalyst. If the catalytic moiety is placed in one of the two extremities of the recognition domain, the cleaved RNA fragment, which mostly maintains its length, can still bind to the catalyst's DNA strand. To avoid losing catalytic turnover and enhance the release of the artificial enzyme, it is important to locate the scission point within the RNA-DNA duplex region. This is because the binding constant between the oligomer and the target is strongly length-dependent, and two shorter RNA fragments can be removed more easily than a longer one. In addition, placing the catalytic head group at the end of the sequence leads to more flexibility and makes the cleaving site hard to control and predict.⁴²

In the last two decades, Strömberg and coworkers have created a series of artificial nucleases that use this strategy by conjugating different catalytic groups with modified oligonucleotide sequences.⁴³ For example, positioning the catalytically active Zn(II) complex of 2,9-dimethylphenanthroline in different sequence regions and using different linkers between the head group and the recognition moiety leads them to achieve efficient and selective cleavage (Figure 1.11).



Structure of the artificial ribonuclease/target RNA complexes:

5' - U C U C G G U - (A)_n - G C U C - 3'

3' - A_mG_mA_mG_mC_mC_mA_m - X - G_mA_mG_m- Y

N_m denotes 2'-OMe nucleotide residue

X = 1-2a and 1-3

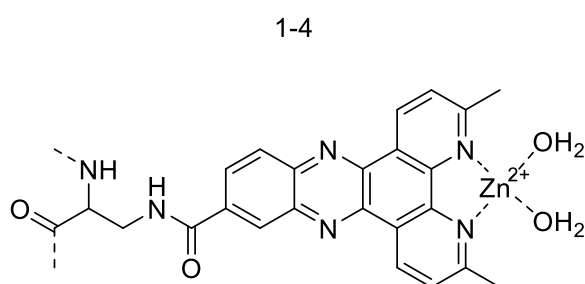
Y = 1-2b

Figure 1.11; Schematic representation of the oligonucleotide-based artificial nucleases studied by Roger Strömberg and coworkers⁴³

They tested each artificial enzyme candidate with different targets, whose interactions with the modified sequence by Watson-Crick base pairing would create different size bulges. No cleavage was detected when all the bases were paired. At pH 7.4 and 37 °C, **1-2a** (oligonucleotide-based artificial nuclease; Figure 1.11) showed the best results, achieving higher selectivity for 3- and 4- adenosine bulges with k_{obs} of $1.4 \pm 0.02 \times 10^{-5} \text{ s}^{-1}$ and $1.7 \pm 0.04 \times 10^{-5} \text{ s}^{-1}$, respectively (substrate and artificial enzyme are equimolar and equal to 4 μM). In the same conditions, the shorter linker used in **1-3** reduced its activity toward the cleavage of larger bulges while enhancing the reaction for the 2-nucleotide AA bulge, showing a k_{obs} of $7.5 \pm 0.02 \times 10^{-6} \text{ s}^{-1}$. By placing the catalytic head group in the 5' end of the recognition domain, limited reactivity with every bulge was observed for **1-2b**. The greater length (including the extra unpaired nucleotide) and the consequent flexibility might

be responsible for the lower rates observed. However, due to its spatial proximity to the larger bulges, **1-2b** showed selectivity toward those.

The promising but limited acceleration provided by **1-2a** has been recently exceeded by the Zn(II) dependent PNA-based artificial ribonuclease **1-4** shown in Figure 1.12.⁴⁴



Structure of the PNAzyme / target RNA complex:

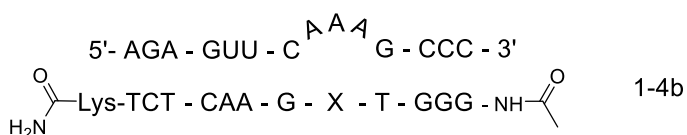
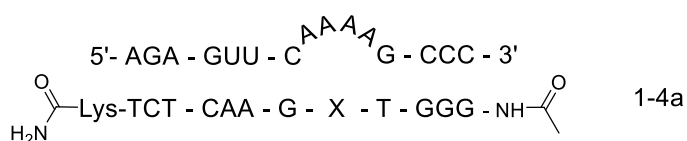


Figure 1.12 Structure of the Zn(II) dependent peptide nucleic acid-based artificial ribonuclease (PNAzyme)⁴⁴

Although previous PNAzymes had already demonstrated high site-specificity, reducing the half-life time of RNA substrate to 20-30 min, their reactivity was extremely dependent on the presence of Cu(II) ions, which is problematic for therapeutic applications.⁴⁵ At pH 7 and 37 °C, **1-4** enhanced the cleavage of the RNA target with 4-nucleotide AAAA (**1-4a**)

and 3-nucleotide AAA (**1-4b**) bulges, reducing their half-life time to 3 and 1 hour, respectively. It is suggested by the authors that the dimethyl-dipyridophenazine's increased rigidity and its interaction with the target can result in a pre-organisation of the RNA bulge, which might favour the cleavage and help to better position the metal ion for the catalysis. When the bulge residues were changed in **1-4b** (AUG, GUA or UUA), a substrate half-life time of 16 min were measured, making this system the most active among Cu(II) and Zn(II)-dependent PNAzymes to date.

These conjugates are just a few examples of the large class of synthetic nucleases proposed.⁴⁶ Even though promising results have been achieved, the efficiency of these systems is still insufficient for most of the potential applications, especially compared with the activity reached by natural enzymes. Optimising the structure of the artificial enzyme, exploring the different combinations of moieties and studying the effect of different links between them are present and future challenges. Among these factors, the catalytic portion plays a crucial and essential role. Many investigations have been done to increase metal ion complexes' activity by designing the ligand scaffolds and providing appropriate functional groups.⁴⁷

1.3.3 Models

RNA and DNA model molecules have been intensively used as substrates to first screen among complexes. The cleavage of phosphodiester molecules with chromophore leaving groups is easy to monitor and can provide a quick measure of catalysts' performance. As summarised in Figure 1.13, 4-nitrophenolate, whose appearance can be followed at 400

nm, is often the leaving group used in the commercially available or synthesised artificial substrates.

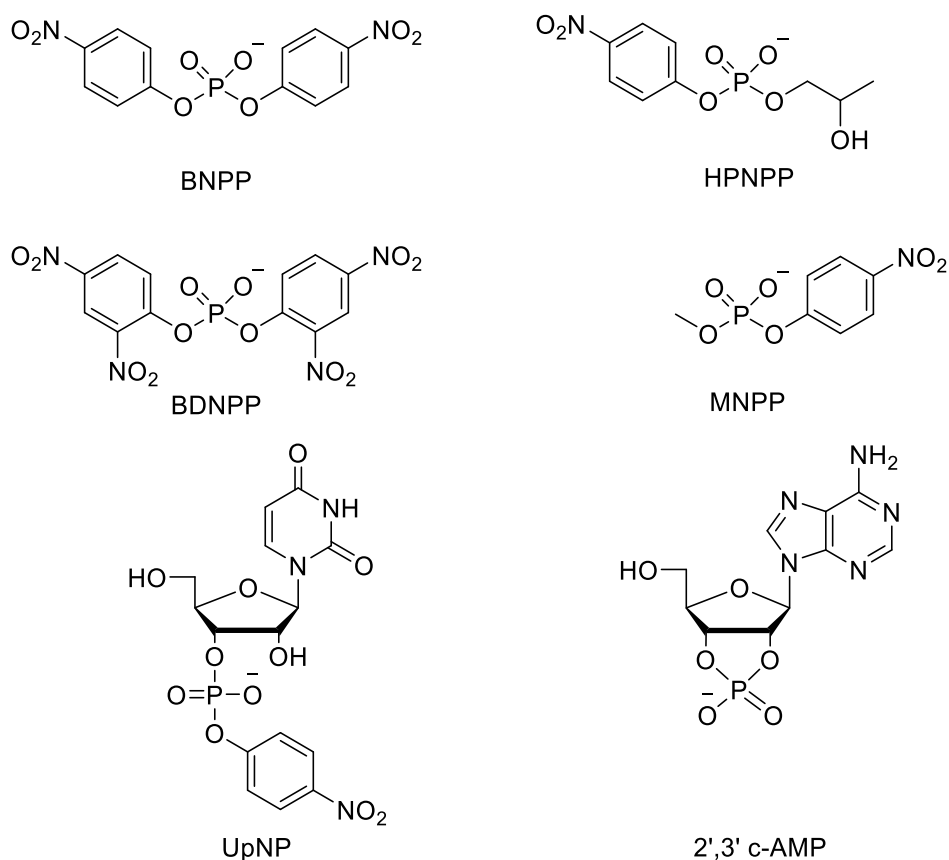


Figure 1.13 Structure of artificial substrate used a DNA (BNPP, BDNPP and MNPP) and RNA (HPNPP, UpNP and 2',3' c-AMP) model molecules

Given its low pK_a of 7.15,⁴⁸ 4-nitrophenolate is an excellent leaving group, especially compared to those of the natural targets (pK_a of 3'OH in DNA and RNA estimated to be approximately 14.3 and 13.5, respectively⁴⁹). Although the most commonly used substrates bis 4-nitrophenyl phosphate (BNPP) and 2-hydroxypropyl 4-nitrophenyl phosphate (HPNPP) are relatively stable to hydrolysis, their half-life times at 25 °C and neutral pH of approximately 100^{50,51} and 22 years (value extrapolated from reference⁵²), respectively, are quite lower than those of the natural targets. For this reason, often complexes have been

tested toward the cleavage of phosphates with worse leaving groups (like phenol or methyl) to replicate better the reaction catalysed by enzymes. The higher stability of the nucleic acids depends on different aspects, which are related to the stable phosphate group itself and their overall macrostructures. Therefore, a direct comparison between the biopolymer and their models cannot be drawn, but there are differences in the reaction participants. To start, the presence of a better leaving group makes BNPP and HPNPP less stable to cleavage compared to their natural counterparts. For RNA, this is partially balanced by the different reactivity of the nucleophile; the 2'-hydroxyl group results more constrained and predisposed to attack the phosphorus than the more flexible 2-hydroxypropyl of the HPNPP. Furthermore, proof of the different reactivity is also shown by the higher pK_a value of the model nucleophile.⁵³

In addition, dinucleotides, cyclic monophosphate or small oligonucleotides strands have been tested to evaluate cleavage selectivity.

1.3.4 Design of the catalytic head group

Among the first active catalysts employed for hydrolysing phosphate diesters, Chin *et al.* proposed a series of Co(III) complexes, whose reactivity was extremely dependent on the ligand structure.⁵⁴ The complexes of the tetramine ligands shown in Figure 1.14 were first studied toward the hydrolysis of BNPP.

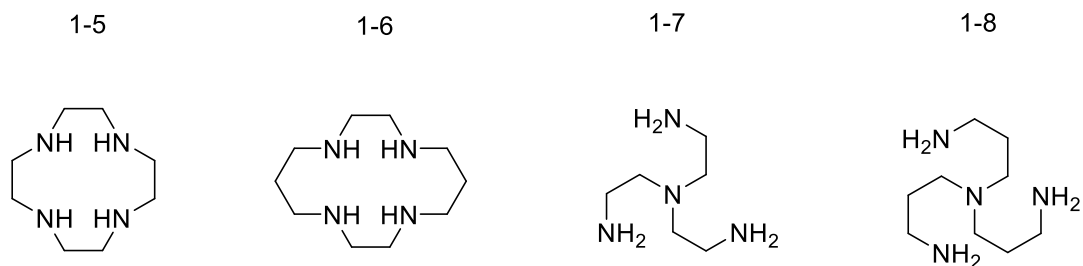


Figure 1.14 Structure of ligands studied as metal ion complexes

At pH 7.0 and 50 °C, the second-order rate constants for the hydrolysis of BNPP catalysed by the Co(III) complexes of **1-5**, **1-7** and **1-8** were $4.38 \times 10^{-1} \text{ M}^{-1} \text{ s}^{-1}$, $8.14 \times 10^{-3} \text{ M}^{-1} \text{ s}^{-1}$ and $2.5 \text{ M}^{-1} \text{ s}^{-1}$, respectively. The authors proposed that substrate cleavage is caused by the intramolecular-like nucleophilic attack of metal bound hydroxide. Surprisingly, the 300-fold difference between **1-8** and **1-7**, which was not ascribed to a different substrate binding constant, revealed that the complex's intrinsic reactivity depends on the ligand's tetramine scaffold. Although the Co(III) complexes were the most reactive catalysts, accelerating the background reaction by 10^5 - 10^8 fold at neutral pH, rather small enhancements were observed when the metal ion was replaced by the more biocompatible Zn(II) ion. Kimura⁵⁵ and Trogler⁵⁶ showed that the complexation of **1-7** and **1-5** to Zn(II) ions caused a rather small enhancement over the background reaction of 2- and 46-fold, respectively. A 15-fold difference in reactivity was observed when [**1-5**:Zn(II)] was compared with the tridentate [**1-9**:Zn(II)], which provided a 550-fold acceleration over the background reaction. The lower rate constants for the Zn(II) complexes of the tetradentate ligands was attributed to the occupation of more of the ion binding sites, which would inhibit substrate coordination. In addition, the complexes' reactivity has been proposed to depend on the ability of the metal ion to deprotonate the bonded water molecule and facilitate the nucleophilic attack

on the phosphorous. As reviewed by Mancin and Tecilla,⁵⁷ complexes of tridentate ligands **1-9** and **1-10** show lower pK_a values and so are more reactive at neutral pH due to the presence of a greater proportion of their active species.

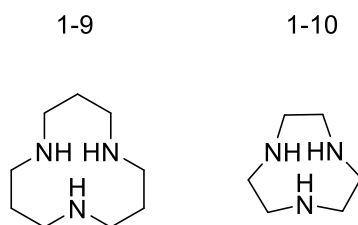


Figure 1.15 Structures of tridentate ligands

By comparing the **1-6** and **1-7**, Tonellato and coworkers also highlighted how the ligand structure impacts the complex reactivity.⁵⁸ Although both tetradentate ligands bind the metal ion and have similar pK_a s for their coordinated water molecules (9.87 and 9.8 for the branched and cyclic ligand, respectively), [**1-7**:Cu(II)] is 3-fold less reactive than [**1-6**:Cu(II)]. The difference could be assigned to the trigonal bipyramidal geometry assumed by **1-7**, further reducing the space for substrate binding compared to the facial coordination mode of **1-6**.

Alternative pyridyl-based ligands were first proposed by Morrow (**1-11**)⁵⁹ and Bashkin (**1-12**)⁶⁰ to avoid the occupation of too many of the coordination sites of divalent metal ions (Figure 1.16).

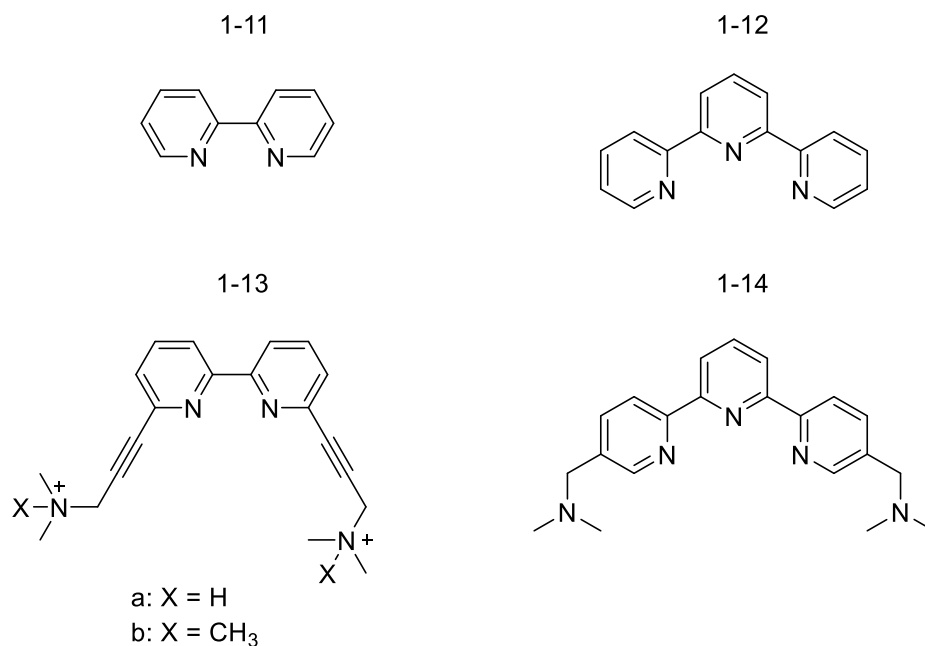
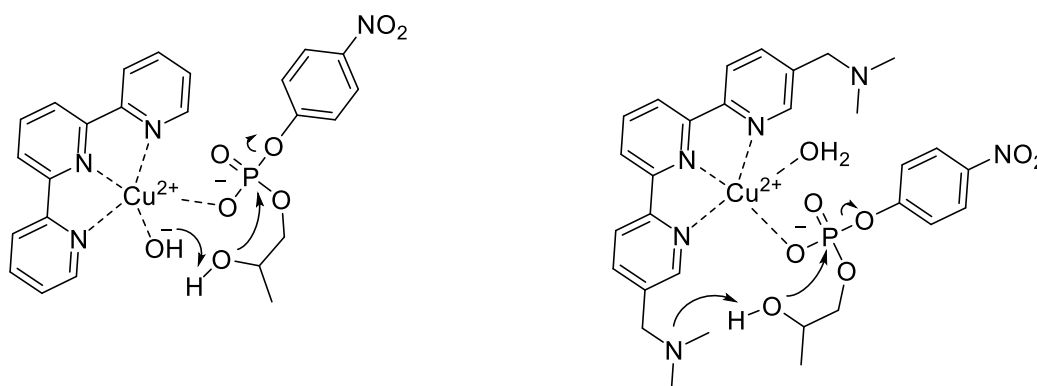


Figure 1.16 Structure of pyridyl-based complexes^{59,60,61}

At 75 °C and pH 6.5, [**1-11**:Cu(II)] (1 mM) leads to a 2000-fold enhancement of BNPP hydrolysis compared to the background reaction. Interestingly, greater reactivity was observed after the ligand scaffold is substituted with ammonium groups.⁶² Although the mixture ethanol:water (19:1) needed to dissolve the complexes affects the catalysis,^{63,64} the Cu(II) complexes of **1-13a** and **1-13b** were 2900 and 2.6 times more reactive than that of **1-11**. As described by the authors, the reactivity of [**1-13a**:Cu(II)] decreases more than 10-fold when the water content reaches 15%, which is ascribed to complex dissociation and competition from water in solvating the phosphate and the ammonium sites, inhibiting the hydrogen bond interactions between the groups. When comparing the Cu (II) complexes of **1-12** and **1-14** toward the hydrolysis of HPNPP, an interesting insight into the catalytic mechanism was proposed by Shanghao *et al.*⁶¹ Although the tertiary amines add a modest enhancement to the observed rate constant (6.7-fold compared to [**1-12**:Cu(II)]), the pH

profile of k_{obs} for [1-14:Cu(II)] reveals an additional base group with a pK_a of approximately 6.5 involved in the catalysis. [1-12:Cu(II)] showed the typical bell-shaped profile with a maximum at pH 9, suggesting that the pK_a of the metal bound water molecule is around pH 8. Due to the tertiary amine that can provide general base catalysis, [1-14:Cu(II)] is more reactive than [1-12:Cu(II)], even if the metal bound hydroxide is not formed at neutral pH. However, moving to alkaline values, the difference between the two complexes is lost, and both the catalysed reactions rely on the participation of the metal bound hydroxide. Scheme 1.4 shows the possible mechanisms for the transesterification of HPNPP at alkaline pH (left) and neutral pH (right).



*Scheme 1.4 Mechanism of the transesterification of HPNPP catalysed by [1-8:Cu(II)] at alkaline pH (left) and [1-10:Cu(II)] at neutral pH (right)*⁶¹

This work encourages using a ligand structure that introduces functional groups that can replace the role of metal bound hydroxide in the cleavage reaction at neutral pH or favour its formation by lowering the pK_a of the metal bound water. A relevant example is the functionalisation of phenanthroline with methyl and amine groups proposed by Chin and coworkers (Figure 1.17).^{65,66}

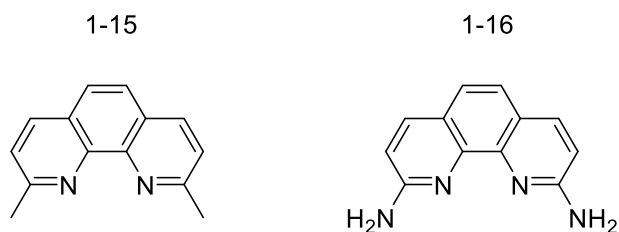


Figure 1.17 Structures of phenanthroline-based ligands proposed by Chin *et al* ⁶⁵

The more rigid structure of **1-15** strongly influences the Lewis acidity of the metal ion, shifting the pK_a of the Cu(II) bound water molecule to 7 (0.8 and 1.2 units lower than **1-11** and **1-12**). As a result, [**1-15**:Cu(II)] (10 mM) reduces the half-life time of Adenylyl-(3'-5')-adenosine (0.5 mM) to 3 min, which is 20 000 and 200 times faster than the analogous complexes of **1-11** and **1-12**, respectively. However, according to the authors, the higher reactivity is not only a consequence of the lower pK_a but might depend on the two methyl groups of the neocuproine ligand being able to decrease the O-Cu-O bond angle and favour the chelation and double lewis activation of the phosphate. Wall *et al.*⁶⁵ were among the first to investigate the influence of primary amine in the second coordination sphere. The hydrolysis of 2',3'-cAMP and BDNPP (0.05 mM) showed a first order dependence on the concentration of the Cu(II) complexes of **1-16**, **1-15** and **1-12** at 25 °C. [**1-16**:Cu(II)] showed the highest reactivity, enhancing the background reaction by 6.3×10^3 (BDNPP) and 3.5×10^4 fold (2',3'-cAMP). Remarkably, 1 mM of catalyst at pH 6 and 25 °C provides over 10^9 -fold rate acceleration over the background base catalysed reaction of the cyclic phosphate. In addition, [**1-16**:Cu(II)] enhances the regiospecific cleavage of 2',3'-cAMP producing 3'-AMP and 2'-AMP in the ratio of 16:1. Although the Lewis acidity of the Cu(II) ion was expected to be reduced by the electron donating amino groups, the reduced pK_a (5.5) of the metal bound water was attributed to the hydrogen bond donating nature of the

substituents that stabilise the metal bound hydroxide (**1-16a**). This hypothesis was corroborated by the increased pK_a (7.7) of **1-16b**, in which the nitrogen groups could only act as hydrogen bond acceptors (Figure 1.18). However, this comparison involves a substantial change in ligand structure, and assigning the overall effect solely to the hydrogen bonding interactions may not be justified.

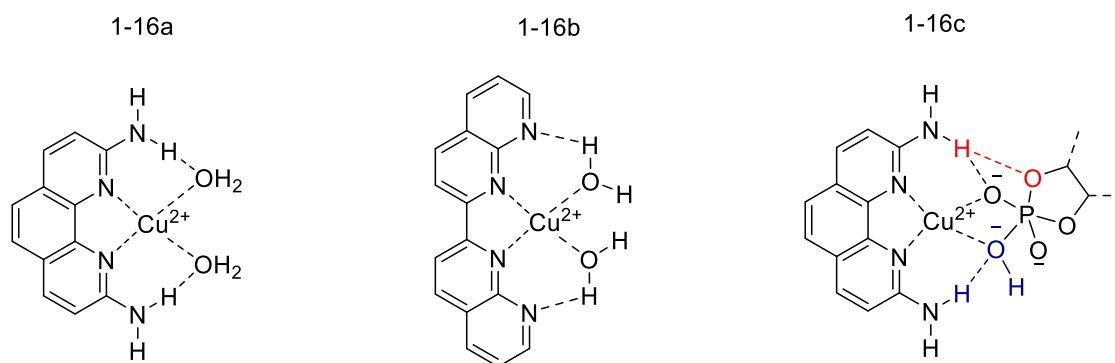


Figure 1.18 Structures of complexes that highlight the impact of different nitrogen sources on the metal bound water pK_a ⁶⁵

The lower pK_a observed for [**1-16**:Cu(II)] and the consequent reduction of the nucleophilicity of the hydroxide seem to be compensated by the hydrogen bond interaction between the amine groups and the phosphate in the transition state (**1-16c**). The authors proposed that the amines modulate the acidity of the hydroxide (blue in **1-16c**) and facilitate the expulsion of the leaving group (red in **1-16c**). This effect, which is greater for substrates with poorer leaving groups, is confirmed by the gaps in reactivity between [**1-16**:Cu(II)] and [**1-15**:Cu(II)]. While only a 20-fold difference is calculated when the catalysts are tested toward the hydrolysis of BDNPP, [**1-16**:Cu(II)] is 600-fold more reactive than [**1-15**:Cu(II)] for hydrolysing 2',3'-cAMP.

Taking inspiration from metalloenzymes that often use more than one cation in their catalytic cavities, the construction of ligand scaffolds able to accommodate multiple metal ions has been widely investigated. An interesting example is Yashiro *et al.*'s work, which compares the activity of mono-, bi- and tri-nuclear Zn(II) complexes having homo-structural features (Figure 1.19).⁶⁷

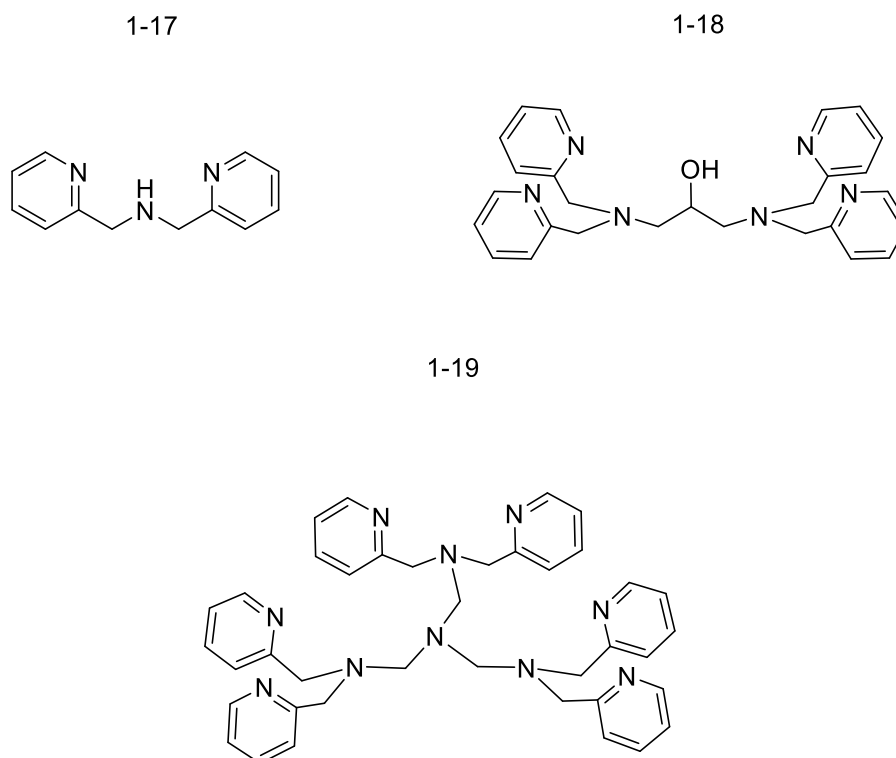


Figure 1.19; Comparison among the structures of ligands designed to form mono-, di- and trimetallic complexes⁶⁷

While the mononuclear bis(pyridin-2-ylmethyl)amine complex [**1-17**:Zn(II)] did not show any detectable activity toward the hydrolysis of several dinucleotides, the presence of two and three Zn(II) centres in [**1-18**:Zn(II)₂] and [**1-19**:Zn(II)₃] provided a substantial rate acceleration over the substrate's background reaction. For example, the dinuclear and trinuclear complex (5 mM) reduced the half-life of CpA to 180 and 16 min at pH 6.5 and

50 °C, respectively. Although relatively small cooperativity was observed after the addition of a third ion (k_{rel} of 12), the cleavage catalysed by [**1-19**:Zn(II)₃] preferentially yielded the 3'-NMP over the 2'-NMP in a ratio 9:1. However, considering the catalytic inefficiency of [**1-17**:Zn(II)], the two metal ions in the dinuclear complex act cooperatively. The strong enhancement might be due to **1-18**'s structure in which the hydroxyl, behaving as an alkoxide bridge in the complex, shields and reduce electrostatic repulsion between the two positively charged metal ions.

The construction of ligand scaffolds able to accommodate two metal ions was also undertaken by Hamilton and coworkers.^{66,68}

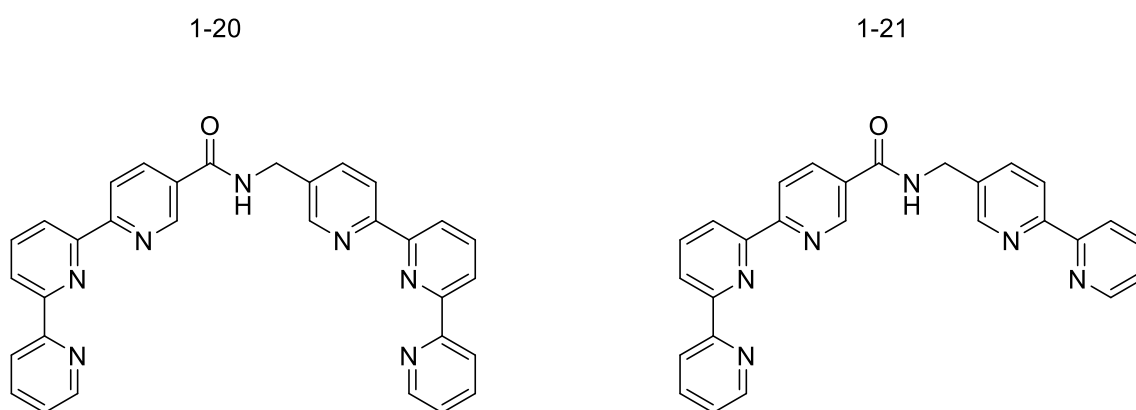
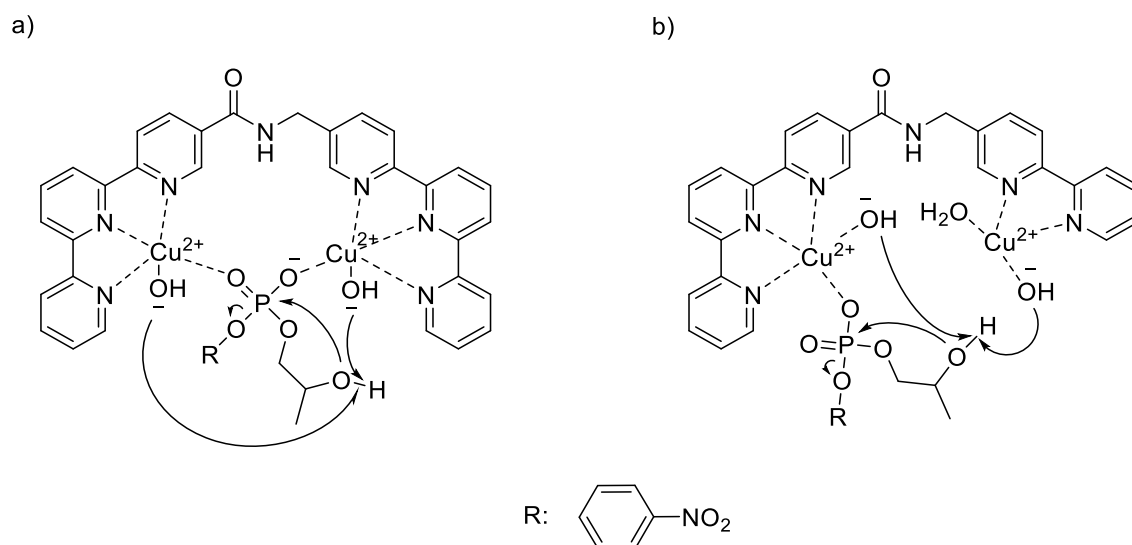


Figure 1.20 Structure of ligands used as dinuclear complexes by Hamilton and coworkers^{66,68}

By conjugating two binding units (terpyridine or bipyridine) with an amide spacer, ligands **1-20** and **1-21** were tested as Cu(II) dinuclear complexes and showed high reactivity toward the hydrolysis of HPNPP and 2',3'-cAMP. As reported for the transesterification of HPNPP at pH 7 and 25 °C, the second metal ion increases the reactivity of [**1-20**:Cu(II)₂] and [**1-21**:Cu(II)₂] by 51- and 67-fold compared to [**1-12**:Cu(II)], respectively, and makes [**1-**

21:Cu(II)₂] 24-fold more reactive than **[1-11:Cu(II)]**. Based on the pH profile of k_{obs} , different cooperative mechanisms were proposed for the two complexes. Double lewis activation and double general base catalysis were proposed for **[1-20:Cu(II)₂]** (Scheme 1.5a), while the reaction enhanced by **[1-21:Cu(II)₂]** would proceed through single Lewis acid activation and as well as double general base catalysis (Scheme 1.5b).



Scheme 1.5 Proposed mechanism for the Cu(II) complexes of 1-13 and 1-14^{66,68}

In addition, **[1-21:Cu(II)₂]** was tested with a series of dinucleotides and showed maximum reactivity at pH 7.5, and gave an unexpected selectivity toward adenine-containing substrates which was attributed to strong π - π stacking interactions between the base and the bipyridyl unit.⁶⁹

Compared to the enhancement provided by the catalysts for the transesterification of RNA-models, unsatisfactory results were achieved for the hydrolysis of DNA-like phosphate groups. In analogy with the natural targets, those molecules lack an intramolecular

nucleophiles and show higher stability toward hydrolysis. In the active centre of alkaline phosphatases, the phosphate monoester coordinated to the Zn(II) ions is first attacked by a serine residue yielding a phosphorylated intermediate which is eventually hydrolysed to reinitiate the catalytic cycle.⁷⁰ Hence, incorporating a hydroxyl group into ligand structures has often been used as a successful strategy to enhance the cleavage of BNPP. For example, Shiro and coworkers investigated the difference in the reactivity of the Zn(II) complexes of **1-23** and **1-5** and **1-22** (Figure 1.14 and Figure 1.21).⁷¹

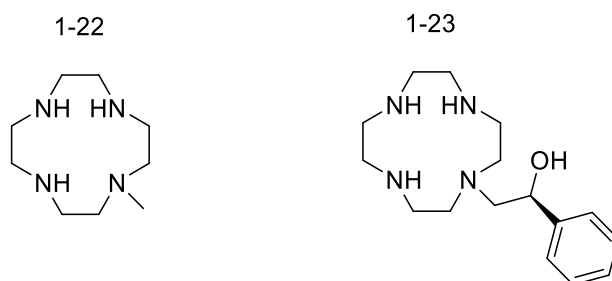
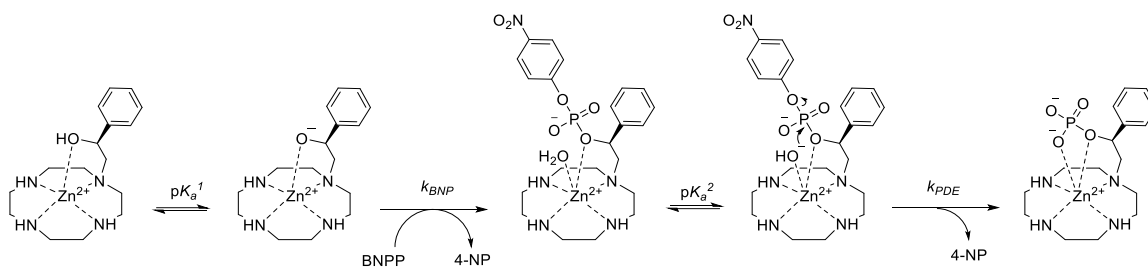


Figure 1.21 Structure of the ligands proposed by Shiro and coworkers⁷¹

In contrast to the reaction catalysed by [**1-5**:Zn(II)] (ligand **1-5** reported in Figure 1.14, page 43) and [**1-22**:Zn(II)], in the presence of [**1-23**:Zn(II)], BNPP is cleaved by transesterification. As reported in Scheme 1.6, once the active catalytic species is formed at pH 7.4, the alkoxide of the ligand attacks the phosphorous, producing a phosphorylated complex, which is eventually hydrolysed by the metal bound hydroxide ($pK_a^2 = 9.0$) at alkaline pH. Although the cleavage proceeds through a different mechanism, with a k_2 of $6.5 \times 10^{-4} \text{ M}^{-1} \text{ s}^{-1}$, [**1-23**:Zn(II)] is 30 and 125 times faster than its analogous [**1-5**:Zn(II)] and [**1-22**:Zn(II)], respectively.



Scheme 1.6 Proposed mechanism of BNPP cleavage catalysed by $[\mathbf{1-23}:\text{Zn}(\text{II})]$ ⁷¹

Catalyst improvement can be achieved by decorating a dinuclear ligand with a nucleophilic group that positively contribute to the activity of complexes. Following this strategy, Bazzicalupi *et al.*⁷² introduced a pendant alcohol to the macrocycle **1-24**, which was used as a ligand to form a dinuclear Zn(II) complex (Figure 1.22).

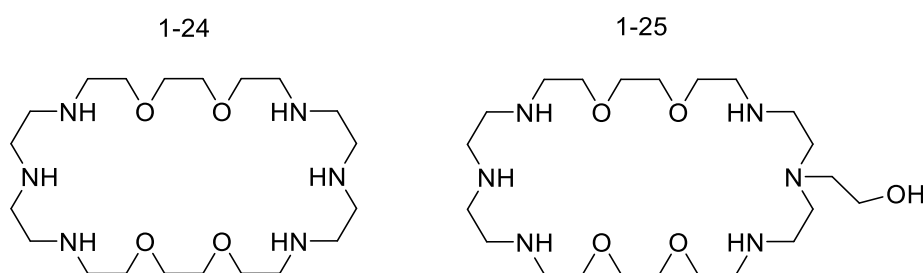


Figure 1.22 Structures of ligand proposed by Bazzicalupi *et al.*⁷²

$[\mathbf{1-25}:\text{Zn}(\text{II})_2]$ showed its highest activity at alkaline pH with k_2 of $8.3 \pm 0.4 \times 10^{-4} \text{ M}^{-1} \text{ s}^{-1}$ recorded for the transesterification of BNPP. Under the same reaction condition, $[\mathbf{1-24}:\text{Zn}(\text{II})_2]$ catalysed the hydrolysis of BNPP 7 times slower. The improvement provided by the small hydroxyl pendant was limited, but $[\mathbf{1-25}:\text{Zn}(\text{II})_2]$ could offer a good model for describing the mechanism of alkaline phosphatase.

1.4 Aims

This project aims to develop more effective catalysts for phosphate diester cleavage in water, building on the concepts that have been described in this introduction and applying them to the development of pyridyl-based Zn(II) complexes.

The second chapter of this thesis focuses on catalysts designed to hydrolyse the phosphodiester bond of DNA. It has been shown that 6'amino groups in the pyridyl substituent of Zn(II) complexes lead to much higher reactivity, and this effect has been ascribed to its hydrogen bond donor properties^{52,73,74}. If this is correct, then stronger hydrogen bond donors will lead to more highly active complexes. To this aim, a comparison between a sulfonamide and a primary amine substitution in *ortho* of the pyridine ring is undertaken (**2-1** and **2-2**, respectively in Figure 1.23).

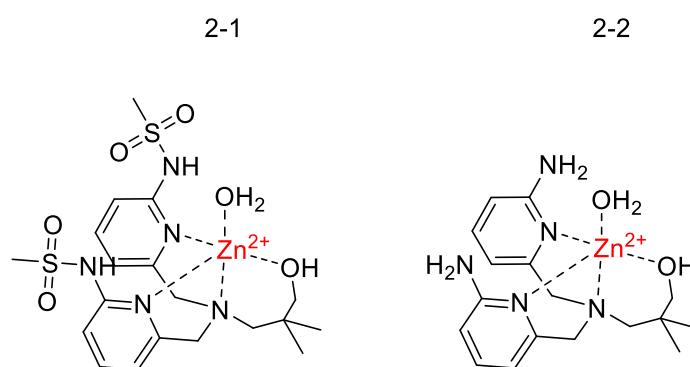


Figure 1.23 Structure of mononuclear complexes studied in Chapter 2

A second question which arises is whether the favourable effects of incorporating more effective ligand based nucleophiles and better hydrogen bond donating substituents on the pyridyl ring combine effectively to make especially effective catalysts. To this aim, we

combined these two aspects in a new family of Zn(II) complexes shown in Figure 1.24 which introduce an amino group to a series of complexes that have nucleophilic side chains of varying effectiveness.

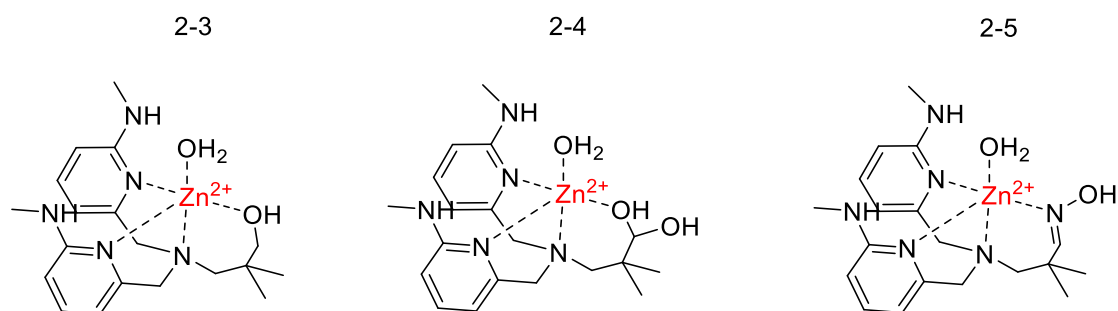


Figure 1.24 Structure of mononuclear complexes discussed in Chapter 2

The third chapter describes how we investigated whether the strength of hydrogen bond donors affects the catalyst's performance (Figure 1.25). A series of mononuclear complexes where the second coordination sphere of the complexes contains aniline-based substituents were used to test this parameter systematically.

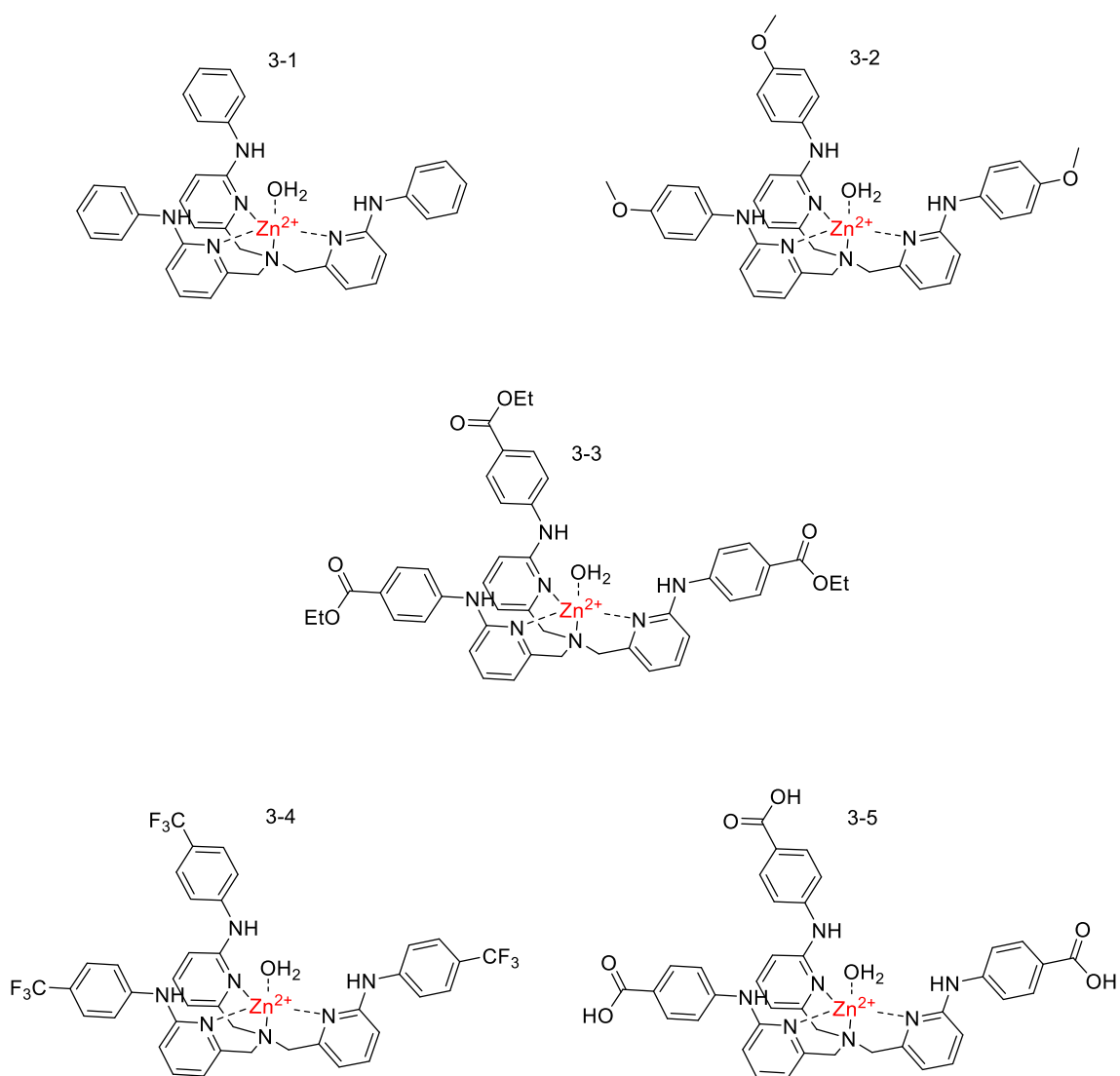


Figure 1.25 Structures of the mononuclear complexes reported in Chapter 3

In chapter four, the effect of aniline substituents on the pyridyl units were examined in the context of a dinuclear complex (Figure 1.26). As these complexes are particularly reactive, this provides the opportunity to examine whether the effect of the new substituent is similar for both activated model compounds, and for RNA fragments such as uridyl-(3-5)guanosine (UpG).

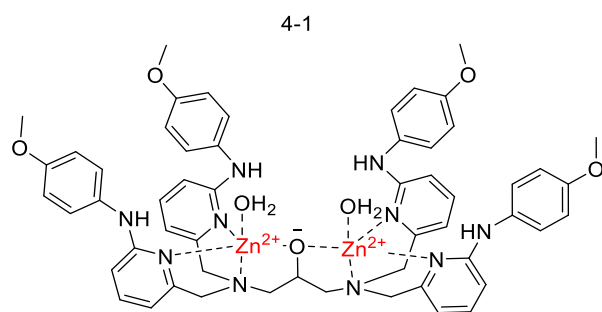


Figure 1.26 Structure of the dinuclear complexes described in Chapter 4

Chapter 2

Optimisation of Zn(II) complexes for the hydrolysis of a phosphate diester model for DNA

2.1 Introduction

The design of the ligand structure has a crucial role in optimising the reactivity of complexes toward the hydrolysis of phosphodiester bond of DNA and DNA-like model molecules. In several studies, researchers have taken inspiration from the findings in the catalytic site of natural systems, and have observed substantial activity enhancements after introducing key groups into the second coordination sphere of the complex.⁵⁷ Enzymes, using the functionalities of their amino acids' side chains, catalyse the reaction by facilitating the nucleophilic attack, providing electrostatic stabilisation of the transition state, intermediates, and the leaving group. For example, nucleophilic amino acids like histidine, serine, threonine and tyrosine can become phosphorylated and create a phosphoenzyme intermediate.¹⁰ Alternatively, ribonuclease catalyses RNA hydrolysis by a concerted general acid-base mechanism, using two histidine residues that behave as proton scavengers.⁷⁵ Those residues have a crucial role in the catalysis and thus, mimicking Nature, ligand structures have often been decorated with thiophenol and imidazole. For example, in 2003, Ichikawa *et al.*⁷⁶ introduced histidine based appendages to their ligand structure and observed a 3.6×10^4 -fold acceleration in the hydrolysis of bis(4-nitrophenyl) phosphate (BNPP) when the Zn(II) complex was used (**2-6** in Figure 2.1). Its maximum activity at physiological pH (tested at 50 °C) was attributed to the mono-deprotonated ionic form of the complex, and the imidazole groups were proposed to have an active role in complexing Zn(II). The coordination of two nitrogen, together with the secondary amine, would indeed provide symmetry to the complex and enhance the hydrophobicity of the active site.

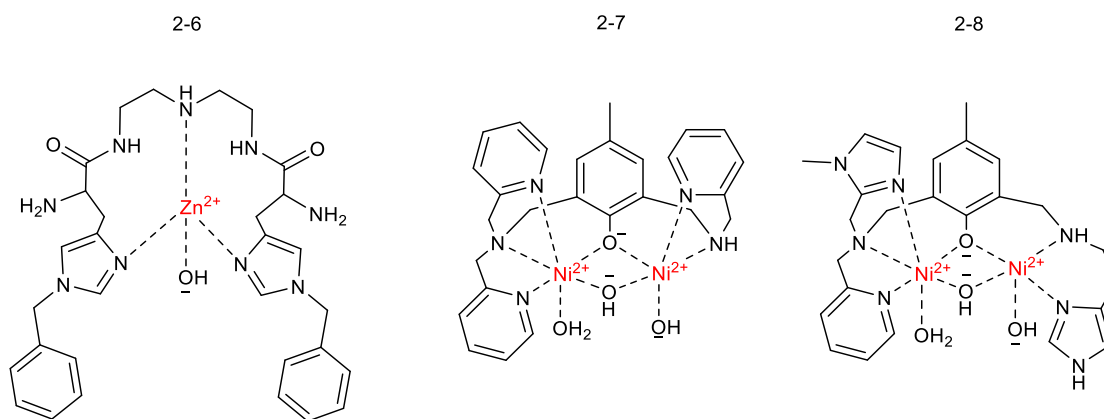


Figure 2.1 Structure of the active species of complexes used for the hydrolysis of DNA-model molecules^{76,77}

Similarly, Neves and coworkers⁷⁷ successfully introduced imidazole into their unsymmetrical dinuclear ligand, which was used as a Ni(II) complex for the hydrolysis of bis(2,4-dinitrophenyl) phosphate (BDNPP) and showed promising results. In their study, comparing the structurally analogous complexes reported in Figure 2.1, at pH 9 and 25 °C, **2-8** was reported to be more reactive than **2-7** toward the cleavage of BDNPP, accelerating the uncatalysed reaction by a factor of 9.95×10^5 (the acceleration provided by **2-7** was 8.8×10^4). The reaction produced 2-equivalents of di-2,4-nitrophenolate and one equivalent of inorganic phosphate. The lower pK_a value of **2-8** (8.6) than **2-7** (9.7), which would result in a higher active species concentration (double deprotonated as reported in Figure 2.1) under the experimental conditions, was proposed to be responsible for the higher reactivity of the former. In addition, the presence of the two 6-membered rings in **2-8**, probably *cis* positioned in the complex-substrate intermediate, would favour proximity and facilitate the nucleophilic attack.

Regarding pyridine-based Zn(II) complexes, a convenient way of introducing functionalities into the ligand structure is to use the 2' position of the pyridine ring. As shown in Figure 2.2, data from Chin's and Williams's group,^{78,79} shows that the presence of methyls and primary amines provide a reactivity enhancement of 5 and 230 fold toward the hydrolysis of BNPP compared to **2-9** respectively. As highlighted by these numbers, the introduction of hydrogen bond donors has the most significant effect.

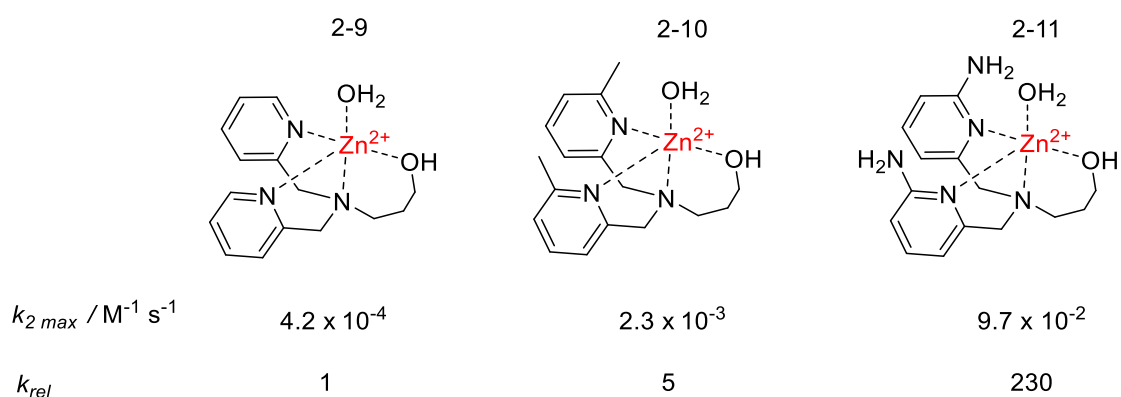


Figure 2.2 Comparison among three complexes with different substitutions in the 2-position of the pyridine rings. The maximum second order rate constant for the BNPP transesterification in the presence of the catalysts are reported below their structures. The values correspond to maximum k_2 value reported for each complex. The rate constant were measured in the following condition: [Buffer] = 50 mM, ionic strength 0.1 M, 25 °C, [BNPP] = 0.05 mM^{78,79}

As further investigated in the following chapters, this approach has also been successfully applied to analogous mononuclear and dinuclear catalysts used for the transesterification of RNA model molecules. The presence of these groups clearly modulates the reactivity of the complexes, which has created curiosity regarding the possible benefits of introducing different hydrogen bond donors. As reported by Breslow and coworkers, thiophenol and imidazole pedants far from the direct Zn(II) coordination sphere were used to decorate the ligand structure of the Zn(II) complexes shown in Figure 2.3.⁸⁰ Although low reactivity was observed at pH 7.0 and 37 °C, the additional groups increase the activity of **2-12** by 9-

and 20- fold (thiophenol and imidazole in **2-13**, respectively) towards the transesterification of the RNA model HPNPP.

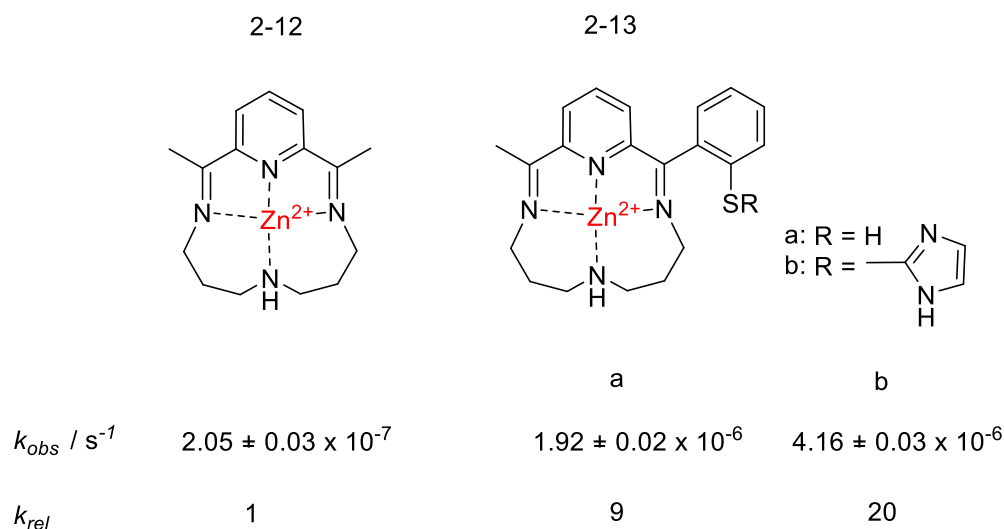


Figure 2.3 Structures of Zn(II) complexes studied by Breslow and coworkers. The rate constants were measured in the following condition: [complex] = 0.5 mM, [HPNPP] = 0.19 mM, [HEPES] = 10 mM, pH 7.0 and 37 °C in 10% (v/v) DMSO in water⁸⁰

As found in many nucleases and phosphatases,^{81,82} arginine residues contribute to the catalytic activity by stabilising the transition state through hydrogen bonding and electrostatic complementarity. Therefore, incorporating the guanidinium group into ligand structures has been exploited to enhance several catalyst's activity. As reported by He *et al.*,⁸³ both the guanidinium-enriched Zn(II) complexes **2-15** and **2-16** (Figure 2.4) were more reactive (by 300- and 600-fold respectively) than the core ligand **2-14** toward the hydrolysis of BNPP at pH 7.2 and 25 °C. The combination of the Zn(II) ions and the positively charged guanidinium groups was believed to lead to a high acceleration for the hydrolysis of plasmid DNA, which was also observed, although not quantified. Surprisingly, the two complexes also demonstrated a remarkable selectivity toward specific

nucleotide sequences although there is no obvious sequence selective component to these complexes.

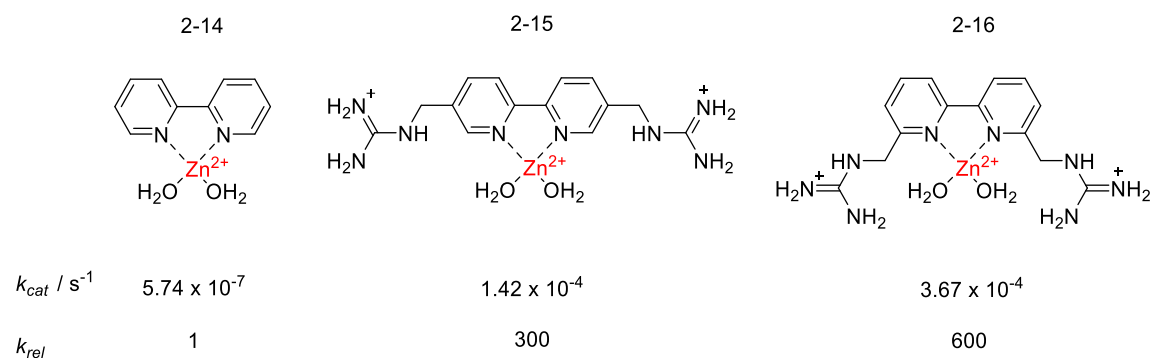


Figure 2.4 Structures of the complexes presented by He *et al.* The rate constants were measured in the following condition: [complex] = 0.05 mM, [BNPP] = 0.05 mM, [Buffer] = 50 mM, ionic strength fixed at 0.1 M by addition of NaCl, pH 7.2 and 25 °C⁸³

The cleavage of DNA, which lacks the intramolecular 2'OH nucleophile present in the ribose units of the RNA, must proceed via an intermolecular attack of a nucleophile. This main difference between the two nucleic acids is a significant contribution to DNA's higher stability towards hydrolysis. Thus, when metal ion complexes are used to tackle this challenge, the incorporation of a nucleophile in the ligand is a common strategy to accelerate the reaction. When the substrate binds to the metal complex, the attack on the phosphorus carried out by the ligand's nucleophile has the characteristic of an intramolecular event. As demonstrated by Chin *et al.*,^{78,84} an alkoxy group in the ligand that coordinates the metal ion can be more reactive than a metal-bound hydroxide in both Zn(II) and Cu(II) complexes. The length of the aliphatic chain and the consequent position of the alkoxy group influences the complex reactivity. For example, the difference in the second-order rate constants for the cleavage of BDNPP catalysed by a series of Cu(II) pyridine complexes (Figure 2.5) illustrates the different impact of this feature.

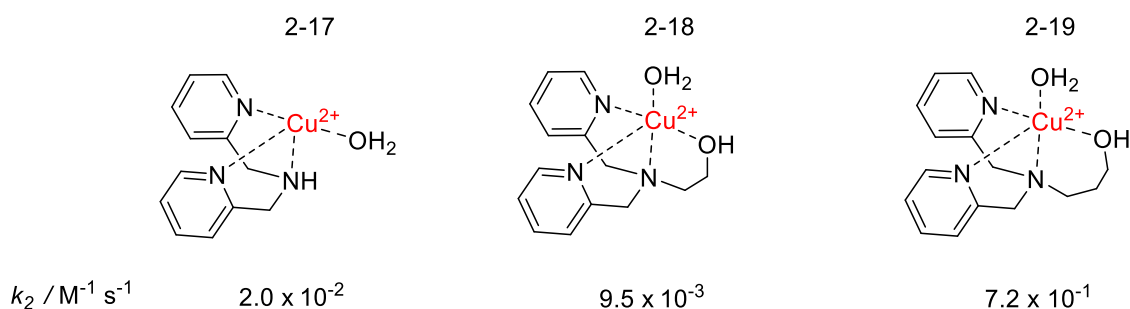


Figure 2.5 Structures and second order rate constants for the cleavage of BDNPP catalysed by the complexes published by Chin *et al.* The rate constants were measured in the following conditions: [BDNPP] = 0.01 mM, [Buffer] = 10 mM, 25 °C ⁸¹

In the presence of the **2-19**, BDNPP cleavage proceeds via transesterification, yielding 2,4-dinitrophenol and the phosphorylated complex, which shows that the metal alkoxide is the nucleophile in this reaction. On the other hand, the alkoxide of the C2-chain ligand does not take part in the reaction, and **2-18** mainly catalysed substrate hydrolysis (90%) with a rate constant similar to **2-17**. The authors suggested that the most active species might be formed by displacing the coordinated alkoxide by hydroxide, which is consistent with the reactivity of **2-18** being about half that of **2-17**. As suggested by crystallography data, the higher reactivity observed for **2-19** could be due to the propylene linker expanding the N(alkylamine)-Cu-O(alkoxide) bond angle, leading to a decrease in the O(alkoxide)-Cu-O(phosphate) bond angle which favours attack of the nucleophilic atom. In turn, the shorter ethylene may prevent the effective delivery of the alkoxide nucleophile, and so hydrolysis through metal ion bound hydroxide is more favourable. Although this strategy has proven to successfully reduce the half-life time of DNA-model molecules, the simple hydroxyl group has limitations. Although the coordination to the metal ion facilitates the alcohol deprotonation at lower pH values by decreasing its pK_a , it could be responsible for reducing

both the alkoxide nucleophilicity and the Lewis acidity of the metal centre. In addition, the transesterification between the substrate and the catalyst yields to a phosphorylated complex that loses its reactivity and catalytic nature.

In the last few years, Williams's group^{79,85} has investigated complexes decorated with alternative nucleophiles which are not directly coordinated to the metal ion. For example, as reported in Figure 2.6, structurally related Zn(II) complexes have shown higher reactivity against the hydrolysis of BNPP when a hydrated aldehyde or an oxime replaces the hydroxyl group in one of the ligand's chains.

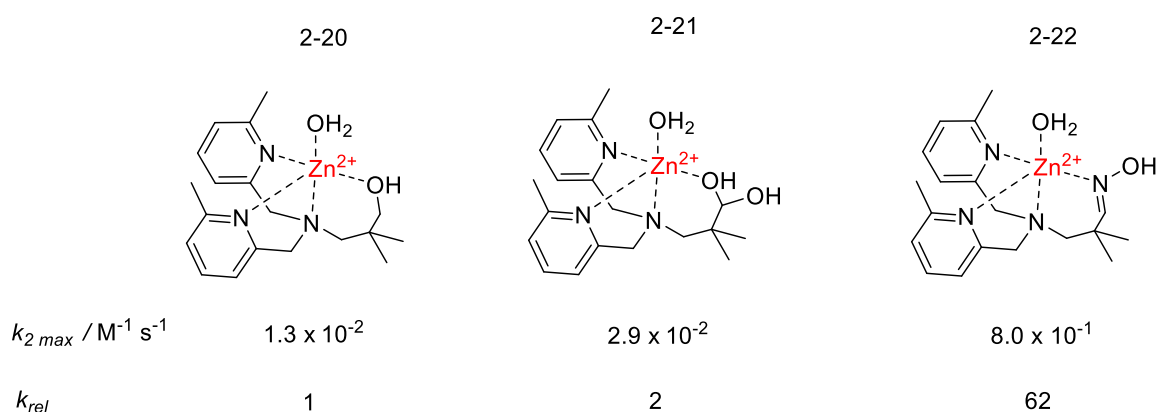


Figure 2.6 Structures and second order rate constants for the cleavage of BNPP catalysed by the complexes published by Williams *et al.* The rate constants were measured in the following condition: [BNPP] = 0.05 mM, [Buffer] = 50 mM, ionic strength fixed at 0.1 M by addition of NaNO₃, 25 °C^{79,85}

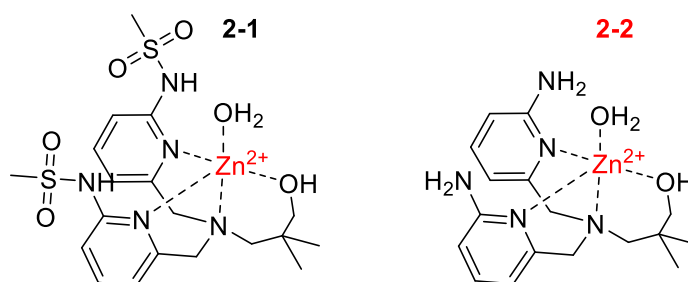
Although a relatively small difference is found between **2-20** and **2-21**, the terminal gem-diol converts the complex from stoichiometric to a catalytic participant of the reaction. In contrast with previous results, which highlighted the importance of the coordination of the nucleophile to the metal ion, the higher reactivity of the hydrated aldehyde suggests that

the attacking nucleophile is the hydroxyl group not directly interacting with the Zn(II) ion. Following this strategy, the design of **2-22** aimed to introduce a better nucleophile into the ligand structure. The oxime can coordinate to the metal centre through the nitrogen, reducing deactivation of the oxygen atom and bringing it and the substrate in close proximity. Although lower reactivity was observed with poor leaving groups, **2-22** is the most active mononuclear complex reported to date toward the hydrolysis of BNPP.

2.2 Result and discussion

As briefly introduced, two main approaches have been followed for designing the ligand structure of pyridine-based mononuclear complexes. Both the functionalisation of the 2' position of the pyridine ring and replacing a hydroxy with more efficient nucleophiles have significantly enhanced catalytic activity. This Chapter first investigates the introduction of a stronger hydrogen bond donor into the ligand by substituting the primary amines (**2-2**) with sulfonamide groups (Figure 2.7a – **2-1**). In the second section a new family of ligands that attempt to combine the two strategies and benefit from a cooperative effect is explored. As shown in Figure 2.7b, the reactivity of three mononuclear complexes (**2-3**, **2-4** and **2-5**) decorated with MeNH as sources of hydrogen bonding and with different nucleophiles incorporated into the ligand are compared.

a) Comparison between sulfonamide and primary amine:



b) Family of new ligands:

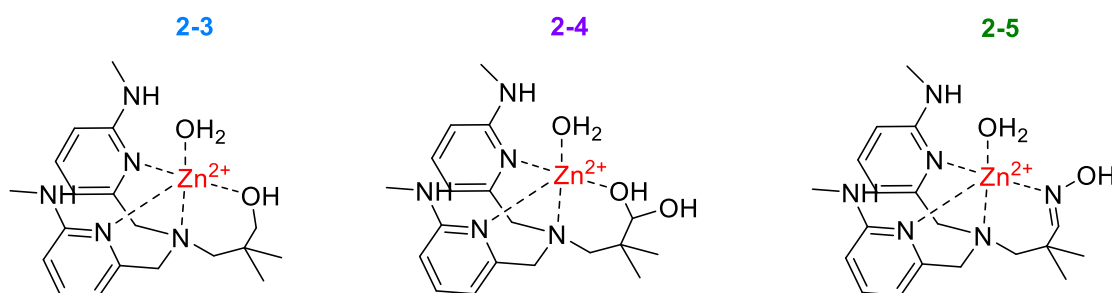


Figure 2.7 Structures of the complexes studied in this Chapter

2.3 Sulfonamide: Hydrogen bond donor or acidic group?

Amides and sulfonamides are among the best candidates to enhance the hydrogen-bonding capacity of ligands. As listed by Hunter,⁸⁶ the hydrogen bond donor capacity (α) for the two groups are similar (2.9 and 2.8 respectively) and significantly greater than the value of an aniline NH (2.1); and almost double the value found for a simple amine (1.5). Previous work,⁸⁷ used a naphthyridine-like structure (**2-23** in Figure 2.8) to constrain the amide geometry for hydrogen bond donation and prevent carbonyl coordination to the metal centre, but resulted in a shutdown of the catalytic activity.

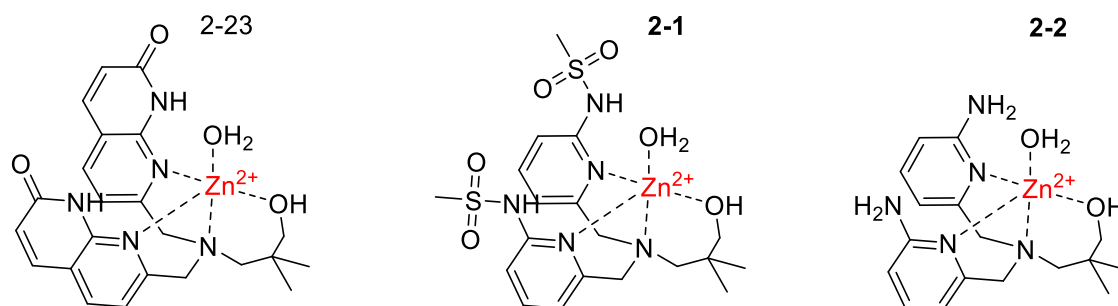
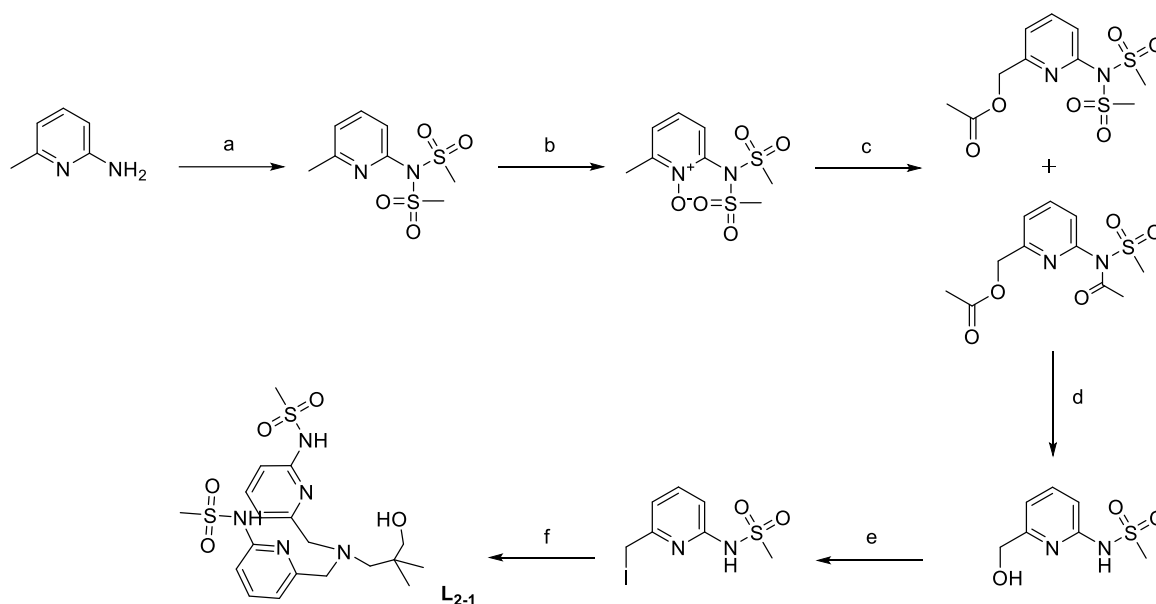


Figure 2.8 Complexes with different hydrogen bond donor groups in the ortho pyridine position

This inactivity might have been due to deprotonation of the amido groups, with the consequent complete loss of hydrogen bonding capacity. However, this particular structure might be especially prone to deprotonation due to the aromatic character of the anion that forms, and so we decided to explore the introduction of sulfonamide groups as hydrogen bond donors. Complex **2-1** was designed, synthesised and studied to discover whether it led to more active complexes, or was similarly deactivating overall.

2.3.1 Synthesis

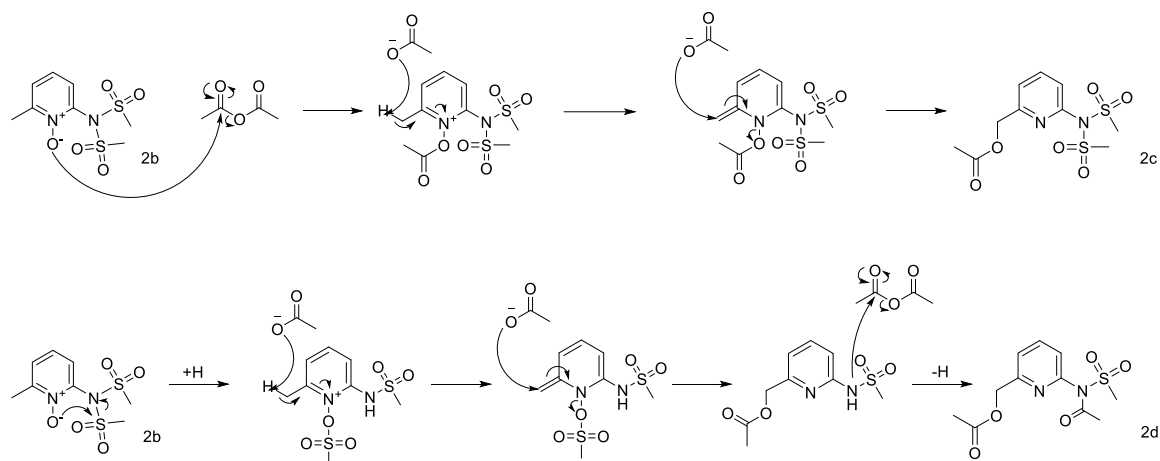
The synthetic procedure for synthesising the sulfonamide-based ligand (**L2-1**) started from 2-amine-6-methyl pyridine and consisted of 5 steps with an overall yield of 18% (Scheme 2.1).



Scheme 2.1 Synthesis of N-(6-(iodomethyl)pyridin-2-yl)methanesulfonamide; a) MeSO₂Cl, Et₃N, DCM, 25°C 2h, 87 % yield; b) mCPBA, DCM, 25°C 18 h, 87% yield; c) Ac₂O, 100 °C 18 h, 55% and 9 % yield; d) KOH, MeOH, 25 °C 1 h; e) I₂, Ph₃P, Imidazole, DCM, 25 °C 18 h, 44 % yield; f) 3-amino-2,2-dimethylpropan-1-ol, DIPEA, dry DMF, 70 °C, 18 h, 40% yield.

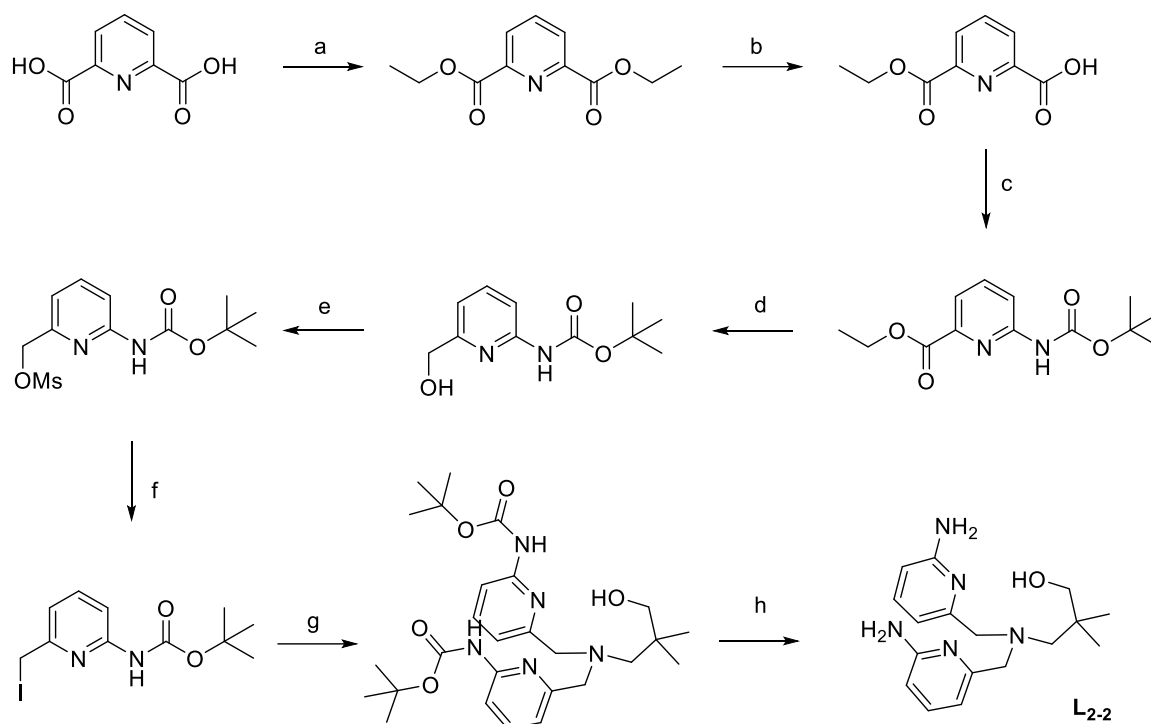
The sulfonamide group was introduced using methanesulfonyl chloride and triethylamine; the reaction led to the di-sulfonamide molecule, which is conveniently more soluble in organic solvents than the mono-functionalised analogue. After N-oxide formation by treatment with *meta*-chloroperoxybenzoic, the Boelke-Held rearrangement at 100 °C yielded two products. The high temperature for this step, used to achieve complete

conversion, also led to different side products, with the major of them the acetylated sulfonamide. A proposed mechanism for both the pathways is shown in Scheme 2.2.



Scheme 2.2 Proposed mechanisms for the Boekelheide reaction, which leads to the formation of 2c and 2d

The addition of potassium hydroxide successfully hydrolysed both the products, and conveniently removed the acetyl group of 2d selectively so that this side product also gave the desired mono sulfonated intermediate. Finally, the iodide derivative, obtained by Appel reaction using iodine, was used to alkylate 3-amino-2,2-dimethylpropan-1-ol in the presence of DIPEA at 70 °C. The aliphatic chain of the ligand was chosen by considering the improvement in the reactivity of the complexes provided by the geminal methyl groups reported in previous work.⁸⁵ The reference compound **L2-2** was obtained by the procedure shown in Scheme 2.3) and followed the synthetic route devised by Søren Svenningsen of the Williams group. The esterification of pyridine-2,6-dicarboxylic acid was performed with sulfuric acid at 80 °C. After the hydrolysis of one ester group, the carboxylic acid was converted to a Boc-protected amine through a Curtius rearrangement.



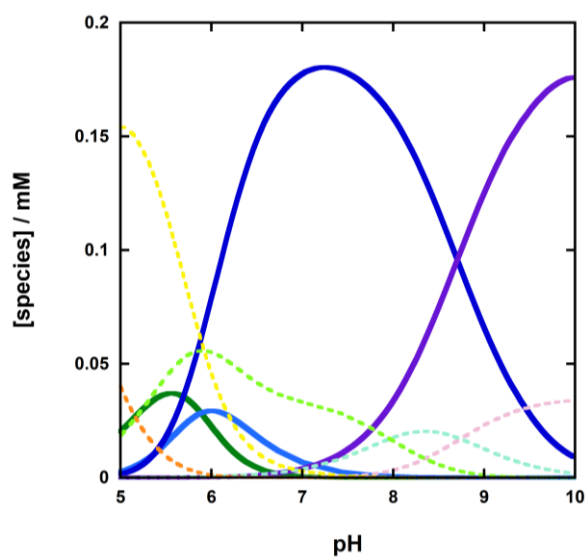
*Scheme 2.3 Synthesis of L2-2: a) H_2SO_4 , EtOH, 80 °C 18 h, 89 % yield; b) NaOH, EtOH:Dioxane (1:2), 100 °C 2 h, 50 % yield; c) Diphenylphosphoryl azide, Et_3N , *t*-BuOH, Toluene, 100 °C 18 h, 69 % yield; d) $NaBH_4$, $CaCl_2$, EtOH, 0-25 °C 18h, 97 % yield; e) $MeSO_2Cl$, Et_3N , THF, 0-25 °C 18h, 95 % yield; f) LiI, THF, 50 °C 2h, 91 % yield; g) 3-amino-2,2-dimethylpropan-1-ol, DIPEA, dry DMF, 70 °C, 18 h, 69 % yield; h) TFA, 25 °C 2 h, 98% yield.*

The ester functionality was then reduced by sodium borohydride in the presence of calcium ions at 0 °C to form the alcohol, which was then converted into a good leaving group by reaction with methanesulfonyl chloride and triethylamine. After the Finkelstein reaction with lithium iodide at 50 °C, the building block was used for the alkylation with 3-amino-2,2-dimethylpropan-1-ol in the presence of DIPEA at 70 °C. Finally, the Boc protecting groups were removed by treatment with trifluoroacetic acid at room temperature, yielding **L2-2**.

2.3.2 Analysis

The sulfonamide-based mononuclear complex **2-1** was tested with BNPP, but at most only a small enhancement above the background rate of hydrolysis was observed in the pH range between 7 and 10. After 14 h at 25 °C at pH 8, based on the 0.6% absorbance increment at 400 nm, we estimated that 1 mM of **2-1** produced approximately 0.4 μM of 4-nitrophenolate (0.9% conversion) corresponding to k_{obs} not higher than $1 \times 10^{-7} \text{ s}^{-1}$. As suggested for the naphthyridine based compounds, this could be due to the intrinsic acidity of sulfonamide groups, which increases once the complex is formed. Consequently, the ligand **L2-1** and **2-1** were studied and compared to **L2-2** and **2-2** by potentiometric titration. The speciation plots for **2-1** and **2-2** were obtained by fitting the potentiometric titration data using Hyperquad and Hyss,⁸⁸ and are compared in Graph 2.1 a and b. At physiological pH, **2-2** (2 mM) is primarily present in its mono deprotonated form, and, given its structure, the proton is probably removed from one of the oxygens coordinated to the Zn(II) ion. The $\text{p}K_{\text{a}}^1$ of 7.32 for **2-2** leads to the most active complex form that accelerates BNPP hydrolysis with a k_2^{max} of $6.79 \pm 0.02 \times 10^{-2} \text{ M}^{-1} \text{ s}^{-1}$. Thanks to the high $\text{p}K_{\text{a}}$ of the amino groups, the ligand retains the presence of stable hydrogen bond donors, and, as shown in the following Chapter, this can positively affect the activity of the catalyst across the pH range of interest. On the other hand, **2-1** (0.2 mM) has almost quantitatively become doubly deprotonated by pH 7 (Graph 2.1a). It is most likely that the sulfonamides are deprotonated, so their strong hydrogen-bond donor capacity is lost, causing the formation of a neutral, less soluble and inactive complex. The proposed deprotonation equilibria and the $\text{p}K_{\text{a}}$ values for **2-1** and **2-2** are presented in Scheme 2.4 and Table 2.1.

a) Speciation plot of **2-1**



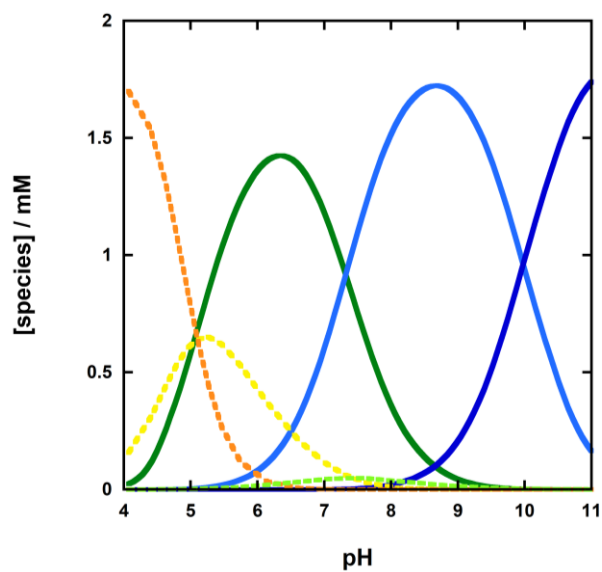
Complex species (solid lines):

- **2-1**
- **(2-1) - H⁺**
- **(2-1) - 2H⁺**
- **(2-1) - 3H⁺**

Ligand species (dashed lines):

- **(L₂₋₁) + 2H⁺**
- **(L₂₋₁) + H⁺**
- **L₂₋₁**
- **(L₂₋₁) - H⁺**
- **(L₂₋₁) - 2H⁺**

b) Speciation plot of **2-2**



Complex species (solid lines):

- **2-2**
- **(2-2) - H⁺**
- **(2-2) - 2H⁺**

Ligand species (dashed lines):

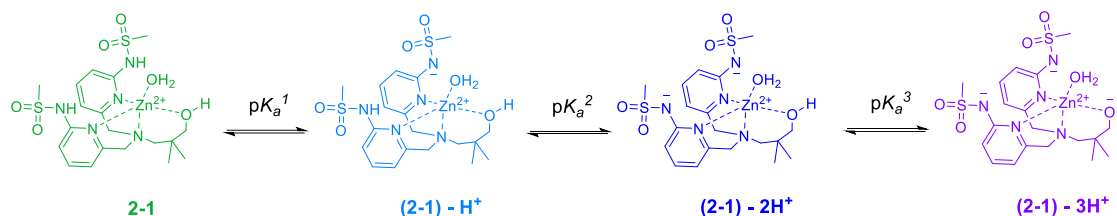
- **(L₂₋₂) + 2H⁺**
- **(L₂₋₂) + H⁺**
- **L₂₋₂**

Graph 2.1 Speciation plots of 2-1 (a) and 2-2 (b). The titration experiment was performed at 25 °C and ionic strength fixed at 0.1 M by addition of NaNO₃; a) [2-1] = 0.2 mM; [2-2] = 2 mM. The difference in the concentration of the complexes is due to the low solubility of 2-1

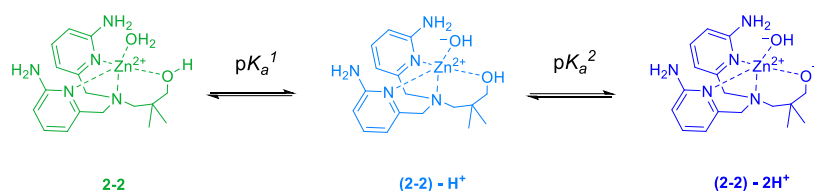
As previously reported in the literature,⁵⁸ the formation of the aliphatic alkoxide at neutral pH strongly affects the catalyst reactivity. As proposed in Scheme 2.4, the

alkoxide in **2-1** is mostly formed at alkaline pH after the deprotonation of the sulfonamides.

Proposed deprotonation equilibria in solution for **2-1**:



Proposed deprotonation equilibria in solution for **2-2**:

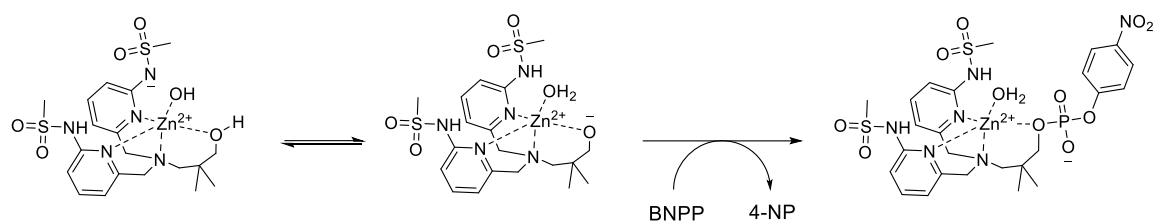


Scheme 2.4 Proposed deprotonation equilibria in the pH range between 5 and 11 for **2-1** and **2-2**

Table 2.1 pK_a values for **2-1** and L_{2-1} , **2-2** and L_{2-2} at 25 °C in 0.1 M NaNO_3

	complex			ligand			
	pK_a^1	pK_a^2	pK_a^3	pK_a^1	pK_a^2	pK_a^3	pK_a^4
2-1	5.58	5.89	8.70	4.41	5.92	7.96	8.74
2-2	7.32	9.98	-	5.24	7.42	-	-

The formation of the additional negative charge might then prevent the substrate binding and decrease the Lewis acidity of the Zn(II) ion. However, the small enhancement over the background reaction could be due to the tautomer of **(2-1)-H⁺**. As shown in Scheme 2.5,



Scheme 2.5 Proposed tautomeric equilibrium of (2-1)-H⁺ that leads to the formation of the active species

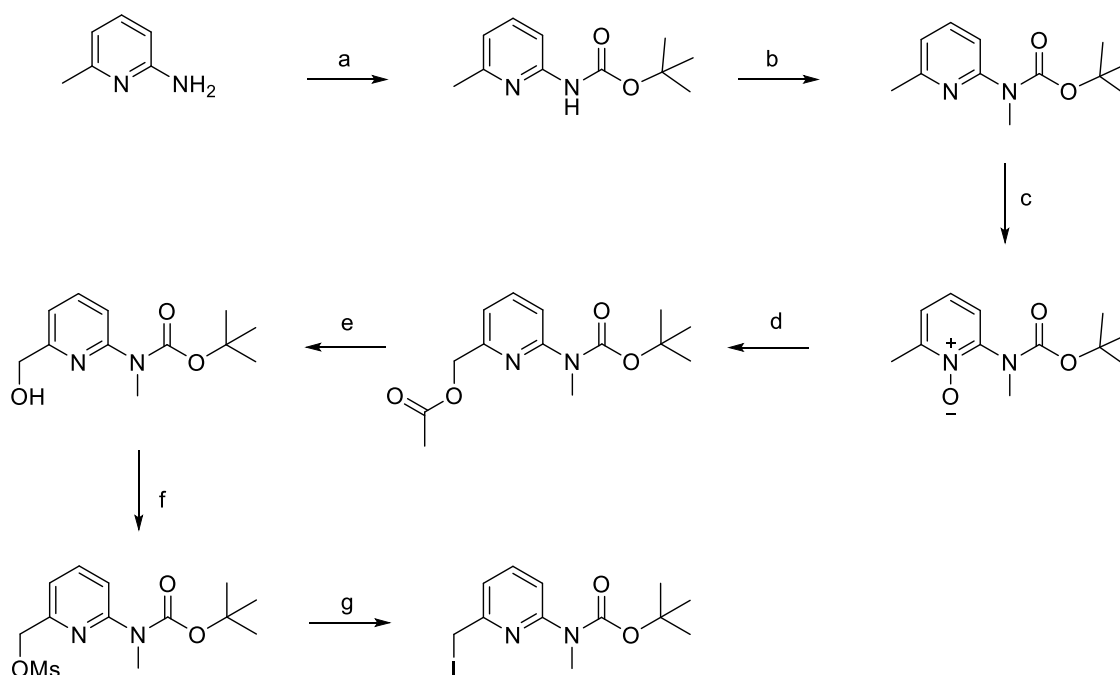
once the active species is formed at neutral pH, the substrate can bind to the complex and benefit from the hydrogen bond donating properties of the sulfonamides. This outcome is consistent with what was previously observed with naphthyridine based ligand and suggests that deprotonation is the main reason for the inactivity. The result has had a significant impact on the work pursued in the following Chapters in which more robust but stable aniline groups have been introduced into the ligand's structure to enhance the phosphodiester hydrolysis. At this point, we turned our attention to addressing the question of how well different forms of structural changes to enhance activity can be combined.

2.4 Methylamine based Zn(II) complexes

As an amino group was the most effective 2-pyridyl substituent known at this point, we decided to combine this with ligand side chains that provide enhanced activity relative to a simple 3-hydroxy propyl side chain. We decided to work with methylamine groups instead of the parent amine partly due to synthetic considerations at the time, but also because one of the target compounds involved aldehyde functional groups, and methylation of the amine was expected to avoid the formation of undesirable imines.

2.4.1 Synthesis

Similarly to the route to the sulfonamide-based building block described earlier, the synthesis starts from the 2-amino-6-methylpyridine as shown in Scheme 2.6.

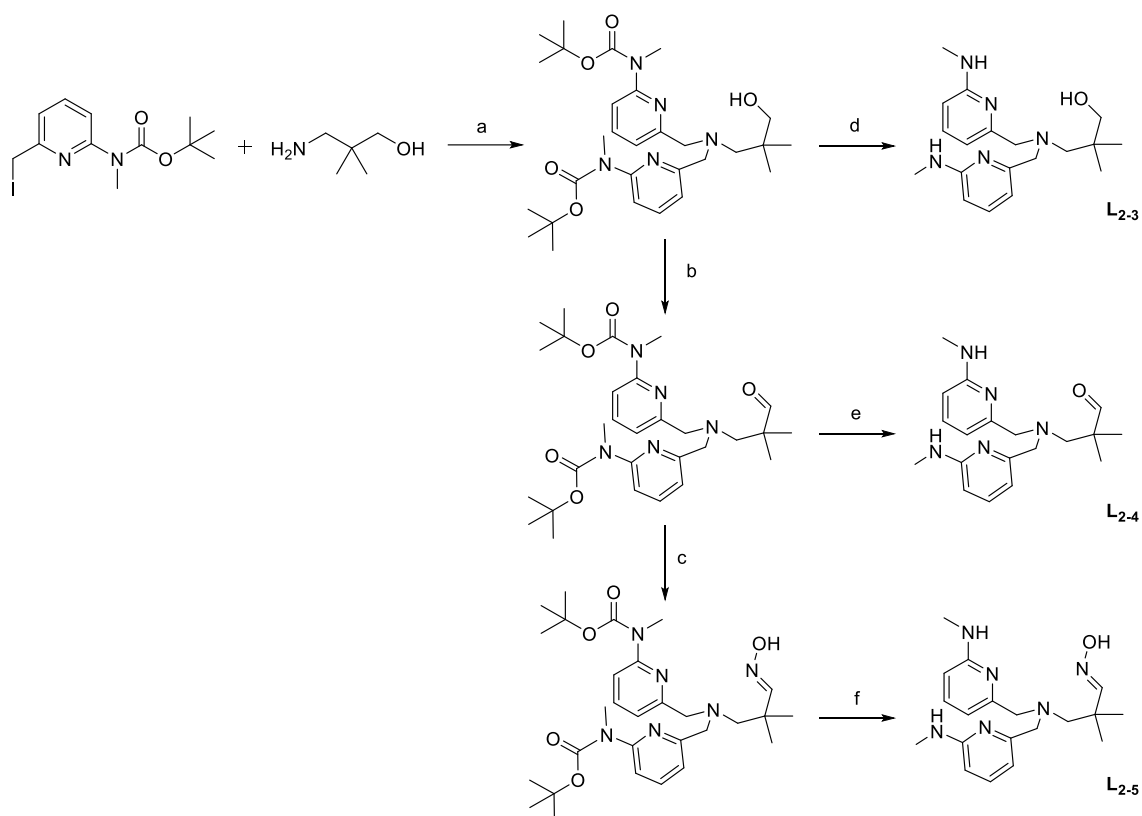


Scheme 2.6 Synthetic procedure of key building block 2t: a) Boc_2O , Et_3N , DMAP, DCM, 25°C 18 h, 80 % yield; b) NaH , MeI , DMF, 25°C 18 h, 97 % yield; c) $m\text{CPBA}$, DCM, 25°C 18 h, 87 % yield; d) Ac_2O , 70°C 18 h, 75 % yield; e) KOH , MeOH , 25°C 1 h, 80 % yield; f) MeSO_2Cl , Et_3N , THF, 25°C 18 h, 98 % yield; g) LiI , THF, 50°C 1 h, 98 % yield.

First, the amine functionality was Boc protected using di-tert-butyl dicarbonate and triethylamine. After the methylation of the protected amine, the building block was oxidised to the N-oxide by *meta*-chloroperoxybenzoic acid. The Boekelheide rearrangement in acetic anhydride at 70°C gave the ester, which was hydrolysed by adding potassium hydroxide to give the hydroxy methyl group in the 6 position. Finally, the hydroxyl group was converted into an iodide through mesylation followed by the Finkelstein reaction. The building block was synthesised with an overall yield of 35%. If

the N-methylation step is not carried out, the Boekelheide rearrangement occurs in poor yield, with substantial amounts of a byproduct forming where the N-oxide reacts with the Boc group.^{87,89}

The series of ligands share one further common step as 3-amino-2,2-dimethyl- propan-1-ol is alkylated with the iodide building block in the presence of DIPEA at 70 °C (Scheme 2.7).



Scheme 2.7 Synthesis of L₂₋₃, L₂₋₄ and L₂₋₅; a) DIPEA, dry DMF, 70 °C 18 h, 75 % yield; b) Dess-Martin periodinane, dry DCM, 25 °C 2h, 65 % yield; c) NH₂OH·HCl, NaOH, water:ethanol (1:1), 25 °C 3h, 93 % yield; d) TFA, DCM, 25 °C 1h, 95 % yield; e) TFA, DCM, 25 °C 1h, 26 % yield; f) TFA, TIS, water, 25 °C 3 h, 59 % yield.

The hydroxyl group was then oxidised in the presence of Dess-Martin periodinane in dry DCM to form the aldehyde. Finally, the oxime was introduced by treating the aldehyde

with $\text{NH}_2\text{OH}\cdot\text{HCl}$ and NaOH . The ligands were then deprotected using trifluoroacetic acid. Apart from **L2-3** (90% yield), the yield of the deprotection steps were low, and loss of the aliphatic chain was observed for **L2-4** and **L2-5**. To avoid ligand decomposition, triisopropylsilane and water were added to the reaction mixture, but only improved the yields for **L2-5** (54% yield). The yield for **L2-4** was 20% and could not be improved. It is not clear why this side chain was so susceptible to decomposition under acidic conditions, although a retro-Mannich type of reaction may be occurring. Given the acidic conditions, where the concentration of tertiary amine is expected to be extremely low, this would be surprising.

2.4.2 Kinetic studies

The mononuclear Zn(II) complexes were tested for their activity in accelerating the hydrolysis of BNPP at 25 °C in water by monitoring the appearance of 4-nitrophenolate at 400 nm. This substrate is a convenient model compound that is often used to evaluate catalysts that are designed to catalyse the hydrolysis of DNA.

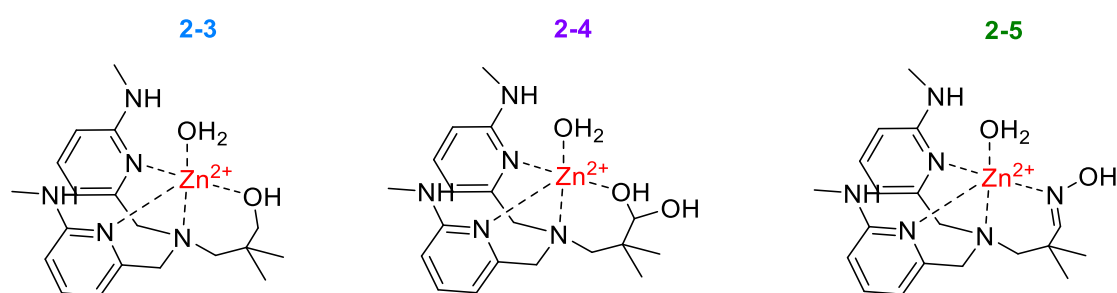
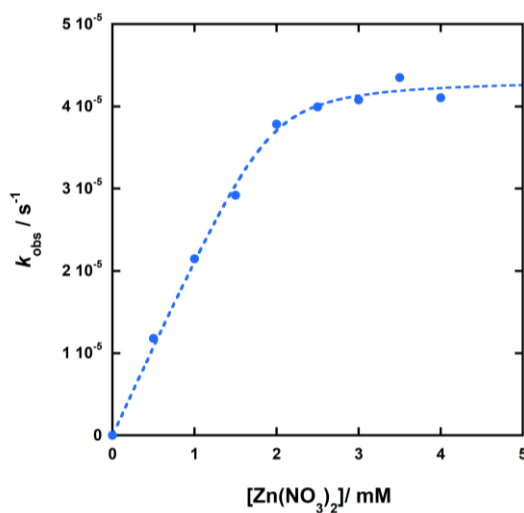


Figure 2.9 Structure of the methylamine-based mononuclear complexes

All three complexes (Figure 2.9) accelerate the hydrolysis of BNPP at pH 7.4 and 25 °C, and the half-life time is reduced from 100 years^{50,51} to 12 h, 19 h and 37 min by 1 mM concentrations of **2-3**, **2-4** and **2-5**, respectively. The introduction of the oxime into the ligand makes **2-5** the most active complex. While **L2-3** and **L2-4** did not provide any detectable enhancement over the background reaction at pH 7 and 25 °C, the transesterification of BNPP (0.05 mM) was catalysed by **L2-5** (1 mM) with an observed rate constant of $1.4 \pm 0.1 \times 10^{-5} \text{ s}^{-1}$. The value found is almost 20-fold lower than that of the reaction catalysed by **2-5** under the same experimental condition. All the ligands show a strong 1:1 binding to the Zn(II) ion, as shown by kinetic experiments performed at different metal ion:ligand ratios as illustrated for **L2-3** in Graph 2.2. Given the strong Zn(II) binding of the ligands, the fitting does not provide an accurate measure of the K_d values, which have been estimated to be approximately equal to $50 \mu\text{M}^{-1}$.

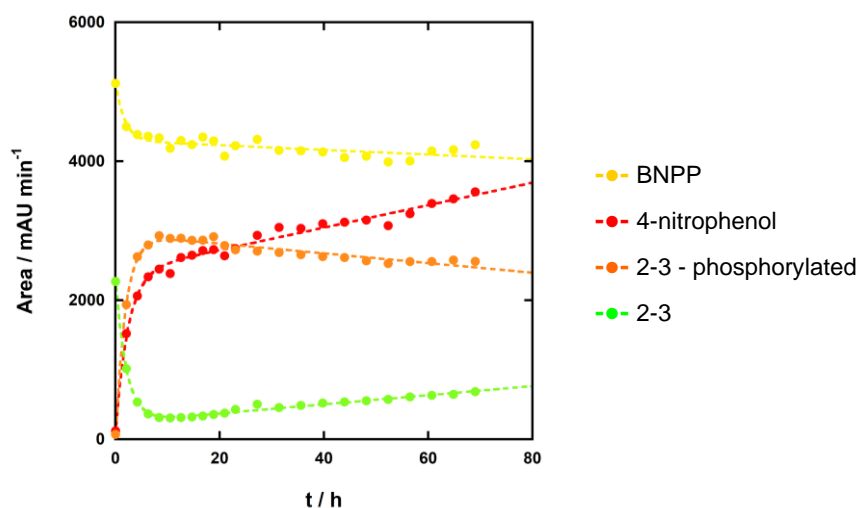


Graph 2.2 Plot of k_{obs} against $\text{Zn}(\text{NO}_3)_2$ equivalent; $[\text{L2-3}] = 2 \text{ mM}$, $[\text{BNPP}] = 0.05 \text{ mM}$, $[\text{HEPES}] = 50 \text{ mM}$ pH 7.4, $[\text{NaNO}_3] = 0.1 \text{ M}$, 25 °C. Data fitted with equation (1)

$$(1) \quad k_{obs} = k_0 \frac{\left([L_{2-n}]_T + [Zn^{2+}] + 1/K_d\right) - \sqrt{\left([L_{2-n}]_T + [Zn^{2+}] + 1/K_d\right)^2 - 4[L_{2-n}]_T[Zn^{2+}]}}{2}$$

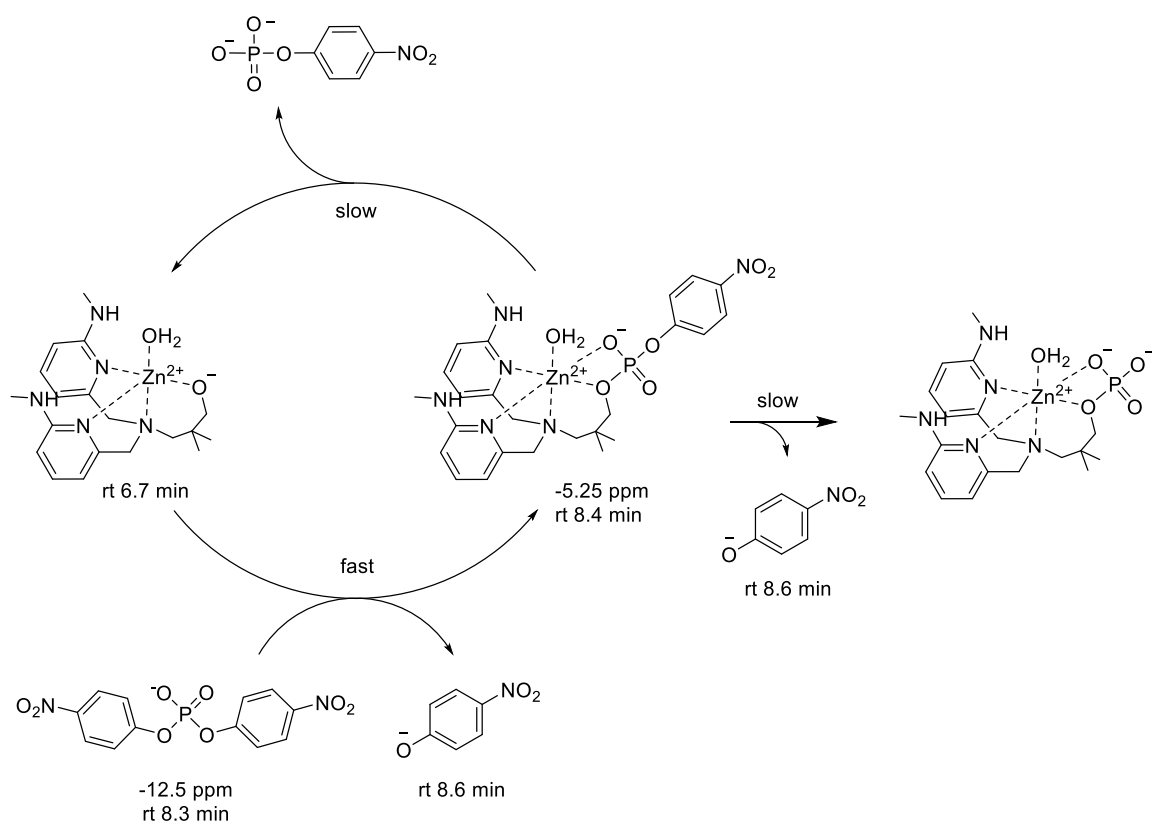
The hydrolysis reaction in the presence of the complexes is not affected by buffer concentration and exhibits a first order dependence on the concentration of BNPP (see experimental section). Given the different types of nucleophiles introduced into the structures of the ligands, the reaction mechanism is expected to differ according to the catalysts used. Therefore, the cleavage of 5 mM BNPP catalysed by 1 mM of **2-n** was investigated by HPLC, LCMS and ³¹P NMR spectroscopy.

The reaction enhanced by **2-3** proceeds by nucleophilic attack of the hydroxyl group with consequent formation of 4-nitrophenol and a phosphorylated complex (Scheme 1.6) which is stable to further hydrolysis. The areas of the peaks for each component of the reaction mixture are reported against time in Graph 2.3. We did not convert the areas into concentration as a calibration curve for the intermediate was not available. In the first 10 h, the formation of 4-nitrophenol (red dots) and the phosphorylated complex (orange dots) mirror the rapid decrease of both the substrate (yellow dots) and **2-3** (green dots). After that time, the drop in active complex concentration leads to a slowdown of the reaction. Although relatively stable, the phosphorylated complex seemed to be partially hydrolysed under the reaction conditions.



Graph 2.3 Variation of the areas of each participant's peak against time for the transesterification of BNPP catalysed by 2-3 at pH 7.4 and 25 °C: BNPP (●), 4-nitrophenol (●), phosphorylated complex (●) and 2-3 (●); [BNPP] = 5 mM, [2-3] = 1 mM, [HEPES] = 50 mM, ionic strength 0.1 M, 40% (v/v) acetonitrile in water

This slow hydrolysis can occur by two pathways in which either the active species is regenerated along with 4-nitrophenyl phosphate, or 4-nitrophenol and a new phosphorylated complex are produced .

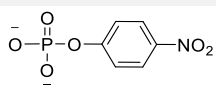


Scheme 1.6 Proposed mechanism of the reaction catalysed by 2-3

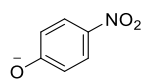
Both processes seem to be occurring, as suggested by the modest rises in the areas of the relevant chromatographic peaks. Four fractions of the HPLC run were collected and the masses are reported in Figure 2.10. Given the proximity among their peaks, 4-nitrophenol and BNPP were collected together in Fraction III. The assignment of the two peaks have been done by single injections of standard solutions (5 mM) of BNPP and 4-nitrophenol using the same HPLC method. Surprisingly both the masses of **L2-3** and its monophosphate derivate were found in Fraction II.

Fraction I - rt: 4 - 5.5 min

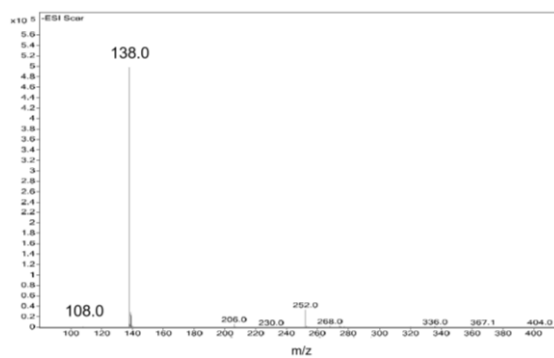
- ESI



Exact Mass: 216.98

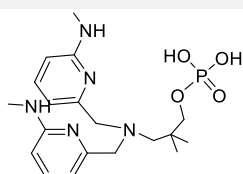


Exact Mass: 138.02

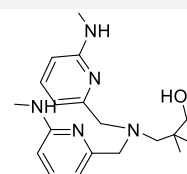


Fraction II - rt: 6 - 7.5

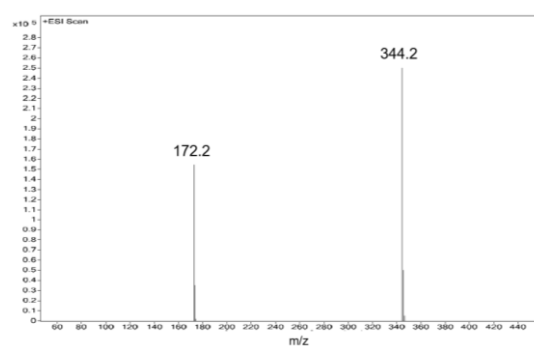
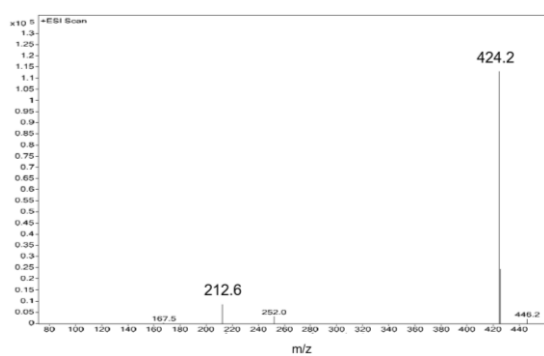
+ ESI



Exact Mass: 423.2035

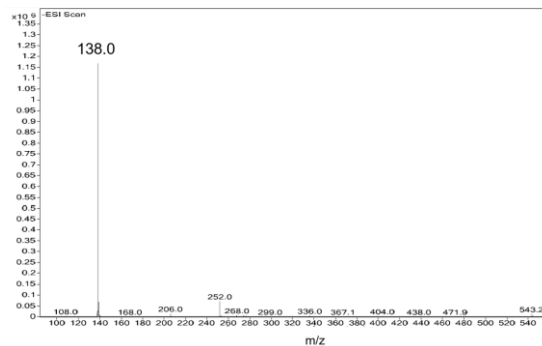
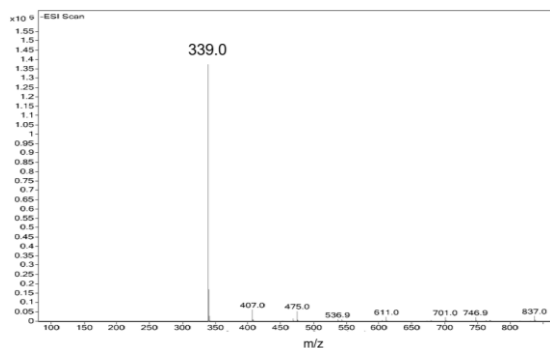
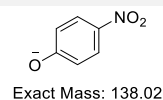
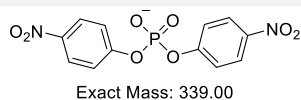


Exact Mass: 343.2372



Fraction III - rt: 7.6 - 9 min

- ESI



Fraction IV - rt: 10 - 12 min

+ ESI

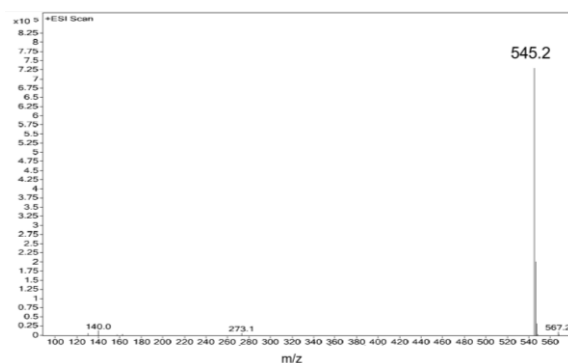
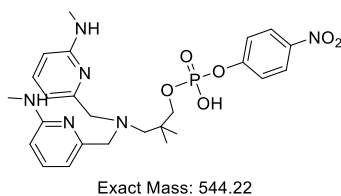


Figure 2.10 Masses of different fractions of HPLC run for the transesterification of BNPP catalysed by 2-3 at 25 °C and pH 7.4. [2-3] = 1 mM, [BNPP] = 5 mM, [HEPES]=50 mM, ionic strength 0.1 M by addition of NaNO₃, 40%(v/v) acetonitrile in water

The values found by LCMS were consistent with the mechanism proposed. **2-3**, which was mostly consumed after 10 h, behaves more as a reagent rather than a catalyst and does not undergo multiple turnovers. After 70 h, only 1 equivalent of BNPP was cleaved, and the

concentration of 4-nitrophenol that is produced was less than 1.5 mM (from the cleavage of BNPP and the hydrolysis of the phosphorylated complex). On the other hand, **2-4**, which was designed to achieve catalytic turnover, cleaves BNPP by overall hydrolysis.

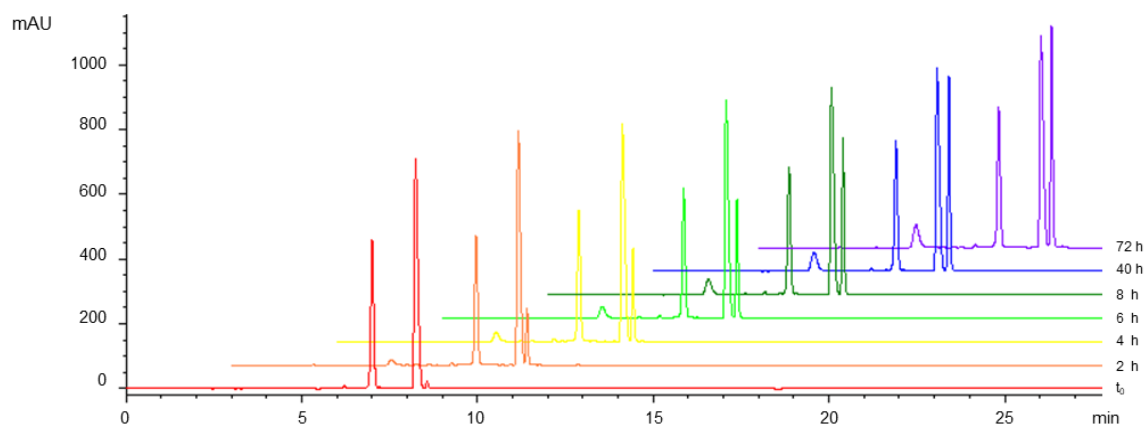
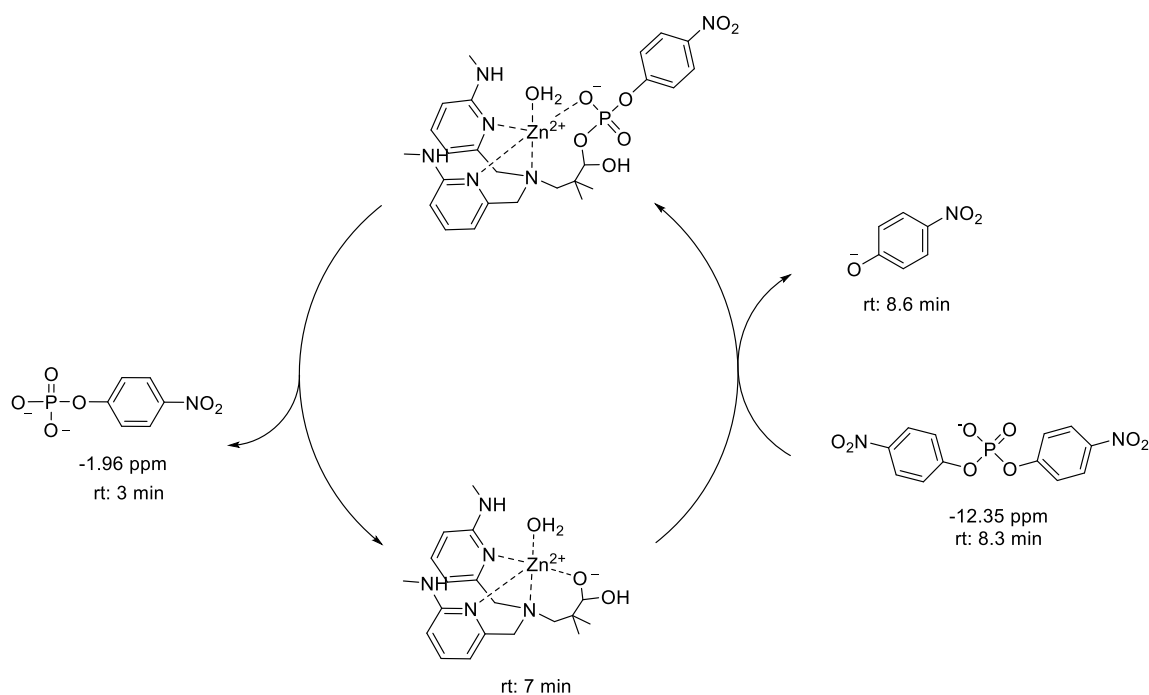


Figure 2.11 Chromatograms of consecutive injections of the reaction mixture for the hydrolysis of BNPP catalysed by **2-4** at pH 7.4 and 25 °C; 4-nitrophenol phosphate (rt: 3 min), **2-4** (rt: 7 min), BNPP (rt: 8.3 min), 4-nitrophenol (rt: 8.6 min); [BNPP] = 5 mM, [**2-4**] = 1 mM, [HEPES] = 50 mM, ionic strength 0.1 M, 40% (v/v) acetonitrile in water



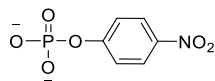
Scheme 2.8 Proposed mechanism for the hydrolysis of BNPP catalysed by **2-4**

As shown in the chromatograms of sequential injections of the reaction mixture (Figure 2.11), the concentration of complex **2-4** does not vary over time as shown by its constant peak area at 7.0 min. Furthermore, the only new components to appear are 4-nitrophenol (rt 8.5 min) and 4-nitrophenyl phosphate (rt 3 min). These data are consistent with the mechanism described in Scheme 2.8.

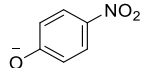
Electrospray ionisation (ESI) mass spectrometry confirmed that the relative molecular masses of the peaks matched the proposed structures (Figure 2.12), and no traces of the phosphorylated complex were found, suggesting the intermediate rapidly hydrolyses back into its active form and rejoins the catalytic cycle.

Fraction I: rt: 4 - 5.5 min

- ESI



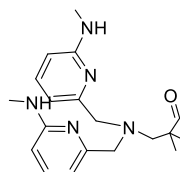
Exact Mass: 216.98



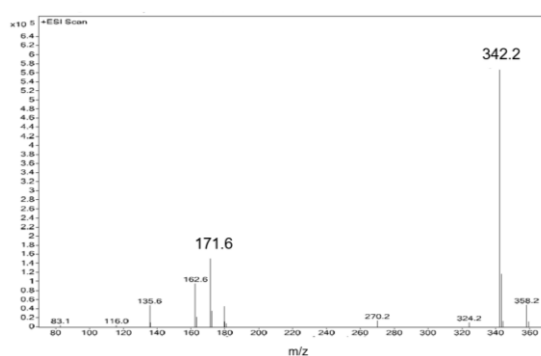
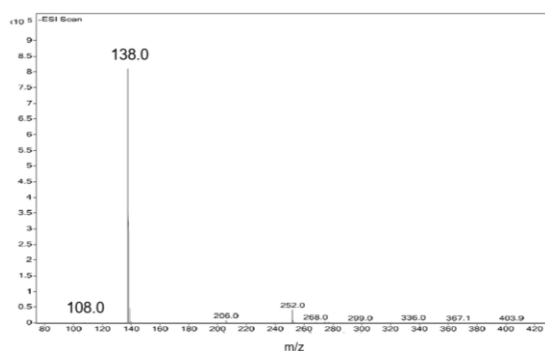
Exact Mass: 138.02

Fraction II: rt: 7 min

+ ESI



Exact Mass: 341.2216



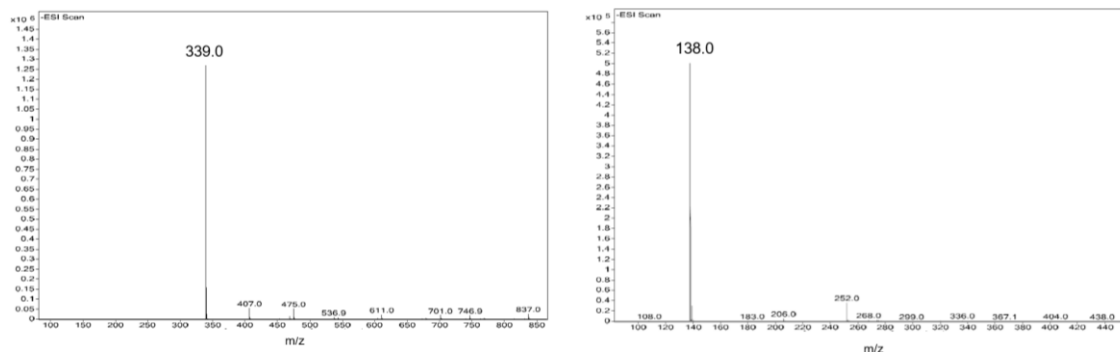
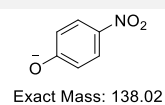
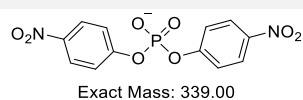


Figure 2.12 Masses of different fractions of the HPLC run after 1 week for the transesterification of BNPP catalysed by **2-4** at 25 °C and pH 7.4. [**2-4**] = 1 mM, [BNPP] = 5 mM, [HEPES]=50 mM, ionic strength 0.1 M by addition of NaNO₃, 40%(v/v) acetonitrile in water

Experiments that use ³¹P NMR to monitor the reaction of BNPP (5 mM) catalysed by **2-3** and **2-4** (1 mM) highlight the difference between the two reactions (Figure 2.13 and Figure 2.14). In the presence of **2-4**, a peak appears at -1.96 ppm which is 4-nitrophenyl phosphate, whereas a phosphorylated complex (-5.3 ppm) was formed when **2-3** catalyses the reaction.

2-3 - ^{31}P NMR experiment

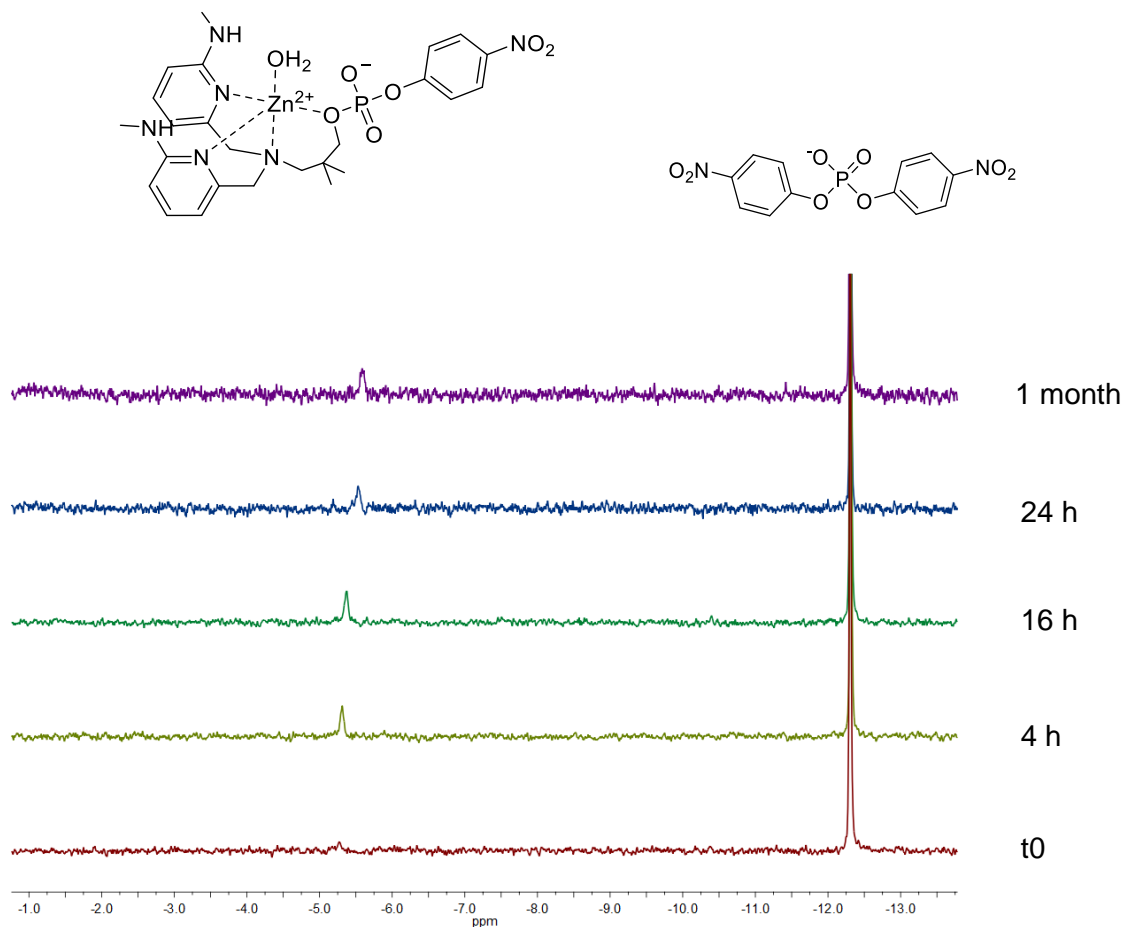


Figure 2.13 Transesterification of BNPP catalysed by **2-3** at pH 7.4 and 25 °C monitored by ^{31}P NMR. [BNPP] = 5 mM, [2-3] = 1 mM, [HEPES] = 50 mM, ionic strength 0.1 M, 40%(v/v) acetonitrile in water

As the HPLC experiment suggests, the product of **2-3** should partially hydrolyse, yielding 4-nitrophenol and the phosphate monoester of the complex. However, except for a small ppm shift, no additional peaks are observed after a month.

2-4 - ^{31}P NMR experiment

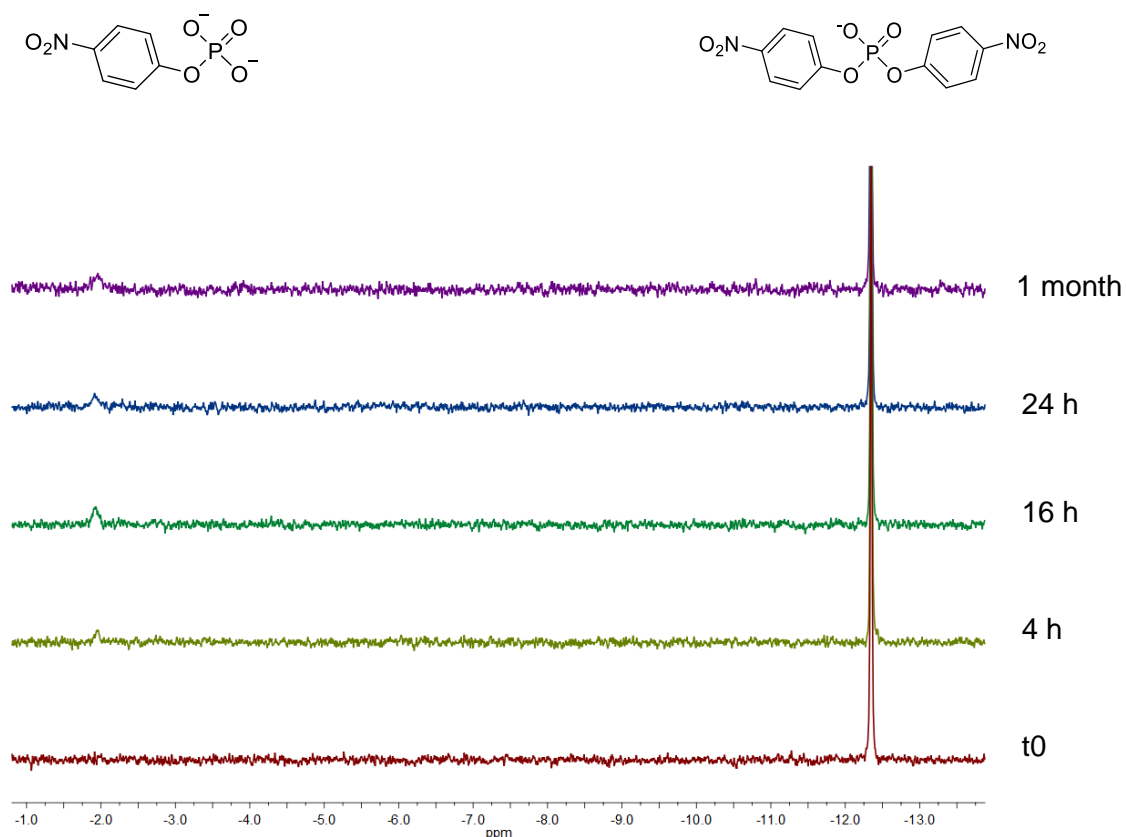
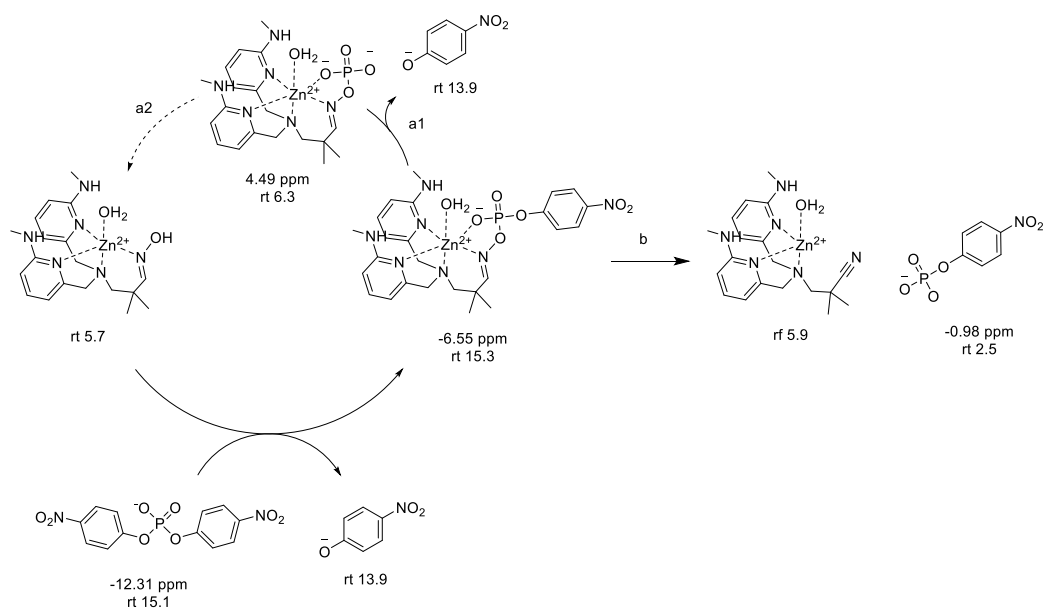


Figure 2.14 Transesterification of BNPP catalysed by 2-4 at pH 7.4 and 25 °C monitored by ^{31}P NMR. [BNPP] = 5 mM, [2-4] = 1 mM, [HEPES] = 50 mM, ionic strength 0.1 M, 40%(v/v) acetonitrile in water

Although **2-4** is catalytic, these experiments showed modest reactivity and a turnover number of only 1.2 after 70 h. This result can be explained by strong inhibition of the catalyst by the phosphate monoester, which could bind tightly to the complex and prevent substrate coordination. However, no shift of the signal for the 4-nitrophenol phosphate was visible by NMR spectroscopy. An inhibition experiment performed in the presence of phenyl phosphate (PP) suggested strong coordination between **2-4** and phosphate monoesters, although precipitation was observed to occur, and no precise measurements

could be made. In the presence of 1 equivalent of PP, no production of 4-nitrophenolate was observed after 18 h. In addition, when mM concentrations of PP were present in the reaction mixture, precipitation occurs, and no reaction was detectable.

A different mechanism is proposed for the reaction enhanced by **2-5**, which cleaves BNPP by transesterification, similarly to **2-3**. The ^{31}P NMR and HPLC data reported in Figure 2.15 and Figure 2.16 reveal that after 30 min, the concentration of 4-nitrophenol (rt 13.9 min) is 1.44 mM, and **2-5** (rt 5.7 min) is fully converted to its phosphorylated form (rt 15.3 min, -6.55 ppm). As hydrolysis of the latter could follow the two pathways described in the proposed mechanism (a and b), the initial production of more than 1 equivalent of 4-nitrophenol might suggest that either the phosphorylated catalyst partially retains its reactivity or is quickly hydrolysed (a1). An alternative explanation could be the fast regeneration of **2-5** through both steps a1 and a2. The additional 4-nitrophenol produced over time mainly comes from the hydrolysis of the complex derivative, confirmed by the decrease of the signal at -6.55 ppm and the peak at 15.3 min. The simultaneous appearance of the three peaks at 2.5, 5.9 and 6.3 min are the 4-nitrophenyl phosphate, phosphate monoester and the cyano derivative of the complex respectively, consistent with this hypothesis. The emerging signal at -0.98 and 5.9 ppm in the NMR experiment are also consistent with the proposed mechanism (Scheme 2.9).



Scheme 2.9 Proposed mechanism for the reaction catalysed by 2-5

^{31}P NMR experiment

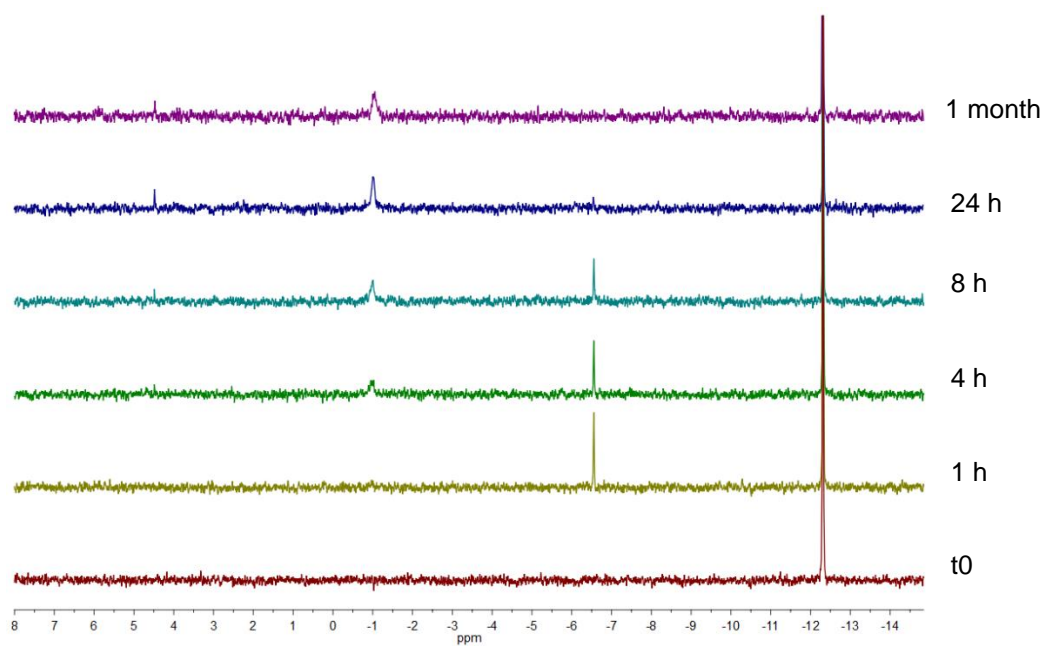
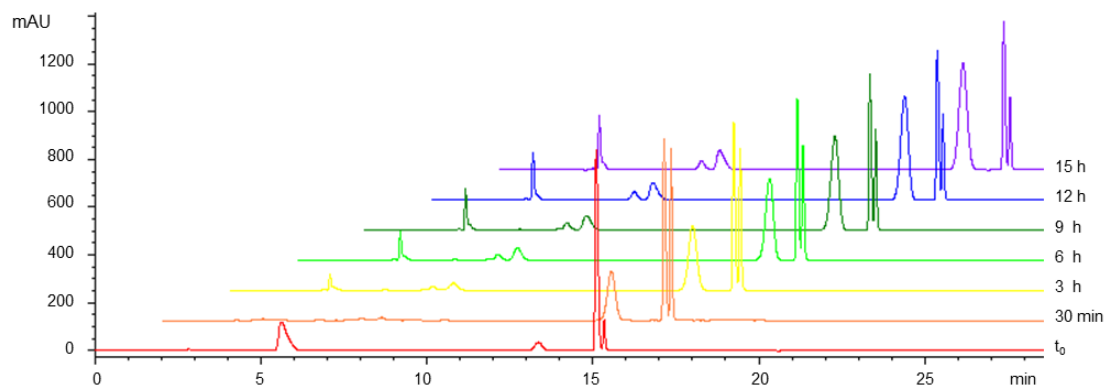
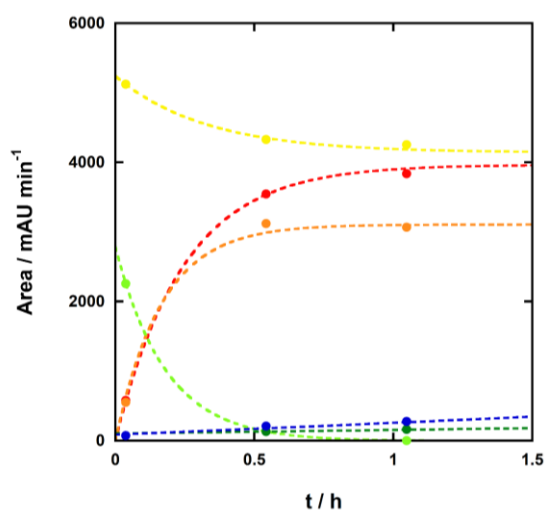


Figure 2.15 Transesterification of BNPP catalysed by 2-5 at pH 7.4 and 25 °C monitored by ^{31}P NMR. $[\text{BNPP}] = 5 \text{ mM}$, $[\text{2-5}] = 1 \text{ mM}$, $[\text{HEPES}] = 50 \text{ mM}$, ionic strength 0.1 M, 40%(v/v) acetonitrile in water

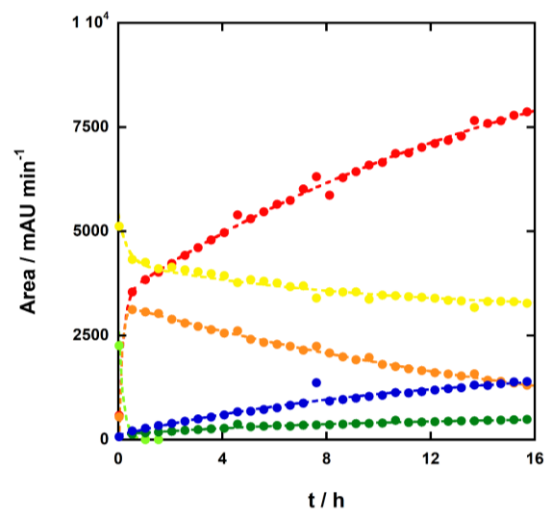
a) HPLC experiment:



b) First hour



c) Overall reaction time



- BNPP
- 4-nitrophenol
- 2-5 - phosphorylated (diester)
- 2-5
- 2-5 - phosphorylated (monoester)*
- 2-5 - CN

*Proposed species

Figure 2.16 Transesterification of BNPP catalysed by 2-5 at pH 7.4 and 25 °C monitored by HPLC (b). 4-nitrophenol phosphate (rt: 2.8 min), 2-5 (rt: 5.7 min), 2-5 – phosphorylated monoester (rt: 4.5 min), 2-5 – CN (rt: 5.9), 4-nitrophenol (rt: 13.9 min), BNPP (rt: 15.1 min), 2-5 – phosphorylated diester (rt: 15.3 min); [BNPP] = 5 mM, [2-5] = 1 mM, [HEPES] = 50 mM, ionic strength 0.1 M, 40%(v/v) acetonitrile in water

Equations used to fit the data in b (phase I):

$$(2) \quad A_t = A_0 + A_f (1 - e^{-k_{obs} t})$$

$$(3) \quad A_t = A_0 + A_f (e^{-k_{obs} t})$$

Equations used to fit the data in c (phase I and phase II):

$$(4) \quad A_t = A_f + (A_0 - A_f) e^{-k_{obs}^2 t} + (A_i - A_f) \frac{k_{obs}^2}{(k_{obs}^1 - k_{obs}^2)} (e^{-k_{obs}^2 t} - e^{-k_{obs}^1 t})$$

where: A_0 : initial area

k_{obs}^1 : observed rate constant phase I

A_f : final area

k_{obs}^2 : observed rate constant phase II

A_i : area due to intermediate

The observed rate constant obtained from least-squares fitting the data with equations (2), (3) and (4) yielded the values reported in Table 2.2 for **2-3**, **2-4** and **2-5**.

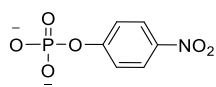
Table 2.2 Observed rate constants obtained by the fitting of equations (2), (3) and (4) to the HPLC experiment

	2-3	2-4	2-5	
	k_{obs} / s^{-1}	k_{obs} / s^{-1}	k_{obs}^1 / s^{-1}	k_{obs}^2 / s^{-1}
4-nitrophenol	$1.1 \pm 0.1 \times 10^{-4}$	$5.25 \pm 0.01 \times 10^{-5}$	$1.8 \pm 0.6 \times 10^{-3}$	$1.5 \pm 0.2 \times 10^{-5}$
BNPP	$1.6 \pm 0.5 \times 10^{-4}$	$5.61 \pm 0.05 \times 10^{-5}$	$4 \pm 2 \times 10^{-3}$	$3.3 \pm 0.6 \times 10^{-5}$
Complex (diester)	$1.4 \pm 0.1 \times 10^{-4}$	-	$2.4 \pm 0.8 \times 10^{-3}$	$1.4 \pm 0.2 \times 10^{-6}$
			k_{obs} / s^{-1}	
Complex	$1.3 \pm 0.4 \times 10^{-4}$	-	$1.54 \pm 0.03 \times 10^{-3}$	
Complex CN	-	-	$3.1 \pm 0.2 \times 10^{-5}$	
Complex (monoester)	-	-	$1.6 \pm 0.5 \times 10^{-5}$	

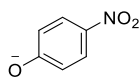
Similar to **2-3** and **2-4**, the fractions of the HPLC run were collected and analysed by electron spray ionisation (Figure 2.17).

Fraction I: rt: 2 - 3 min

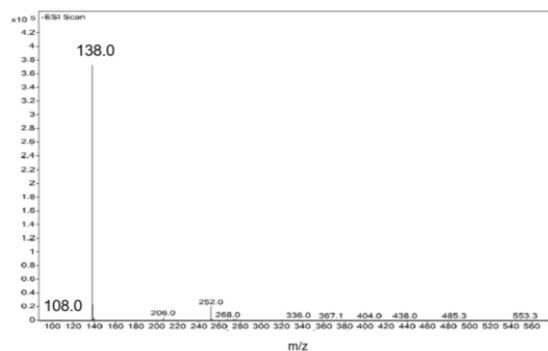
- ESI



Exact Mass: 216.98

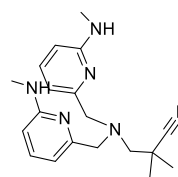


Exact Mass: 138.02

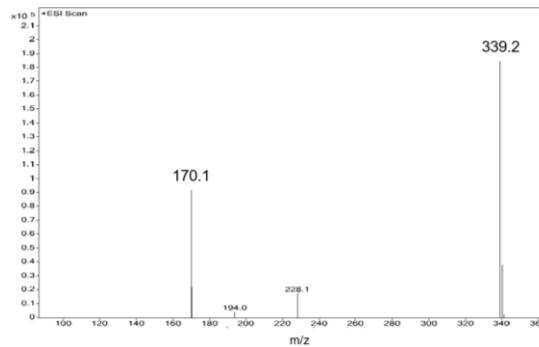


Fraction II: rt: 5 - 6 min

+ ESI

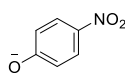


Exact Mass: 338.22

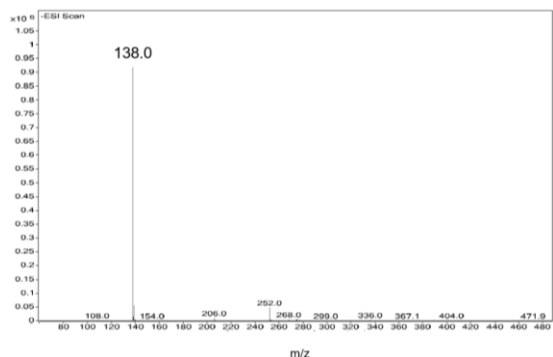


Fraction III: rt: 13 - 14 min

- ESI

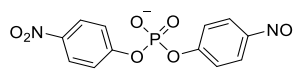


Exact Mass: 138.02



Fraction IV: rt: 15 - 16 min

- ESI



Exact Mass: 339.00

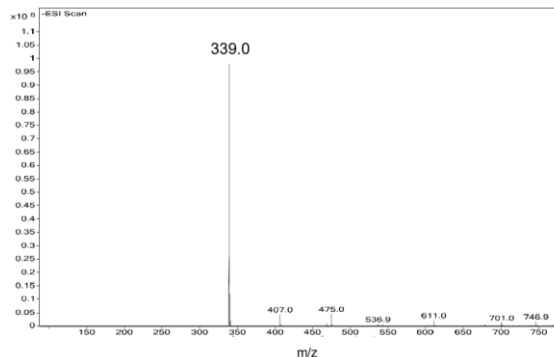


Figure 2.17 Masses of different fractions of the HPLC run after 1 week for the transesterification of BNPP catalysed by 2-5 at 25 °C and pH 7.4. [2-5] = 1 mM, [BNPP] = 5 mM, [HEPES]=50 mM, ionic strength 0.1 M by addition of NaNO_3 , 40%(v/v) acetonitrile in water.

LCMS analysis did not show any presence of **2-5**. After 2 weeks, the only mass identified by electrospray MS was that of the CN-derivate of the complex, suggesting that the hydrolysis of the phosphoryl complex mainly followed path b (as also confirmed by NMR).

After 16 h, **2-5** (1 mM) consumed almost 2 mM of BNPP, which is double the amount cleaved by **2-3** and **2-4** in more than 70 h. This higher rate enhancement provided by introducing the better nucleophile is also helped by weak binding with the monophosphate ester produced during the reaction. As highlighted by an experiment to measure whether PP inhibits the reaction (Figure 2.18a), increasing the concentration of the inhibitor in the reaction mixture led to a decrease in the relative rate constants for the transesterification of BNPP (0.05 mM) catalysed by 0.5 mM of **2-5** at pH 7.5, 8 and 9 and 25 °C. High concentrations of the inhibitor were required to strongly affect the reaction, reflecting a relative weak binding constant between the monoesters and the catalyst. In contrast, the equivalent experiment performed with **2-3** (2 mM) showed that an equal concentration of the monoester is enough to deactivate the complex (Figure 2.18b).

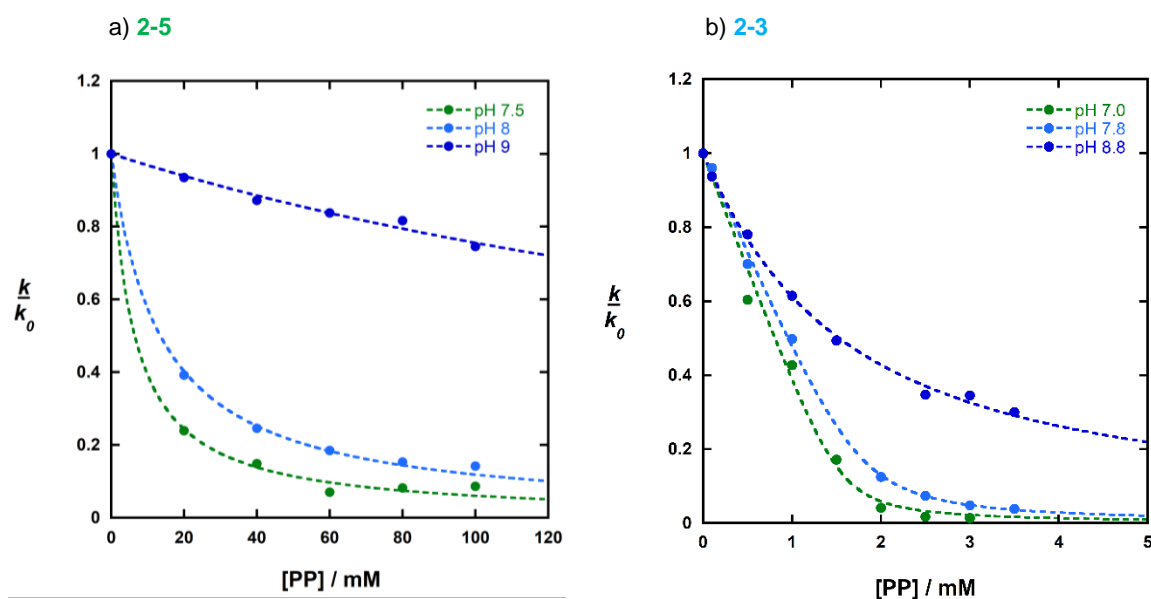


Figure 2.18 PP inhibition plot for the transesterification of BNPP catalysed by **2-5** (a) and **2-3** (b) at pH 7.5 (●), 8 (●) and 9 (●) and 25 °C; a) [**2-5**] = 0.5 mM, [BNPP] = 0.05 mM, [Buffer] = 50 mM, ionic strength 0.1 M by NaNO₃ addition. b) [**2-3**] = 2 mM, [BNPP] = 0.05 mM, [Buffer] = 50 mM, ionic strength 0.1 M by NaNO₃ addition.

$$(5) \quad \frac{k_{obs}}{k_0} = \frac{K_i^{obs}}{[I] + K_i^{obs}}$$

Table 2.3 K_i values

$$(6) \quad \frac{k_{obs}}{k_0} = \frac{1}{2} (1 - x - y + \sqrt{(1 + x + y)^2 - 4x})$$

where:

$$x = \frac{[I]}{[Cx]_T} \quad y = \frac{K_i^{obs}}{[Cx]_T}$$

	K_i^{obs} / mM	
	2-3	2-5
pH 7	0.03 ± 0.02	-
pH 7.5	-	6.4 ± 0.5
pH 8	0.04 ± 0.01	13.5 ± 0.4
pH 9	0.68 ± 0.06	310 ± 10

The PP profiles shown in Figure 2.18a and b were fitted with equations (5) and (6), respectively, yielding the observed inhibition constants reported in Table 2.3.

The dependence of the rate of BNPP cleavage on complex concentration under pseudo first order conditions (excess complex) was also evaluated. As reported in Figure 2.19, the reaction is first order in **2-3** and **2-4** (0.5 – 3 mM), but a downwards curvature is observed with increasing concentration of **2-5** (0.1 – 2 mM).

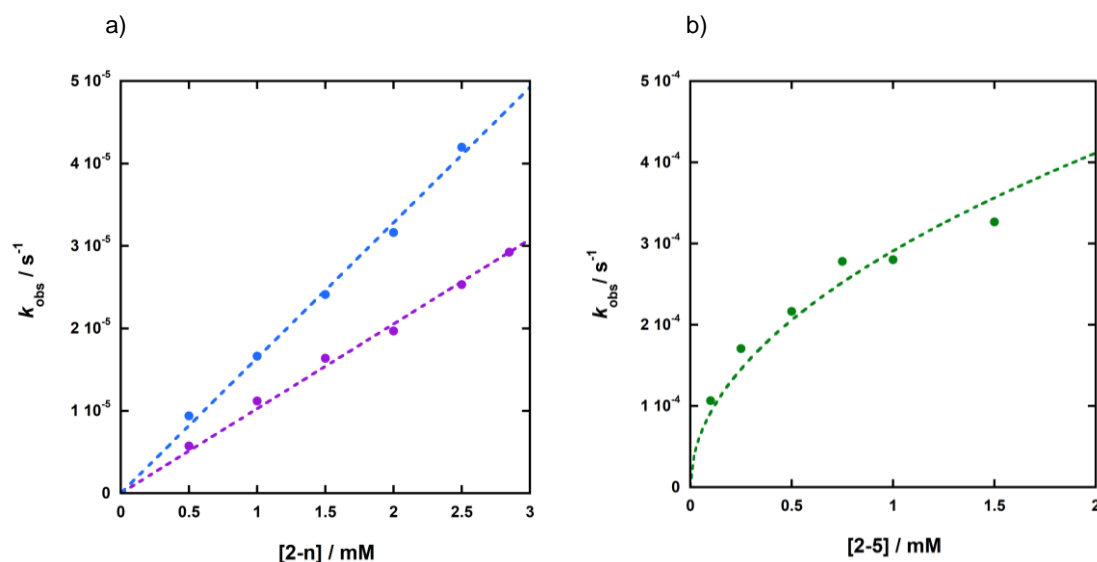
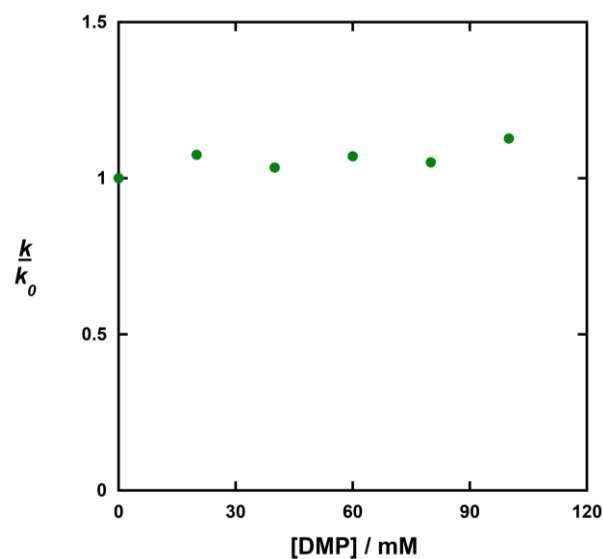
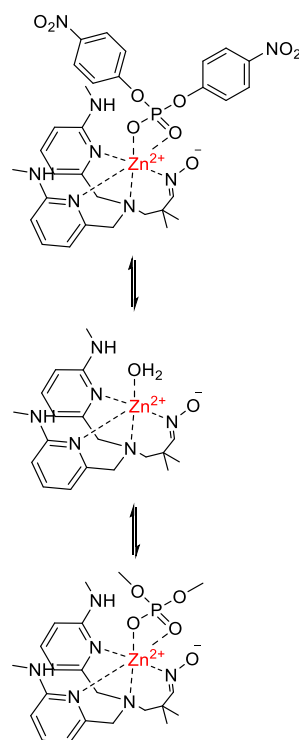


Figure 2.19 Plots of the observed rate constants for the hydrolysis of BNPP at pH 7.4 and 25 °C against the concentration of the 2-n; a) First order dependence of k_{obs} on $[2-3]$ (●) and $[2-4]$ (●); b) Dependence of k_{obs} on $[2-5]$; $[\text{BNPP}] = 0.05 \text{ mM}$, $[\text{HEPES}] = 50 \text{ mM}$, ionic strength at 0.1 M by addition of NaNO_3

The observed curvature could indicate that the substrate becomes fully bound to the complex at higher concentrations, but it would require a binding constant between the diester and the complex that is around $2\,000 \text{ M}^{-1}$; this is very high for a mononuclear Zn complex in aqueous solution, and inconsistent with the much weaker values observed for PP binding reported in Table 2.3 (as monoesters usually bind to Zn complexes much more tightly than diesters). In addition, an analogous experiment with dimethyl phosphate (DMP) at pH 7.4 showed that increasing the diester concentration caused no variation of the relative rate constant (Graph 2.4), confirming a weaker binding with diesters.

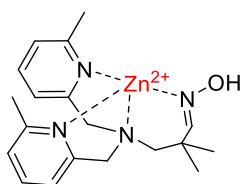


Graph 2.4 DMP Inhibition plot. $[2-5] = 0.25 \text{ mM}$, $[BNPP] = 0.05 \text{ mM}$, $[\text{HEPES}] = 50 \text{ mM}$ pH 7.4, ionic strength at 0.1 M by addition NaNO_3



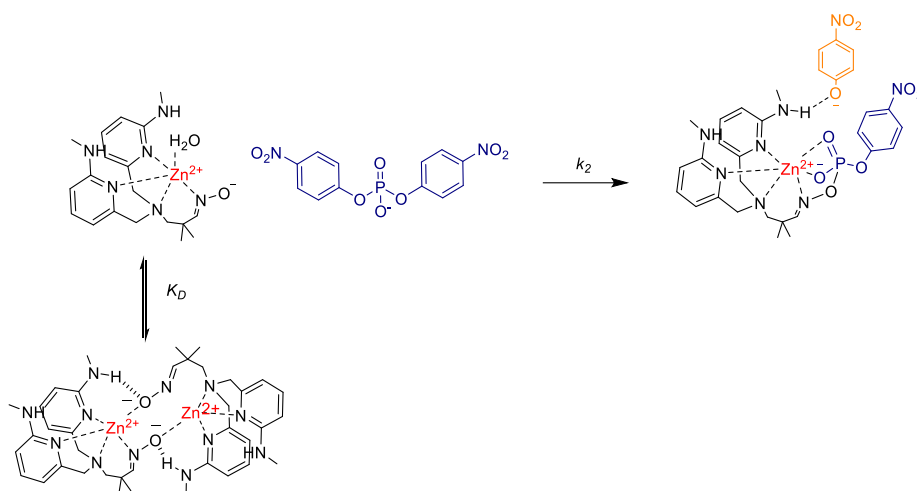
Scheme 2.10 Inhibition equilibrium

The trend, observed in the pH range between 7 and 11, could be due to complex dimerisation, as proposed by Williams *et al.* when a related complex containing an oxime was studied (**2-22** in Figure 2.20).⁸⁵ Dimerisation is also common with Co(II) and Cu(II) mononuclear complexes and, from similar equilibria to the one described in Scheme 2.11, equation (7) was used to fit the profile.^{90,91}



$$(7) \quad k_{obs} = k_2 \frac{-K_D + \sqrt{K_D^2 + 8K_D[Cx]_T}}{4}$$

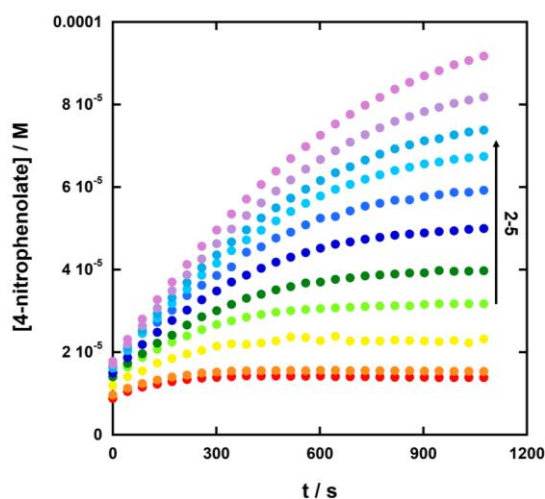
Figure 2.20 Structure of 2-22



Scheme 2.11 Dimerisation equilibrium in competition with BNPP cleavage

However, for **2-5** this approach did not lead us to a good measurement of k_2 and K_D , suggesting that the complex exists predominantly in the dimer form under these experimental conditions. If this is the case, then the two parameters are not defined independently, and cannot be determined from the plot of the observed rate constant against the total concentration of complex (see below). Therefore, an investigation of the reaction was undertaken at lower catalyst concentration, where the ground state of the complex would have a larger proportion of the monomer present. To maintain the pseudo first order condition, the substrate was kept at 1 mM, while the complex varied from 0.009 to 0.1 mM.

The increasing concentrations of 4-nitrophenolate over time are reported in Graph 2.5a. Each curve represents the transesterification of BNPP at pH 8.3 and 25 °C enhanced by the presence of a specific catalyst concentration (increasing from the bottom to the top). As observed for the turnover experiment, after the conversion of 1 equivalent of substrate, the excess of 4-nitrophenolate comes from the subsequent slow hydrolysis of the phosphorylated complex. To avoid monitoring this additional reaction, we monitor the 4-nitrophenolate appearance up to a concentration equivalent to that of the complex for each experiment. As highlighted in Figure 2.21a for the experiment at 0.07 mM of **2-5**, the exponential rise equation (3) (page 93) was not a very accurate fit for the data, with the residuals showing a systematic deviation from the data, suggesting the reaction was not first order. Unlike **2-22**, which showed a K_D of $110 \pm 10 \text{ M}^{-1}$, these data suggested that **2-5** was mostly present in its dimeric form even at the lower concentrations. By applying the proposed model and by fitting the data numerically with the software Barkeley Madonna (Figure 2.21b), we obtain an approximate K_D value of $5 \times 10^5 \text{ M}^{-1}$ and a k_2 of $14 \pm 2 \text{ M}^{-1} \text{ s}^{-1}$ (pH 8.3 and 25 °C).



Graph 2.5 Plot of the appearance of 4-nitrophenolate over time. Transesterification of BNPP (0.001 M) catalysed by 2-5 (9×10^{-6} - 1×10^{-4} M) at pH 8.3 and 25 °C; [BNPP] = 1 mM, [EPPES] = 50 mM, ionic strength at 0.1 M by addition of NaNO_3

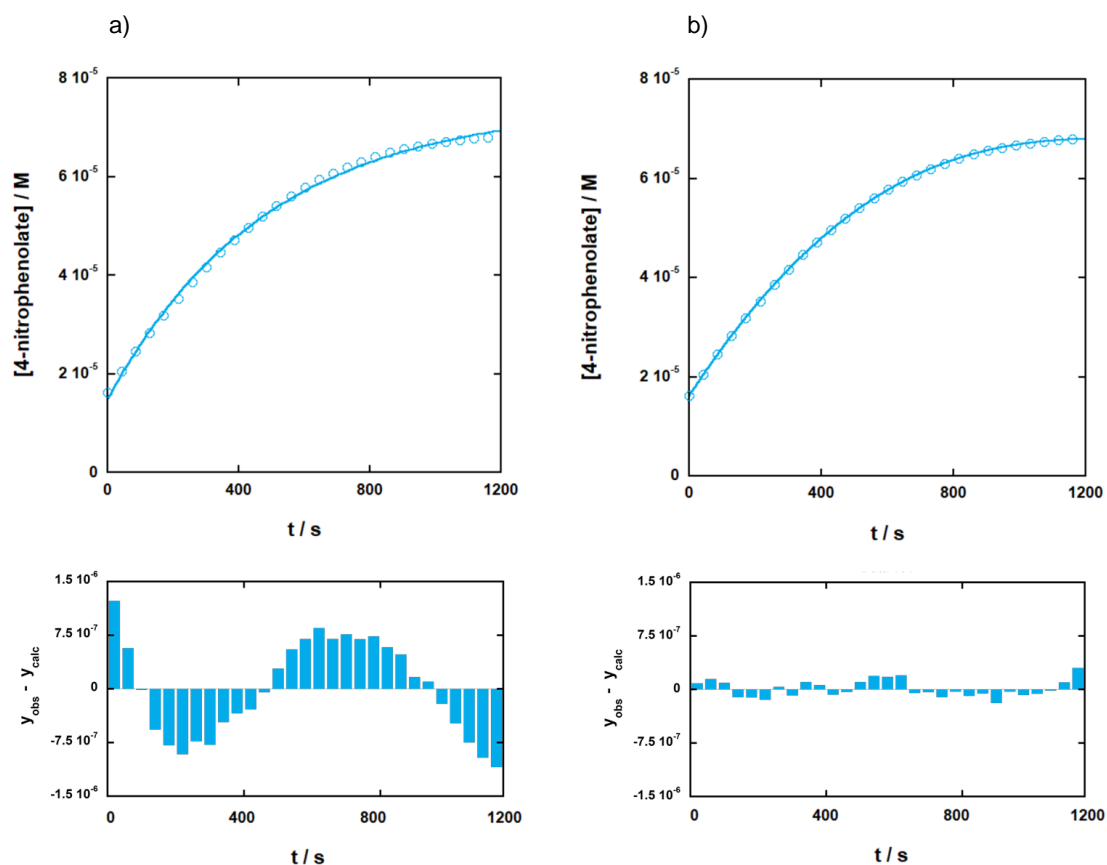


Figure 2.21 Appearance of 4-nitrophenolate over time for the transesterification of BNPP (1 mM) catalysed by 3-5 (0.07 mM) at 25 °C and pH 8.3; a) Fitting of the data by exponential rise equation; b) Fitting of the data by Berkeley Madonna

Due to the high value found for K_D , it is apparent that in pseudo-first order conditions (excess of complex), **2-5** is mostly dimerised, and the concentration of dimer (C_{x2}) in terms of the concentration of total complex (C_T) can be approximated by equation (8). Given the equilibrium defined by equation (9), the monomer concentration can be expressed in terms of total complex (C_T) as described in equation (10).

$$(8) \quad [C_T] = 2 [Cx_2] \qquad (9) \quad K_D = \frac{[Cx_2]}{[Cx][Cx]} = \frac{[Cx_2]}{[Cx]^2}$$

$$(10) \quad [Cx] = \sqrt{\frac{[Cx_2]}{K_D}} = \sqrt{\frac{[C_T]}{2K_D}}$$

The observed rate constant (k_{obs}) is related to the dimerisation constant (K_D) and the second order rate constant for the reaction of the monomer with the substrate (k_2) by:

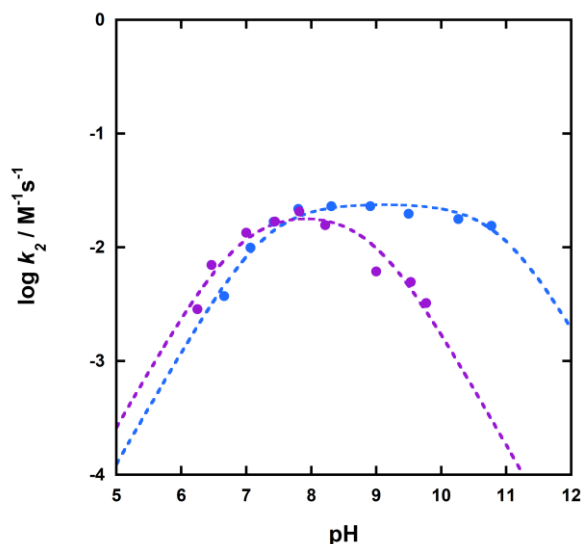
$$(11) \quad k_{obs} = k_2 [Cx] = k_2 \sqrt{\frac{[C_T]}{2K_D}} = k_0 \sqrt{[C_T]} \qquad \text{where:} \quad k_0 = \frac{k_2}{\sqrt{2K_D}}$$

The data were fitted by equation (11) which yielded $k_0 = 0.011 \text{ M}^{-0.5} \text{ s}^{-1}$ at pH 8.3. The second order rate constant k_2 was then calculated using the K_D value obtained from the experiments at low complex concentration (5×10^5) and found to be equal to $11 \text{ M}^{-1} \text{ s}^{-1}$ in good agreement with the value of $14 \text{ M}^{-1} \text{ s}^{-1}$ deduced from the numerical fitting of the reaction progress at low complex concentration. Using the value of $14 \text{ M}^{-1} \text{ s}^{-1}$ for k_2 led to

a value of $8 \times 10^5 \text{ M}^{-1}$ for K_D . These analyses suggest that this reaction scheme explains the data under both sets of reaction conditions satisfactorily, and led to an acceptable evaluation of the rate and dimerisation constants.

The dashed line in Figure 2.19b illustrates the fit of the same equation at pH 7.4 and 25 °C and is indistinguishable from the fit obtained of equation (11) to these data. The values of k_2 and K_D obtained from equation (7) had an error which was much greater than their values, but when combined together according to equation (10), gave exactly the same value of k_0 . This suggests that our assumption that the dimer is essentially fully dimerised under these conditions is reasonable. At the lowest concentration of 0.1 mM we used for these experiments, $K_D = 5 \times 10^5 \text{ M}^{-1}$ would indicate that only 10% of the complex exists as the monomer, and this seems likely to be an upper limit. If this value is lower, the value for k_2 would be higher, compensating for the lower concentration of active monomer present.

Plotting the second order rate constant k_2 for **2-3** and **2-4** against the pH revealed the bell shape profile reported in Graph 2.6. The data are in good agreement with equation (12), which defines a maximum k_2 value and two kinetic $\text{p}K_a^1$ and $\text{p}K_a^2$ that define a singly ionised species as the active form (values reported in Table 2.4). Although the second $\text{p}K_a$ is less pronounced for **2-3**, the profile of **2-4** showed that the formation of the double deprotonated form of the catalyst strongly reduced its activity. This hypothesis is consistent with the potentiometric titration data, which yielded the speciation plots reported in Figure 2.22. The $\text{p}K_a$ s for all the complexes reported in Table 2.4 are in good agreement with the kinetic values. In particular, the data confirmed that **2-3** and **2-4** reach their highest k_2 when the single deprotonated complex was formed.



Graph 2.6 pH profile of the second order rate constant k_2 for the cleavage of BNPP catalysed by 2-3 and 2-4 at 25 °C; $[BNPP] = 0.05 \text{ mM}$, $[Buffer] = 50 \text{ mM}$, ionic strength at 0.1 M by addition of NaNO_3

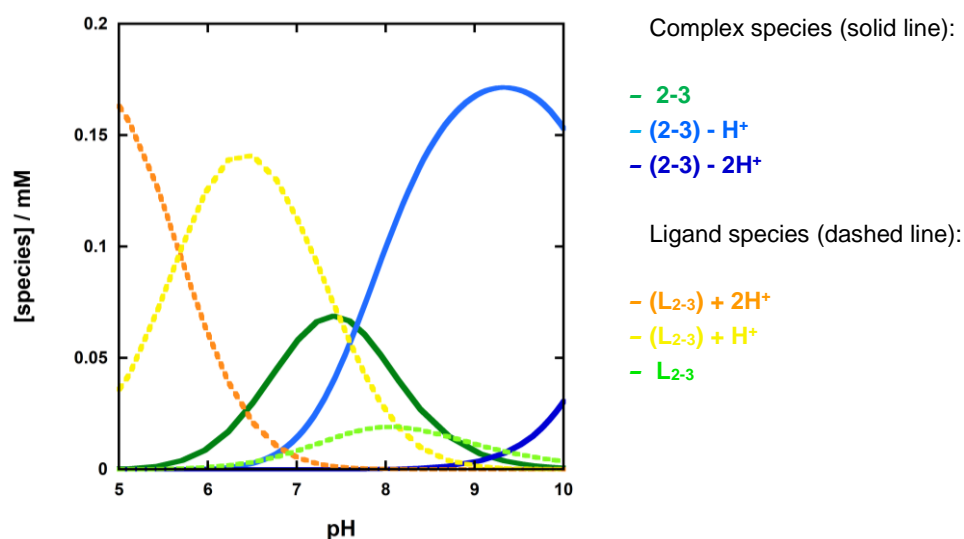
Table 2.4 Values of k_2 and pK_a obtained by fitting equation (12) to the pH profile of the second order rate constant k_2

Complex	$k_2^{\text{max}} / \text{M}^{-1} \text{s}^{-1}$	pK_a^1		pK_a^2	
		Kinetic	Titration	Kinetic	Titration
2-3	$2.4 \pm 0.2 \times 10^{-2}$	7.3 ± 0.1	7.68	10.9 ± 0.3	10.71
2-4	$2.1 \pm 0.4 \times 10^{-2}$	6.9 ± 0.2	6.79	8.9 ± 0.2	8.72

$$(12) \quad k_2 = k_2^{\text{max}} [Cx] \frac{K_a^1 [H^+]}{(K_a^1 K_a^2 + K_a^1 [H^+] + [H^+]^2)}$$

A measured macroscopic pK_a cannot be assigned to a specific microscopic deprotonation, and we cannot identify where the proton was removed unambiguously. However, either the metal bound water or the hydroxyl group can likely be deprotonated under the experimental conditions.

a) Speciation plot of **2-3**



b) Speciation plot of **2-4**

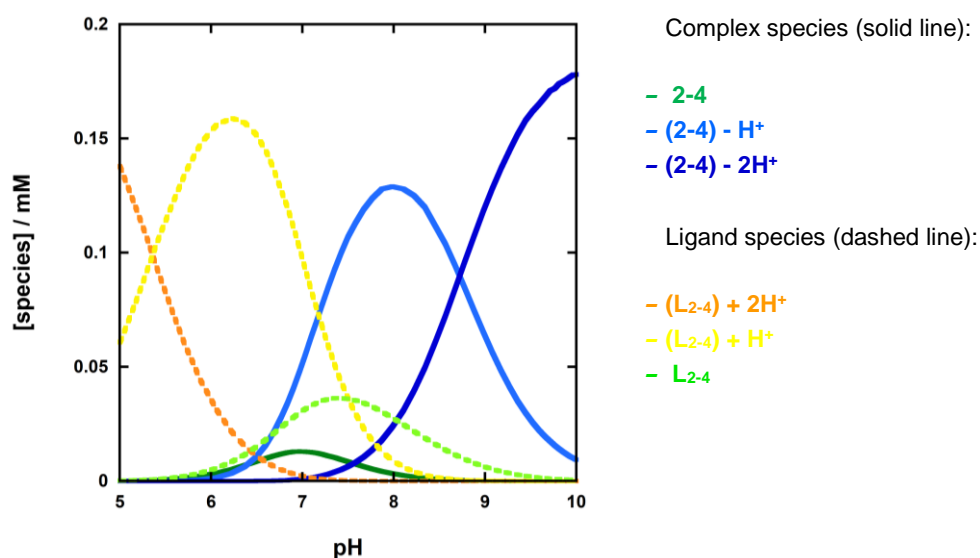
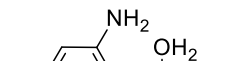


Figure 2.22 Speciation plots of 2-3 (a) and 2-4 (b). The titration experiment was performed at 25 °C and ionic strength fixed at 0.1 M by addition of NaNO₃; a) [2-3] = 2 mM; [2-4] = 0.2 mM; The difference in the concentration of the complexes is due to the low solubility of 2-4 and 2-5.

As previously reported by Mareque-Rivas *et al.*,⁹² a primary amino group in the second coordination sphere of closely related tetradentate complexes can stabilise the metal bound hydroxide by hydrogen bonding, causing a shift of the metal bound water's pK_a to a lower

value. For complexes with analogous scaffolds to that of **2-3**, it has been suggested that the presence of substituents in the ortho pyridyl position (**2-11**) would likely affect the water deprotonation rather than the alkoxy group.^{93,87} Here we report the kinetic pK_a values of the equivalent ligand **2-11** compared to **2-2** and **2-3** (Table 2.5). Due to the similarities between the values found, the complexes appeared to behave likewise. If the first deprotonation is mainly associated with the formation of the metal bound hydroxide, the secondary and primary amines in **2-3** and **2-2** impact the pK_a of water similarly. However, a small shift to a lower value for pK_a^1 was observed for **2-2** and **2-3**. A more alkaline value of pK_a^2 , which corresponds to the deprotonation of the hydroxyl group, was found for **2-3** and **2-4**.

2-2



2-11

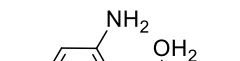


Table 2.5 kinetic pK_a of 2-3, 2-2 and 2-11

Complex	pK_a^1	pK_a^2
2-3	7.3 ± 0.1	10.9 ± 0.3
2-2	6.97 ± 0.05	10.68 ± 0.06
2-11*	7.90	10.2
*from reference ⁹³		

Figure 2.23 Structure of mononuclear Zn(II) complexes with primary amine groups in the ortho pyridyl position

The shift might be due to the two methyl groups that would affect the hydroxyl group more than the water molecule. **2-11** is the most reactive among these complexes and has k_2^{\max} of $9.7 \times 10^{-2} \text{ M}^{-1} \text{ s}^{-1}$ which is most closely approached at pH 9. However, comparing the kinetic data at pH 7.4, **2-3**, **2-2** and **2-11** had approximately similar reactivity toward the cleavage of BNPP with k_2 values of $2.4 \pm 0.2 \times 10^{-2}$, $6.5 \pm 0.2 \times 10^{-2}$ and $2.5 \times 10^{-2} \text{ M}^{-1} \text{ s}^{-1}$, respectively. Although **2-3** and **2-2** formed the single deprotonated active species at lower

pH, their maximum activity was reduced. The deprotonation of the metal bound hydroxyl is central for the catalyst reactivity, but coordination with the Zn(II) centre reduces the alkoxide's nucleophilic activity toward the phosphorous. Hence, the relatively lower k_2^{\max} values of **2-3** and **2-2** compared to **2-11**, which are modulated by their ligand structures, might result from the Zn(II) coordination which decreased the strength of the nucleophile.

The speciation plot and the kinetic pH profile of **2-4** showed that the active form of the catalyst is present as the dominant species over a narrower pH range than for **2-3**. This is primarily due to a 2-units difference in pK_a^2 . As for **2-3**, it was difficult to identify the microscopic nature of the ionic species formed with certainty. However, we propose that the second electron-withdrawing hydroxyl group might be responsible for lowering the second pK_a . Due to proximity, the metal bound hydroxide is more affected than the coordinated water molecule; hence, the pK_a^2 of 8.7 might be due to the deprotonation of the former. This result is in good agreement with values reported by Bonomi *et al.*⁹⁴ for their analogous mononuclear ligands in which the pK_a of an alcohol group was proposed to be reduced by introducing electron-withdrawing groups (**2-23** and **2-24** in Figure 2.24 and Table 2.6)

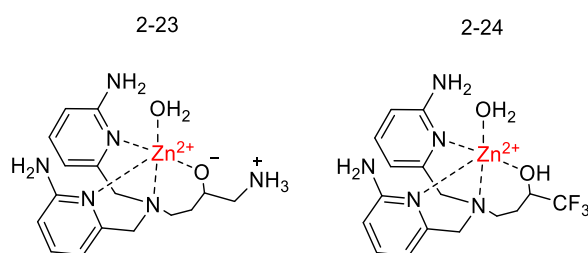


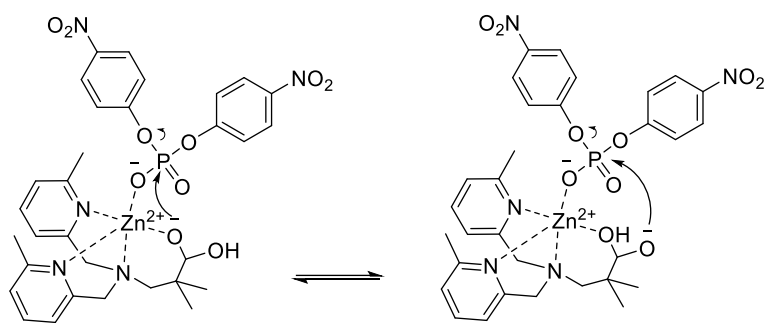
Figure 2.24 Complexes proposed by Bonomi *et al.*

Table 2.6 Kinetic pK_a and k_2^{\max} calculated for **2-23** and **2-24**

Complex	pK_a^1	pK_a^2	$k_2 / M^{-1} s^{-1}$
2-4	6.9	8.9	2.1×10^{-2}
2-23*	7.3	8.4	2.2×10^{-2}
2-24*	7.7	8.6	1.5×10^{-3}

*from reference⁹⁴

The similar pK_a^1 measured for **2-3** and **2-4** are consistent with this analysis. No enhancement over the reaction catalysed by **2-3** was observed when the hydroxyl group was replaced by the gem-diol. However, when Williams and coworkers reported the incorporation of an aldehyde into the ligand structure, **2-21** promoted the catalytic hydrolysis of BNPP two times faster than **2-20** (reported in the chapter introduction - Figure 2.6).⁷⁹ As demonstrated by the k_2 values reported in Table 2.6, lowering the hydroxyl pK_a might reflect a decrease in the alkoxide nucleophilicity. Due to the higher k_2 , the reaction catalysed by **2-21** was proposed to proceed by the nucleophilic attack of the non-coordinated hydroxyl group. In particular, given the tautomeric equilibrium, if the Zn(II) coordinates to the hydroxyl group, a greater Lewis acid activation was provided to the substrate (Scheme 2.12). Although the reaction catalysed by our novel complex might proceed through an analogous mechanism, the same reactivity observed for **2-3** and **2-4** seems to suggest that this hypothesis is unnecessary. In this work, the hydrate anion is likely to be present at higher concentrations than the alkoxy anion, in which case the alkoxy needs to be more reactive to lead to the same overall reactivity. For **2-3**, the most acidic site for the first deprotonation is likely to be the Zn(II) bound water that can be stabilised by the amino groups; for **2-4**, both the Zn(II) bound water and the side chain could be the preferred site, and so each will be present as the anionic form. These differences in pK_a might mask a more significant difference in reactivity of the nucleophilic side chains than is apparent from the pH rate profile.



Scheme 2.12 Tautomeric equilibrium of 2-21

The pH dependence of k_{obs} for the BNPP transesterification catalysed by **2-5** at different concentrations are reported in Figure 2.25a, and the pH dependence of the values for k_2 derived from fitting the data at each pH to equation (13) are reported in Figure 2.25b.

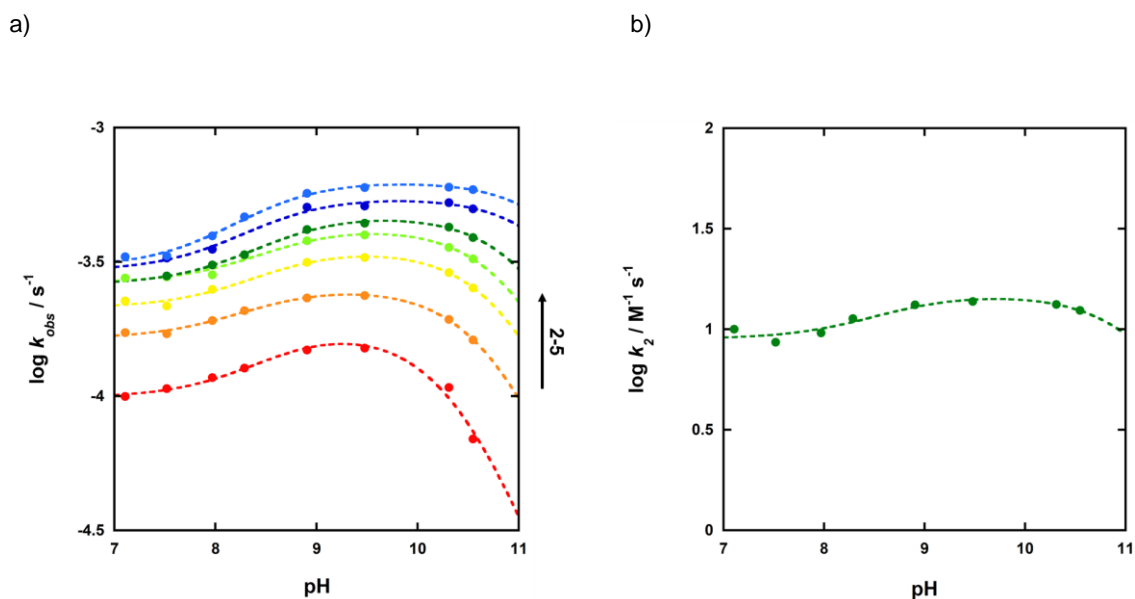


Figure 2.25 pH dependence of the k_{obs} at increasing complex concentration (a) and k_2 (b) for the transesterification of BNPP catalysed by 2-5 at 25 °C. [BNPP] = 0.05 mM, [Buffer] = 50 mM, ionic strength at 0.1 M by addition of NaNO_3

$$(13) \quad y = \frac{k_0''[H^+]K_a^1 + k_0'K_a^1K_a^2[H^+]^2}{1 + [H^+]K_a^1 + K_a^1K_a^2[H^+]^2}$$

Table 2.7 k_{obs} and pK_a values at different concentration of **2-5**

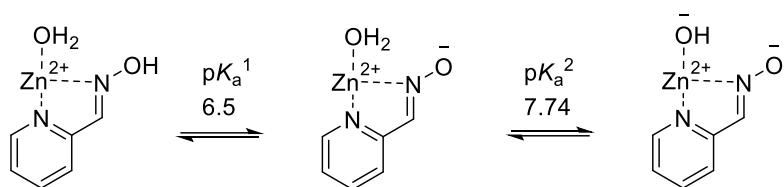
[2-5] / mM	k_{obs}' / s^{-1}	k_{obs}'' / s^{-1}	pK_a^1	pK_a^2
0.10	$9.90 \pm 0.60 \times 10^{-5}$	$1.8 \pm 0.2 \times 10^{-4}$	8.5 ± 0.3	10.4 ± 0.1
0.25	$1.64 \pm 0.03 \times 10^{-4}$	$2.6 \pm 0.1 \times 10^{-4}$	8.4 ± 0.3	10.8 ± 0.1
0.50	$2.13 \pm 0.08 \times 10^{-4}$	$3.5 \pm 0.2 \times 10^{-4}$	8.5 ± 0.2	10.9 ± 0.1
0.75	$2.64 \pm 0.09 \times 10^{-4}$	$4.3 \pm 0.2 \times 10^{-4}$	8.6 ± 0.2	11.0 ± 0.1
1.00	$2.60 \pm 0.06 \times 10^{-4}$	$4.8 \pm 0.1 \times 10^{-4}$	8.5 ± 0.1	11.2 ± 0.1
1.50	$2.90 \pm 0.30 \times 10^{-4}$	$5.5 \pm 0.3 \times 10^{-4}$	8.4 ± 0.3	11.6 ± 0.4
2.00	$3.00 \pm 0.10 \times 10^{-4}$	$6.3 \pm 0.2 \times 10^{-4}$	8.3 ± 0.1	11.7 ± 0.3

Table 2.8 k_2 and pK_a values for **2-5** gained by fitting the data with equation (13)

	$k_2' / M^{-1} s^{-1}$	$k_2'' / M^{-1} s^{-1}$	pK_a^1	pK_a^2
2-3	9.0 ± 0.6	15 ± 1	8.6 ± 0.4	11.2 ± 0.3

(13) considers two ionisations and two rate constants. The rate constant and pK_a values obtained from Figure 2.25a and b are reported in Table 2.7 and Table 2.8, respectively. While almost no change was observed for pK_a^1 , increasing the concentration of **2-5** from 0.1 to 2 mM led to a shift of pK_a^2 . The pH profile also suggested the existence of two active species. The first active ionised species, formed below pH 7, undergoes deprotonation at approximately pH 8.6 ± 0.4 (pK_a^1), leading to the second active form of the catalyst. Eventually, deprotonation (pK_a^2) of the latter causes the decrease in reactivity at pH 11.2 ± 0.3 .

As reported by Breslow and Chipman,⁹⁵ binding Zn(II) to 2-pyridinealdoxime reduces the pK_a of the oxime from 10.4 to 6.5. The pK_a of the water bound to the Zn(II) ion is less affected by the ionisation of the oxime than by the ionisation of an OH group directly coordinated to the Zn(II) ion, as might be expected.



Scheme 2.13 Equilibria proposed by Breslow and Chipman for the 2-pyridinealdoxime

In contrast to **2-3** and **2-4**, the first pK_a of the catalyst, which should be at $pH < 7$, does not measure the deprotonation of the metal bound water. In agreement with the report of Breslow and Chipman, we proposed that at $pH\ 7$, the catalyst is already in its single deprotonated form (**2-5**)-H⁺, with the proton being removed from the oxime group. Then, the two kinetic pK_a s obtained from the pH profiles correspond to the further deprotonations that yield (**2-5**)-2H⁺ and (**2-5**)-3H⁺. While the double deprotonated form of the catalyst is still reactive, further deprotonation deactivates the complex. A similar result was reported by Yatsimirsky and coworkers on their Zn(II) complex **2-25** tested toward the hydrolysis of esters and phosphate triesters.⁹⁶ The pH profile (in the 7-11 range) of the rate constant for the phenol acetates hydrolysis catalysed by **2-25**, structurally similar to **2-5**, was characterised by two kinetic pK_a of 8.5 and 10.5. Although the most active species to hydrolyse the acetate was (**2-25**)-3H⁺, the pK_a values are in agreement with our findings.

2-25

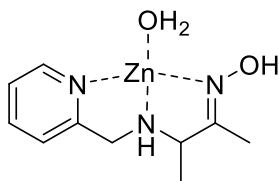
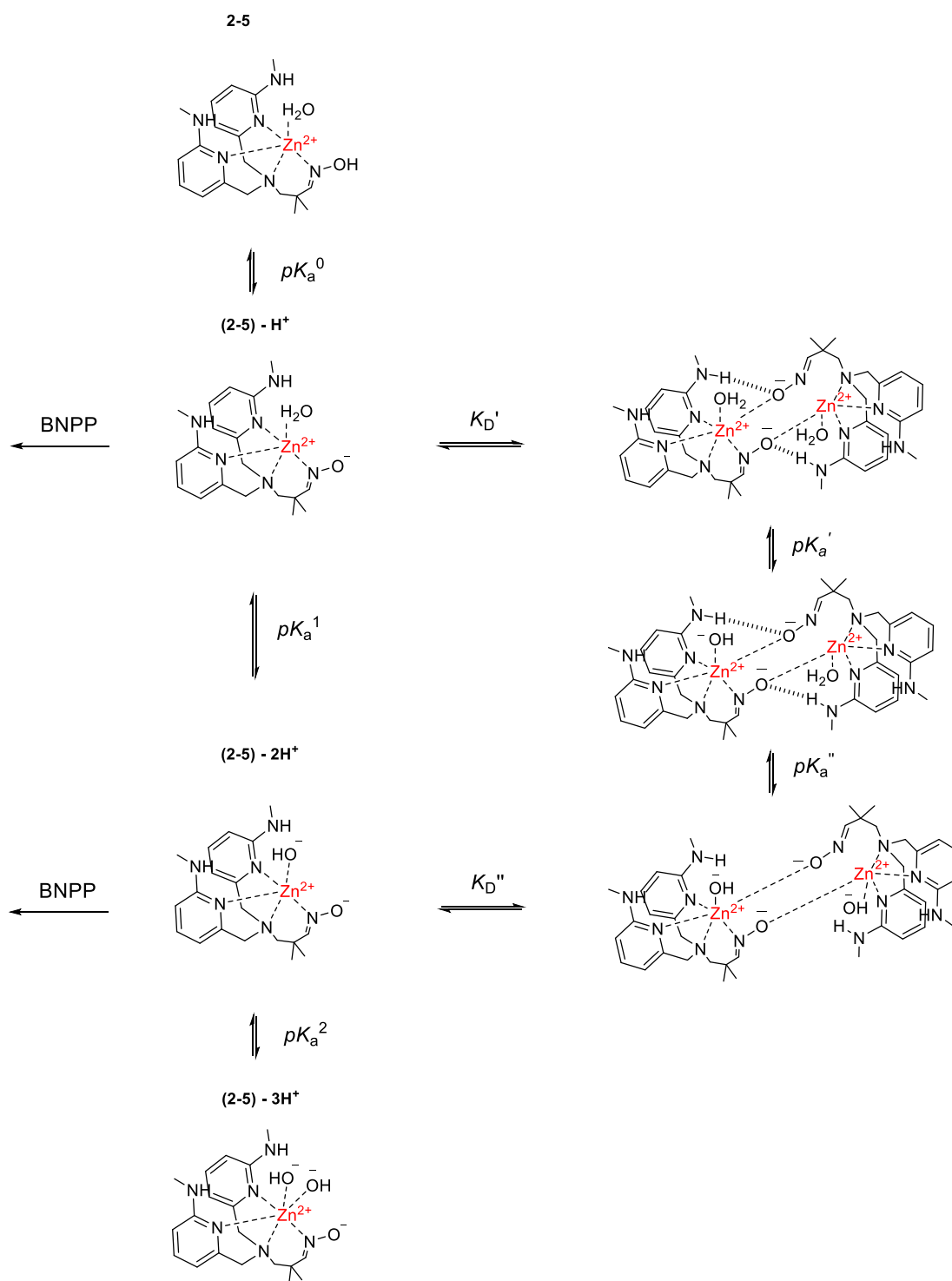


Figure 2.26 Structure of the catalyst proposed by Yatsimirsky and coworkers

The proposed equilibria of **2-5** are shown in Scheme 2.13. We expected the single deprotonated species to be the most active form of the complex due to a likely decrease in substrate affinity caused by further deprotonations. In contrast to acetate hydrolysis, it is uncommon for a catalyst tested with a phosphate diester to exhibit more than one active species. For carbonyl ester cleavage, the presence of an additional nucleophile coordinated to the metal usually leads to an increase in the catalyst reactivity, as observed for **2-25**. In the reactions, initial coordination of the substrate to the complex is not believed to be part of the mechanism, and so as the reactivity of the nucleophile increases, so does the rate of the reaction.

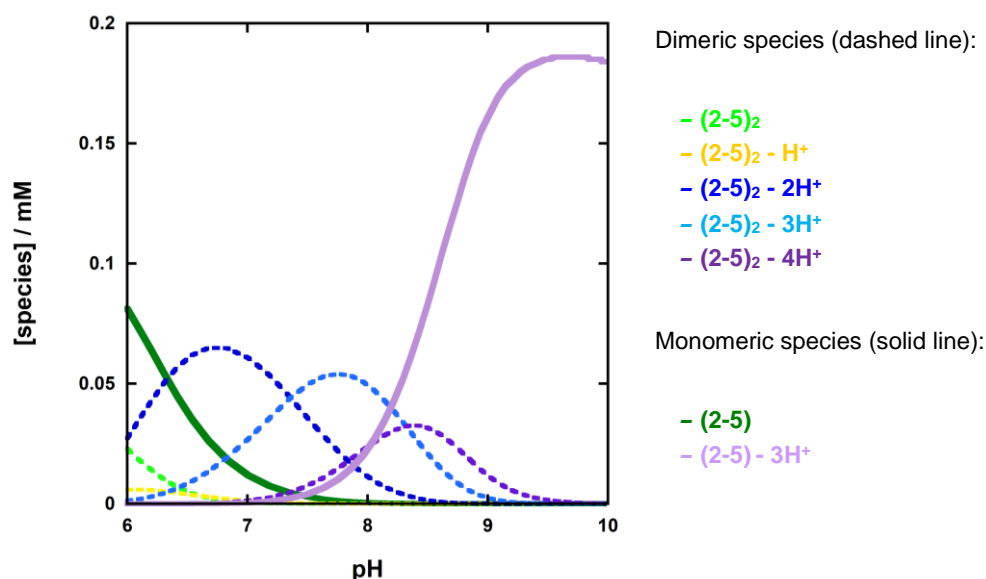
Although we considered no variation of the dimerisation constant across the pH range, the deprotonation of **2-5** might partially influence the equilibria between $(\mathbf{2-5})\text{-}2\text{H}^+$ and its dimeric form. As reported in Scheme 2.14, after the first $\text{p}K_{\text{a}}$, the additional negatively charged hydroxide groups might partially prevent the doubly and triply deprotonated forms of **2-5** from engaging in dimerisation. Therefore, if $(\mathbf{2-5})\text{-H}^+$ and $(\mathbf{2-5})\text{-}2\text{H}^+$ retained part of the complex reactivity, the observed maximum of k_2 at higher pH might be due to compensation between the two major events happening in solution.



Scheme 2.14 Proposed deprotonation and dimerisation equilibria for 2-5

Although **(2-5)**-2H⁺ might be less reactive than **(2-5)**-H⁺, the former might be more in its monomeric form than the latter.

To attempt to gain further information that could help interpret the profile, we titrated both **L2-5** and **2-5** at 0.2 mM total concentration. Although the data for **L2-5** could be analysed using a simple scheme to describe its sequential deprotonation, a more elaborate scheme was required for **2-5** to take into account dimerisation. However, introducing a large number of species affect the validity of the model. For this reason, we reduced the possible species in the pH range studied based on the kinetic data and proposed Scheme 2.14. Although titrations of **2-5** at higher concentrations would have favoured the dimer formation only and tested the model more thoroughly (the experiment at 2 mM was attempted, but precipitation occurred), we assumed that under the experimental condition, the single and the double deprotonated form of **2-5** mainly engaged in dimerisation. However, we did not expect **(2-5)**-3H⁺ to dimerise, and only **(2-5)**₂-2H⁺ **(2-5)**₂-3H⁺ and **(2-5)**₂-4H⁺ species were considered. The speciation plot is reported in Graph 2.7.



Graph 2.7 Speciation plot of 2-5. The titration experiment was performed at 25 °C and ionic strength fixed at 0.1 M by addition of NaNO_3 ; $[\text{2-5}] = 0.2 \text{ mM}$.

Table 2.9 pK_a values of the dimeric form of 2-5

	pK_a^1	pK_a^2	pK_a^3
$(\text{2-5})_2$	6.6	7.4	8.3

As proposed by the speciation plot, the major species at pH 7 is the dimer of the single deprotonated form of **2-5**, and moving to more alkaline pH, consecutive deprotonations lead to $(\text{2-5})_2\text{-3H}^+$ and $(\text{2-5})_2\text{-4H}^+$. It is worth noting that increasing the number of negative charges seems to reduce the abundance of the dimeric species. Compared to $(\text{2-5})_2\text{-2H}^+$, the additional metal bound hydroxides in $(\text{2-5})_2\text{-3H}^+$ and $(\text{2-5})_2\text{-4H}^+$ might affect the complex dimerisation as confirmed by the reduction of the maximum of their distributions. Although we were interested in the monomeric species of the catalyst, the speciation plot of the dimers helps us to understand where the correspondent monomer would form. For example, the speciation of $(\text{2-5})_2\text{-4H}^+$, which has its maximum at pH 8.5, suggested that in the same

pH region at lower concentration **(2-5)**-2H⁺ would be the major species. Good agreement was found between the speciation plot and the kinetic data at lower pH. Over pH 7, the speciation plot confirmed that **(2-5)**-H⁺, which is affected by dimerisation to form **(2-5)**₂-2H⁺, was the most abundant form, and its reactivity is defined by the second order rate constant equal to $5.7 \pm 0.4 \text{ M}^{-1} \text{ s}^{-1}$. According to Graph 2.7, the pK_a of **(2-5)**₂-4H⁺ is at pH 8.3, and a similar value would be expected of the equivalent monomer **(2-5)**-2H⁺. This result was confirmed by the pH profile, in which the kinetic pK_a¹ of 8.6 ± 0.4 led to a k_2 of $15 \pm 1 \text{ M}^{-1} \text{ s}^{-1}$. However, compared to the kinetic data, which showed a second pK_a of 11.2 ± 0.3 , the increase in the speciation distribution of **(2-5)**-3H⁺ was observed at lower pH (approximately 9.5). Although we could not explain this discrepancy between our model, based on the kinetic data, and the potentiometric titration, we excluded the possibility that the higher reactivity at pH 9.5 was due to the highly negatively charged **(2-5)**-3H⁺, which would strongly inhibit the phosphate binding to the complex. It is worth highlighting that the potentiometric titration is influenced by dimerisation and the experimental concentration of the complex (kept low at 0.2 mM). Both factors have made the titration fitting laborious and complicated.

The presence of the secondary amines in the *ortho* position seemed to favour the dimerisation considerably more strongly than the methyl groups and the second order rate constant was only 19-fold higher than that measured for **2-22** ($k_2 = 0.80 \text{ M}^{-1} \text{ s}^{-1}$). The difference observed between **2-5** and **2-22** was modest compared to previously reported literature.^{78,79,89,97} The introduction of primary amine groups in the *ortho* position of the pyridyl ring has often greatly improved the catalyst reactivity. In Figure 2.27 is a comparison between the reactivity of mononuclear catalysts designed for the hydrolysis of

DNA model molecules and dinuclear complexes, which have been studied for the hydrolysis of RNA model molecules. As highlighted by the relative rate constants, while the gap between the mononuclear catalysts is 40, the dinuclear complex enriched with primary amines is 1400-fold more reactive than its equivalent **2-26**. This large difference was explained to be due to the hydrogen bond donor capacity of the groups, which stabilise the formation of the metal-bound hydroxide and enhance the substrate binding.

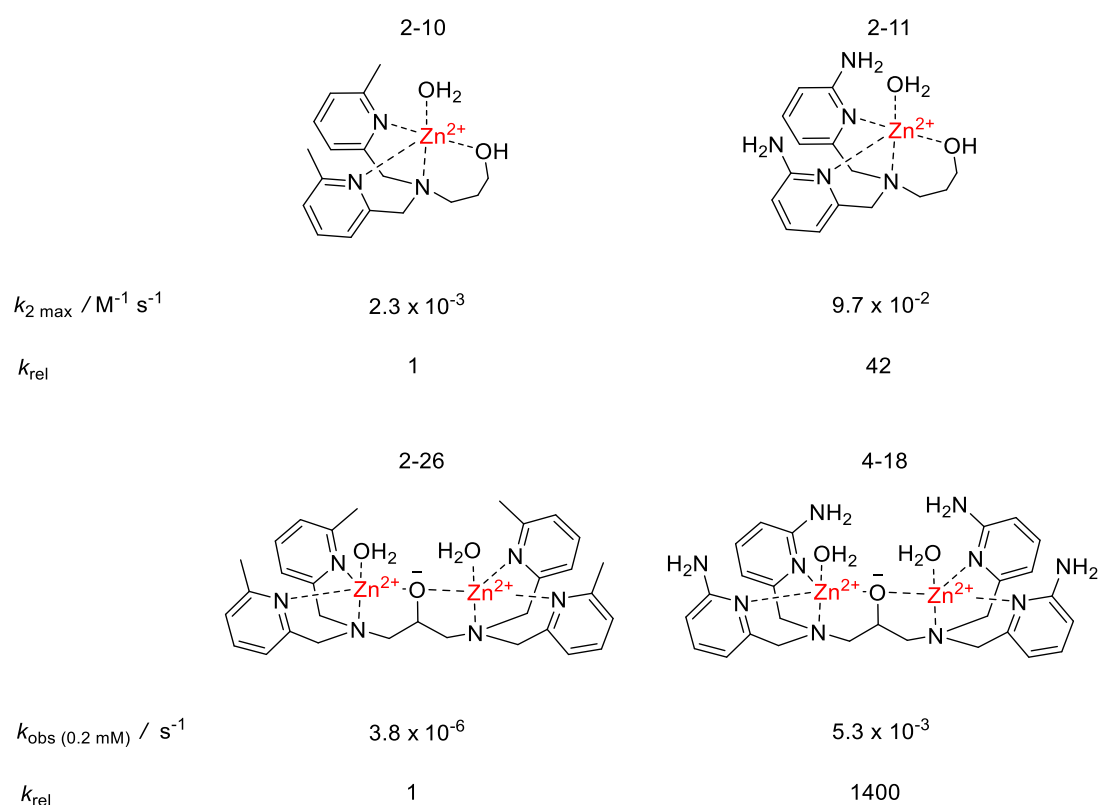
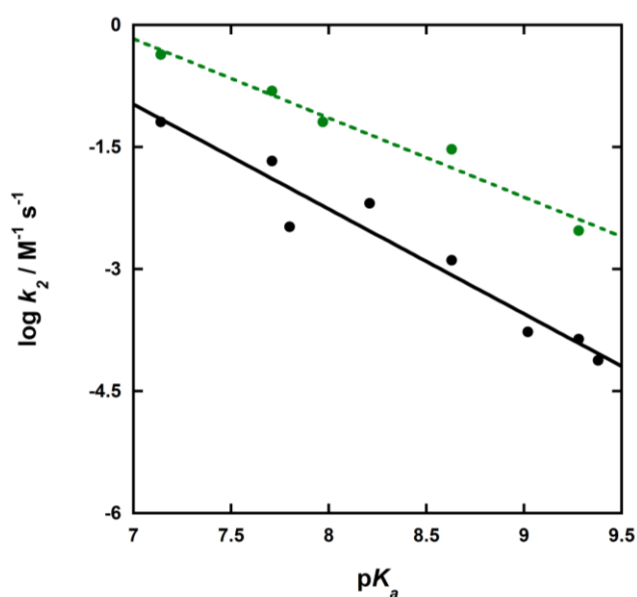


Figure 2.27 Difference in reactivity of mononuclear and dinuclear catalyst reported in literature

To test if **2-5** is a promising candidate for the cleavage of substrates less reactive than BNPP (and potentially DNA), we monitored the transesterification of five methyl aryl phosphate diesters (Figure 2.28) with different leaving groups. The presence and the position of substituents in the aromatic ring strongly influenced the $\text{p}K_{\text{a}}$ of the leaving group.



Graph 2.8 Comparison between the k_2 dependence over the pK_a of the leaving group for the transesterification of methyl aryl phosphate diester between 2-22 (black solid line) and 2-5(●), at pH 8.3 and 25 °C; [substrate] = 0.05 mM, pH 8.3 [EPPS] = 50 mM, ionic strength at 0.1 M by addition of NaNO₃

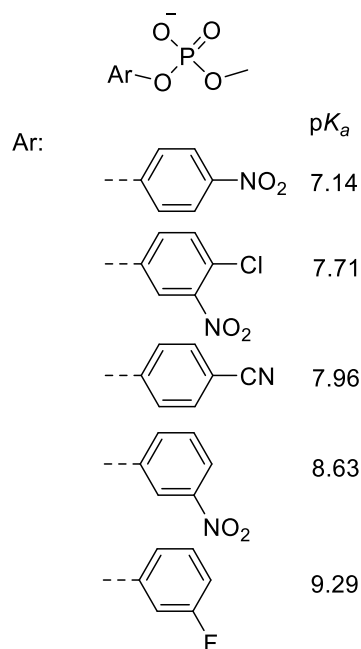


Figure 2.28 Methyl aryl Phosphate diesters

The reaction catalysed by **2-5** proceeds by the transesterification of the substrates, releasing the phenolate. The second order rate constant for the cleavage of 4-nitrophenyl methyl phosphate in the presence of **2-5** at pH 8.3 and 25 °C is equal to $4.3 \pm 0.5 \text{ M}^{-1} \text{ s}^{-1}$, which is 30 times lower than the value found for BNPP. As reported in Graph 2.8, increasing the pK_a of the leaving group reduces the second order rate constant. The linear least-squares fitting of the data produced a β_{LG} of -0.97 ± 0.1 . Due to mesomeric contribution, 4-NO₂ and 4-CN groups offer much greater stability to the phenolate than the other substituents. For this reason, previous studies have shown that a more appropriate analysis of the cleavage of the methyl phenyl phosphodiester was done by omitting these two substrates.⁷ In our case, the two approaches did not yield different results (β_{LG} of -1.07 ± 0.1), and the k_2 for the transesterification of all the substrates stay approximately on the same line. In an

analogous experiment in the presence of **2-22**, a steeper dependence of the k_2 was found by Williams and coworkers (β_{LG} of -1.3 ± 0.1). The slope β_{LG} is a measure of the ability of the transition state to accommodate the charge buildup on the leaving group's oxygen. For a specific reaction, this value is greatly affected by the local environment. As reported by Herschlag and Zalatan for phosphate diester hydrolysis catalysed by alkaline phosphatase, the predicted β_{LG} are -0.43, -1.11 and -0.85 for an associative, dissociative and synchronous transition state, respectively. The β_{LG} value found for the cleavage of methyl aryl phosphate diester catalysed by **2-5** is higher than the value found for hydroxide (tested at 42 °C, β_{LG} of -0.94 ± 0.05), but smaller than the one found for **2-22**. In addition, the fractional effective charge in the transition state, calculated by the ratio of β_{LG}/β_{eq} (β_{eq} equal to -1.73^{98}) is equal to 0.61, suggesting a concerted reaction with a loose transition state. The equivalent parameter for **2-22** is 0.75, suggesting that **2-5** has a less advanced transition state as far as bond cleavage to the leaving group is concerned than **2-22**. Although this is a relatively small variation, we cannot exclude that the secondary amine might play a role in stabilising the charge on the leaving group and favouring its departure. However, the huge drop in reactivity between the most (4-NO₂) and the least (3-F) activated substrate (95-fold difference in k_2) highlights the limitation of the catalyst for the hydrolysis of nucleic acids (which have leaving groups with much higher pK_{as}).

2.5 Conclusions

This Chapter highlights the impact of the ligand structure on modulating catalyst performance. Although tempting as a strategy, the introduction of stronger hydrogen bond donor groups in the *ortho* position of the pyridine rings disrupts the effectiveness of the complex due to competing deprotonation. With first and second pK_{as} of 5.58 and 5.89, the double deprotonated species (with the two protons probably coming from the sulfonamide groups) is dominant at physiological pH. The formation of this neutral complex leads to reduced solubility and reactivity.

As discussed in the second half of the Chapter, we confirmed the importance of stable hydrogen bond donors, which determine a 57-fold enhancement over the cleavage of BNPP catalysed by **2-9** (Figure 2.29).⁷⁸

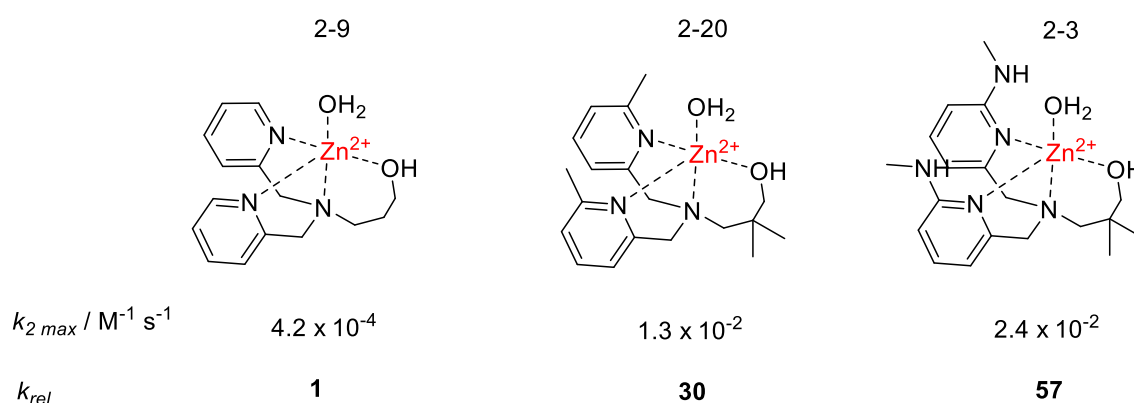
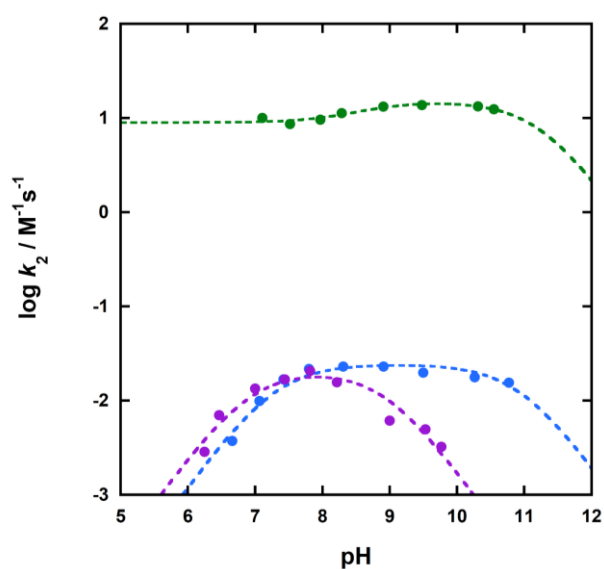
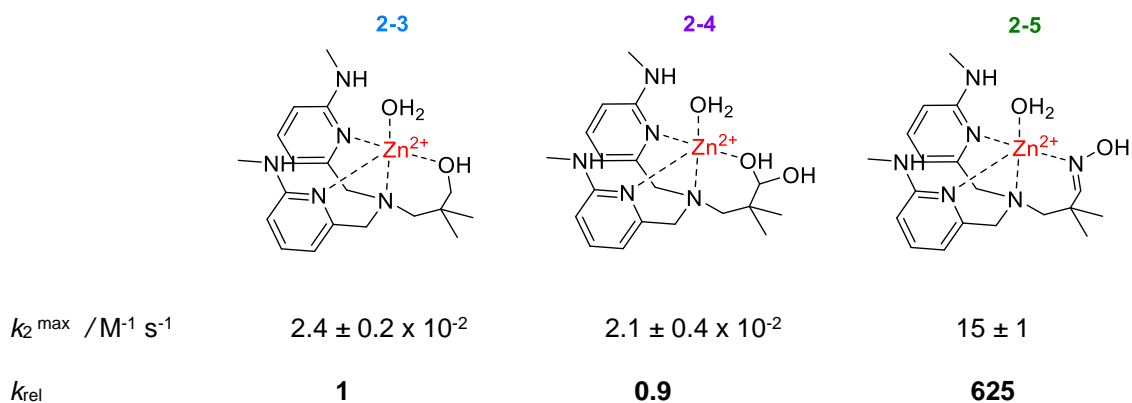


Figure 2.29 Structure and reactivity of mononuclear complex tested with BNPP at 25 °C

In addition, we investigated how the combination of hydrogen bond donors in the *ortho* position and different nucleophiles in the ligand chain would affect the complex behaviour

and reactivity. The pH dependence of the k_2 calculated for **2-3**, **2-4** and **2-5** are compared in Graph 2.9.



Graph 2.9 pH profile of the second order rate constant k_2 for the cleavage of BNPP catalysed by **2-3**, **2-4** and **2-5** at 25 °C; [BNPP] = 0.05 mM, [Buffer] = 50 mM, ionic strength at 0.1 M by addition of NaNO_3 .

While the gem-diol in the aliphatic chain did not provide any benefit in terms of reactivity and efficiency (and yielded only low turnover numbers), the oxime group had a huge impact

on the catalyst. The presence of an oxyanion not deactivated by coordination with the metal ion, and not decreasing the Lewis acidity of the Zn(II) ion, seem to combine to provide a large enhancement of the reactivity of the complex. In comparison, **2-5** is 625-fold faster than **2-3**. Surprisingly, the difference between the two catalyst is higher than that found between **2-20** and **2-22** (64-fold)^{79,85}.

Although this is the highest k_2 ever recorded for a mononuclear Zn(II) complex ($15 \pm 1 \text{ M}^{-1} \text{ s}^{-1}$), the observed rate constant for **2-5** is strongly influenced by dimerisation. Compared to **2-22** (K_D of $9 \pm 1 \text{ mM}$), **2-5** show an approximately 4500-times smaller value of $5 \mu\text{M}$ (Figure 2.30).

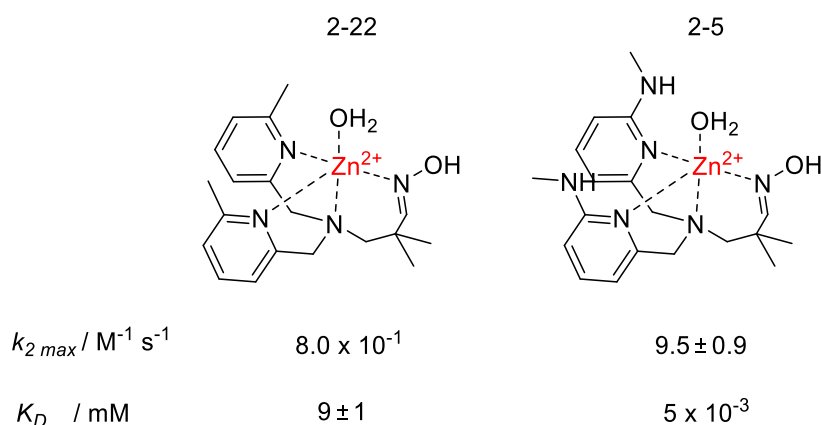


Figure 2.30 Comparison between the kinetic parameter calculated for 2-22 and 2-5

As shown in Figure 2.31, by providing a hydrogen bond, the secondary amine might be responsible for the observed stronger dimerisation of **2-5**. The much larger effect on dimerisation (4 500-fold) than reactivity (about 10 fold) can be accounted for the formation of a dimer where both coordinated oxime anions are stabilised by two sets of hydrogen bond interactions. For the reaction, the interactions may enhance the effective Lewis acidity

of the metal ion centre, but the oxygen of the phosphate that is coordinated may not be the site of the greatest charge change during the reaction – and so enhanced Lewis activity could have a reduced effect.

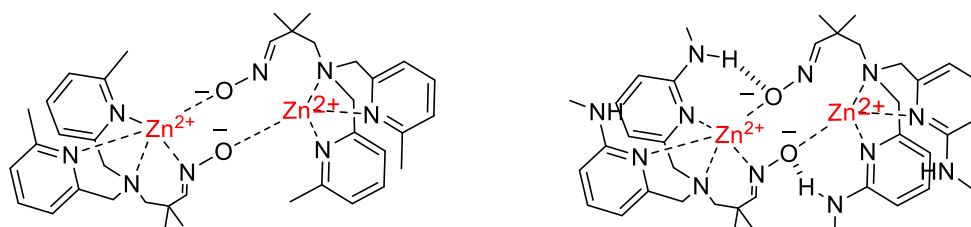


Figure 2.31 Dimeric structure of 2-22(left) and 2-5 (right)

Although consistent, our calculation of k_2 is strongly influenced by the K_D value extrapolated from the data obtained with limiting complex concentrations. Therefore, to obtain a more definitive measure and confirm the intrinsic catalyst reactivity, the investigation of the catalyst reactivity at even lower concentrations would need to be considered. As previously reported, in excess of BNPP, the lowest concentration of the catalyst used was 9 μM , and, in this experimental condition, we monitored the appearance of only 1 equivalent of 4-nitrophenolate. The increment in the absorbance at 400 nm due to the production of 9 μM of the product is small. Hence, decreasing the catalyst concentration and, consequently, the detectable phenol produced would not be practical due to the low sensitivity of the method. A possible alternative to confirm the reactivity of the monomer would then be to use a substrate with a fluorescent leaving group. Fluorescent spectroscopy, more sensitive than UV-vis, would then allow the screening of lower concentrations.

Dimerisation could also be reduced or avoided by changing the ligand structure or anchoring the latter to a support. For example, aliphatic thiolated chains, able to self-assemble on the surface of gold nanoparticles, have often been conjugated with catalytic head groups. Mancin and Scrimin have developed series of nanoparticle-based catalysts and investigated their activity as enzyme mimics.⁹⁹ Recently Sousa and coworkers¹⁰⁰ have incorporated La(III) complexes into electrospun polycaprolactone fibres, widely used in bioengineering applications,¹⁰¹ for hydrolysing BDNPP by heterogeneous catalysis. Similarly, the conjugation of **L2-5** to other systems can be a valid future application of **2-5** in catalysis. Both these approaches might be useful to limit dimerisation and evaluate the benefit of combining the hydrogen bond donor groups in the second coordination sphere and the stronger nucleophile present in the ligand structure. Possible strategies to modify the ligand structure are highlighted in red in Figure 2.32.

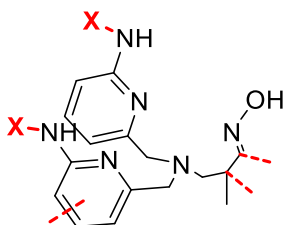


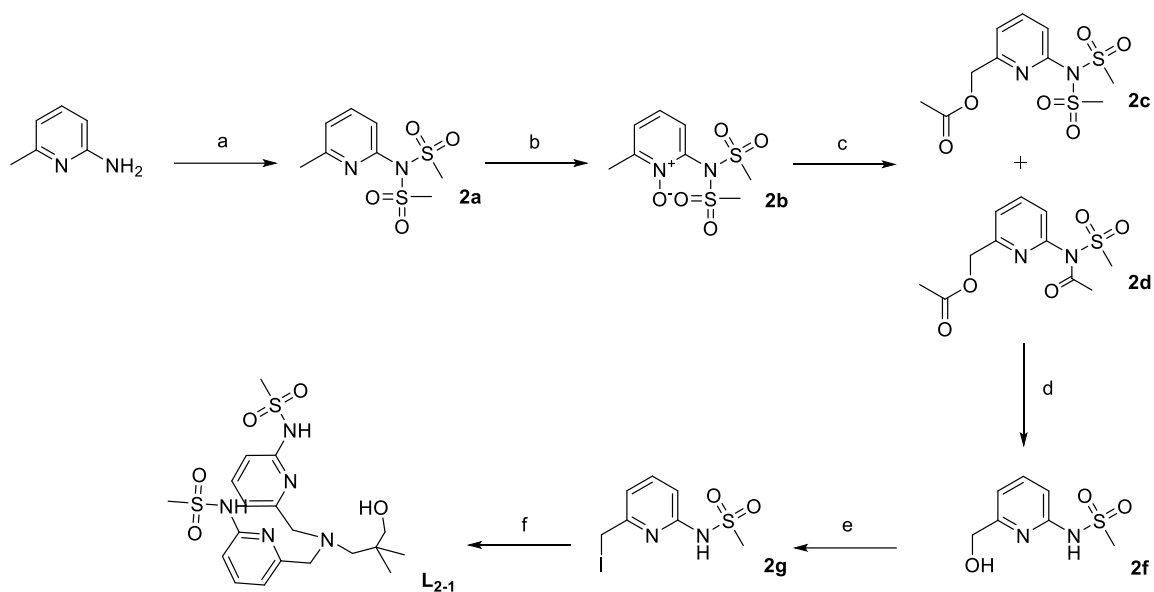
Figure 2.32 Possible strategies to modify **L2-5**

While bulkier groups might be introduced in 2' position of the pyridyl ring or in α to the oxime to limit the complex dimerisation, by using any other position of the pyridyl ring or the β to the oxime, it would be possible to connect the catalytic group to a different moiety.

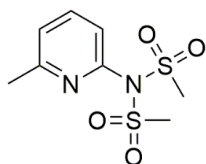
2.6 Experimental

2.6.1 Synthesis

L₂₋₁



Scheme 2.15 Synthesis of *N*-(6-(iodomethyl)pyridin-2-yl)methanesulfonamide; a) MeSO_2Cl , Et_3N , DCM, 25°C 2 h, 87 % yield; b) *m*CPBA, DCM, 25°C 18 h, 87% yield; c) Ac_2O , 100°C 18 h, 55% and 9 % yield; d) KOH, MeOH, 25°C 1 h; e) I_2 , Ph_3P , Imidazole, DCM, 25°C 18 h, 44 % yield; f) 3-amino-2,2-dimethylpropan-1-ol, DIPEA, dry DMF, 70°C , 18 h, 40% yield.



2a N-(6-methylpyridin-2-yl)-N-(methanesulfonyl)methanesulfonamide

2-Amino-6-methylpyridine (15 g, 138 mmol) was dissolved in 250 mL of DCM at 0°C .

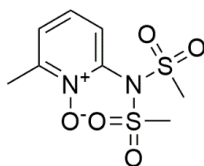
Methanesulfonyl chloride (48 g, 416 mmol) and triethylamine (77 mL, 554 mmol) were

added, and the solution mix was left reacting for 2 h at room temperature. 100 mL of DCM were added to the mixture, and the organic layer washed with NH₄Cl saturated solution of (50 mL x 3) and brine (100 mL). The organic layer was dried over MgSO₄, and the solvent was removed under reduced pressure. The product was purified using silica gel chromatography (EtOAc-Hexane, 7:3) to yield a white solid (32 g, 120 mmol; 87% Yield).

¹H NMR (400 MHz, CDCl₃): δ 7.72 (t, J= 8 Hz, 1H - CH py), 7.25 (d, J= 8 Hz, 1H - CH py), 7.14 (d, J= 8 Hz, 1H - CH py), 3.59 (s, 6H - SO₂(CH₃)₂), 2.57 (s, 3H - CH₃).

¹³C NMR (101 MHz, CDCl₃): δ 159.53(C py), 147.71 (C py), 139.35 (CH py), 124.96 (CH py), 122.13 (CH py), 44.17 (SO₂(CH₃)₂), 24.40 (CH₃).

MS (ES-TOF): [M+H]⁺ Obs. m/z: 265.03



2b 2-methyl-6-(N-(methylsulfonyl)methylsulfonamido)pyridine 1-oxide

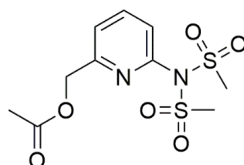
To a stirred solution of **2a** (32 g, 120 mmol) in DCM (200 mL), *meta*-chloro peroxybenzoic acid (≤ 77%) (41 g, 181 mmol) was added at 0 °C. After 18 h at room temperature, the solvent was evaporated under reduced pressure. The solid was dissolved in DCM (500 mL), and the organic layer was washed with saturated NaHCO₃ (4 × 100 mL) and was dried over MgSO₄. After solvent removal under reduced pressure, the crude product was purified using silica gel chromatography (EtOAc-DCM, 1:1) and obtained as white solid (13 g, 55 mmol, 87 % yield).

¹H NMR (400 MHz, CDCl₃): δ 7.37-7.34 (m, 1H - CH py), 7.21 (t, J= 8 Hz, 1H - CH py), 7.14 (d, J= 8 Hz, 1H - CH py), 3.61 (s, 6H - (SO₂(CH₃)₂), 2.55 (s, 3H - CH₃).

¹³C NMR (101 MHz, CDCl₃): δ 127.96 (CH py), 127.18 (CH py), 124.75 (CH py), 45.03 (SO₂(CH₃)₂), 18.33 (CH₃).

MS (ES-TOF): [M+H]⁺ Obs. m/z: 265.0

[M+Na]⁺ Obs. m/z: 287.0

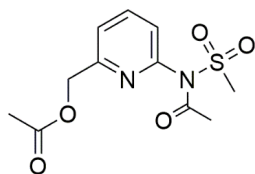


2c (6-(N-(methylsulfonyl)methylsulfonyl)pyridin-2-yl)methyl acetate

2b (25 g, 91 mmol) was dissolved in acetic anhydride (150 mL), and the reaction mixture was stirred for 18 h at 100 °C. The solvent was removed under reduced pressure, and the crude was purified by silica gel chromatography (EtOAc-DCM, 1:1). A white solid (16 g, 50 mmol) was obtained with a 55% yield.

¹H NMR (400 MHz, CDCl₃): δ 7.87 (t, J= 8 Hz, 1H - CH py), 7.47 (d, J= 8 Hz, 1H - CH py), 7.27 (d, J= 8 Hz, 1H - CH py), 5.23 (s, 2H - OCH₂), 3.58 (s, 6H - (SO₂(CH₃)₂), 2.17 (s, 3H - CH₃).

¹³C NMR (101 MHz, CDCl₃): δ 170.62 (CO), 156.69 (C py), 147.92 (C py), 140.08 (CH py), 124.29 (CH py), 123.00 (CH py), 65.98 (OCH₂), 44.17 ((SO₂CH₃)₂), 21.03 (CH₃COO).

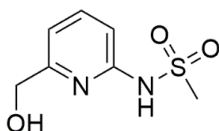


2d (6-(N-(methylsulfonyl)acetamido)pyridin-2-yl)methyl acetate

2b (25 g, 91 mmol) was dissolved in acetic anhydride (150 mL), and the reaction mixture was stirred for 18h at 100 °C. The solvent was removed under reduced pressure, and the crude was purified by silica gel chromatography (EtOAc-DCM, 1:1), yielding the product as white solid (2.3 g, 8 mmol; 9% yield).

¹H NMR (400 MHz, CDCl₃): δ 7.9 (t, J= 8 Hz, 1H - CH py), 7.47 (d, J= 8 Hz, 1H - CH py), 7.40 (d, J= 8 H, 1H - CH py), 5.21 (s, 2H - OCH₂), 3.45 (s, 3H - (SO₂CH₃), 2.17 (s, 3H - CH₃COO), 1.99 (s, 3H - CH₃CON).

¹³C NMR (101 MHz, CDCl₃): δ 171.15 (NCO), 170.60 (CO), 157.03 (C py), 149.58 (C py), 139.95 (CH py), 124.72 (CH py), 122.79 (CH py), 66.03 (OCH₂) 41.69 (SO₂CH₃), 25.12 (CH₃CON), 21.03 (CH₃CO).



2e N-(6-(hydroxymethyl)pyridin-2-yl)methanesulfonamide

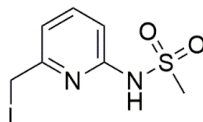
2c (16 g, 50 mmol) and **2d** (2.3 g, 8 mmol) were dissolved in MeOH (150 mL) at 0 °C. NaOH (7 g, 174 mmol) was dissolved in 10 mL of water and added dropwise to the solution. The reaction mixture was left stirring at room temperature, and after 1 h, 50 mL of 1 M solution of HCl in MeOH were added. The solvent was removed under reduced pressure, and the solid obtained dissolved in 80 mL of EtOH. The organic layer was filtered off and

concentrated by rotary evaporator. The operation was repeated three times to remove traces of salts. A yellow oil was obtained and used without further purification (10 g, 50 mmol).

¹H NMR (400 MHz, D₂O): δ 7.87-7.83 (m, 1H - CH py), 7.13 (d, J= 8 Hz, 1H - CH py), 6.94 (d, J= 8 Hz, 1H - CH py), 4.65 (s, 2H - CH₂), 3.11 (s, 3H - (SO₂CH₃)). OH signal not observed.

¹³C NMR (101 MHz, D₂O): δ 153.91 (C py), 143.56 (CH py), 114.21 (CH py), 112.07 (CH py), 60.41 (HOCH₂), 40.15 (SO₂CH₃).

HRMS (ES-TOF): [M+H]⁺ Calc. m/z: 203.0493 - Obs. m/z: 203.0485;



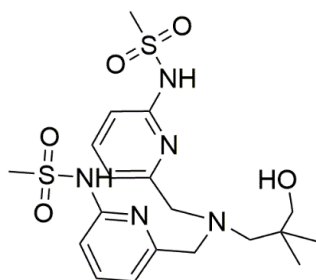
2f N-(6-(iodomethyl)pyridin-2-yl)methanesulfonamide

To a solution of iodine (15 g, 60 mmol) and imidazole (4 g, 60 mmol) in 50 mL of dry DCM, triphenylphosphine (16 g, 60 mmol) was added at 0 °C under argon. The mixture was left reacting for 30 min. **2e** (10 g, 50 mmol) in 50 mL of dry DCM was finally added to the reaction mixture, which was left stirring for 18 h at room temperature. The solution was washed with water (20 mL x 2) and 10% Na₂S₂O₃ solution (20 mL), dried over MgSO₄ and the solvent removed under reduced pressure. The product was obtained pure by silica gel chromatography (EtOAc-DCM, 1:4) with a 44% yield (6.8 g, 21 mmol).

¹H NMR (400 MHz, CDCl₃): δ 7.62 (t, J=8 Hz, 1H - CH py), 7.10 (d, J= 8 Hz, 1H - CH py), 6.03 (d, J= 8 Hz, 1H - CH py), 4.41 (s, 2H - CH₂), 3.27 (s, 3H - SO₂CH₃).

¹³C NMR (101 MHz, CDCl₃): δ 150.72 (C py), 139.96 (CH py), 118.12 (CH py), 111.19 (CH py), 41.64 (SO₂CH₃), 5.28 (ICH₂).

HRMS (ES-TOF): [M+H]⁺ Calc. m/z: 312.9502 - Obs. m/z: 312.9507



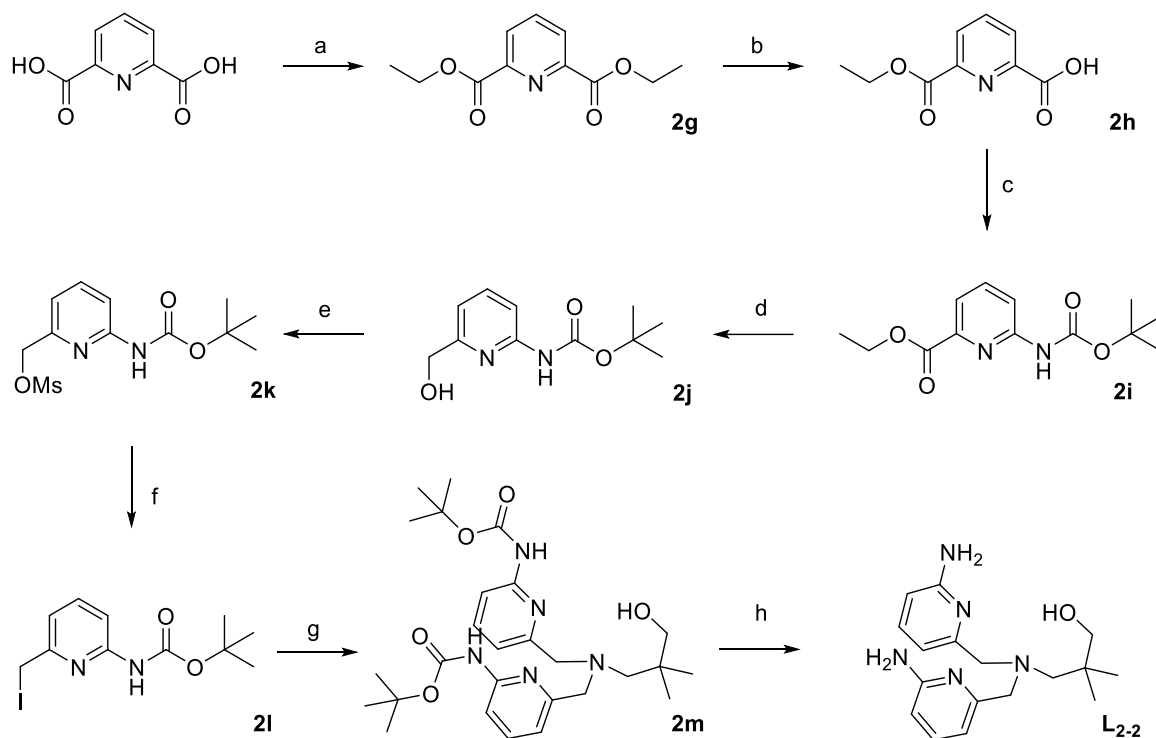
L2-1

3-Amino-2,2-dimethylpropanol (140 mg, 1.3 mmol) was added to a solution of **2f** (1.1 g, 3.4 mmol) in 20 mL of dry DMF. DIPEA (690 μ L, 43.5 mmol) was added to the mixture, which was left stirring overnight at 70 °C. The solvent was evaporated under reduced pressure, and the product was purified by using silica gel chromatography (EtOAc) and obtained in 40% Yield (250 mg, 0.53 mmol).

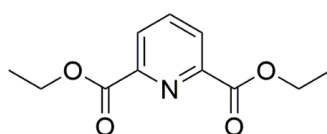
¹H NMR (400 MHz, CDCl₃): δ 7.80 (t, J= 8 H, 1H, Py), 7.15 (d, J= 8 H, 1H, Py), 7.01 (d, J= 8 H, 1H, Py), 3.89 (s, 4H, NCH₂-Py), 3.25 (s, 6H, SO₂CH₃), 3.14 (s, 2H, OCH₂), 2.61 (s, 2H, NCH₂), 0.64 (s, 6H, CH₃). OH signal not observed.

¹³C NMR (101 MHz, CDCl₃): δ 140.89 (CH-Py), 113.36 (CH-Py), 113.14 (CH-Py), 69.36 (HOCH₂), 63.92 (NCH₂), 60.33 (NCH₂-Py), 41.05 (SO₂CH₃), 23.23 (CH₃).

HRMS (ES-TOF): [M+H]⁺ Calc. m/z: 471.1610 - Obs. m/z: 472.1705

L₂-2

Scheme 2.16 Synthesis of **L₂-2**: a) H_2SO_4 , EtOH, 80 °C 18 h, 89 % yield; b) NaOH, EtOH:Dioxane (1:2), 100 °C 2 h, 50 % yield; c) Diphenylphosphoryl azide, Et_3N , *t*-BuOH, Toluene, 100 °C 18 h, 69 % yield; d) NaBH_4 , CaCl_2 , EtOH, 0-25 °C 18h, 97 % yield; e) MeSO_2Cl , Et_3N , THF, 0-25 °C 18h, 95 % yield; f) LiI, THF, 50 °C 2h, 91 % yield; g) 3-amino-2,2-dimethylpropan-1-ol, DIPEA, dry DMF, 70 °C, 18 h, 69 % yield; h) TFA, 25 °C 2 h, 98% yield.

**2g diethyl pyridine-2,6-dicarboxylate**

To a suspension of pyridine-2,6-dicarboxylic acid (13 g, 78 mmol) in 150 mL of ethanol, 2.1 mL of sulfuric acid was added dropwise. The reaction was left stirring overnight at 80 °C. The following day, the mixture was concentrated by rotary evaporation and then diluted with 200 mL of a saturated solution of NaHCO_3 . The product was extracted by DCM (3 x

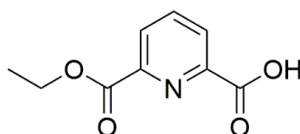
30 mL), and the combined organic layers were dried over MgSO₄. The solvent evaporation by reduced pressure yielded a colourless oil (15.5 g, 70 mmol; 89%) used without further purification.

¹H NMR (400 MHz, CDCl₃): δ 8.26 (d, J = 7.8 Hz, 2H - CH py), 7.99 (t, J = 7.8 Hz, 1H - CH py), 4.47 (q, J = 7.1 Hz, 4H - CH₂), 1.43 (t, J = 7.1 Hz, 6H - CH₃).

¹³C NMR (101 MHz, CDCl₃): δ 164.72 (CO), 148.68 (C - py), 138.34 (CH - py), 127.93 (CH - py), 62.44 (CH₂), 14.30 (CH₃).

HRMS (ES-TOF): [M+H]⁺ Calc. m/z: 224.0917 - Obs. m/z: = 224.0917;

[M+Na]⁺ Calc. m/z: 246.0737 - Obs. m/z: = 246.0743;



2h 6-(ethoxycarbonyl)picolinic acid

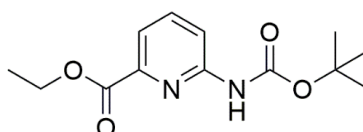
NaOH (2.8 g, 69.6 mmol) was left dissolving in 80 mL of ethanol by sonication for 1 h. Next, the NaOH solution was added dropwise to a solution of 1g (15.5 g, 69.6 mmol) in 220 mL of dioxane:ethanol (10:1). The solution was left stirring for 2 h at 100 °C, cooled to approximately 50 °C and concentrated. 250 mL of water were poured into the round bottom flask, and the unreacted starting material was removed by CHCl₃ (3 x 50 mL). By adding HCl (0.1 M), the water phase pH was lowered to 1, and the product was extracted by CHCl₃ (3 x 50 mL). The organic layers were combined, treated with MgSO₄ and dried under low pressure. A pure white solid was obtained with a 50% yield (6.68 g, 34.2 mmol).

¹H NMR (400 MHz, CDCl₃): δ 8.40 (dd, J = 7.8, 1.1 Hz, 1H - CH py), 8.36 (dd, J = 7.8, 1.1 Hz, 1H - CH py), 8.12 (t, J = 7.8 Hz, 1H - CH py), 4.49 (q, J = 7.1 Hz, 2H - CH₂), 1.45 (t, J = 7.1 Hz, 3H - CH₃), OH signal not observed.

¹³C NMR (101 MHz, CDCl₃): δ 163.78 (CO), 163.68 (CO), 147.19 (C - py), 146.52 (C - py), 139.74 (CH - py), 128.86 (CH - py), 126.83 (CH - py), 62.61 (CH₂), 14.37 (CH₃).

HRMS (ES-TOF): [M+H]⁺ Calc. m/z: 196.0604 - Obs. m/z: = 196.0601;

[M+Na]⁺ Calc. m/z: 218.0424- Obs. m/z: = 218.0420;



2i ethyl 6-((tert-butoxycarbonyl)amino)picolinate

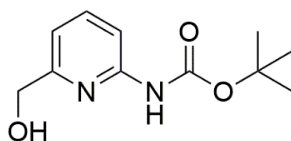
To **2h** (6.68 g, 34 mmol) and Et₃N (10.5 mL, 75 mmol) dissolved in Toluene (220 mL), t-BuOH (2.3 mL, 239 mmol) and di-phenyl phosphoryl azide (11 mL, 51 mmol) were added. The temperature of the stirring mixture was then increased and kept at 100 °C for 15 h. The reaction solution was concentrated by rotary evaporation and diluted by 300 mL of EtOAc. The organic layer was washed with a saturated solution of NaHCO₃ (3 x 70 mL), Brine solution (70 mL) and finally dried over MgSO₄. The solvent was removed by reduced pressure, and the crude product was purified by flash chromatography (EtOAc/hexane (1:9)). The yellow oil obtained crystallised under high vacuum (6.22 g, 23 mmol; 69 %)

¹H NMR (400 MHz, CDCl₃): δ 8.13 (dd, J = 7.0, 2.0 Hz, 1H - CH py), 7.87 – 7.68 (m, 2H - CH py), 7.58 (s, 1H - NH), 4.44 (q, J = 7.1 Hz, 2H - CH₂), 1.50 (s, 9H - (CH₃)₃), 1.41 (t, J = 7.1 Hz, 3H - CH₃).

¹³C NMR (101 MHz, CDCl₃): δ 164.98 (CO), 152.45 (C py), 152.02 (C py), 146.33 (CONH), 139.14 (CH py), 120.05 (CH py), 116.09 (CH py), 81.40 (C), 62.02 (CH₂), 28.31 ((CH₃)₃), 14.43 (CH₃).

HRMS (ES-TOF): $[M+H]^+$ Calc. m/z : 267.1339 - Obs. m/z : = 267.1352;

$[M+Na]^+$ Calc. m/z : 289.1159 - Obs. m/z : = 289.1169;



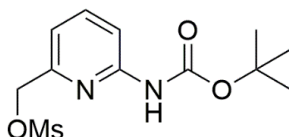
2j tert-butyl (6-(hydroxymethyl)pyridin-2-yl)carbamate

2i (6.22 g, 23 mmol) and CaCl_2 (2.74 g, 25 mmol) were dissolved in ethanol at 0 °C. NaBH_4 (5.2 g, 138 mmol) was added portion-wise, and the mixture was left stirring for 2 h at 0 °C and then overnight at room temperature. 400 mL of water were poured into the round bottom flask, and the product was extracted from the aqueous phase with CHCl_3 (3 x 100 mL). The combined organic layers were washed with brine (150 mL), treated with MgSO_4 and concentrated *in vacuum*. The product was purified by flash chromatography (Hexane/EtOAc (3:2)) and obtained as a colourless oil with 97% yield (5.1 g, 23 mmol).

^1H NMR (400 MHz, CDCl_3): δ 7.82 (d, J = 8.3 Hz, 1H - CH), 7.65 (t, J = 7.9 Hz, 1H - CH), 7.33 (s, 1H - NH), 6.89 (d, J = 7.4 Hz, 1H - CH), 4.65 (s, 2H - CH_2), 3.53 (s, 1H - OH), 1.52 (s, 9H - $(\text{CH}_3)_3$).

^{13}C NMR (101 MHz, CDCl_3): δ 157.50 (C py), 152.33 (C py), 151.17 (CONH), 139.09 (CH py), 115.06 (CH py), 110.61 (CH py), 81.33 (C), 63.85 (CH_2), 28.38 ($(\text{CH}_3)_3$).

HRMS (ES-TOF): $[M+H]^+$ Calc. m/z : 225.1234 - Obs. m/z : = 225.1238;



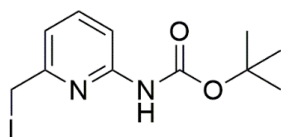
2k (6-((tert-butoxycarbonyl)amino)pyridin-2-yl)methyl methanesulfonate

To a solution of **2j** (3.7 g, 16 mmol) and MeSO₄Cl (1.5 mL, 20 mmol) in THF (120 mL), Et₃N (3.4 mL, 25 mmol) was added dropwise at 0 °C. The mixture was stirred for 15 h at room temperature. The suspension formed was filtered off, and the filtrate was concentrated *in vacuum*. The mixture was taken with a saturated solution of NH₄Cl (250 mL), and the product was extracted by Et₂O (3 x 50 mL). The combined organic layers were washed with a saturated solution of NH₄Cl (80 mL), treated with MgSO₄ and dried under reduced vacuum, yielding a pale yellow oil. The product was used without further purification (4.75 g, 16 mmol; 95%).

¹H NMR (400 MHz, CDCl₃): δ 7.93 (d, J = 8.4 Hz, 1H - CH), 7.71 (t, J = 7.9 Hz, 1H - CH), 7.34 (s, 1H - NH), 7.10 (d, J = 7.4 Hz, 1H - CH), 5.17 (s, 2H - CH₂), 3.04 (s, 3H - SO₂CH₃), 1.51 (s, 9H - (CH₃)₃).

¹³C NMR (101 MHz, CDCl₃): δ 152.29 (C py), 151.94 (C py), 151.75 (CONH), 139.39 (CH py), 117.24 (CH py), 112.41 (CH py), 81.48 (C), 71.26 (CH₂), 38.30 (SO₂CH₃), 28.36 ((CH₃)₃).

HRMS (ES-TOF): [M+H]⁺ Calc. m/z: 302.0936 - Obs. m/z: = 302.0930;

**2l tert-butyl (6-(iodomethyl)pyridin-2-yl)carbamate**

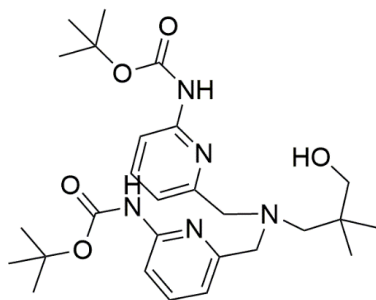
To a round bottom flask loaded with a solution of **2k** (4.8 g, 16 mmol) in THF, LiI (4.2 g, 31 mmol) was added. The reaction mixture was left stirring for 2 h at 50 °C. After pouring 180 mL of a saturated solution of NH₄Cl, the product was extracted from the aqueous layer

by Et₂O (3 x 50 mL). The combined organic layers were washed with 50 mL of NH₄Cl saturated solution, 50 mL of 10% (w) Na₂S₂O₃ solution, and then dried over MgSO₄. The solvent was removed by high vacuum, yielding a yellow oil (4.8 g, 14 mmol; 91%).

¹H NMR (400 MHz, CDCl₃): δ 7.79 (d, *J* = 8.3 Hz, 1H - CH py), 7.58 (t, *J* = 7.9 Hz, 1H - CH py), 7.01 (d, *J* = 7.4 Hz, 1H - CH py), 4.37 (s, 2H - CH₂), 1.52 (d, *J* = 6.7 Hz, 9H - (CH₃)₃).

¹³C NMR (101 MHz, CDCl₃): δ 156.51 (C py), 151.63 (C py), 139.23 (CH py), 117.32 (CH py), 111.30 (CH py), 28.37 (((CH₃)₃)), 6.16 (CH₂).

HRMS (ES-TOF): [M+H]⁺ Calc. m/z: 335.0251 - Obs. m/z: = 335.0251;



2m di-tert-butyl((((3-hydroxy-2,2-dimethylpropyl)azanediyl)bis(methylene))bis(pyridine-6,2-diyl))dicarbamate

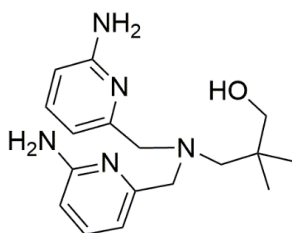
A solution of **2l** (4.8 g, 14 mmol) and 3-amino-2,2-dimethylpropanol (667 mg, 6.5 mmol) in DMF (70 mL) was prepared in a 100 mL round bottom flask. DIPEA (3.4 mL, 19 mmol) was added to the latter, and the reaction mixture was left stirring overnight at 70 °C. 200 mL of brine were poured into the DMF solution, and the crude product was extracted from the aqueous phase by DCM (3 x 50 mL). The organic layers were combined, washed with brine (50 mL) and treated with MgSO₄. The solvent is finally removed by rotary evaporator.

The product is obtained pure after flash chromatography (DCM/EtOAc (9:1)) with a 69% Yield (2.3 g, 4.5 mmol).

¹H NMR (400 MHz, CDCl₃): δ 7.80 (d, J = 8.3 Hz, 2H - CH py), 7.59 (t, J = 7.9 Hz, 2H - CH py), 7.35 (s, 2H - NH), 6.93 (d, J = 7.4 Hz, 2H - CH py), 3.68 (s, 4H - CH₂), 3.33 (s, 2H - CH₂OH), 2.58 (s, 2H - CH₂N), 1.52 (s, 18H - (CH₃)₃), 0.91 (s, 6H -CH₃). OH signal not observed.

¹³C NMR (101 MHz, CDCl₃): δ 157.22 (C py), 152.51 (C py), 151.51 (CONH), 138.81 (CH py), 117.90 (CH py), 110.58 (CH py), 81.08 (C), 72.42 (OCH₂), 65.82 (NCH₂), 61.88 (CH₂), 28.41 ((CH₃)₃), 24.83 (CH₃).

HRMS (ES-TOF): [M+H]⁺ Calc. m/z: 516.3180 - Obs. m/z: 516.3189;



L2-2

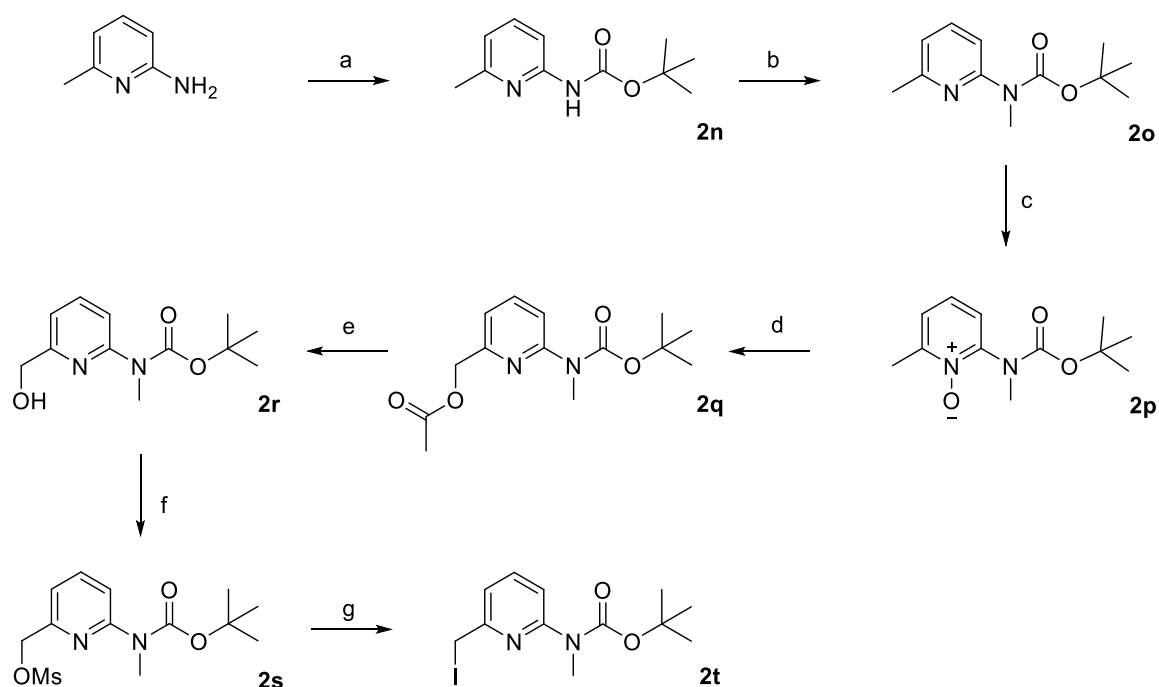
2m (200 mg, 0.39 mmol) was dissolved in 3 mL of TFA and stirred for 3 h at room temperature. The TFA in excess was removed by blowing nitrogen, and the remaining oil was dissolved in water (10 mL). The aqueous phase, which was first washed with Et₂O (3 x 5 mL), was basified by adding concentrated NaOH. The product is then extracted from the water layer by DCM (3 x 10 mL). The combined organic layers were treated with MgSO₄ and dried under *in vacuum*. The desired compound was obtained as a pale yellow oil in 98% yield (120 mg, 0.38 mmol).

^1H NMR (400 MHz, CDCl_3): δ 7.36 (dd, J = 8.0, 7.5 Hz, 2H – CH py), 6.71 (d, J = 7.3 Hz, 2H – CH py), 6.36 (d, J = 8.1 Hz, 2H – CH py), 4.60 (s, 4H – NH_2), 3.65 (s, 4H – CH_2), 3.35 (s, 2H – CH_2OH), 2.56 (s, 2H – NCH_2), 0.89 (s, 6H – CH_3). OH signal not observed.

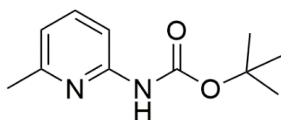
^{13}C NMR (101 MHz, CDCl_3): δ 158.00 (C py), 157.36 (C py), 138.54 (C py), 113.04 (s), 107.12 (s), 71.72 (OCH_2), 64.95 (NCH_2), 62.30 (CH_2), 36.82 ($(\text{CH}_3)_3$), 24.98 (CH_3).

HRMS (ES-TOF): $[\text{M}+\text{H}]^+$ Calc. m/z : 316.2132 - Obs. m/z : 316.2146;

Methyl amine building block



Scheme 2.17 Synthetic procedure of key building block 2t: a) Boc_2O , Et_3N , DMAP, DCM, 25°C 18 h, 80 % yield; b) NaH , MeI , DMF, 25°C 18 h, 97 % yield; c) $m\text{CPBA}$, DCM, 25°C 18 h, 87 % yield; d) Ac_2O , 70°C 18 h, 75 % yield; e) KOH , MeOH , 25°C 1 h, 80 % yield; f) MeSO_2Cl , Et_3N , THF, 25°C 18 h, 98 % yield; g) LiI , THF, 50°C 1 h, 98 % yield.



2n 2-(tert-butoxycarbonylamino)-6-methylpyridine

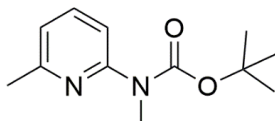
2-Amine-6-methylpyridine (9 g, 81.5 mmol) was dissolved in DCM (200 mL). Di-tert-butyl dicarbonate (18 g, 81.5 mmol) and triethylamine (12.5 mL, 89.6 mmol) were added to the solution. A catalytic amount of 4-dimethylaminopyridine (570 mg, 10%) was added, and the reaction mixture was stirred overnight at room temperature. The solvent was removed under reduced pressure, and the product was purified and obtained as white crystals (13.6 g, 65.2 mmol, 80% yield) using silica gel chromatography (EtOAc-hexane, 1:4).

¹H NMR (400 MHz, CDCl₃): δ 8.07 (s, 1H, NH), 7.71 (d, J= 8 Hz, 1H - CH py), 7.52 (t, J= 8 Hz, 1H - CH py), 6.77 (d, J= 8 Hz, 1H - CH py), 2.41 (s, 3H - CH₃), 1.47 (s, 9H - (CH₃)₃).

¹³C NMR (101 MHz, CDCl₃): δ 156.87 (CO), 152.78 (C py), 151.63 (C py), 138.55 (CH py), 117.96 (CH py), 109.33 (CH py), 80.72 (C Boc), 28.36 ((CH₃)₃), 24.04 (CH₃).

MS (ES-TOF): [M+H]⁺ Obs. m/z: 209.1

[M+Na]⁺ Obs. m/z: 231.1



2o 2-(methyl-tert-butoxycarbonylamino)-6-methylpyridine

Sodium hydride 60% in mineral oil (5.2 g, 130.4 mmol) was suspended in 80 mL of dry DMF under argon. A solution of **2n** (13.6 g, 65.2 mmol) in dry DMF (80 mL) was then

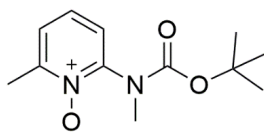
added at 0 °C. After slow addition of methyl iodide (4.87 mL, 78.24 mmol), the reaction mixture was stirred overnight at room temperature. The reaction was quenched with 200 mL of water, and the product was extracted with Et₂O (3 × 50 mL). The combined organic layers were washed with saturated NaHCO₃ (3 × 50 mL), brine (3 × 50 mL) and dried over MgSO₄. The solvent was removed under reduced pressure yielding a colourless oil (14 g, 63.2 mmol, 97 % yield), used without further purification.

¹H NMR (400 MHz, CDCl₃): δ 7.43 (t, J= 8 Hz, 1H - CH py), 7.33 (d, J= 8 Hz, 1H - CH py), 6.78 (d, J= 8 Hz, 1H - CH py), 3.32 (s, 3H - NCH₃), 2.41 (s, 3H - CH₃), 1.44 (s, 9H - (CH₃)₃).

¹³C NMR (101 MHz, CDCl₃): δ 156.41 (CO), 154.57 (C py), 154.44 (C py), 137.05 (CH py), 118.61 (CH py), 116.30 (CH py), 80.72 (C Boc), 34.32 (NCH₃), 28.28 ((CH₃)₃), 24.24 (CH₃).

MS (ES-TOF): [M+H]⁺ Obs. m/z: 223.1

[M+Na]⁺ Obs. m/z: 245.1



2p 2-(methyl-tert-Butoxycarbonylamino)-6-methylpyridine-N-oxide

To a solution of **2o** (14 g, 63.2 mmol) in 200 mL of DCM at 0 °C, *meta*-chloroperoxybenzoic acid (21.2 g, 94.8 mmol) was added. The reaction mixture was stirred at room temperature. After 18 h, the solvent was removed under reduced pressure. Next, the solid was dissolved in Et₂O (150 mL), which was washed with saturated NaHCO₃ (3 × 100 mL). The product was finally extracted from the water phase with DCM (4 × 50 mL).

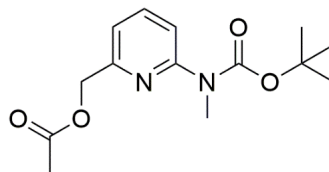
The combined organic layers were dried over MgSO_4 , and the solvent was removed under high vacuum. A white solid was obtained (13 g, 55 mmol, 87% yield) and used without further purification.

^1H NMR (400 MHz, CDCl_3): δ 7.19-7.16 (m, 2H - CH py), 7.11 (t, J = 8 Hz, 1H - CH py), 3.18 (s, 3H - NCH_3), 2.52 (s, 3H - CH_3), 1.41 (s, 9H - $(\text{CH}_3)_3$).

^{13}C NMR (101 MHz, CDCl_3): δ 154.37 (CO), 149.95 (C py), 154.26 (C py), 124.59 (CH py), 124.40 (CH py), 123.56 (CH py), 81.40 (C Boc), 34.78 (NCH_3), 28.79 ($(\text{CH}_3)_3$), 18.31 (CH_3).

MS (ES-TOF): $[\text{M}+\text{H}]^+$ Obs. m/z : 239.1

$[\text{M}+\text{Na}]^+$ Obs. m/z : 261.1



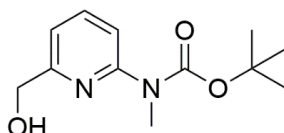
2q 2-(methyl-tert-butoxycarbonylamino)-6-acetylpyridine

2p (13 g, 55 mmol) was dissolved in 100 mL of acetic anhydride, and the reaction solution was left stirring overnight at 70 °C. The solvent was removed under reduced pressure and co-evaporated with toluene. The product (11.6 g, 41.2 mmol) was obtained pure after silica gel chromatography (DCM-EtOAc, 9:1) with a 75% yield.

^1H NMR (400 MHz, CDCl_3): δ 7.62-7.60 (m, 2H - CH py), 7.03-7.01 (m, 1H - CH py), 5.15 (s, 2H - OCH_2), 3.38 (s, 3H - NCH_3), 2.16 (s, 3H - CH_3CO), 2.52 (s, 3H - CH_3), 1.51 (s, 9H - $(\text{CH}_3)_3$).

¹³C NMR (101 MHz, CDCl₃): δ 170.85 (OCO), 154.93 (CO), 154.54 (C py), 153.74 (C py), 137.64 (CH py), 118.26 (CH py), 116.17 (CH py), 81.34 (C Boc), 66.79 (OCH₂), 34.29 (NCH₃) 28.47 ((CH₃)₃), 21.14 (CH₃CO).

MS (ES-TOF): [M+H]⁺ Obs. m/z: 281.1



2r 2-(methyl-tert-Butoxycarbonylamino)-6-methanopyridine

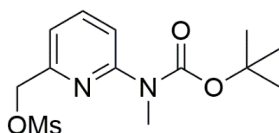
A saturated solution of potassium hydroxide (10 mL) was added to **2q** (11.6 g, 41.2 mmol) dissolved in 60 mL of MeOH. After 1 h of stirring at room temperature, the solution was concentrated by rotary evaporator, 150 mL of water were added to the mixture, and the product was extracted with DCM (3 x 70 mL). The organic layers were dried over MgSO₄ and the solvent removed under reduced pressure; the obtained colourless oil (7.85 g, 33 mmol, 80% yield) was used without further purification.

¹H NMR (400 MHz, CDCl₃): δ 7.64-7.52 (m, 2H - CH py), 6.93-6.91 (m, 1H - CH py), 4.695 (d, J= 4 Hz, 2H - HOCH₂), 3.40 (s, 3H - NCH₃), 1.52 (s, 9H - (CH₃)₃). OH signal not observed.

¹³C NMR (101 MHz, CDCl₃): δ 156.90 (C py), 154.44 (C py), 137.82 (CH py), 117.54 (CH py), 115.49 (CH py), 81.51 (C Boc), 63.92 (HOCH₂), 34.32 (NCH₃) 28.46 ((CH₃)₃).

MS (ES-TOF): [M+H]⁺ Obs. m/z: 239.1

[M+Na]⁺ Obs. m/z: 261.1



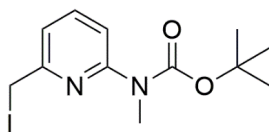
2s 2-(methyl-tert-Butoxycarbonylamino)-6-mesyloxy-3-methylpyridine

2r (7.8 g, 33 mmol) and triethylamine (7 mL, 49.5 mmol) were dissolved in 100 mL of THF. Methanesulfonyl chloride (3 mL, 39.6 mmol) was added at 0 °C, and the mixture was left stirring for 18 h at room temperature. The reaction was quenched with 200 mL of saturated NH₄Cl, and the product was extracted with DCM (3 x 100 mL). The organic layer was dried over MgSO₄, and the solvent was removed by rotary evaporator, yielding a yellow oil (10 g, 32.4 mmol, 98 % yield) used without further purification.

¹H NMR (400 MHz, CDCl₃): δ 7.73-7.63 (m, 2H - CH py), 7.14 (d, J=8 Hz, 1H - CH py), 5.25 (s, 2H - HOCH₂), 3.38 (s, 3H - NCH₃), 3.07 (s, 3H - OSO₂CH₃), 1.52 (s, 9H - (CH₃)₃).
¹³C NMR (101 MHz, CDCl₃): δ 155.13 (CO), 154.45 (C py), 151.32 (C py), 138.00 (CH py), 119.01 (CH py), 117.59 (CH py), 81.64 (C Boc), 71.74 (OCH₂), 38.24 (OSO₂CH₃), 34.24 (NCH₃) 28.44 ((CH₃)₃).

MS (ES-TOF): [M+H]⁺ Obs. m/z: 317.1

[M+Na]⁺ Obs. m/z: 339.1



2t 2-(methyl-tert-Butoxycarbonylamino)-6-iodomethyl-3-methylpyridine

LiI (9 g, 64.8 mmol) was added to a solution of **2s** (10 g, 32.4 mmol) in dry THF (120 mL). The reaction mixture was stirred for 1 h at 50 °C and then quenched with 250 mL of

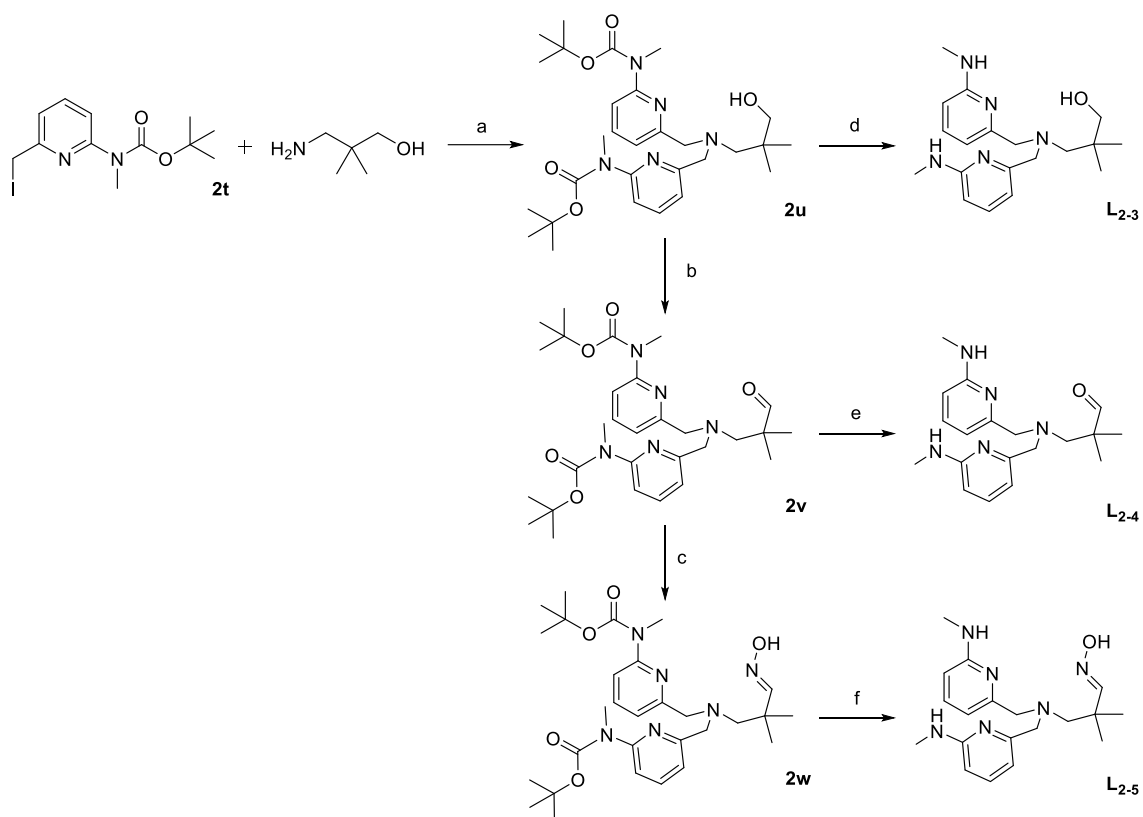
saturated NH_4Cl . The product was extracted with DCM (3 x 50 mL), and the combined organic layers were washed with 10% $\text{Na}_2\text{S}_2\text{O}_3$ solution (50 mL) and were dried over MgSO_4 . The solvent was evaporated under reduced pressure, and an orange oil was obtained (11 g, 31.8 mmol, 98% yield) and used without further purification.

^1H NMR (400 MHz, CDCl_3): δ 7.58-7.52 (m, 2H - CH py), 7.08-7.06 (m, 1H - CH py), 4.44 (s, 2H - ICH_2), 3.40 (s, 3H - NCH_3), 1.52 (s, 9H - $(\text{CH}_3)_3$).

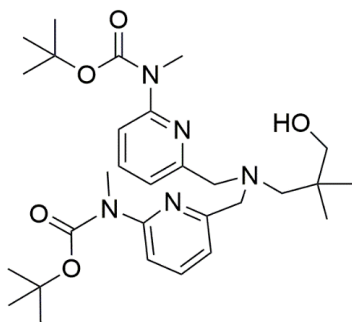
^{13}C NMR (101 MHz, CDCl_3): δ 155.96 (C py), 154.88 (C py), 137.87 (CH py), 117.94 (CH py), 117.82 (CH py), 81.40 (C Boc), 34.34 (NCH_3), 28.44 ($(\text{CH}_3)_3$), 6.85 (ICH_2).

MS (ES-TOF): $[\text{M}+\text{H}]^+$ Obs. m/z: 349.0

Methyl amine based ligands



Scheme 2.18; Synthesis of L_{2-3} , L_{2-4} and L_{2-5} ; a) DIPEA, dry DMF, 70 °C 18 h, 75 % yield; b) Dess-Martin periodinane, dry DCM, 25 °C 2h, 65 % yield; c) $\text{NH}_2\text{OH} \cdot \text{HCl}$, NaOH, water:ethanol (1:1), 25 °C 3h, 93 % yield; d) TFA, DCM, 25 °C 1h, 95 % yield; e) TFA, DCM, 25 °C 1h, 26 % yield; f) TFA, TIS, water, 25°C 3 h, 59 % yield.



2u

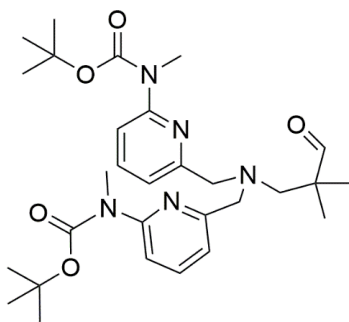
3-Amino-2,2-dimethylpropanol (1.5 g, 14.5 mmol) was added to a solution of **2t** (11 g, 31.8 mmol) dissolved in 80 mL of dry DMF. DIPEA (7.6 mL, 43.5 mmol) was added to the mixture, and stirred overnight at 70 °C under argon. The solution was poured in water (200 mL), and the product was extracted with DCM (3 x 40 mL). The combined organic layers were washed with water (2 x 30 mL), dried over MgSO₄ and concentrated under reduced pressure. The product was purified by silica gel chromatography (EtOAc-Hex, 3:7), and a yellow oil was obtained in 75% yield (5.9 g, 11 mmol).

¹H NMR (400 MHz, CDCl₃): δ 7.57-7.56 (m, 4H - CH py), 7.02-7.00 (m, 2H - CH py), 5.38 (s, 1H - OH), 3.78 (s, 4H - NCH₂ py), 3.42 (s, 6H - NCH₃), 3.30 (s, 2H - HOCH₂), 2.73 (s, 2H - CH₂N), 1.52 (s, 9H - (CH₃)₃), 0.91 (s, 6H - CH₃).

¹³C NMR (101 MHz, CDCl₃): δ 156.58 (CO), 154.9 (C py), 154.66 (C py), 137.38 (CH py), 118.86 (CH py), 117.61 (CH py), 81.21 (C Boc), 72.92 (CH₂OH), 66.02 (NCH₂), 61.74 (CH₂N py), 34.43 (CH₃N), 28.50 ((CH₃)₃), 24.59 (CH₃).

MS (ES-TOF): [M+H]⁺ Obs. m/z: 544.3

[M+Na]⁺ Obs. m/z: 566.3



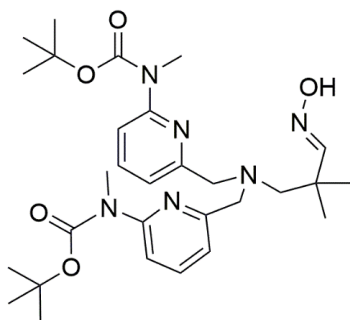
2v

Dess-martin periodinane (5.1 g, 12.1 mmol) was added to a solution of **2u** (5.9 g, 11 mmol) in dry DCM (100 mL) at 0 °C under argon. After 2 h at room temperature, the reaction mixture was poured with 150 mL of water; the product was extracted with DCM (3 x 50 mL), and the organic layers were washed with water (2 x 50 mL) and were dried over MgSO₄. The solution was concentrated under reduced pressure, and the crude was purified by silica gel chromatography (EtOAc-DCM, 1:9), yielding a yellow oil (3.9 g, 7.15 mmol, 65% Yield).

¹H NMR (400 MHz, CDCl₃): δ 9.36 (s, 1H, CHO), 7.60-7.50 (m, 4H - CH py), 7.13-7.11 (m, 2H - CH py), 3.74 (s, 4H - CH₂N py), 3.39 (s, 6H - CH₃N), 2.93 (s, 2H - CH₂N), 1.51 (s, 9H - (CH₃)₃), 1.02 (s, 6H - CH₃).

¹³C NMR (101 MHz, CDCl₃): δ 206.63 (CHO), 157.43 (C py), 154.62 (C py), 137.42 (CH py), 118.54 (CH py), 117.51 (CH py), 81.18 (C Boc), 61.78 (CH₂N), 61.41 (CH₂N py), 34.42 (CH₃N), 28.49 ((CH₃)₃), 20.47 (CH₃).

MS (ES-TOF): [M+H]⁺ Obs. m/z: 542.3



2w

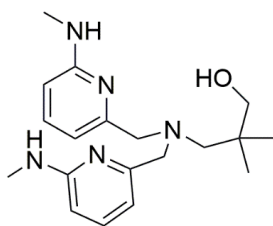
$\text{NH}_2\text{OH}\cdot\text{HCl}$ (275 mg, 4 mmol) and NaOH (158 mg, 4 mmol) were dissolved in 10 mL of a mix MeOH :water (1:1) and then added to a solution of **2v** (2 g, 3.6 mmol) in 25 mL of MeOH . The reaction was stirred for 3 h at 60 °C, and then NaCl saturated (100 mL) was added. The product was extracted with Et_2O (3 x 20 mL). The organic layer was dried over MgSO_4 , and the solvent was removed under reduced pressure. The colourless oil (1.9 g, 3.34 mmol, 93% Yield) was used without further purification.

^1H NMR (400 MHz, CDCl_3): δ 8.05 (s, 1H, CNOH), 7.57 (t, J = 8 Hz, 2H - CH py), 7.49 (d, J = 8 Hz, 2H - CH py), 7.18 (d, J = 8 Hz, 2H - CH py), 3.78 (s, 4H, CH_2N py), 3.38 (s, 6H - CH_3N), 2.77 (s, 2H - CH_2N), 1.50 (s, 9H - $(\text{CH}_3)_3$), 1.01 (s, 6H - CH_3).

^{13}C NMR (101 MHz, CDCl_3): δ 158.59 (CNOH), 157.43 (CO), 154.65 (C py), 154.55 (C py), 137.33 (CH py), 118.67 (CH py), 117.44 (CH py), 81.13 (C Boc), 64.63 (CH_2N), 61.69 (CH_2N py), 34.46 (CH_3N), 28.48 ($(\text{CH}_3)_3$), 3.92 (CH_3).

MS (ES-TOF): $[\text{M}+\text{H}]^+$ Obs. m/z : 557.3

$[\text{M}+\text{Na}]^+$ Obs. m/z : 579.3



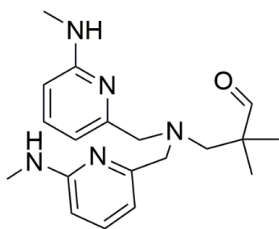
L2-3

2u (200 mg, 0.37 mmol) was dissolved in 3 mL of TFA and left reacting for 3 h at room temperature. The TFA in excess was removed by blowing N_2 , and the remaining oil was dissolved in water (10 mL). The aqueous phase, which was first washed with Et_2O (3 x 5 mL), was basified by adding concentrated NaOH. The product is then extracted from the water layer by DCM (3 x 10 mL). The combined organic layers were treated with $MgSO_4$ and dried under a high vacuum. The desired compound was obtained as a pale yellow oil in 95% yield (120 mg, 0.35 mmol).

1H NMR (400 MHz, $CDCl_3$): δ 7.45 (t, $J = 7.8$ Hz, 2H - CH py), 6.66 (d, $J = 7.3$ Hz, 2H - CH py), 6.32 (d, $J = 8.5$ Hz, 2H - CH py), 3.76 (s, 4H - CH_2N py), 3.42 (s, 2H - CH_2N), 2.92 (d, $J = 5.0$ Hz, 6H - CH_3N), 2.64 (s, 2H - CH_2), 0.91 (s, 6H - CH_3). NH and OH signals not observed.

^{13}C NMR (101 MHz, $CDCl_3$) δ 154.78 (C py), 148.44 (C py), 144.29 (CH py), 111.51 (CH py), 107.96 (CH py), 69.71 (CH_2O), 65.12 (CH_2N), 57.52 (CH_2N py), 37.27 (C), 29.06 (NCH_3), 24.07 (CH_3).

HRMS (ES-TOF): $[M+H]^+$ Calc. m/z: 344.2445 Obs. m/z: 344.2458



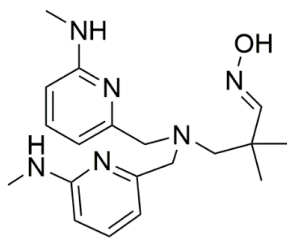
L2-4

2v (250 mg, 0.46 mmol) was dissolved in 4 mL of DCM:TFA (1:1), and the mixture was stirred for 35 min at room temperature. After TFA and DCM evaporation by N₂ blowing, the crude was dissolved in 10 mL of water, and the solution was basified by adding NaOH (1 M) until alkaline pH (8-9) was reached. The product was extracted from the aqueous phase with DCM (3 x 10 mL). The combined organic layers were dried over MgSO₄ and concentrated *in vacuum*. Finally, the crude was purified by the auto column CombiFlash NextGen 100 applying a gradient from 0 to 5% of MeOH in DCM for 20 min, followed by 10 min isocratic (5 % of MeOH in DCM), yielding a pale yellow oil (41 mg, 0.12 mmol, 26% Yield).

¹H NMR (400 MHz, CDCl₃): δ 9.34 (s, 1H - CHO), 7.41 (t, J= 8 Hz, 2H - CH py), 6.75 (d, J= 8 H, 2Hz, 2H - CH py), 6.24 (d, J= 8 Hz, 2H - CH py), 4.54 (m, 2H - NH), 3.62 (s, 4H - CH₂N py), 2.895 (d, 6H - CH₃N), 2.88 (s, 2H - CH₂N), 1.00 (s, 6H - CH₃).

¹³C NMR (101 MHz, CDCl₃): δ 207.03 (CHO), 159.34 (C py), 158.22 (C py), 138.06 (CH py), 112.12 (CH py), 103.85 (CH py), 62.04 (CH₂N), 61.68 (CH₂N py), 29.41 (CH₃N), 20.53 (CH₃).

HRMS (ES-TOF): [M+H]⁺ Calc. m/z: 342.2288 - Obs. m/z: 342.2272



L2-5

A mixture of TFA (2.85 mL), TIS (0.15 mL) in 5 mL of DCM was prepared and added to **2w** (200 mg, 0.36 mmol) solution in DCM (2 mL). After 4 h of stirring at room temperature, the TFA solution was evaporated by N₂. The crude was then purified using the auto column CombiFlash[®] NextGen 100 applying a gradient from 0 to 5% of MeOH in DCM for 10 min, followed by 30 min isocratic (5 % of MeOH in DCM), yielding a yellow oil (117 mg, 0.21 mmol, 59% Yield).

¹H NMR (400 MHz, CDCl₃): δ 9.91 (s, 2H, NH), 7.79 (t, J= 8 Hz, 2H - CH py), 7.24 (s, 1H - HOCN), 6.89 (d, J= 8 Hz, 2H - CH py), 6.61 (d, J= 8 Hz, 2H - CH py), 3.93 (s, 4H - CH₂N py), 2.96 (s, 6H - CH₃N), 2.80 (s, 2H - CH₂N), 1.08 (s, 6H - (CH₃)₃).

¹³C NMR (101 MHz, CDCl₃): δ 158.91 (CNOH), 157.63 (C py), 157.54 (C py), 138.30 (CH py), 111.71 (CH py), 103.42 (CH py), 64.24 (NCH₂), 61.4 (NCH₂ py), 29.3 (NCH₃), 24.00 (CH₃).

HRMS (ES-TOF): [M+H]⁺ Calc. m/z: 357.2397 - Obs. m/z: 357.2383

2.6.2 UV - Kinetic experiment

The kinetic experiments were carried out using Milli-Q® water at 25 °C. The buffers used were MES (5.5 < pH < 6.7) HEPES (6.9 < pH < 8.2), EPPS (7.4 < pH < 8.6), CHES (8.7 < pH < 9.9) and CAPS (9.8 < pH < 11.0). All the solutions were prepared with analytical grade buffers keeping the ionic strength at 0.1 M by adding NaNO₃. The reaction was either performed in a quartz cuvette using the Cary 300 UV-Vis-NIR spectrophotometers or wells of a quartz plate using the FluoroStar Omega plate reader. At pH 7 or above, the reaction progress was monitored at 400 nm, following the appearance of *p*-nitrophenolate; in the pH range 5-7, the reaction was monitored by detecting the formation of *p*-nitrophenol at 318 nm using scanning kinetic methods or HPLC. A typical experiment was started by introducing a volume 20 µL of 5 mM BNPP to the reaction solution. The latter was prepared by mixing the zinc complex (0.05 – 2 mM - created *in situ* by adding specific aliquots of 5-50 mM Zn(NO₃)₂ and ligand stock solutions) with 1 mL of 0.1 M Buffer and the appropriate volume of 0.1 M NaNO₃ to reach 2 mL. The ligand solution was prepared with DMSO and the Zn(NO₃)₂ with 0.1 M NaNO₃ in water.

2.6.3 HPLC – Kinetic experiment

Kinetic experiments monitored by HPLC used the following method:

- Turnover experiment for **2-3** and **2-4**:

Gradient: 5-95% acetonitrile in 10 min, injected volume: 10 µL; Absorbance registered at 350 nm. Column: Synergi 4 µm Polar-RP 80 A, LC Column 150 x 4.6 mm, Phenomenex.

- Turnover experiment for **2-5**:

20 % acetonitrile for 10 min followed by a gradient 20-95 % acetonitrile in 5 min, injected volume: 10 μ L; Absorbance registered at 350 nm. Column: Synergi 4 μ m Polar-RP 80 A,LC Column 150 x 4.6 mm, Phenomenex.

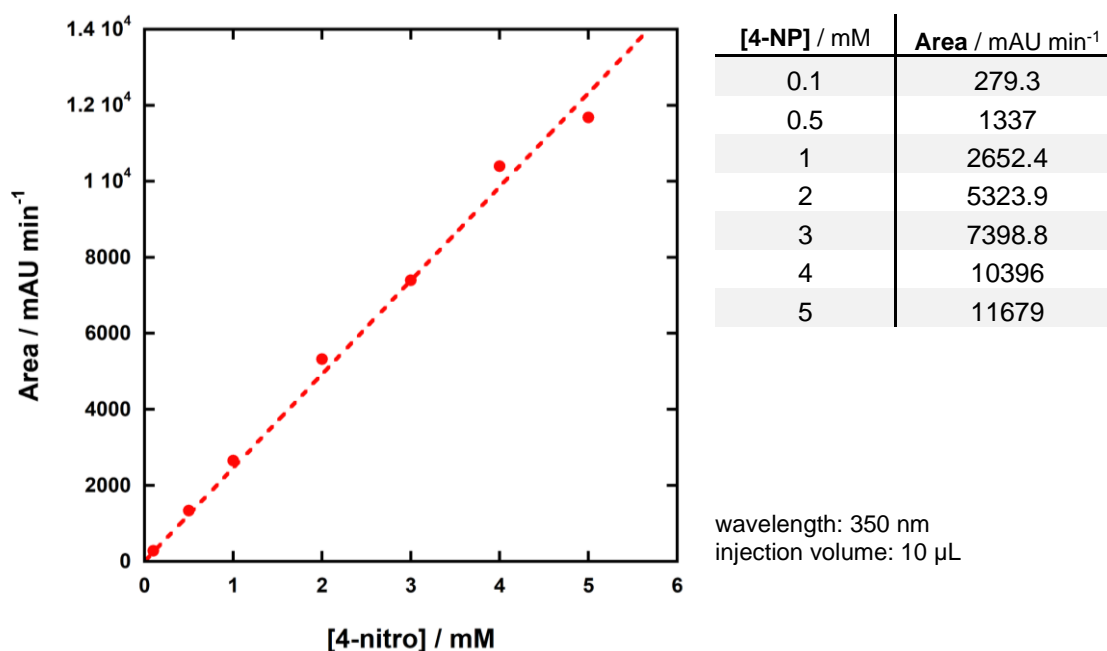
- Substrate screening with **2-5**:

Gradient: 5-95% acetonitrile in 15 min, injected volume: 20 μ L; Absorbance registered at 280 nm. Column: Synergi 4 μ m Polar-RP[®] 80 A,LC Column 150 x 4.6 mm, Phenomenex. Kinetex[®] 5 μ m C18 100 Å, LC Column, Phenomenex.

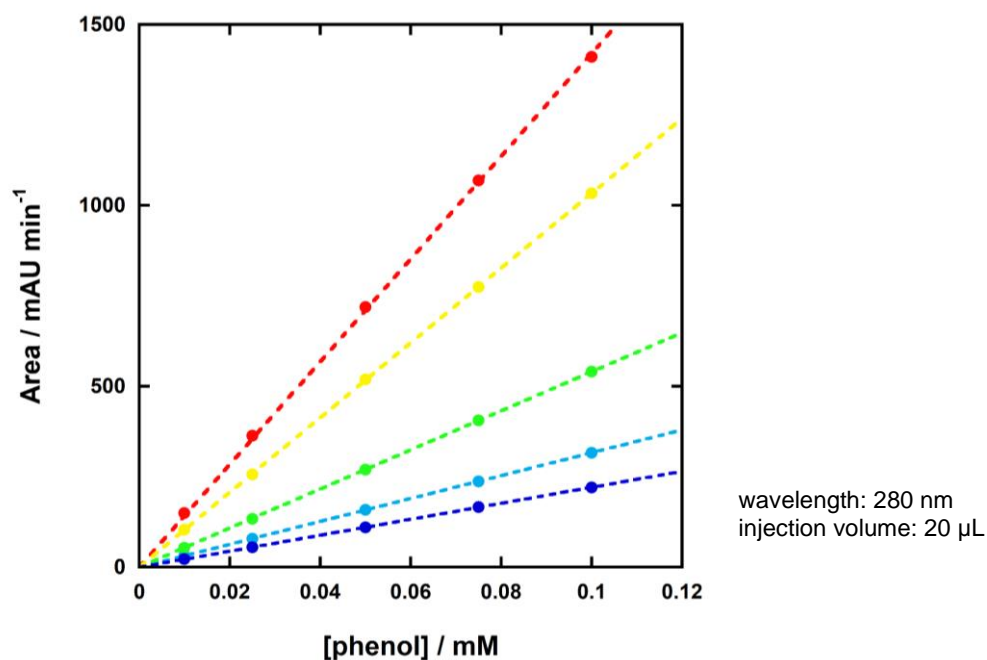
- **2-4** analysis in pseudo first-order condition:

Gradient: 5-95% acetonitrile in 15 min, injected volume: 20 μ L; Absorbance registered at 318 nm. Column: Synergi 4 μ m Polar-RP 80 A,LC Column 150 x 4.6 mm, Phenomenex.

Calibration curve of 4-nitrophenol for the HPLC experiment in excess of substrate:



Calibration curves of phenols used for the substrate screening experiment performed by HPLC:



mM	4-CN / rt 9.1	3-NO ₂ / rt 10.4 min	3-NO ₂ -4 Cl / rt 11.6 min	4-NO ₂ / rt 10.0 min	3-F / rt 10.1 min
0.01	149.39	104.08	53.93	31.45	21.99
0.025	363.54	256.45	133.37	78.83	54.6
0.05	719.07	518.92	269.56	158.53	109.94
0.075	1068.8	774.84	405.54	237.19	166.28
0.1	1410.2	1033.4	540.72	316.29	220.79
slope: / mAU mM ⁻¹	14203 ± 65	10337 ± 11	5403 ± 7	3163 ± 2	2209 ± 4

In general, the experiments were initiated by adding a volume of 5 mM BNPP solution to the reaction solution composed of complex (formed *in situ*), buffer, 0.1 M NaNO₃ in water. To both the eluents, 0.1 % of TFA was added.

2.6.4 Data

- k_{obs} vs [2-n]:

[Buffer] = 50 mM, [NaNO₃] = 0.1 M, [BNPP]=0.05 mM, 25 °C;

2-3:

[2-3] / mM	k_{obs} / s^{-1}			
	pH 6.66	pH 7.06	pH 7.40	pH 7.80
0.5	$2.30 \pm 0.02 \times 10^{-6}$	$4.36 \pm 0.02 \times 10^{-6}$	$9.38 \pm 0.04 \times 10^{-6}$	$1.08 \pm 0.05 \times 10^{-5}$
1.0	$4.59 \pm 0.03 \times 10^{-6}$	$9.41 \pm 0.03 \times 10^{-6}$	$1.66 \pm 0.04 \times 10^{-5}$	$2.14 \pm 0.01 \times 10^{-5}$
1.5	$6.45 \pm 0.04 \times 10^{-6}$	$1.44 \pm 0.01 \times 10^{-5}$	$2.41 \pm 0.01 \times 10^{-5}$	$3.07 \pm 0.03 \times 10^{-5}$
2.0	$7.53 \pm 0.04 \times 10^{-6}$	$1.90 \pm 0.01 \times 10^{-5}$	$3.16 \pm 0.01 \times 10^{-5}$	$4.42 \pm 0.03 \times 10^{-5}$
2.5	$9.93 \pm 0.28 \times 10^{-6}$	$2.48 \pm 0.01 \times 10^{-5}$	$4.20 \pm 0.01 \times 10^{-5}$	$5.42 \pm 0.06 \times 10^{-5}$

[2-3] / mM	k_{obs} / s^{-1}		
	pH 8.30	pH 8.91	pH 9.51
0.5	$2.04 \pm 0.12 \times 10^{-5}$	$1.59 \pm 0.02 \times 10^{-5}$	$1.05 \pm 0.01 \times 10^{-5}$
1.0	$3.92 \pm 0.09 \times 10^{-5}$	$3.04 \pm 0.01 \times 10^{-5}$	$2.31 \pm 0.02 \times 10^{-5}$
1.5	$4.19 \pm 0.09 \times 10^{-5}$	$4.07 \pm 0.02 \times 10^{-5}$	$2.99 \pm 0.02 \times 10^{-5}$
2.0	$5.96 \pm 0.56 \times 10^{-5}$	$5.18 \pm 0.03 \times 10^{-5}$	$3.95 \pm 0.02 \times 10^{-5}$
2.5	$7.72 \pm 0.08 \times 10^{-5}$	$5.75 \pm 0.04 \times 10^{-5}$	-

2-4:

[2-4] / mM	k_{obs} / s^{-1}
	pH 7.40
0.50	$4.88 \pm 0.32 \times 10^{-6}$
1.00	$1.01 \pm 0.01 \times 10^{-5}$
1.50	$1.50 \pm 0.05 \times 10^{-5}$
2.00	$1.92 \pm 0.03 \times 10^{-5}$
2.50	$2.36 \pm 0.09 \times 10^{-5}$
2.85	$2.60 \pm 0.12 \times 10^{-5}$

2-5:

[2-5] / mM	k_{obs} / s^{-1}			
	pH 7.11	pH 7.52	pH 7.97	pH 8.29
0.10	$9.98 \pm 0.04 \times 10^{-5}$	$1.07 \pm 0.04 \times 10^{-4}$	$1.17 \pm 0.03 \times 10^{-4}$	$1.27 \pm 0.02 \times 10^{-4}$
0.25	$1.72 \pm 0.01 \times 10^{-4}$	$1.71 \pm 0.04 \times 10^{-4}$	$1.91 \pm 0.03 \times 10^{-4}$	$2.08 \pm 0.01 \times 10^{-4}$
0.50	$2.26 \pm 0.01 \times 10^{-4}$	$2.17 \pm 0.01 \times 10^{-4}$	$2.50 \pm 0.01 \times 10^{-4}$	$2.74 \pm 0.01 \times 10^{-4}$
0.75	$2.75 \pm 0.12 \times 10^{-4}$	$2.78 \pm 0.05 \times 10^{-4}$	$2.83 \pm 0.01 \times 10^{-4}$	$3.34 \pm 0.03 \times 10^{-4}$
1.00	$3.07 \pm 0.08 \times 10^{-4}$	$2.80 \pm 0.08 \times 10^{-4}$	$3.08 \pm 0.05 \times 10^{-4}$	$3.36 \pm 0.03 \times 10^{-4}$
1.50	$3.82 \pm 0.14 \times 10^{-4}$	$3.27 \pm 0.05 \times 10^{-4}$	$3.52 \pm 0.05 \times 10^{-4}$	$2.74 \pm 0.07 \times 10^{-4}$
2.00	$3.30 \pm 0.12 \times 10^{-4}$	$3.33 \pm 0.09 \times 10^{-4}$	$3.95 \pm 0.06 \times 10^{-4}$	$4.65 \pm 0.08 \times 10^{-4}$

[2-5] / mM	k_{obs} / s^{-1}			
	pH 8.91	pH 9.48	pH 10.31	pH 10.55
0.10	$1.49 \pm 0.01 \times 10^{-4}$	$1.51 \pm 0.01 \times 10^{-4}$	$1.08 \pm 0.01 \times 10^{-4}$	$6.92 \pm 0.11 \times 10^{-5}$
0.25	$2.32 \pm 0.02 \times 10^{-4}$	$2.37 \pm 0.02 \times 10^{-4}$	$1.93 \pm 0.02 \times 10^{-4}$	$1.62 \pm 0.03 \times 10^{-4}$
0.50	$3.15 \pm 0.03 \times 10^{-4}$	$3.28 \pm 0.02 \times 10^{-4}$	$2.89 \pm 0.02 \times 10^{-4}$	$2.53 \pm 0.02 \times 10^{-4}$
0.75	$3.79 \pm 0.04 \times 10^{-4}$	$3.98 \pm 0.03 \times 10^{-4}$	$3.58 \pm 0.03 \times 10^{-4}$	$3.25 \pm 0.03 \times 10^{-4}$
1.00	$4.17 \pm 0.04 \times 10^{-4}$	$4.41 \pm 0.06 \times 10^{-4}$	$4.26 \pm 0.04 \times 10^{-4}$	$3.90 \pm 0.04 \times 10^{-4}$
1.50	$5.06 \pm 0.04 \times 10^{-4}$	$5.10 \pm 0.04 \times 10^{-4}$	$5.26 \pm 0.07 \times 10^{-4}$	$4.98 \pm 0.08 \times 10^{-4}$
2.00	$5.68 \pm 0.09 \times 10^{-4}$	$5.98 \pm 0.08 \times 10^{-4}$	$6.00 \pm 0.09 \times 10^{-4}$	$5.88 \pm 0.10 \times 10^{-4}$

- pH profile

[Buffer] = 50 mM, [NaNO₃] = 0.1 M, [BNPP]=0.05 mM, 25 °C;

2-3:

pH	$k_2 / M^{-1} s^{-1}$	$\log k_2$
6.66	$3.73 \pm 0.11 \times 10^{-3}$	-2.43
7.06	$9.93 \pm 0.05 \times 10^{-3}$	-2.00
7.42	$1.68 \pm 0.01 \times 10^{-2}$	-1.78
7.80	$2.17 \pm 0.02 \times 10^{-2}$	-1.66
8.31	$2.30 \pm 0.03 \times 10^{-2}$	-1.64
8.91	$2.30 \pm 0.02 \times 10^{-2}$	-1.64
9.50	$1.98 \pm 0.01 \times 10^{-2}$	-1.70
10.26	$1.77 \pm 0.02 \times 10^{-2}$	-1.75
10.77	$1.55 \pm 0.01 \times 10^{-2}$	-1.81

2-4:

pH	$k_2 / M^{-1} s^{-1}$	$\log k_2$
6.40	$7.00 \pm 0.65 \times 10^{-3}$	-2.155
6.20	$2.86 \pm 0.08 \times 10^{-3}$	-2.544
7.00	$1.34 \pm 0.29 \times 10^{-2}$	-1.872
7.40	$1.68 \pm 0.43 \times 10^{-2}$	-1.774
8.00	$2.07 \pm 0.14 \times 10^{-2}$	-1.685
8.40	$1.57 \pm 0.75 \times 10^{-2}$	-1.805
9.50	$4.96 \pm 0.38 \times 10^{-3}$	-2.305
10.00	$3.24 \pm 0.23 \times 10^{-3}$	-2.490

2-5:

pH	$k_0 / s^{-1} M^{-1/2}$	$k_2 / M^{-1}s^{-1}$	$\log k_2$
7.11	$1.001 \pm 0.017 \times 10^{-2}$	10.0 ± 0.2	1.000
7.52	$8.626 \pm 0.432 \times 10^{-3}$	8.6 ± 0.4	0.936
7.97	$9.599 \pm 0.376 \times 10^{-3}$	9.6 ± 0.4	0.982
8.29	$1.129 \pm 0.051 \times 10^{-2}$	11.3 ± 0.5	1.053
8.91	$1.324 \pm 0.023 \times 10^{-2}$	13.2 ± 0.2	1.122
9.48	$1.376 \pm 0.025 \times 10^{-2}$	13.8 ± 0.2	1.139
10.31	$1.328 \pm 0.018 \times 10^{-2}$	13.3 ± 0.2	1.123
10.55	$1.241 \pm 0.042 \times 10^{-2}$	12.4 ± 0.4	1.094

k_{obs} vs [BNPP]:

[EPPS] = 50 mM pH 7.4, [NaNO₃] = 0.1 M, 25 °C;

BNPP / mM	k_{obs} / s^{-1}		
	2-3 / 2 mM	2-4 / 1 mM	2-5 / 1 mM
0.010	$4.53 \pm 0.03 \times 10^{-5}$	$5.32 \pm 0.03 \times 10^{-6}$	$2.51 \pm 0.51 \times 10^{-4}$
0.025	$4.62 \pm 0.02 \times 10^{-5}$	$6.95 \pm 0.08 \times 10^{-6}$	$3.11 \pm 0.43 \times 10^{-4}$
0.050	$4.40 \pm 0.02 \times 10^{-5}$	$9.24 \pm 0.02 \times 10^{-6}$	$2.85 \pm 0.10 \times 10^{-4}$
0.075	$4.50 \pm 0.02 \times 10^{-5}$	$1.14 \pm 0.07 \times 10^{-5}$	$2.94 \pm 0.04 \times 10^{-4}$
0.100	$4.63 \pm 0.01 \times 10^{-5}$	$1.26 \pm 0.06 \times 10^{-5}$	$2.77 \pm 0.02 \times 10^{-4}$
0.125	$4.49 \pm 0.03 \times 10^{-5}$	-	$2.77 \pm 0.02 \times 10^{-4}$
0.150	$4.67 \pm 0.03 \times 10^{-5}$	$1.64 \pm 0.10 \times 10^{-5}$	$2.68 \pm 0.03 \times 10^{-4}$
0.175	-	-	$2.79 \pm 6.92 \times 10^{-4}$
0.200	-	-	$2.90 \pm 8.91 \times 10^{-4}$

- k_{obs} vs [HEPES]:

[NaNO₃] = 0.1 M, [BNPP] = 0.05 mM, 25 °C;

HEPES / M	k_{obs} / s^{-1}		
	2-3 / 2 mM	2-4 / 1 mM	2-5 / 1 mM
0.005	$2.34 \pm 0.01 \times 10^{-5}$	$1.13 \pm 0.10 \times 10^{-5}$	$2.26 \pm 0.01 \times 10^{-4}$
0.010	$2.78 \pm 0.01 \times 10^{-5}$	$1.18 \pm 0.08 \times 10^{-5}$	$3.08 \pm 0.01 \times 10^{-4}$
0.025	$3.08 \pm 0.01 \times 10^{-5}$	$1.06 \pm 0.07 \times 10^{-5}$	$3.37 \pm 0.01 \times 10^{-4}$
0.050	$3.19 \pm 0.01 \times 10^{-5}$	$9.68 \pm 0.05 \times 10^{-6}$	$3.42 \pm 0.04 \times 10^{-4}$
0.075	$3.22 \pm 0.01 \times 10^{-5}$	$9.94 \pm 0.08 \times 10^{-6}$	$3.45 \pm 0.05 \times 10^{-4}$
0.100	$3.23 \pm 0.01 \times 10^{-5}$	$1.15 \pm 0.08 \times 10^{-5}$	$3.29 \pm 0.03 \times 10^{-4}$

- PP inhibition experiment

[Buffer] = 50 mM, [NaNO₃] = 0.1 M, [2-n] = 1 mM, [BNPP]=0.05 mM, 25 °C;

2-3:

[PP] / mM	pH 7.05		pH 7.98		pH 9.05	
	k_{obs} / s^{-1}	k/k_0	k_{obs} / s^{-1}	k/k_0	k_{obs} / s^{-1}	k/k_0
0.0	$2.15 \pm 0.01 \times 10^{-5}$	1.00	$4.56 \pm 0.02 \times 10^{-5}$	1.00	$6.35 \pm 0.03 \times 10^{-5}$	1.00
0.1	$2.02 \pm 0.01 \times 10^{-5}$	0.94	$4.38 \pm 0.02 \times 10^{-5}$	0.96	$5.95 \pm 0.02 \times 10^{-5}$	0.94
0.5	$1.30 \pm 0.01 \times 10^{-5}$	0.60	$3.19 \pm 0.02 \times 10^{-5}$	0.70	$4.96 \pm 0.02 \times 10^{-5}$	0.78
1.0	$9.20 \pm 0.03 \times 10^{-6}$	0.43	$2.27 \pm 0.03 \times 10^{-5}$	0.50	$3.90 \pm 0.01 \times 10^{-5}$	0.61
1.5	$3.70 \pm 0.01 \times 10^{-6}$	0.17	$9.46 \pm 0.37 \times 10^{-6}$	0.21	$3.13 \pm 0.01 \times 10^{-5}$	0.49
2.0	$9.02 \pm 0.07 \times 10^{-7}$	0.04	$5.71 \pm 0.03 \times 10^{-6}$	0.13	$2.06 \pm 0.01 \times 10^{-5}$	0.32
2.5	$3.83 \pm 0.09 \times 10^{-7}$	0.02	$3.38 \pm 0.02 \times 10^{-6}$	0.07	$2.20 \pm 0.01 \times 10^{-5}$	0.35
3.0	$3.11 \pm 0.06 \times 10^{-7}$	0.01	$2.19 \pm 0.01 \times 10^{-6}$	0.05	$2.19 \pm 0.01 \times 10^{-5}$	0.35
3.5	-	-	$1.76 \pm 0.01 \times 10^{-6}$	0.04	$1.91 \pm 0.01 \times 10^{-5}$	0.30

2-5:

[PP] / mM	pH 7.6		pH 8.0		pH 9.0	
	k_{obs} / s^{-1}	k/k_0	k_{obs} / s^{-1}	k/k_0	k_{obs} / s^{-1}	k/k_0
0	$7.88 \pm 0.03 \times 10^{-4}$	1.00	$2.30 \pm 0.01 \times 10^{-4}$	1.00	$2.98 \pm 0.00 \times 10^{-4}$	1.00
20	$1.89 \pm 0.04 \times 10^{-4}$	0.24	$9.01 \pm 0.07 \times 10^{-5}$	0.39	$2.79 \pm 0.04 \times 10^{-4}$	0.93
40	$1.17 \pm 0.01 \times 10^{-4}$	0.15	$5.66 \pm 0.01 \times 10^{-5}$	0.25	$2.60 \pm 0.01 \times 10^{-4}$	0.87
60	$5.53 \pm 0.01 \times 10^{-5}$	0.07	$4.25 \pm 0.01 \times 10^{-5}$	0.18	$2.49 \pm 0.01 \times 10^{-4}$	0.84
80	$6.43 \pm 0.01 \times 10^{-5}$	0.08	$3.52 \pm 0.01 \times 10^{-6}$	0.15	$2.43 \pm 0.01 \times 10^{-4}$	0.82
100	$6.81 \pm 0.01 \times 10^{-5}$	0.09	$3.26 \pm 0.01 \times 10^{-6}$	0.14	$2.22 \pm 0.01 \times 10^{-4}$	0.75

- **Zn(II) binding**

[HEPES] = 50 mM pH 7.4, [NaNO₃] = 0.1 M, [2-n] = 1 mM, [BNPP]=0.05 mM, 25 °C;

2-3:

Zn(NO ₃) ₂		k_{obs} / s^{-1}
mM	eq	
0.0	0.00	$4.25 \pm 0.06 \times 10^{-7}$
0.5	0.25	$1.18 \pm 0.01 \times 10^{-5}$
1.0	0.50	$2.15 \pm 0.01 \times 10^{-5}$
1.5	0.75	$2.92 \pm 0.01 \times 10^{-5}$
2.0	1.00	$3.78 \pm 0.02 \times 10^{-5}$
2.5	1.25	$3.99 \pm 0.01 \times 10^{-5}$
3.0	1.50	$4.08 \pm 0.01 \times 10^{-5}$
3.5	1.75	$4.35 \pm 0.02 \times 10^{-5}$
4.0	2.00	$4.11 \pm 0.02 \times 10^{-5}$

2-4:

Zn(NO ₃) ₂		k_{obs} / s^{-1}
mM	eq	
0.0	0.00	$3.87 \pm 0.46 \times 10^{-7}$
0.05	0.05	$1.16 \pm 0.11 \times 10^{-6}$
0.10	0.10	$1.46 \pm 0.10 \times 10^{-6}$
0.50	0.50	$6.65 \pm 0.26 \times 10^{-5}$
1.00	1.00	$1.14 \pm 0.08 \times 10^{-5}$
1.50	1.50	$1.15 \pm 0.11 \times 10^{-5}$
2.00	2.00	$1.13 \pm 0.06 \times 10^{-5}$
2.50	2.50	$1.20 \pm 0.09 \times 10^{-5}$
3.00	3.00	$1.20 \pm 0.09 \times 10^{-5}$

2-5:

Zn(NO ₃) ₂		k_{obs} / s^{-1}
mM	eq	
0.00	0.00	$6.08 \pm 0.19 \times 10^{-7}$
0.05	0.05	$1.37 \pm 0.04 \times 10^{-6}$
0.10	0.10	$1.67 \pm 0.02 \times 10^{-6}$
0.50	0.50	$2.24 \pm 0.03 \times 10^{-5}$
1.00	1.00	$2.67 \pm 0.01 \times 10^{-5}$
1.50	1.50	$2.80 \pm 0.01 \times 10^{-5}$
2.00	2.00	$2.92 \pm 0.02 \times 10^{-5}$
2.50	2.50	$2.98 \pm 0.02 \times 10^{-5}$
3.00	3.00	$2.97 \pm 0.01 \times 10^{-5}$

- **k_{obs} vs [DMP]**

[HEPES] = 50 mM pH 7.4, [2-5] = 1 mM, [BNPP]=0.05 mM, ionic strength at 0.1 M by addition of NaNO₃, 25 °C;

[DMP] / mM	k_{obs} / s^{-1}	k/k_0
0	$1.694 \pm 0.017 \times 10^{-4}$	1.00
20	$1.776 \pm 0.015 \times 10^{-4}$	1.05
40	$1.706 \pm 0.016 \times 10^{-4}$	1.01
60	$1.774 \pm 0.019 \times 10^{-4}$	1.05
80	$1.787 \pm 0.019 \times 10^{-4}$	1.05
100	$1.864 \pm 0.020 \times 10^{-4}$	1.10

- **k_2 vs pK_a of leaving group**

[EPPS] = 50 mM pH 8.3, [2-5] = 1 mM, [substrate] = 0.05 mM, ionic strength at 0.1 M by addition of NaNO₃, 25 °C;

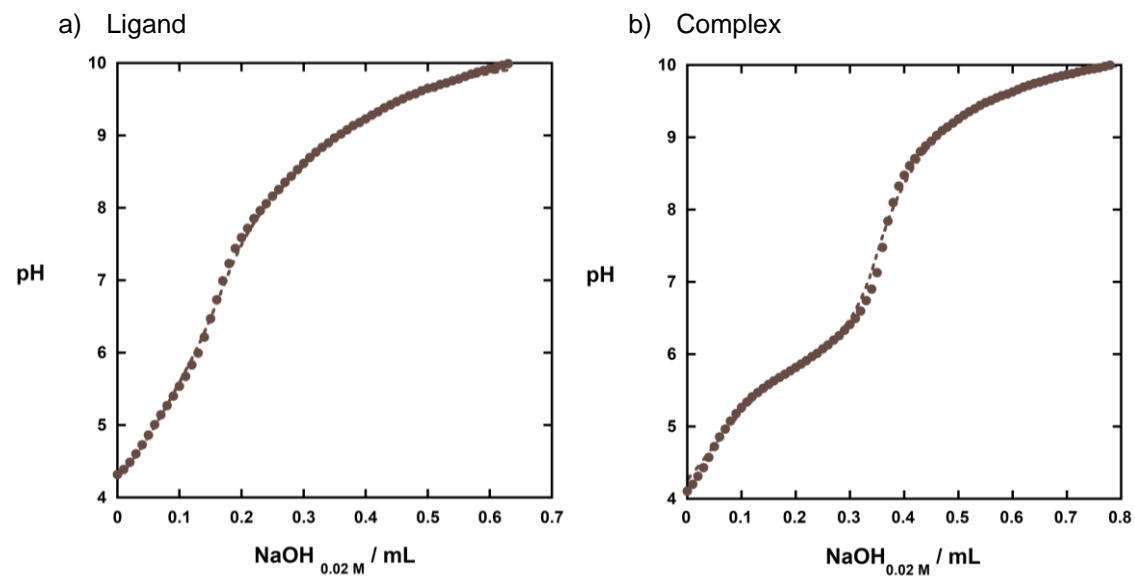
pK _a	k_{obs} / s^{-1}	$k_0 / s^{-1} M^{-1/2}$	$k_2 / M^{-1} s^{-1}$	log k_2
7.14	$1.37 \pm 0.15 \times 10^{-5}$	$4.33 \pm 0.47 \times 10^{-4}$	$4.33 \pm 0.47 \times 10^{-1}$	-0.36
7.71	$4.90 \pm 0.33 \times 10^{-6}$	$1.55 \pm 0.11 \times 10^{-4}$	$15.51 \pm 1.06 \times 10^{-2}$	-0.81
7.97	$2.04 \pm 0.06 \times 10^{-6}$	$6.46 \pm 0.20 \times 10^{-5}$	$6.46 \pm 0.20 \times 10^{-2}$	-1.19
8.63	$9.38 \pm 0.14 \times 10^{-7}$	$2.97 \pm 0.04 \times 10^{-5}$	$2.97 \pm 0.04 \times 10^{-2}$	-1.53
9.28	$9.38 \pm 0.14 \times 10^{-8}$	$2.97 \pm 0.04 \times 10^{-6}$	$2.97 \pm 0.04 \times 10^{-3}$	-2.53

2.6.5 Potentiometric titration

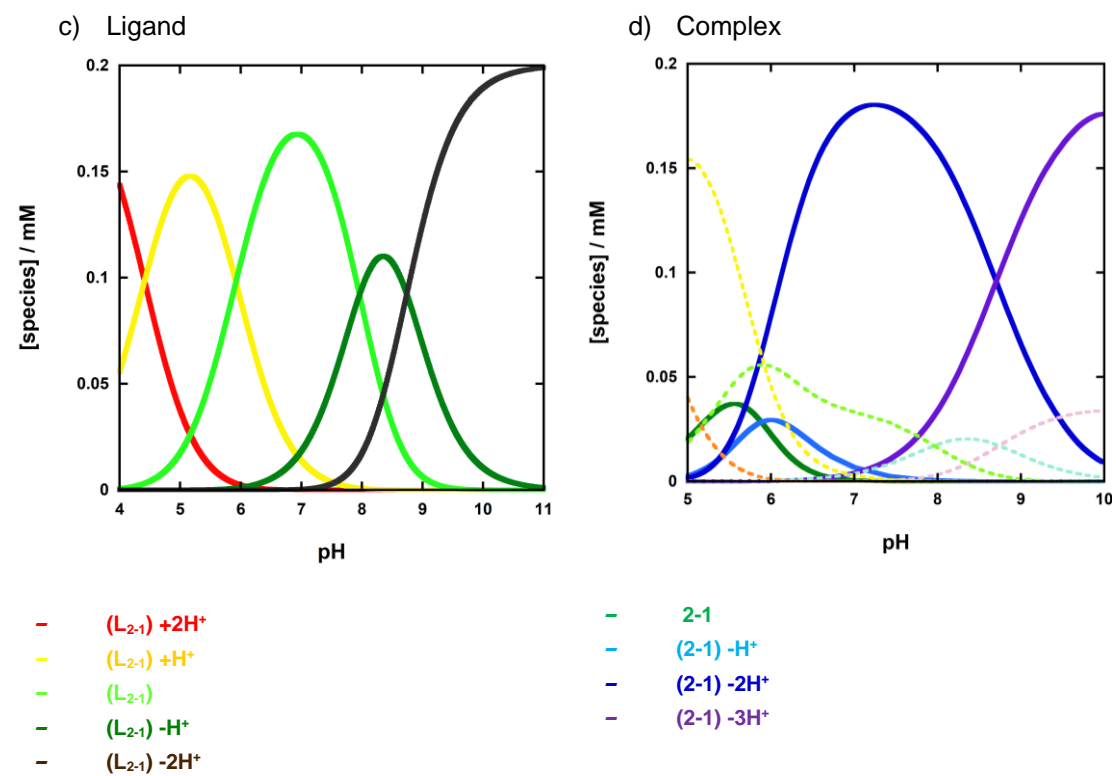
The titration experiments were carried out at 25 °C, and the pH was measured by Mettler-Toledo pH meter calibrated with Thermo Scientific buffer packs at pH 4.00, 7.01 and 10.06 at 25 °C. To the ligand or complex (0.2 mM), dissolved in 10 mL of 0.1 M NaNO₃, 2 equivalents of HCl (40 µL of 0.1 N from a standardised HCl solution purchased from Alfa Aesar) were added. The titration was performed by adding aliquots of 10 µL of 0.02 M NaOH (equal to 1/10 of equivalent) with a Hamilton gas-tight glass syringe (500 µL). The 0.02 M NaOH solution was prepared from a standardised 1 N solution of NaOH purchased from Alfa Aesar. The 0.2 M NaOH solution concentration was evaluated by titration against 10 ml of a 0.2 mM of potassium hydrogen phthalate as a primary standard and then used to titrate the 0.01 N HCl solution. The solutions were all prepared with deionised water. The measures were then processed by Hypspec and Hyss, and the data fitting yielded the speciation plots reported below. The titration plots of the complexes were fitted using the log β values obtained for the relative ligands.

2-1

Titration curve:

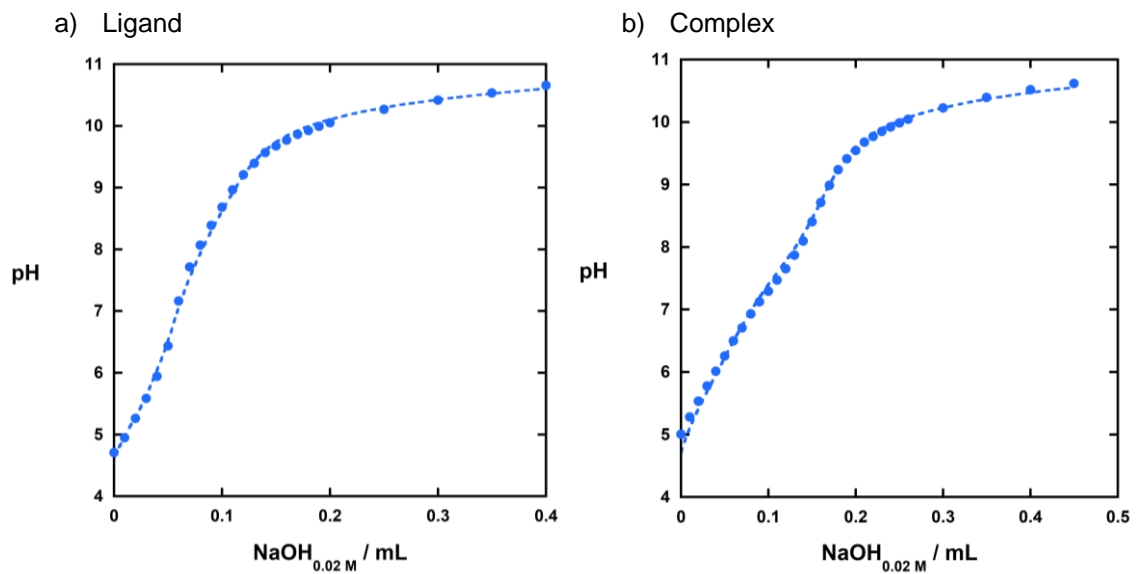


Speciation plot:

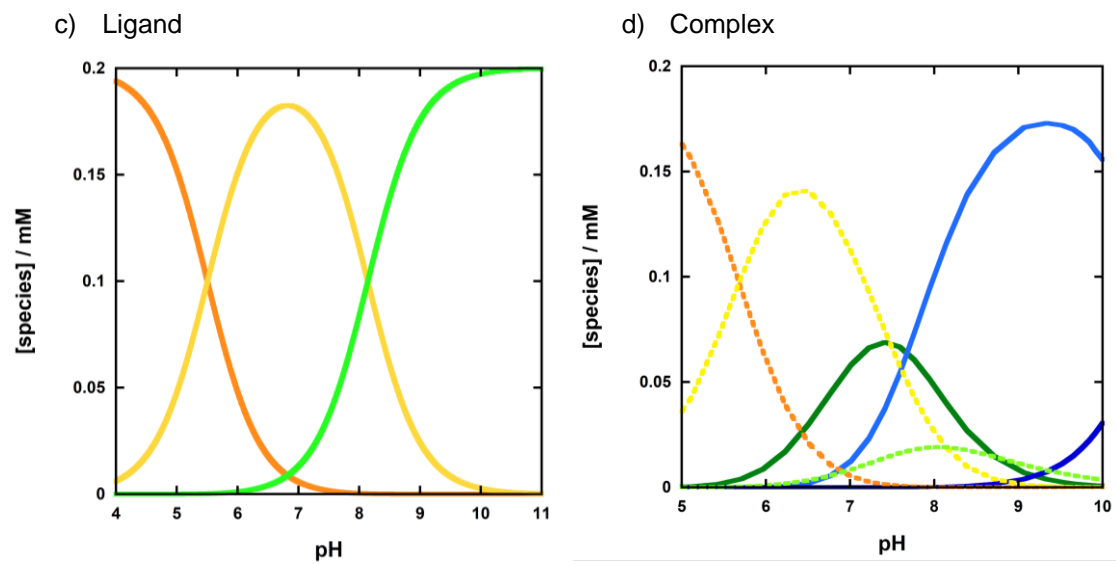


2-3

Titration curve:



Speciation plot:

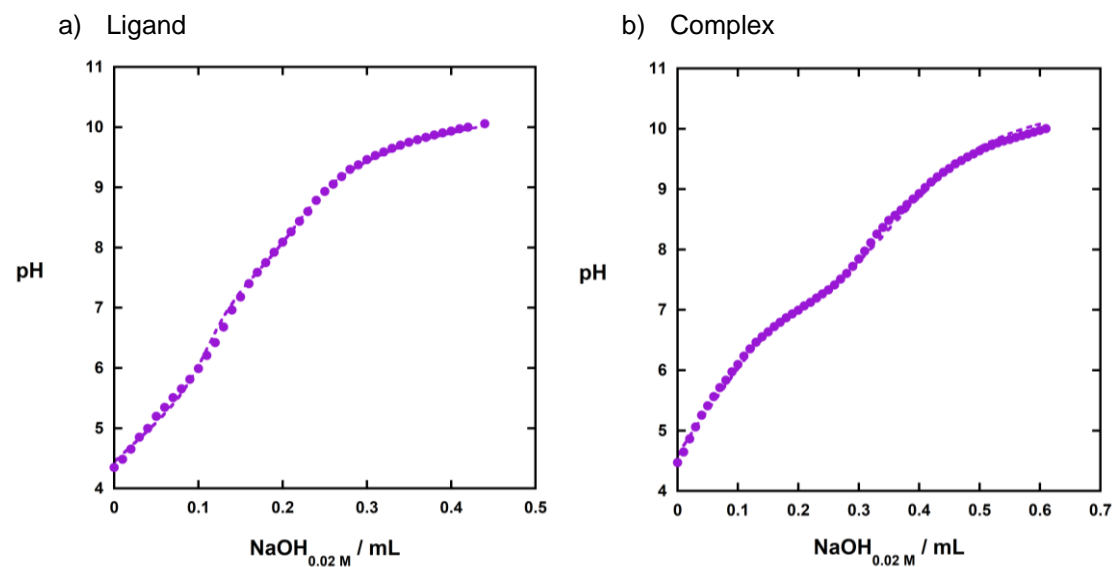


- $(L_{2-3}) + 2H^+$
 - $(L_{2-3}) + H^+$
 - L_{2-3}

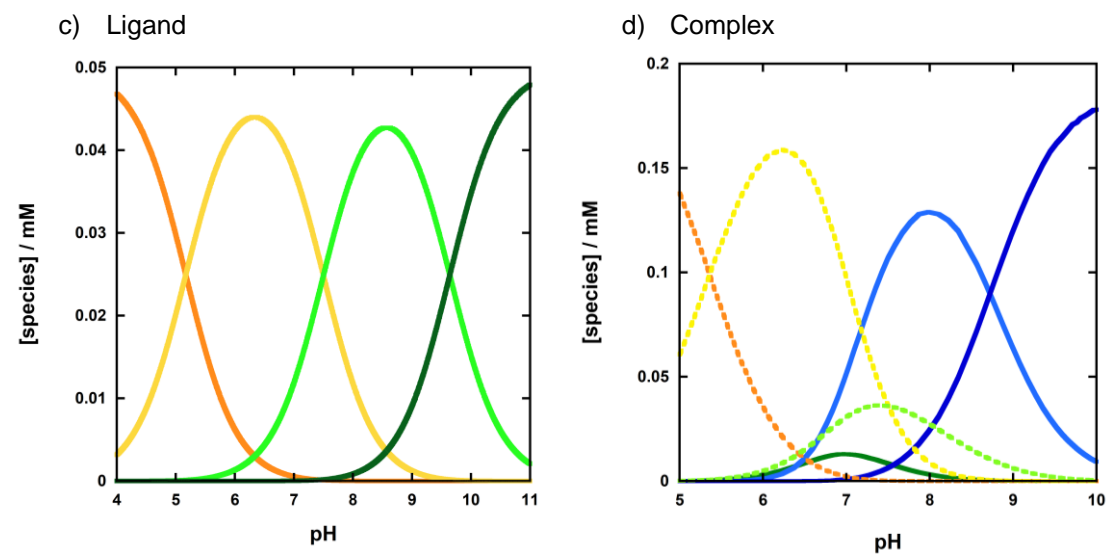
- 2-3
 - $(2-3) - H^+$
 - $(2-3) - 2H^+$

2-4

Titration curve:



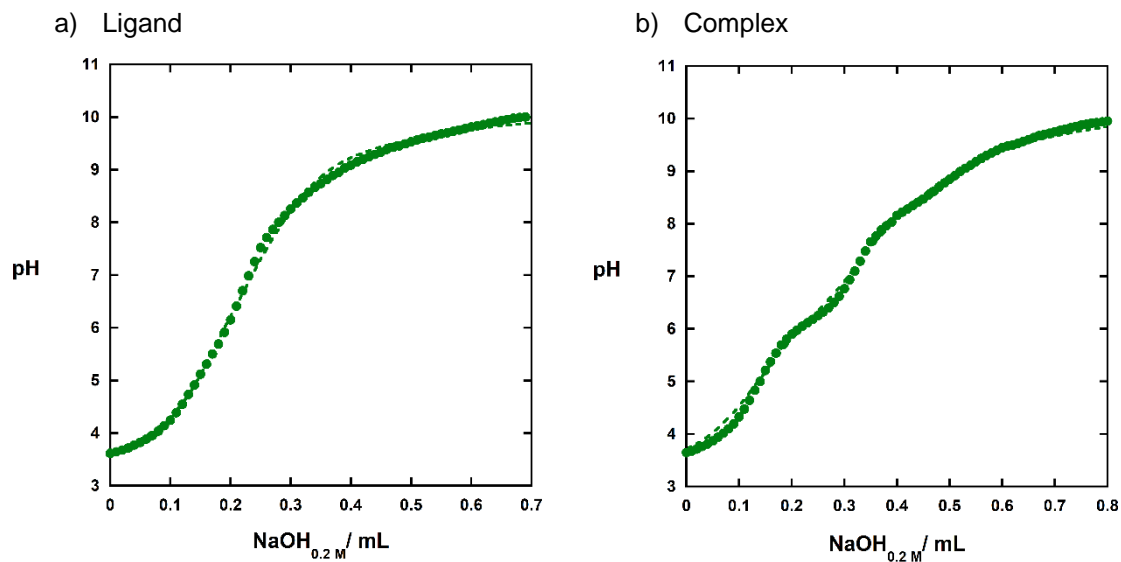
Speciation plot:



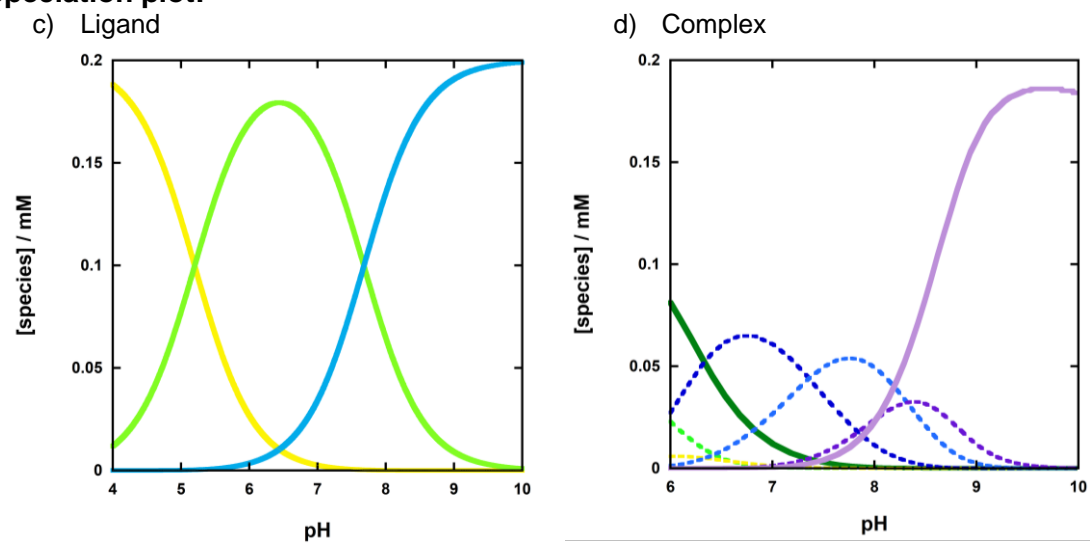
- $(L_{2-4}) + 2H^+$
 - $(L_{2-4}) + H^+$
 - L_{2-4}
 - $(L_{2-4}) - H$

- $2-4$
 - $(2-4) - H^+$
 - $(2-4) - 2H^+$

Titration curve:



Speciation plot:



— $(L_{2-5}) + 2H^+$
 — $(L_{2-5}) + H^+$
 — L_{2-5}

Dimeric species:
 (dashed line)

— $(2-5)_2$
 — $(2-5)_2 - H^+$
 — $(2-5)_2 - 2H^+$
 — $(2-5)_2 - 3H^+$
 — $(2-5)_2 - 4H^+$

Monomeric species:
 (solid lines)

— $(2-5)$
 — $(2-5) - 3H^+$

Chapter 3

Mononuclear Zn (II) complexes for the cleavage of phosphate diester models for RNA

3.1 Introduction

A wide range of metal ion complexes have been studied to explore their ability to enhance the cleavage of the phosphodiester bonds in RNA.⁴⁷ As described in Chapter 1, RNA has lower stability toward hydrolysis than DNA. Intramolecular transesterification can occur through the 2' hydroxyl group attacking the phosphate group, and the half-life time of RNA is approximately 3×10^5 times lower than that of DNA.^{2,3} Given these structural and mechanistic differences, the complexes used to catalyse the cleavage of RNA do not need to deliver a nucleophile efficiently, as is required to accelerate DNA cleavage. As highlighted in Chapter 2, a ligand based nucleophile can enhance the reaction rate, but the ensuing transesterification between the ligand and the substrate creates a de-activated catalyst and affects its performance by reducing the turnover number. In the case of artificial enzymes for RNA cleavage, this issue can be avoided, and generally, better catalyst efficiency is achieved.⁵²

It is firmly established that phosphate diester cleavage is accelerated strongly by metal ions. For example, Zn(II) ions in hydrolases coordinate to water molecules, decreasing their pK_a so that hydroxide is generated at neutral pH and enhances nucleophilic attack.^{2,58} Furthermore, the microenvironment of an enzyme pocket is strongly affected by all the amino acid residues capable of hydrogen bonding to the substrate, facilitating its coordination to the metal ion cores.^{10,12,75} Although their role has not been completely defined, functional groups capable of hydrogen bonding have been suggested to strengthen substrate binding, stabilise the transition state, and help leaving group departure. Also, the

interaction between the metal ion-bound water and the hydrogen bond donating groups of arginine, lysine, histidine, and serine might influence hydroxide formation.¹⁰²

While designing the ligand structure of complexes to mimic this local environment, substantial work has focused on quantifying the effect on the reaction rate provided by the second coordination sphere. To investigate this, De Rosales and coworkers have studied the impact of introducing primary amines into the second coordination sphere of tris(2-pyridylmethyl)amine (tpa) based Zn(II) complexes on the pK_a of the metal bound water molecule (Figure.3.1).⁹²

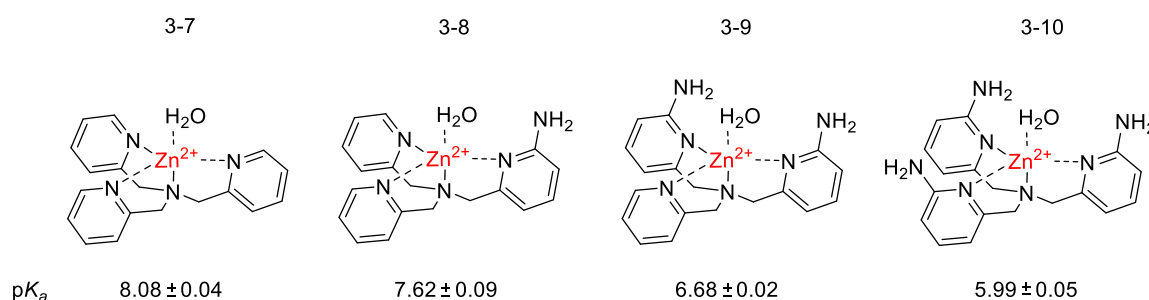


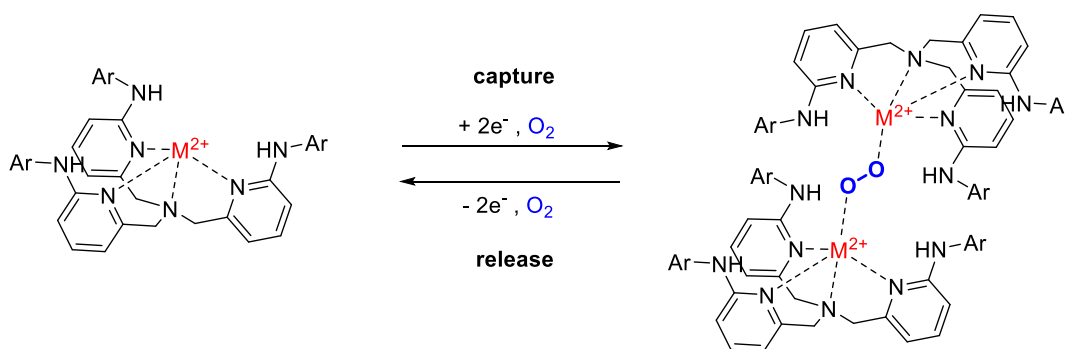
Figure.3.1 Structures of mononuclear complexes and relative pK_a of Zn(II) bound water molecule. ⁹²

Given their electron donating nature, the amino groups are expected to make the Zn(II) centre more electron rich and, consequently, a poorer Lewis acid. This would lower the acidity of a Zn(II) bound water molecule. However, the primary amines cooperate with the Zn(II) Lewis acidity to polarise the O-H bond and stabilise the hydroxide over the water molecule. As a result, an approximately 0.7 pK_a unit decrease per hydrogen bond donor was observed, and **3-10** showed the lowest value of 5.99 ± 0.05 . This demonstrates that Zn-bound water acidity is strongly influenced by the shape and binding site of the ligand, as

well as the environmental effects. A similar trend is also reflected in the complexes' ability to coordinate phosphate esters and catalyse their hydrolytic reactions.¹⁰³ Complex **3-9** showed a higher affinity toward phenyl phosphate than **3-7**. The monophosphate is expected to replace the neutral water molecule more easily than the negatively charged hydroxide. Although **3-9** ionises at a lower pH than **3-7**, the trend confirms that the amine hydrogen bonding provides significant stabilisation on the negatively charged oxygen of the phosphate. Williams and coworkers reported a study on the amine enriched tpa Zn(II) complexes, comparing the activity of **3-7** and **3-10** toward the hydrolysis of the RNA model 2-hydroxypropyl 4-nitrophenyl phosphate (HPNPP)⁵². Complex **3-10** was highly effective (with a k_c of $2 \times 10^5 \text{ M}^{-1} \text{ s}^{-1}$) and accelerates the background reaction 750-fold faster than **3-7** (k_c of $3 \times 10^3 \text{ M}^{-1} \text{ s}^{-1}$). The contribution provided by the amino groups is comparable to the core Zn(II) ion in **3-7**, further confirming the influence on catalysis of the microenvironment around the metal centre.

Providing the ligand structure with alternative functionalities is crucial for testing this hypothesis further. As reported in Chapter 2, introducing stronger hydrogen bond donors, such as amides and sulfonamides, has not proven effective due to their deprotonation at neutral pH. Therefore, groups that are more effective hydrogen bond donors but with a high pK_a are required.

Szymczak *et al.* have recently focused their attention on 6-phenylamino substituted tpa copper and zinc complexes as models to understand oxygenase and oxidase enzymes.^{104,105} They reported promising results in dioxygen capture via the formation of dimerised complexes and the reverse dioxygen release, as reported in Scheme 3.1.



Scheme 3.1 Reversible O_2 capture and release equilibrium of tpa based complexes^{104,105}

The performance of the complex was influenced by the introduction of different para-substituted aniline groups in the *ortho* position of pyridyl rings. They suggested that the effect was due to the secondary amine's hydrogen bond strength modulated by the *para* substitution. As summarised in Figure 3.2, the highest stability of the adduct was reached when the ligand structure was enriched with 4-(trifluoromethyl)anilines.

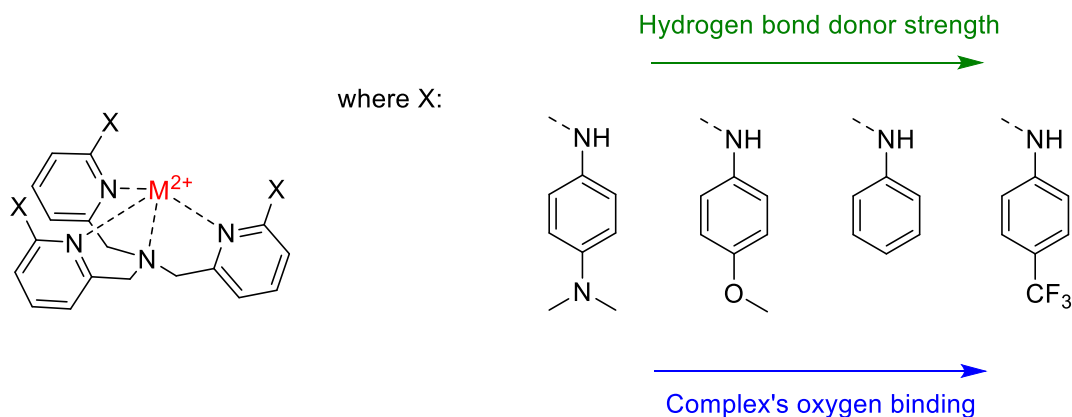


Figure 3.2 Impact on oxygen binding of the secondary amines' hydrogen bond strength¹⁰²

Enriching the ligand structure with aromatic amines provides the complex with stronger H-bond donors that are not strongly acidic, also creating a hydrophobic pocket whose effect would be interesting to investigate.

3.2 Results and discussion

This Chapter reports the synthesis and kinetic evaluation of 6-aniline substituted tris(2-pyridylmethyl)amine mononuclear Zn(II) complexes that efficiently enhance the transesterification of the phosphodiester bond. We also investigate how *para* functionalisation of the aniline rings perturbs the complex reactivity. Although five mononuclear complexes have been obtained (Figure 3.3), this Chapter focuses on structures **3-1**, **3-2**, **3-3** and **3-4**. Complex **3-5** did not show any reactivity and so was not investigated further.

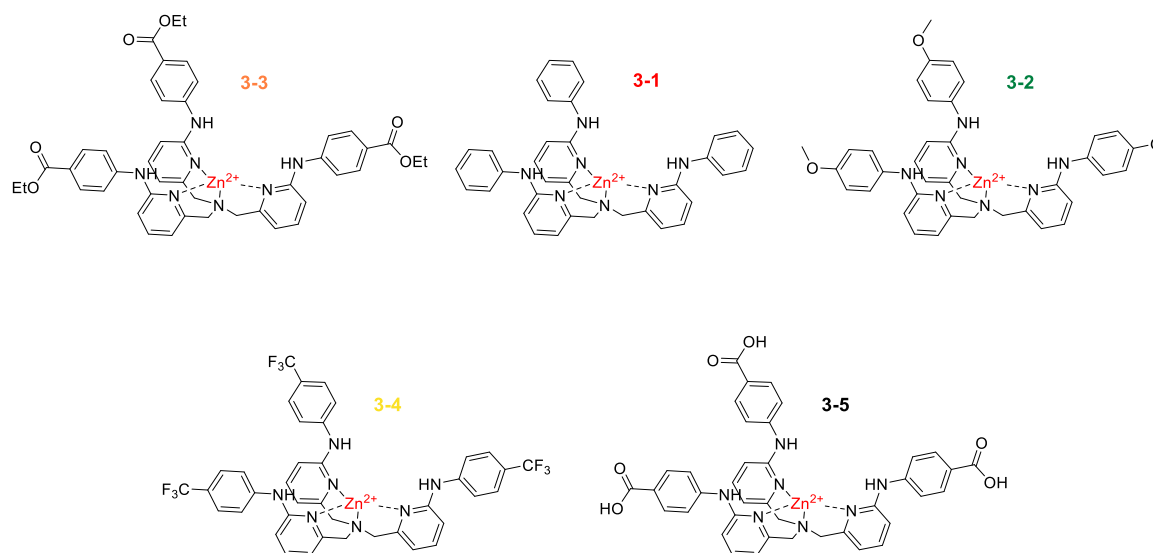
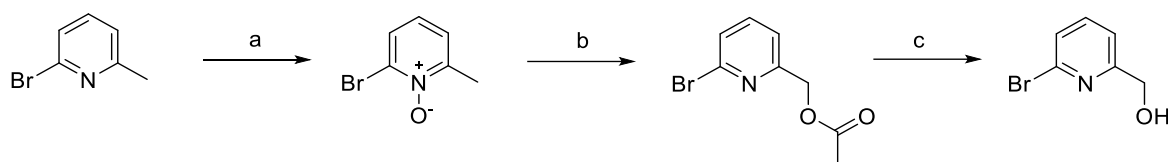


Figure 3.3 Mononuclear Zn(II) complexes

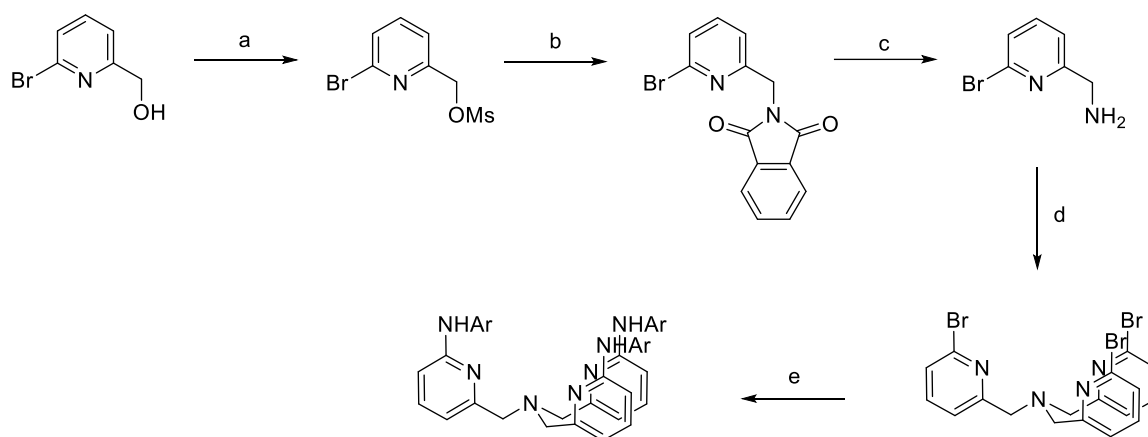
3.2.1 Synthesis

Szymczak's group approached the synthesis of these ligands starting from (6-bromo-2-pyridyl)methanol to obtain a versatile tris((6-bromo-2-pyridylmethyl)amine intermediate, which can eventually be converted by Buchwald-Hartwig cross-coupling into the final ligands.¹⁰⁴ We followed the same core strategy,¹⁰⁶ but modified the route to the key intermediate. Thanks to our collaboration with the Research Institute of Sweden (RISE), a new and upscaled method was developed to obtain (6-bromo-2-pyridyl)methanol, as shown in Scheme 3.2.



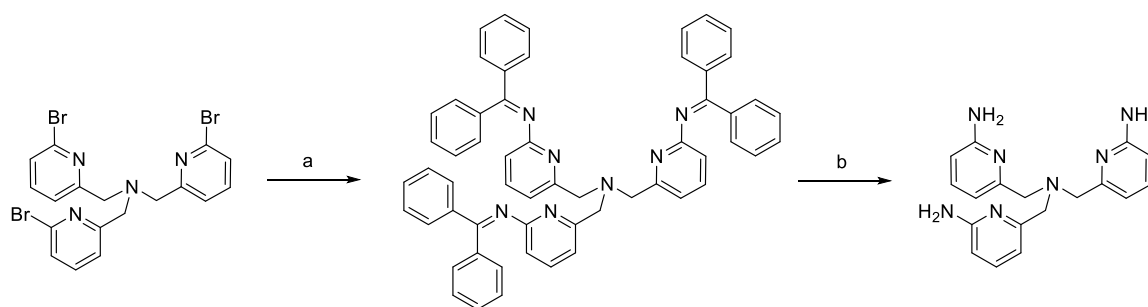
Scheme 3.2 Large scale synthesis of (6-bromo-2-pyridyl)methanol: a) AcOOH , AcOH $70\text{ }^{\circ}\text{C}$, 15 h, 40 % yield; b) Ac_2O , H_2SO_4 , $70\text{ }^{\circ}\text{C}$, 15 h; c) KOH , MeOH , r.t. 1 h, 55 % yield

The Boekelheide rearrangement of the 2-bromo-6-methylpyridine, conveniently activated by peracetic acid, yields (6-bromo-2-pyridyl)methyl acetate, which was then hydrolysed. The synthesis was performed and optimised on a large scale using 1.7 moles of starting material with an overall yield of 40%. The synthetic route does not include any purification by flash chromatography in its steps. The updated method used for synthesising the family of ligands is shown in Scheme 3.3.



Scheme 3.3 General method for the synthesis of the ligands; a) MsCl, Et₃N, THF, r.t. 18 h, 90 % yield; b) Potassium Phthalimide, DMF-DCM, r.t. 3 h; c) 38% HBr, 120 °C, 15 h, two steps-yield of 49%; d) (6-bromo-2-pyridyl)methyl methanesulfonate, NaOH, MeOH-H₂O, 70 °C, 18 h, 60% yield; e) NH₂Ar, Pd(OAc)₂, BINAP, Cs₂CO₃, Toluene, 100 °C, 20 h

The hydroxyl group of (6-bromo-2-pyridyl)methanol is efficiently mesylated and converted to a primary amine by a nucleophilic substitution with potassium phthalimide and subsequent hydrolysis. Alkylation of (6-bromo-2-pyridyl)methanamine with (6-bromo-2-pyridyl)methyl methanesulfonate provided tris((6-bromo-2-pyridyl)methyl)amine. The final ligands were furnished by Buchwald-Hartwig reactions with the relevant substituted anilines.



Scheme 3.4 Synthetic route for (6-bromo-2-pyridyl)methanamine and (6-bromo-2-pyridyl)methyl methane sulfonate; a) Benzophenone imine, Pd(OAc)₂, BINAP, Cs₂CO₃, Toluene, 100 °C, 24 h, 70 % yield; b) HCl, THF, r.t. 1h, 87% yield

To synthesise the previously studied 6-((bis((6-amino-2-pyridyl)methyl)amino)methyl)pyridin-2-amine, tris((6-bromo-2-pyridyl)methyl)amine was cross-coupled with benzophenone imine followed by acidic hydrolysis as shown in Scheme 3.4.

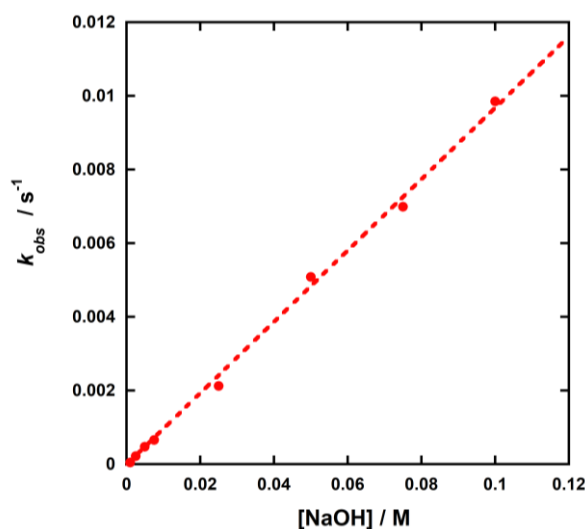
3.2.2 Kinetic studies

Reaction conditions

Replacing the primary amino groups with more bulky and apolar anilines leads to challenges in terms of water solubility. The complexes show poor aqueous solubility under the usual reaction conditions, which involve 0.1 M NaNO₃ and 0.05 M sulfonate buffer. These salts are generally used to keep ionic strength and pH constant, and were retained. Hence, the complexes have been studied using an aqueous solution containing 40% (v/v) of acetonitrile.

Reducing the medium polarity can alter the phosphodiester cleavage reaction, especially when higher percentages of organic solvents are used. The presence of dipolar aprotic solvents, leading to nucleophilic dehydration, could activate the alkoxide or hydroxide involved in the reaction. Furthermore, Yatsimirsky and coworkers proposed that an organic-rich mixture of water might be a good model for the environment of an active site.¹⁰⁷ They suggested that introducing an organic cosolvent, like DMSO and DMF, would imitate the solvating properties of the peptides and create a rather polar medium. The group followed the alkaline hydrolysis of BNPP and NPDPP in aqueous DMSO, acetonitrile and dioxane mixtures, discovering a general medium effect. Increasing the percentage of the organic cosolvent up to 60-70% (v/v) gave barely any change or a slight decrease of the

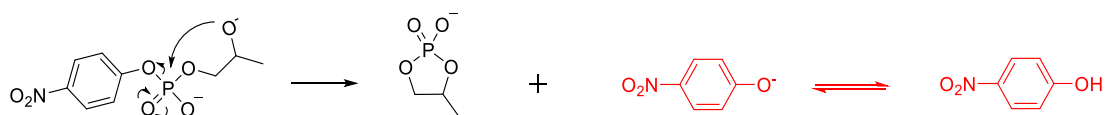
reaction rate, but when the percentage was raised over 70%, the reaction is 10-40 times faster in organic-rich media than in water. This suggests that a higher percentage of acetonitrile than we have used with the **3-n** complexes is required to lead to a significant change in the reactivity of the phosphate diester. A series of experiments have been designed to test this hypothesis, starting from determining the second order rate constant for the based-catalysed HPNPP transesterification under these reaction conditions.



Graph 3.1 Second-order plot for the alkaline transesterification of HPNPP in 40 %(v/v) acetonitrile in water. [HPNPP] = 0.05 mM, ionic strength at 0.1 M by addition of NaNO₃

The linear least-squares fitting of the data gives a second-order rate constant equal to $9.6 \pm 0.1 \times 10^{-2} \text{ M}^{-1} \text{ s}^{-1}$, which is in close agreement with the value reported by Williams and coworkers ($7.0 \pm 0.4 \times 10^{-2} \text{ M}^{-1} \text{ s}^{-1}$)⁵² in fully aqueous condition, and confirms that no large alteration in reactivity is caused by the new medium. The leaving group of the HPNPP is a 4-nitrophenolate, and the catalytic reaction is usually monitored by following the appearance of its peak at 400 nm (Scheme 3.5). The formation of the 4-nitrophenolate was confirmed by HPLC analysis, where product formation is followed (rt, 8 min; method: 1

mL/min, acetonitrile 5-95% in 10 min, 25 °C). However, the addition of acetonitrile perturbs the deprotonation equilibrium of the 4-nitrophenol, shifting its pK_a from 7.15⁴⁸ to 7.90 ± 0.01 , as demonstrated by UV titration (Figure 3.4). The absorbance values at 400 nm were reported against the pH and the fitting of the data by equation (14) yielded the new constant. The 0.75 unit shift is consistent with a decrease of the medium polarity.



Scheme 3.5 Transesterification of HPNPP. In red, the deprotonation equilibrium of the 4-nitrophenol

$$(14) \quad Abs_{400nm} = Abs_{400nm}^i \frac{[H^+]}{[H^+] + K_a} + Abs_{400nm}^f \frac{K_a}{[H^+] + K_a}$$

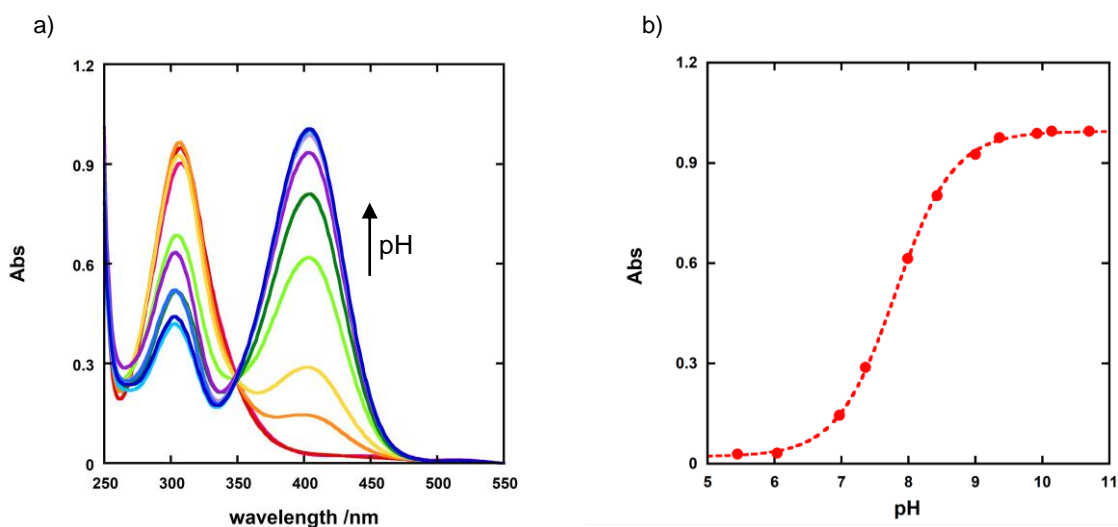


Figure 3.4a) UV-spectra of 0.05 mM 4-nitrophenol solutions at different pH, using 50 mM Buffer. Increasing the pH (red to blue) the absorbance band shows a maximum at 400 nm, assigned to 4-nitrophenolate; b) Titration curve obtained by the absorbance value at 400 nm, plotted against the pH. Buffer used: MES, HEPES, CHES and CAPS

As reported by Barbosa *et al.* in their study on the preferential solvation of carboxylic acids in acetonitrile and water mixtures, up to 3 pK unit shifts can be observed by changing the

acetonitrile from 10 to 70% (w/w).¹⁰⁸ Similarly, the 40% (v/v) mixture, which can preferentially enhance the solvation of the neutral rather than the charged species, alters the pK_a of 4-nitrophenol and causes the reported shift. To assess the impact caused by the acetonitrile on the reactivity of the catalysts, **3-10** (Figure 3.5), which has been studied extensively in fully aqueous solution,⁵² was investigated at increasing percentages of the organic solvent. The HPNPP transesterification catalysed by **3-10** at pH 7.4 and 25 °C was followed at 30, 40 and 50% (v/v) of acetonitrile in water, monitoring the 4-nitrophenolate peak appearance at 400 nm over time (Figure 3.6a).

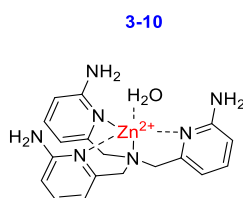


Figure 3.5 Structure of 3-10

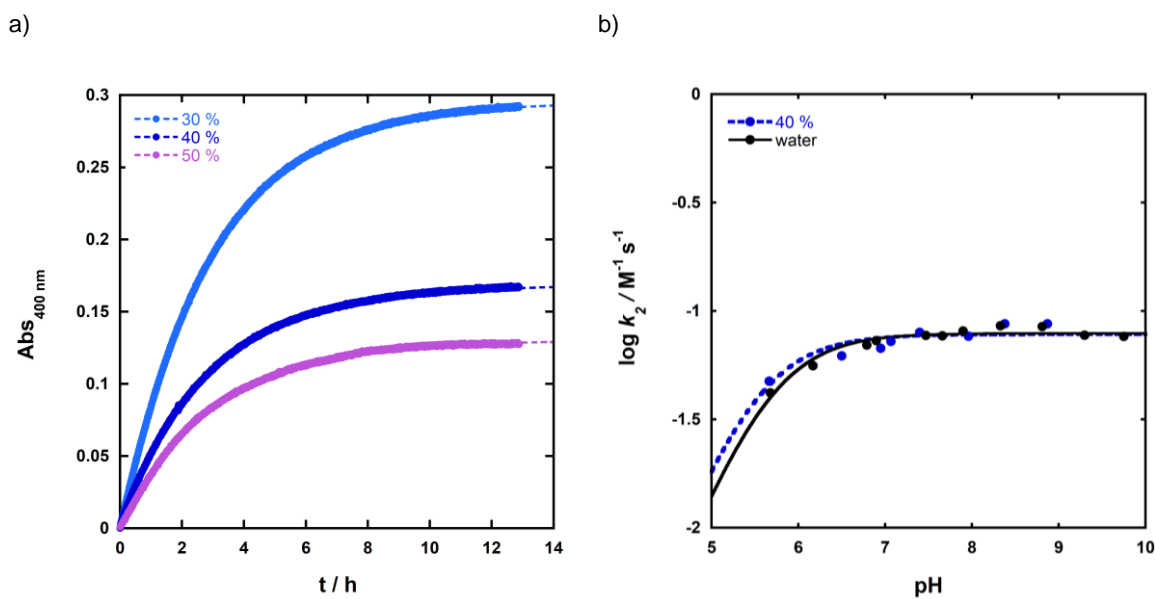


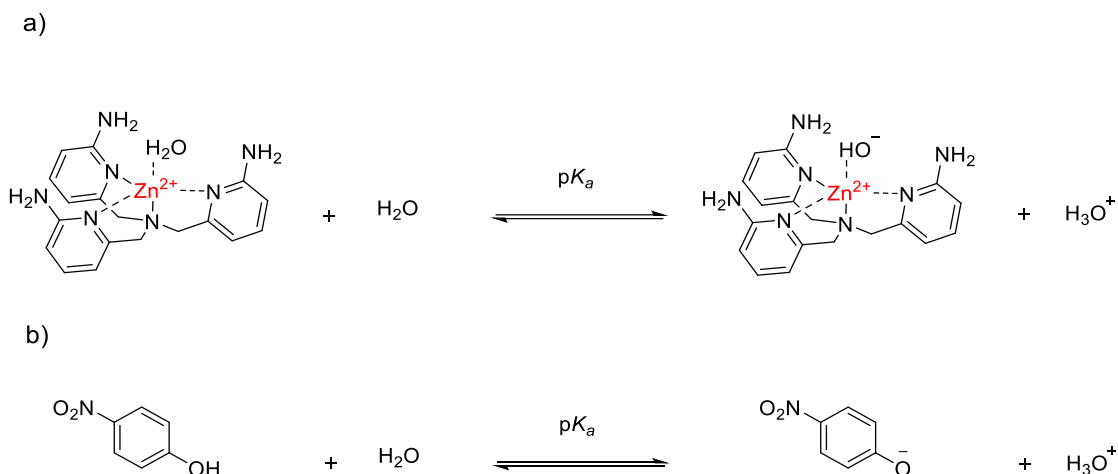
Figure 3.6 a) HPNPP transesterification catalysed by **3-10** at pH 7.4 and 25 °C in a reaction mixture containing 30(light blue), 40 (blue) and 50 (purple)% (v/v) of acetonitrile in water. Appearance of 4-nitrophenolate peak at 400nm over time. The data fitting through equation (2) yielded the k_{obs} reported in the table. [HPNPP] = 0.05 mM, [**3-10**] = 1 mM, [HEPES] = 50 mM, ionic strength (0.1 M) regulated by addition of $NaNO_3$. b) Comparison between pH rate profiles for the transesterification of 0.05 mM HPNPP catalysed by **3-10** at 25 °C in water (●)⁵² and 40%(v/v) acetonitrile in water (●). [Buffer]=50 mM and ionic strength fixed at 0.1 M by addition of $NaNO_3$

$$(2) \quad [P] = [P_{\infty}] (1 - e^{-k_{obs} t}) \quad (15) \quad k_2 = k_2^{max} \frac{K_a}{K_a + [H^+]}$$

Table 3.1 k_{obs} values gained by fitting the data reported in graph a by equation (2)

ACN (v/v) %	k_{obs} / s^{-1}
30	$9.58 \pm 0.03 \times 10^{-5}$
40	$9.68 \pm 0.01 \times 10^{-5}$
50	$9.59 \pm 0.01 \times 10^{-5}$

Due to the perturbation of 4-nitrophenol pK_a previously discussed, the three curves' endpoints differ, but no alteration of k_{obs} was detected (Figure 3.6 and Table 3.1). The pH rate profile for the second order rate constant for the transesterification of HPNPP catalysed by **3-10** was not changed significantly by added acetonitrile as shown by the overlap between the data reported in the literature (black dots) and the new values (blue dots) in Figure 3.6b. The pH values were measured by pH electrode InLab Micro at the end of the experiment. Fitting equation (15) to the data gives a second-order limiting rate constant of $7.8 \pm 0.2 \times 10^{-2} M^{-1} s^{-1}$ and kinetic pK_a of 5.5 ± 0.1 which are in close agreement with the literature values for the reaction under fully aqueous conditions: $7.9 \pm 0.1 \times 10^{-2} M^{-1} s^{-1}$ and 5.7 ± 0.1 . The kinetic pK_a extrapolated from the pH profile, which refers to the dissociation equilibrium involving the complex's aqua and hydroxy form (Scheme 3.6a), was barely affected by the addition of acetonitrile.



Scheme 3.6 Deprotonation equilibria of 3-10 (a) and 4-nitrophenol (b)

In contrast with the equilibrium of nitrophenol (Scheme 3.6b), there is no change in the overall charge for the complex's dissociation. Therefore, the equilibrium was not influenced by the dielectric constant variation but rather by the solute-solvent interaction and the ability of the medium to solvate one or the other charged species.

The lack of alteration in reaction rate with this solvation change can be compared with reports for related processes. Selmeçzi *et al.* have also investigated HPNPP transesterification, catalysed by their binuclear Zn(II) complexes in water/DMSO (70/30) mixture and DMSO.¹⁰⁹ The transesterification rate was 34-fold higher in DMSO than in the aqueous mixture, and different mechanisms were proposed for the two different conditions. Sigel and coworkers have observed that 50% (v/v) of dioxane in water enhanced the Zn(II)-promoted dephosphorylation of ATP by a factor of 15, which they explained in terms of an increased stabilisation of metal ion complexes with ligands having a negatively charged oxygen as a donor group.¹¹⁰ Anhydrous ethanol and methanol have also been used for

mimicking the presumed lower dielectric constant of enzymatic active site and have shown a remarkable increase in the reaction rate for the catalysis of HPNPP by a dinuclear Zn(II) complex.⁶⁴ However, these examples either involved more highly charged substrates or much higher fractions of the organic component to show large differences relative to the fully aqueous conditions than we have used (molar fraction of acetonitrile χ_i less than 20%). This suggests that our data were not significantly perturbed by the solvent composition and the effects observed can be expected to be applicable to fully aqueous solution too.

Active complexes

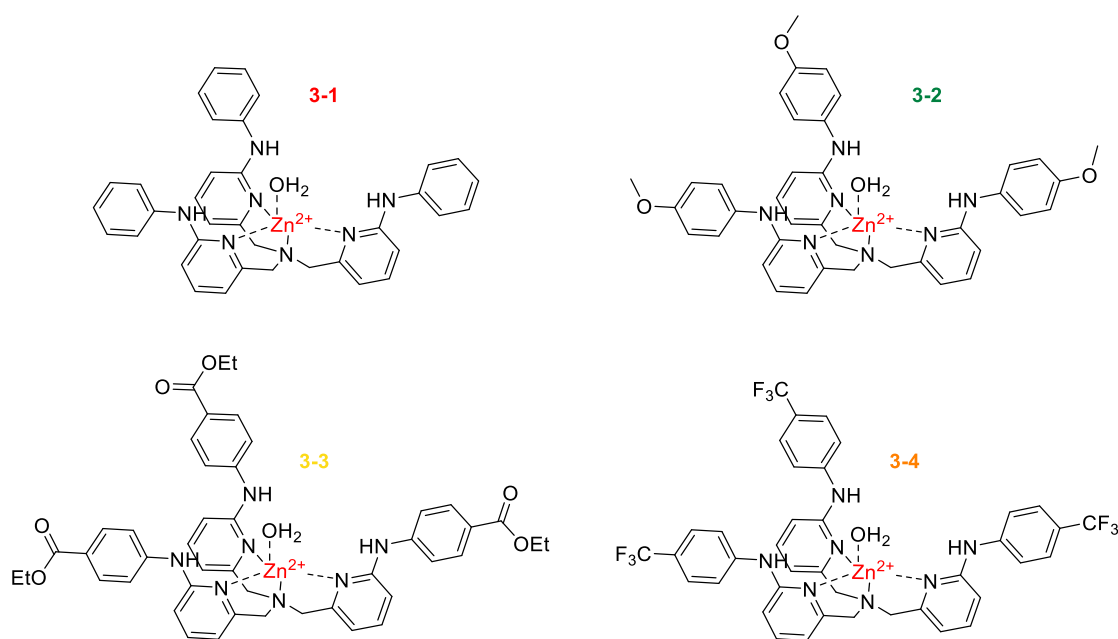


Figure 3.7 Structure of the different catalysts

Similarly to the tris(pyridin-2-ylmethyl)amine complex, **3-1** and **3-2** exhibited strong binding with Zn(II). The complexation properties were evaluated by monitoring the UV spectra of the compounds during a ZnCl₂ titration at pH 7, 7.4 and 8 (Figure 3.8a and b for

3-1 and **3-2** at pH 7.4). Under these conditions, the binding of the Zn(II) to the ligand was found to be sufficiently strong that the stoichiometry was well defined, but the binding constant cannot be readily determined.

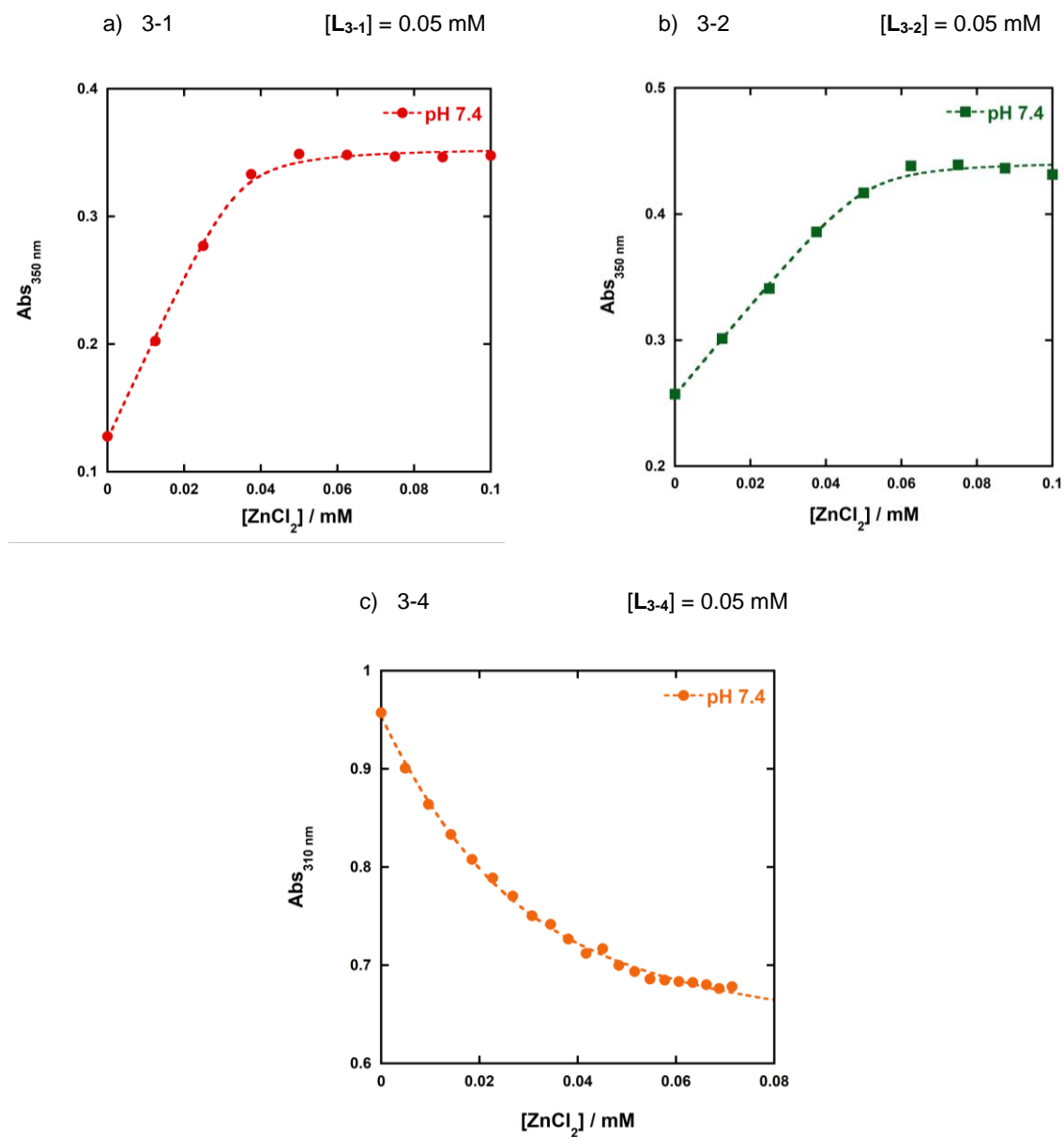


Figure 3.8 Zn(II) titration of 3-1(a), 3-2 (b) and 3-4 (c) at pH 7.4. $[3-n] = 0.05 \text{ mM}$, $[ZnCl_2] = 0 - 0.1 \text{ mM}$, $[HEPES] = 50 \text{ mM}$

$$(16) \quad Abs = Abs_0 \frac{\left([L_{3-n}]_T + [Zn^{2+}] + \frac{1}{K_d}\right) - \sqrt{\left([L_{3-n}]_T + [Zn^{2+}] + \frac{1}{K_d}\right)^2 - 4[L_{3-n}]_T[Zn^{2+}]}}{2}$$

This confirmed tight binding between the ligand and Zn(II) even at a concentration 10 times lower than the one used in the experimental kinetic conditions. In contrast to this result, the ZnCl₂ titration of **L3-4** showed a weak but persistent 1:1 binding within the pH range studied (7-8), as reported for the experiment at pH 7.4 in Figure 3.8c, and the fitting of equation (1) give a binding constant of $70 \pm 20 \text{ mM}^{-1}$. A pH dependent Zn(II) binding behaviour was found for **L3-3** (Figure 3.9). At lower pH (Figure 3.9a) the titration plot displayed a sharp change of absorbance at 326 nm by addition of 0.5 eq of ZnCl₂, suggesting the formation of a 2:1 (ligand:Zn(II)) adduct. This unexpected behaviour was partially lost at pH 7.4 and 8 (Figure 3.9b and c), where the complexation curves, although different, showed a weak 2:1 binding. The data were fitted to a 2:1 (**L3-3**:Zn(II)) model by Bindfit, the online tool for supramolecular chemistry research and analysis offered by Thordarson,¹¹¹ which yielded the binding constants reported in Table 3.2. Even though the adduct was formed, the kinetic experiment, where the ratio between ligand and Zn(NO₃)₂ was kept 2:1, did not show any effect on the system reactivity. The observed rate constant k_{obs} for transesterification of 0.05 mM HPNPP catalysed by 0.25 mM **3-3** at pH 7 is $3.592 \pm 0.002 \times 10^{-5} \text{ s}^{-1}$, which was approximately 2-fold higher than the value found when the same concentration of ligand and half an equivalent of Zn(NO₃)₂ are used ($1.642 \pm 0.001 \times 10^{-5} \text{ s}^{-1}$).

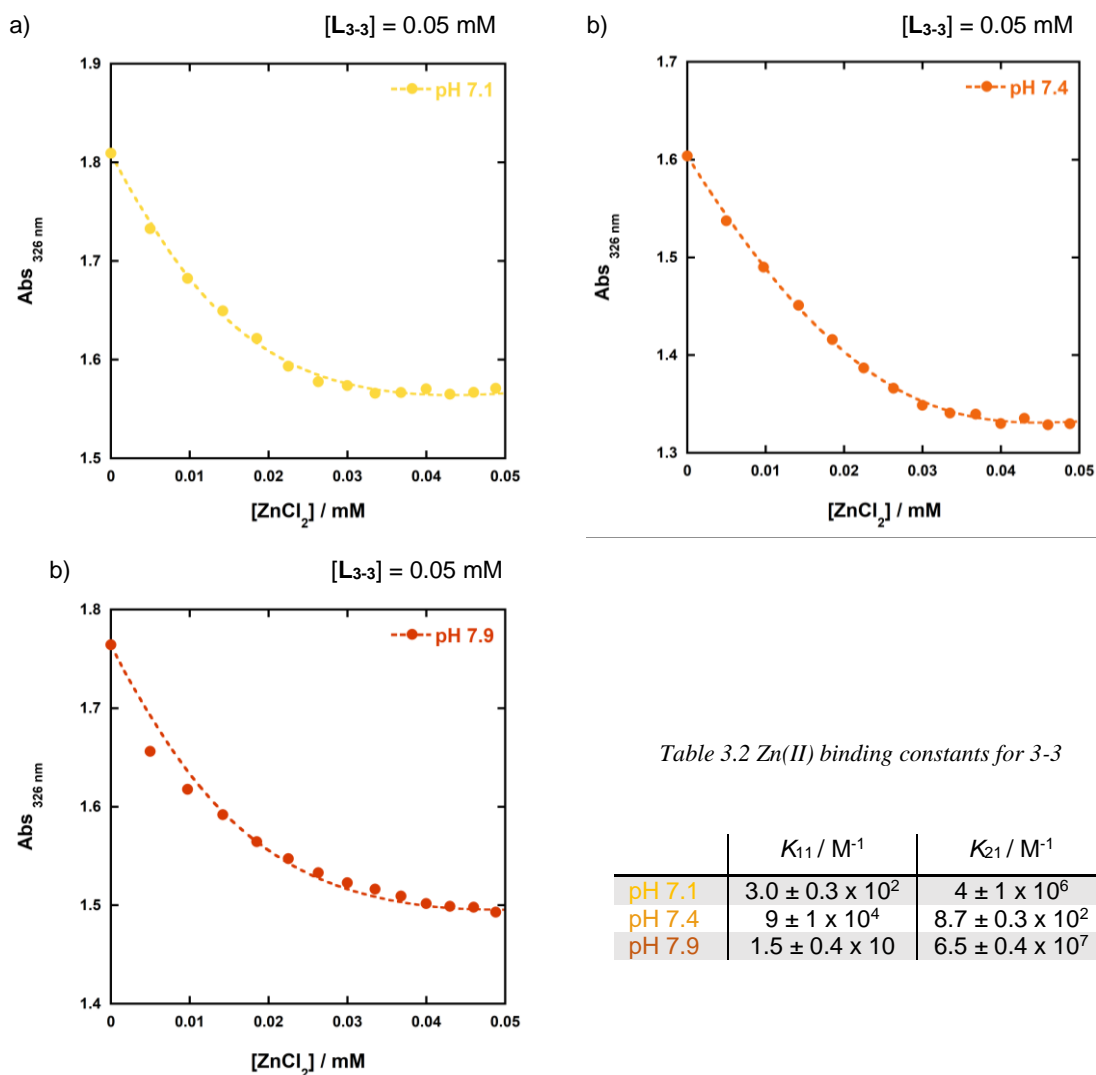


Figure 3.9 Zinc titration experiments. Plots of Absorbance at 326 nm against the equivalent ZnCl_2 (0 - 0.75 mM) at pH 7 (a), 7.4 (b) and 8 (c); $[L_{3-3}] = 0.05 \text{ mM}$, $[\text{Buffer}] = 50 \text{ mM}$, 40% (v/v) acetonitrile in water

As described below, given the linear dependence of k_{obs} on the complex concentration, the rate is more likely to be due to the concentration of **3-3** being equal to 0.125 mM (equal to the Zn(II) concentration) than a poorly active dimeric adduct.

The complexes undergo multiple turnovers as shown by a ^{31}P NMR experiment (Figure 3.10): 1.5 mmol of HPNPP were efficiently cleaved by 0.1 mM of **3-2** at pH 7.4, producing

the cyclic diester, whose stability to hydrolysis has been monitored and confirmed over 7 days. The disappearance of the substrate signal at -5.27 ppm (triplet - Figure 3.10c) matched the rise of the doublet of triplets characteristic of the above mentioned product at 19.65 ppm (Figure 3.10b), suggesting the cleavage of HPNPP did not include the formation of an intermediate.

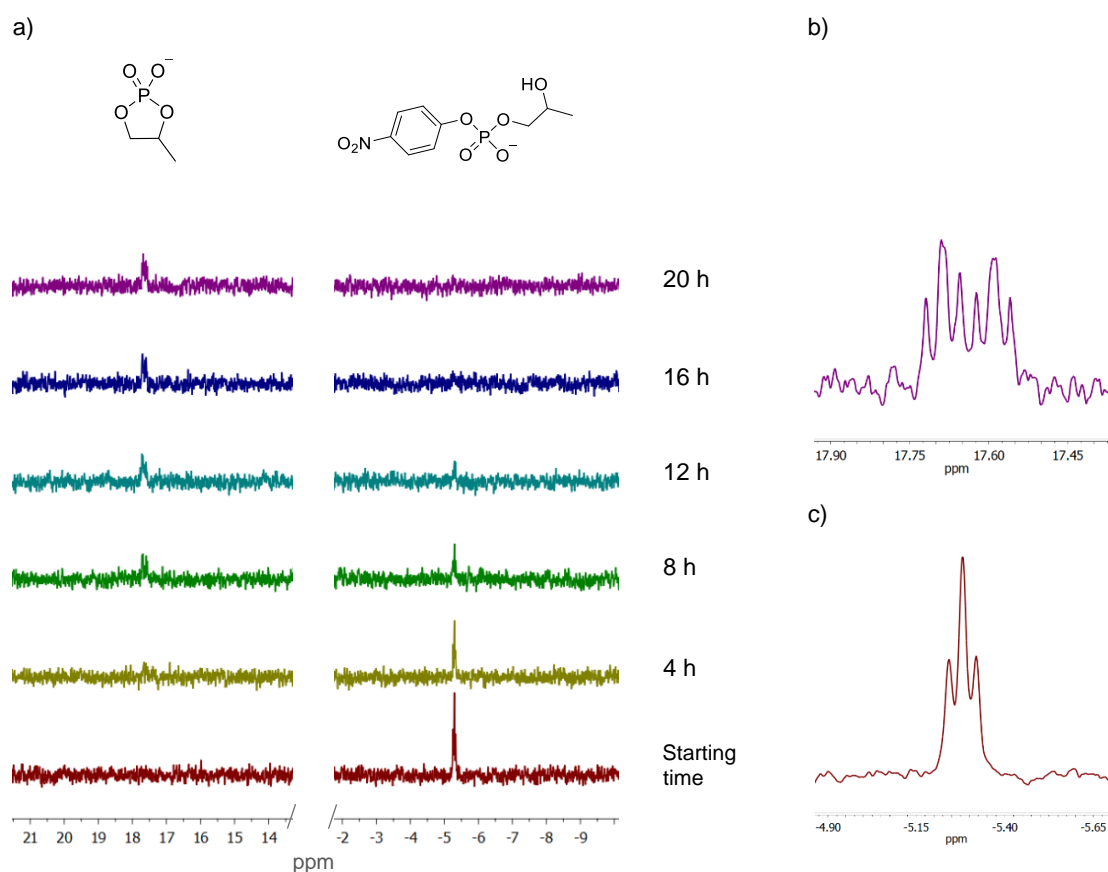
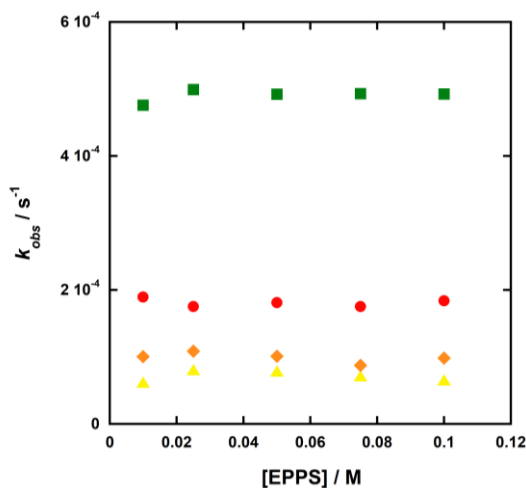


Figure 3.10 ^{31}P NMR experiment. Transesterification of 1.5 mM HPNPP catalysed by 0.1 mM of 3-2 at pH 7.3 and 25°C ([HEPES] = 50 mM, ionic strength at 0.1 M by addition of NaNO_3); a) ^{31}P NMR spectra over time; b) product signal after 7 days; c) substrate signal at t_0

As seen for the previously reported complex **3-10**, the cleavage reaction of HPNPP catalysed by **3-1**, **3-2**, **3-3** and **3-4** displayed a first order dependence on the substrate (0.01

- 0.1 mM, experimental paragraph) and was independent of buffer concentration (0.01 - 0.1 M, Graph 3.2), excluding the involvement of general acid or base catalysis.



Graph 3.2 Plot of observed rate constants for the transesterification of HPNPP at pH 7.4 and 25°C catalysed by 3-1 (●), 3-2 (■), 3-3 (▲) and 3-4 (◆) reported against EPPS concentration; (ionic strength at 0.1 M by addition of NaNO₃, [HPNPP]=0.05 mM, [3-n] = 0.5 mM)

When **3-1** and **3-2** were used as catalysts, the observed rate constants similarly showed a first order behaviour against the complex concentration (0.1 - 2 mM, Figure 3.11a). Although there is a similar dependence at lower concentrations for **3-3** and **3-4**, a deviation from linearity was observed over 1 mM as shown in Figure 3.11 b and c. All the complexes revealed second order rate constant values higher than the one observed for **3-10**. With a k_2 of $1.10 \pm 0.01 \text{ M}^{-1} \text{ s}^{-1}$, **3-2** was found to be the most active catalyst, followed by **3-1**, **3-4** and **3-3** (k_2 values are reported in Table 3.3).

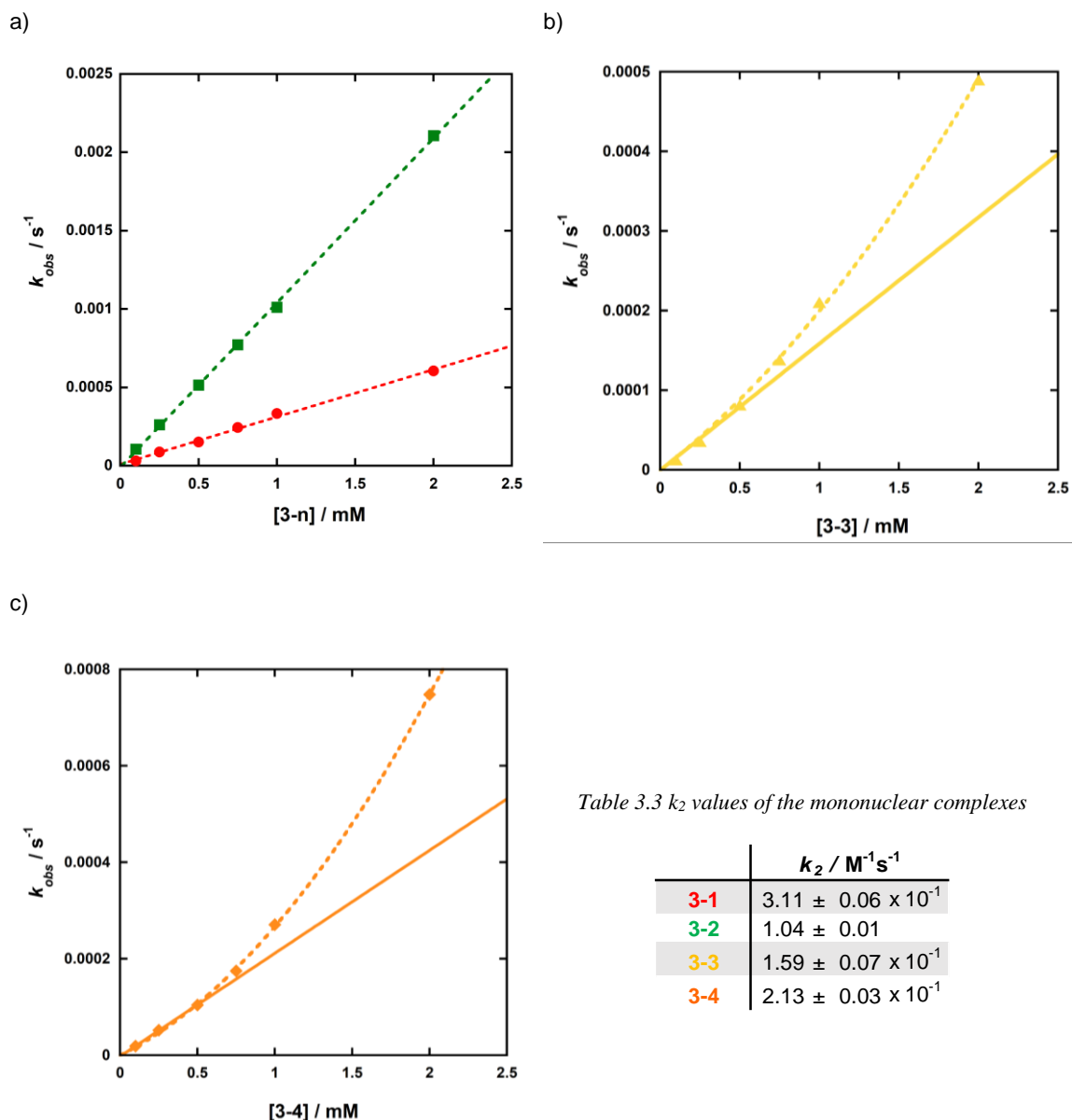
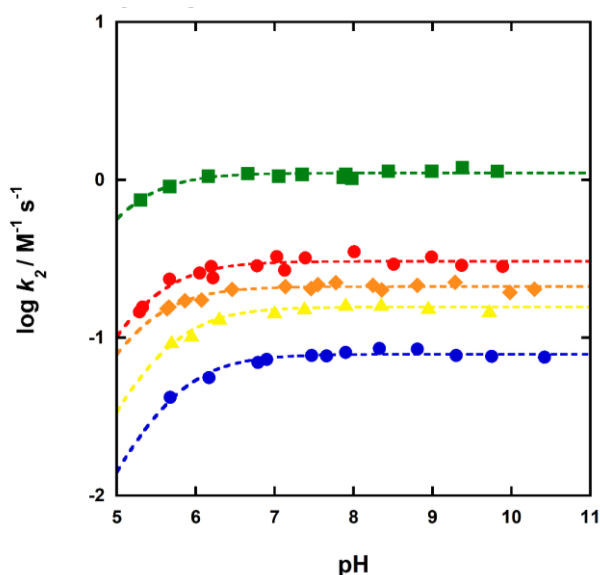


Figure 3.11 a) Plots of the observed rate constants for the transesterification of HPNPP at pH 7.4, 25°C in 40% (v/v) acetonitrile in water against the complex concentration: a) 3-1 (●), 3-2 (■), b) 3-3 (▲) and c) 3-4 (◆) ([EPPS] = 50 mM, [HPNPP] = 0.5 mM, ionic strength at 0.1 M by addition of NaNO₃)

The data showed that a 1 mM solution of **3-2** could reduce the half-life time of HPNPP to about 12 min at pH 7.4, making the complex 10-fold more reactive than **3-10**.

Considering a linear dependence of k_{obs} on the complex concentration in the pH range between 5 and 11, we plotted the second order rate constants for **3-1** (red dots), **3-2** (green squares), **3-3** (orange triangles) and **3-4** (yellow diamonds) against the pH in Graph 3.3.



$$(15) \quad k_2 = k_2^{\max} \cdot \frac{K_a}{K_a + [H^+]}$$

Graph 3.3 pH profile of second order rate constant for **3-1** (●), **3-2** (■), **3-3** (▲), **3-4** (◆) and **3-10** (●), [HPNPP] = 0.05 mM [Buffer] = 50 mM, ionic strength at 0.1 M by addition of NaNO₃ and 25°C

Table 3.4 Second order rate constants for the transesterification of HPNPP at pH 7.4 ([EPPS] = 50 mM, ionic strength at 0.1 M by addition of NaNO₃ catalysed by the mononuclear complexes

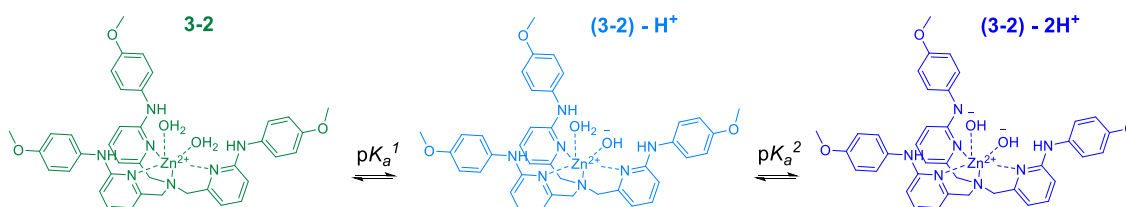
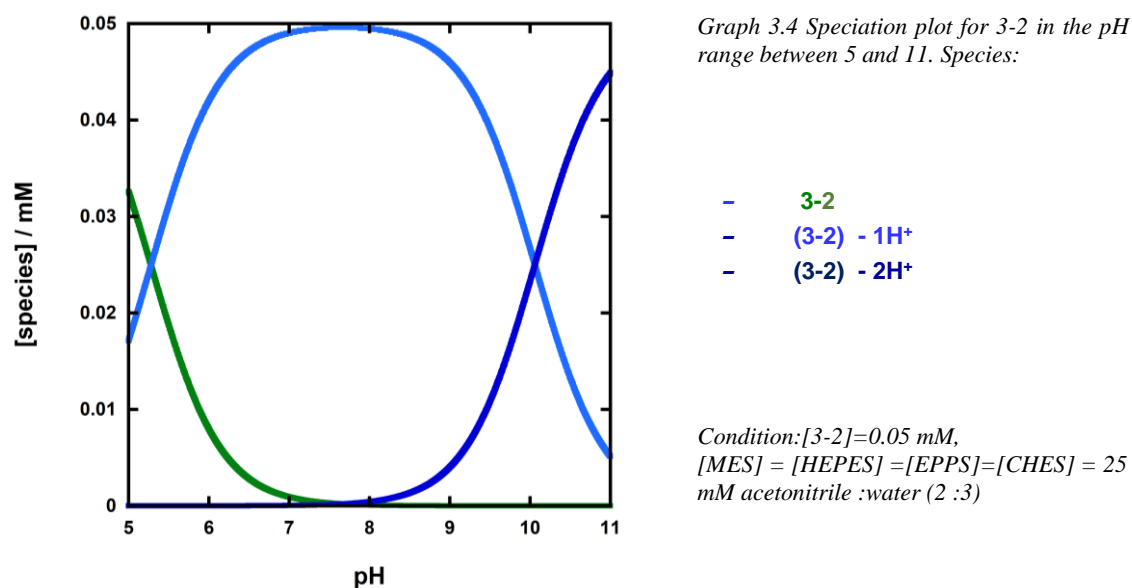
Complex	$k_2^{\max} / \text{M}^{-1} \text{s}^{-1}$	$\text{p}K_a$
3-1	0.30 ± 0.01	5.30 ± 0.05
3-2	1.10 ± 0.02	5.04 ± 0.05
3-3	0.16 ± 0.01	5.39 ± 0.06
3-4	0.21 ± 0.01	5.23 ± 0.05
3-10	$0.080 \pm 0.001^*$	$5.66 \pm 0.05^*$
3-10	0.078 ± 0.003	5.51 ± 0.10

*Literature value in water

The nonlinear least-squares fitting of these data with equation (15) yielded the kinetic $\text{p}K_a$ and k_2 values reported in Table 3.4. As a comparison, the following plot also includes the

pH rate profile for **3-10** (blue dots), which showed analogous behaviour. Thus, the first data interpretation would suggest that the complex, once deprotonated, reaches its maximum activity, making the Zn-hydroxo form its most active species.

As confirmed by UV titration experiments, the hydroxo form is indeed the major species in the pH range between 6 and 10. The experiment was performed following the change in the UV spectra while raising the pH by NaOH addition. The theoretical fit of the raw data, carried out with HypSpec and HySS,⁸⁸ defined the speciation plot shown in Graph 3.4 for **3-2**. The pK_a values for all the mononuclear complexes and those of the relative ligands are described in Table 3.5



Scheme 3.7 Proposed deprotonation equilibria for 3-2

Table 3.5 pK_a values obtained from the UV-titration curved fitted with the Hypspec software

	complex		ligand		
	pK_a^1	pK_a^2	pK_a^1	pK_a^2	pK_a^3
3-1	5.32	10.12	5.68	8.49	10.08
3-2	5.04	10.3	5.34	7.84	10.64
3-3	5.54	8.50	6.98	9.50	11.18
3-4	5.43	10.08	6.25	7.84	10.05

The high values of the second order rate constants reported in Table 3.3 might be due to tight substrate binding or high reactivity of the adduct substrate:complex (or a combination of the two aspects). To measure the real improvement provided by the formation of the adduct, inhibition experiments have been performed using as an inhibitor dimethyl phosphate (DMP) at pH 6 and 7 or phenyl phosphate (PP) at pH 7, 8 and 9. Unfortunately, due to precipitation, **3-3** and **3-4** were tested only using DMP. However, the analogous measure for **3-10** confirmed the values reported in the literature with good agreement.⁵² The following graphs present the study for **3-1** (Figure 3.11a - b) and **3-2** (Figure 3.11c - d). First, the analysis was performed measuring the observed rate constant k in the presence of different concentrations of the inhibitor; the value was then normalised by the observed rate constant k_0 (measured in the absence of the inhibitor) and reported against the concentration of either DMP or PP.

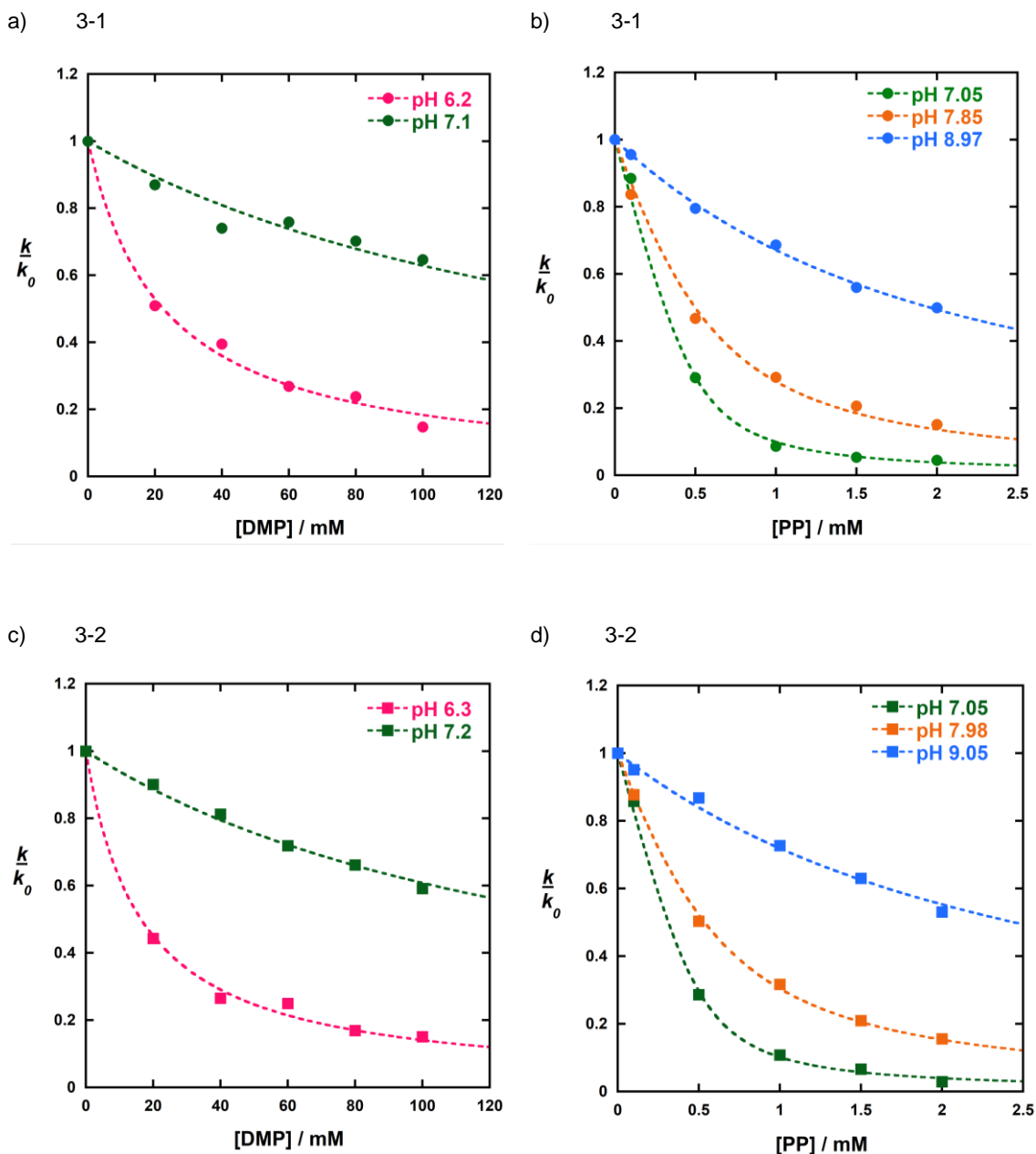
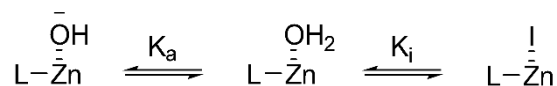


Figure 3.12 Inhibition studies for 3-1 : a) k_{obs}/k_0 reported against the concentration of DMP at pH 6.2 (●) and 7.1 (●); the dashed lines are the least square fits of equation (8) to the data; b) k_{obs}/k_0 reported against the concentration of PP at pH 7.1 (●), 7.9 (●) and 9.0 (●); the dashed lines are the least square fits of equation (10); Inhibition study for 3-2: c) k_{obs}/k_0 reported against the concentration of DMP at pH 6.3 (■) and 7.2 (■); the dashed lines are the least square fits of equation (8) to the data; d) k_{obs}/k_0 reported against the concentration of PP at pH 7.1 (■), 8.0 (■) and 9.1 (■) the dashed lines are the least square fits of equation (10); experimental condition: [3-n]=0.5 mM, [HPNPP]=0.05 mM, [Buffer] = 50 mM, ionic strength at 0.1 M by addition of NaNO₃, 25 °C, 40%(v/v) acetonitrile in water.

The presence of an additional ester in solution introduced a further equilibrium in the reaction scheme. The inhibitor competes with the substrate for binding the complex, and as expected, increasing the concentration reduces the reaction rate and the ratio k/k_0 . This effect was most evident in the presence of the tightly-binding monoester PP, while it required higher concentrations of DMP to be detected. Based on the pH dependence of k_2 , the kinetic pK_a of **3-1** and **3-2** were equal to 5.30 ± 0.05 and 5.04 ± 0.05 respectively, and under these experimental conditions the mono-deprotonated form of the complexes were the main species. If the hydroxy form was also the active species, for pH values over the pK_a of the complexes, the presence of the DMP and PP would perturb the reaction rate in the same way regardless of the pH. As shown in the graphs, the ratio k/k_0 strongly depended on the pH, suggesting the inhibitors and the substrate did not bind to the hydroxy but to the aqua form of the complex. In these experimental conditions, the concentration of active aqua form Cx depends on both the deprotonation and inhibition equilibrium (Scheme 3.8).



Scheme 3.8 Inhibition binding compared to the deprotonation equilibrium of the bound water molecule

$$(17) \quad [Cx]_T = [Cx \cdot OH^-] + [Cx] + [Cx \cdot I]$$

$$K_a = \frac{[Cx \cdot OH^-][H^+]}{[Cx]} \qquad K_i = \frac{[Cx][I]}{[Cx \cdot I]}$$

Taking into account K_a and K_i , the expression of the total concentration of the complex $[Cx]_T$ (17) can be rearranged in the following equation (18),

$$(18) \quad [Cx]_T = [Cx] + \frac{[I]_T [Cx]}{[Cx] + K_i} + \frac{K_a [Cx]}{[H^+]}$$

which, for $K_i \gg [Cx]$ (relative to $[I] \gg [Cx]$), can be simplified as shown in equation (19):

$$(19) \quad [Cx]_T = [Cx] + \frac{[I]_T [Cx]}{K_i} + \frac{K_a [Cx]}{[H^+]}$$

The concentration $[Cx]$ in the presence of inhibitor is then expressed by equation (20).

$$(20) \quad [Cx] = \frac{K_i [H^+]}{K_i [H^+] + [H^+][I] + K_a K_i}$$

In the absence of an inhibitor, the observed rate constant k_0 of the reaction is given by equation (21), which can be rearranged expressing the ratio k_{obs}/k_0 proportional to Cx (equation (22)):

$$(21) \quad k_0 = k_{obs} = k [Cx] = k \frac{[H^+]}{[H^+] + K_a} [Cx]_T$$

$$(22) \quad \frac{k [Cx]}{k_0} = \frac{[H^+] + K_a}{[H^+][Cx]_T} [Cx]$$

where $k [Cx] = k_{obs}$ is the observed rate constant at a specific concentration of Cx. Substituting (20) in equation (22), the ratio k_{obs}/k_0 is defined by the hyperbolic function (23).

$$(23) \quad \frac{k_{obs}}{k_0} = \frac{K_i^{obs}}{[I] + K_i^{obs}} \quad \text{where:} \quad (24) \quad K_i^{obs} = \frac{[H^+] + K_a}{[H^+]} K_i$$

As the concentration of PP and complex used in the experiments were of the same order of magnitude, no approximations can be made and, therefore, expression (23) can only be used to fit the data when DMP was used. Equation (25), obtained similarly from (18), was used to fit the PP data. The more laborious calculations used are reported by Feng *et al.*⁵²

$$\frac{k_{obs}}{k_0} = \frac{1}{2} (1 - x - y + \sqrt{(1 + x + y)^2 - 4x}) \quad (25) \quad \text{where:}$$

$$x = \frac{[I]}{[Cx]_T}$$

$$y = \frac{K_i^{obs}}{[Cx]_T}$$

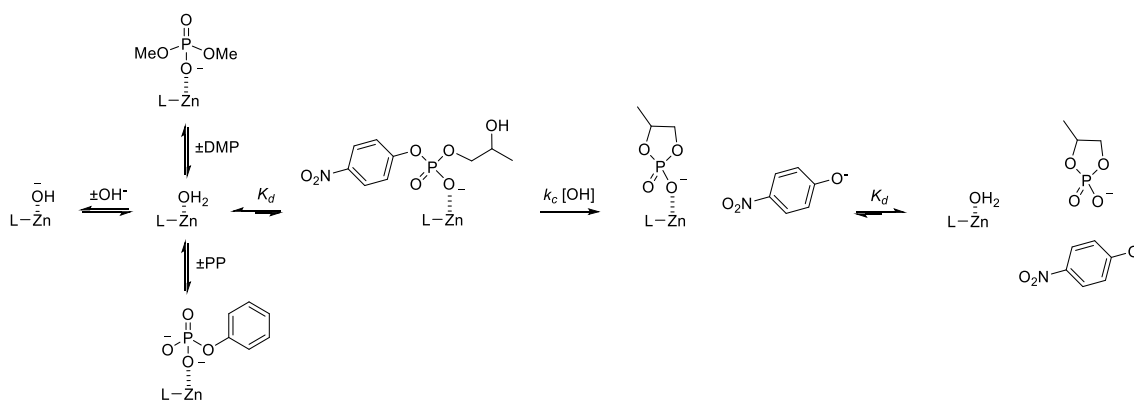
The K_i values for the binding of PP and DMP for the mononuclear complexes and **3-10** are reported in Table 3.6.

Table 3.6 Inhibition binding constants of the PP and DMP for 3-n obtained from the equation (9)

Complex	K_i	
	PP / μM	DMP / mM
3-1	0.34 ± 0.02	2.58 ± 0.06
3-2	0.24 ± 0.01	1.03 ± 0.14
3-3	-	5.45 ± 0.39
3-4	-	4.51 ± 0.03
3-10	1.93 ± 0.33	$10 \pm 2^*$

*Literature value

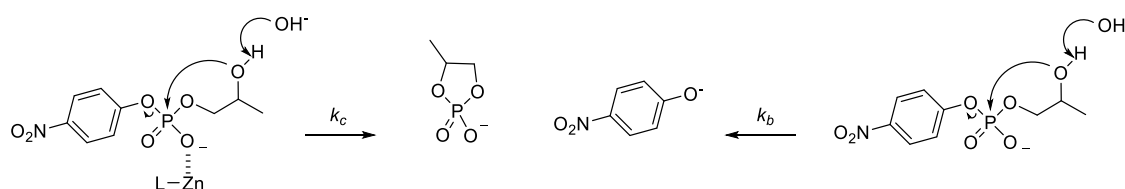
The proposed mechanism of the transesterification of HPNPP catalysed by the mononuclear complexes is shown in Scheme 3.9.



Scheme 3.9 Proposed mechanism of the transesterification of HPNPP catalysed by the mononuclear complexes

As demonstrated by the inhibition experiments, the substrate bound to the aqua form of the complex underwent base-catalysed transesterification. The behaviour of k_2 was explained considering two simultaneous events; while moving to higher pH values, the increase of the hydroxide concentration compensates for the proportional decrease of the protonated species and, therefore, the observed plateau results from the combination of descendent (active catalyst) and ascendant (hydroxide) linear concentration trends. The inhibition

constants obtained from the DMP experiments were taken as a good approximation for the substrate binding constant K_d . As reported in the proposed mechanism (Scheme 3.9), the catalyst activity might either depend on a strong binding of the substrate to the complex active form or the intrinsic reactivity of the substrate:complex adduct. This study gave an insight into the moiety that would represent the conjugated catalytic headgroup of the artificial enzymes designed for the cleavage of RNA or DNA. As the binding to the nucleic acid would rely on the recognition portion of the macro catalyst, the complex would be responsible only for the cleavage. Therefore, if the reported activity of the complexes is mainly the result of a high binding constant (low value of K_d) and not k_c , their use in the artificial enzymes would be less effective. The benefit on the reaction rate given by the coordination was calculated by comparing the k_c , rate constant when the adduct substrate-complex is formed, with k_b , the base catalysed rate constant of the background reaction (Scheme 3.10).



Scheme 3.10 Two possible reaction pathways

The rate of the reaction is described by:

$$(26) \quad \text{rate} = k_c [Cx \cdot S][OH^-]$$

where $[C_x \cdot S]$ is the concentration of the activated subtracted-complex adduct. Considering the substrate binding equilibrium and the relative constant K_d (27), $[C_x \cdot S]$ is given by equation (28):

$$(27) \quad K_d = \frac{[C_x \cdot H_2O][S]}{[C_x \cdot S]}$$

$$(28) \quad [C_x \cdot S] = \frac{[C_x \cdot H_2O][S]}{K_d}$$

Since the equilibrium between the aqua and hydroxy form of the complex (Scheme 3.11), expressing $[C_x \cdot H_2O]$ and $[C_x \cdot OH^-]$ as functions of the pK_a by (30) and (31),



Scheme 3.11 Equilibrium between the aqua and hydroxy form of the complex

$$(29) \quad K_{eq} = \frac{[C_x \cdot H_2O][OH^-]}{[C_x \cdot OH^-]}$$

$$(30) \quad [C_x \cdot H_2O] = \frac{[H^+]}{[H^+] + K_a} \cdot [C_x]_T$$

$$(31) \quad [C_x \cdot OH^-] = \frac{K_a}{[H^+] + K_a} \cdot [C_x]_T$$

equation (29) can be rearranged in:

$$(32) \quad K_{eq} = \frac{[H^+][OH^-]}{[K_a]} = \frac{K_w}{K_a}$$

The reaction rate equation can then be reorganised by substituting in equations (28) and (32), as follows:

$$rate = k_c \frac{[Cx \cdot H_2O][S]}{K_d} [OH^-] = k_c \frac{K_{eq}}{K_d} [Cx \cdot OH^-][S] = k_c \frac{K_w}{K_d K_a} [Cx \cdot OH^-][S]$$

Above the pK_a of the complex, approximating $[Cx \cdot OH^-] = [Cx]_T$:

$$rate = k_c \frac{K_w}{K_d K_a} [Cx]_T [S] = k_2 [Cx]_T [S] \quad (33) \quad \text{hence:} \quad k_c = k_2 \frac{K_d K_a}{K_w} \quad (34)$$

where k_2 is the second order rate constant obtained experimentally.

The catalytic rate constants calculated by equation (34) are reported in Table 3.7. The rate accelerations provided by the HPNPP coordination to the novel complexes were significant and higher than that reported for **3-10**.

Table 3.7 Catalytic rate constants and acceleration of the transesterification of HPNPP catalysed by the mononuclear complexes

Complex	$k_c / M^{-1} s^{-1}$	k_c / k_b
3-1	4×10^5	6×10^6
3-2	1×10^6	1.5×10^7
3-3	2.5×10^5	4×10^6
3-4	3×10^5	4.5×10^6
3-10*	2×10^5	3×10^6

*Literature value

Although the K_d derived from the inhibition experiments was smaller than that found for the reference catalyst, the aryl substitution in all the complexes seemed to stabilise the transition state of the reaction. With the highest k_c value of $1 \times 10^6 s^{-1} M^{-1}$, **3-2** was nearly

10 times more reactive than **3-10**. All the complexes exhibited a higher reactivity than **3-10**, but the difference among the calculated k_c values of the novel catalysts is not big. Figure 3.13a, b and c show the Hammett plots of k_c reported against the σ^+ , σ and σ^- values,¹¹² respectively, of the substituents in the para position of the aniline ring. The plots highlights that the reactivity of the complex decreases as the strength of the hydrogen bond donor increases, and similar gradients are obtained by linear least square fitting of the data.

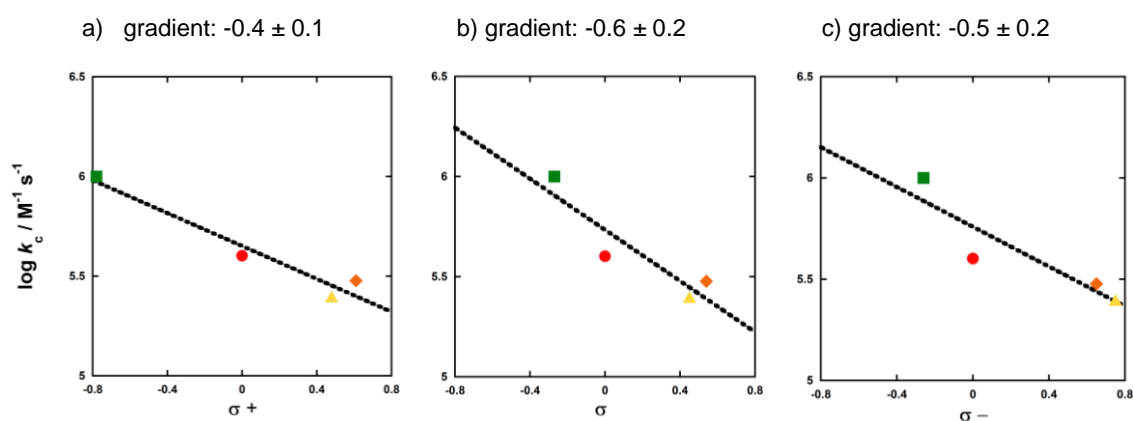


Figure 3.13 Hammett plots of k_c reported against the σ^- values of the para substituent of the aniline rings for the mononuclear complexes: **3-1** (●), **3-2** (■), **3-3** (▲) and **3-4** (◆); a) k_c values reported against σ^+ ; b) k_c values reported against σ ; c) k_c values reported against σ^-

This trend contrasts with that reported by Szymczak *et al.*,¹⁰⁴ where electron withdrawing groups lead to tighter binding, and seems to conflict with the assumption that a stronger hydrogen bond donor in the second coordination sphere would increase the reactivity of the catalysts. However, precipitation and sequential deactivation of **3-3** and **3-4** was observed when small PP concentrations were used. As reported in Figure 3.14a for **3-3**, the variation of the absorbance value at 400 nm over time was perturbed by precipitation in the presence of 0.1 mM (orange curve) and 0.5 mM (yellow curve) of inhibitor. As a reference, the curve for the HPNPP transesterification catalysed by **3-3** (0.5 mM) at pH 7 and 25 °C

is reported in red in the same graph (k_{obs} of $9.01 \pm 0.01 \times 10^{-5} \text{ s}^{-1}$). Although only an approximate k_{obs} value can be extrapolated for the experiment at 0.5 mM of PP ($\sim 10^{-6} \text{ s}^{-1}$), 0.1 mM of the inhibitor led to a 33% reduction of the observed rate constant. Therefore, assuming a linear inhibition trend (solid line in Figure 3.14b), if each 0.1 mM addition would cause a 33% reduction of k_{obs} , approximately 0.3 mM of PP should be necessary to shut down the catalyst's effect. Therefore, if a total complex concentration of 0.3 mM is used in equation (10), a good fit of the partial inhibition profile is obtained. This result contrasts with the PP inhibition experiments previously shown for **3-1** and **3-2**, suggesting that the catalytically active form of **3-3** (and **3-4**) might be further reduced in the experimental conditions. Unfortunately, the precipitation made this study unclear and, to some extent, unreliable, but this hypothesis cannot be excluded. As in the case of the sulfonamide substituents discussed in Chapter 2, the presence of electron-withdrawing groups might increase the acidity of the secondary amines in **3-3** and **3-4**. The formation of a deprotonated species would then decrease the concentration of the catalytically active form and lead to the underestimation of k_2 .

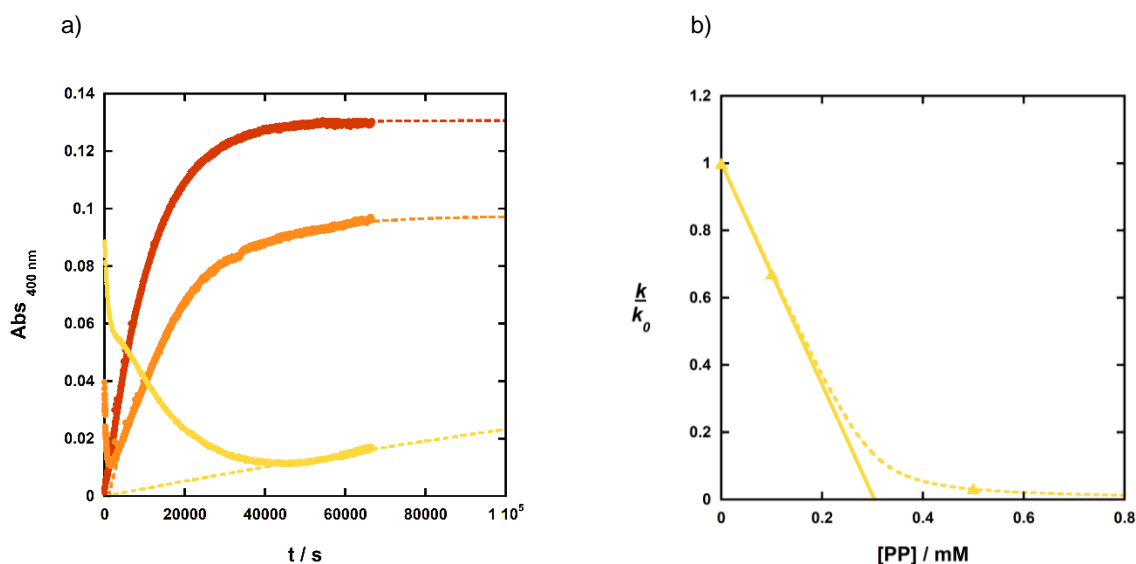


Figure 3.14 Attempt of PP inhibition experiment for the transesterification of HPNPP catalysed by **3-3** at 25 °C and pH 7.4; a) Absorbance at 400 nm over time. [PP] = 0 mM (red curve), 0.1 mM (orange curve) and 0.5 mM (yellow curve) b) Inhibition plot of the relative rate constant against the PP concentration; [3-3] = 0.5 mM, [EPPS] = 50 mM, ionic strength at 0.1 M by addition of NaNO₃, 40% (v/v) acetonitrile in water.

However, assuming that k_{obs} at pH 7 and 25 °C is due to a reduced catalyst concentration of approximately 0.3 mM, the second order rate constant for **3-3** would be $3 \times 10^{-1} \text{ M}^{-1} \text{ s}^{-1}$, equal to that of **3-1** and still 4 times smaller than the value obtained for **3-2**. The similarities between these values might suggest that the activity of the complexes might largely be due to the ligand scaffold. This hypothesis is also supported by the shallow gradient observed in the Hammett's plots of Figure 3.13a, b and c. The hydrophobic cavity, absent in **3-10**, could be responsible for the reactivity enhancement, which is lowered by additional effects in **3-3** and **3-4**. However, if the amine deprotonation were to occur in the pH range studied, the UV-titrations of the complexes would probably show a distinct change in their UV spectra while moving toward alkaline values. As reported in the experimental section, those changes were modest and seemed to be more likely related to the deprotonation of water molecules coordinated to the metal ions.

To test if the cavity was mainly responsible for the observed rate enhancement, we compared tetradentate to tridentate coordinating ligands. **3-6** was synthesised and studied (Figure 3.15). The catalyst presented two pyridyl moieties analogously functionalised with anisidine (equivalent to **3-2**) and an aliphatic chain enriched with a primary hydroxyl group.

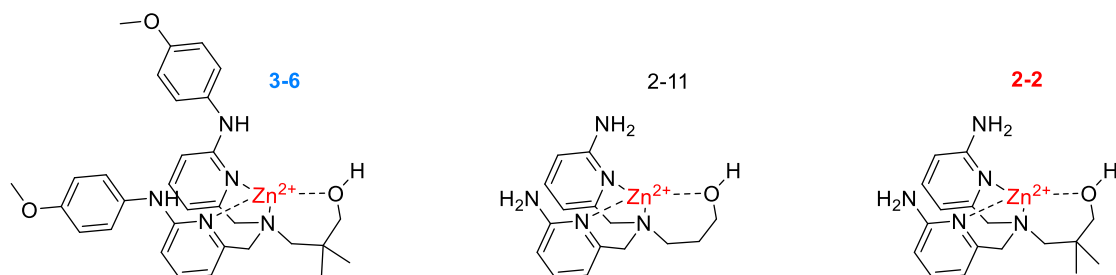


Figure 3.15 Structure of mononuclear complex for the cleavage of BNPP

As the complex has a nucleophile in its ligand structure, it was used as a catalyst for the cleavage of BNPP. At pH 7.4 and 25 °C, **3-6** displayed a first order dependence on complex (0.1 – 2.5 mM; Figure 3.16a) and substrate concentration (0.02 – 0.15 mM; Figure 3.16b); Figure 3.16c demonstrates that the reaction was not catalysed by the buffer concentration in the 0.05 – 0.1 M range. The second-order rate constant k_2 obtained for **3-6** was $4.8 \pm 0.5 \times 10^{-2} \text{ M}^{-1} \text{ s}^{-1}$, which is only 2-fold higher than the value reported in the literature for the comparable complex **2-11** where amines replace the anisidine groups.⁷⁸

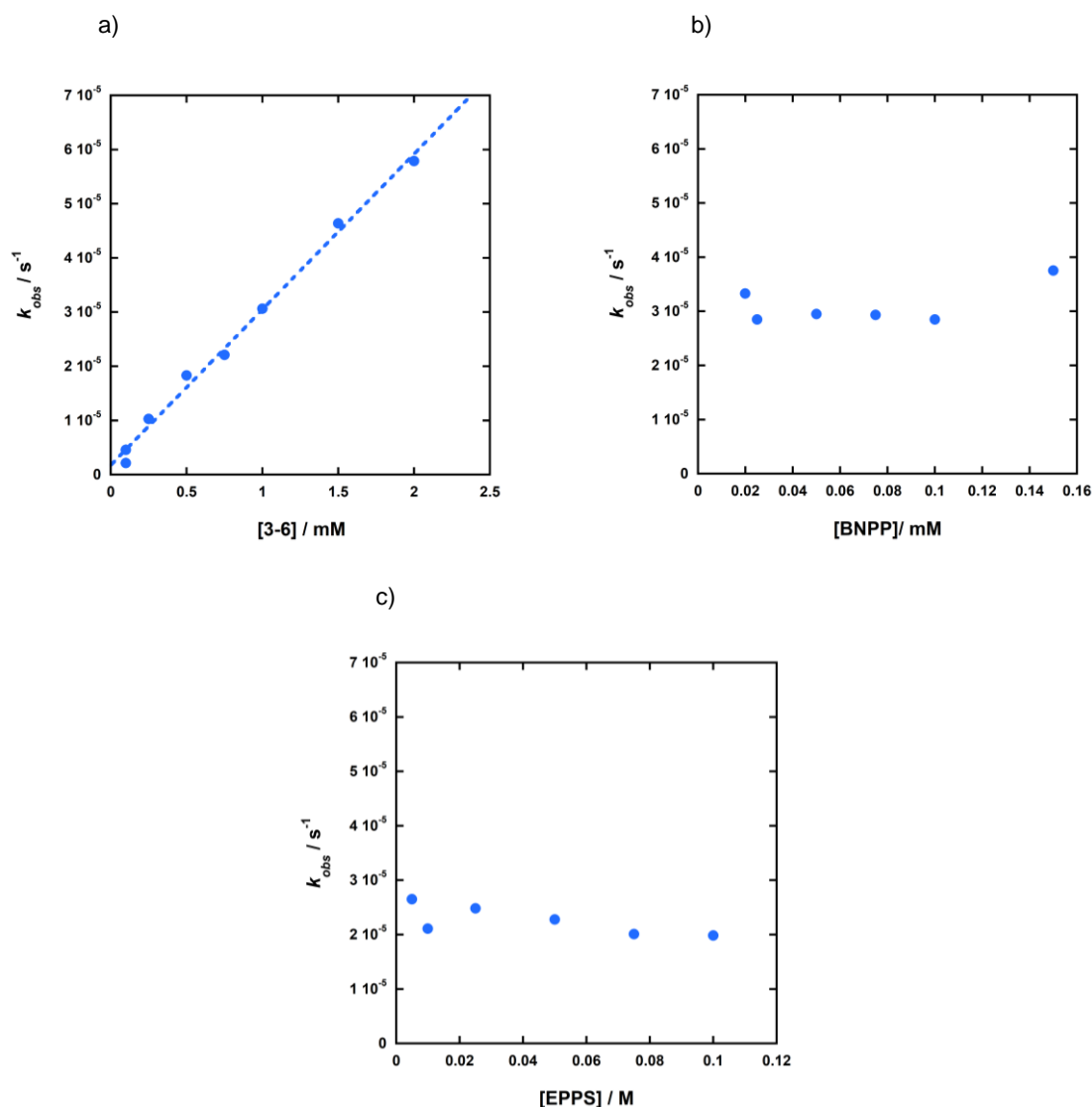


Figure 3.16 Plots of observed rate constants for the transesterification of HPNPP at pH 7.4 and 25°C catalysed by 3-6: a) First order dependence of k_{obs} against the concentration of 3-6 ($[EPPS] = 50$ mM, $[NaNO_3] = 0.1$ M, $[HPNPP] = 0.05$ mM); b) First order dependence of k_{obs} against the substrate ($[EPPS] = 50$ mM, $[NaNO_3] = 0.1$ M, $[3-6] = 0.5$ mM); c) Independence of k_{obs} on EPPS concentration ($[NaNO_3] = 0.1$ M, $[HPNPP] = 0.05$ mM, $[3-6] = 0.5$ mM);

Although the catalysts have an equivalent carbon backbone, **3-6** has two methyl groups attached to the aliphatic chain. As mentioned in Chapter 2, previous studies published by Tirel *et al.*⁸⁵ confirm that having a methylated side chain leads to an unexpected increase of k_2 , and a rate acceleration of about 5-fold was observed when the two mononuclear complexes were compared (**2-20** and **2-10** reported in Figure 3.17). This result might be

due to the perturbation of the local solvation shell or indirect steric effects that influence the zinc coordination site and increase its Lewis acidity. Therefore, the higher reactivity observed with **3-6** could be attributed to both the anisidine in *ortho* and the two methyl groups in the side chain.

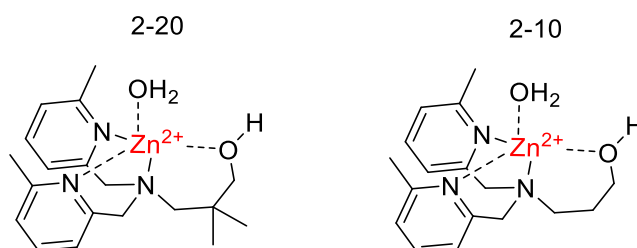
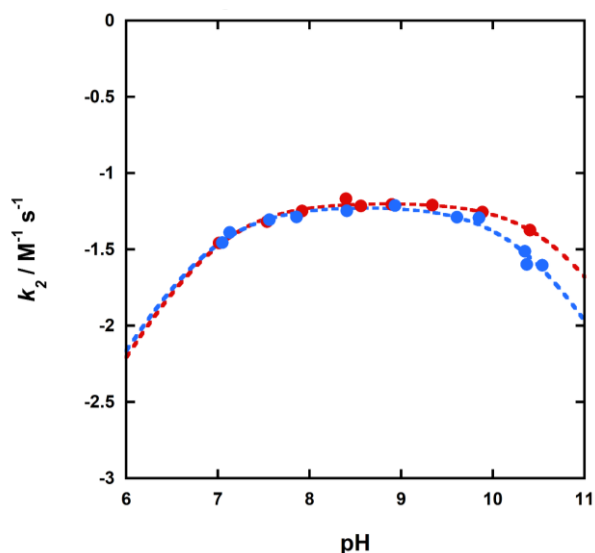


Figure 3.17 Structure of mononuclear complexes reported in the literature

2-2, obtained as described in Chapter 2, was studied to make a more reliable comparison. The hydrolysis of BNPP catalysed by **2-2** was not affected by the buffer concentration (5 – 100 mM) and showed a first order dependence on catalyst (0.1 – 2 mM) and substrate concentration (0.01 – 0.1 mM) (as reported in the experimental section). The pH profile of the second order rate constant for **3-6** (light blue dots) and **2-2** (red dots) is reported in Graph 3.5:



Graph 3.5 Plot of the pH profile of the second order rate constant of the hydrolysis of BNPP catalysed by 3-6 (●) and 2-2 (●) at 25°C, in 40% (v/v) acetonitrile in water; [3-6]=1 mM, [BNPP]=0.05 mM, [Buffer]=50 mM, ionic strength at 0.1 M by addition of NaNO₃

$$(35) \quad k_2 = k_2^{\max} [Cx] \frac{K_a^1[H^+]}{(K_a^1K_a^2 + K_a^1[H^+] + [H^+]^2)}$$

Table 3.8 Vales of the second-order rate constants k_2 , pK_a^1 and pK_a^2 obtained from the nonlinear least-square fitting of the pH profile kinetic data for 3-6 and 2-2 with equation (35). The pK_a values are compared with those obtained from the titration curves

Complex	$k_2^{\max} / M^{-1} s^{-1}$	pK_a^1		pK_a^2	
		Kinetic	Titration	Kinetic	Titration
3-6	$6.13 \pm 0.27 \times 10^{-2}$	6.90 ± 0.08	6.92	10.33 ± 0.05	9.88
2-2	$6.50 \pm 0.15 \times 10^{-2}$	6.97 ± 0.05	7.35	10.68 ± 0.06	9.98

By the nonlinear least-square fitting of these data with equation (35), the maximum activity of the complex k_2^{\max} , the first and the second deprotonation of the catalyst (K_a^1 and K_a^2), which lead respectively to the active and inactive form of the catalyst, were obtained (Table 3.8).

The pK_a values reported in Table 3.8 are in good agreement with those derived from the speciation plots obtained from UV- and potentiometric titrations. Under the experimental condition, **3-6** and **2-2** surprisingly exhibited approximately the same reactivity. The presence of the bulky anisidine groups did not appear to provide any benefit against the hydrolysis of BNPP and, considering the reduced water solubility of the complex, precluded the use of **3-6**. Due to the absence of the intramolecular hydroxyl, BNPP is less reactive than HPNPP, and the rate constant of its spontaneous hydrolysis is estimated to be $1 \times 10^{-10} \text{ s}^{-1}$ at pH 7 and 25 °C.^{51,54} Under the same conditions, 1 mM of **3-6** and **2-2** hydrolysed the substrate at a rate respectively of $4.95 \pm 0.01 \cdot 10^{-5} \text{ s}^{-1}$ and $4.36 \pm 0.01 \cdot 10^{-5} \text{ s}^{-1}$, providing an acceleration of 3.1 and 2.7×10^6 . The hydrolysis of the DNA model proceeds through the attack of an intermolecular nucleophile, which, in the presence of **3-6** or **2-2**, is the hydroxyl group in the ligand small aliphatic chain. As previously described, the main product of the transesterification is a new phosphate that bonds a 4-nitrophenyl unit and the Zn(II) complex together. The ^{31}P NMR experiment reported in Figure 3.18 in the presence of **2-2** demonstrates that after 18 h at pH 7.4 and 25 °C, when a substrate excess was used, a relative stable diester is formed. After 28 days, the NMR showed the presence of the substrate (-12.37 ppm), the 4-nitrophenyl phosphate (-1.58 ppm) and the diester intermediate (-5.27 ppm), whose resistance to hydrolysis prevented catalytic turnover.

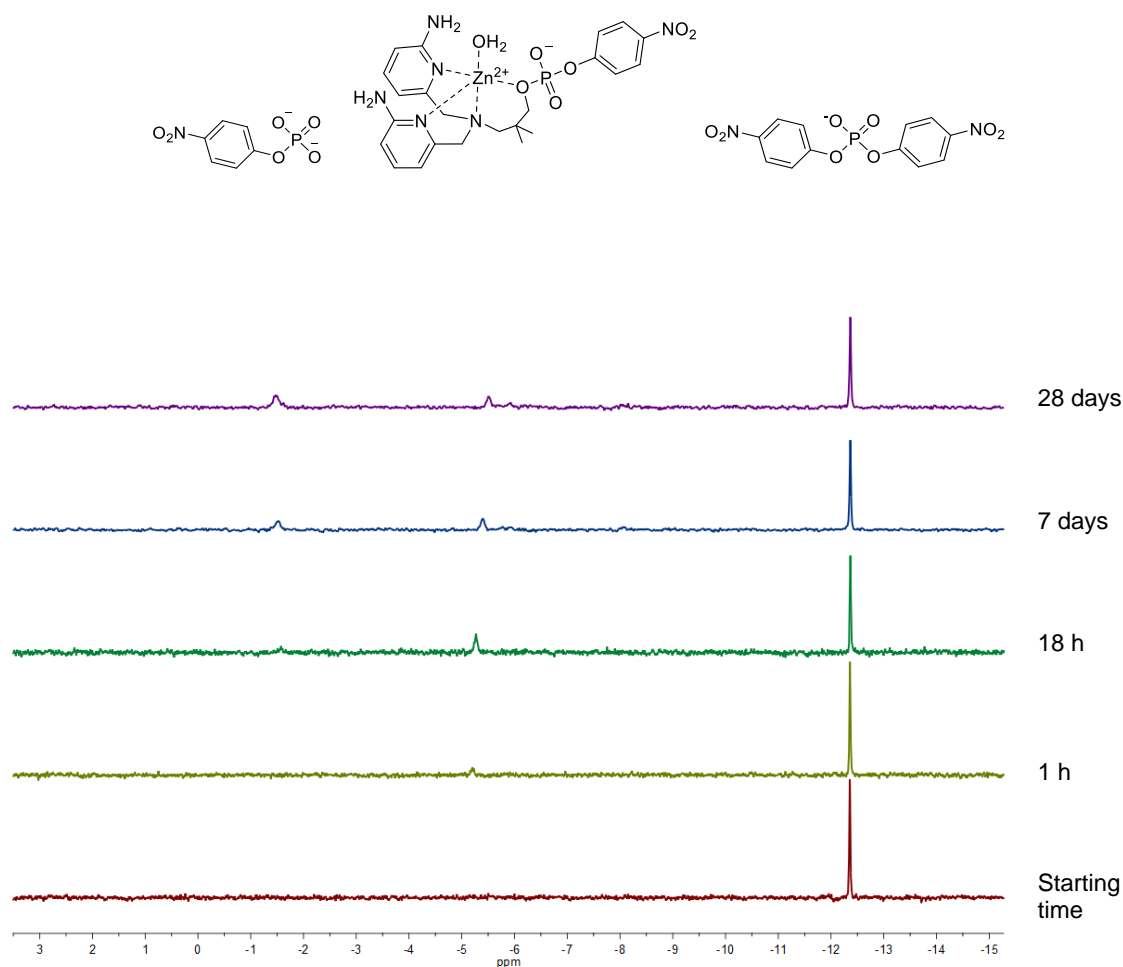
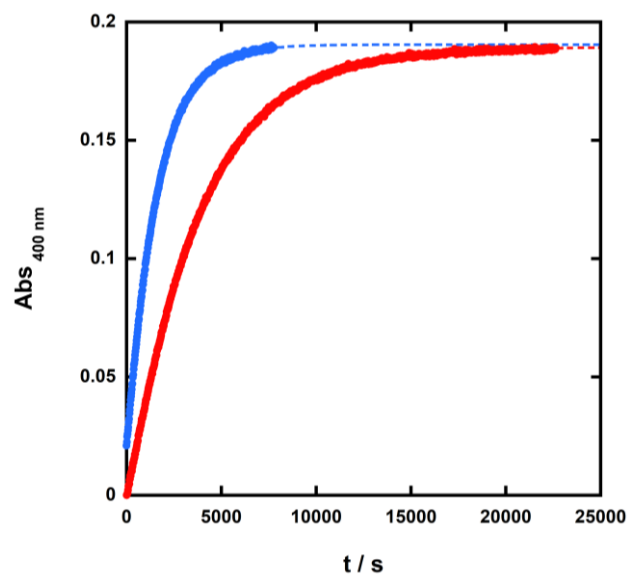


Figure 3.18 ^{31}P NMR spectra of the hydrolysis of 5 mM BNPP catalysed by 2 mM of 2-2 at pH 7.4 and 25°C ; [HEPES] = 50 mM, $[\text{NaNO}_3]$ = 0.1 M;

Although there are similarities between the two molecules, the cleavage of BNPP and HPNPP proceed through two different pathways. Testing **3-6** against BNPP suggested that the aromatic amine substitution provided no further enhancement, and to confirm this evidence, HPNPP hydrolysis was also investigated. Graph 3.6 shows the 4-nitrophenolate appearance followed at 400 nm over time. The k_{obs} values at pH 7.4 and 25 °C in the presence of **3-6** or **2-2** (1 mM) were respectively $6.25 \pm 0.01 \cdot 10^{-4} \text{ s}^{-1}$ and $2.64 \pm 0.01 \cdot 10^{-4} \text{ s}^{-1}$.



Graph 3.6 Plot of the absorbance values at 400nm over time caused by the appearance of 4-nitrophenolate. The reaction is the cleavage of HPNPP at 25 °C and pH 7.4 in 40% (v/v) acetonitrile in water catalysed by 3-6(●) and 2-2(●) ([complex]=1 mM; [HPNPP]=0.05 mM; [HEPES]=50 mM ;ionic strength at 0.1 M by addition of NaNO₃)

Although not evident with BNPP, the difference in reactivity was clear when the complexes were used to catalyse HPNPP cleavage.

3.3 Conclusion

In conclusion, we reported a family of highly reactive mononuclear Zn(II) complex that accelerate the transesterification of HPNPP catalytically.

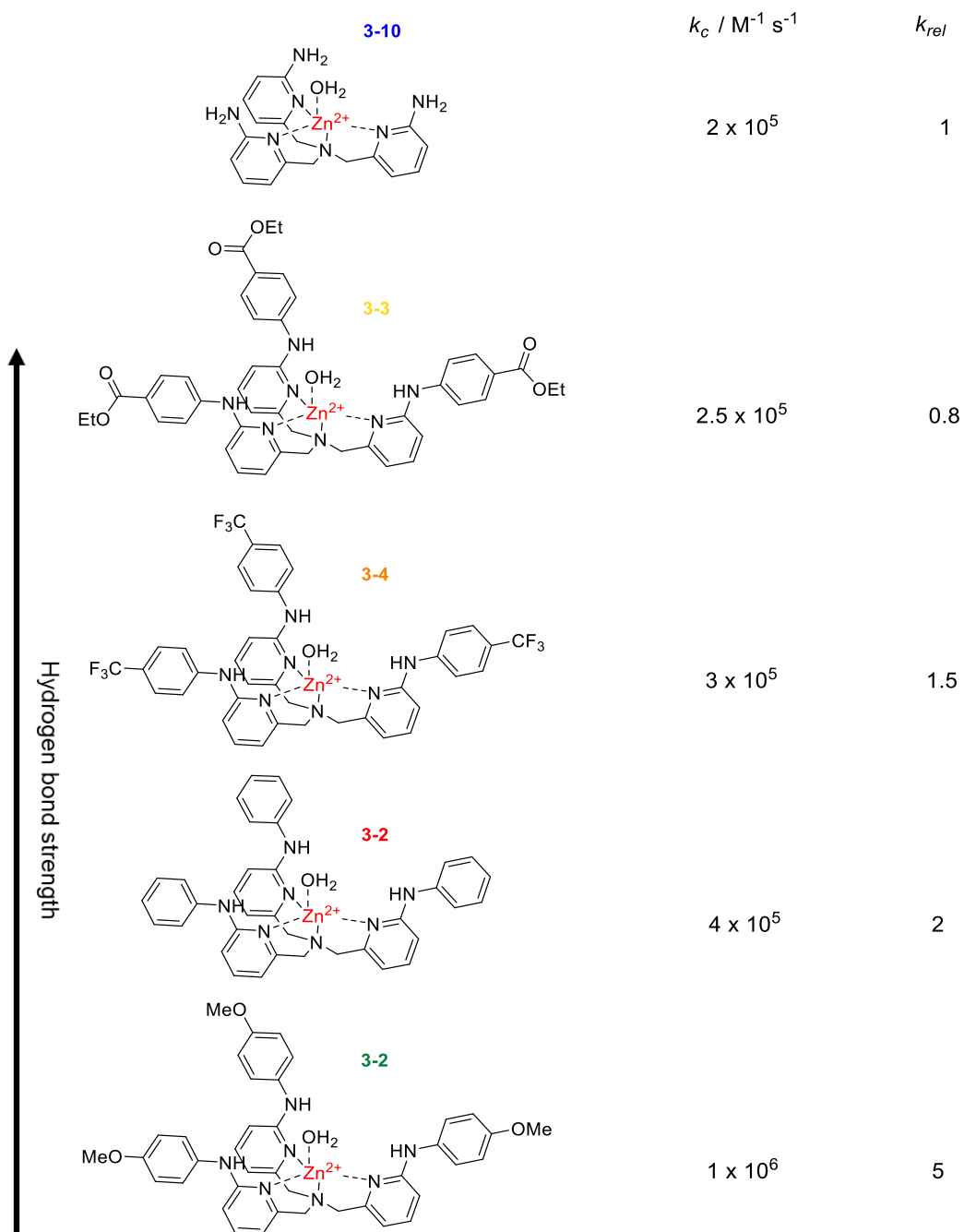


Figure 3.19 comparison among the proposed complexes

Although bigger differences were observed among the second order rate constants, Figure 3.19 highlights similar k_c values to the reference **3-10**. This is due to a greater substrate binding (lower K_d) which confirm that the higher reactivity of the catalysts (compared to **3-10**) depends on more efficient stabilisation of both the ground and the transition state. In contrast to what was reported by Szymczak *et al.*,¹⁰⁴ we observed that the stronger hydrogen bond donor groups in the second coordination sphere led to a decrease in catalyst reactivity. We cannot exclude that the different result might be due to possible dimerisation of **3-3** and **3-4**, absent in **3-1** and **3-2**, which might give a decrease in the concentration of the active species of the catalyst. In addition, while the aniline-based complexes were studied in fully organic solvents in Szymczak's work, the aqueous medium might have altered the previously observed trend.

To understand if the ligand scaffold was responsible for the higher reactivity observed, we synthesised and studied the analogous tridentate complex **3-6**, compared to **2-2**.

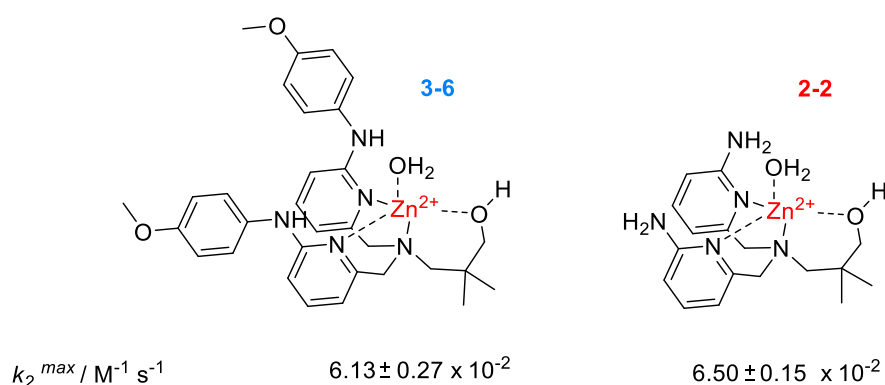


Figure 3.20 Comparison of mononuclear complexes tested toward the transesterification of BNPP (0.05 mM) at 25 °C

As summarised in Figure 3.20, the two complexes were tested toward the BNPP transesterification at 25 °C and showed approximately the same k_2 . Therefore, no additional benefit was provided by introducing the anisidine ring in the ortho-position of the pyridyl ring. Interestingly, when comparing the reactivity of the analogous tridentate and tridentate complexes in the same reaction conditions toward the HPNPP cleavage, two different trends are observed (Figure 3.21). The lack of one of the coordinating pyridyl nitrogen, decreasing the electron density over the Zn(II) ion and enhancing its Lewis acidity, is expected to affect the rate constant positively. Following the expected behaviour, **2-2** results 2-fold faster than **3-10**. By contrast, the k_2 of **3-6** is approximately 2/3 of the value found for **3-2**, suggesting that the reactivity could be more sensitive to the particular geometry of the catalyst than the coordination itself.

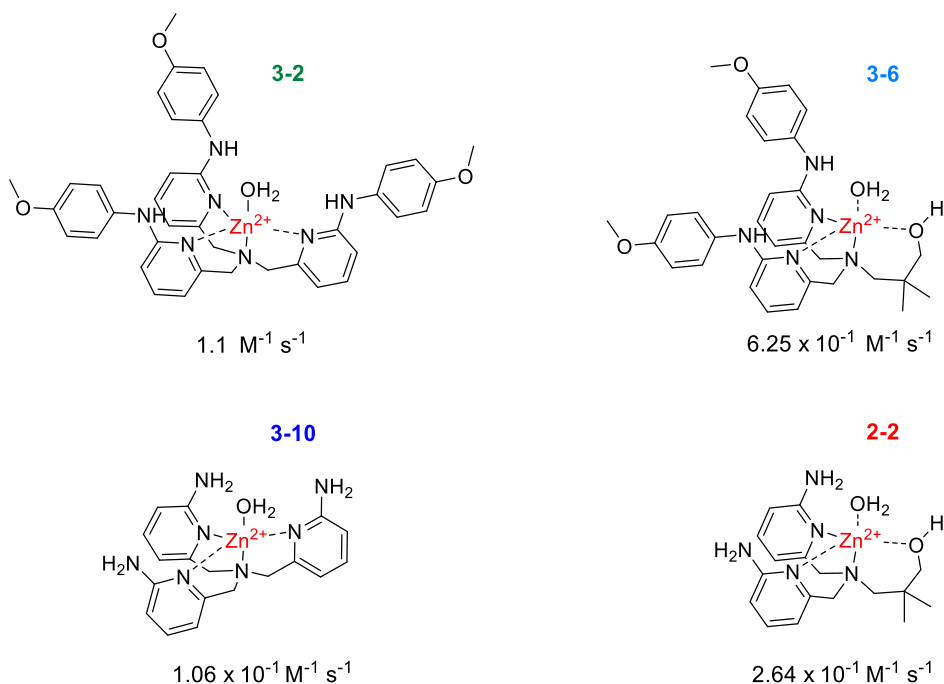


Figure 3.21 k_2 value for the amine- and aniline-based tridentate and tetradentate complexes

Especially considering the modest improvement provided by **3-6** (compared to **2-2**), the result could suggest the highly reactive **3-2** may provide a wider hydrophobic pocket (than the one formed by the tridentate) that is mainly responsible for the rate acceleration. Although the *para*-substitution and the hydrogen bond strength of the anisidine substituents influence their intrinsic reactivity, the slight difference of the k_c figures among all the mononuclear complexes reinforces this hypothesis.

Although we established that the additional acetonitrile does not affect the measurement of the activity of the catalysts, the **3-n** family of complexes might also be tested in a fully aqueous solution by implementing their water solubility. This can be achieved by introducing inert sulfonate groups far from the coordination site, as shown in Figure 3.22a. In addition, to achieve both activity and selectivity, the highly effective anisidine substituents might be introduced in the bis(pyridin-2-ylmethyl)amine coordination site of artificial hydrolyses (Figure 3.22b). The conjugation of bis(pyridin-2-ylmethyl)amine with PNA sequences is already under investigation in Williams' group, thanks to the collaboration with Strömberg and coworkers.

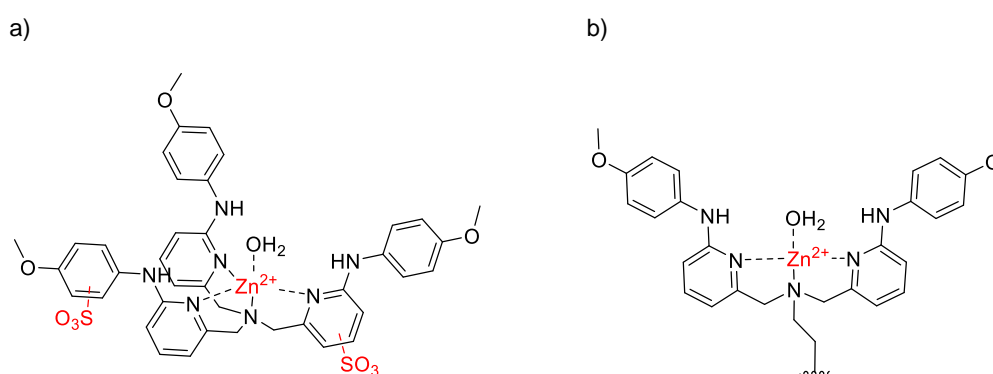
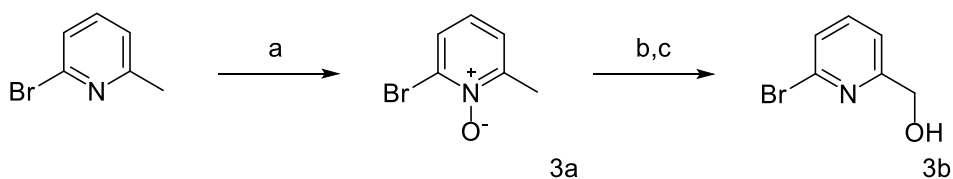


Figure 3.22 a) possible strategy to increase the solubility of the complexes by introducing sulfonate groups; b) Artificial enzyme obtained by conjugation of anisidine decorated bis(pyridin-2-ylmethyl)amine unit to PNA sequences

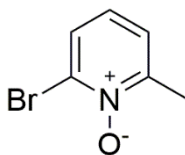
3.4 Experimental

3.4.1 Synthesis

Large scale synthesis of building block 3b



Scheme 3.12 a) AcOOH , AcOH , 70°C , 3 h, 84% yield; b) Ac_2O , H_2SO_4 , 80°C , 30 min; c) NaOH , $\text{H}_2\text{O-MeOH}$ r.t., 18 h, 55% yield



3a 2-bromo-6-methylpyridin-1-ium-1-olate

A solution of 2-bromo-6-methylpyridine (300 g, 1.7 mol) in acetic acid (2 vol, 600 mL) was left stirring and heated to 70°C . 40% peracetic acid (500 mL, 3.4 mol) was added dropwise, monitoring the temperature of the reaction mixture and avoiding a rapid increase. After 3 h, the crude was concentrated *in vacuo* (approx. 450 mL) and then diluted with water (200 mL). The aqueous phase was basified by adding 40% (w) potassium hydroxide solution (600 mL) and the product extracted by DCM (4 x 600 mL). The combined organic layers were washed with 200 mL of water and dried over MgSO_4 . After solvent evaporation

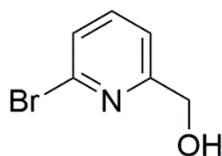
under reduced pressure, the product was recrystallised from TBME (200 mL) and obtained as white crystal (276 g, 1.47 mol; 84%).

¹H NMR (500 MHz, CDCl₃): δ 7.52 (d, *J* = 8.15 Hz, 1H - CH py), 7.20 (d, *J* = 7.9 Hz, 1H - CH py), 6.98 (d, *J* = 7.9 Hz, 1H - CH py), 2.55 (s, 3H - CH₃).

¹³C NMR (125 MHz, CDCl₃): δ 150.86 (C py), 133.20 (C py), 128.45 (CH py), 125.01 (CH py), 124.83 (CH py), 19.03 (CH₃).

MS (ES-TOF): [M+H]⁺ Obs. m/z: 188.0

[2M+H]⁺ Obs. m/z: 374.9



3b (6-Bromo-pyridin-2-yl)methanol

To acetic anhydride (2.5 vol, 550 mL) at 70 °C, **3a** (276 g, 1.5 mol) and 96% sulphuric acid (3.9 mL, 73.5 mmol) were added dropwise. A rapid increase in temperature was observed after the latter's addition, and 130 °C were reached. After 30 min, the reaction mixture was cooled down and quenched with water (140 mL). The acetic acid was then removed *in vacuo*, and the brown crude dissolved in methanol (150 mL). Potassium hydroxide solution (20 M) was added dropwise until pH 11 was reached, and the reaction was left stirring overnight at room temperature. The solution was diluted with water (1 L), and the product was extracted from the aqueous phase by DCM (500 mL). The water phase was further extracted with DCM (4 x 300 mL), and the combined organic layers were dried

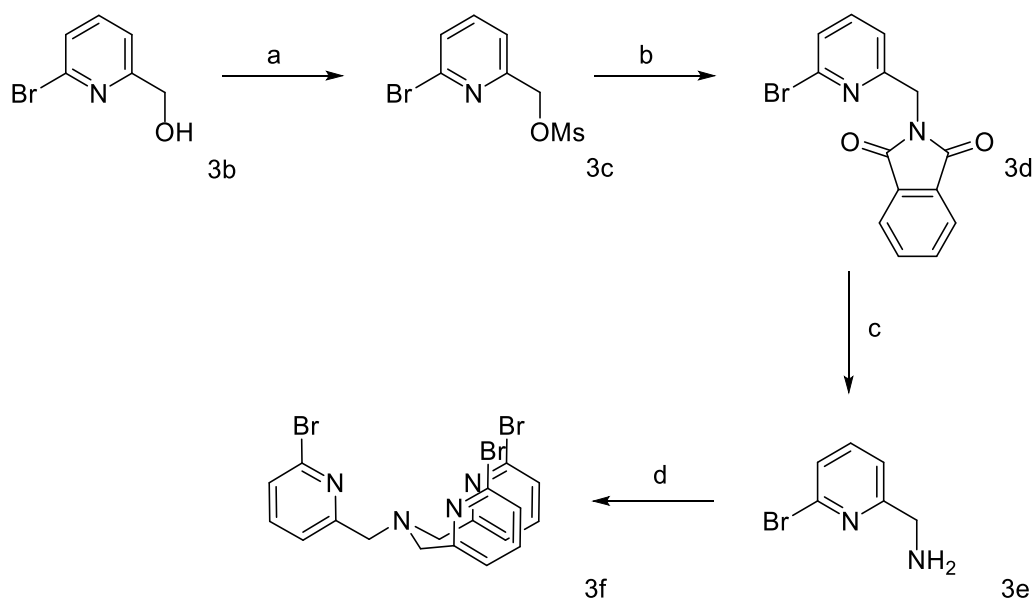
over MgSO_4 . After solvent evaporation *in vacuo*, the product was purified by silica block (heptane-heptane/ethyl acetate (4:1)) and obtained as yellow solid (151 g, 0.8 mol; 55%).

^1H NMR (400 MHz, CDCl_3): δ 7.54 (t, $J = 7.7$ Hz, 1H - CH py), 7.38 (d, $J = 7.8$ Hz, 1H - CH py), 7.28 (d, $J = 7.6$ Hz, 1H - CH py), 4.74 (d, $J = 4.3$ Hz, 2H - CH_2), 3.31 (t, $J = 4.9$ Hz, 1H - OH).

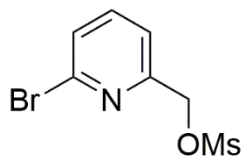
^{13}C NMR (101 MHz, CDCl_3): δ 161.40 (C py), 141.49 (C py), 139.21 (CH py), 126.77 (CH py), 119.45 (CH py), 64.32 (CH_2).

MS (ES-TOF): $[\text{M}+\text{H}]^+$ Calc. m/z : 188.0 - Obs. m/z : 188.0

Synthesis of ligand 3f



Scheme 3.13 a) MeSO_2Cl , Et_3N , THF, 90% yield; b) Potassium phthalimide, DMF; c) HBr, 120 °C; d) NaOH, (6-bromopyridin-2-yl)methyl methanesulfonate, H_2O -MeOH, 100 °C, 60% yield



3c (6-bromopyridin-2-yl)methyl methanesulfonate

To a THF solution (80 mL) of **3b** (6.0 g, 32 mmol) and methanesulfonyl chloride (2.9 mL, 38 mmol) at 0 °C, trimethylamine (6.6 mL, 48 mmol) was added dropwise. The cloudy solution was left stirring overnight at room temperature. The precipitate was removed by filtration, and the filtrate was concentrated under reduced pressure. The concentrated mixture was quenched with a saturated ammonium chloride solution (200 mL), and the product was extracted with diethyl ether (50 mL x 3). The combined organic layers were washed with ammonium chloride saturated solution (100 mL), brine (90 mL) and dried over MgSO₄. The solvent was evaporated under reduced pressure and the yellow oil obtained (7.5 g, 29 mmol; 90%) was used without further purification.

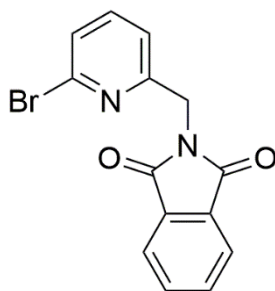
¹H NMR (400 MHz, CDCl₃): δ 7.62 (t, 1H - CH py), 7.48 (d, *J* = 7.9 Hz, 1H - CH py), 7.44 (d, *J* = 7.6 Hz, 1H - CH py), 5.28 (s, 2H - CH₂), 3.12 (s, 3H - SO₂CH₃).

¹³C NMR (101 MHz, CDCl₃): δ 155.11 (C py), 141.9 (C py), 139.54 (CH py), 128.26 (CH py), 121.13 (CH py), 70.48 (CH₂), 38.27 (SO₂CH₃).

MS (ES-TOF): [M+H]⁺ Calc. m/z: 265.9 - Obs. m/z: 265.9

[M+Na]⁺ Calc. m/z: 287.9 - Obs. m/z: 287.9

[M+K]⁺ Calc. m/z: 303.9 - Obs. m/z: 303.9.



3d 2- [(6-bromopyridin-2-yl)methyl]-2,3-dihydro-1H-isoindole-1,3-dione

To a round-bottom flask containing a solution of **3c** (3.6 g, 14 mmol) in 20 mL of DMF, potassium phthalimide (5.1 g, 27 mmol) was added portion-wise. The mixture was left stirring for 3 h at room temperature. The precipitate was filtrated off, and the filtrate was poured into 120 mL of a basic water solution (pH > 11). The product was extracted from the water phase by DCM (3 x 30 mL), and the combined organic layers were washed with brine (30 mL x 2) and dried over MgSO₄. The evaporation of the solvent under vacuum yielded a white solid (wet weight: 4.4 g), which was used without further purification.

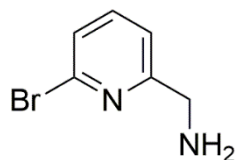
¹H NMR (400 MHz, CDCl₃): δ 7.86 - 7.83 (m, 2H - CH pht), 7.75 – 7.68 (m, 2H - CH pht), 7.45 (t, *J* = 7.7 Hz, 1H - CH py), 7.32 (d, *J* = 7.8 Hz, 1H - CH py), 7.13 (d, *J* = 7.6 Hz, 1H - CH py), 4.94 (s, 2H - CH₂).

¹³C NMR (101 MHz, CDCl₃): δ 167.91 (CO pht), 156.88 (C py), 141.86 (C py), 139.10 (CH py), 134.30 (CH pht), 132.04 (C pht), 127.03 (CH py), 123.62 (CH pht), 119.97 (CH py), 42.45 (CH₂).

MS Ref. mass: 316.0; Obs. mass: [M+H]⁺ = 317.0, [2M+H]⁺ = 632.9.

MS (ES-TOF): [M+H]⁺ Calc. m/z: 317.0 - Obs. m/z: 317.0

[2M+H]⁺ Calc. m/z: 633.0 - Obs. m/z: 632.9.



3e 1-(6-bromopyridin-2-yl)methanamine

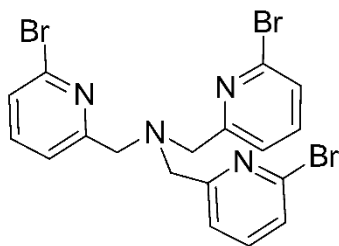
3d (4.43 g; 13^{*} mmol) was dissolved in 50 mL (433 mmol) of 48% (wt.) HBr, and the solution was left stirring overnight at 120 °C. The mixture was brought to room temperature, and the HBr was partially neutralised by dropwise addition of NaOH (14 g; 350.0 mmol) in 30 mL of water. The pH was then brought to 5 by Na₂CO₃ (6.3 g, 60 mmol), and the water phase was washed with DCM (30 mL x 3). Finally, the water phase was basified by 0.1 M NaOH solution (10 mL), and the product was then extracted with DCM (50 mL x 3). The combined organic layers were dried over MgSO₄, and the solvent was evaporated by reduced pressure. The product was obtained as a yellow oil (1.3 g, 7 mmol).

¹H NMR (400 MHz, CDCl₃): δ 7.49 (t, *J* = 7.7 Hz, 1H - CH py), 7.33 (d, *J* = 7.8 Hz, 1H - CH py), 7.24 (d, *J* = 7.2 Hz - CH py), 3.93 (s, 2H - CH₂), 1.67 (s, 2H).

¹³C NMR (101 MHz, CDCl₃): δ 163.93 (C py), 141.92 (C py), 139.09 (CH py), 126.28 (CH py), 120.08 (CH py), 47.52 (CH₂).

MS (ES-TOF): [M+H]⁺ Calc. m/z: 187.0 - Obs. m/z: 187.0

[2M+H]⁺ Calc. m/z: 373.0 - Obs. m/z: 372.9.



3f tris[(6-bromopyridin-2-yl)methyl]amine

To a mixture of **3c** (3.9 g, 15 mmol) and **3e** (1.3 g, 7 mmol) and methanol (4 mL), NaOH (1.1g, 27 mmol) in 12 mL of water was added dropwise. The reaction was left stirring overnight at 100 °C. The biphasic mixture was diluted with 100 mL of brine, and the crude product was extracted from the water phase with DCM (30 mL x 3). The combined organic layers were dried over MgSO₄ and the solvent was evaporated under reduced pressure. The product was then crystallised from toluene (2.1 g, 4 mmol; 60%).

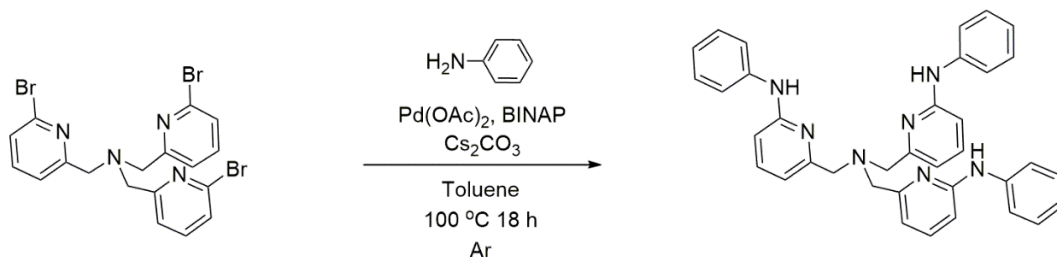
¹H NMR (400 MHz, CDCl₃): δ 7.60 – 7.46 (m, 6H - CH py), 7.34 (dt, *J* = 7.7, 3.8 Hz, 3H-CH py), 3.87 (s, 6H - CH₂).

¹³C NMR (101 MHz, CDCl₃): δ 160.72 (C py), 141.58 (C py), 138.97 (CH py), 126.61 (CH py), 121.93 (CH py), 59.55 (CH₂).

HRMS (ES-TOF): [M+H]⁺ Calc. m/z: 524.8920 - Obs. m/z: 524.8907

Ligands synthesis

3g 6-[[bis({[6-(phenylamino)pyridine-2-yl]methyl})amino]methyl]-N-phenylpyridin-2-amine



A 100 mL round bottom flask charged with **3f** (500 mg, 0.95 mmol), $\text{Pd}(\text{OAc})_2$ (19 mg, 0.085 mmol), $\pm\text{BINAP}$ (80 mg, 0.128 mmol) and Cs_2CO_3 (1.86 g, 5.7 mmol), was filled with argon. To the powders mixture, an argon-saturated solution of aniline (796 mg, 8.55 mmol) in toluene (40 mL) was added and the solution was left stirring overnight at $100\text{ }^\circ\text{C}$. The mixture was cooled to room temperature and filtered off over Celite[®]. The filtrate was concentrated under reduced pressure and the product was obtained pure (241 mg; 0.43 mmol; 45%) after silica gel chromatography (DCM-DCM/ethyl acetate (3:2)).

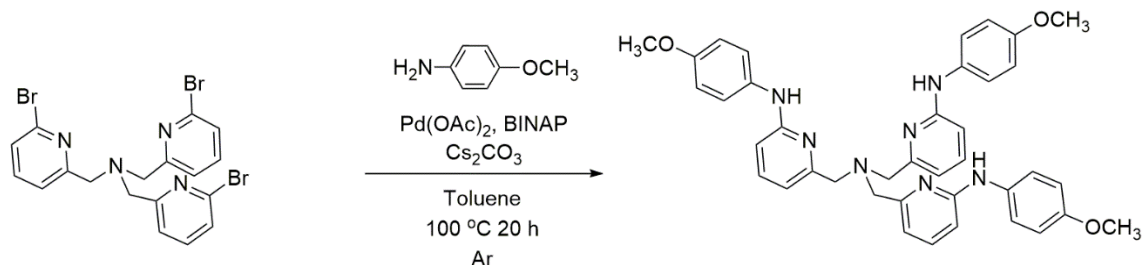
^1H NMR (400 MHz, CDCl_3): δ 7.48 (t, $J = 8, 5.7$ Hz, 3H - CH py), 7.36 – 7.27 (m, 12H-CH ar), 7.12 (d, $J = 7.4$ Hz, 3H - CH py), 7.02 (tt, $J = 6.7, 1.8$ Hz, 3H - CH ar), 6.75 (d, $J = 8.2$ Hz, 3H - CH py), 6.51 (s, 3H - NH), 3.83 (s, 6H - CH_2) .

^{13}C NMR (101 MHz, CDCl_3): δ 158.83 (C py), 155.41 (C ar), 140.84 (C py), 138.24 (CH py), 129.36 (CH ar), 122.61 (CH ar), 120.12 (CH ar), 114.05 (CH py), 106.40 (CH py), 60.35 (CH_2).

HRMS (ES-TOF): $[\text{M}+\text{H}]^+$ Calc. m/z: 564.2870 - Obs. m/z: 564.2878

$[\text{M}+2\text{H}]^{2+}$ Calc. m/z: 282.6472 - Obs. m/z: 282.6487

3h 6-[[bis({6-[(4-methoxyphenyl)amino]pyridine-2-yl)methyl}amino)methyl]-N-(4-methoxyphenyl) pyridine-2-amine



A 100 mL round bottom flask charged with **3f** (500 mg, 0.95 mmol), Pd(OAc)₂ (19 mg, 0.085 mmol), ±BINAP (80 mg, 0.128 mmol) and Cs₂CO₃ (1.86 g, 5.7 mmol), was filled with argon. To the powders mixture, an argon-saturated solution of p-anisidine (1.05 g, 8.55 mmol) in toluene (40 mL) was added, and the solution was left stirring for 20 h at 100 °C. The mixture was cooled to room temperature and filtered off over Celite®. The filtrate was concentrated under reduced pressure, and the product was obtained pure (310 mg, 0.47 mmol; 50%) after silica gel chromatography (DCM-DCM/ethyl acetate (2:3)).

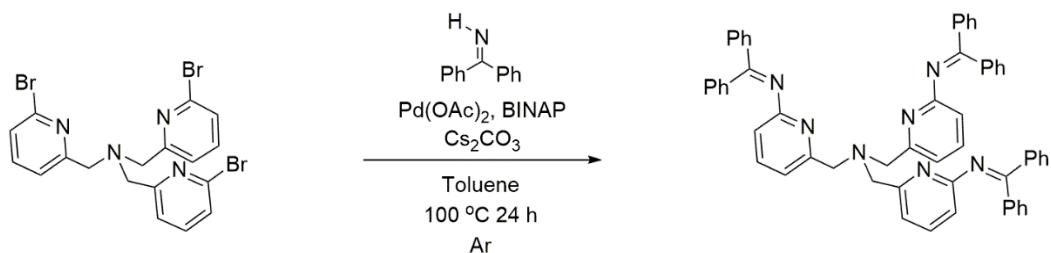
¹H NMR (400 MHz, CDCl₃): δ 7.41 (t, *J* = 7.8 Hz, 3H - CH py), 7.26 – 7.22 (dd, 6H - ar), 7.05 (d, *J* = 7.3 Hz, 3H - CH py), 6.93 – 6.83 (m, 6H - ar), 6.55 (d, *J* = 8.2 Hz, 3H - CH py), 6.34 (s, 1H - NH), 3.80 (d, 6H - CH₂), 3.79 (s, 9H - CH₃).

¹³C NMR (101 MHz, CDCl₃): δ 158.79 (C py), 156.75 (C ar), 156.21 (C py), 138.20 (CH py), 133.71 (C py), 123.88 (CH ar), 114.72 (CH ar), 113.31 (CH py), 105.26 (CH py), 60.35 (CH₂), 55.70 (OCH₃).

HRMS (ES-TOF): [M+H]⁺ Calc. m/z: 654.3214 - Obs. m/z: 654.3207

[M+2H]²⁺ Calc. m/z: 327.6657 - Obs. m/z: 372.6642

3i tris({6-[(diphenylmethylidene)amino]pyridine-2-yl)methyl)amine



3f (650 mg, 1.24 mmol), Pd(OAc)₂ (25 mg, 0.11 mmol), \pm BINAP (104 mg, 0.167 mmol) and Cs₂CO₃ (1.35 g, 7.56 mmol) were introduced into a round bottom flask, which was then filled with argon. An Ar-sparged solution of benzophenone imine (2.12 g, 7.44 mmol) in 80 mL of toluene was added to the mixture. The solution was heated at 100 °C and left stirring under argon atmosphere for 24 h. The crude mixture was cooled down at room temperature and filtered off over celite. The filtrate was kept, and the solvent was evaporated under reduced pressure. The crude product was purified by silica gel chromatography (DCM-DCM/ethyl acetate (2:3)), obtaining the desired compound as a yellow solid (720 mg, 0.87 mmol; 70%).

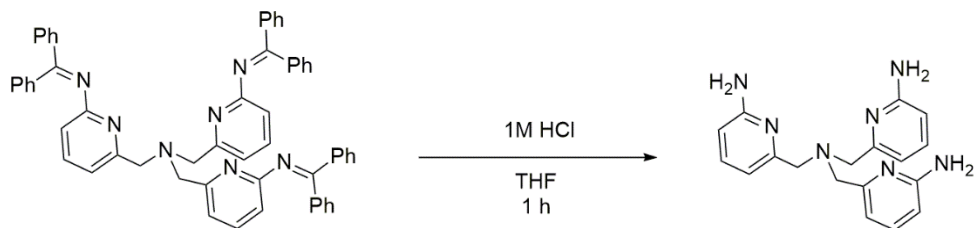
¹H NMR (400 MHz, CDCl₃): δ 7.80 (d, J = 7.3 Hz, 6H - CH ph), 7.47 (t, J = 7.3 Hz, 3H - CH py), 7.43 – 7.36 (m, 9H - CH ph), 7.17 – 7.05 (m, 15H - CH ph), 6.96 (d, J = 7.4 Hz, 3H - CH py), 6.45 (d, J = 7.7 Hz, 3H - CH py), 3.40 (s, 6H - CH₂).

¹³C NMR (101 MHz, CDCl₃): δ 170.42 (CN), 162.90 (C py), 159.15 (C py), 138.99 (C ph), 137.57 (CH py), 136.44 (C ph), 131.29 (CH ph), 129.89 (CH ph), 129.30 (CH ph), 128.85 (CH ph), 128.22 (CH ph), 127.91 (CH ph), 118.08 (CH py), 113.50 (CH py), 59.68 (CH₂).

MS (ES-TOF): [M+H]⁺ - Obs. m/z: 828.4

[M+2H]²⁺ Obs. m/z: 414.7

3j 6-({bis[(6-aminopyridin-2-yl)methyl]amino}methyl)pyridin-2-amine



1 M HCl (3 mL) was added to a solution of **3i** (720 mg, 0.87 mmol) in THF (10 mL), which was left stirring for an hour at room temperature. The solution was diluted with 20 mL of water and then washed with diethyl ether (20 mL x 4). The water phase was basified by adding 1 M NaOH (3.5 mL), and the product was extracted with ethyl acetate (3 x 20 mL). The combined organic layers were dried over MgSO₄ and the solvent evaporated by reduced pressure, yielding a yellow powder (254 mg, 0.75 mmol; 87 %).

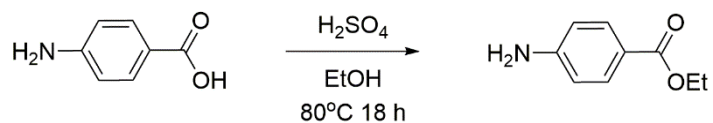
¹H NMR (400 MHz, d-DMSO): δ 7.34 (t, J = 7.7 Hz, 3H - CH py), 6.75 (d, J = 7.2 Hz, 3H - CH py), 6.28 (d, J = 8.1 Hz, 3H - CH py), 5.81 (s, 6H - NH₂), 3.47 (s, 6H - CH₂).

¹³C NMR (101 MHz, d-DMSO): δ 159.14 (C py), 157.57 (C py), 137.43 (CH py), 109.56 (CH py), 105.98 (CH py), 59.59 (CH₂).

HRMS (ES-TOF): [M+H]⁺ Calc. m/z: 336.1958 - Obs. m/z: 336.1938

[M+2H]²⁺ Calc. m/z: 168.6029 - Obs. m/z: 168.6012

3k Ethyl-4-aminobenzoate



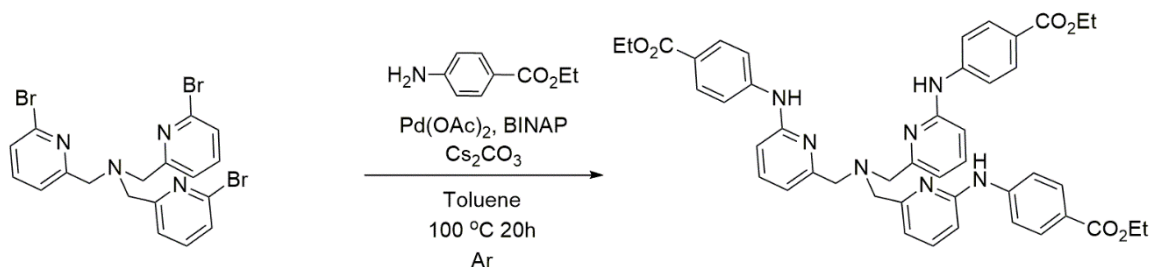
4-aminobenzoic acid (5 g, 36.4 mmol) was dissolved in ethanol (90 mL), and the solution was heated at 80°C . 98 % sulphuric acid (2.5 mL, 46 mmol) was added dropwise to the solution, which was left stirring overnight at 80°C . The mixture was partially concentrated by rotary evaporator and then diluted with 50 mL of water. The sulphuric acid was neutralised by dropwise addition of NaOH solution (1.5 g in 20 mL of water) and a saturated solution of sodium bicarbonate (70 mL). The product was then extracted from the water phase with DCM (3 x 50 mL). The combined organic layers were washed with brine (90 mL) and dried over MgSO_4 . The solvent was removed under vacuum, and the desired product was obtained as a white solid with 92% Yield (5.54 g, 33.5 mmol).

^1H NMR (400 MHz, CDCl_3): δ 8.01 – 7.70 (m, 2H - CH), 6.74 – 6.52 (m, 2H - CH), 4.32 (q, $J = 7.1$ Hz, 2H - CH_2), 4.03 (s, 2H - NH_2), 1.36 (t, $J = 7.1$ Hz, 3H - CH_3).

^{13}C NMR (101 MHz, CDCl_3): δ 166.83 (CO), 150.82 (CN), 131.69 (CH), 120.31 (C), 113.92 (CH), 60.45 (OCH_2), 14.57 (CH_3).

HRMS (ES-TOF): $[\text{M}+\text{H}]^+$ Calc. m/z : 166.0890 - Obs. m/z : 166.0870.

3l Ethyl 4-[[6-({bis[6-([4-(ethoxycarbonyl)phenyl]amino)pyridine-2-yl)methyl]amino} methyl)pyridine-2-yl]amino}benzoate



A 100 mL round bottom flask charged with **3f** (500 mg, 0.95 mmol), Pd(OAc)₂ (19 mg, 0.085 mmol), \pm BINAP (80 mg, 0.128 mmol) and Cs₂CO₃ (1.86 g, 5.7 mmol), was filled with argon. To the powders mixture, an Ar-sparged solution of **3k** (1.41 g, 8.5 mmol) in toluene (40 mL) was added, and the solution was left stirring for 20 h at 100 °C. The mixture was cooled to room temperature and filtered off over Celite[®]. The filtrate was concentrated under reduced pressure, and the product was obtained pure (473 mg, 0.60 mmol; 64%) after silica gel chromatography (DCM-DCM/ethyl acetate (3:2)).

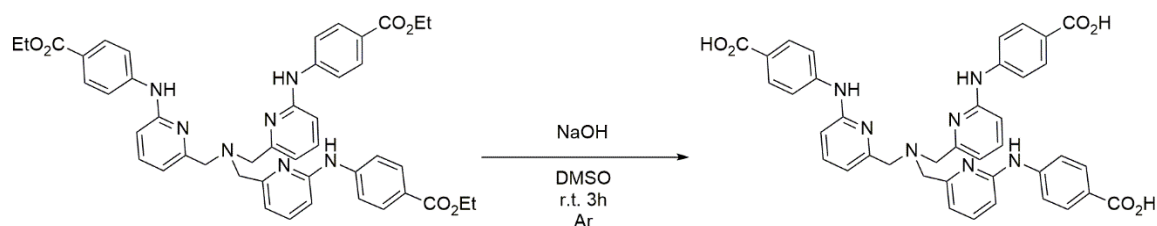
¹H NMR (400 MHz, CDCl₃): δ 8.07 – 7.84 (m, 6H - CH ar), 7.54 (t, J = 7.8 Hz, 3H - CH py), 7.49 – 7.42 (m, 6H - CH ar), 7.19 (d, J = 7.4 Hz, 3H - CH py), 6.78 (d, J = 8.1 Hz, 3H - CH py), 6.72 (s, 3H - NH₂), 4.35 (q, J = 7.1 Hz, 6H - OCH₂), 3.87 (s, 6H - CH₂), 1.38 (t, J = 7.1 Hz, 9H - CH₃).

¹³C NMR (101 MHz, CDCl₃): δ 166.56 (CO), 158.75 (C py), 154.04 (C py), 145.32 (C ar), 138.37 (CH py), 131.22 (CH ar), 123.26 (C ar), 117.27 (CH ar), 115.37 (CH py), 108.43 (CH py), 60.71 (OCH₂), 60.33 (CH₂), 14.56 (CH₃).

HRMS (ES-TOF): [M+H]⁺ Calc. m/z: 780.3504 - Obs. m/z: 780.3504

[M+2H]²⁺ Calc. m/z: 390.6802 - Obs. m/z: 390.6797

3m 4,4',4''-(((nitrilotris(methylene))tris(pyridine-6,2-diyl))tris(azanediy))tribenzoic acid



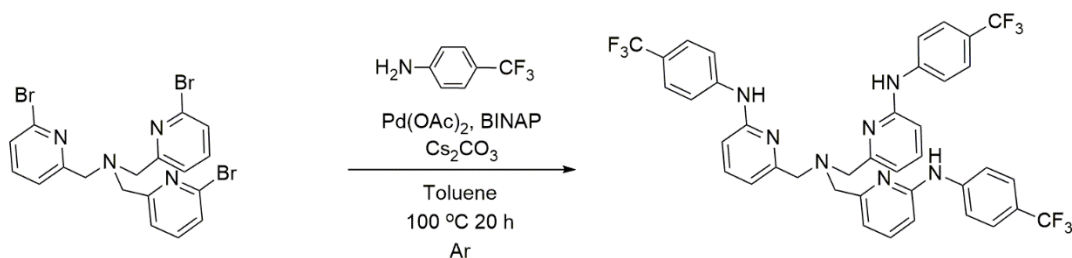
3l (250 mg, 0.32 mmol) was dissolved in 5 mL of DMSO. Following the addition of 1 M NaOH (3 mL), the solution was left stirring at room temperature for 3 h. The crude mixture was concentrated by rotary evaporator and then dissolved in 5 mL of methanol. The excess of NaOH, which precipitated as white salt, was removed by filtration. Next, the filtrate was concentrated, and the procedure was repeated two more times. Finally, after adding 10 mL of water, the product precipitated as white solid and was recovered by filtration (132 mg, 19.2 mmol; 60%).

¹H NMR (400 MHz, MeOD): δ 7.73 (d, J = 8.2 Hz, 6H - CH ar), 7.56 (t, J = 7.7 Hz, 3H - CH py), 7.47 (d, J = 7.9 Hz, 6H - CH ar), 6.92 (d, J = 7.1 Hz, 3H - CH py), 6.79 (d, J = 8.2 Hz, 3H - CH py), 4.44 (s, 6H - CH₂).

¹³C NMR (101 MHz, CDCl₃): δ 168.80 (C), 155.16 (C), 145.38 (C), 138.36 (CH py), 130.36 (CH ar), 122.65 (C), 117.09 (CH ar), 114.63 (CH py), 111.08 (CH py), 59.18 (CH₂).

HRMS (ES-TOF): [M+H]⁺ Calc. m/z: 696.2583- Obs. m/z: 696.2565

**3n 4,4',4''-(((nitrilotris(methylene))tris(pyridine-6,2-diyl))tris(azanediyl))
tribenzoic acid**



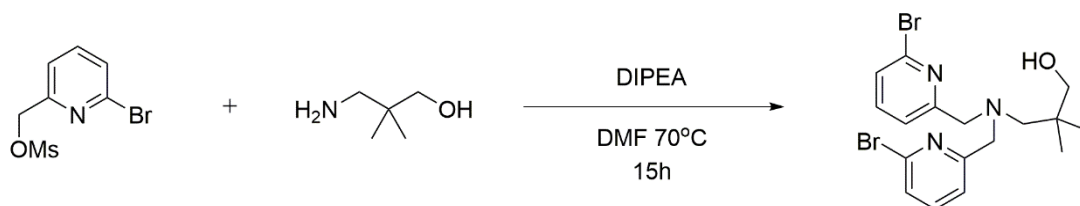
3f (500 mg, 0.95 mmol), Pd(OAc)₂ (19 mg, 0.085 mmol), \pm BINAP (78 mg, 0.13 mmol) and Cs₂CO₃ (1.85 g, 5.70 mmol) were introduced into a round bottom flask, which was then filled with argon. An Ar-sparged solution of 4-(trifluoromethyl)aniline (1.08 mL, 8.55 mmol) in 40 mL of toluene was added to the mixture. While heating to 100 °C, the solution turned from orange to red and from red to green. The reaction mixture was left stirring under Argon atmosphere for 20 h. TLC and LCMS showed full conversion of the starting material. The crude mixture was cooled down at room temperature and filtered off over celite. The filtrate was kept, and the solvent was evaporated under vacuum. The crude product was purified by auto column CombiFlash NextGen 100 using as eluent 3 CV of 20% ethyl acetate in hexane, followed by 15 CV gradient up to 50% of ethyl acetate in hexane. The product was collected between 10-15 CV. (510 mg, 0.66 mmol; 70%).

¹H NMR (400 MHz, CDCl₃): δ 7.58 – 7.46 (m, 15H - 3 CH py, 12 CH ar), 7.18 (d, J = 7.4 Hz, 3 CH py), 6.74 (d, J = 8.2 Hz, 3 CH py), 6.63 (s, 3H - NH), 3.87 (s, 6H - CH₂).

¹³C NMR (101 MHz, CDCl₃): δ 158.63 (C), 154.17 (C), 144.09 (C), 138.40 (CH py), 126.52 (q, J = 3.7 Hz - OCF₃), 117.96 (CH), 115.18 (CH), 108.18 (CH), 60.30 (CH₂).

HRMS (ES-TOF): [M+H]⁺ Calc. m/z: 768.2497- Obs. m/z: 768.2502

[M+Na]⁺ Calc. m/z: 790.2311- Obs. m/z: 790.2307

3o 3-{bis[(6-bromopyridin-2-yl)methyl]amino}-2,2-dimethylpropan-

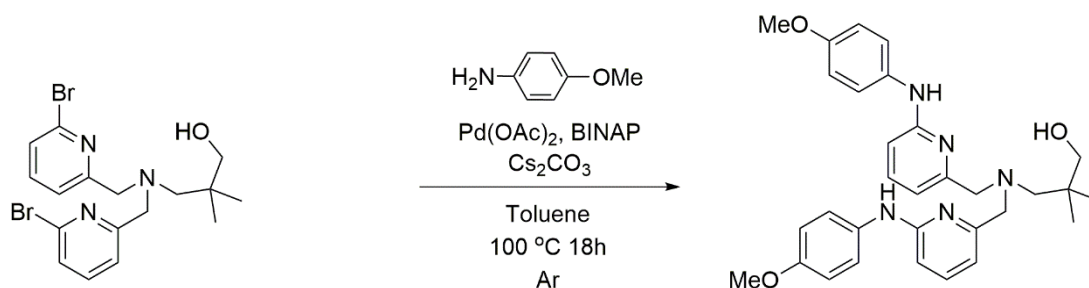
To a solution of **3c** (4.11 g, 15.46 mmol) in DMF (50 mL), 3-amino-2,2-dimethyl-1-propanol (633 mg, 6.11 mmol) and DIPEA (3.4 mL, 19.32 mmol) were added. The reaction mixture was then left stirring for 15 h at 70 °C. 300 mL of brine were poured into the solution, and the product was extracted from the water phase with DCM (3 x 70 mL). The organic layers were combined, dried over MgSO₄, and concentrated under vacuum. The product was purified by silica gel chromatography (hexane/ethyl acetate (7:3)) and obtained as a white powder (1.07 g, 2.41 mmol) in 40 % yield.

¹H NMR (400 MHz, CDCl₃): δ 7.50 (t, *J* = 7.7 Hz, 2H - CH py), 7.35 (t, *J* = 7.8 Hz, 4H - CH py), 4.69 (s, 1H - OH), 3.83 (s, 4H - CH₂), 3.34 (s, 2H - OCH₂), 2.67 (s, 2H - NCH₂ chain), 0.90 (s, 6H - CH₃).

¹³C NMR (101 MHz, CDCl₃): δ 160.53 (C py), 141.59 (C py), 139.01 (CH py), 126.71 (CH py), 122.32 (CH py), 71.95 (OCH₂ chain), 65.61 (NCH₂ chain), 62.15 (NCH₂), 36.86 (C chain), 24.55 (CH₃).

HRMS (ES-TOF): [M+H]⁺ Calc. m/z: 442.0124 - Obs. m/z: 442.0110

3p 3-[bis({6-[(4-methoxyphenyl)amino]pyridine-2-yl}methyl)amino]-2,2-dimethylpropan-1-ol



3o (670 mg, 1.51 mmol), $\text{Pd}(\text{OAc})_2$ (30.5 mg, 0.09 mmol), \pm BINAP (127 mg, 0.135 mmol) and Cs_2CO_3 (2.95 g, 9.06 mmol) were added to a 100 mL round bottom flask. To the powder mixture, an argon saturated solution of p-anisidine (1.12 g, 9.06 mmol) in toluene (40 mL) was added, and the reaction was left stirring for 18 h at $100\text{ }^\circ\text{C}$. The crude was then filtered off over Celite[®] and concentrated by rotary evaporator. The product was obtained pure (470 mg, 0.89 mmol) after silica gel chromatography column (hexane/ethyl acetate (3:2)) with 60 % yield.

¹H NMR (400 MHz, CDCl_3): δ 7.38 (t, $J = 7.8\text{ Hz}$, 2H - CH py), 7.22 (d, $J = 8.9\text{ Hz}$, 4H - CH an), 6.88 (d, $J = 8.9\text{ Hz}$, 4H - CH an), 6.75 (d, $J = 7.3\text{ Hz}$, 2H - CH py), 6.57 (d, $J = 8.3\text{ Hz}$, 2H - CH py), 6.54 (s, 2H - NH an), 3.80 (s, 6H - OCH_3), 3.72 (s, 4H - NCH_2), 3.41 (s, 2H - OCH_2), 2.65 (s, 2H - NCH_2 chain), 0.94 (s, 6H - CH_3).

¹³C NMR (101 MHz, CDCl_3): δ 157.97 (C an), 156.96 (C py), 156.25 (C an), 138.29 (CH py), 133.45 (C py), 124.19 (CH an), 114.64 (CH an), 113.57 (CH py), 105.20 (CH py), 72.22 (OCH_2 chain), 65.48 (NCH_2 chain), 62.34 (NCH_2), 55.65 (OCH_3), 36.78 (C chain), 24.94 (CH_3 chain).

HRMS (ES-TOF): $[\text{M}+\text{H}]^+$ Calc. m/z : 528.2969 - Obs. m/z : 528.2969;

3.4.2 UV- Kinetic experiment

The kinetic experiments were carried out at 25 °C in a mixture of 40% (v/v) acetonitrile in water. The latter was prepared as a single batch and used for all the stock solutions. The buffers used were MES (5.5 < pH < 6.7) HEPES (6.9 < pH < 8.2), EPPS (7.4 < pH < 8.6), CHES (8.7 < pH < 9.9) and CAPS (9.8 < pH < 11.0). All the solutions were prepared with analytical grade buffers keeping the ratio of water to acetonitrile constant and fixing the ionic strength at 0.1 M. The reactions were performed in a quartz cuvette using a Cary 300 UV-Vis-NIR spectrophotometers. At pH 7 or above, the reaction progress was monitored at 400 nm, following the appearance of p-nitrophenolate; in the pH range 5-7, the evaluation was done detecting the formation of p-nitrophenol at 318 nm by scanning kinetic method or HPLC. A typical experiment was started by introducing a volume of 5 mM HPNPP to the reaction solution. The latter was prepared by mixing the zinc complex (0.05 – 2 mM - created *in situ* by adding specific aliquots of 5-50 mM $\text{Zn}(\text{NO}_3)_2$ and ligand stock solutions) with 1 mL of 0.1 M buffer and the appropriate volume of 0.1 M NaNO_3 to reach 2 mL. The ligand solution was prepared with DMSO and the $\text{Zn}(\text{NO}_3)_2$ with 0.1 M NaNO_3 in 40% (v/v) acetonitrile in water.

Regarding the inhibition experiments, a similar method was used. The complex concentration was fixed at 0.5 mM, the buffer at 0.05 M and the substrate at 0.05 mM. A volume of 10 mM phenyl phosphate (PP - prepared using as solvent 0.1 M NaNO_3 in 40% (v/v) acetonitrile in water) was introduced into the reaction solution as an additional element in the over mentioned procedure. In the case of DMP, the concentration of the inhibitor was taken into account to keep constant the ionic strength. The stock solutions

(buffer, $\text{Zn}(\text{NO}_3)_2$ and DMP) were prepared in 40% (v/v) acetonitrile in water and the ionic strength was controlled with an additional solution of NaNO_3 in water/ acetonitrile (1 M). The buffer and the DMP were prepared at 0.2 M. All the components were added into the cuvette and the final volume was reached by adding water/ acetonitrile mixture.

3.4.3 HPLC- Kinetic experiment

DMP inhibition studies and kinetic experiments in pseudo-first order conditions (complex excess) below pH 7 were run by HPLC. The reaction progress was evaluated by measuring the appearance of p-nitrophenol (r.t. 9). A generic experiment was initiated by addition of 10 μL of 5 mM HPNPP to 1 mL reaction solution composed of: 1 mM complex (formed *in situ*), 50 mM buffer, 0.1 M NaNO_3 and optional DMP (20-100 mM) in 40% (v/v)

Kinetic experiments were run by HPLC using the following method:

- Pseudo first-order conditions (complex excess) at $\text{pH} \leq 7$:

Gradient: 5-95 % ACN in 10 min, run length: 30 min; injected volume: 20 μL ; Absorbance registered at 318 nm. Column: Kinetex[®] 5 μm C18 100 Å, LC Column,

3.4.4 Data

pH profile

[Buffer] = 50 mM , [NaNO₃] = 0.1 M, [HPNPP]=0.05 mM, 25 °C and 40% (v/v) acetonitrile in water;

3-1:

pH	k_{obs} / s^{-1}	[3-1] / M	$k_2 / M^{-1} s^{-1}$	log k_2
5.29	$1.46 \pm 0.07 \times 10^{-4}$	1×10^{-3}	$1.46 \pm 0.07 \times 10^{-1}$	-0.835
5.33	$7.83 \pm 0.13 \times 10^{-6}$	5×10^{-5}	$1.57 \pm 0.03 \times 10^{-1}$	-0.805
5.64	$1.62 \pm 0.14 \times 10^{-4}$	1×10^{-3}	$1.62 \pm 0.14 \times 10^{-1}$	-0.790
5.69	$1.76 \pm 0.02 \times 10^{-5}$	5×10^{-5}	$3.51 \pm 0.04 \times 10^{-1}$	-0.454
6.05	$1.28 \pm 0.01 \times 10^{-5}$	5×10^{-5}	$2.57 \pm 0.01 \times 10^{-1}$	-0.591
6.2	$2.82 \pm 0.04 \times 10^{-4}$	1×10^{-3}	$2.82 \pm 0.04 \times 10^{-1}$	-0.549
6.22	$1.20 \pm 0.02 \times 10^{-5}$	5×10^{-5}	$2.40 \pm 0.04 \times 10^{-1}$	-0.620
6.78	$1.43 \pm 0.01 \times 10^{-5}$	5×10^{-5}	$2.86 \pm 0.03 \times 10^{-1}$	-0.543
7.03	$3.41 \pm 0.02 \times 10^{-4}$	1×10^{-3}	$3.41 \pm 0.02 \times 10^{-1}$	-0.467
7.13	$1.34 \pm 0.01 \times 10^{-5}$	5×10^{-5}	$2.68 \pm 0.03 \times 10^{-1}$	-0.572
7.39	$3.70 \pm 0.01 \times 10^{-4}$	1×10^{-3}	$3.70 \pm 0.01 \times 10^{-1}$	-0.432
8.01	$3.69 \pm 0.05 \times 10^{-4}$	1×10^{-3}	$3.69 \pm 0.00 \times 10^{-1}$	-0.433
8.51	$3.07 \pm 0.01 \times 10^{-4}$	1×10^{-3}	$3.07 \pm 0.01 \times 10^{-1}$	-0.513
8.99	$3.44 \pm 0.01 \times 10^{-4}$	1×10^{-3}	$3.44 \pm 0.01 \times 10^{-1}$	-0.463
9.37	$2.88 \pm 0.01 \times 10^{-4}$	1×10^{-3}	$2.88 \pm 0.01 \times 10^{-1}$	-0.541
9.89	$2.83 \pm 0.01 \times 10^{-4}$	1×10^{-3}	$2.83 \pm 0.01 \times 10^{-1}$	-0.549

3-2:

pH	k_{obs} / s^{-1}	[3-2] / M	$k_2 / M^{-1} s^{-1}$	log k_2
5.30	$3.730 \pm 0.009 \times 10^{-5}$	5×10^{-5}	0.746 ± 0.002	-0.127
5.67	$4.550 \pm 0.023 \times 10^{-5}$	5×10^{-5}	0.910 ± 0.004	-0.041
6.16	$5.288 \pm 0.024 \times 10^{-5}$	5×10^{-5}	1.058 ± 0.003	0.024
6.66	$5.495 \pm 0.020 \times 10^{-5}$	5×10^{-5}	1.099 ± 0.004	0.041
7.05	$5.292 \pm 0.024 \times 10^{-5}$	5×10^{-5}	1.058 ± 0.005	0.025
7.35	$5.409 \pm 0.043 \times 10^{-4}$	5×10^{-4}	1.082 ± 0.006	0.034
7.87	$1.070 \pm 0.010 \times 10^{-4}$	1×10^{-4}	1.070 ± 0.001	0.030
7.90	$5.421 \pm 0.072 \times 10^{-4}$	5×10^{-4}	1.084 ± 0.002	0.035
7.98	$1.022 \pm 0.010 \times 10^{-3}$	1×10^{-3}	1.022 ± 0.010	0.009
8.44	$1.137 \pm 0.100 \times 10^{-3}$	1×10^{-3}	1.137 ± 0.100	0.056
8.99	$5.698 \pm 0.011 \times 10^{-4}$	5×10^{-4}	1.140 ± 0.002	0.057
9.38	$5.983 \pm 0.003 \times 10^{-4}$	5×10^{-4}	1.197 ± 0.001	0.078
9.82	$5.674 \pm 0.007 \times 10^{-4}$	5×10^{-4}	1.135 ± 0.001	0.055

3-3:

pH	k_{obs} / s^{-1}	[3-3] / M	$k_2 / M^{-1} s^{-1}$	log k_2
5.69	$4.731 \pm 0.028 \times 10^{-5}$	4.4×10^{-4}	$1.075 \pm 0.006 \times 10^{-1}$	-0.969
5.95	$5.207 \pm 0.029 \times 10^{-5}$	4.4×10^{-4}	$1.183 \pm 0.007 \times 10^{-1}$	-0.927
6.30	$6.680 \pm 0.176 \times 10^{-5}$	4.4×10^{-4}	$1.336 \pm 0.035 \times 10^{-1}$	-0.874
7.00	$7.316 \pm 0.018 \times 10^{-5}$	5×10^{-4}	$1.463 \pm 0.004 \times 10^{-1}$	-0.835
7.38	$7.749 \pm 0.003 \times 10^{-5}$	5×10^{-4}	$1.550 \pm 0.001 \times 10^{-1}$	-0.810
7.90	$8.183 \pm 0.001 \times 10^{-5}$	5×10^{-4}	$1.637 \pm 0.001 \times 10^{-1}$	-0.786
8.35	$8.179 \pm 0.003 \times 10^{-5}$	5×10^{-4}	$1.636 \pm 0.001 \times 10^{-1}$	-0.786
8.95	$7.791 \pm 0.005 \times 10^{-5}$	5×10^{-4}	$1.558 \pm 0.001 \times 10^{-1}$	-0.807
9.72	$7.454 \pm 0.004 \times 10^{-5}$	5×10^{-4}	$1.491 \pm 0.001 \times 10^{-1}$	-0.827

3-4:

pH	k_{obs} / s^{-1}	[3-4] / M	$k_2 / M^{-1} s^{-1}$	log k_2
5.64	$6.559 \pm 0.033 \times 10^{-5}$	4.4×10^{-4}	$1.525 \pm 0.008 \times 10^{-1}$	-0.817
5.66	$6.264 \pm 0.042 \times 10^{-5}$	4.0×10^{-4}	$1.566 \pm 0.011 \times 10^{-1}$	-0.805
5.87	$7.381 \pm 0.019 \times 10^{-5}$	4.4×10^{-4}	$1.716 \pm 0.004 \times 10^{-1}$	-0.765
6.08	$6.933 \pm 0.024 \times 10^{-5}$	4.0×10^{-4}	$1.733 \pm 0.006 \times 10^{-1}$	-0.761
6.46	$8.709 \pm 0.180 \times 10^{-5}$	4.4×10^{-4}	$2.025 \pm 0.042 \times 10^{-1}$	-0.693
7.14	$1.055 \pm 0.001 \times 10^{-4}$	5×10^{-4}	$2.111 \pm 0.001 \times 10^{-1}$	-0.676
7.46	$8.808 \pm 0.033 \times 10^{-5}$	4.4×10^{-4}	$2.048 \pm 0.008 \times 10^{-1}$	-0.689
7.48	$6.264 \pm 0.040 \times 10^{-5}$	4×10^{-4}	$1.875 \pm 0.010 \times 10^{-1}$	-0.727
7.55	$1.084 \pm 0.004 \times 10^{-4}$	5×10^{-4}	$2.168 \pm 0.001 \times 10^{-1}$	-0.664
7.78	$2.232 \pm 0.003 \times 10^{-4}$	1×10^{-3}	$2.232 \pm 0.001 \times 10^{-1}$	-0.651
8.25	$2.150 \pm 0.002 \times 10^{-4}$	1×10^{-3}	$2.150 \pm 0.002 \times 10^{-1}$	-0.668
8.36	$8.031 \pm 0.195 \times 10^{-5}$	4×10^{-4}	$2.008 \pm 0.049 \times 10^{-1}$	-0.697
8.81	$2.150 \pm 0.002 \times 10^{-4}$	1×10^{-3}	$2.150 \pm 0.002 \times 10^{-1}$	-0.668
9.29	$2.244 \pm 0.001 \times 10^{-4}$	1×10^{-3}	$2.244 \pm 0.001 \times 10^{-1}$	-0.649
9.98	$9.691 \pm 0.008 \times 10^{-5}$	5×10^{-4}	$1.938 \pm 0.002 \times 10^{-1}$	-0.713
10.29	$2.033 \pm 0.004 \times 10^{-4}$	1×10^{-3}	$2.033 \pm 0.004 \times 10^{-1}$	-0.692

· k_{obs} vs [3-n]:

[EPPS] = 50 mM , [NaNO₃] = 0.1 M, [HPNPP]=0.05 mM, 25 °C and 40% (v/v) acetonitrile in water;

[2-n] / mM	k_{obs} / s^{-1}			
	3-1	3-2	3-3	3-4
0.1	$3.13 \pm 0.002 \times 10^{-5}$	$1.071 \pm 0.001 \times 10^{-4}$	$1.280 \pm 0.001 \times 10^{-5}$	$1.888 \pm 0.001 \times 10^{-5}$
0.25	$8.870 \pm 0.005 \times 10^{-5}$	$2.615 \pm 0.001 \times 10^{-4}$	$3.592 \pm 0.002 \times 10^{-5}$	$5.192 \pm 0.003 \times 10^{-5}$
0.5	$1.522 \pm 0.001 \times 10^{-4}$	$5.146 \pm 0.002 \times 10^{-4}$	$8.187 \pm 0.005 \times 10^{-5}$	$1.044 \pm 0.001 \times 10^{-4}$
0.75	$2.444 \pm 0.008 \times 10^{-4}$	$7.724 \pm 0.003 \times 10^{-4}$	$1.382 \pm 0.001 \times 10^{-4}$	$1.749 \pm 0.001 \times 10^{-4}$
1	$3.338 \pm 0.012 \times 10^{-4}$	$1.012 \pm 0.001 \times 10^{-3}$	$2.104 \pm 0.003 \times 10^{-4}$	$2.709 \pm 0.003 \times 10^{-4}$
2	$6.052 \pm 0.009 \times 10^{-4}$	$2.107 \pm 0.005 \times 10^{-3}$	$4.936 \pm 0.018 \times 10^{-4}$	$7.480 \pm 0.022 \times 10^{-4}$

k_{obs} vs [HPNPP]:

[EPPS] = 50 mM pH 7.4 , [NaNO₃] = 0.1 M, [3-n] = 0.5 mM, 25 °C and 40% (v/v) acetonitrile in water;

[HPNPP] / mM	$k_{\text{obs}} / \text{s}^{-1}$			
	3-1	3-2	3-3	3-4
0.01	$1.451 \pm 0.003 \times 10^{-4}$	$3.814 \pm 0.015 \times 10^{-4}$	$8.995 \pm 0.024 \times 10^{-5}$	$1.170 \pm 0.001 \times 10^{-4}$
0.025	$1.630 \pm 0.002 \times 10^{-4}$	$4.445 \pm 0.004 \times 10^{-4}$	$8.607 \pm 0.001 \times 10^{-5}$	$1.087 \pm 0.001 \times 10^{-4}$
0.05	$1.522 \pm 0.001 \times 10^{-4}$	$4.559 \pm 0.004 \times 10^{-4}$	$8.187 \pm 0.005 \times 10^{-5}$	$1.209 \pm 0.001 \times 10^{-4}$
0.075	$1.576 \pm 0.001 \times 10^{-4}$	$4.561 \pm 0.004 \times 10^{-4}$	$8.155 \pm 0.003 \times 10^{-5}$	$1.219 \pm 0.001 \times 10^{-4}$
0.1	$1.756 \pm 0.001 \times 10^{-4}$	$4.564 \pm 0.004 \times 10^{-4}$	$7.804 \pm 0.001 \times 10^{-5}$	$1.186 \pm 0.005 \times 10^{-4}$

k_{obs} vs [Buffer]:

pH 7.4, [NaNO₃] = 0.1 M, [HPNPP] = 0.05 mM, 25 °C and 40% (v/v) acetonitrile in water;

[HEPES] / M	$k_{\text{obs}} / \text{s}^{-1}$			
	3-1 /1mM	3-2 /1mM	3-3 /0.5 mM	3-4 /0.5 mM
0.01	$3.791 \pm 0.005 \times 10^{-4}$	$9.521 \pm 0.041 \times 10^{-4}$	$6.254 \pm 0.003 \times 10^{-4}$	$1.005 \pm 0.001 \times 10^{-4}$
0.025	$3.508 \pm 0.010 \times 10^{-4}$	$9.985 \pm 0.012 \times 10^{-4}$	$8.134 \pm 0.004 \times 10^{-4}$	$1.087 \pm 0.001 \times 10^{-4}$
0.05	$3.625 \pm 0.008 \times 10^{-4}$	$9.848 \pm 0.010 \times 10^{-4}$	$7.912 \pm 0.005 \times 10^{-4}$	$1.013 \pm 0.001 \times 10^{-4}$
0.075	$3.505 \pm 0.006 \times 10^{-4}$	$9.867 \pm 0.007 \times 10^{-4}$	$7.203 \pm 0.005 \times 10^{-4}$	$8.753 \pm 0.001 \times 10^{-5}$
0.1	$3.676 \pm 0.006 \times 10^{-4}$	$9.851 \pm 0.010 \times 10^{-4}$	$6.588 \pm 0.007 \times 10^{-4}$	$9.846 \pm 0.002 \times 10^{-5}$

● **PP inhibition experiment**

[Buffer] = 50 mM, [NaNO₃] = 0.1 M, [3-n] =1 mM, [HPNPP]=0.05 mM, 25 °C and 40% (v/v) acetonitrile in water;

[PP] / mM	3-1					
	pH 7.1		pH 7.9		pH 9.0	
	k_{obs} / s^{-1}	k/k_0	k_{obs} / s^{-1}	k/k_0	k_{obs} / s^{-1}	k/k_0
0	$1.572 \pm 0.003 \times 10^{-4}$	1.00	$1.810 \pm 0.001 \times 10^{-4}$	1.00	$1.548 \pm 0.001 \times 10^{-4}$	1.00
0.1	$1.391 \pm 0.002 \times 10^{-4}$	0.88	$1.515 \pm 0.001 \times 10^{-4}$	0.84	$1.479 \pm 0.001 \times 10^{-4}$	0.96
0.5	$4.571 \pm 0.004 \times 10^{-5}$	0.29	$8.456 \pm 0.005 \times 10^{-5}$	0.47	$1.213 \pm 0.000 \times 10^{-4}$	0.78
1	$1.356 \pm 0.004 \times 10^{-5}$	0.09	$5.288 \pm 0.002 \times 10^{-5}$	0.29	$1.056 \pm 0.001 \times 10^{-4}$	0.68
1.5	$8.397 \pm 0.004 \times 10^{-6}$	0.05	$3.737 \pm 0.024 \times 10^{-5}$	0.21	$8.594 \pm 0.007 \times 10^{-5}$	0.56
2	$7.039 \pm 0.130 \times 10^{-6}$	0.04	$2.733 \pm 0.001 \times 10^{-5}$	0.15	$6.783 \pm 0.009 \times 10^{-5}$	0.44

[PP] / mM	3-2					
	pH 7.1		pH 8.0		pH 9.1	
	k_{obs} / s^{-1}	k/k_0	k_{obs} / s^{-1}	k/k_0	k_{obs} / s^{-1}	k/k_0
0	$4.497 \pm 0.005 \times 10^{-4}$	1.00	$4.405 \pm 0.002 \times 10^{-4}$	1.00	$4.865 \pm 0.005 \times 10^{-4}$	1.00
0.1	$3.859 \pm 0.020 \times 10^{-4}$	0.95	$3.866 \pm 0.001 \times 10^{-4}$	0.88	$4.628 \pm 0.005 \times 10^{-4}$	0.95
0.5	$1.287 \pm 0.001 \times 10^{-4}$	0.87	$2.218 \pm 0.008 \times 10^{-4}$	0.50	$4.223 \pm 0.003 \times 10^{-4}$	0.87
1	$4.847 \pm 0.010 \times 10^{-5}$	0.73	$1.396 \pm 0.000 \times 10^{-4}$	0.32	$3.536 \pm 0.002 \times 10^{-4}$	0.73
1.5	$2.985 \pm 0.005 \times 10^{-5}$	0.63	$0.925 \pm 0.000 \times 10^{-5}$	0.21	$3.066 \pm 0.002 \times 10^{-5}$	0.63
2	$8.213 \pm 0.051 \times 10^{-6}$	0.53	$6.861 \pm 0.000 \times 10^{-5}$	0.16	$2.581 \pm 0.001 \times 10^{-6}$	0.53

- **DMP inhibition:**

[Buffer] = 50 mM, [NaNO₃] = 0.1 M, [3-n] = 0.5 mM, [HPNPP] = 0.05 mM, 25 °C and 40% (v/v) acetonitrile in water;

[DMP] / mM	3-1			
	pH 7.1		pH 6.2	
	k_{obs} / s^{-1}	k/k_0	k_{obs} / s^{-1}	k/k_0
0	$4.02 \pm 0.01 \times 10^{-4}$	1.00	$2.82 \pm 0.04 \times 10^{-4}$	1.00
20	$3.50 \pm 0.02 \times 10^{-4}$	0.87	$1.44 \pm 0.02 \times 10^{-4}$	0.51
40	$2.98 \pm 0.02 \times 10^{-4}$	0.74	$1.11 \pm 0.03 \times 10^{-4}$	0.39
60	$3.06 \pm 0.02 \times 10^{-4}$	0.76	$7.58 \pm 0.20 \times 10^{-5}$	0.27
80	$2.83 \pm 0.02 \times 10^{-4}$	0.70	$6.72 \pm 0.12 \times 10^{-5}$	0.24
100	$2.42 \pm 0.03 \times 10^{-4}$	0.60	$4.15 \pm 0.08 \times 10^{-5}$	0.15

[DMP] / mM	3-2			
	pH 7.1		pH 6.3	
	k_{obs} / s^{-1}	k/k_0	k_{obs} / s^{-1}	k/k_0
0	$8.885 \pm 0.012 \times 10^{-4}$	1	$3.13 \pm 0.23 \times 10^{-4}$	1.00
20	$8.004 \pm 0.008 \times 10^{-4}$	0.90	$1.39 \pm 0.04 \times 10^{-4}$	0.44
40	$7.218 \pm 0.013 \times 10^{-4}$	0.81	$8.29 \pm 0.51 \times 10^{-5}$	0.27
60	$6.382 \pm 0.009 \times 10^{-4}$	0.72	$7.80 \pm 0.50 \times 10^{-5}$	0.25
80	$5.874 \pm 0.005 \times 10^{-4}$	0.66	$5.29 \pm 0.34 \times 10^{-5}$	0.17
100	$5.255 \pm 0.004 \times 10^{-4}$	0.59	$4.71 \pm 0.37 \times 10^{-5}$	0.15

[DMP] / mM	3-3			
	pH 7.1		pH 6.3	
	k_{obs} / s^{-1}	k/k_0	k_{obs} / s^{-1}	k/k_0
0	$4.690 \pm 0.003 \times 10^{-5}$	1	$3.96 \pm 0.01 \times 10^{-5}$	1.00
20	$4.254 \pm 0.015 \times 10^{-5}$	0.91	$2.40 \pm 0.00 \times 10^{-5}$	0.61
40	$3.902 \pm 0.004 \times 10^{-5}$	0.83	$1.65 \pm 0.04 \times 10^{-5}$	0.42
60	$3.810 \pm 0.004 \times 10^{-5}$	0.81	$1.35 \pm 0.03 \times 10^{-5}$	0.34
80	$3.472 \pm 0.005 \times 10^{-5}$	0.74	$1.11 \pm 0.03 \times 10^{-5}$	0.28
100	$3.316 \pm 0.005 \times 10^{-5}$	0.71	$0.98 \pm 0.02 \times 10^{-5}$	0.25

[DMP] / mM	3-4			
	pH 7.1		pH 6.3	
	k_{obs} / s^{-1}	k/k_0	k_{obs} / s^{-1}	k/k_0
0	$7.631 \pm 0.002 \times 10^{-5}$	1	$6.23 \pm 0.03 \times 10^{-5}$	1.00
20	$7.170 \pm 0.003 \times 10^{-5}$	0.71	$4.41 \pm 0.00 \times 10^{-5}$	0.71
40	$6.474 \pm 0.002 \times 10^{-5}$	0.48	$2.97 \pm 0.03 \times 10^{-5}$	0.48
60	$6.301 \pm 0.002 \times 10^{-5}$	0.38	$2.34 \pm 0.02 \times 10^{-5}$	0.38
80	$5.599 \pm 0.004 \times 10^{-5}$	0.28	$1.76 \pm 0.03 \times 10^{-5}$	0.28
100	$5.336 \pm 0.002 \times 10^{-5}$	0.25	$1.53 \pm 0.03 \times 10^{-5}$	0.25

- **Kinetic data for 3-6**

- **pH profile:**

[Buffer] = 50 mM , [NaNO₃] = 0.1 M, [BNPP]=0.05 mM, 25 °C and 40% (v/v)

acetonitrile in water;

pH	k_{obs} / s^{-1}	[3-6] / M	$k_2 / M^{-1} s^{-1}$
7.05	$3.501 \pm 0.669 \times 10^{-5}$	1×10^{-4}	$3.501 \pm 0.669 \times 10^{-2}$
7.13	$2.040 \pm 0.002 \times 10^{-5}$	5×10^{-4}	$4.081 \pm 0.002 \times 10^{-2}$
7.56	$4.958 \pm 0.008 \times 10^{-5}$	1×10^{-3}	$4.958 \pm 0.008 \times 10^{-2}$
7.86	$2.578 \pm 0.008 \times 10^{-5}$	5×10^{-4}	$5.156 \pm 0.008 \times 10^{-2}$
7.94	$4.220 \pm 0.666 \times 10^{-5}$	1×10^{-3}	$4.220 \pm 0.666 \times 10^{-2}$
8.41	$5.654 \pm 0.004 \times 10^{-4}$	1×10^{-3}	$5.654 \pm 0.004 \times 10^{-2}$
8.93	$6.146 \pm 0.159 \times 10^{-5}$	1×10^{-3}	$6.146 \pm 0.159 \times 10^{-2}$
9.61	$2.572 \pm 0.114 \times 10^{-5}$	5×10^{-4}	$5.144 \pm 0.229 \times 10^{-2}$
9.85	$5.102 \pm 0.003 \times 10^{-4}$	1×10^{-3}	$5.102 \pm 0.003 \times 10^{-2}$
10.35	$3.079 \pm 0.006 \times 10^{-4}$	1×10^{-3}	$3.079 \pm 0.006 \times 10^{-2}$
10.37	$2.517 \pm 0.001 \times 10^{-4}$	1×10^{-3}	$2.517 \pm 0.001 \times 10^{-2}$
10.54	$1.244 \pm 0.001 \times 10^{-5}$	5×10^{-4}	$2.488 \pm 0.002 \times 10^{-2}$

- k_{obs} vs [3-6]:

[EPPS] = 50 mM , [NaNO₃] = 0.1 M, [BNPP]=0.05 mM, 25 °C and 40% (v/v) acetonitrile in water;

[3-6] / mM	k_{obs} / s^{-1}
0.10	$3.361 \pm 0.028 \times 10^{-6}$
0.25	$1.029 \pm 0.001 \times 10^{-5}$
0.50	$1.831 \pm 0.001 \times 10^{-5}$
0.75	$2.212 \pm 0.002 \times 10^{-5}$
1.00	$3.062 \pm 0.005 \times 10^{-5}$
1.50	$4.639 \pm 0.009 \times 10^{-5}$
2.00	$5.789 \pm 0.005 \times 10^{-5}$
2.50	$8.002 \pm 0.014 \times 10^{-5}$

- k_{obs} vs [BNPP]:

[3-6] = 0.5 mM, [EPPS] = 50 mM , [NaNO₃] = 0.1 M, 25 °C and 40% (v/v) acetonitrile in water;

[BNPP] / mM	k_{obs} / s^{-1}
0.01	$3.327 \pm 0.008 \times 10^{-5}$
0.025	$2.849 \pm 0.005 \times 10^{-5}$
0.05	$2.949 \pm 0.003 \times 10^{-5}$
0.075	$2.935 \pm 0.002 \times 10^{-5}$
0.1	$2.851 \pm 0.003 \times 10^{-5}$

- k_{obs} vs [HEPES]:

[3-6] = 0.5 mM, [NaNO₃] = 0.1 M , [BNPP] = 0.05 mM, 25 °C and 40% (v/v) acetonitrile in water;

[HEPES] / M	k_{obs} / s^{-1}
0.005	$2.653 \pm 0.029 \times 10^{-5}$
0.010	$2.110 \pm 0.001 \times 10^{-5}$
0.025	$2.483 \pm 0.003 \times 10^{-5}$
0.050	$2.279 \pm 0.003 \times 10^{-5}$
0.075	$2.011 \pm 0.001 \times 10^{-5}$
0.100	$1.984 \pm 0.002 \times 10^{-5}$

● Kinetic data for 2-2

- pH profile:

[2-2] = 1 mM, [Buffer] = 50 mM , [NaNO₃] = 0.1 M, [BNPP]=0.05 mM, 25 °C and 40% (v/v) acetonitrile in water;

pH	k_{obs} / s^{-1}	[2-2] / M	$k_2 / M^{-1} s^{-1}$
7.02	$3.481 \pm 0.333 \times 10^{-5}$	1×10^{-3}	$3.481 \pm 0.333 \times 10^{-2}$
7.54	$4.809 \pm 0.445 \times 10^{-5}$	1×10^{-3}	$4.809 \pm 0.445 \times 10^{-2}$
7.92	$5.641 \pm 0.130 \times 10^{-5}$	1×10^{-3}	$5.641 \pm 0.130 \times 10^{-2}$
8.40	$6.791 \pm 0.024 \times 10^{-5}$	1×10^{-3}	$6.791 \pm 0.024 \times 10^{-2}$
8.56	$6.097 \pm 0.003 \times 10^{-5}$	1×10^{-3}	$6.097 \pm 0.003 \times 10^{-2}$
8.90	$6.243 \pm 0.013 \times 10^{-4}$	1×10^{-3}	$6.243 \pm 0.013 \times 10^{-2}$
9.34	$6.170 \pm 0.011 \times 10^{-5}$	1×10^{-3}	$6.170 \pm 0.011 \times 10^{-2}$
9.89	$5.558 \pm 0.002 \times 10^{-5}$	1×10^{-3}	$5.558 \pm 0.002 \times 10^{-2}$
10.41	$4.228 \pm 0.003 \times 10^{-4}$	1×10^{-3}	$4.228 \pm 0.003 \times 10^{-2}$

- k_{obs} vs [2-2]:

[EPPS] = 50 mM , [NaNO₃] = 0.1 M, [BNPP]=0.05 mM, 25 °C and 40% (v/v)

acetonitrile in water;

[2-2] / mM	k_{obs} / s^{-1}
0.10	$2.151 \pm 0.003 \times 10^{-6}$
0.25	$4.029 \pm 0.001 \times 10^{-6}$
0.50	$1.082 \pm 0.002 \times 10^{-5}$
0.75	$1.665 \pm 0.001 \times 10^{-5}$
1.00	$1.801 \pm 0.001 \times 10^{-5}$
1.50	$3.896 \pm 0.010 \times 10^{-5}$
2.00	$4.429 \pm 0.004 \times 10^{-5}$

- k_{obs} vs [BNPP]:

[2-2] = 1 mM, [EPPS] = 50 mM , [NaNO₃] = 0.1 M, [complex] = 0.5 mM, 25 °C

and 40% (v/v) acetonitrile in water;

[BNPP] / mM	k_{obs} / s^{-1}
0.01	$1.527 \pm 0.003 \times 10^{-5}$
0.025	$1.476 \pm 0.003 \times 10^{-5}$
0.05	$1.846 \pm 0.004 \times 10^{-5}$
0.075	$1.760 \pm 0.001 \times 10^{-5}$
0.1	$2.284 \pm 0.001 \times 10^{-5}$

- k_{obs} vs [HEPES]:

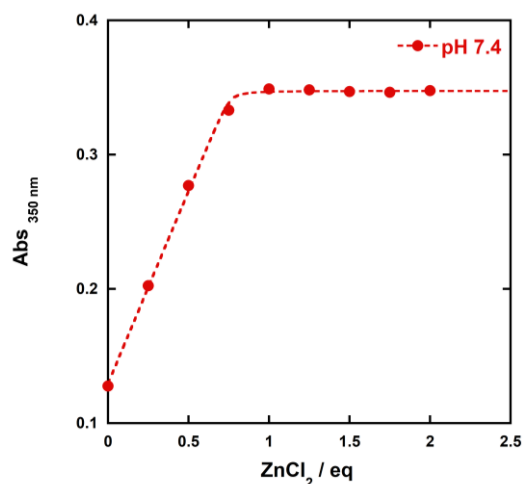
[2-2] = 1 mM, [NaNO₃] = 0.1 M, [BNPP] = 0.05 mM, 25 °C and 40% (v/v)

acetonitrile in water;

[HEPES] / M	k_{obs} / s^{-1}
0.005	$1.848 \pm 0.019 \times 10^{-5}$
0.010	$2.204 \pm 0.001 \times 10^{-5}$
0.025	$2.119 \pm 0.003 \times 10^{-5}$
0.050	$2.165 \pm 0.002 \times 10^{-5}$
0.075	$2.020 \pm 0.001 \times 10^{-5}$
0.100	$2.070 \pm 0.002 \times 10^{-5}$

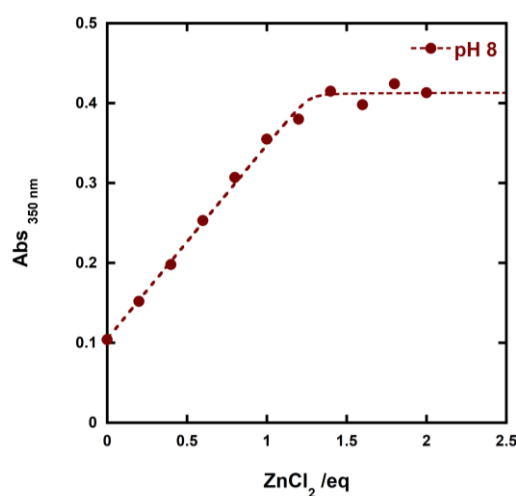
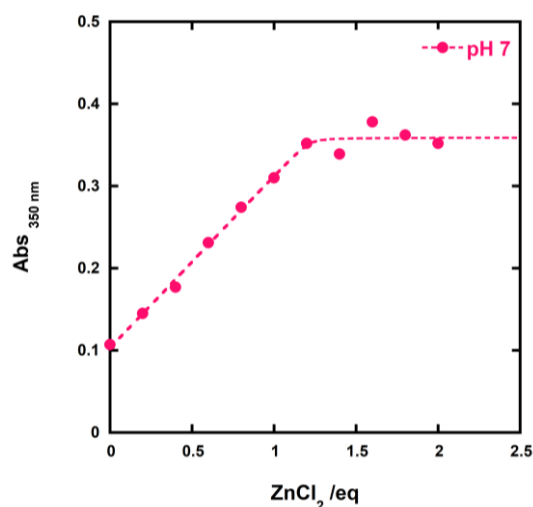
3.4.5 Zinc binding - Graph of Absorbance at 350 nm against the equivalent of ZnCl_2

3-1



Abs _{350 nm}	ZnCl ₂ / mmol	ZnCl ₂ / eq
0.1277	0	0
0.2024	0.025	0.25
0.2769	0.050	0.5
0.3332	0.075	0.75
0.3490	0.100	1
0.3483	0.125	1.25
0.3470	0.150	1.5
0.3464	0.175	1.75
0.3477	0.200	2

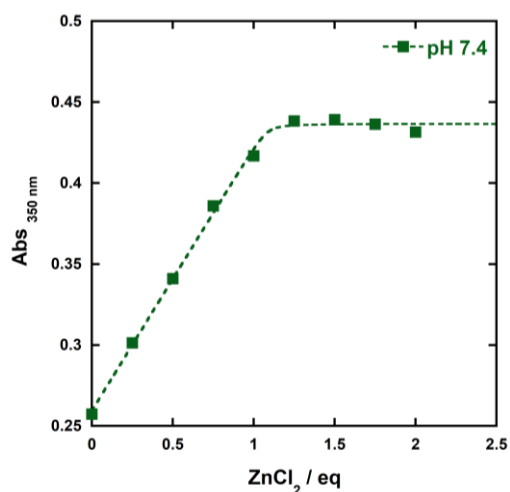
The zinc titration experiment at pH 7.4 was performed using a UV Spectrophotometer. Condition: $[3-1] = 0.05 \text{ mM}$, $[\text{HEPES}] = 50 \text{ mM}$, $V_{\text{tot}} = 2 \text{ mL}$, 40% (v/v) acetonitrile in water; addition: $10 \mu\text{L}$ of $[\text{ZnCl}_2] = 2.5 \text{ mM}$, 40% (v/v) acetonitrile in water;



The zinc titration experiments at pH 7 and 8 were performed using a plate reader. Condition: $[3-1] = 0.05 \text{ mM}$, $[\text{ZnCl}_2] = 0 - 0.1 \text{ mM}$, $[\text{HEPES}] = 50 \text{ mM}$, $V_{\text{tot}} = 300 \mu\text{L}$, 40% (v/v) acetonitrile in water;

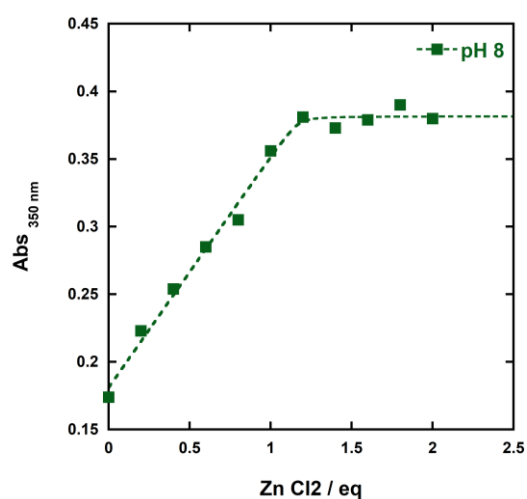
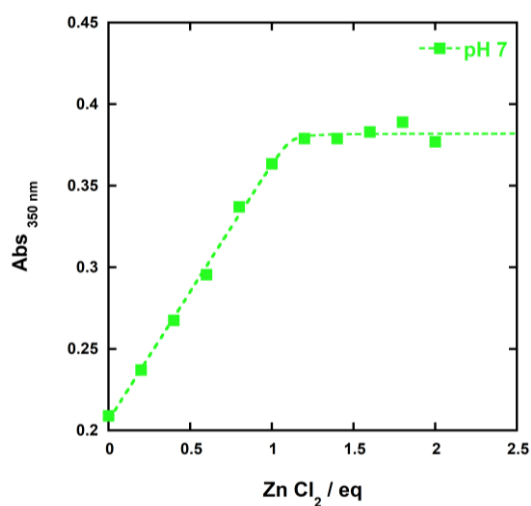
ZnCl ₂ /eq		0	0.2	0.4	0.6	0.8	1	1.2	1.4	1.6	1.8	2
Abs 350 nm	pH 7	0.107	0.145	0.177	0.231	0.274	0.31	0.352	0.339	0.378	0.362	0.352
	pH 8	0.104	0.152	0.198	0.253	0.307	0.355	0.38	0.415	0.398	0.424	0.413

3-2



Abs _{350 nm}	ZnCl ₂ / mmol	ZnCl ₂ / eq
0.2573	0	0
0.3013	0.025	0.25
0.3410	0.050	0.5
0.3859	0.075	0.75
0.4168	0.100	1
0.4383	0.125	1.25
0.4391	0.150	1.5
0.4364	0.175	1.75
0.4315	0.200	2

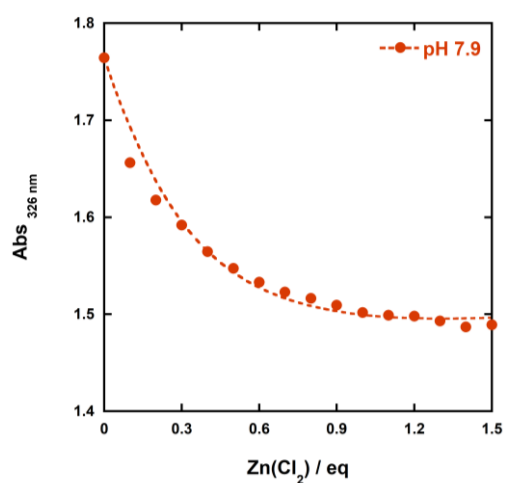
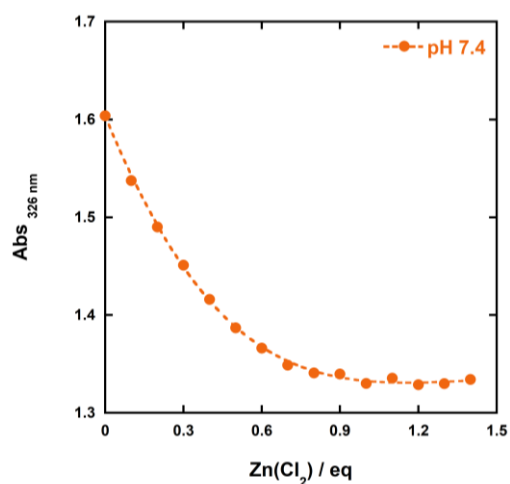
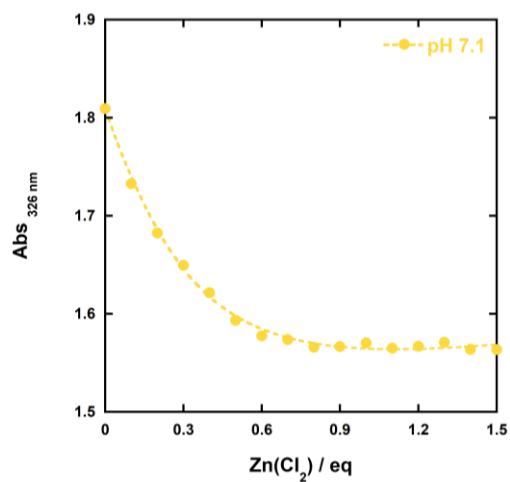
The zinc titration experiment at pH 7.4 was performed using a 2 mL cuvette with a UV Spectrofotometer. Condition: [3-2] = 0.05 mM, [HEPES] = 50 mM, V_{tot} = 2 mL, 40% (v/v) acetonitrile in water; addition: 10 μ L of [ZnCl₂] = 2.5 mM, 40% (v/v) acetonitrile in water;



The zinc titration experiments at pH 7 and 8 were performed using a plate reader. Condition: [3-2] = 0.05 mM, [ZnCl₂] = 0 - 0.1 mM, [HEPES] = 50 mM, V_{tot} = 300 μ L, 40% (v/v) acetonitrile in water;

ZnCl ₂ /eq	0	0.2	0.4	0.6	0.8	1	1.2	1.4	1.6	1.8	2
Abs _{350 nm} pH 7	0.209	0.237	0.267	0.296	0.337	0.364	0.379	0.378	0.383	0.389	0.377
Abs _{350 nm} pH 8	0.174	0.223	0.254	0.285	0.305	0.356	0.381	0.373	0.379	0.39	0.38

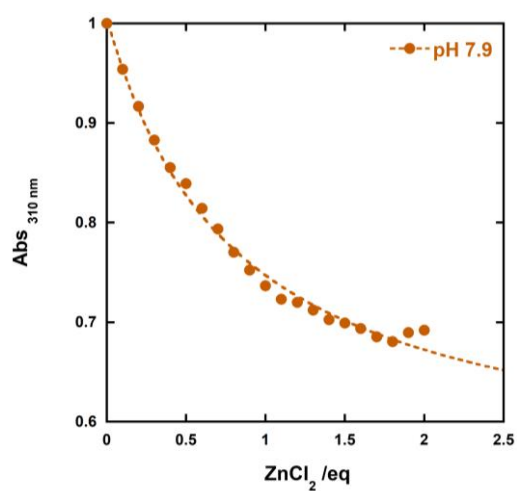
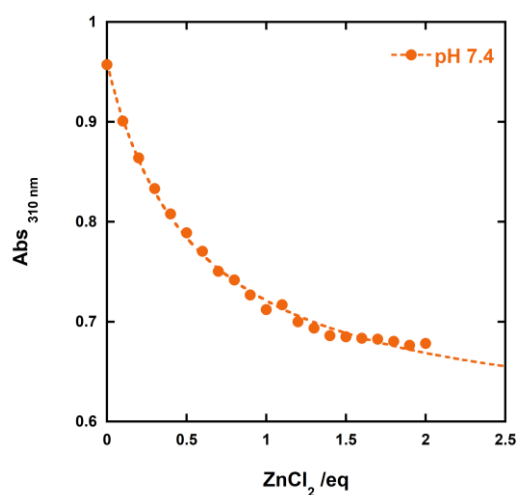
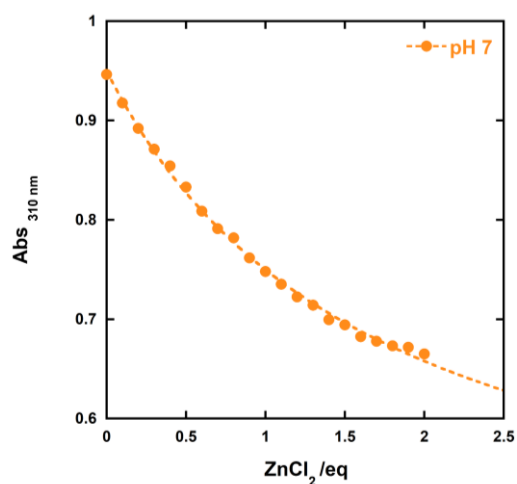
3-3



ZnCl ₂ / eq	Absorbance _{326 nm}		
	pH 7.1	pH 7.4	pH 7.9
0	1.809	1.634	1.764
0.1	1.733	1.538	1.656
0.21	1.683	1.490	1.618
0.31	1.650	1.451	1.592
0.41	1.622	1.416	1.565
0.51	1.593	1.387	1.547
0.62	1.578	1.366	1.533
0.72	1.574	1.349	1.523
0.82	1.566	1.341	1.516
0.92	1.567	1.340	1.509
1.03	1.570	1.330	1.502
1.13	1.565	1.336	1.499
1.23	1.567	1.329	1.498
1.34	1.571	1.330	1.493
1.44	1.564	1.334	1.487
1.54	1.564	1.634	1.489

The zinc titration experiments were performed using a 0.75 mL cuvette with a UV Spectrophotometer. Condition: [3-3] = 0.05 mM, [Buffer] = 50 mM, V_{tot} = 2 mL, 40% (v/v) acetonitrile in water; addition: 10 μ L of [ZnCl₂] = 2.5 mM, [3-3] = 0.05 mM, [Buffer] = 50 mM 40% (v/v) acetonitrile in water;

3-4



ZnCl ₂ /eq	Absorbance _{310 nm}		
	pH 7	pH 7.4	pH 7.9
0.0	0.946	0.957	0.946
0.1	0.918	0.901	0.918
0.2	0.892	0.864	0.892
0.3	0.871	0.833	0.871
0.4	0.854	0.808	0.854
0.5	0.833	0.789	0.833
0.6	0.809	0.770	0.809
0.7	0.791	0.750	0.791
0.8	0.782	0.742	0.782
0.9	0.762	0.727	0.762
1.0	0.748	0.712	0.748
1.1	0.735	0.717	0.735
1.2	0.722	0.700	0.722
1.3	0.714	0.693	0.714
1.4	0.700	0.686	0.700
1.5	0.694	0.685	0.694
1.6	0.682	0.683	0.682
1.7	0.678	0.682	0.678
1.8	0.673	0.680	0.673
1.9	0.672	0.676	0.672
2.0	0.665	0.678	0.665

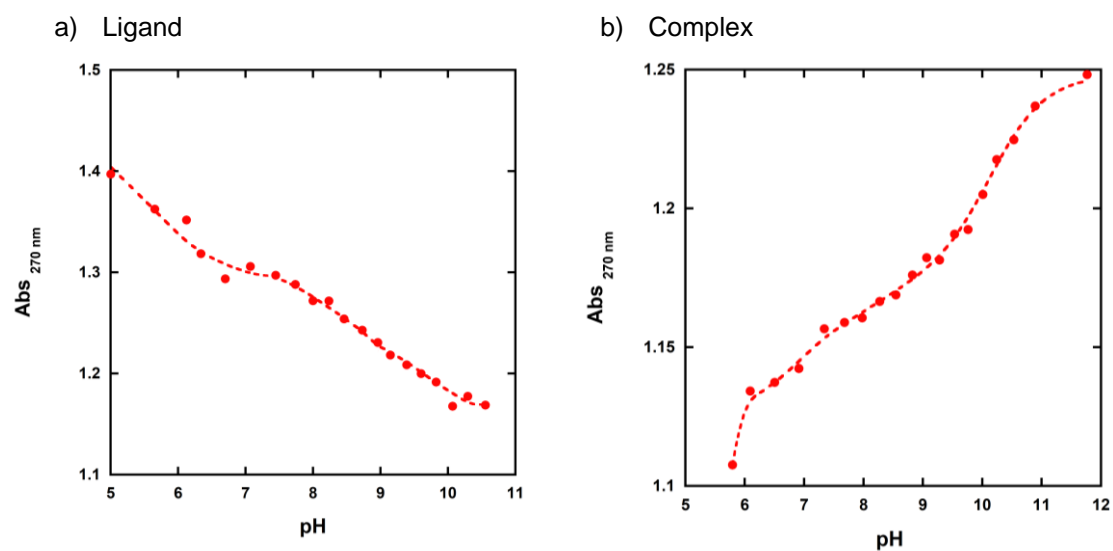
The zinc titration experiments were performed using a 0.75 mL cuvette with a UV Spectrofotometer. Condition: [3-4] = 0.05 mM, [Buffer] = 50 mM, V_{tot} = 2 mL, 40% (v/v) acetonitrile in water; addition: 10 μ L of [ZnCl₂] = 2.5 mM, [3-3] = 0.05 mM, [Buffer] = 50 mM 40% (v/v) acetonitrile in water;

3.4.6 UV - Titration

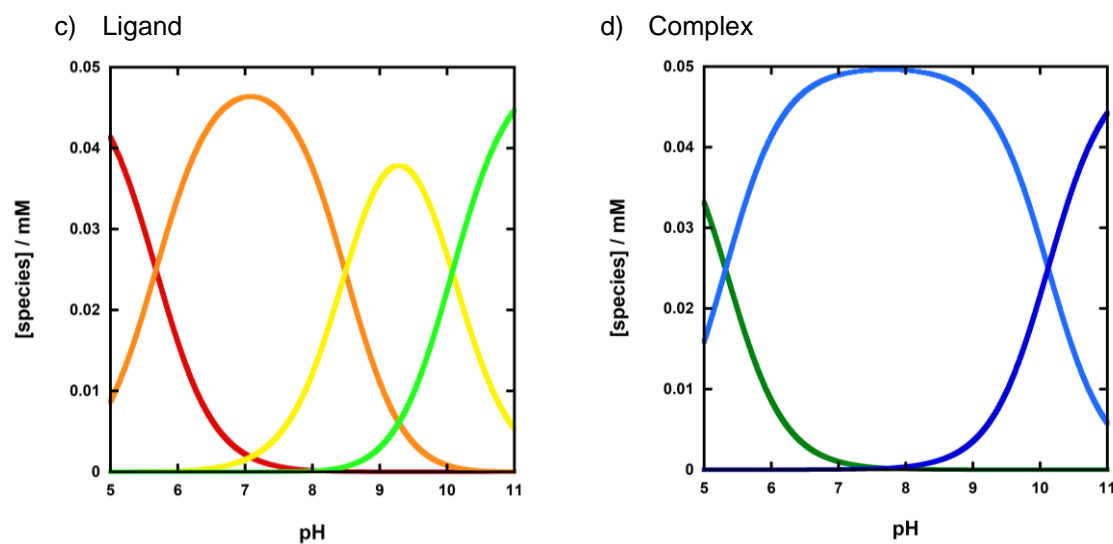
The titration experiments were carried out at 25°C and the pH was measured by Mettler-Toledo pH meter calibrated with Thermo Scientific buffer packs at pH 4.00, 7.01 and 10.06 at 25 °C. Cary 50 UV-Vis spectrophotometer was used to register the spectrum. All the UV-titrations were performed at the same experimental conditions. To keep the **L3-n** and **3-n** concentration constant during the titration, both the analyte and the titrant solutions were prepared at 0.05 mM of the ligand or complex. In addition, both the solutions were made at 40%(v/v) of acetonitrile in water. In the analyte solution (0.5 mL), MES, EPPS, CHES and CAPS were at the same concentration (25 mM) and the pH range between 5 and 12 was investigated by consecutive addition of 10 µL of the titrant (0.25 M NaOH). Each base addition was followed by recording the UV spectrum and measuring the pH of the analyte solution. A reduced volume cuvette with 0.5 cm path length was used for all the experiments. The absorbance values of an appropriate wavelength were then reported against the pH and processed by Hyperspec and Hyss. The fitting of the data yielded the speciation plots reported below. The titration plots of the **3-n** were fitted using the log β values obtained for the relative **L3-n**.

3-1

Titration curve:



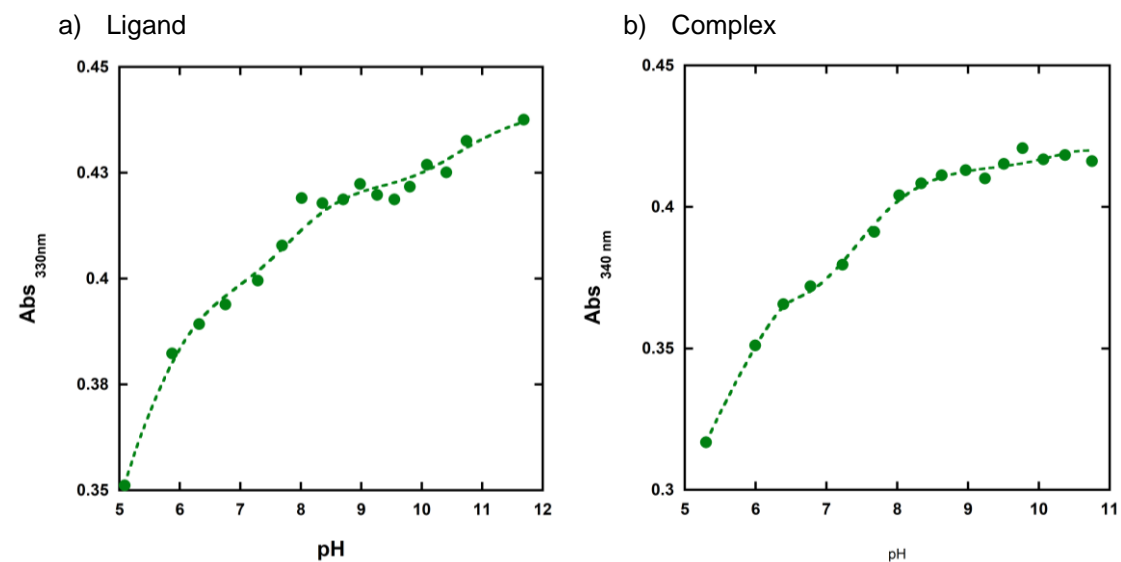
Speciation curve:



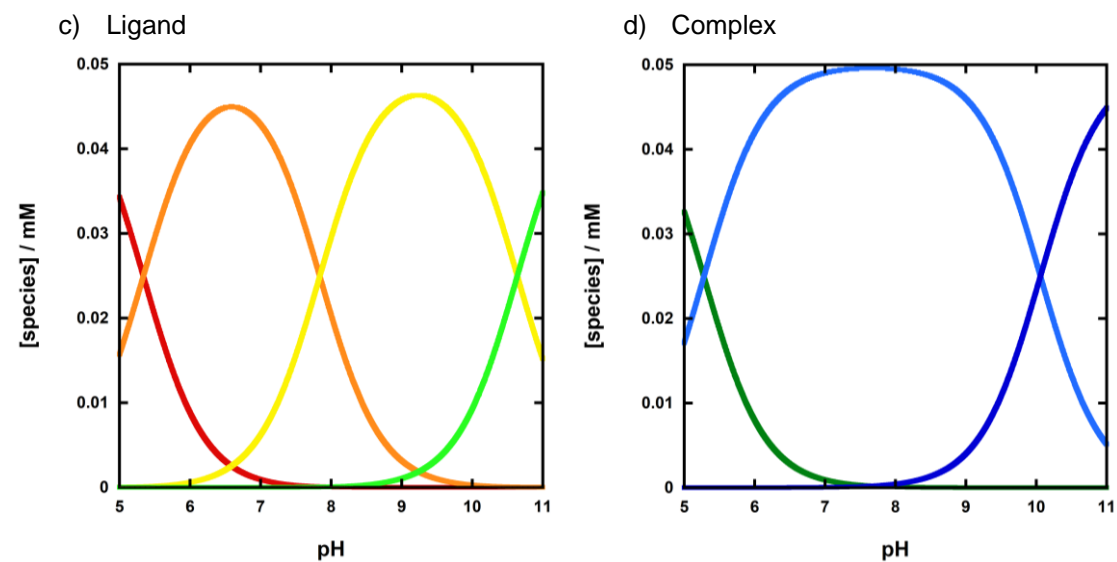
- $(L_{3-1}) + 3H^+$
 - $(L_{3-1}) + 2H^+$
 - $(L_{3-1}) + H^+$
 - L_{3-1}

- $3-1$
 - $(3-1) - H^+$
 - $(3-1) - 2H^+$

Titration curve:



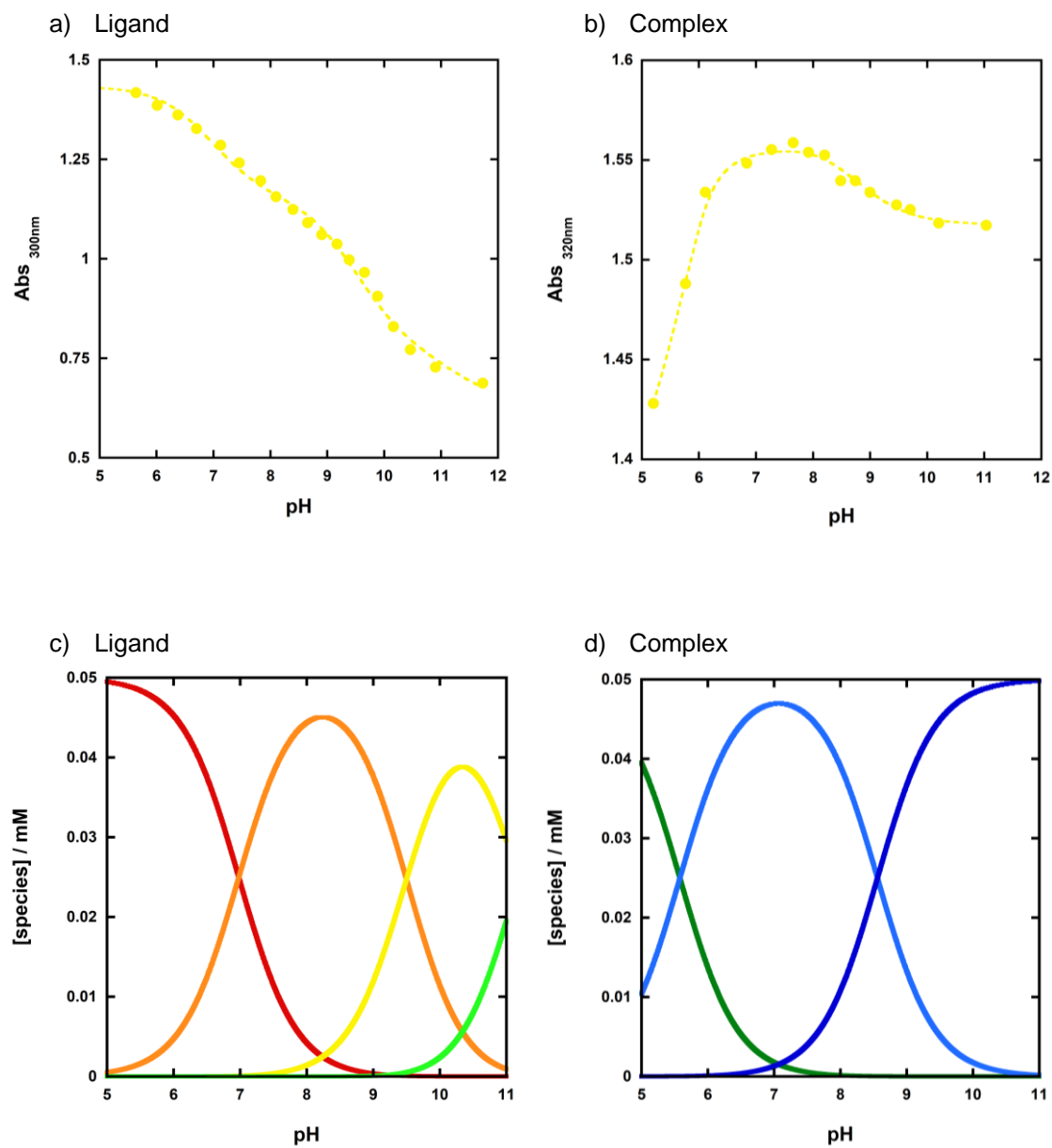
Speciation curve:



- $(L_{3-2}) + 3H^+$
 - $(L_{3-2}) + 2H^+$
 - $(L_{3-2}) + H^+$
 - L_{3-}

- $3-2$
 - $(3-2) - H^+$
 - $(3-2) - 2H^+$

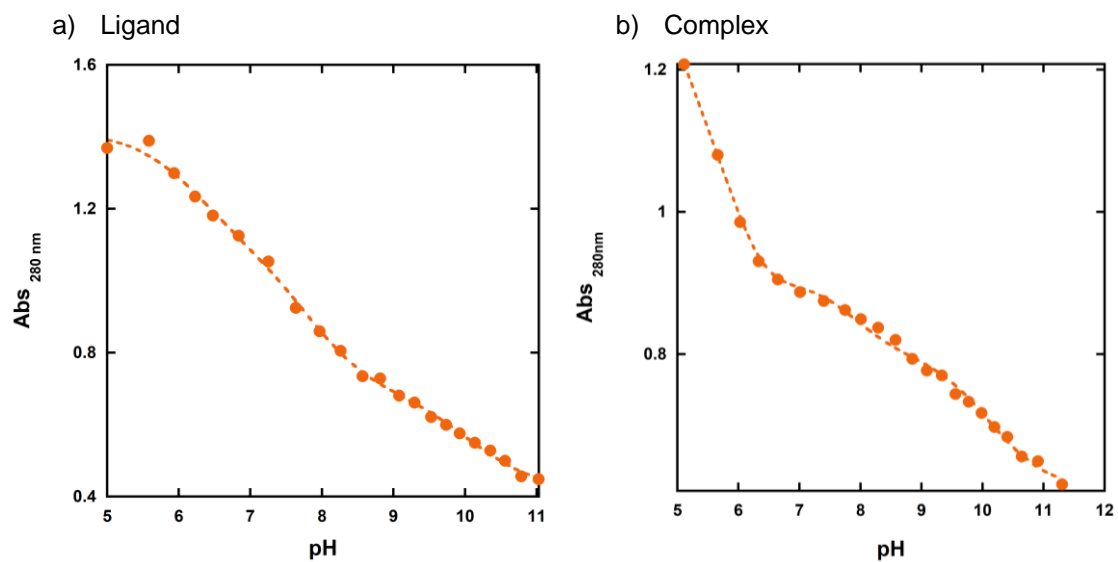
Titration curve:



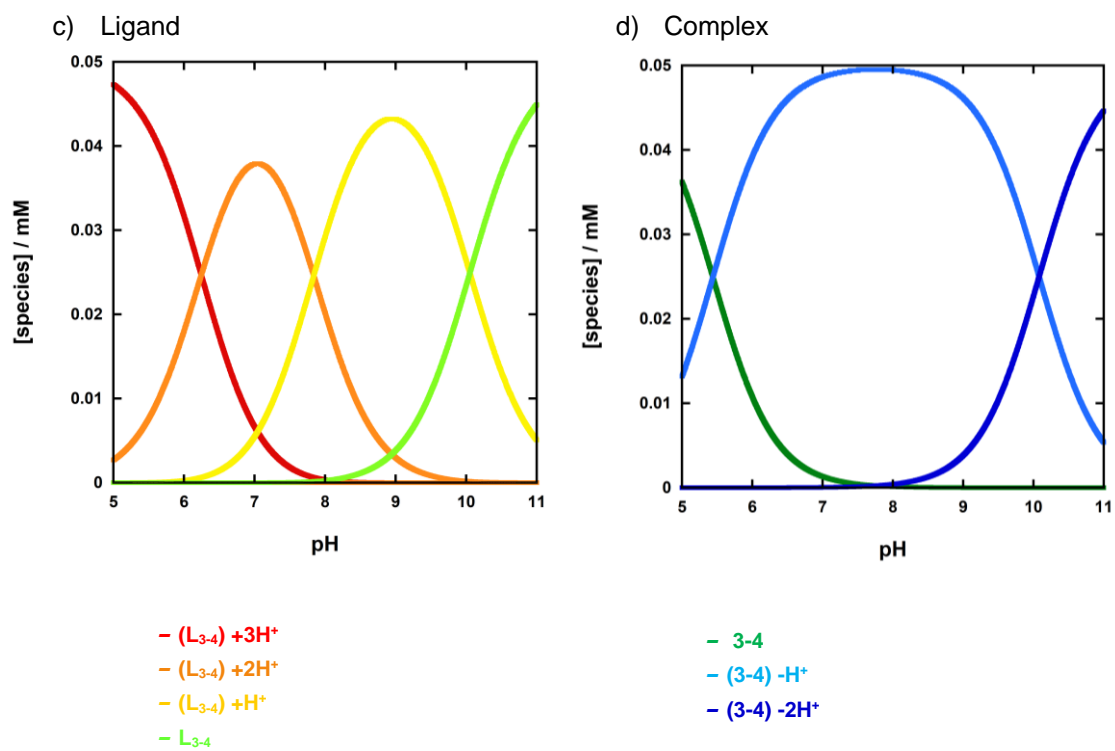
— $(L_{3-3}) + 3H^+$
 — $(L_{3-3}) + 2H^+$
 — $(L_{3-3}) + H^+$
 — L_{3-3}

— $3-3$
 — $(3-3) - H^+$
 — $(3-3) - 2H^+$

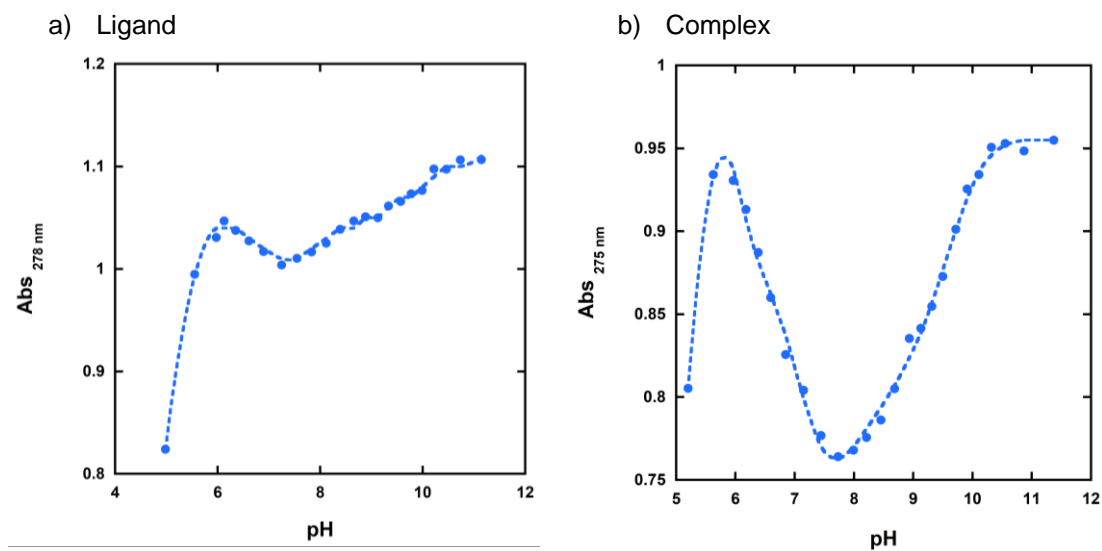
Titration curve:



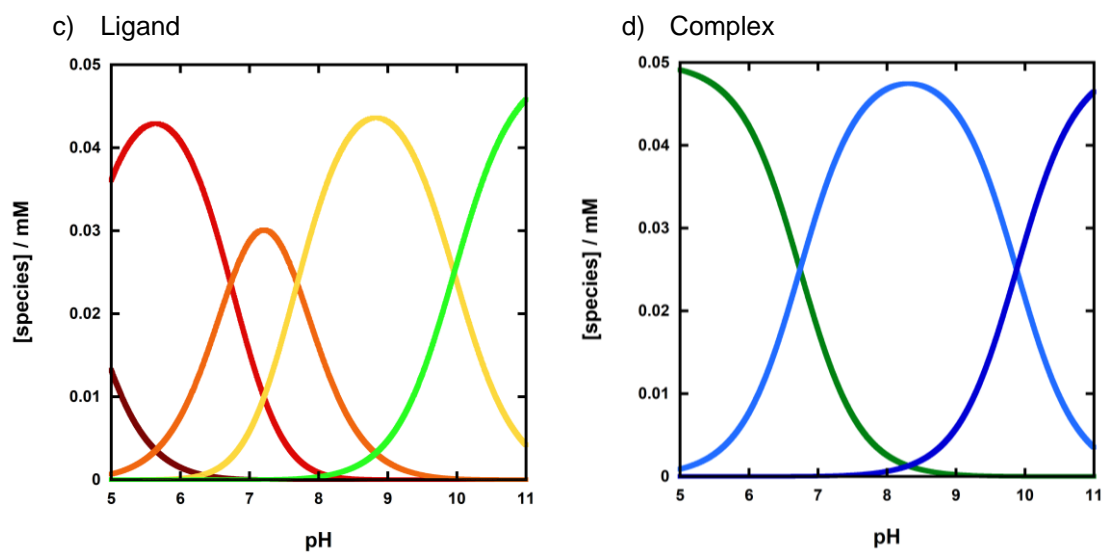
Speciation plot:



Titration curve:



Speciation plot:



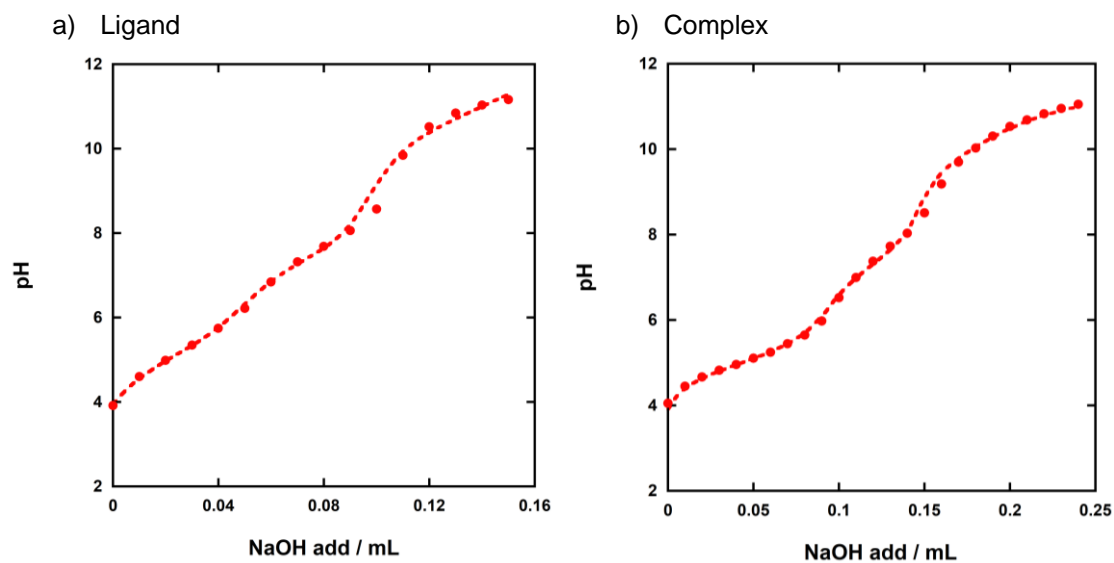
- $(L_{2-6}) + 4H^+$
 - $(L_{2-6}) + 3H^+$
 - $(L_{2-6}) + 2H^+$
 - $(L_{2-6}) + H^+$
 - L_{2-6}

- 3-6
 - $(3-6) - H^+$
 - $(3-6) - 2H^+$

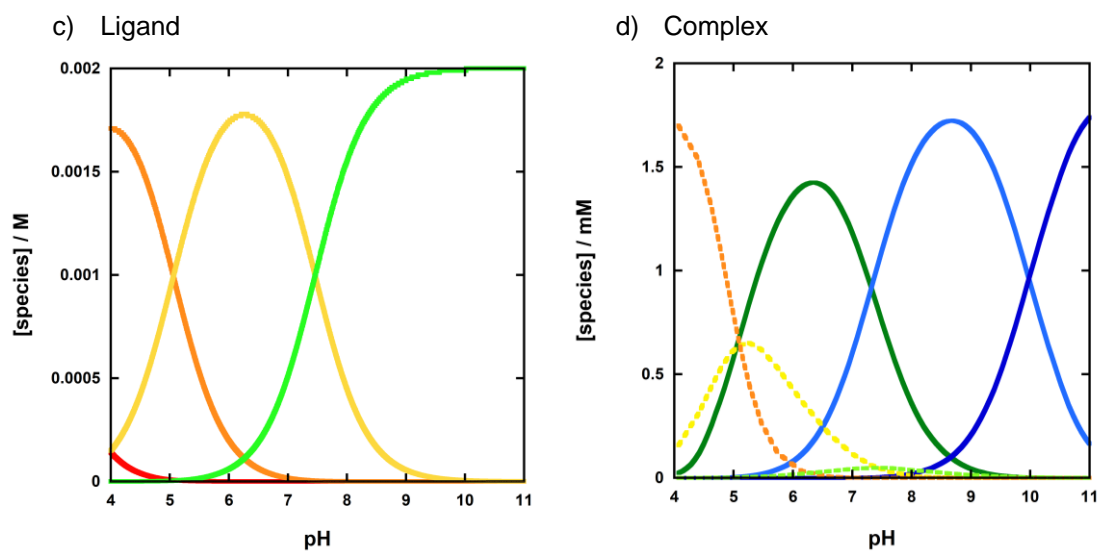
3.4.7 Potentiometric Titration

The titration experiments were carried out at 25°C and the pH was measured by Mettler-Toledo pH meter calibrated with Thermo Scientific buffer packs at pH 4.00, 7.01 and 10.06 at 25 °C. To the ligand or complex (0.02 mmol), dissolved in 10 mL of 0.1 M NaNO₃, 2 equivalents of HCl (40 µL of 1 N standardised HCl solution purchased from Alfa Aesar) were added. The titration was performed by adding aliquots of 10 µL of 0.2 M NaOH (equal to ½ of equivalent) with a Hamilton gas tight glass syringe (500 µL). The 0.2 M NaOH solution was prepared from a standardised 1 N solution of NaOH purchased from Alfa Aesar. The concentration of the 0.2 M NaOH solution was evaluated by titration against 10 ml of a 2 mM of potassium hydrogen phthalate as a primary standard, and then used to titrate the 1 N HCl solution. The solutions were all prepared with deionised water. The measures then processed by Hypspec and Hyss and the fitting of the data yielded the speciation plots reported below. The titration plots of the **2-2** were fitted using the log β values obtained for the relative **L₂₋₂**.

Titration curve:



Speciation plot:



- $(L_{2-2}) + 3H^+$
 - $(L_{2-2}) + 2H^+$
 - $(L_{2-2}) + H^+$
 - L_{2-2}

- $(L_{2-2}) + 2H^+$
 - $(L_{2-2}) + H^+$
 - L_{2-2}
 - $2-2$
 - $(2-2) - H^+$
 - $(2-2) - 2H^+$

Chapter 4

Investigations of the activity of a dinuclear Zn(II) complex towards phosphate diester models for RNA and DNA

4.1 Introduction

Often enzymes use more than one metal ion cofactor for catalysing a wide range of chemical reactions. Although the metal ions have different roles and can provide a more structural function, the activity of the natural catalysts has often been correlated to their cooperative action.^{75,113} For example, the positively charged metals enhance the substrate binding by electrostatic interaction with the anionic phosphate and stabilise the transition state for the phosphoryl transfer. In addition, by binding to metal sites, the reaction can be accelerated by the simultaneous double Lewis acid activation of the phosphate, deprotonation of the incoming nucleophile and stabilisation of leaving group.¹¹⁴ Taking inspiration from Nature, the development and investigation of ligands able to bring two metal ions into close proximity is a winning approach to achieve faster catalysis. The improvement observed for the dinuclear complexes might result from the cooperative action of the metal ions on stabilising the transition state for the cleavage reaction, but might also reflect the stronger substrate binding gained by the more significant positive charge under subsaturating conditions.²² High cooperativity was found for the first time by Young *et al.*¹¹⁵ when two units of 1,4,7-triazacyclononane (TACN) were joined together by a naphthalene linker (*Figure 4.1*). The Cu(II) complex **4-3**, although most active at lower pH, was 500 times more reactive toward the hydrolysis of the dinucleotide ApA at 50 °C than expected for its mononuclear components, based on the analogue **4-2**. The ligand structure strongly modulates the mode of action of the two metal centres; for example, if the right geometry is created, the two ions might cooperatively coordinate the phosphorous, resulting in double Lewis acid activation. Alternatively, the phosphorous might coordinate only to one ion, while the additional metal centre might favour the nucleophilic attack by

deprotonating the metal-bound water molecule. Cooperative interactions were facilitated by introducing a tether to overcome the electrostatic repulsion between the positive charges and create a scaffold for chelating the ions with the most advantageous relative positions.

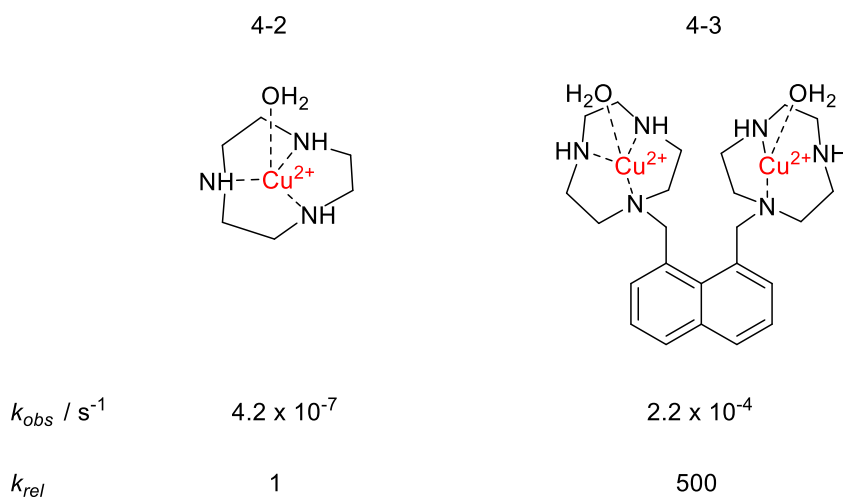


Figure 4.1 Comparison between structures and reactivities of mononuclear and dinuclear complexes tested toward the hydrolysis of ApA at pH 7.3 and 50 °C; conditions: [ApA]=0.05 mM, [complex] = 2 mM, [HEPES] = 10 mM

Morrow and Richard have studied a striking example in their dinuclear Zn(II) complexes for RNA-like substrates transesterification.¹¹⁶ As reported in Figure 4.2 and Table 4.1, the different dinuclear Zn(II) complexes, obtained by combining two 1,4,7-triazacyclononane (TACN) with different linkers, are all more reactive toward the HPNPP cleavage at pH 7.6 and 25 °C than **4-4**. However, the second order rate constants determined for **4-7**, **4-8** and **4-9** are only a few fold higher than the value found for **4-4**, suggesting that the subunits of these systems act independently. On the other hand, **4-6** (k_2 of $2.5 \times 10^{-1} \text{ M}^{-1} \text{ s}^{-1}$) is 120-fold more reactive than **4-4**, which is 60-fold greater than a dinuclear complex in which the TACN units act autonomously. This strong cooperativity may be due to the alkoxide group,

which reduces the metal ions' electronic repulsion. A similar role is played by the carboxylic acid of Asp and Glu residues, or the water and hydroxide molecule often present in the dinuclear catalytic sites of metalloenzymes.^{10,75,117}

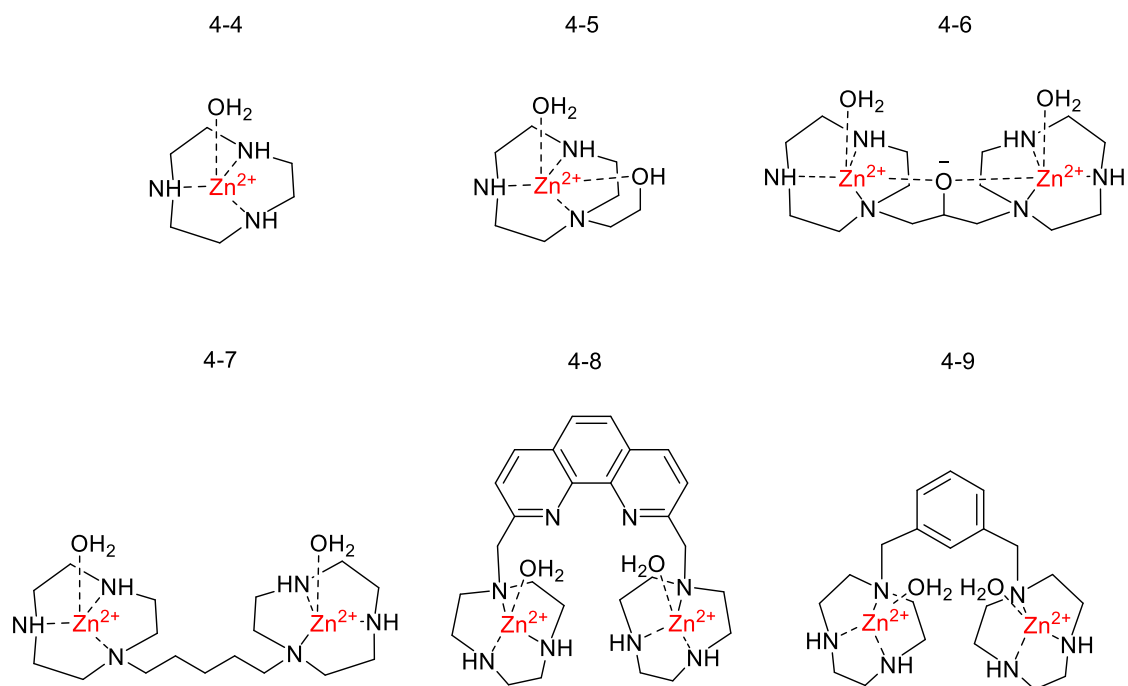


Figure 4.2 Structure of mononuclear and dinuclear Zn(II) complexes studied by Richard and Morrow¹¹⁶

Table 4.1 k_2 and k_{rel} values of the complexes reported in Figure 4.2 for the transesterification of HPNPP at pH 7.6 and 25 °C, conditions: [HPNPP]=0.038 mM, [Buffer] = 20 mM, ionic strength at 0.1 M by addition of NaNO₃¹¹⁶

	4-4	4-5	4-6	4-7	4-8	4-9
$k_2 / \text{M}^{-1} \text{s}^{-1}$	2.1×10^{-3}	1.3×10^{-3}	2.5×10^{-1}	1.1×10^{-2}	8.9×10^{-3}	5.8×10^{-3}
k_{rel}	1	0.6	120	5	4	3

The higher reactivity of **4-6** might also be attributed to a lower kinetic pK_a and a more robust interaction with the substrate. As the authors reported the same year,¹¹⁸ the pH profile of the second order rate constant for **4-5** and **4-6** shows a downward break associated

with the formation of metal ion hydroxide complexes. The author's interpretation is that the metal bound hydroxide participates in the substrate cleavage as a general base catalyst making the deprotonated complex the most active species. Exhibiting a lower pK_a than both the mononuclear analogues, at physiological conditions **4-6** is a better catalyst because it is primarily present in its hydroxide form. In addition, inhibition studies reveal that **4-6** binds diethyl phosphate 6 times stronger than **4-5**, suggesting a similar interaction strength with the substrate. Although this confirms that the high value of k_2 is partially due to ground state interactions, the higher binding constant is not solely responsible for the difference in catalytic efficiency. Further electrostatic stabilisation is proposed to occur when proceeding from the Michaelis complex to the transition state for phosphate cleavage. A similar result was also found when **4-6** was tested toward the hydrolysis of the more RNA-like substrate uridylyl-3'-5'-uridine (UpU)¹¹⁹. A 2.1 kcal/mol greater stabilisation of the transition state was found for the UpU cleavage, suggesting a modest stabilisation of the leaving group's negative charge by interaction with **4-6**. The pH profile of the second order rate constant at 25 °C, showing a k_2^{\max} of $6.8 \times 10^{-3} \text{ M}^{-1} \text{ s}^{-1}$ and a kinetic pK_a of 7.8, demonstrates that the reaction proceeds by the same ionic form of the substrate catalyst complex. Both the ground state adduct and the transition state for converting the latter to products are stabilised at higher pH.

As highlighted in Chapter 3, changes in the medium polarity can affect reactions due to the different solvation of the ground-state starting materials and the transition state participants. The effective dielectric constant in proteins' and enzymes' cavities is reduced compared to bulk water, and although strong hydrogen bond interactions enhance both substrate binding and catalysis, the active site has been estimated to be rather non-aqueous.¹¹⁰ The reduced

solvent polarity might also be responsible for the high acceleration provided by the natural systems, which artificial catalysts have not been able to replicate yet.^{63,110} Brown and coworkers have reported extremely high acceleration of the metal ions-catalysed acyl and phosphoryl transfer reactions in light alcohols.⁶⁴ For example, while the **4-10**'s activity toward the transesterification of HPNPP (k_2 of $16.9 \pm 0.7 \text{ M}^{-1} \text{ s}^{-1}$ - Figure 4.3) is 6500 times higher than that of methoxide in methanol, the corresponding reactions in water show that the complex is 3 times less reactive than hydroxide.^{58,120} A 1000-fold difference between these activities in these different solvents highlights how a reduced solvent polarity positively affects metal ions catalysis. In contrast with Morrow's and Richard's findings, the opposite trend was detected when studying dinuclear complexes with or without the hydroxyl group in the ligand linker.¹²¹

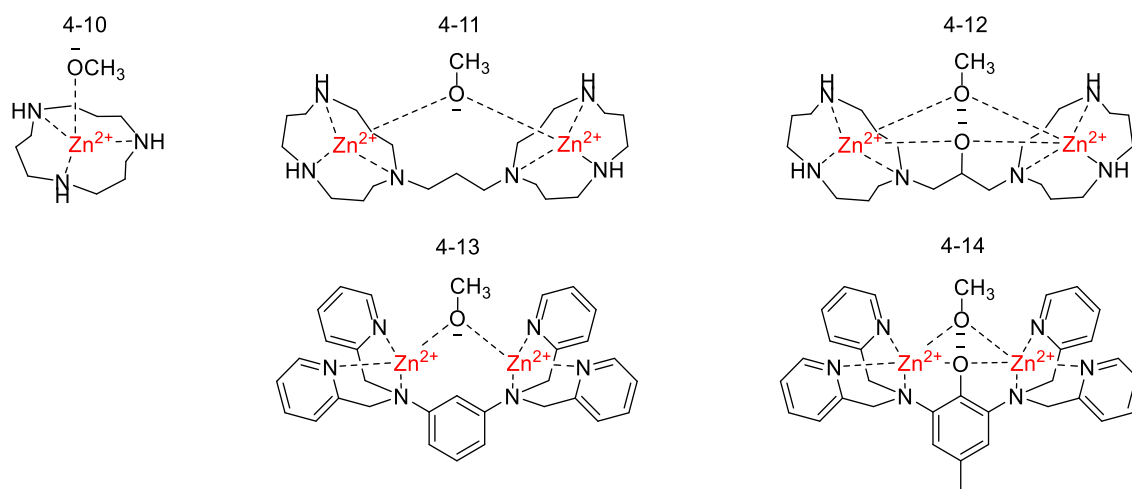
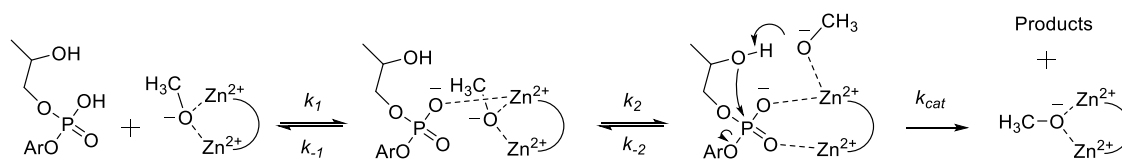


Figure 4.3 Structures of dinuclear Zn(II) complexes studied by Brown and coworkers¹²¹

Figure 4.3 shows two families of catalysts studied by the group. Exceptional accelerations of the reaction rate were observed for all the complexes when tested at 25 °C in methanol. With a k_2 of $275\,000 \text{ M}^{-1} \text{ s}^{-1}$, **4-11** accelerates the transesterification of HPNPP by 10^{12} fold

relative to the background reaction and is 10^8 and 1.5×10^4 more reactive than methoxide and its mononuclear analogue **4-10**, respectively. The high cooperativity, which makes **4-11** the most active Zn(II) catalyst reported to date, is lost entirely when the reaction is catalysed by **4-12** with a k_2 of $7.6 \text{ M}^{-1} \text{ s}^{-1}$ (2-fold less reactive than **4-10**). The pH profile of the second order rate constant for **4-11** revealed kinetic pK_a values of 9.3 and 11.2 that suggest that the kinetically dominant form of the catalysts is the singly deprotonated form. As proposed by the authors, the mechanism involves a bimolecular binding step, followed by intramolecular rearrangement to further activate the phosphate by additional coordination to the second metal ion. The final step is the intramolecular nucleophilic attack enhanced by the methoxide yielding the cyclic phosphate and 4-nitrophenolate (Scheme 4.1). Mechanistic investigations using substrates with good leaving groups have suggested a larger k_{cat} than k_2 term and identified the formation of the activated phosphate-complex adduct as the rate limiting step.



Ar = 4-nitrophenyl

Scheme 4.1 Proposed mechanism for the HPNPP transesterification catalysed by **3-10** ¹²¹

A comparable mechanism is predicted for **4-12** (pK_a 9.65), but the 37 000 times lower k_2 might be due to either the net positive charge (inferior to that on **4-11**) or the higher coordination numbers of the metal ions, both of which make the substrate binding weaker. For the bis(pyridin-2-ylmethyl)amine (bpa) based complexes, **4-13** exhibits a k_2 of $9\,100 \text{ M}^{-1} \text{ s}^{-1}$, roughly 160 times higher than **4-14** (k_2 of $58.8 \text{ M}^{-1} \text{ s}^{-1}$).

According to the pH measures, the kinetic active form is the adduct in which the complex binds the substrate and a deprotonated methanol molecule is coordinated to one or two Zn(II) ions. The result suggests that the anionic bridging group is only necessary for dinuclear complexes in water to compensate for the unfavourable electrostatic interactions and heavier solvating property of the metal ions, which affect the catalysis and are caused by the medium.

By replicating the presumed conditions of the enzymatic cavities, Brown and coworkers offer a closer look at the impact of the protein on these catalytic components. Although this method gives more realistic models and insights into catalysis, its use for designing artificial enzymes has limitations. Aqueous metal ion complexes have provided good rate accelerations for RNA and DNA model molecule cleavage, but less evidence of their effectiveness with natural substrates can be found in literature. For example, Caccipaglia *et al.*^{122,123} have studied di- and trinuclear Cu(II) complexes of 1,5,9-triazacyclododecane ligands fused to the upper rim of calix[4]arene scaffolds aimed to cleave dinucleotides and single-stranded six residues RNA sequences (**4-15** and **4-16** in Figure 4.4). Although selectivity for substrates having a uracil base at the 5'-hydroxyl terminus (UpG and UpU) is observed with the former, a preference for cleaving the phosphate diester bond between a cytosine and adenine residue is detected with single-stranded RNA.

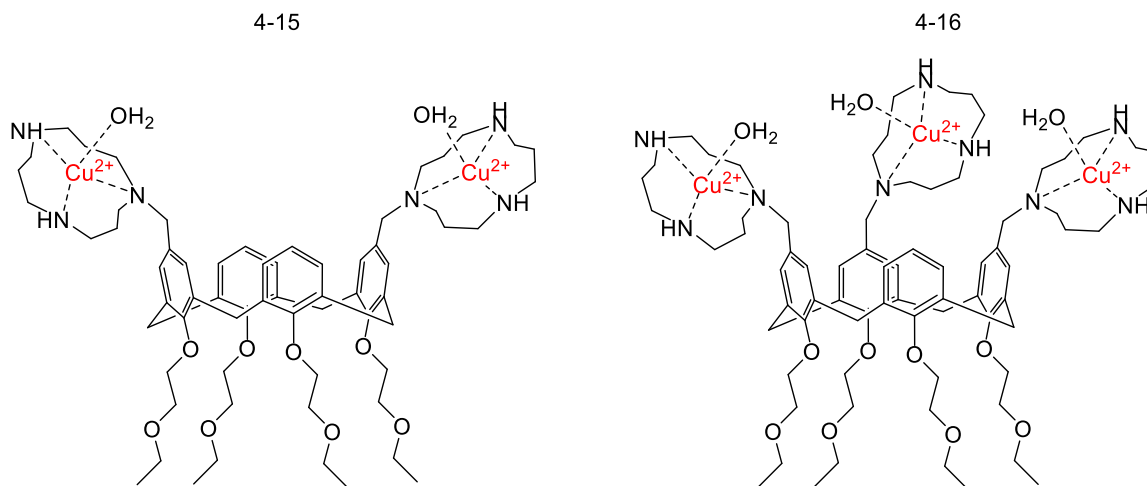


Figure 4.4 Structures of decorated calix[4]arene systems used for the hydrolysis of RNA

The different selectivity is unexpected and makes those macrocycles unpredictable for use with natural targets.

As explained in Chapter 1, substantial effort has been dedicated to conjugating catalytic moieties to recognition units of modified oligonucleotides sequences to achieve efficiency and selectivity at once. For example, Strömberg and coworkers have used this methodology.^{43,44} The catalytic head group is often attached via a linker at the middle of the sequence and surrounded by a bulge of 3 or 5 unpaired nucleotides, experiencing a more apolar but still aqueous microenvironment. Although the adduct folding reduces the medium polarity of the transesterification, such systems do not replicate the strong hydrophobicity of the protein active sites. Hence, the conclusion drawn by Brown can only partially apply to those systems, and the studies of aqueous metal complexes seem to be the most reliable method to improve the catalytic moieties and propose alternatives to enzymes.

Based on the encouraging results from their studies on the tris(pyridin-2-ylmethyl)amine (tpa) mononuclear complex, in 2006, Williams and coworkers introduced 2-amino substituents to the pyridine units of a dinuclear complex.⁹⁷ Similarly to the previous examples reported in the chapter, two bpa units are joined together via a 2-propanol chain (Figure 4.5).

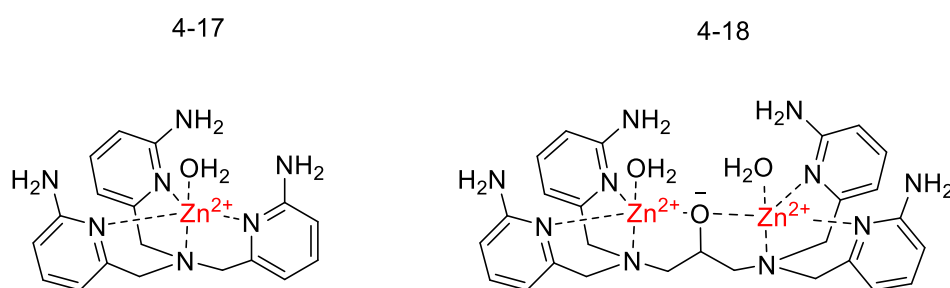


Figure 4.5 Structure of mono and dinuclear Zn(II) complexes proposed by Williams and coworkers^{52,97}

In contrast with Morrow and Richard's catalysts, which is most active at alkaline pH, **4-18** exhibits an astonishing activity at physiological pH and 25 °C. 0.2 mM of **4-18** reduces the half-life time of HPNPP (0.05 mM) to approximately a minute. With a k_2 of 53 M⁻¹ s⁻¹, 670 and 240-times higher than **4-17** and **4-6** respectively, **4-18** is highly effective and shows strong cooperativity between the two metal ion centres. The three orders of magnitude difference between **4-18** and its analogous dinuclear complex lacking the 2-amino substituents reveals the importance of amines' hydrogen bond donating properties, which stabilises binding of the phosphate substrate. Hence, this increase is due equally to a stronger substrate binding and a higher reactivity of the substrate-catalyst complex. The coordination of the phosphate ester to both the Zn(II) ions revealed by X-ray analysis might be responsible for the high cooperativity observed. The phosphate, benefiting from a double

Lewis acid activation, would also position the oxygen atoms in a hydrogen-bonding distance of the amino groups. **4-18** was also tested with a wide range of unactivated substrates,¹²⁴ enhancing their hydrolysis with 10⁶-fold rate acceleration, similar to that observed for HPNPP.

4.2 Result and discussion

Based on these well-established precedents of constructing a carefully designed dinucleating ligand that can encourage two metal ions centres to cooperate, we investigated the effect of enriching this dinculeating ligand with anisidine substitutions. This builds on the promising result for the mononuclear complexes described in the previous chapter. (Figure 4.6).

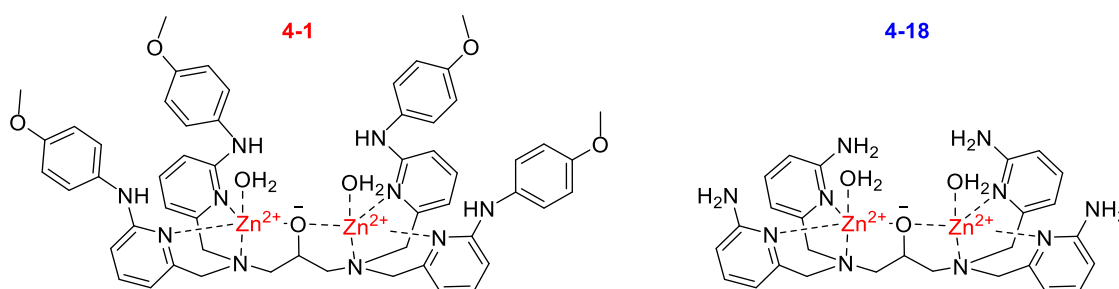
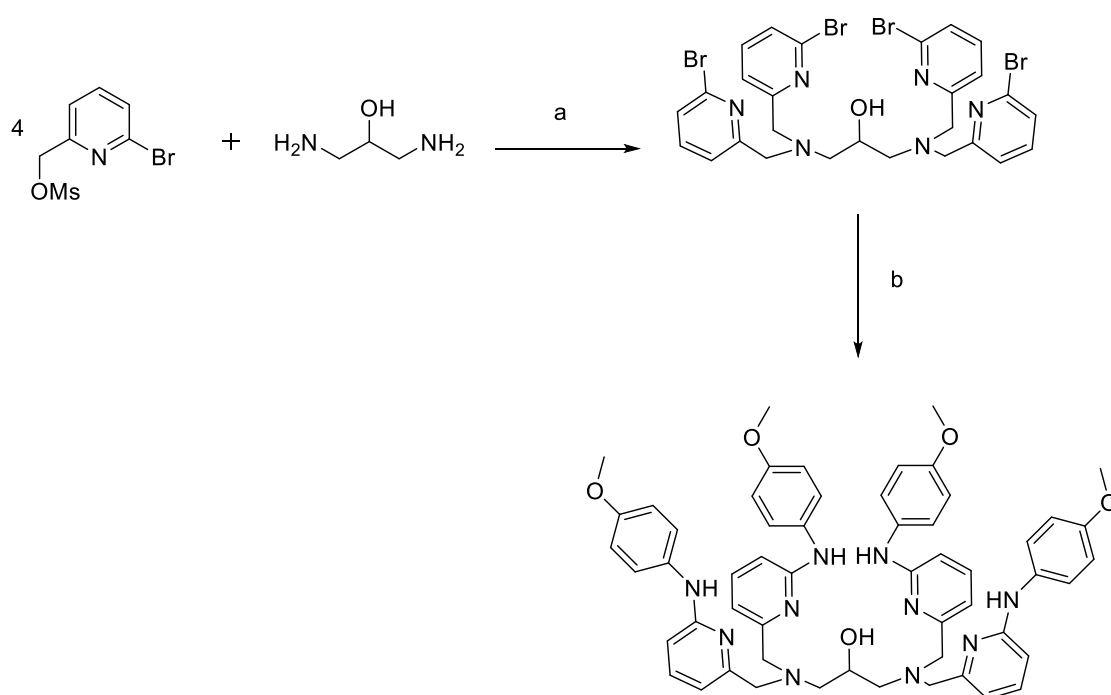


Figure 4.6 Structure of the dinuclear complex 4-1

We investigated and analysed the effect of cooperativity between the metal ions translated into **4-1**'s activity for the cleavage of RNA and DNA model molecules and the dinucleotide uridyl-(3-5)guanosine (UpG).

4.2.1 Synthesis

The dinuclear ligand was obtained by a synthetic procedure analogous to that followed for the mononuclear complexes. The precursor bromo ligand was obtained as a white solid (53% yield) by the 4-fold alkylation of 1,3-diaminopropan-2-ol with (6-bromo-2-pyridyl)methyl methanesulfonate. A Buchwald-Hartwig cross-coupling *p*-anisidine yielded the desired ligand, as shown in Scheme 4.2.¹²⁵



Scheme 4.2 Synthetic strategy; a) DIPEA, DMF, 70 °C, 18 h, 57 % yield; b) *p*-anisidine, Pd(OAc)₂, ±BINAP, Cs(CO₃)₂, toluene, 100 °C, 18 h, 53% yield

4.2.2 Kinetic studies

As for the mononuclear complexes, **4-1** showed poor water solubility and the same percentage of acetonitrile was used to test the catalyst activity. The addition of 40% (v/v) of acetonitrile did not influence the activity of the reference compound **4-18**, which has been synthesised (experimental section) and tested in the new reaction conditions. At pH 7.4 and 25 °C in 40% (v/v) acetonitrile in water **4-18** (0.2 mM) accelerated the transesterification of HPNPP (0.05 mM) with a k_{obs} of $1.7 \pm 0.5 \times 10^{-2} \text{ s}^{-1}$, which is in very good agreement with the value reported in literature ($1.4 \times 10^{-2} \text{ s}^{-1}$).

4-1 has been studied with different substrates, which are used to mimic both RNA and DNA transesterification, so this chapter is divided into three main sections in which **4-1** activity is tested with HPNPP, BNPP and UpG.

Transesterification of HPNPP

The transesterification of HPNPP was very strongly enhanced by **4-1**. Under pseudo-first order conditions, the half-life time of HPNPP (0.05 mM) at pH 7.4 and 25 °C (0.05 M buffer and 0.1 M ionic strength) was reduced to approximately 0.2 seconds in the presence of 0.2 mM of **4-1**, corresponding to an observed rate acceleration of 10^8 fold. Under similar reaction conditions, **4-18** catalysed HPNPP cleavage with an observed rate constant of $1.4 \times 10^{-2} \text{ s}^{-1}$, 285 times less reactive than **4-1**. Given the high reactivity, the kinetic characterisation was mainly performed in the complex concentration range of 5 - 100 μM .

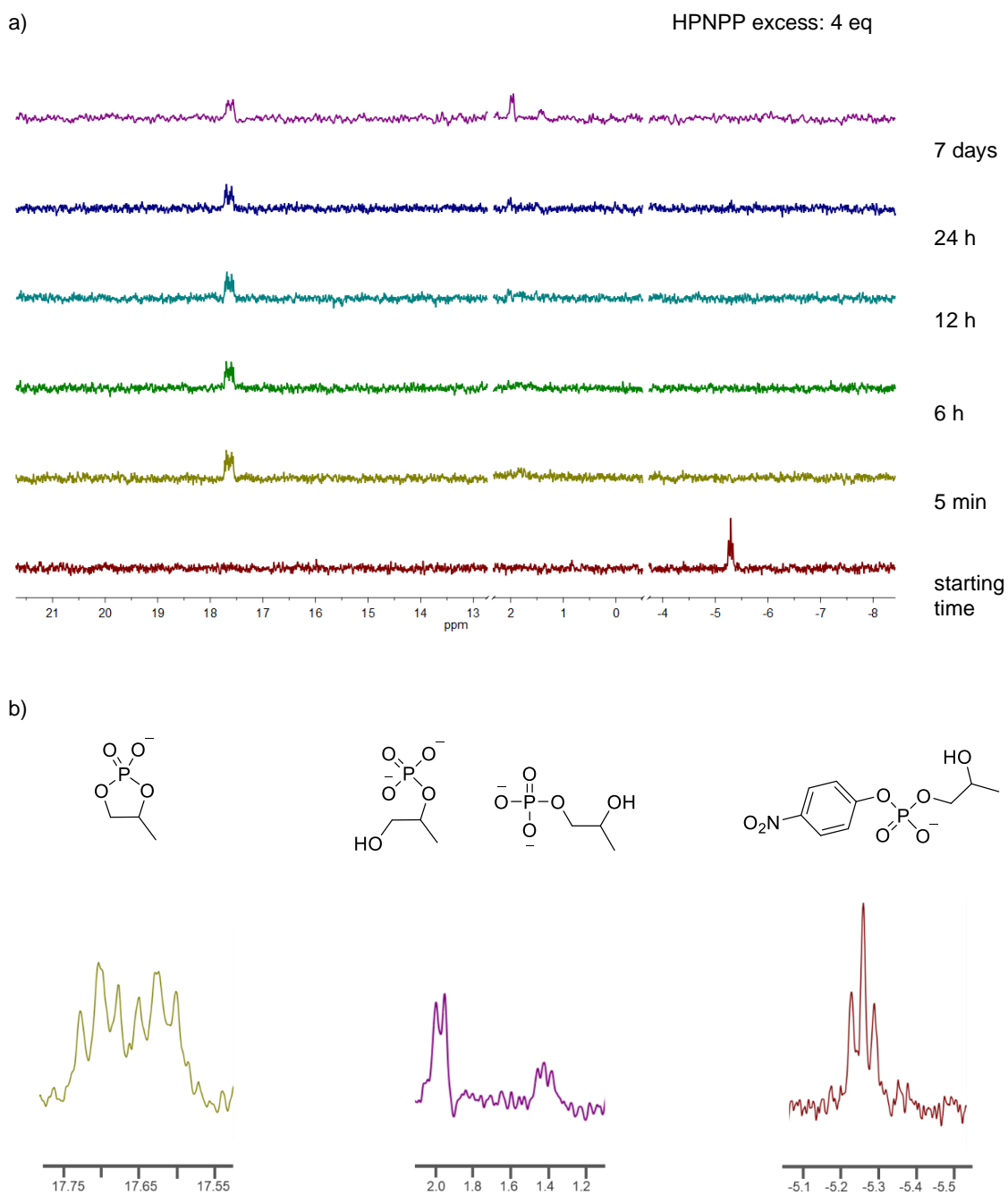
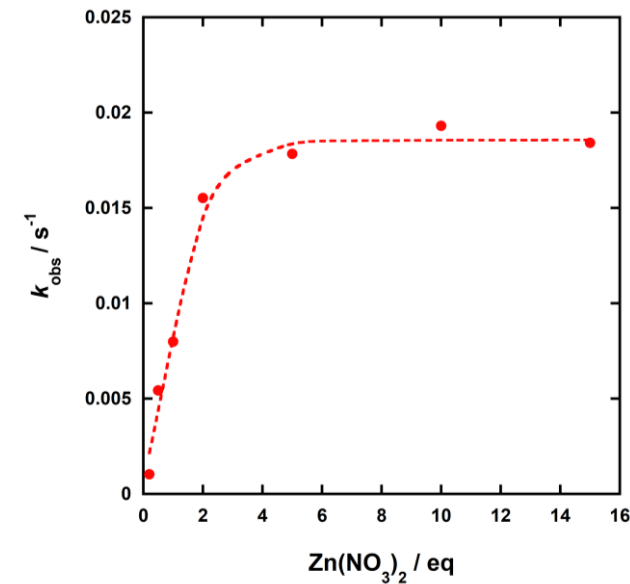


Figure 4.7 ^{31}P NMR experiment for the transesterification of HPNPP catalysed by 4-1 at pH 7.4 and 25 °C; a) Consecutive spectra of the solution; b) enlargement of the substrates' and product's signals; $[4-1] = 0.5 \text{ mM}$, $[\text{HPNPP}] = 2 \text{ mM}$, $[\text{HEPES}] = 50 \text{ mM}$, ionic strength at 0.1 M by addition of NaNO_3

As shown by the ^{31}P NMR experiment of a solution of HPNPP (2 mM) and **4-1** (0.5 mM) at pH 7.4 and 25 °C (Figure 4.7), the dinuclear catalyst not only catalysed the cyclisation

of HPNPP but enhanced the ring opening, leading to the production of the two monophosphate isomers. After 5 min (the time required to prepare the machine for the measurement), the spectrum did not show any traces of the triplet at -5.25 ppm assigned to HPNPP, while complete conversion was confirmed by the doublet of triplets at 17.66 ppm corresponding to the cyclic phosphate. Although the second step was slow, after 1 week the two doublets of the final monophosphates emerged at 2 and 1.4 ppm.

Measuring the observed rate constants as Zn(II) was titrated into **L4.1** (0.05 mM) showed that two equivalents of Zn(II) bonded tightly to the ligand to form the fully active species, as shown in Graph 4.1. The data have been fitted to a 2:1 model by Bindfit, the online tool for supramolecular chemistry research and analysis offered by Thordarson,¹¹¹ which yielded a K_{11} and K_{12} binding constants of $4 \pm 1 \times 10^3$ and $6 \times 10^6 \text{ M}^{-1}$.



Graph 4.1 Plot of k_{obs} vs $\text{Zn}(\text{NO}_3)_2$ equivalent at 25 °C and pH 7.4. [**L4.1**] = 0.05 mM, [HPNPP] = 0.05 mM, [EPPS] = 50 mM, ionic strength at 0.1 M by addition of NaNO_3

Like the mononuclear complexes, the reaction catalysed by **4-1** showed a first order dependence on the substrate, as confirmed by the experiments performed at pH 8 and 9 (0.01 – 0.1 mM - Figure 4.8a). Additional kinetic data demonstrated the catalytic nature of the complex, which in the presence of 10 and 5 equivalents of HPNPP (red and blue curves in Figure 4.8b respectively) efficiently underwent multiple turnovers and was not affected by product inhibition. ^{31}P NMR experiments confirmed the catalytic activity. When 25 equivalents of HPNPP are added to a solution of **4-1** (0.05 mM) at pH 7.4 and 25 °C, it efficiently catalysed the diester transesterification to completion.

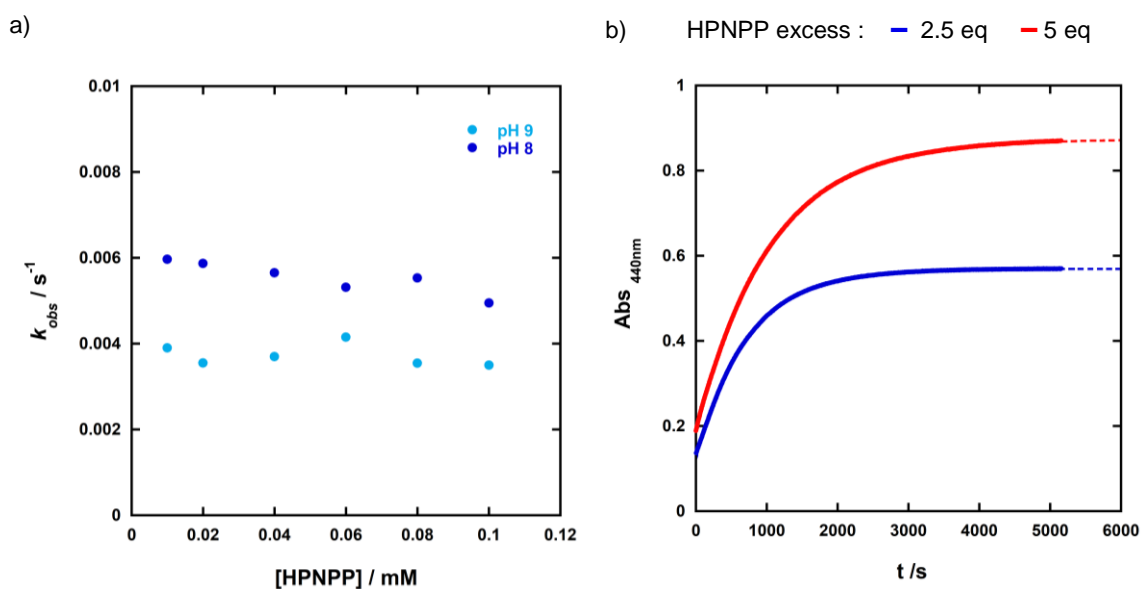


Figure 4.8 a) Plot of k_{obs} against the concentration of HPNPP at pH 9 and 8 catalysed by **4-1** at 25 °C; $[\text{4-1}] = 0.05 \text{ mM}$, $[\text{Buffer}] = 50 \text{ mM}$ (EPPS, CHES), ionic strength 0.1 M by addition of NaNO_3 , 40 % (v/v) acetonitrile in water; b) Turnover experiment of the transesterification of HPNPP catalysed by **4-1** at pH 8 and 25 °C; $[\text{4-1}] = 0.025 \text{ mM}$, $[\text{EPPS}] = 50 \text{ mM}$, ionic strength 0.1 M by addition of NaNO_3 , 40 % (v/v) acetonitrile in water

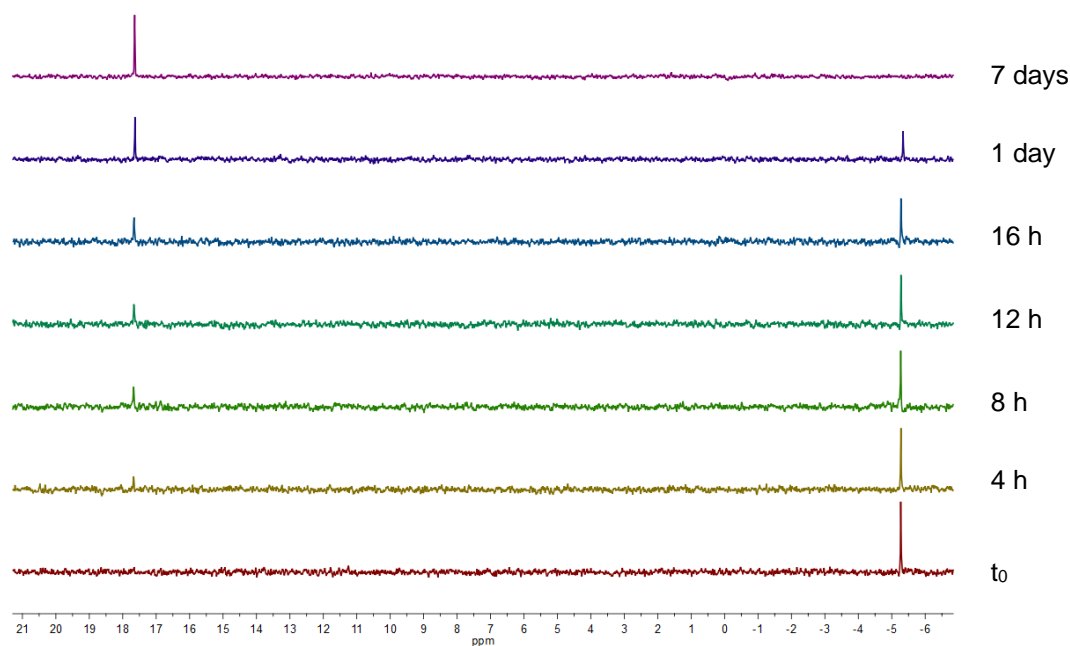


Figure 4.9. ^{31}P NMR experiment of the HPNPP transesterification catalysed by **4-1** at pH 7.4 and 25 °C. [HPNPP]=1.25 mM, [4-1] = 0.05 mM, [EPPS] = 50 mM, ionic strength 0.1 M, 25 °C, 40% (v/v) acetonitrile in water

The reaction was followed by monitoring the disappearance of the substrate signal at -5.3 ppm and the simultaneous appearance of the cyclic phosphate diester product at 17.8 ppm (Figure 4.9). However in the ^{31}P NMR turnover experiment, traces of HPNPP were still present after 1 day (with a 1:1 ratio of **4-1** and substrate, the half-life of HPNPP was approximately 1 minute). Strong inhibition could result from the production of phosphate monoesters derived from the opening of the initial cyclic product (as reported in Figure 4.7). Monophosphates bind tightly to metal ions, and inhibition was confirmed when the HPNPP (0.05 mM) cleavage catalysed by **4-1** (0.05 mM) was tested at increasing PP concentration (0 – 0.1 mM). As reported in Graph 4.2 for pH 7, 8 and 9.1, less than one equivalent of PP completely inhibits catalytic activity. Similarly to the previous Chapters,

the inhibition profiles were fitted with equation (6) and yielded the observed K_i reported in Table 4.2.

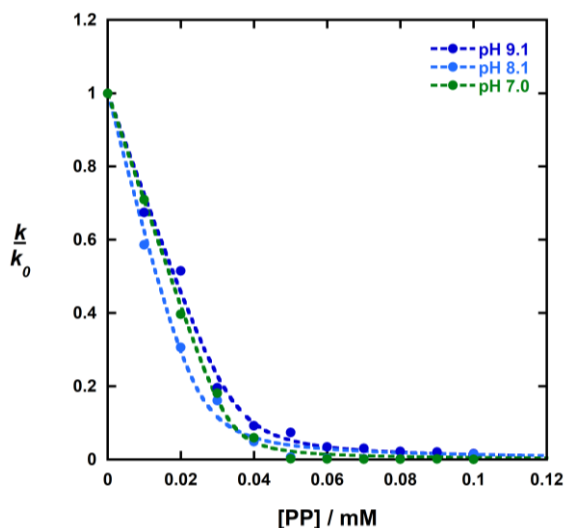


Table 4.2 K_i^{obs} obtained from graph 1.2

	$K_i^{obs} / \mu\text{M}$
pH 7.0	0.9 ± 0.3
pH 8.1	1.1 ± 0.3
pH 9.1	0.4 ± 0.1

Graph 4.2 PP Inhibition profile of the transesterification of HPNPP catalysed by 4-1. $[4-1] = 0.05 \text{ mM}$, $[\text{HPNPP}] = 0.05 \text{ mM}$, $[\text{Buffer}] = 50 \text{ mM}$ (HEPES/EPPS/CHES), ionic strength at 0.1 M by addition of NaNO_3 , 40% acetonitrile (v/v) in water

Although the ring opening would lead to the appearance of two additional signals in the spectrum, the quantity needed to reduce the reaction rate is small ($[4-1] = 0.05 \text{ mM}$) and maybe undetectable due to the sensitivity of the instrument being too low.

The transesterification of HPNPP catalysed by **4-1** was also followed at different buffer concentrations to test for general acid and base catalysis. Although no buffer catalysis was observed, some of the buffer molecules used to control the experiment pH inhibit the reaction. The structure of the commonly used buffers are shown in Figure 4.10:

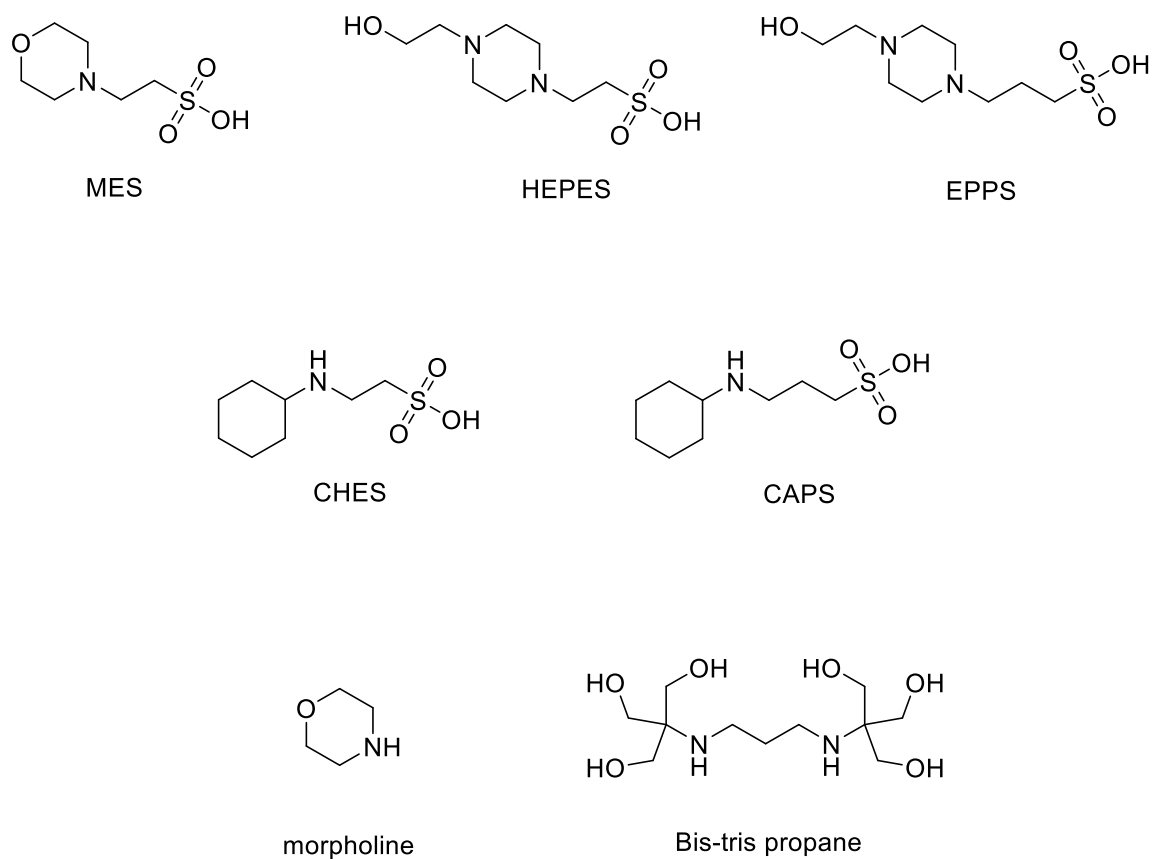


Figure 4.10 Structure of some commonly used buffers

As shown for pH 7.4, 9 and 10 (Figure 4.11a, b and c), an increase in EPPS, CHES and CAPS concentration led to a decrease of the observed rate constant. This result was also observed when using small amine-based molecules as the buffer, such as morpholine and bis tris-propane, discounting the possibility that the sulfonate group was responsible for the phenomenon (Figure 4.11d).

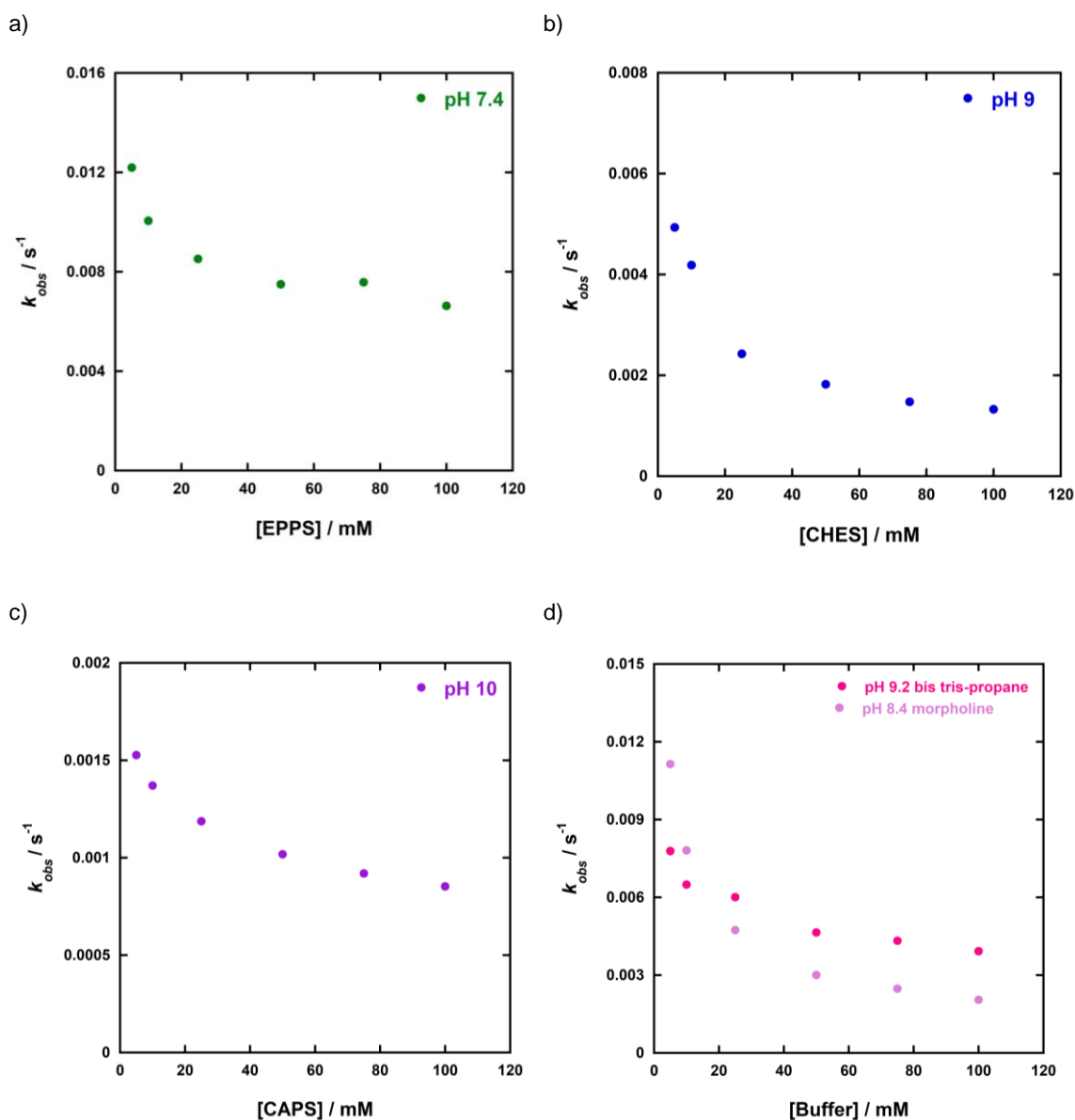


Figure 4.11 Plot of k_{obs} for the HPNPP transesterification against buffers concentrations at 25 °C, 40%(v/v) acetonitrile in water. $[4-1] = 0.05$ mM, $[HPNPP] = 0.05$ mM, ionic strength 0.1 M ($NaNO_3$), at a) pH 7.4 (HEPES); b) pH 9 (CHES); c) pH 10 (CAPS); d) Comparison between morpholine and bis trispropane

Although the reactivity was decreased, it is worth noting that the complex was not entirely deactivated by high concentrations of the buffering molecules; for example, from Figure 4.11c at pH 10 and a CAPS concentration of 100 mM, **4-1** (0.05 mM) cleaved HPNPP (0.05 mM) with a k_{obs} of 8.53 ± 0.05 s⁻¹, correspondent to a half-life time of 13 min (with the

most active mononuclear complex **3-2** similar values were obtained for a catalyst concentration of 1 mM).

Buffer inhibition was also observed by Chin and coworkers when they used 1,10-phenanthroline-2,9-diamine as Cu(II) complex (**1-16** in Figure 4.12) toward the hydrolysis of BDNPP and 2'-3'-cAMP.⁶⁵ As the rate was decelerated by any buffer tested (not listed), the catalyst itself was used to control the experimental pH. Although good control was achieved (changes smaller than 0.1 units), the absence of buffer limited the study to a pH range centred around the pK_a of the complex. Similarly, in their studies with **4-12** and **4-14** in methanol, Brown and coworkers¹²¹ observed that iPr-morpholine, triethylamine, 2-picoline and tetramethylpiperidine, used as buffers, affected the observed rate constant of the HPNPP transesterification.

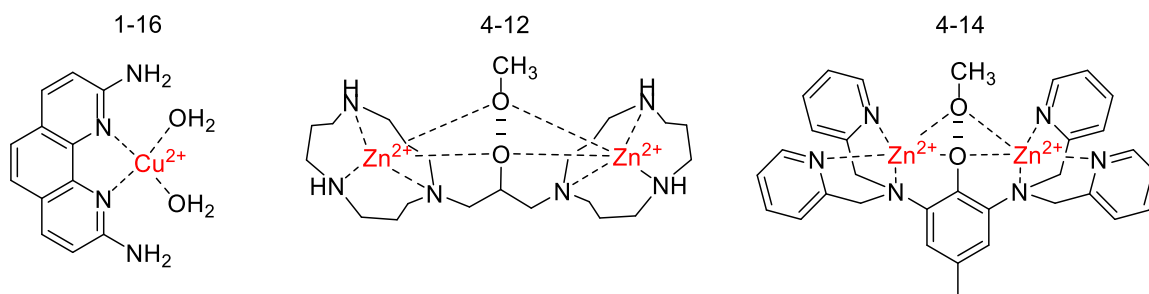
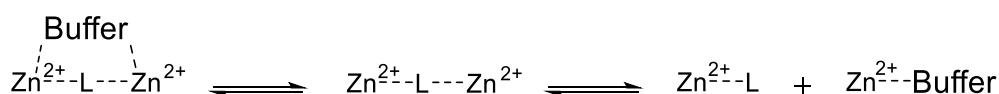


Figure 4.12 mononuclear and dinuclear complexes previously studied.

In particular, while a linear inhibition trend was observed for all the buffers (5 -25 mM) tested with **4-14**, **4-12** was inhibited only by iPr-morpholine and triethylamine. The ratio between the k_0 (the theoretical rate constant in the absence of buffer) and the k_{25mM} (measured rate constant at 25 mM of buffer) varied from 1.22 to 1.56 for **4-14**. From the

inhibition plot of iPr-morpholine for the HPNPP transesterification catalysed by **4-12**, which showed a downward curvature, an inhibition constant of 76.4 mM was obtained. The small range of buffers concentration and the different experimental conditions (fully organic solutions and different buffers) limits the comparison with **4-1**. However, we cannot exclude that at buffer concentration higher than 25 mM, the inhibition of **4-12** and **4-14** would follow a similar trend to that observed for **4-1**.

As reviewed by Ferreira *et al.* in 2015,¹²⁶ bis tris-propane was reported to participate in tight complexation with Zn(II) ions, the literature for MES and HEPES was found not to be in agreement, and EPPS has been shown to have low affinity toward Zn(II). Furthermore, there is no evidence in the literature of complexation for CHES and CAPS. Even though the sulfonate buffers did not inhibit the catalysts reported in the previous Chapters, it should be noted that, due to the high reactivity of **4-1**, an unusually low concentration (0.05 mM) was used for the kinetic experiments. Therefore, additional experiments were conducted to investigate whether the buffer molecules were responsible for stopping the complex formation, competing with the ligand for the Zn ions, or preventing the substrate binding by interacting with the complex (Scheme 4.3).



Scheme 4.3 Possible inhibition equilibrium pathways

The substrate transesterification (0.05 mM) seemed to be similarly decelerated by CHES in the presence of either 0.05 mM or 0.1 mM of the complex at pH 9 and 25 °C (Figure

4.13a); in addition to this, no difference in the inhibition profile was seen in the presence of a 10-fold excess of Zn(II), showing that the behaviour was not dependent on the metal-binding properties of the sulfonate (Figure 4.13b).

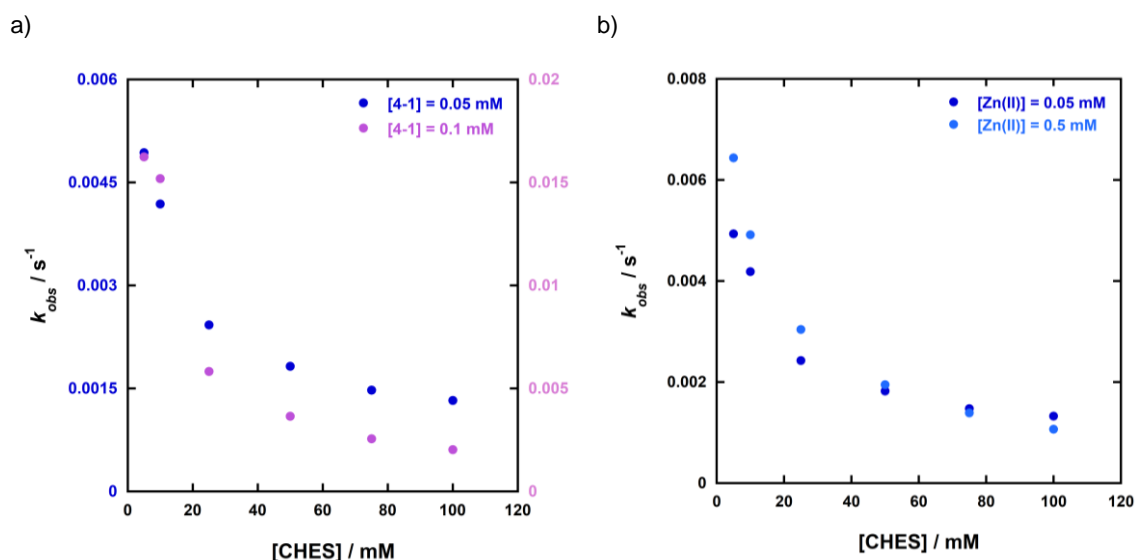


Figure 4.13 CHES inhibition plots for the transesterification of HPNPP catalysed by 4-1 at pH 9 and 25 °C a) comparison between the experiment performed at 0.05 (●) and 0.1 (●) mM of 4-1; [HPNPP] = 0.05 mM, ionic strength at 0.1 M by addition of NaNO₃, 40%(v/v) acetonitrile in water; b) comparison between the experiment performed at 0.05 (●) and 0.5 (●) mM of Zn(NO₃)₂; [L₄₋₁] = 0.05 mM [HPNPP] = 0.05 mM, ionic strength at 0.1 M by addition of NaNO₃, 40%(v/v) acetonitrile in water; the blue dots in both the graphs are obtained from the same experiment

The tight binding exhibited by **4-1** reported in Graph 4.1 was similarly consistent with this analysis. This evidence could suggest an inhibition pathway in which the presence of the additional molecule in solution can partially prevent substrate coordination to the complex. Although consistent, the inhibition profile also depended on both the particular buffer used and the pH. Different inhibition plots were obtained when EPPS was utilised for the experiment at pH 7.4, 8 and 8.4 (Figure 4.14). Figure 4.14a shows the observed rate constant against the EPPS concentration. The profile at 7.4 seems to differ from the analogous ones obtained at the two higher pH values. Equation (36), derived for

competitive inhibition, was used to fit the data at pH 8 and 8.4, but an additional variable was needed for fitting the data at pH 7.4, as the presence of the buffer did not seem to lead to zero activity at high concentrations (equation (37)). The rate constant k_0 in the buffer absence is extrapolated from the fitting and is equal to a at pH 8 and 8.4, and $a + b$ at pH 7.4. Similar inhibition constants were found at higher pH. Although this difference could depend on the proportion of the protonated and deprotonated EPPS species, especially considering that its pK_a is equal to 8, it could also be related to the complex itself; different catalyst species may form in the pH range studied, and they could have a different interaction with the buffering molecules.

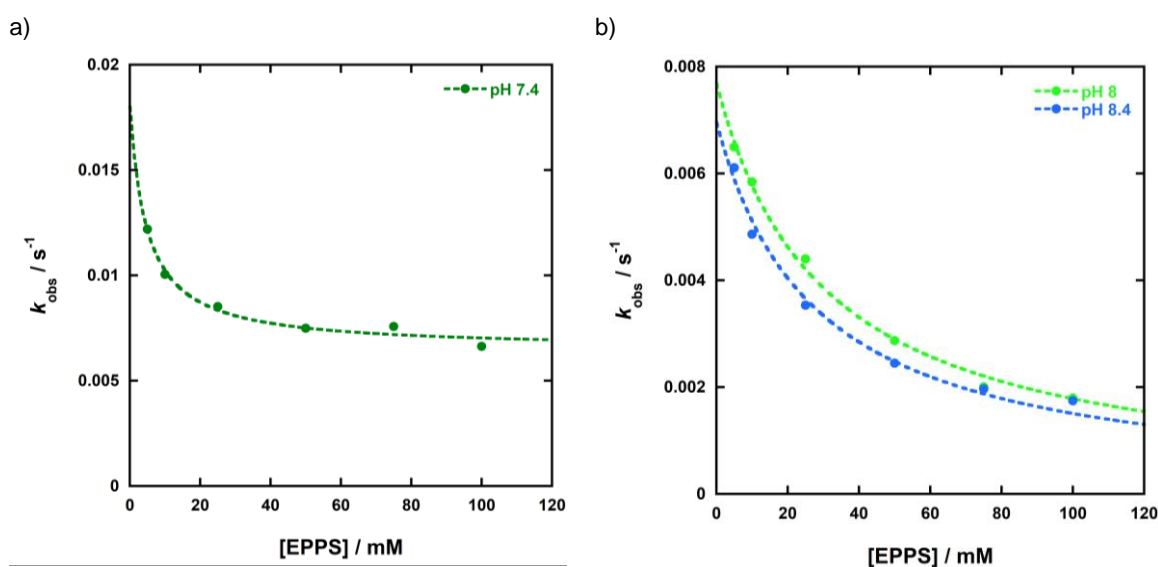


Figure 4.14 EPPS inhibition plot for the HPNPP transesterification catalysed by 4-1 at 25 °C, a) pH 7.4 (●); b) pH 8 (●); pH 8.4 (●). $[4-1] = 0.05 \text{ mM}$, $[\text{HPNPP}] = 0.05 \text{ mM}$, ionic strength 0.1 M (NaNO_3), 40%(v/v) acetonitrile in water

$$(36) \quad k_{obs} = \frac{a \cdot K_b}{K_b + [B]} + b$$

$$(37) \quad k_{obs} = \frac{a \cdot K_b}{K_b + [B]}$$

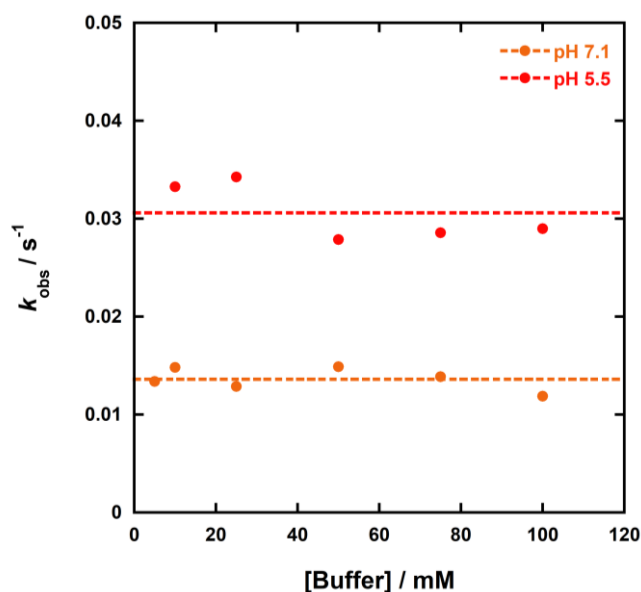
where:

$$k_0 = a + b$$

$$k_0 = a$$

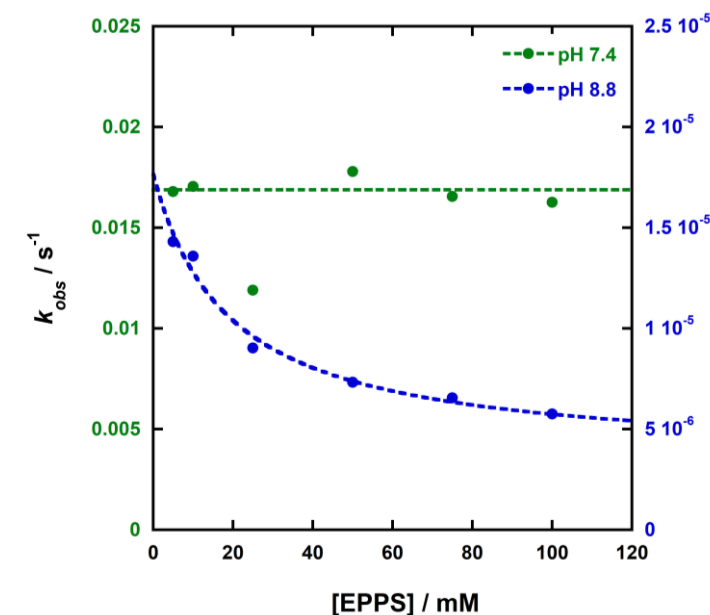
K_b : observed buffer inhibition constant
 $[B]$: buffer concentration

Interestingly, at lower pH, as reported in Graph 4.3 for pH 5.5 and 7.1, varying the concentration of HEPES or MES did not affect the rate of the reaction. Given the high similarity between the structures of HEPES and EPPS, it is unlikely that the different behaviour observed for such a slight pH difference (0.3 units) was caused by the particular choice of the buffer. This was supported by the experiment at pH 5.5, in which a structurally similar molecule stabilises the pH and does not display inhibition (Figure 4.10).



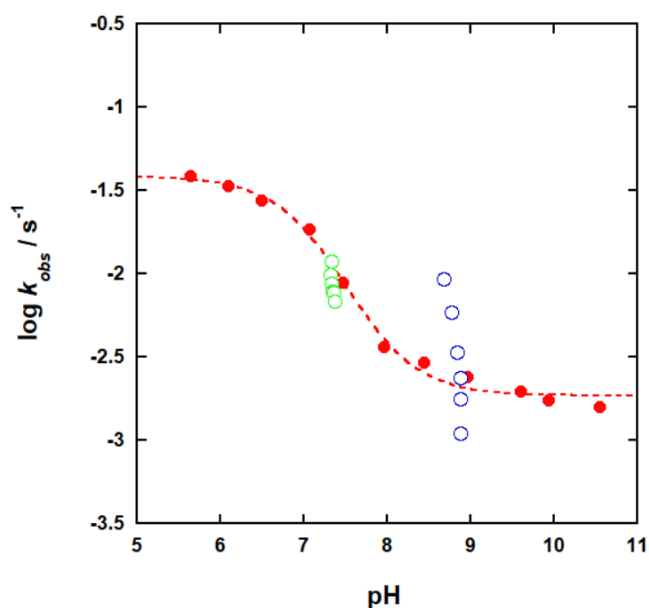
Graph 4.3 Plot of k_{obs} for the HPNPP transesterification against sulphonate buffers concentrations at 25 °C, 40%(v/v) acetonitrile in water. $[4-1] = 0.05$ mM, $[HPNPP] = 0.05$ mM, ionic strength 0.1 M ($NaNO_3$), at pH 7.1 by using HEPES (●); pH 5.5 by using MES(●)

We also tested the buffer effect on the HPNPP (0.05 mM) transesterification at 25 °C catalysed by **4-18** (0.2 mM) at pH 7.4 and 8.8 using EPPS (5-100 mM). While no inhibition was detected at pH 7.4 (green dots), a similar reduction of the k_{obs} was observed at pH 8.8 (blue dots - Graph 4.4). At lower pH, our result is in good agreement with what was previously reported. When the HPNPP cleavage enhanced by **4-18** was tested in water at pH 7.4, no buffer catalysis or inhibition was observed. Moreover, given the unexpected phenomenon of buffer inhibition, the analysis at higher pH was not performed at the time. The trend at pH 8.8 suggested the buffer similarly influences the reaction catalysed by **4-18**. Therefore, we cannot exclude that the observed inhibition is due to the common ligand scaffold for **4-1** and **4-18**.



Graph 4.4 Plot of k_{obs} for the HPNPP transesterification against EPPS concentrations at 25 °C, 40%(v/v) acetonitrile in water. $[4-I] = 0.05$ mM, $[HPNPP] = 0.05$ mM, ionic strength 0.1 M ($NaNO_3$), at pH 7.4 (●); pH 8.8 (●)

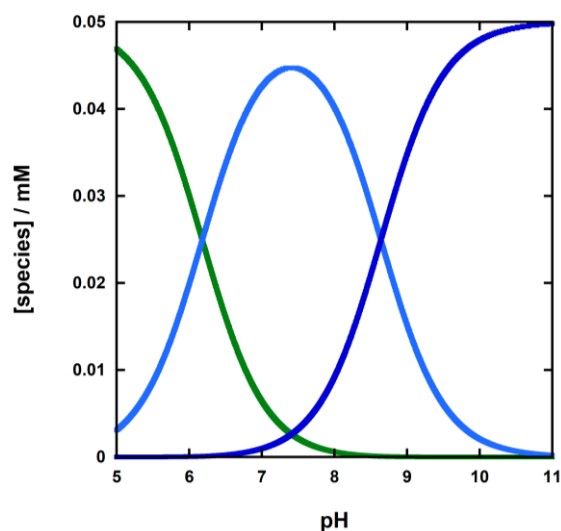
Although good buffer capacity should be reached in the concentration range studied (5-100 mM), we noticed variations of the experimental pH associated with the concentration of the buffers. Therefore, to understand if the decrease in reactivity were due to buffer inhibition or the experimental pH, we plotted in the pH profile of the k_{obs} measured at a buffer concentration equal to 50 mM (red dots) and the logarithmic values of k_{obs} at different buffer concentration (green and blue circles; 5 – 100 mM; pH of the stock solutions was 7.4 and 8.9, respectively).



Graph 4.5 Comparison between the pH profile of k_{obs} (Buffer at 50 mM ; ●) and the logarithmic values of k_{obs} measured at different EPPS concentrations (5-100 mM ; ○ – stock solution pH 7.4; ○ – stock solution pH 8.8) at 25 °C. [4-1] = 0.05 mM, [HPNPP] = 0.05 mM, ionic strength at 0.1 mM by addition of NaNO₃, 40%(v/v) acetonitrile in water

A sigmoidal equation was used to fit the red data measured at a buffer concentration of 50 mM, yielding a kinetic pK_a of 7.5 ± 0.1 and two observed rate constants of $3.8 \pm 0.3 \times 10^{-2}$ and $1.8 \pm 0.1 \times 10^{-3} s^{-1}$. The green and blue circles are the logarithmic k_{obs} value at increasing EPPS concentrations (top: 5 mM – bottom: 100 mM). While there was only a small variation for the green data centred at pH 7.4, varying the EPPS concentration determined a big change at pH 8.8. In particular, the rate constant measured at EPPS concentration of 5 mM is 8-fold higher than the values at 100 mM. The experiment highlighted that the change in the k_{obs} was pH-dependent and due mainly to the buffer concentration at higher pH. Consequently, the inhibition exhibited by a particular buffer at a specific pH might conceal the real profile of the observed rate constant in the range studied. According to Graph 4.5, only one pK_a is defined kinetically.

However, as demonstrated by a UV-titration experiment, different species of **4-1** are formed in the pH range between 5 and 11. The speciation plot displayed in Graph 4.6 was derived from the titration plot, in which the absorbance values at 275 nm were monitored over the pH range between 5 and 11 (experimental section). The theoretical fit and the speciation plot are obtained respectively with Hypspec and HySS.⁸⁸ Although accurate at higher pH, the complex's speciation plot does not consider the ligand's protonation below pH 5.5, which would eventually prohibit the complex formation. The data suggest that once **4-1** is formed (below pH 6), it undergoes two major deprotonations whose pK_a s are reported in Table 4.3, and it is present in at least three forms. Apart from the hydroxyl group, which coordinated the two ions and whose deprotonation is simultaneous with complex formation, the deprotonations of the coordinated water molecules are the most plausible events happening in solution.



Graph 4.6 Speciation plot for **4-1** in the pH range between 5 and 11. Species:

- **4-1**
- **(4-1) - 1H⁺**
- **(4-1) - 2H⁺**

[**4-1**]=0.05 mM, [MES]=[HEPES]=[EPPS]=[CHES] = 25 mM 40 % (v/v) acetonitrile in water

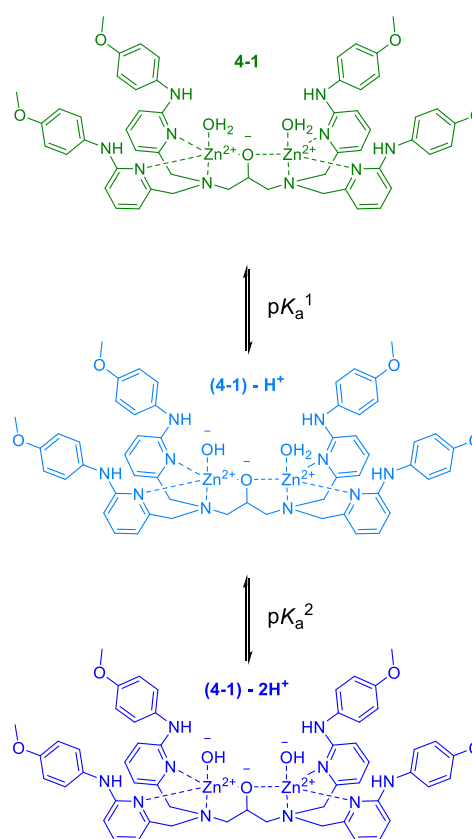
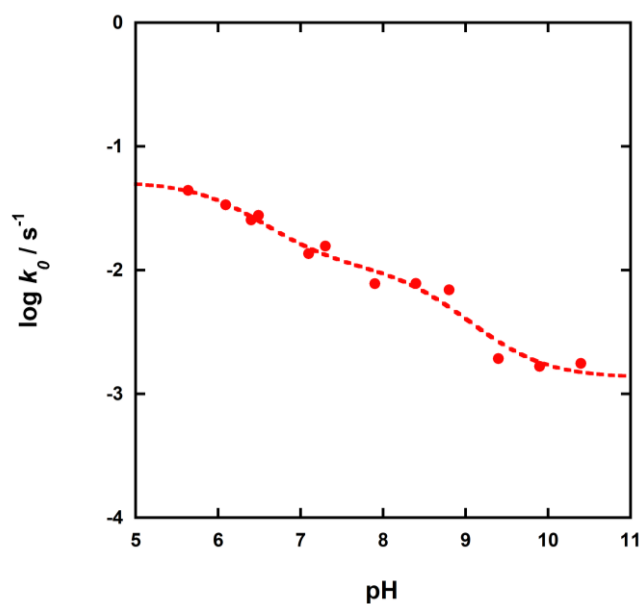


Table 4.3 pK_a values of **L4-1** and **4-1**

	complex		ligand		
	pK_a^1	pK_a^2	pK_a^1	pK_a^2	pK_a^3
4-1	6.18	8.64	5.04	7.28	10.38

All three species seemed to retain their activity, as confirmed by the pH profile reported in Graph 4.7, derived from the buffer inhibition plots described above. In contrast with Graph 4.5, we calculated k_0 at a theoretical buffer concentration equal to zero by extrapolating the y axis intercept value obtained from the fitting of each plot. The k_0 values were then reported against the average pH of each buffer inhibition experiment.



Graph 4.7. pH profile of the actual rate constant k_0 for the HPNPP transesterification at 25 °C, 40%(v/v) acetonitrile in water. Data fitted by equation . $[4-1] = 0.05$ mM, $[HPNPP] = 0.05$ mM, ionic strength 0.1 M ($NaNO_3$) and theoretical buffer concentration equal to zero

$$(38) \quad k_0 = \frac{k_0''' + k_0''[H^+]K_a^1 + k_0'K_a^1K_a^2[H^+]^2}{1 + [H^+]K_a^1 + K_a^1K_a^2[H^+]^2}$$

Table 4.4 k_0 and pK_a values obtained by fitting the data with equation (38)

	$k_0' / M^{-1} s^{-1}$	$k_0'' / M^{-1} s^{-1}$	$k_0''' / M^{-1} s^{-1}$	pK_a^1	pK_a^2
4-1	$5 \pm 1 \times 10^{-2}$	$1.1 \pm 0.3 \times 10^{-2}$	$1.3 \pm 0.3 \times 10^{-3}$	6.2 ± 0.4	8.6 ± 0.3

Equation (38), which is used to fit the data, considers three observed rate constants and two pK_a s, whose values of 6.2 ± 0.4 and 8.6 ± 0.3 were in good agreement with the result gained from the UV-titration.

Surprisingly, the hydrolysis of HPNPP proceeds fastest at lower pH and decreases while the pH is increased. For example, the HPNPP half-life time in the presence of **4-1** (0.05

mM) at pH 6.1 and 10.5 is reduced respectively to 19 and 360 seconds (approx. 6 min), which corresponds to a 20-fold difference in the relative k_0 values. Thus, the most active species seems to be the neutral one, while any further deprotonations seem to reduce the system reactivity. This result differed from the previously reported dinuclear complex **4-6**.^{119,127} The catalyst proposed by Richards and Morrow was most active toward the transesterification of HPNPP, UpU and UpNPP after the deprotonation of the metal bound water molecule (pK_a of 7.8). For **4-1**, the metal bound hydroxide formation seems to reduce the catalyst reactivity and, compared to **4-6**, at physiological pH **4-1** (0.05 mM) promote the HPNPP cleavage 1200-times faster (the difference at pH 9.3 is reduced to 60).

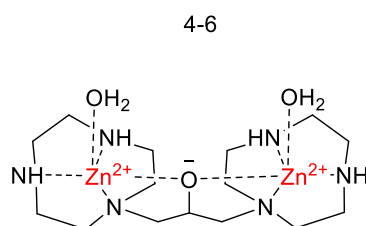
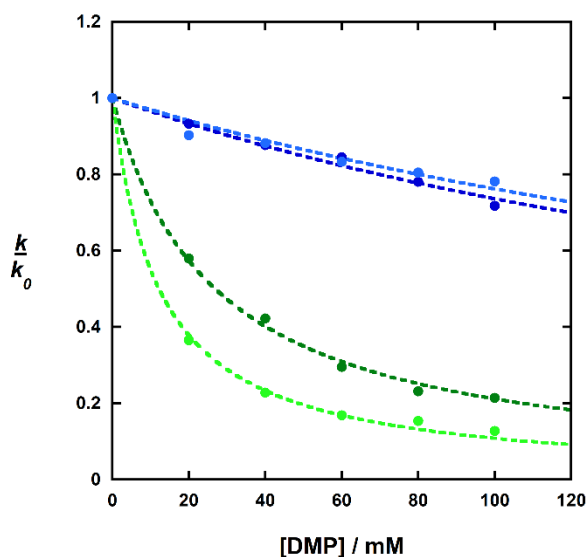


Figure 4.15 Dinuclear complex proposed by Morrow and Richards^{119,127}

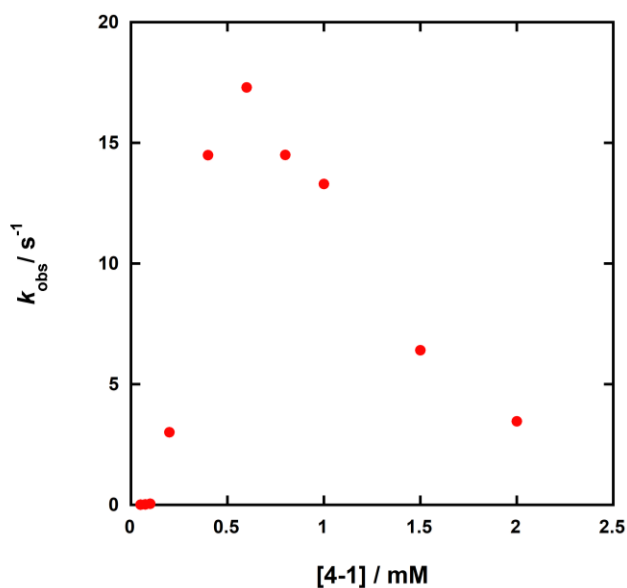
The formation of different species across the pH range was also confirmed by the inhibition studies (Graph 4.8) performed in the presence of dimethyl phosphate (DMP). As explained in Chapter 2, an additional phosphate in solution perturbs the reaction pathway by interacting with the complex, preventing the substrate from binding to the active complex species.



Graph 4.8 DMP inhibition plot at pH 7.1 (●), 7.5 (●), 8 (●) and 9 (●) at 25 °C, 40%(v/v) acetonitrile in water. $[4-1] = 0.05$ mM, $[HPNPP] = 0.05$ mM, $[Buffer] = 50$ mM, ionic strength 0.1 M by addition of $NaNO_3$; the buffers used were: EPPS for pH 7.5 and 8, and CHES for pH 9

High concentrations of DMP were needed to perturb the rate constant at all the pHs studied. However, two distinctive trends were observed. At lower pHs, the complex reactivity seemed to be strongly affected by DMP (K_i^{obs} of 12.1 ± 0.5 and 26.8 ± 0.8 mM for pH 7 and 7.5), while experiments at pH 8 and 9 showed almost no inhibition (K_i^{obs} of 279 ± 11 and 320 ± 22 mM, respectively). In good agreement with the pH profile and the UV-titration, this result is consistent with the hypothesis that different active species are formed, and the difference in reactivity could be due to their interaction mode with the substrate. Consequently, if DMP binding is taken as a good approximation for the substrate binding, the higher k_0 at lower pH could reflect a stronger substrate binding constant.

The transesterification of HPNPP (0.05 mM) has also been measured by working at different **4-1** concentrations at pH 7.4 and 25 °C. As reported in Graph 4.9, no clear dependence was observed. The maximum value of 17.3 ± 0.6 s⁻¹ is reached at 0.6 mM.



Graph 4.9 Plots of the observed rate constants for the transesterification of HPNPP at pH 7.4, 25°C in 40% (v/v) acetonitrile in water against **4-1** concentration; [HPNPP] = 0.05 mM, [HEPES] = 10 mM

The observed behaviour is not readily accounted for. Deviation from linearity was reported in literature for mononuclear and dinuclear complexes. When Brown and coworkers studied **4-19** in methanol and ethanol for the HPNPP transesterification, although a linear trend was reported for lower catalyst concentration (≤ 1 mM), the plot showed an upward curvature consistent with a bimolecular process.¹²⁸

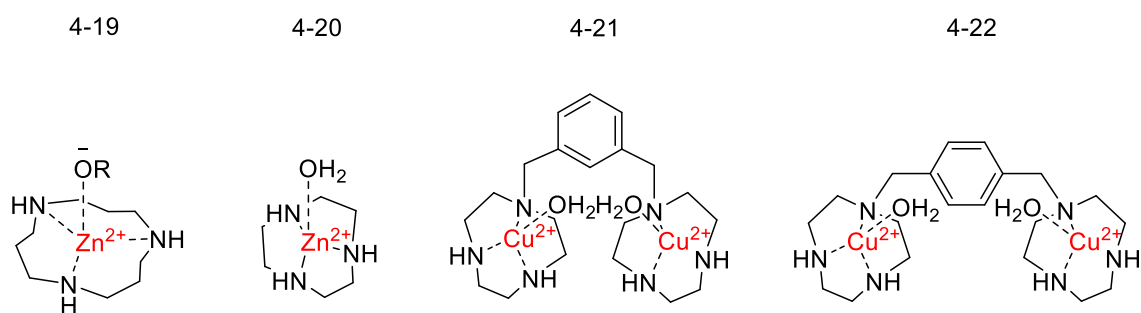


Figure 4.16 Structure of complexes proposed by Brown (4-19) and Morrow¹²⁸ (4-20, 4-21 and 4-22)^{129,130}

Earlier work from Morrow and coworkers on **4-20**,¹²⁹ used to enhance the hydrolysis of ApUp at 64 °C and pH 7.6, reported a similar dependence on the complex concentration. In particular, k_{obs} increased rapidly with the catalyst concentration, reaching a maximum of $2.3 \times 10^{-5} \text{ s}^{-1}$ at 0.25 mM and then decreasing with a further increase of concentration. When **4-21** and **4-22** were studied toward the hydrolysis of the GpppG anhydride at pH 7.3 and 37 °C, saturation kinetics at higher concentrations of both catalysts were reported.¹³⁰ The group proposed the formation of a 2:1 adduct of the dinuclear complex and the substrate. While **4-22** would promote the hydrolysis of GpppG through both 1:1 and a 2:1 adduct (with the latter being 20-fold more reactive than the former), **4-21** would hydrolyse the substrate only via the 2:1 complex. Although striking similarities among those reports and our results on **4-1**, the different experimental conditions (alcohols used as a solvent by Brown and the different substrates tested in the following examples) make a direct comparison impracticable. However, the common aspect of the proposed mechanisms for the reaction catalysed by the previously reported catalysts considered the participation of more than one catalyst unit.

For **4-1**, the formation of a cluster of multiple units of the complex that can cooperate to form a species that is more reactive than the monomer is a possible hypothesis. While the reaction could be accelerated by aggregation to form especially active catalytic sites in the lower concentration range, a limiting point is reached at 0.6 mM when further aggregation limits the substrate binding leading to an overall drop in activity. The aggregate formation could create a relatively hydrophobic environment which, similarly to biological systems and the observations made in light alcohols,⁶⁴ could be responsible for the high reactivity observed.

This hypothesis has been tested by UV-vis and Fluorescence spectroscopy. UV spectra recorded at different concentrations of **4-1** (0.1 – 500 μM) at 25 $^{\circ}\text{C}$, pH 8 and ionic strength at 0.1 M by addition of NaNO_3 are shown in Figure 4.17a. The residual band at 0.1 μM of **4-1** (bright light green - Figure 4.17a) is due to the presence of 0.1 M of NaNO_3 . Plotting the absorbance at 270 and 350 nm against the complex concentration revealed no variation from the Beer-Lambert equation (Figure 4.17b).

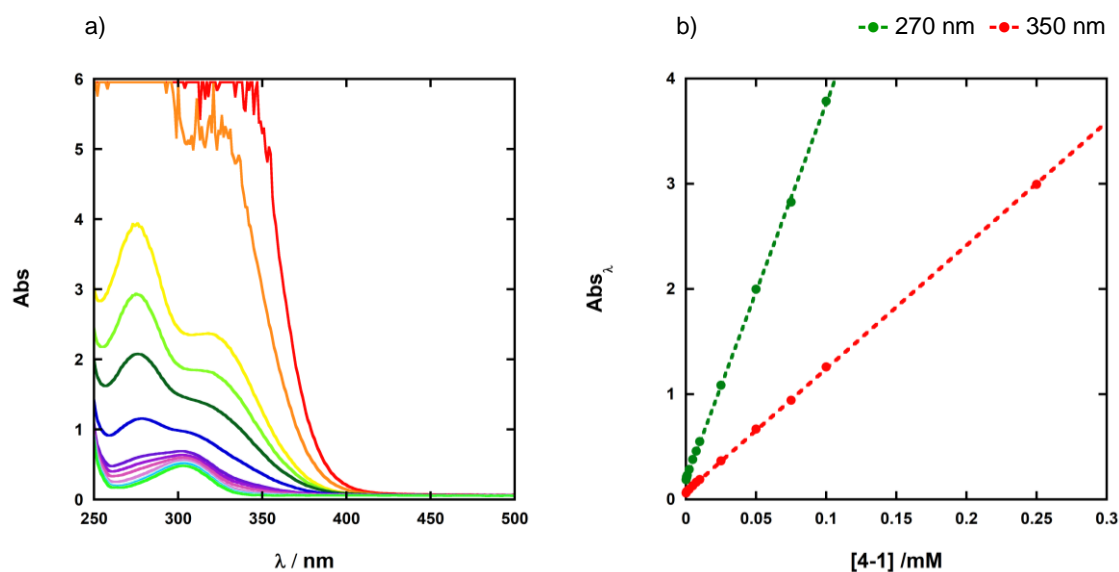


Figure 4.17 Aggregation investigation at 25 $^{\circ}\text{C}$ and pH 8; a) UV-spectra of solutions at different concentrations of **4-1**; b) Absorbance at 270 and 250 nm reported against the logarithmic value of **[4-1]**; $[\text{EPPS}] = 50 \text{ mM}$, ionic strength at 0.1 M by addition of NaNO_3

This method is often used to calculate the critical aggregation concentration (CAC) of macrosystems,¹³¹ such as micelles or vesicles, and a deviation from linearity might imply a change in the aggregation status of these systems. In the concentration range studied, the data for **4-1** did not suggest that an adduct was forming. However, following the aggregation of a relatively small molecule might not be possible with this method. Furthermore, if the adduct is already formed at concentrations lower than 0.1 μM , the event

cannot be monitored by UV spectroscopy. To overcome this problem and explore a lower concentrations range, we performed the following experiment with pyrene.

Pyrene can be used as a fluorescent probe to investigate agglomerate formation in solution.¹³² The pyrene fluorescent band is sensitive to the local environment and, moving from an aqueous to a hydrophobic phase, the ratio between the two intensities at 384 and 373 nm usually changes. Although the fluorescent probe is often used with nano and micro dimensional supramolecular assemblies, in the case of **4-1**, the nature of the ligand could lead to the formation of a relatively big hydrophobic pocket upon aggregation.

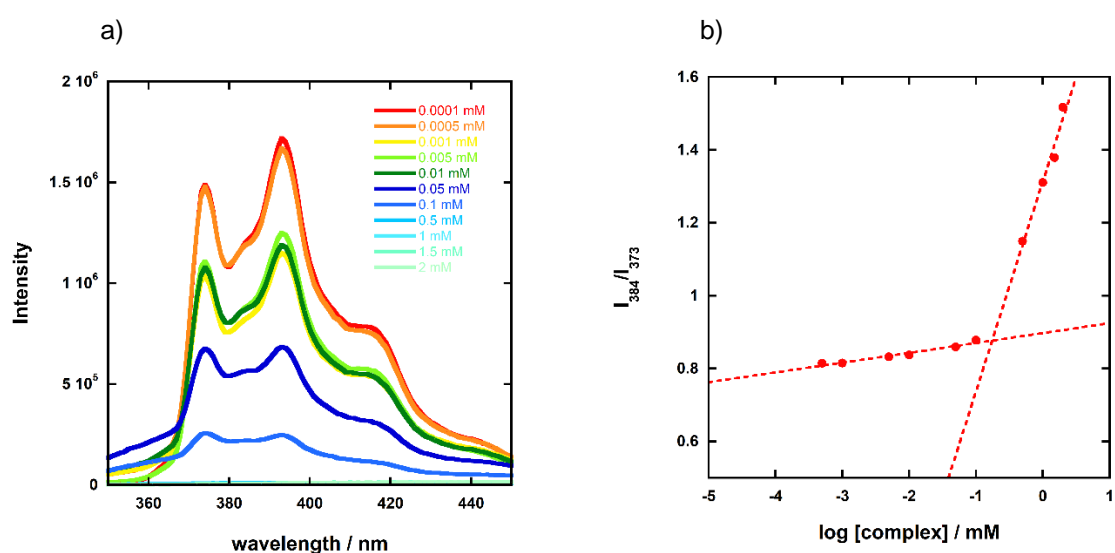


Figure 4.18 a) Study of the variation of the fluorescent band of pyrene at increasing concentration of 4-1; b) Plot of the ratio of the intensities recorded at 384 and 373 nm reported against 4-1 concentration. [pyrene] = 2.5 · 10⁻⁴ mM, [Buffer] = 50 mM, ionic strength 0.1 M, 40% (v/v) acetonitrile in water

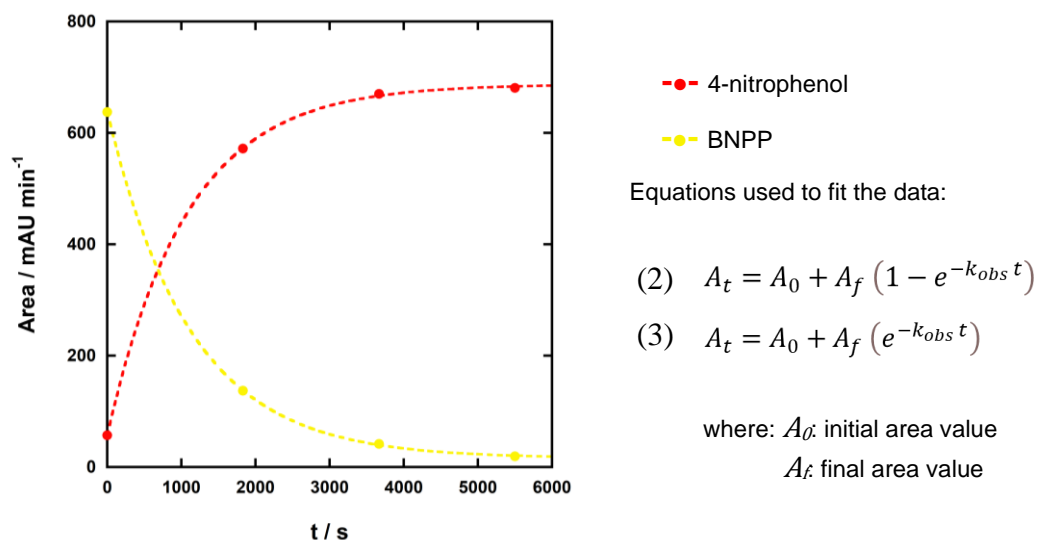
The change in the fluorescent spectrum of a solution of 2.5 x 10⁻⁴ mM of pyrene was recorded at different complex concentrations (Figure 4.18a); even though a significant change in the ratio I₃₈₄/I₃₇₃ is observed for concentrations over 0.1 mM (Figure 4.18b), this

behaviour seemed to be due to a total quenching of the pyrene fluorescence. In light of the result, this experiment did not clearly support the hypothesis that an aggregate forms but the rapid disappearance of any pyrene fluorescence is an intriguing aspect that may suggest a change in solution.

Hydrolysis of BNPP

Given the substantial rate enhancement provided by **4-1** for the transesterification of HPNPP, the complex was also tested with BNPP to discover whether this provided useful insights into its unusual catalytic behaviour. BNPP is inherently less reactive phosphate diester as it does not have an intramolecular nucleophile and is often used as a convenient (although crude) test substrate for DNA. Although the ligand in **4-1** does not possess nucleophilic sites, it is possible that there are metal bound water sites that can fulfil this role or that the bound substrate is sufficiently activated that intermolecular attack of hydroxide or water is effective enough to lead to a significant catalytic effect.

At pH 7.4 and 25 °C, 1 mM of **4-1** enhances the hydrolysis of BNPP by a factor of 10^8 -fold, reducing its half-life to less than 4 min. In pseudo first order conditions, HPLC confirmed that the catalysed reaction leads to 4-nitrophenol and that no phosphorylated derivatives of **4-1** are formed during the reaction time.



Graph 4.10 HPLC experiment of the cleavage of BNPP at pH 7.4 and 25 °C; Area of the peaks of 4-nitrophenol (●) and BNPP (●); $[4-1] = 0.5 \text{ mM}$, $[BNPP] = 0.05 \text{ mM}$, $[HEPES] = 50 \text{ mM}$, ionic strength 0.1 M by addition of NaNO_3 , 40 % (v/v) of acetonitrile in water

Similarly, when working with an excess of catalyst, the hydrolysis is first order on the substrate (0.01-0.25 mM). However, **4-1** does not catalyse the hydrolysis of an excess of BNPP efficiently. The reaction of **4-1** with 5 equivalents of BNPP at pH 7.1 and 25 °C was monitored by HPLC, and only one equivalent of 4-nitrophenolate was produced after 1 h.

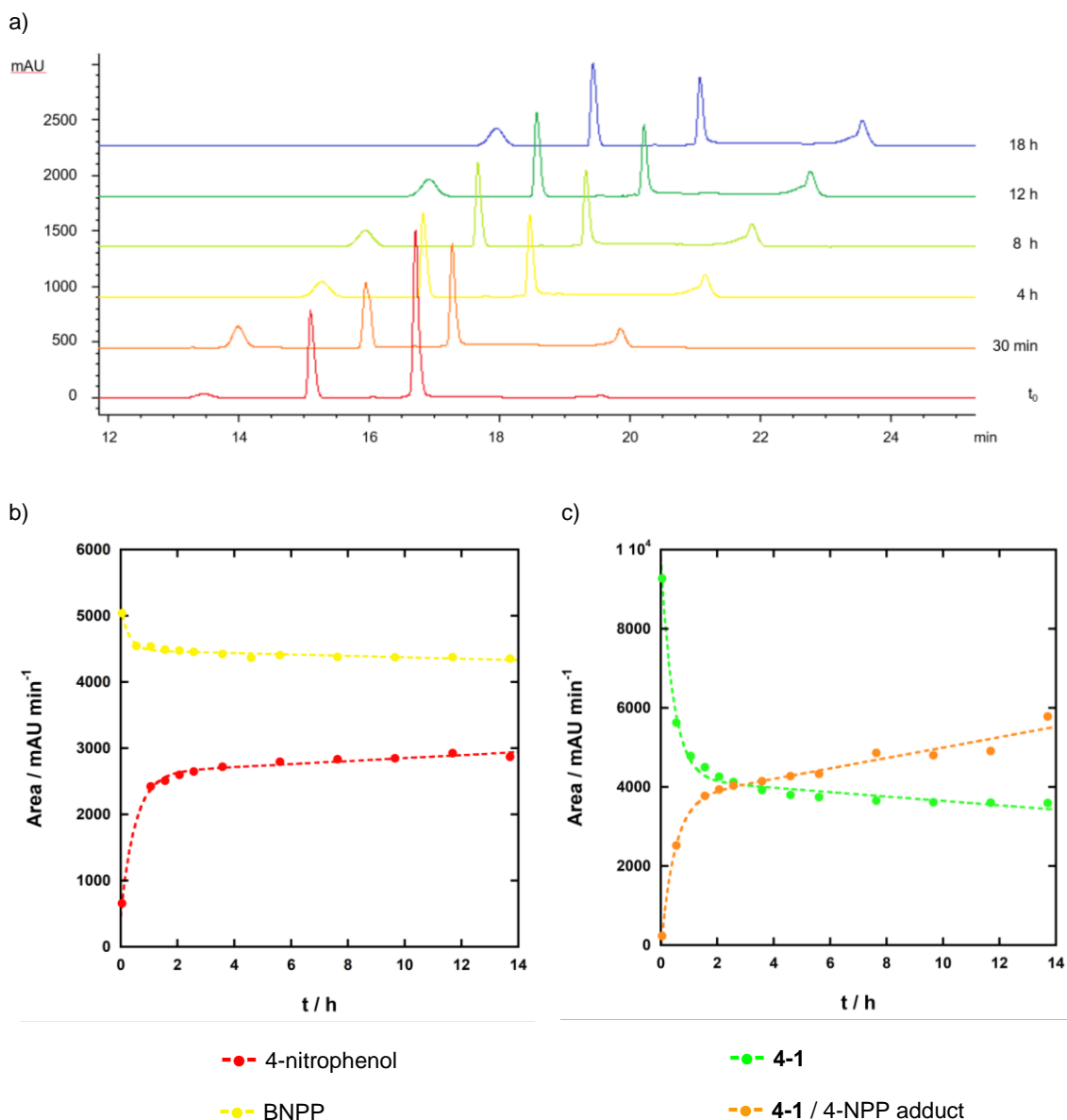
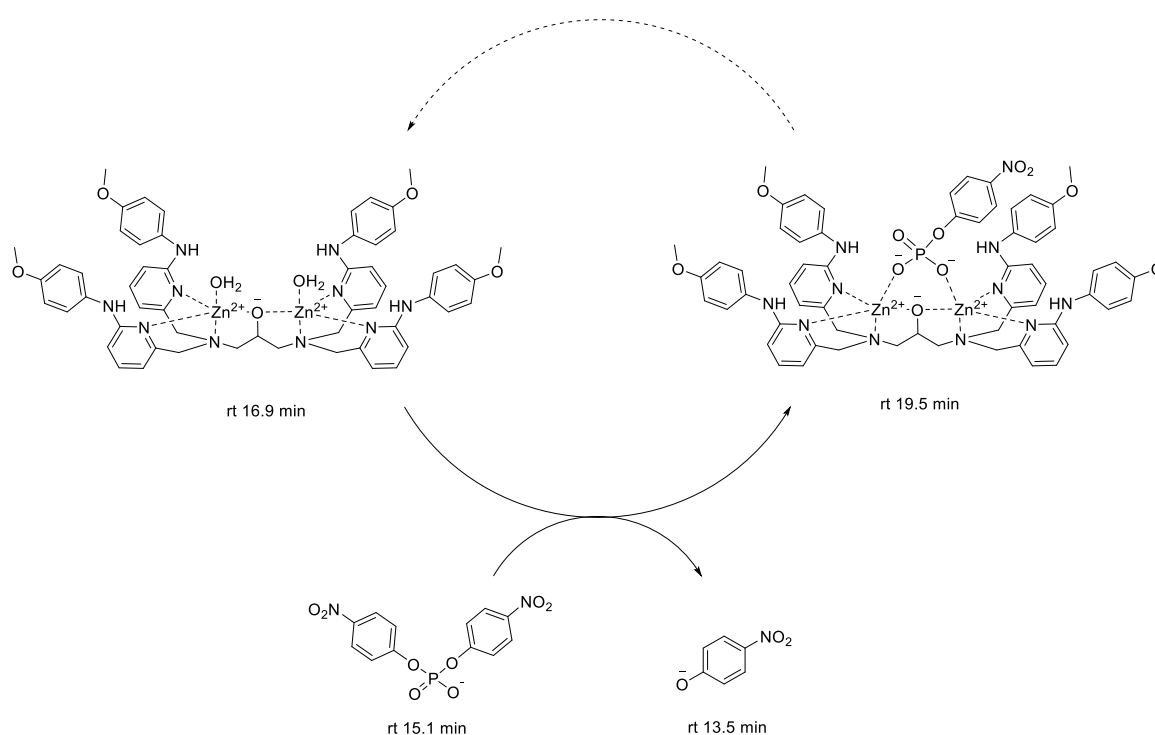


Figure 4.19 HPLC experiment of the hydrolysis of BNPP catalysed by 4-1 at pH 7.1 and 25 °C: a) reported chromatograms at different reaction time, retention times: BNPP 15.1 min, 4-1 16.9 min, 4-nitrophenol 13.5 min; b) Area of BNPP's (●) and 4-nitrophenol's (●) peak over time; c) Area of 4-1 (●) and 4-1's / 4-NPP adduct's (●) peak over time; [4-1] = 1 mM, [BNPP] = 5 mM, [HEPES] = 50 mM, ionic strength 0.1 M, 40%(v/v) acetonitrile in water

Figure 4.19, which shows chromatograms of the reaction mixture taken over 18 h, confirms that **4-1** does not undergo multiple turnovers. The product (r.f. 13.5 min), substrate (r.f. 15.1 min) and complex (r.f. 16.9 min) peaks change over the first hour, but strong product inhibition seems to affect the catalyst performance with no significant differences after 18

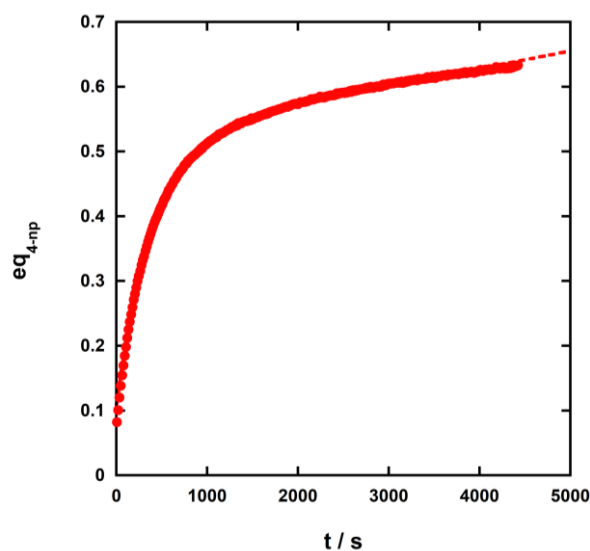
h (1.2 final equivalents of 4-nitrophenol). The areas of four observed peaks are reported in Figure 4.19b and Figure 4.19c. The unexpected decrease of the peak for **4-1** could be due to the formation of a new species (appearing at 19.5 min), representing **4-1** firmly bound to the 4-nitrophenyl monophasphate. In addition, a baseline alteration close to the peak might have altered the area of **4-1**/4-NPP adduct, which increased more rapidly than the other values. The proposed mechanism based on the HPLC experiment is described in Scheme 4.4:



Scheme 4.4 Proposed mechanism for the hydrolysis of BNPP catalysed by 4-1 based on the HPLC and LCMS experiment

Monitoring the reaction by UV spectroscopy provided a similar result as shown in Graph 4.11. Reducing the catalyst and substrate concentration (0.5 and 2.5 mM, respectively) but maintaining the same ratio, we observed that after 1 h, less 4-nitrophenolate was produced

(approximately 0.6 equivalent) at pH 7.1 and 25 °C. In contrast with the HPLC, when working with a lower catalyst concentration, the monophosphate produced by the reaction seems to affect **4-1**'s performance. The TIC scan of the LCMS experiment reported in Figure 4.20, although not quantitative, confirmed the partial conversion of the substrate after 24 h.



Graph 4.11. Equivalents of 4-nitrophenolate reported over time produced during the hydrolysis of BNPP catalysed by **4-1** at pH 7.4 and 25 °C. [**4-1**] = 0.5 mM, [BNPP] = 2.5 mM; [HEPES] = 50 mM, ionic strength 0.1 M by addition of NaNO₃, 40% (v/v) acetonitrile in water

The observed *burst effect* can be explained by the growth of the monophosphate concentration, leading to a decrease of active complex that would cause a reactivity decrease.

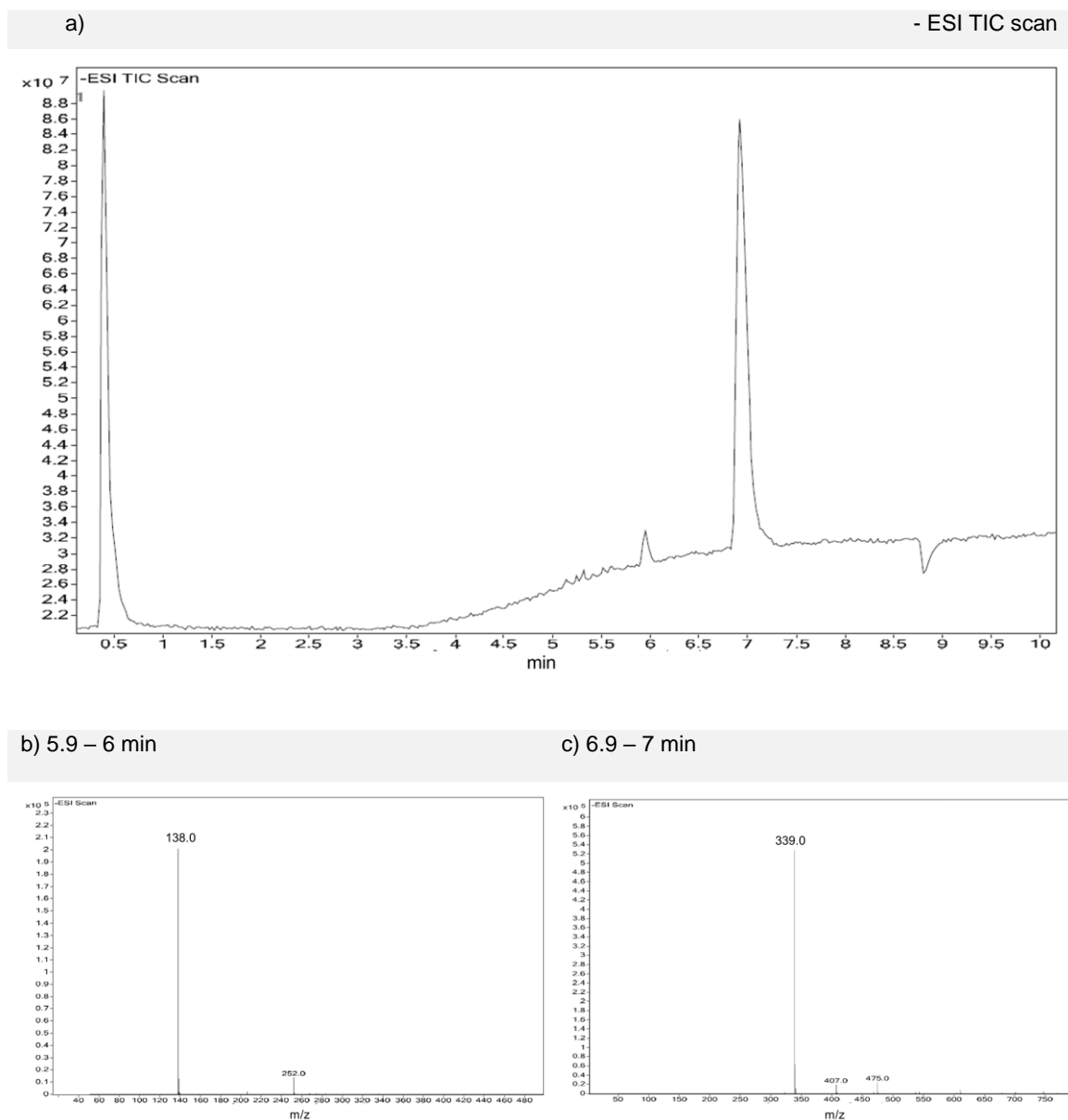


Figure 4.20 LCMS experiment of the turnover experiment; a) -ESI TIC scan, b) mass of the peak at 6 min (4-nitro phenolate; c) mass of the peak at 7 min (BNPP)

Despite the lack of efficient turnover, it should be noted that the observed rate constant reached by **4-1** is higher or comparable to those measured with mononuclear catalysts provided with "intramolecular" nucleophiles. As described in Chapter 2, the presence of different nucleophiles changed the cleaving mechanism of BNPP; while **2-3** and **2-5**

catalysed the transesterification of the substrate, **2-4** enhanced the hydrolysis. **4-1** behaved similarly to **2-4** (gem diol as nucleophile), and 4-nitrophenol phosphate inhibited both. At pH 7 and 25 °C, the observed rate constant for the cleavage of BNPP catalysed by 1 mM of **4-1** is 10-fold higher than observed for **2-5** (oxime as nucleophile), whose reactivity was not inhibited by monophosphate but strongly affected by dimerisation.

As previously carried out for HPNPP, the activity of **4-1** towards BNPP hydrolysis was also tested in the pH range between 6 and 10. Varying the buffer concentration (5-75 mM) led to a reduction of the k_{obs} . In particular, while no deviation can be observed at lower pH (< 7.4), moving to higher pH, a decrease is noticeable. However, in contrast to the data for HPNPP, these variations were due to unexpected pH shifts associated with the specific buffer concentrations of the experiment. For example, as highlighted by Figure 4.21a, a specific buffer concentration corresponds to a pH (light green dots) and leads to a corresponding k_{obs} (dark green dots). Although partial inhibition cannot be excluded over 75 mM, the reactivity changes correlate with the particular pH of each measurement.

Six experiments (pH of the stock solutions: 7, 7.4, 8, 8.5, 9 and 9.5) were carried out where the buffer concentration was varied from 5 to 75 mM. The k_{obs} of each experiment were plotted against the measured pH in one single plot (Figure 4.21b). For example, the green dots in Figure 4.21b are the logarithmic values of the k_{obs} reported in Figure 4.21a. Except for those at 75 mM over pH 7.4 (empty squares), all the data (red dots and green dots) lie on the same curve, suggesting that the changes in the observed rate constant for the hydrolysis reaction were due to the sensitivity to the pH of the solution rather than the buffer concentration. The fitting with equation (39) of the observed bell-shaped pH profile

reveals the presence of two kinetic pK_a s at 6.2 ± 0.1 and 7.68 ± 0.05 , which suggests that a singly deprotonated form of **4-1** was the active species for this reaction.

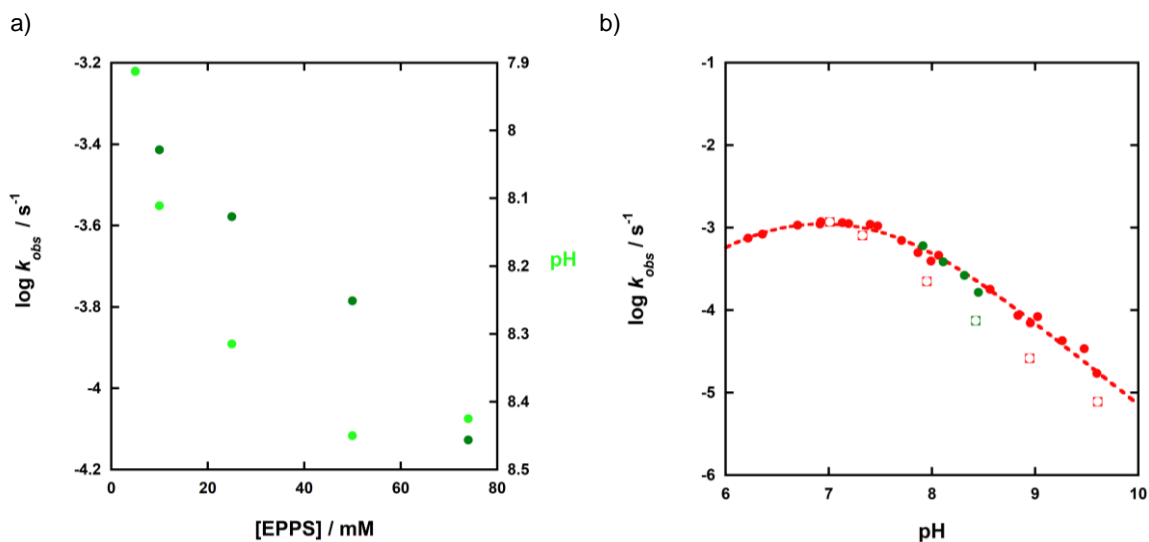


Figure 4.21 a) Plot of $\log k_{obs}$ against the EPPS concentration in the pH range 7.9-8.5 and 25 °C for the hydrolysis of BNPP catalysed by **4-1**, $[4-1] = 0.5$ mM, $[BNPP] = 0.05$ mM, ionic strength 0.1 M, 40%(v/v) of acetonitrile in water ; b) Plot of the pH profile of k_{obs} at different buffers concentration (5-75 mM) at 25 °C, $[4-1] = 0.5$ mM, $[BNPP] = 0.05$ mM, ionic strength 0.1 M, 40%(v/v) of acetonitrile in water

$$(39) \quad k_{obs} = k_{obs}^{max} \frac{K_a^1[H^+]}{(K_a^1K_a^2 + K_a^1[H^+] + [H^+]^2)}$$

Although different trends are observed for HPNPP and BNPP, **4-1** is most active at physiological pH. According to UV-titration (Graph 4.6), in the pH range between 6 and 7.5, **4-1** is mostly present in the form reported in Figure 4.22.

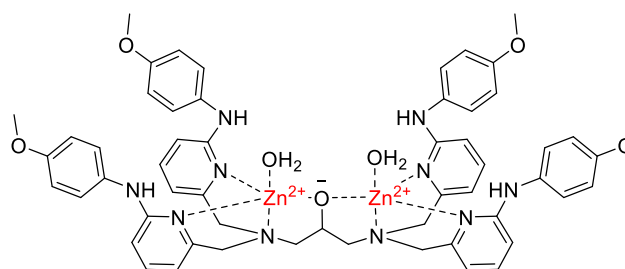
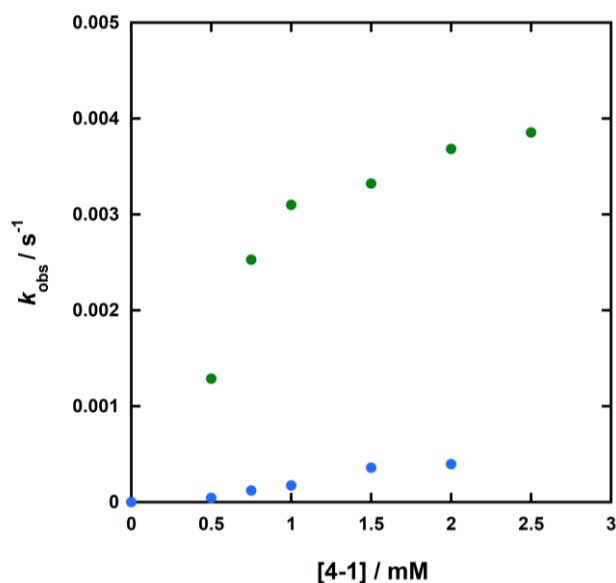


Figure 4.22 Active form of **4-1**

In contrast to what was observed for HPNPP, the analysis with BNPP revealed that further deprotonation deactivated the catalyst. Furthermore, the dinuclear complex is less reactive toward the cleavage of BNPP, which is cleaved by **4-1** (1 mM) 4300-fold slower than HPNPP at pH 7 and 25 °C (substrate concentration of 0.05 mM).

The effect of varying the concentration of **4-1** (0.5 - 2.5 mM) on the hydrolysis of BNPP at pH 7 and 9 and 25 °C was also measured (Graph 4.12). In agreement with the pH profile, the reaction proceeded faster at lower pH. However, the dependence was not simply first order at both pHs. Similarly to the transesterification of HPNPP (Graph 4.9) at the lower concentrations, there was a sigmoidal dependence on the concentration of **4-1**. However, when the rate constant reaches its maximum value, it levels off rather than dropping ($k_{\text{obs}} = 3.86 \pm 0.03 \cdot 10^{-3} \text{ s}^{-1}$ at 2.5 mM at pH 7). Given the low solubility of the complex, higher concentrations than 2.5 mM have not been investigated, and the possible subsequent decrease noted with the RNA model molecule might be missed by this analysis (the sigmoidal increase occurs over a greater change in concentration than for the HPNPP reactions).



Graph 4.12 Plot of the k_{obs} against the concentration of 4-1 for the hydrolysis of BNPP at pH 7(●) and 9(●), 25 °C; [BNPP] = 0.05 mM, [Buffer] = 50 mM (HEPES, CHES); ionic strength at 0.1 M by addition of NaNO_3 , 40% (v/v) acetonitrile in water

Transesterification of UpG

Although the RNA and DNA model molecules allow for convenient monitoring of reactions which helps provide detailed data of the activity of a complex, their value is limited by the structural differences with their relative nucleic acids. For example, these substrates are not suitable for investigating the complex ability for stabilising the leaving group; by using these models, such information is not gained because of the high stability of p-nitrophenolate.

Using nucleotides is an essential step to investigate whether the catalyst could have applications for biological purposes. The transesterification of UpG has been tested in the presence of **4-1** at pH 7.4 and 25 °C. The dinuclear complex (1 mM) accelerates the reaction substantially, reducing the half-life of UpG to approximately 30 min. Under similar

conditions, **4-18**,⁹⁷ is 3 times less reactive for catalysing the hydrolysis of Uridyl-(3-5)uridine (UpU). The reaction was followed by monitoring the area of UpG and the guanosine peaks of HPLC chromatograms taken at different times. Figure 4.23a shows the relative area ($\text{UpG}_t/\text{UpG}_0$ and G_t/G_∞) of the peaks at 3.7 (substrate – red dots) and 3.4 (product – green dots) over time.

Proposed mechanism:

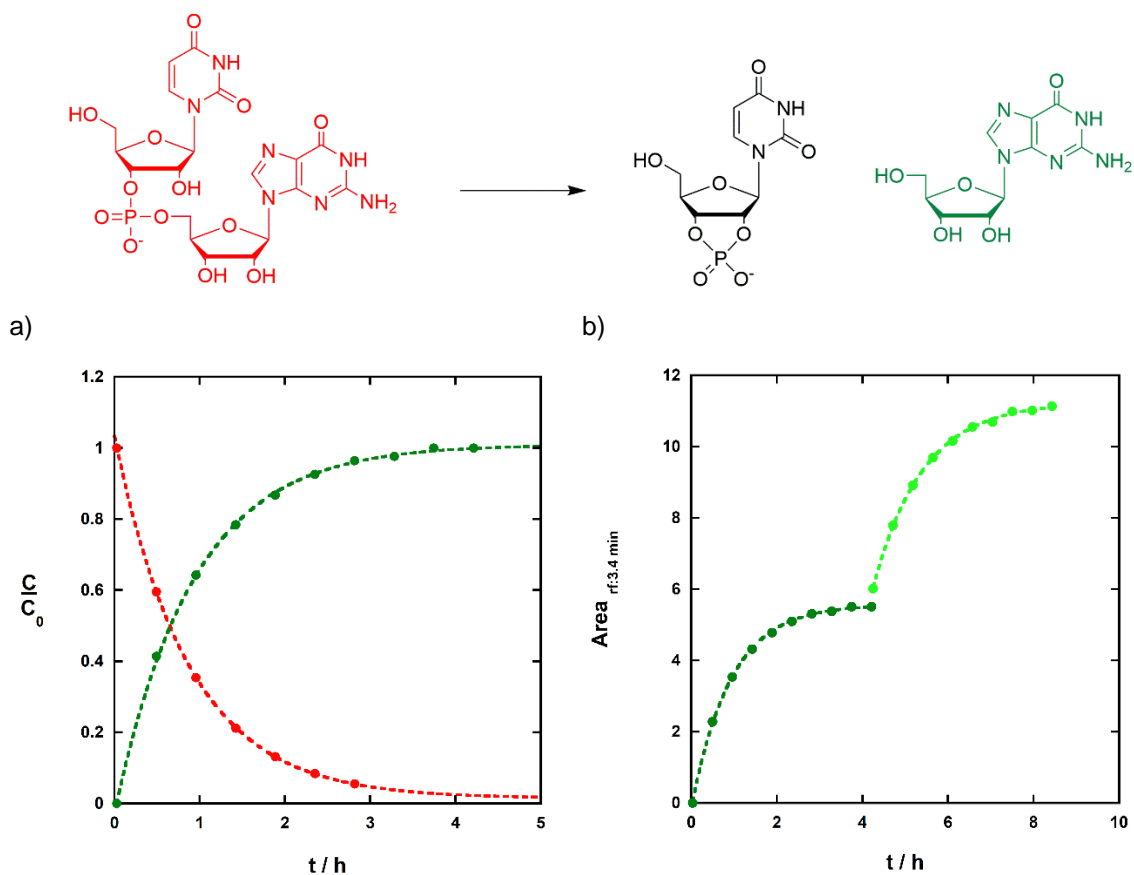
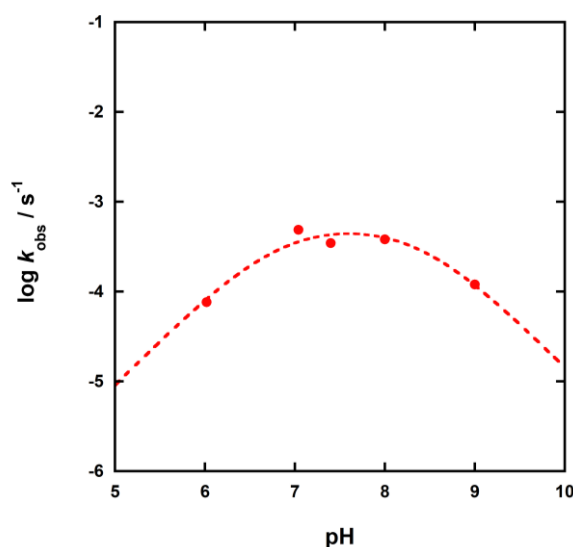


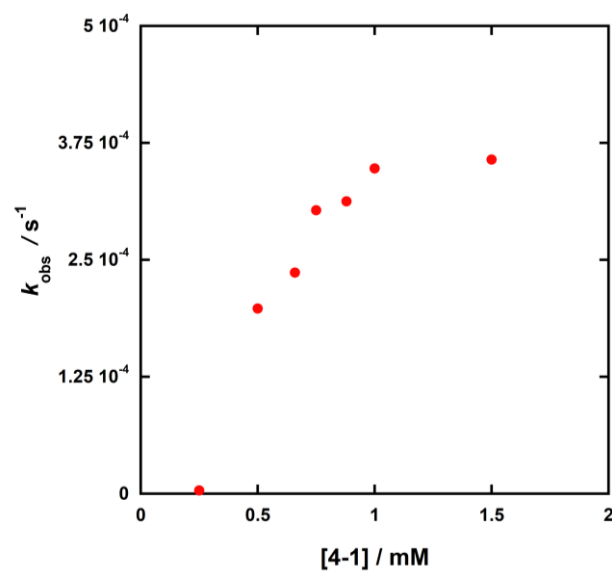
Figure 4.23 HPLC experiment of the transesterification of UpG catalysed by 4-1 at pH 7.4 25 °C; [4-1] = 1 mM, [UpG] = 0.05 mM, [HEPES] = 50 mM, ionic strength 0.1 M, 40% (v/v) acetonitrile in water a) Relative area of the substrate ($\text{UpG}_t/\text{UpG}_0$ - ●) and product (G_t/G_∞ - ●) over time. An exponential rise function fits the data; b) Area of product peak (rf: 3.4 min) over time. The first (●) and second (●) additions are reported in the plot. An exponential rise function fits the data; to have an equivalent initial substrate concentration, the second addition of UpG is done considering the volume reduction after the first 10 measures.

After a second addition of UpG (light green dots in Figure 4.23b), the reaction continues with a similar rate constant showing that the complex retains its activity for the duration of these experiments. In contrast to **4-18**,⁹⁷ the substrate is entirely cleaved by the catalyst, and no traces are visible after 5 h. The pH rate profile of the observed rate constant for the transesterification of UpG (0.05 mM and 1 mM of **4-1**) shows a maximum at pH 7.4. The bell-shaped pH profile shows ionisations at $\text{pH } 6.8 \pm 0.3$ and at $\text{pH } 8.4 \pm 0.3$ (Graph 4.13). Once again, this result qualitatively agrees with the speciation plot (obtained from the UV-titration) and resembles both the HPNPP and BNPP transesterification trends.



Graph 4.13 pH profile of k_{obs} for the transesterification of UpG catalysed by **4-1** at 25°C ; $[\text{UpG}] = 0.05 \text{ mM}$, $[\text{4-1}] = 1 \text{ mM}$, $[\text{Buffer}] = 50 \text{ mM}$, ionic strength at 0.1 M by addition of NaNO_3

When the reaction was followed at different catalyst concentrations, no simple dependence on **4-1** was observed. Once again, as reported for both the model molecules, the observed rate constant for the UpG transesterification shows a sigmoidal dependence on increasing the catalyst concentration, reaching a maximum at 1 mM (Graph 4.14).



Graph 4.14 Plot of the k_{obs} against 4-1 concentration for the transesterification of UpG at pH 7.4 and 25 °C; $[UpG] = 0.05 \text{ mM}$, $[HEPES] = 50 \text{ mM}$, ionic strength 0.1 M, 40 % (v/v) acetonitrile in water

4.3 Conclusion

In conclusion, we have reported a dinuclear Zn(II) complex, which showed the highest reactivity to date in aqueous solutions. Compared to the most reactive dinuclear Zn(II) catalysts reported to date, at neutral pH and 25 °C, **4-1** (0.2 mM) is 100 000- and 850-fold more reactive than **4-6** and **4-18**, respectively, toward the hydrolysis of HPNPP.^{97,116}

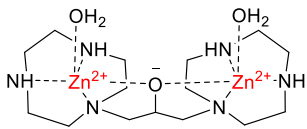
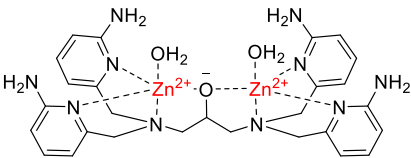
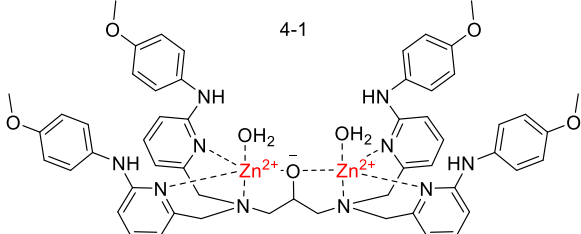
	HPNPP	UpN	BNPP
	$k_{\text{obs}} / \text{s}^{-1}$ (at 0.6 mM)	$k_{\text{obs}} / \text{s}^{-1}$ (1 mM)	$k_{\text{obs}} / \text{s}^{-1}$ (1 mM)
<p>4-6</p> 	1.5×10^{-4}	7×10^{-7}	-
<p>4-18</p> 	2×10^{-2}	1.2×10^{-4}	-
<p>4-1</p> 	17.3 ± 0.6	$3.5 \pm 0.2 \times 10^{-4}$	$3.1 \pm 0.1 \times 10^{-3}$

Figure 4.24 Comparison among reported dinuclear catalysts

Although **4-1** is less reactive for cleaving the unactivated UpG, at pH 7.4 and 25 °C, the presence of the catalyst reduced the half-life time of the dinucleotide (0.05 mM) is 30 min. Under similar experimental conditions, **4-6** and **4-18** reduced the half life time of UpU

(estimated to be 180 years) to 16500 (approximately 11 days) and 90 min, respectively. As we would not expect any nucleobase selectivity, we estimated that **4-1** is 500- and 3-fold more reactive than **4-6** and **4-18**.

In addition, given the high reactivity observed with the RNA-model molecules, we tested the catalyst toward the hydrolysis of BNPP. It is worth noting that catalysts lacking a nucleophile in their ligand structure have relatively small reactivity toward the hydrolysis of BNPP. For this reason, the reaction with BNPP catalysis was not previously investigated with **4-6** and **4-18**. However, at pH 7.4 and 25 °C, the observed rate constant in the presence of **4-1** (1 mM) is $3.1 \pm 0.1 \times 10^{-3} \text{ s}^{-1}$, comparable to the observed reactivity of the mononuclear catalyst enriched with an oxime (**2-5** in Chapter 2).

Surprisingly, **4-1** is more active at neutral rather than alkaline pH. The pH dependence of k_{obs} at 25 °C for the three reactions are reported in Figure 4.25a.

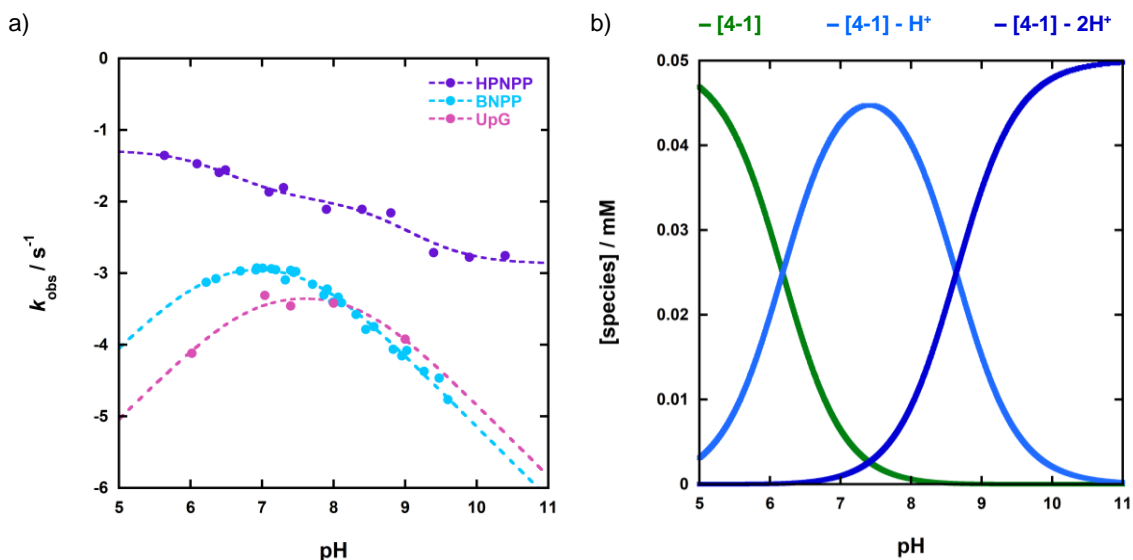


Figure 4.25 a) pH dependence of the observed rate constant for the cleavage of HPNPP (●), BNPP (●) and UpG (●) catalysed by 4-1 at 25 °C; HPNPP: [4-1] = 0.05 mM, [HPNPP] = 0.05 mM, BNPP: [4-1] = 0.5 mM, [BNPP] = 0.05 mM; UpG: [4-1] = 1 mM, [UpG] = 0.05 mM, [Buffer] = 50 mM; all the solutions were prepared at ionic strength of 0.1 M by addition of NaNO₃ in 40 % (v/v) acetonitrile in water; b) speciation plot of 4-1 (0.05 mM) at 25 °C; [MES]=[EPPS]=[CHES]=[MES]=25 mM; ionic strength at 0.1 M by addition of NaNO₃

Due to the different stability of the substrates, the same concentration of catalyst was not used to produce the pH profiles shown in Figure 4.25a. Although a comparison between the various $k_{\text{obs}}^{\text{max}}$ is not feasible, the kinetic $\text{p}K_{\text{a}}$ values extrapolated from the fitting can be compared (Table 4.5). The speciation plot and the $\text{p}K_{\text{a}}$ s (from UV-titration) of **4-1** are also reported in Figure 4.25b and Table 4.5.

Table 4.5 Kinetic $\text{p}K_{\text{a}}$ values extrapolated by the fitting of the pH profile of the k_{obs} of HPNPP, BNPP and UpG cleavage compared with the $\text{p}K_{\text{a}}$ values obtained by the UV-titration

	$\text{p}K_{\text{a}}^1$	$\text{p}K_{\text{a}}^2$
HPNPP	6.2 ± 0.4	8.6 ± 0.3
BNPP	6.2 ± 0.1	7.6 ± 0.1
UpG	6.6 ± 0.2	8.4 ± 0.3
Titration	6.18	8.64

For the transesterification of HPNPP, **4-1** was most active in its neutral form, and the two deprotonations led to the formations of species that retained part of the catalyst reactivity. In contrast, both BNPP and UpG cleavage were enhanced by the single deprotonated form of **4-1** (corresponding to the complex bound to one water molecule and one hydroxide). The second deprotonation of **4-1** led to the double deprotonated form of the catalyst, which was not active for the BNPP hydrolysis and UpG transesterification. While good agreement was found between the kinetic pK_a values of the RNA model molecules, the second pK_a for the hydrolysis of BNPP is lower. This shift might be due to the different mechanism between the reaction, which in the case of BNPP involved the participation of an intermolecular hydroxide.

As previously reported, the dependence of the rate constant on the catalyst concentration is peculiar but common among the reactions tested. As shown in Figure 4.26 a and b, for the cleavage of all the substrates, the initial increase of the catalyst concentration determines a rapid enhancement of the k_{obs} . However, while the rate levels off for the BNPP and UpG cleavage over 1 mM, the transesterification of HPNPP catalysed by **4-1** reaches a maximum at 0.6 mM. Over 0.6 mM, the k_{obs} decrease as the catalyst concentration increases.

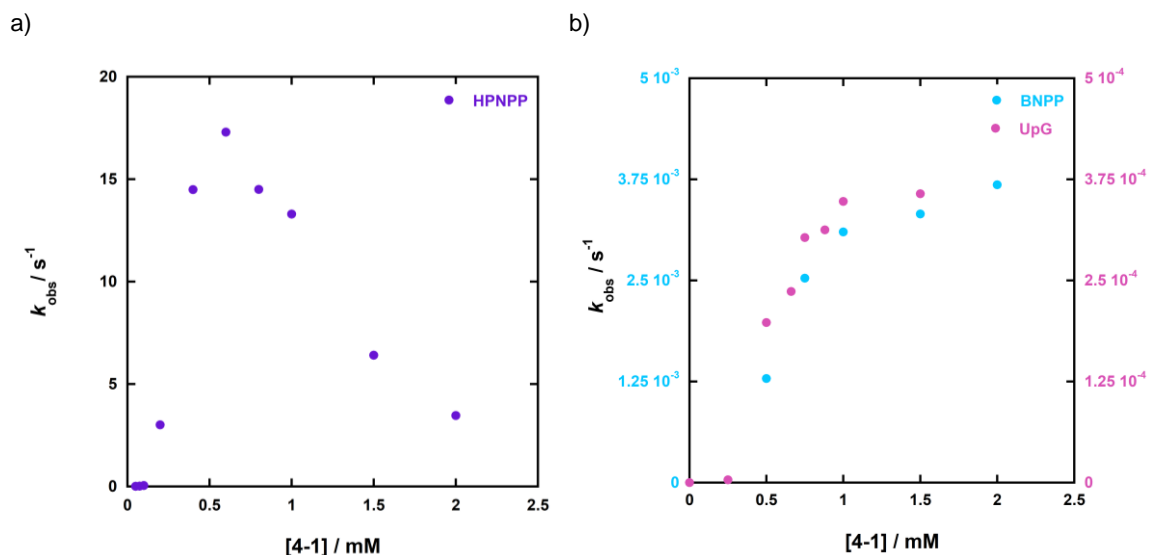


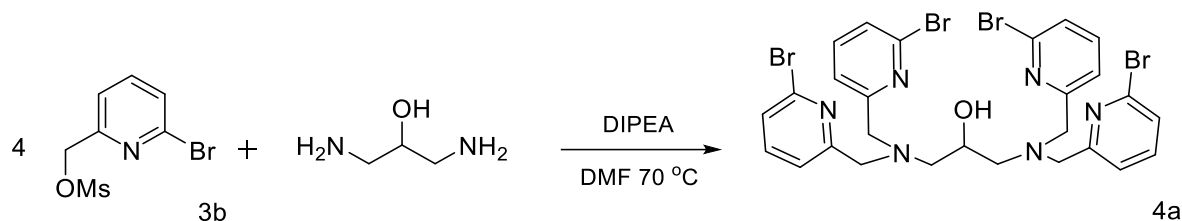
Figure 4.26 Dependence of k_{obs} on $[4-1]$ for the transesterification of HPNPP (a - ●) and UpG (b - ●), and the hydrolysis of BNPP at pH 7.4 and 25 °C (b - ●); a: $[HPNPP] = 0.05$ mM, $[HEPES] = 10$ mM, 40 % (v/v) acetonitrile in water; b) $[substrate] = 0.05$ mM, $[HEPES] = 50$ mM, ionic strength at 0.1 M by addition of $NaNO_3$, 40 % (v/v) acetonitrile in water

In the presence of **4-1** (1 mM) the half-life time of HPNPP, BNPP and UpG is 0.05, 216 (4 min) and 1991 (33 min) seconds. Although we could not fully confirm our hypothesis of a macro adduct forming by spectroscopy analysis, the full quenching of the pyrene fluorescent band at **4-1** concentration higher than 0.1 mM might suggest a change in solution.

4.4 Experimental

4.4.1 Synthesis

4a 1,3-bis(bis((6-bromopyridin-2-yl)methyl)amino)propan-2-ol



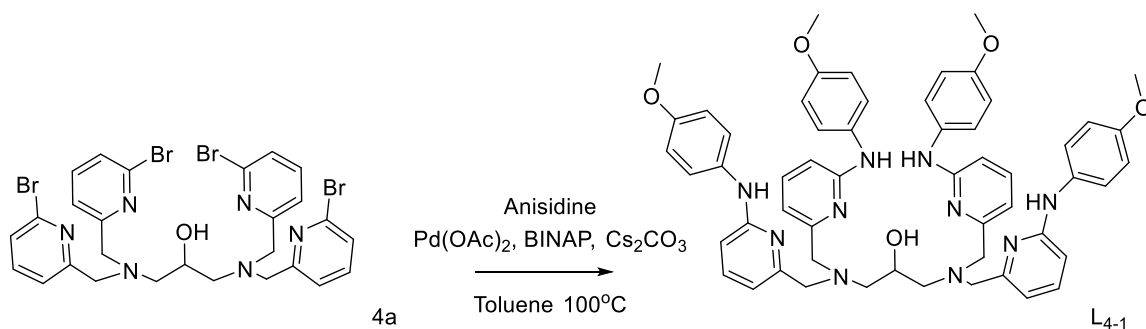
To a solution of **3b** (2.95 g, 11 mmol), synthesised following the strategy described in Chapter 2, in DMF (mL), 1,3-diamino-2-propanol (207 mg, 2.3 mmol) was added. The reaction was started by adding DIPEA (2.4 mL, 14 mmol) and was left stirring at 70 °C. After 18 h, the solution was concentrated under vacuum, diluted with 100 mL of brine and the product was mainly extracted from the aqueous phase by DCM (50 mL x 3). The latter were combined, dried under MgSO₄ and concentrated by rotary evaporation. Finally, the crude mixture was purified by flash chromatography (EtOAc/Hexane 2:3), and 1 g of product was obtained pure with a 57% yield.

¹H NMR (400 MHz, CDCl₃): δ 7.46 (t, *J* = 7.7 Hz, 4H - CH py), 7.35 (d, *J* = 7.5 Hz, 4H - CH py), 7.29 (d, *J* = 7.8 Hz, 4H - CH py), 4.59 – 4.42 (m, 1H - OH), 3.96 – 3.74 (m, 1H - CH-OH, 8H - NCH₂), 2.68 (dd, *J* = 13.3, 3.7 Hz, 2H - CH₂), 2.58 (dd, *J* = 13.3, 8.1 Hz, 2H - CH₂).

¹³C NMR (101 MHz, CDCl₃): δ 161.07 (C py), 141.41 (C py), 138.92 (CH py), 126.42 (CH py), 121.88 (CH py), 67.11 (CH), 60.24 (CH₂), 58.87 (CH₂).

HRMS (ES-TOF): $[M+H]^+$ Calc. m/z : 766.8980 - Obs. m/z : 766.8970;

L4-1 1,3-bis(bis((6-((4-methoxyphenyl)amino)pyridin-2-yl)methyl)amino)propan-2-ol



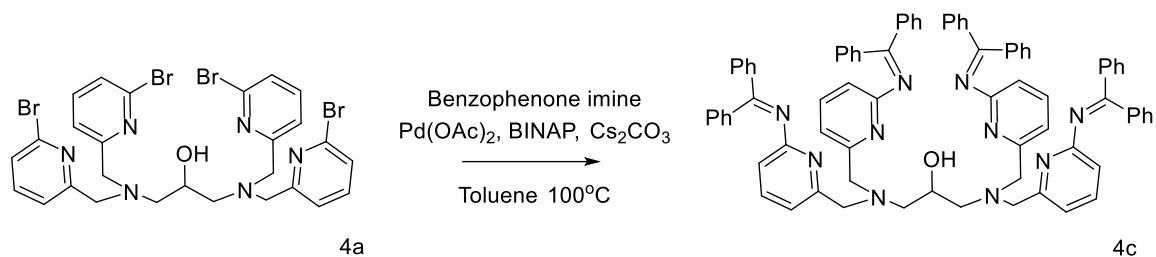
A 100 mL round bottom flask charged with **4a** (650 mg, 0.84 mmol), $\text{Pd}(\text{OAc})_2$ (23 mg, 0.10 mmol), \pm BINAP (95 mg, 0.152 mmol) and Cs_2CO_3 (2.2 g, 6.7 mmol), was filled with argon. An argon-saturated solution of p-anisidine (1.25 g, 10.1 mmol) in toluene (60 mL) was added to the powders mixture, and the solution was left stirring for 24 h at 100°C . The mixture was cooled to room temperature and filtered off over Celite[®]. The filtrate was concentrated under reduced pressure, and the product was obtained pure (424 mg, 0.45 mmol; 53%) after silica gel chromatography (DCM-DCM/EtOAc (2:3)).

^1H NMR (400 MHz, CDCl_3): δ 7.34 (t, $J = 7.8$ Hz, 4H - CH py), 7.17 (d, $J = 8.8$ Hz, 8H - CH ar), 6.85 (d, $J = 8.8$ Hz, 8H - CH ar), 6.77 (d, $J = 7.3$ Hz, 4H - CH py), 6.53 (d, $J = 8.2$ Hz, 4H - CH py), 4.08 – 3.90 (m, 1H - CH), 3.87 – 3.66 (m, 8H - NCH_2 , 12H - OCH_3), 2.88 – 2.76 (m, 2H - CH_2), 2.67 (dd, $J = 13.2, 7.7$ Hz, 2H - CH_2). OH and NH signals not observed.

^{13}C NMR (101 MHz, CDCl_3): δ 156.71 (C), 156.11 (C), 138.03 (CH py), 123.91 (CH ar), 114.55 (CH ar), 113.49 (CH py), 105.05 (CH py), 60.66 (CH_2), 59.06 (CH_2), 55.52 (OCH_3).

HRMS (ES-TOF): $[M+H]^+$ Calc. m/z : 939.4670- Obs. m/z : 939.4658;

4b 1,3-bis(bis((6-((diphenylmethylene)amino)pyridin-2-yl)methyl)amino)propan-2-ol ¹³³



4a (500 mg, 0.95 mmol), $\text{Pd}(\text{OAc})_2$ (19 mg, 0.09 mmol), $\pm\text{BINAP}$ (78 mg, 0.13 mmol) and Cs_2CO_3 (1.85 g, 5.7 mmol) were introduced into a roundbottom flask, which was then filled with argon. To the mixture, an Ar-sparged solution of benzophenone imine (1.08 mL, 8.55 mmol) in 40 mL of toluene was added. The reaction mixture was left stirring under Argon atmosphere for 20 h but the LCMS showed the presence of partially reacted compounds. $\text{Pd}(\text{OAc})_2$ (6 mg, 0.03 mmol), $\pm\text{BINAP}$ (27 mg, 0.04 mmol) and Cs_2CO_3 (620 mg, 1.90 mmol) were further added and the reaction was left stirring for 15 h. The crude mixture was cooled down at room temperature and filtered off over Celite[®]. The filtrate was kept and the solvent was evaporated under vacuum. The crude product was purified by silica gel chromatography (DCM/EtOAc (1:1)-EtOAc), and obtained pure as a yellow solid (199 mg, 0.19 mmol; 20%).

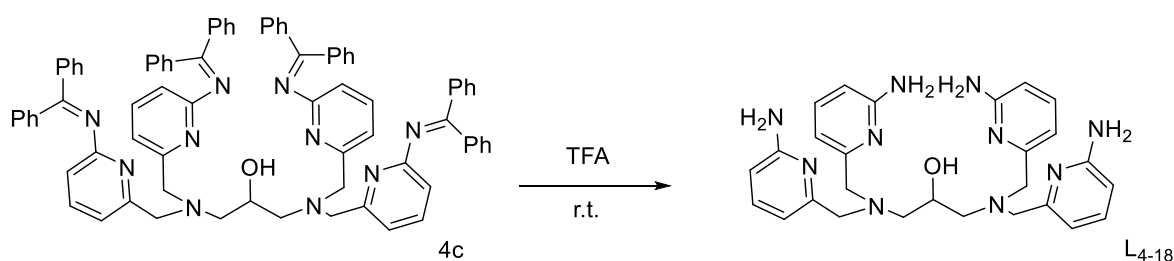
¹H NMR (400 MHz, CDCl_3): δ 7.78 (d, $J = 7.4$ Hz, 8H - CH ar), 7.47 (t, $J = 7.3$ Hz, 4H - CH py), 7.38 (t, $J = 7.5$ Hz, 8H - CH ar), 7.32 (t, $J = 7.7$ Hz, 4H - CH ar), 7.14 (m, $J = 7.6$

Hz, 20H - CH ar), 6.87 (d, J = 7.4 Hz, 4H - CH py), 6.39 (d, J = 7.8 Hz, 4H - CH py), 3.81 (s, 1H - OCH), 3.57 (dd, J = 30.9, 14.4 Hz, 8H - CH₂), 2.37 (m, J = 5.5 Hz, 4H - CH₂ chain). OH signal not observed.

¹³C NMR (101 MHz, CDCl₃): δ 170.28 (CN), 162.92 (C ar), 158.74 (C ar), 138.99 (C py), 137.69 (CH ar), 136.35 (C py), 131.26 (CH py), 129.88 (CH ar), 129.36 (CH ar), 128.91 (CH ar), 128.20 (CH ar), 127.94 (CH ar), 118.07 (CH py), 113.51 (CH py), 67.03 (CH), 60.40 (CH₂), 58.62 (CH₂).

MS (ES-TOF): [M+H]⁺ Obs. m/z: 1171.6
[M+Na]⁺ Obs. m/z: 1193.5

L4-18 1,3-bis(bis((6-aminopyridin-2-yl)methyl)amino)propan-2-ol



4b (50 mg, 0.04 mmol) was dissolved in 3 mL of TFA and left reacting for 3 h at room temperature. The excess of TFA was removed by blowing nitrogen, and the remaining oil was dissolved in water (10 mL). The aqueous phase, which was first washed with Et₂O (3 x 5 mL), was basified by adding concentrated NaOH. The product is then extracted from the water layer by DCM (3 x 10 mL). Finally, the combined organic layers were treated with MgSO₄ and filtered off a sintered funnel. The filtrate was dried under high vacuum. The desired compound was obtained as a pale yellow oil in 97% yield (21 mg, 0.04 mmol).

¹H NMR (400 MHz, MeOD): δ 7.37 (t, J = 7.8 Hz, 4H - CH py), 6.68 (d, J = 7.2 Hz, 4H - CH py), 6.40 (d, J = 8.1 Hz 4H - CH py), 3.92 (m, 1H - CH), 3.57 (s, 8H - NCH₂), 3.48 (d, J = 7.0 Hz, 15H), 2.62 (dd, J = 13.2, 4.3 Hz, 2H - CH₂), 2.47 (dd, J = 13.1, 7.5 Hz, 2H - CH₂). OH and NH₂ signals not observed.

¹³C NMR (101 MHz, MeOD): δ 160.43 (C py), 158.22 (C py), 139.62 (CH py), 113.22 (CH py), 108.42 (CH py), 68.65 (OCH), 61.67 (NCH₂), 60.21 (CH₂).

HRMS (ES-TOF): [M+H]⁺ Calc. m/z : 515.2995 - Obs. m/z : 515.3008;

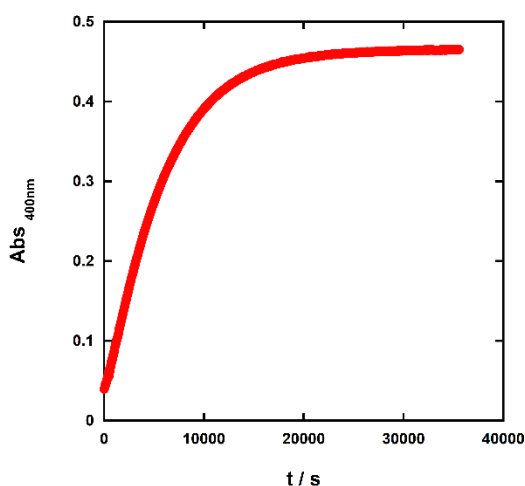
4.4.2 UV-kinetic experiment

The kinetic experiments were carried out in a mixture in 40% (v/v) acetonitrile in water at 25 °C. The aqueous phase was prepared in one batch and used for all the stock solutions. The buffers used were MES (5.5 < pH < 6.7) HEPES (6.9 < pH < 8.2), EPPS (7.4 < pH < 8.6), CHES (8.7 < pH < 9.9) and CAPS (9.8 < pH < 11.0). All the solutions were prepared with analytical grade buffers keeping the ratio of water/ acetonitrile constant and fixing the ionic strength at 0.1 M. The reaction was performed in quartz cuvettes using Cary 300 UV-Vis-NIR spectrophotometers or in a quartz plate using POLARstar OMEGA plate reader. At pH 7 or above, the reaction progress was monitored at 400 nm, following the appearance of p-nitrophenolate; in the pH range 5-7, the evaluation was done detecting the formation of p-nitrophenol at 318 nm by the scanning kinetic method or HPLC analysis. A typical experiment was started by introducing 20 μ L of 5 mM HPNPP solution to the reaction mixture. The latter was prepared by mixing the zinc complex (0.05 – 2 mM - created *in situ* by adding specific aliquots of 5-50 mM Zn(NO₃)₂ and ligand stock solutions) with 1 mL of 0.1 M Buffer and the appropriate volume of 0.1 M NaNO₃ to reach 2 mL. The ligand

solution was prepared with DMSO and the $\text{Zn}(\text{NO}_3)_2$ with 0.1 M NaNO_3 in 40% (v/v) acetonitrile in water.

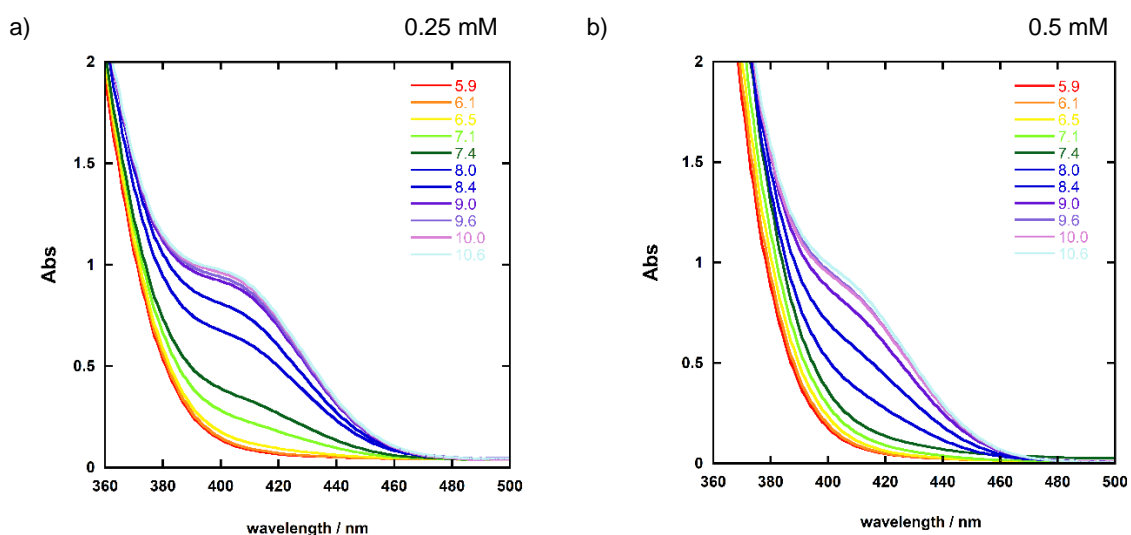
A similar method was used for the inhibition experiments. The complex concentration was fixed at 0.05 mM, the buffer at 0.05 M and the substrate at 0.05 mM. A volume of 10 mM phenyl phosphate (PP - prepared using as solvent 0.1 M NaNO_3 in 40% (v/v) acetonitrile in water) was introduced into the reaction solution as an additional element in the over mentioned procedure. In the case of dimethyl phosphate (DMP), the concentration of the inhibitor was taken into account to keep constant the ionic strength. The stock solutions (buffer, $\text{Zn}(\text{NO}_3)_2$ and DMP) were prepared in 40% (v/v) acetonitrile in water and the ionic strength was controlled with an additional solution of NaNO_3 in water/ acetonitrile (1 M). The buffer and the DMP were prepared at 0.2 M. All the components were added adequately into the cuvette, and the final volume was reached by adding water/ acetonitrile mixture. The Buffer inhibition experiments were carried out working with 0.2 M Buffer stock solution, adjusting the ionic strength with 1 M NaNO_3 .

Working with a higher concentration of **4-1** (>0.5 mM), minor absorbance variations at 400 nm were recorded during the reaction monitoring. This peculiar aspect has been observed for both HNPnPP and BNPP. For example, as shown in Graph 4.15 for the hydrolysis of BNPP catalysed by 1 mM of the dinuclear complex at pH 9.0 and 25 °C, the final absorbance value reaches a maximum of 0.465. Given the 4-nitrophenol's pK_a of 7.8 in 40% (v/v) acetonitrile in water, at pH 9, assuming the reaction completion, 0.05 mM of the product deprotonated form would produce an absorbance approximately of 1.



Graph 4.15 Plot of the recorded absorbance at 400nm overtime for the hydrolysis of BNPP catalysed by **4-1** at pH 9 and 25 °C; [**4-1**] = 1 mM, [BNPP] = 0.05 mM, [CHES] = 50 mM, ionic strength 0.1 M in 40%(v/v) acetonitrile in water

An investigation was carried out to check whether the smaller variation resulted from a partial product formation or a change in the chemical-physical property of the 4-nitrophenol. Using the POLARstar OMEGA plate reader, different solutions were prepared and analysed from pH 5.9 to 10.6 at a 4-nitrophenol concentration of 0.05 mM in the presence of **4-1** (0.25, 0.5, 0.75 and 1 mM – Figure 4.27).



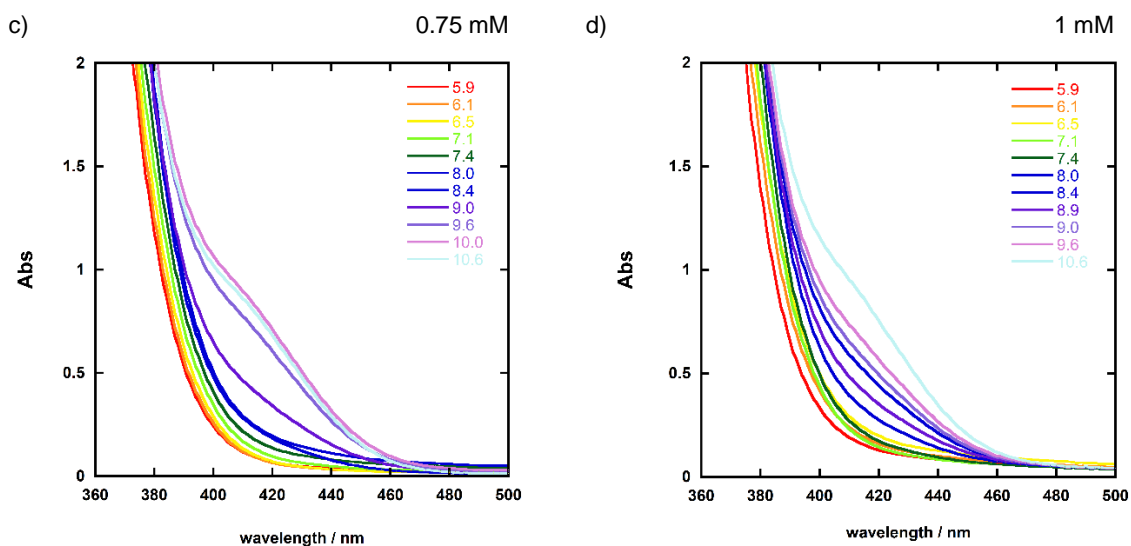


Figure 4.27 4-nitrophenol titration at different **4-I** concentrations; conditionios: [4-nitrophenol] = 0.05 mM, [Buffer] = 50 mM, ionic strength 0.1 M in 40% (v/v) acetonitrile in water. a) [**4-I**] = 0.25 mM; b) [**4-I**] = 0.5 mM; c) [**4-I**] = 0.75 mM; d) [**4-I**] = 1 mM

The pK_a values obtained from the plots in Figure 4.28, considering the absorbance at 400nm, are reported in Table 4.6. When the complex concentration is lower than 0.5 mM, no substantial deviation from the pK_a measured in the complex absence is observed. However, the solution prepared with a complex concentration of 0.75 and 1 mM present an alteration which might suggest a shift of the deprotonation equilibrium to higher pH.

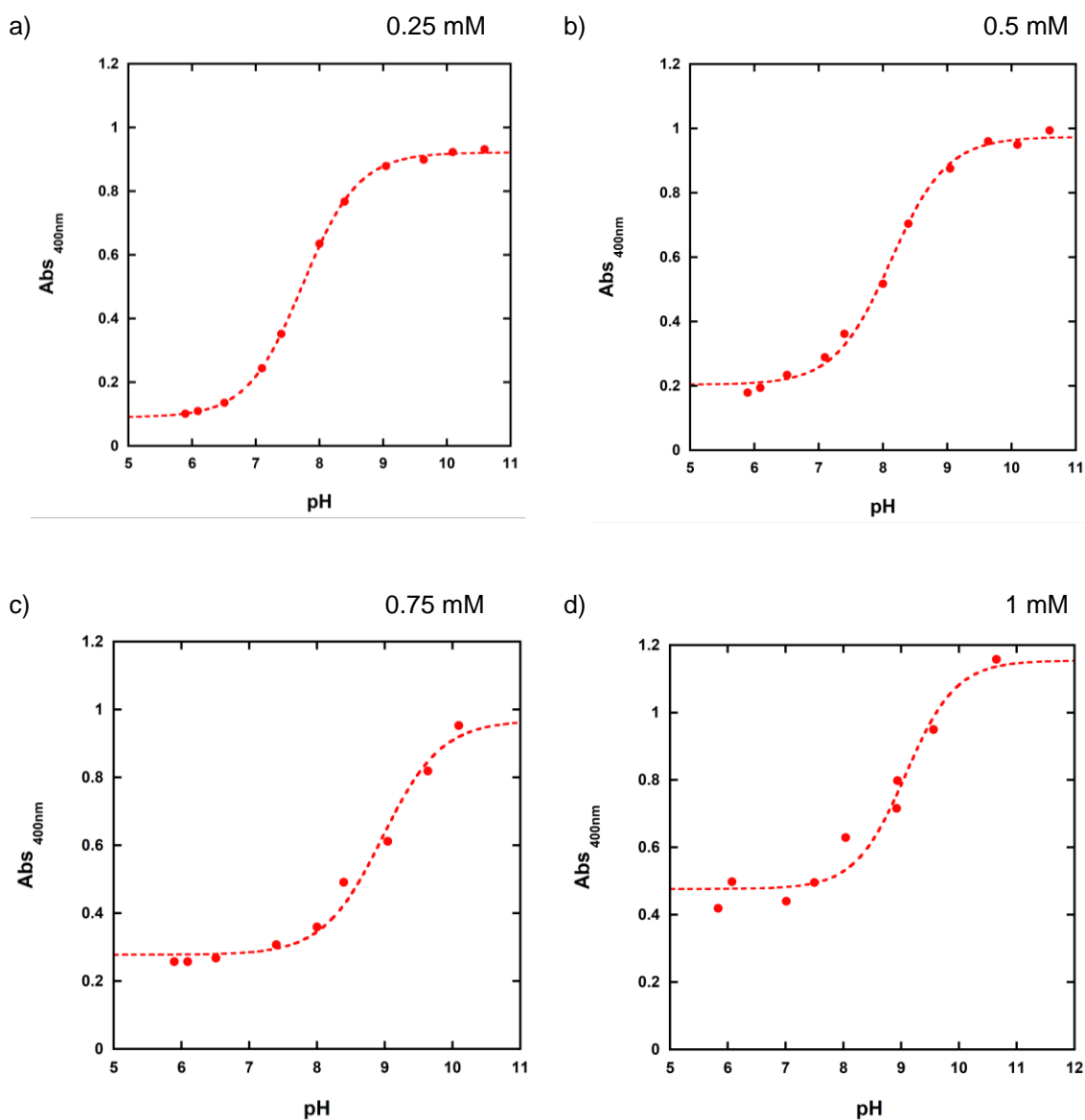


Figure 4.28 Absorbance at 400 nm against the pH at different **4-I** concentrations; conditionios: [4-nitrophenol] = 0.05 mM, [Buffer] = 50 mM, ionic strength 0.1 M in 40% (v/v) acetonitrile in water. a) [**4-I**] = 0.25 mM; b) [**4-I**] = 0.5 mM; c) [**4-I**] = 0.75 mM; d) [**4-I**] = 1 mM

Table 4.6 Measured pK_a values at different **4-I** concentrations

	[4-I] / mM				
	-	0.25	0.5	0.75	1
pK_a	7.80 ± 0.01	7.73 ± 0.01	8.12 ± 0.05	$8.9 \pm 0.1^*$	$9.1 \pm 0.1^*$

*the values obtained at [4-I] of 0.75 and 1 mM are an estimate of the real values as the endpoint of the sigmoidal is not fully reached

The values reported in Table 4.6 are reliable for the solution at 0.25 and 0.5 mM, but not well defined sigmoidal curves can be drawn through the data at 0.75 and 1 mM, as the ending point does not seem to be reached at pH 10.6. Although only speculative conclusions can be drawn, the high concentration of complex might be responsible for an alteration of the molar extinction coefficient of the 4-nitrophenol and also might unexpectedly influence its pK_a . However, this experiment confirms the legitimacy of our method and excludes a partial substrate conversion.

4.4.3 HPLC – kinetic experiment

A generic experiment was initiated by adding a volume of a stock solution of substrate to the reaction solution composed of **4-1** (formed *in situ*), buffer (50 mM), in 40% (v/v) acetonitrile in water.

Kinetic experiments were run by HPLC using the following method:

- Turnover experiment with BNPP and HPNPP:

Gradient: 5-95% ACN in 10 min, injected volume: 10 μ L; Absorbance registered at 350 nm. Column: Synergi 4 μ m Polar-RP[®] 80 A, LC Column 150 x 4.6 mm, Phenomenex.

- Pseudo first-order conditions (complex excess) at $\text{pH} \leq 7$ with HPNPP:

Gradient: 5-95 % ACN in 10 min, injected volume: 20 μ L; Absorbance registered at 318 nm. Column: Kinetex[®] 5 μ m C18 100 Å, LC Column,

- Monitoring of UpG transesterification catalysed by **4-1**:

Gradient: 5-30% ACN in 10 min, injected volume: 10 μ L; Absorbance registered at 260 nm. Column: Synergi 4 μ m Polar-RP 80 A, LC Column 150 x 4.6 mm, Phenomenex.

4.4.4 Data

HPNPP transesterification:

- Zn(II) binding**

[4-1] = 0.05 mM, [EPPS] = 50 mM pH 7, [HPNPP]=0.05 mM, ionic strength at 0.1 M by addition of NaNO₃, 25 °C and 40% (v/v) acetonitrile in water;

Zn(NO ₃) ₂		k_{obs} / s^{-1}
mM	eq	
0.01	0.2	$1.04 \pm 0.02 \times 10^{-3}$
0.025	0.5	$9.60 \pm 0.08 \times 10^{-3}$
0.05	1.0	$6.98 \pm 1.43 \times 10^{-3}$
0.075	1.5	$1.61 \pm 0.15 \times 10^{-2}$
0.1	2.0	$1.49 \pm 0.08 \times 10^{-2}$
0.25	5.0	$1.78 \pm 0.02 \times 10^{-2}$
0.5	10.0	$1.93 \pm 0.01 \times 10^{-2}$
0.75	15.0	$1.84 \pm 0.02 \times 10^{-2}$

- k_{obs} vs [HPNPP]

[4-1] = 0.05 mM, [EPPS] = 50 mM, ionic strength at 0.1 M by addition of NaNO₃, 25

°C and 40% (v/v) acetonitrile in water;

[HPNPP] / mM	$k_{\text{obs}} / \text{s}^{-1}$	
	pH 8.0	pH 9.0
0.01	$5.97 \pm 0.04 \times 10^{-3}$	$3.90 \pm 0.14 \times 10^{-3}$
0.02	$5.87 \pm 0.03 \times 10^{-3}$	$3.55 \pm 0.03 \times 10^{-3}$
0.04	$5.65 \pm 0.04 \times 10^{-3}$	$3.70 \pm 0.03 \times 10^{-3}$
0.06	$5.32 \pm 0.01 \times 10^{-3}$	$4.15 \pm 0.05 \times 10^{-3}$
0.08	$5.53 \pm 0.03 \times 10^{-3}$	$3.55 \pm 0.03 \times 10^{-3}$
0.1	$4.95 \pm 0.02 \times 10^{-3}$	$3.50 \pm 0.03 \times 10^{-3}$

- pH profile

[4-1] = 0.05 mM, [HPNPP]=0.05 mM, ionic strength at 0.1 M by addition of NaNO₃, 25

°C and 40% (v/v) acetonitrile in water;

[Buffer] /mM	$k_{\text{obs}} / \text{s}^{-1}$					
	pH 5.5	pH 6.4	pH 6.7	pH 7.1	pH 7.3	pH 7.9
5	$2.35 \pm 0.27 \times 10^{-2}$	$1.97 \pm 0.22 \times 10^{-2}$	$2.57 \pm 0.33 \times 10^{-2}$	$1.34 \pm 0.06 \times 10^{-2}$	$1.18 \pm 0.02 \times 10^{-2}$	$6.50 \pm 0.13 \times 10^{-3}$
10	$3.33 \pm 0.36 \times 10^{-2}$	$3.38 \pm 0.39 \times 10^{-2}$	$2.29 \pm 0.24 \times 10^{-2}$	$1.48 \pm 0.06 \times 10^{-2}$	$0.99 \pm 0.02 \times 10^{-2}$	$5.84 \pm 0.13 \times 10^{-3}$
25	$3.43 \pm 0.11 \times 10^{-2}$	$0.86 \pm 0.16 \times 10^{-2}$	$2.08 \pm 0.29 \times 10^{-2}$	$1.29 \pm 0.04 \times 10^{-2}$	$0.87 \pm 0.02 \times 10^{-2}$	$4.40 \pm 0.15 \times 10^{-3}$
50	$2.79 \pm 0.07 \times 10^{-2}$	$2.98 \pm 0.38 \times 10^{-2}$	$1.86 \pm 0.18 \times 10^{-2}$	$1.49 \pm 0.06 \times 10^{-2}$	$0.79 \pm 0.02 \times 10^{-2}$	$2.87 \pm 0.03 \times 10^{-3}$
75	$2.86 \pm 0.12 \times 10^{-2}$	$2.24 \pm 0.20 \times 10^{-2}$	$2.29 \pm 0.14 \times 10^{-2}$	$1.39 \pm 0.05 \times 10^{-2}$	$0.77 \pm 0.02 \times 10^{-2}$	$2.00 \pm 0.05 \times 10^{-3}$
100	$2.90 \pm 0.25 \times 10^{-2}$	$3.86 \pm 0.38 \times 10^{-2}$	$1.55 \pm 0.13 \times 10^{-2}$	$1.19 \pm 0.04 \times 10^{-2}$	$0.68 \pm 0.01 \times 10^{-2}$	$1.80 \pm 0.03 \times 10^{-3}$

[Buffer] /mM	$k_{\text{obs}} / \text{s}^{-1}$				
	pH 8.4	pH 8.8	pH 9.4	pH 9.9	pH 10.4
5	$6.11 \pm 0.09 \times 10^{-3}$	$4.93 \pm 0.05 \times 10^{-3}$	$1.66 \pm 0.01 \times 10^{-3}$	$1.53 \pm 0.01 \times 10^{-3}$	$1.57 \pm 0.01 \times 10^{-3}$
10	$4.86 \pm 0.06 \times 10^{-3}$	$4.19 \pm 0.04 \times 10^{-3}$	$1.43 \pm 0.01 \times 10^{-3}$	$1.37 \pm 0.01 \times 10^{-3}$	$1.38 \pm 0.01 \times 10^{-3}$
25	$3.53 \pm 0.04 \times 10^{-3}$	$2.43 \pm 0.02 \times 10^{-3}$	$1.19 \pm 0.01 \times 10^{-3}$	$1.19 \pm 0.01 \times 10^{-3}$	$1.15 \pm 0.01 \times 10^{-3}$
50	$2.45 \pm 0.02 \times 10^{-3}$	$1.82 \pm 0.01 \times 10^{-3}$	$1.01 \pm 0.01 \times 10^{-3}$	$1.02 \pm 0.01 \times 10^{-3}$	$9.64 \pm 0.05 \times 10^{-4}$
75	$1.97 \pm 0.01 \times 10^{-3}$	$1.48 \pm 0.01 \times 10^{-3}$	$9.07 \pm 0.07 \times 10^{-4}$	$9.20 \pm 0.06 \times 10^{-4}$	$8.64 \pm 0.05 \times 10^{-4}$
100	$1.75 \pm 0.01 \times 10^{-3}$	$1.33 \pm 0.01 \times 10^{-3}$	$8.33 \pm 0.04 \times 10^{-4}$	$8.53 \pm 0.05 \times 10^{-4}$	$7.88 \pm 0.05 \times 10^{-4}$

- **Morpholine and bis tris-propane inhibition**

[4-1] = 0.05 mM, [HPNPP]=0.05 mM, ionic strength at 0.1 M by addition of NaNO₃, 25 °C and 40% (v/v) acetonitrile in water;

[Buffer] / mM	k_{obs} / s^{-1}	
	pH 8.4 morpholine	pH 9.2 bis tris-propane
5	1.114 ± 0.003 × 10 ⁻²	7.79 ± 0.02 × 10 ⁻³
10	7.814 ± 0.012 × 10 ⁻³	6.49 ± 0.03 × 10 ⁻³
25	4.739 ± 0.008 × 10 ⁻³	6.01 ± 0.02 × 10 ⁻³
50	3.008 ± 0.004 × 10 ⁻³	4.65 ± 0.01 × 10 ⁻³
75	2.481 ± 0.004 × 10 ⁻³	4.33 ± 0.01 × 10 ⁻³
100	2.050 ± 0.001 × 10 ⁻³	3.92 ± 0.01 × 10 ⁻³

- **CHES inhibition**

[HPNPP]=0.05 mM, ionic strength at 0.1 M by addition of NaNO₃, 25 °C and 40% (v/v) acetonitrile in water;

[CHES] / mM	k_{obs} / s^{-1}	
	[4-1] = 0.1 mM	[Zn(NO ₃) ₂] = 0.5 mM [L ₄₋₁] = 0.05 mM
5	1.62 ± 0.11 × 10 ⁻²	6.44 ± 0.16 × 10 ⁻³
10	1.52 ± 0.06 × 10 ⁻²	4.91 ± 0.11 × 10 ⁻³
25	5.83 ± 0.16 × 10 ⁻³	3.04 ± 0.03 × 10 ⁻³
50	3.65 ± 0.03 × 10 ⁻³	1.95 ± 0.01 × 10 ⁻³
75	2.56 ± 0.02 × 10 ⁻³	1.39 ± 0.01 × 10 ⁻³
100	2.03 ± 0.01 × 10 ⁻³	1.07 ± 0.01 × 10 ⁻³

- **DMP inhibition**

[4-1] = 0.05 mM, [Buffer] = 50 mM, [HPNPP]=0.05 mM, ionic strength at 0.1 M by addition of NaNO₃, 25 °C and 40% (v/v) acetonitrile in water;

[DMP] / mM	pH 7.1		pH 7.5		pH 7.9		pH 8.9	
	k_{obs} / s^{-1}	k/k_0	k_{obs} / s^{-1}	k/k_0	k_{obs} / s^{-1}	k/k_0	k_{obs} / s^{-1}	k/k_0
10	$1.27 \pm 0.29 \times 10^{-2}$	1.000	$3.81 \pm 0.17 \times 10^{-3}$	1.000	$3.644 \pm 0.03 \times 10^{-3}$	1.000	$3.01 \pm 0.04 \times 10^{-3}$	1.000
20	$4.62 \pm 0.27 \times 10^{-3}$	0.365	$2.43 \pm 0.06 \times 10^{-3}$	0.580	$3.397 \pm 0.02 \times 10^{-3}$	0.932	$2.71 \pm 0.02 \times 10^{-3}$	0.903
40	$2.89 \pm 0.05 \times 10^{-3}$	0.228	$1.73 \pm 0.02 \times 10^{-3}$	0.422	$3.194 \pm 0.04 \times 10^{-3}$	0.877	$2.65 \pm 0.02 \times 10^{-3}$	0.882
60	$2.13 \pm 0.05 \times 10^{-3}$	0.168	$1.11 \pm 0.14 \times 10^{-3}$	0.295	$3.077 \pm 0.04 \times 10^{-3}$	0.845	$2.50 \pm 0.03 \times 10^{-3}$	0.833
80	$1.94 \pm 0.02 \times 10^{-3}$	0.153	$0.90 \pm 0.10 \times 10^{-4}$	0.231	$2.842 \pm 0.03 \times 10^{-3}$	0.780	$2.42 \pm 0.02 \times 10^{-3}$	0.804
100	$1.62 \pm 0.02 \times 10^{-3}$	0.128	$0.90 \pm 0.32 \times 10^{-4}$	0.214	$2.613 \pm 0.02 \times 10^{-3}$	0.717	$2.35 \pm 0.04 \times 10^{-3}$	0.781

- k_{obs} vs [4-1]

[HEPES] = 10 mM pH 7.4, [HPNPP] = 0.05 mM 25 °C and 40% (v/v) acetonitrile in water;

[4-1] /mM	k_{obs} / s^{-1}
0.05	$9.51 \pm 1.23 \times 10^{-3}$
0.075	$2.02 \pm 0.11 \times 10^{-2}$
0.1	$4.82 \pm 0.29 \times 10^{-2}$
0.2	3.01 ± 0.08
0.4	$1.45 \pm 0.09 \times 10$
0.6	$1.73 \pm 0.06 \times 10$
0.8	$1.45 \pm 0.08 \times 10$
1	$1.33 \pm 0.09 \times 10$
1.5	6.41 ± 0.37
2	3.46 ± 0.16

- PP inhibition

[4-1] = 0.05 mM, [Buffer] = 50 mM, [HPNPP]=0.05 mM, ionic strength at 0.1 M by addition of NaNO₃, 25 °C and 40% (v/v) acetonitrile in water;

[PP] / mM	pH 7.01		pH 8.10		pH 9.10	
	k_{obs} / s^{-1}	k/k_0	k_{obs} / s^{-1}	k/k_0	k_{obs} / s^{-1}	k/k_0
0	$8.98 \pm 0.12 \times 10^{-3}$	1.0000	$2.62 \pm 0.05 \times 10^{-3}$	1.000	$9.98 \pm 0.17 \times 10^{-4}$	1.000
0.01	$6.37 \pm 0.41 \times 10^{-3}$	0.7095	$1.54 \pm 0.02 \times 10^{-3}$	0.586	$6.73 \pm 0.16 \times 10^{-4}$	0.674
0.02	$3.56 \pm 0.10 \times 10^{-3}$	0.3968	$8.02 \pm 0.14 \times 10^{-4}$	0.306	$5.14 \pm 0.18 \times 10^{-4}$	0.515
0.03	$1.63 \pm 0.03 \times 10^{-3}$	0.1811	$4.22 \pm 0.08 \times 10^{-4}$	0.161	$1.96 \pm 0.14 \times 10^{-4}$	0.196
0.04	$5.35 \pm 0.13 \times 10^{-4}$	0.0596	$1.28 \pm 0.01 \times 10^{-4}$	0.049	$9.24 \pm 0.07 \times 10^{-5}$	0.093
0.05	$1.99 \pm 0.07 \times 10^{-5}$	0.0022	$1.78 \pm 0.20 \times 10^{-5}$	0.007	$7.35 \pm 0.15 \times 10^{-5}$	0.074
0.06	$1.70 \pm 0.09 \times 10^{-5}$	0.0019	$9.11 \pm 0.05 \times 10^{-6}$	0.003	$3.45 \pm 0.04 \times 10^{-5}$	0.035
0.07	$1.20 \pm 0.08 \times 10^{-5}$	0.0013	$6.79 \pm 0.21 \times 10^{-6}$	0.003	$3.05 \pm 0.02 \times 10^{-5}$	0.031
0.08	$1.19 \pm 0.08 \times 10^{-5}$	0.0013	$4.84 \pm 0.03 \times 10^{-6}$	0.002	$2.22 \pm 0.04 \times 10^{-5}$	0.022
0.09	$1.41 \pm 0.08 \times 10^{-5}$	0.0016	$5.49 \pm 0.28 \times 10^{-6}$	0.002	$2.07 \pm 0.02 \times 10^{-5}$	0.021
0.1	$3.08 \pm 0.16 \times 10^{-6}$	0.0003	$3.88 \pm 0.02 \times 10^{-6}$	0.001	$1.63 \pm 0.04 \times 10^{-5}$	0.016

BNPP hydrolysis:

- k_{obs} vs [4-1]

[4-1] = 0.05 mM, [Buffer] = 50 mM, [BNPP]=0.05 mM, ionic strength at 0.1 M by addition of NaNO₃, 25 °C and 40% (v/v) acetonitrile in water;

[4-1] / mM	k_{obs} / s^{-1}	
	pH 7.1	pH 9.0
0.5	$1.29 \pm 0.01 \times 10^{-3}$	$4.54 \pm 0.05 \times 10^{-5}$
0.75	$2.53 \pm 0.01 \times 10^{-3}$	$1.22 \pm 0.01 \times 10^{-4}$
1	$3.10 \pm 0.05 \times 10^{-3}$	$1.74 \pm 0.02 \times 10^{-4}$
1.5	$3.32 \pm 0.05 \times 10^{-3}$	$3.60 \pm 0.01 \times 10^{-4}$
2	$3.68 \pm 0.06 \times 10^{-3}$	$3.97 \pm 0.01 \times 10^{-4}$
2.5	$3.86 \pm 0.03 \times 10^{-3}$	-

- **pH profile**

[4-1] = 0.05 mM, [BNPP]=0.05 mM, ionic strength at 0.1 M by addition of NaNO₃, 25 °C and 40% (v/v) acetonitrile in water;

[Buffer] /mM	HEPES - pH 7		EPPS - pH 7.4 / 8 / 8.4					
	k_{obs} / s^{-1}	pH	k_{obs} / s^{-1}	pH	k_{obs} / s^{-1}	pH	k_{obs} / s^{-1}	pH
5	$7.46 \pm 0.03 \times 10^{-4}$	6.22	$8.37 \pm 0.04 \times 10^{-4}$	6.36	$1.05 \pm 0.03 \times 10^{-3}$	7.47	$6.01 \pm 0.01 \times 10^{-4}$	7.91
10	$1.07 \pm 0.01 \times 10^{-3}$	6.70	$1.18 \pm 0.03 \times 10^{-3}$	6.93	$7.03 \pm 0.02 \times 10^{-4}$	7.71	$3.86 \pm 0.02 \times 10^{-4}$	8.11
25	$1.11 \pm 0.03 \times 10^{-3}$	6.92	$1.12 \pm 0.02 \times 10^{-3}$	7.19	$4.98 \pm 0.01 \times 10^{-4}$	7.87	$2.64 \pm 0.02 \times 10^{-4}$	8.32
50	$1.15 \pm 0.02 \times 10^{-3}$	7.13	$1.10 \pm 0.05 \times 10^{-3}$	7.40	$3.94 \pm 0.02 \times 10^{-4}$	7.99	$1.64 \pm 0.15 \times 10^{-4}$	8.45
75	$1.17 \pm 0.05 \times 10^{-3}$	7.01	$8.04 \pm 0.00 \times 10^{-4}$	7.33	$2.24 \pm 0.15 \times 10^{-4}$	7.95	$7.46 \pm 0.17 \times 10^{-5}$	8.43

[Buffer] /mM	CHES - pH 9 / 9.5			
	k_{obs} / s^{-1}	pH	k_{obs} / s^{-1}	pH
5	$4.63 \pm 0.02 \times 10^{-4}$	8.07	$8.34 \pm 0.01 \times 10^{-5}$	9.02
10	$1.79 \pm 0.01 \times 10^{-4}$	8.56	$4.26 \pm 0.01 \times 10^{-5}$	9.26
25	$8.64 \pm 0.01 \times 10^{-5}$	8.83	$3.42 \pm 0.03 \times 10^{-5}$	9.48
50	$7.01 \pm 1.69 \times 10^{-5}$	8.95	$1.72 \pm 0.14 \times 10^{-5}$	9.60
75	$2.62 \pm 0.14 \times 10^{-5}$	8.95	$7.77 \pm 0.00 \times 10^{-6}$	9.61

UpG transesterification:

- **k_{obs} vs [4-1]:**

[HEPES] = 50 mM pH 7.4, [UpG] = 0.05 mM, ionic strength at 0.1 M by addition of NaNO₃, 25 °C and 40% (v/v) acetonitrile in water;

[4-1] /mM	k_{obs} / s^{-1}
0.25	$3.47 \pm 0.41 \times 10^{-6}$
0.5	$1.98 \pm 0.07 \times 10^{-4}$
0.66	$2.36 \pm 0.06 \times 10^{-4}$
0.75	$3.03 \pm 0.10 \times 10^{-4}$
0.88	$3.13 \pm 0.12 \times 10^{-4}$
1	$3.48 \pm 0.17 \times 10^{-4}$
1.5	$3.57 \pm 0.02 \times 10^{-4}$

- **pH profile**

[4-1] = 1 mM, [Buffer] = 50 mM, [UpG] = 0.05 mM, ionic strength at 0.1 M by addition of NaNO₃, 25 °C and 40% (v/v) acetonitrile in water;

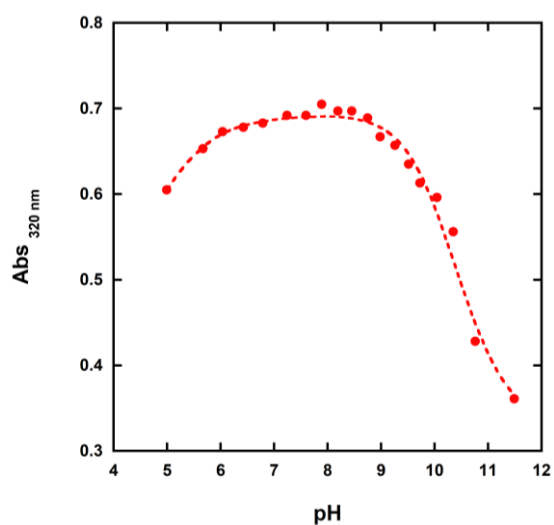
pH	k_{obs} / s^{-1}	$\log k_{obs}$
6.02	$7.63 \pm 0.28 \times 10^{-5}$	-4.117
7.04	$4.88 \pm 0.27 \times 10^{-4}$	-3.312
7.40	$3.44 \pm 0.14 \times 10^{-4}$	-3.463
8.00	$3.83 \pm 0.73 \times 10^{-4}$	-3.417
9.00	$1.20 \pm 0.23 \times 10^{-5}$	-3.921

4.4.5 UV titration

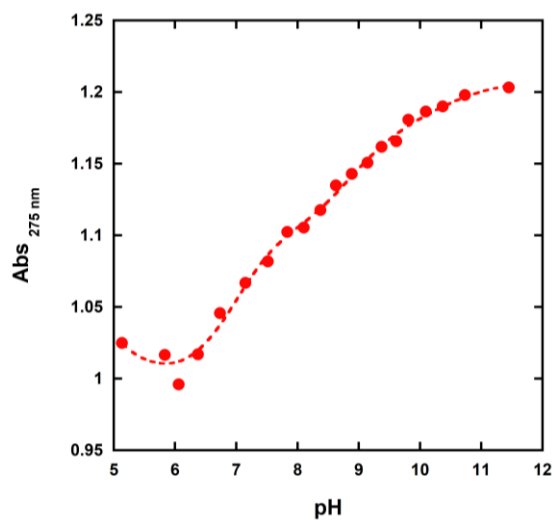
The titration experiments were carried out at 25°C and the pH was measured by Mettler-Toledo pH meter calibrated with Thermo Scientific buffer packs at pH 4.00, 7.01 and 10.06 at 25 °C. Cary 50 UV-Vis spectrophotometer was used to register the spectrum. All the UV-titrations were performed at the same experimental conditions. To keep the **L4-1** and **4-1** concentration constant during the titration, both the analyte and the titrant solutions were prepared at 0.05 mM of the ligand or complex. In addition, both the solutions were made at 40%(v/v) of ACN in water. In the analyte solution (0.5 mL), MES, EPPS, CHES and CAPS were at the same concentration (25 mM) and the pH range between 5 and 12 was investigated by consecutive addition of 10 µL of the titrant (0.25 M NaOH). Each base addition was followed by recording the UV spectrum and measuring the pH of the analyte solution. A reduced volume cuvette with 0.5 cm path length was used for all the experiments. The absorbance values of an appropriate wavelength were then reported against the pH and processed by Hyperspec and Hyss. The fitting of the data yielded the speciation plots reported below. The titration plots of the **L4-1** were fitted using the log β values obtained for the relative **4-1**.

Titration curve:

e) Ligand

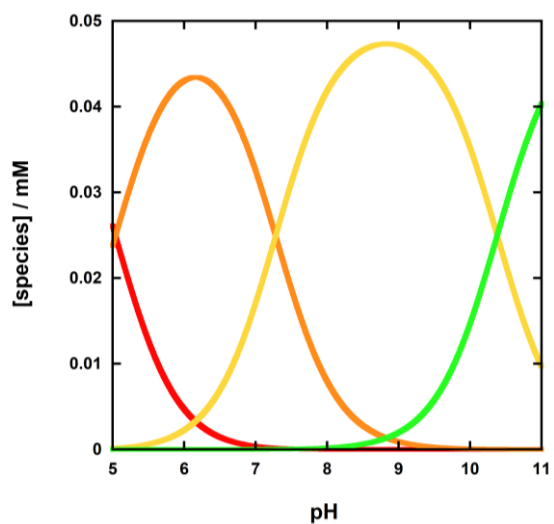


f) Complex

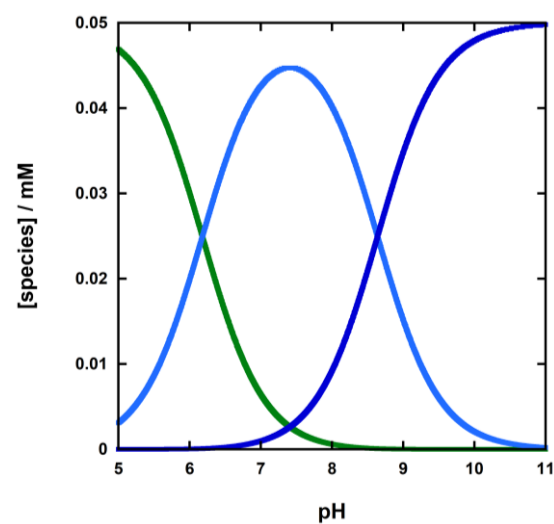


Speciation plot:

g) Ligand



h) Complex



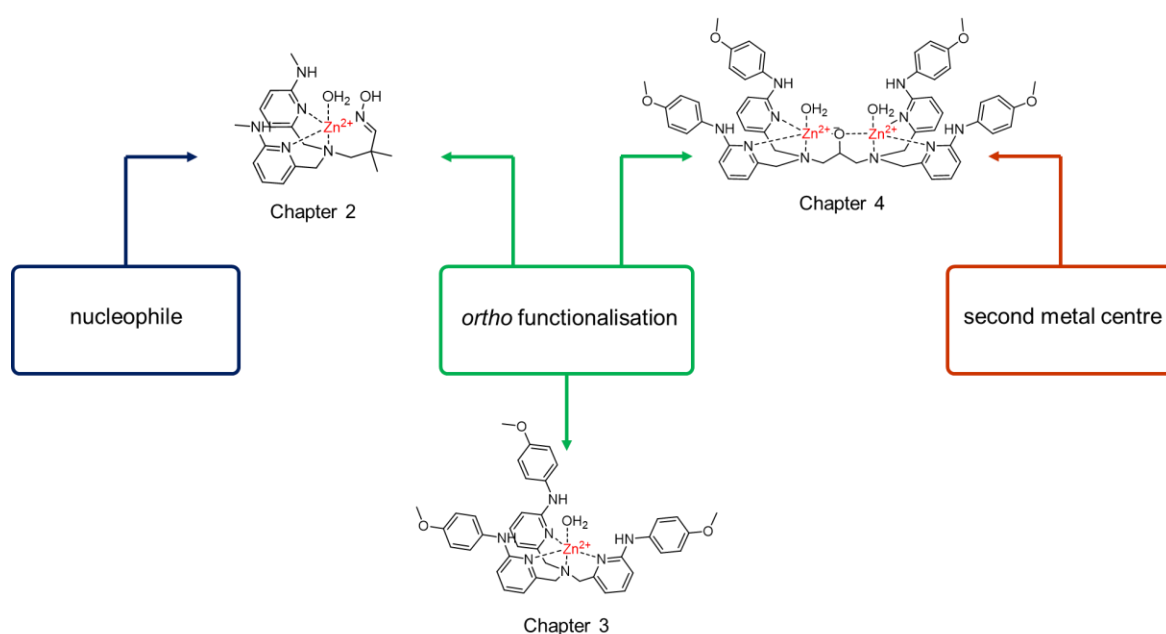
- $(L_{4-1}) + 3H^+$
 - $(L_{4-1}) + 2H^+$
 - $(L_{4-1}) + H^+$
 - L_{4-1}

- $4-1$
 - $(4-1) - H^+$
 - $(4-1) - 2H^+$

Chapter 5

Conclusions

In this work, we presented a wide range of Zn(II) complexes designed to enhance the cleavage of the phosphodiester bond. In addition, we demonstrated the improvement in the catalyst reactivity provided by functional groups carefully introduced into the ligands scaffold. As summarised in Scheme 5.1, three main strategies and their combination have been used to improve the performance of the pyridyl-based catalysts.



Scheme 5.1 Combination of the strategies used for the design of the catalysts studied in this work

Functional groups can be readily introduced in the ortho pyridyl position, creating a second coordination sphere around the metal ion. We demonstrated the importance of introducing stable hydrogen bond donor groups that are not easily deprotonated under physiological conditions. While the acidic sulfonamide substituents determined the deactivation of the catalyst, the amine and the novel aniline-based groups used to enrich the structure of the ligand improved the catalysis. In addition, increasing the strength of the hydrogen bond donor did not lead to higher reactivity. As highlighted in Chapter 3, the anisidine group is

the most effective substitution, and a 1000-fold enhancement was measured compared to the unsubstituted analogue.⁵²

As reported in Chapter 2 for catalysts designed to hydrolyse DNA models, a large enhancement is provided by introducing a nucleophile in the ligand chain. In this work, we confirmed that the presence of an oxime as a nucleophile has a huge impact on the catalyst reactivity: the cleavage of BNPP was 625-fold faster in the presence of **2-5** than the analogue **2-3** (hydroxyl group nucleophile). Furthermore, as highlighted by Scheme 5.1, by introducing a secondary amine in the ortho position as well as the oxime in the aliphatic chain of the ligand, we tested the cooperativity between these modifications. Although the difference with the methyl-substituted analogue **2-11** is only 19-fold, the combination of these two strategies has led to the most active mononuclear complex toward the hydrolysis of BNPP reported so far. Future work might concern the test of **2-5** toward the hydrolysis of different substrates, which release fluorescent leaving groups, allowing the study at a lower catalyst concentration ($< 9 \mu\text{M}$) and confirming the monomer reactivity.

Finally, in Chapter 4, we showed that the addition of a second metal centre could enhance the activity enormously. Introducing anisidine groups into a dinuclear ligand scaffold yielded the most active catalyst toward the hydrolysis of HPNPP in aqueous conditions. Strong cooperation was observed between the two metal ions, and 0.6 mM of **4-1** at pH 7.4 and 25 °C accelerates the hydrolysis of HPNPP 30 000-times faster than its mononuclear analogue **3-2**. High reactivity was also observed when the complex was tested with BNPP and UpG, showing its ability to catalyse the cleavage of less activated substrates.

The promising results reported in this work encourage the investigation of mononuclear and dinuclear complexes as catalytic head groups of artificial restriction enzymes. By following the strategy exploited by Strömberg and coworkers,⁴⁴ these systems might be conjugated to a PNA recognition domain, benefiting from both efficiency and selectivity. Although **4-1** was less reactive toward the transesterification of the UpG than HPNPP, we cannot exclude that the enhanced binding due to the recognition domain might improve the catalyst performance.

Given the unprecedented reactivity of **4-1** toward the transesterification of HPNPP, a possible application of the catalyst might also expand to other research fields which do not target natural substrates. For example, to mimic signal transduction across lipid membranes, a synthetic molecular transducer able to move across the bilayer was proposed by Hunter and Williams.¹³⁴ In particular, the recognition event on the outer side of the membrane would determine the translocation of the transducer on the inner site. To confirm the translocation and amplify the signal, the transducer was equipped with a catalytic head group able to accelerate the hydrolysis of an ester encapsulated inside the vesicle, monitored by the release of its fluorescent leaving group. Following a similar approach, and to obtain a quicker response to the translocation, a derivate of the active **4-1** might be conjugated to the transducer to catalyse the cleavage of encapsulated phosphates.

References

- (1) D. Voet and J. G. Voet. *Biochemistry*; New York: J. Wiley & Sons, 1995.
- (2) Williams, N. H.; Takasaki, B.; Wall, M.; Chin, J. Structure and Nuclease Activity of Simple Dinuclear Metal Complexes: Quantitative Dissection of the Role of Metal Ions. *Acc. Chem. Res.* **1999**, 32 (6), 485–493. <https://doi.org/10.1021/ar9500877>.
- (3) Schroeder, G. K.; Lad, C.; Wyman, P.; Williams, N. H.; Wolfenden, R. The Time Required for Water Attack at the Phosphorus Atom of Simple Phosphodiester and of DNA. *Proc. Natl. Acad. Sci.* **2006**, 103 (11), 4052–4055. <https://doi.org/10.1073/pnas.0510879103>.
- (4) Westheimer, F. H. Why Nature Chose Phosphates. *Science* (80-.). **1987**, 235 (4793), 1173–1178. <https://doi.org/10.1126/science.2434996>.
- (5) Davis, B. D. On the Importance of Being Ionized. *Arch. Biochem. Biophys.* **1958**, 78, 497–509.
- (6) Kamerlin, S. C. L.; Williams, N. H.; Warshel, A. Dineopentyl Phosphate Hydrolysis: Evidence for Stepwise Water Attack. *J. Org. Chem.* **2008**, 73 (18), 6960–6969. <https://doi.org/10.1021/jo801207q>.
- (7) Zalatan, J. G.; Herschlag, D. Alkaline Phosphatase Mono- and Diesterase Reactions: Comparative Transition State Analysis. *J. Am. Chem. Soc.* **2006**, 128 (4), 1293–1303. <https://doi.org/10.1021/ja056528r>.
- (8) Pia Jarvinen, Mikko Oivanen, and H. L. Interconversion and Phosphoester Hydrolysis of 2',5'- and 3',5'-Dinucleoside Monophosphates: Kinetics and Mechanisms. *J. Org. Chem.* **1991**, 56, 5396–5401. <https://doi.org/10.1021/jo00018a037>.
- (9) Lönnberg, H.; Strömberg, R.; Williams, A. Compelling Evidence for a Stepwise

- Mechanism of the Alkaline Cyclisation of Uridine 3'-Phosphate Esters. *Org. Biomol. Chem.* **2004**, 2 (15), 2165–2167. <https://doi.org/10.1039/b406926a>.
- (10) Strater, N.; Lipscomb, W. N.; Klabunde, T.; Krebs, B. Two-Metal Ion Catalysis in Enzymatic Acyl- and Phosphoryl-Transfer Reactions. *Angew. Chemie (International Ed. English)* **1996**, 35 (18), 2024–2055. <https://doi.org/10.1002/anie.199620241>.
 - (11) Williams, N. H.; Takasaki, B.; Wall, M.; Chin, J. Structure and Nuclease Activity of Simple Dinuclear Metal Complexes: Quantitative Dissection of the Role of Metal Ions. *Acc. Chem. Res.* **1999**, 32 (6), 485–493. <https://doi.org/10.1021/ar9500877>.
 - (12) Sigel, R. K. O.; Pyle, A. M. Alternative Roles for Metal Ions in Enzyme Catalysis and the Implications for Ribozyme Chemistry. *Chem. Rev.* **2007**, 107 (1), 97–113. <https://doi.org/10.1021/cr0502605>.
 - (13) Sigel, H.; Fischer, B. E.; Prijs, B. Biological Implications from the Stability of Ternary Complexes in Solution. I Mixed-Ligand Complexes with Manganese(II) and Other 3d Ions. *J. Am. Chem. Soc.* **1977**, 99 (13), 4489–4496. <https://doi.org/10.1021/ja00455a047>.
 - (14) Sigel, H.; Wyss, K.; Fischer, B. E.; Prijs, B. Metal Ions and Hydrogen Peroxide. I Catalase-like Activity of Cu²⁺ in Aqueous Solution and Its Promotion by the Coordination of 1, 2'-Bipyridyl. *Inorg. Chem.* **1979**, 18 (5), 1354–1358. <https://doi.org/10.1021/ic50195a040>.
 - (15) Shevelev, I. V.; Hübscher, U. The 3'-5' Exonucleases. *Nat. Rev. Mol. Cell Biol.* **2002**, 3 (5), 364–375. <https://doi.org/10.1038/nrm804>.
 - (16) Beese, L. S.; Steitz, T. A. Structural Basis for the 3'-5' Exonuclease Activity of Escherichia Coli Dna Polymerase α : A Two Metal Ion Mechanism. *Struct. Insights into Gene Expr. Protein Synth.* **2020**, 10 (1), 245–253. https://doi.org/10.1142/9789811215865_0025.
 - (17) Sands, J.; Kruger, K.; Zaug, A. J.; Gottschling, D. E.; Cech, T. R.; Grabowski, P. J. Self-Splicing RNA: Autoexcision and Autocyclization of the Ribosomal RNA

- Intervening Sequence of Tetrahymena. *Cell* **1982**, *31* (1), 147–157. [https://doi.org/10.1016/0092-8674\(82\)90414-7](https://doi.org/10.1016/0092-8674(82)90414-7).
- (18) Trawick, B. N.; Daniher, A. T.; Bashkin, J. K. Inorganic Mimics of Ribonucleases and Ribozymes: From Random Cleavage to Sequence-Specific Chemistry to Catalytic Antisense Drugs. *Chem. Rev.* **1998**, *98* (3), 939–960. <https://doi.org/10.1021/cr960422k>.
- (19) Bergstrom, D. E.; Gerry, N. P. Precision Sequence-Specific Cleavage of a Nucleic Acid by a Minor-Groove-Directed Metal-Binding Ligand Linked through N-2 of Deoxyguanosine. *J. Am. Chem. Soc.* **1994**, *116* (26), 12067–12068. <https://doi.org/10.1021/ja00105a063>.
- (20) Carroll, D. Progress and Prospects: Zinc-Finger Nucleases as Gene Therapy Agents. *Gene Ther.* **2008**, *15* (22), 1463–1468. <https://doi.org/10.1038/gt.2008.145>.
- (21) Tullius, T. D. Metals and Molecular Biology Thomas. *ACS Symp. Ser.* **1989**, *Chapter 1*.
- (22) Williams, N. H.; Cheung, W.; Chin, J. Reactivity of Phosphate Diesters Doubly Coordinated to a Dinuclear Cobalt(III) Complex: Dependence of the Reactivity on the Basicity of the Leaving Group. *J. Am. Chem. Soc.* **1998**, *120* (32), 8079–8087. <https://doi.org/10.1021/ja980660s>.
- (23) Adli, M. The CRISPR Tool Kit for Genome Editing and Beyond. *Nat. Commun.* **2018**, *9* (1). <https://doi.org/10.1038/s41467-018-04252-2>.
- (24) Epinat, J. C.; Amould, S.; Chames, P.; Rochaix, P.; Desfontaines, D.; Puzin, C.; Patin, A.; Zanghellini, A.; Pâques, F.; Lacroix, E. A Novel Engineered Meganuclease Induces Homologous Recombination in Yeast and Mammalian Cells. *Nucleic Acids Res.* **2003**, *31* (11), 2952–2962. <https://doi.org/10.1093/nar/gkg375>.
- (25) Wolfe, S. A.; Nekludova, L.; Pabo, C. O. DNA RECOGNITION BY Cys2His2 ZINC FINGER PROTEINS. *Annu. Rev. Biophys. Biomol. Struct.* 1999. **2000**, *3*, 183–212.

- (26) Gamsjaeger, R.; Liew, C. K.; Loughlin, F. E.; Crossley, M.; Mackay, J. P. Sticky Fingers: Zinc-Fingers as Protein-Recognition Motifs. *Trends Biochem. Sci.* **2007**, *32* (2), 63–70. <https://doi.org/10.1016/j.tibs.2006.12.007>.
- (27) Kim, Y. G.; Cha, J.; Chandrasegaran, S. Hybrid Restriction Enzymes: Zinc Finger Fusions to Fok I Cleavage Domain. *Proc. Natl. Acad. Sci. U. S. A.* **1996**, *93* (3), 1156–1160. <https://doi.org/10.1073/pnas.93.3.1156>.
- (28) Li, L.; Wu, L. P.; Clarke, R.; Chandrasegaran, S. C-Terminal Deletion Mutants of the FokI Restriction Endonuclease. *Gene* **1993**, *133* (1), 79–84. [https://doi.org/10.1016/0378-1119\(93\)90227-T](https://doi.org/10.1016/0378-1119(93)90227-T).
- (29) Waugh, D. S.; Sauer, R. T. Single Amino Acid Substitutions Uncouple the DNA Binding and Strand Scission Activities of Fok I Endonuclease. *Proc. Natl. Acad. Sci. U. S. A.* **1993**, *90* (20), 9596–9600. <https://doi.org/10.1073/pnas.90.20.9596>.
- (30) Wah, D. A.; Hirsch, J. A.; Dorner, L. F.; Schildkraut, I.; Aggarwal, A. K. Structure of the Multimodular Endonuclease FokI Bound to DNA. *Nature* **1997**, *388* (6637), 97–100. <https://doi.org/10.1038/40446>.
- (31) Boch, J.; Scholze, H.; Schornack, S.; Landgraf, A.; Hahn, S.; Kay, S.; Lahaye, T.; Nickstadt, A.; Bonas, U. Breaking the Code of DNA Binding Specificity of TAL-Type III Effectors. *Science* (80-.). **2009**, *326* (5959), 1509–1512. <https://doi.org/10.1126/science.1178811>.
- (32) Christian, M.; Cermak, T.; Doyle, E. L.; Schmidt, C.; Zhang, F.; Hummel, A.; Bogdanove, A. J.; Voytas, D. F. Targeting DNA Double-Strand Breaks with TAL Effector Nucleases. *Genetics* **2010**, *186* (2), 756–761. <https://doi.org/10.1534/genetics.110.120717>.
- (33) Li, T.; Huang, S.; Zhao, X.; Wright, D. A.; Carpenter, S.; Spalding, M. H.; Weeks, D. P.; Yang, B. Modularly Assembled Designer TAL Effector Nucleases for Targeted Gene Knockout and Gene Replacement in Eukaryotes. *Nucleic Acids Res.* **2011**, *39* (14), 6315–6325. <https://doi.org/10.1093/nar/gkr188>.

- (34) Thurtle-Schmidt, D. M.; Lo, T. W. Molecular Biology at the Cutting Edge: A Review on CRISPR/CAS9 Gene Editing for Undergraduates. *Biochem. Mol. Biol. Educ.* **2018**, *46* (2), 195–205. <https://doi.org/10.1002/bmb.21108>.
- (35) Anders, C.; Niewoehner, O.; Duerst, A.; Jinek, M. Structural Basis of PAM-Dependent Target DNA Recognition by the Cas9 Endonuclease. *Nature* **2014**, *513* (7519), 569–573. <https://doi.org/10.1038/nature13579>.
- (36) O’Geen, H.; Yu, A. S.; Segal, D. J. How Specific Is CRISPR/Cas9 Really? *Curr. Opin. Chem. Biol.* **2015**, *29*, 72–78. <https://doi.org/10.1016/j.cbpa.2015.10.001>.
- (37) Nishimasu, H.; Cong, L.; Yan, W. X.; Ran, F. A.; Zetsche, B.; Li, Y.; Kurabayashi, A.; Ishitani, R.; Zhang, F.; Nureki, O. Crystal Structure of Staphylococcus Aureus Cas9. *Cell* **2015**, *162* (5), 1113–1126. <https://doi.org/10.1016/j.cell.2015.08.007>.
- (38) Huang, X.; Sun, W.; Cheng, Z.; Chen, M.; Li, X.; Wang, J.; Sheng, G.; Gong, W.; Wang, Y. Structural Basis for Two Metal-Ion Catalysis of DNA Cleavage by Cas12i2. *Nat. Commun.* **2020**, *11* (1). <https://doi.org/10.1038/s41467-020-19072-6>.
- (39) Schultz, R. N. Z. and P. G. A Hybrid Sequence-Selective Ribonuclease S. *J. Am. Chem. Soc.* **1988**, *110* (19), 6592–6594.
- (40) Zuckermann, R. N.; Schultz, P. G. Site-Selective Cleavage of Structured RNA by a Staphylococcal Nuclease-DNA Hybrid. *Proc. Natl. Acad. Sci.* **1989**, *86* (6), 1766–1770. <https://doi.org/10.1073/pnas.86.6.1766>.
- (41) Bashkin, J. K.; Frolova, E. I.; Sampath, U. S. Sequence-Specific Cleavage of HIV MRNA by a Ribozyme Mimic. *J. Am. Chem. Soc.* **1994**, *116* (13), 5981–5982. <https://doi.org/10.1021/ja00092a064>.
- (42) Komiyama, M.; Sumaoka, J. Progress towards Synthetic Enzymes for Phosphoester Hydrolysis. *Curr. Opin. Chem. Biol.* **1998**, *2* (6), 751–757. [https://doi.org/10.1016/S1367-5931\(98\)80113-0](https://doi.org/10.1016/S1367-5931(98)80113-0).
- (43) Åtröm, H.; Williams, N. H.; Strömberg, R. Oligonucleotide Based Artificial

- Nuclease (OBAN) Systems. Bulge Size Dependence and Positioning of Catalytic Group in Cleavage of RNA-Bulges. *Org. Biomol. Chem.* **2003**, *1* (9), 1461–1465. <https://doi.org/10.1039/b212216b>.
- (44) Luige, O.; Bose, P. P.; Stulz, R.; Steunenberg, P.; Brun, O.; Andersson, S.; Murtola, M.; Strömberg, R. Zn²⁺-Dependent Peptide Nucleic Acid-Based Artificial Ribonucleases with Unprecedented Efficiency and Specificity. *Chem. Commun.* **2021**, *57* (83), 10911–10914. <https://doi.org/10.1039/d1cc04383h>.
- (45) Luige, O.; Murtola, M.; Ghidini, A.; Strömberg, R. Further Probing of Cu²⁺-Dependent PNAzymes Acting as Artificial RNA Restriction Enzymes. *Molecules* **2019**, *24* (4), 1–12. <https://doi.org/10.3390/molecules24040672>.
- (46) Niittymäki, T.; Lönnberg, H. Artificial Ribonucleases. *Org. Biomol. Chem.* **2006**, *4* (1), 15–25. <https://doi.org/10.1039/b509022a>.
- (47) Desbouis, D. -S. pd.; Troitsky, I. P.; Belousoff, M. J.; Spiccia, L.; Graham, B. Copper(II), Zinc(II) and Nickel(II) Complexes as Nuclease Mimetics. *Coord. Chem. Rev.* **2012**, *256* (11–12), 897–937. <https://doi.org/10.1016/j.ccr.2011.12.005>.
- (48) Lide, D. R. *CRC Handbook of Chemistry and Physics*, 88th ed.; Taylor & Francis, 2007, Ed.; 2007.
- (49) Åström, H.; Limén, E.; Strömberg, R. Acidity of Secondary Hydroxyls in ATP and Adenosine Analogues and the Question of a 2',3'-Hydrogen Bond in Ribonucleosides. *J. Am. Chem. Soc.* **2004**, *126* (45), 14710–14711. <https://doi.org/10.1021/ja0477468>.
- (50) Younas, A. J. K. and M. The Reactivity of Phosphate Esters. Diester Hydrolysis. **1970**, *B* (0), 510–513. <https://doi.org/10.1039/J29700000510>.
- (51) Chin, J. Developing Artificial Hydrolytic Metalloenzymes by a Unified Mechanistic Approach. *Acc. Chem. Res.* **1991**, *24* (5), 145–152. <https://doi.org/10.1021/ar00005a004>.

- (52) Feng, G.; Mareque-Rivas, J. C.; Torres Martín De Rosales, R.; Williams, N. H. A Highly Reactive Mononuclear Zn(II) Complex for Phosphodiester Cleavage. *J. Am. Chem. Soc.* **2005**, *127* (39), 13470–13471. <https://doi.org/10.1021/ja054003t>.
- (53) Padovani, M.; Williams, N. H.; Wyman, P. Mononuclear Co(III)-Complex Promoted Phosphate Diester Hydrolysis: Dependence of Reactivity on the Leaving Group. *J. Phys. Org. Chem.* **2004**, *17* (6-7 SPEC.ISS.), 472–477. <https://doi.org/10.1002/poc.770>.
- (54) Chin, J.; Banaszczyk, M.; Jubian, V.; Zou, X. Co(III) Complex Promoted Hydrolysis of Phosphate Diesters: Comparison in Reactivity of Rigid Cis-Diaquotetraazacobalt(III) Complexes. *J. Am. Chem. Soc.* **1989**, *111* (1), 186–190. <https://doi.org/10.1021/ja00183a029>.
- (55) Koike, T.; Kimura, E.; Kimura, E. Roles of Zinc(II) Ion in Phosphatases. A Model Study with Zinc(II)-Macrocyclic Polyamine Complexes. *J. Am. Chem. Soc.* **1991**, *113* (23), 8935–8941. <https://doi.org/10.1021/ja00023a048>.
- (56) Rosch, M. A. De; Trogler, W. C. Hydrolysis of Phosphodiester with Ni (II), Cu (II), Zn (II), Pd (II), and Pt (II) Complexes. *Inorg. Chem.* **1990**, *29*, 2409–2416.
- (57) Mancin, F.; Tecilla, P. Zinc(II) Complexes as Hydrolytic Catalysts of Phosphate Diester Cleavage: From Model Substrates to Nucleic Acids. *New J. Chem.* **2007**, *31* (6), 800–817. <https://doi.org/10.1039/b703556j>.
- (58) Bonfá, L.; Gatos, M.; Mancin, F.; Tecilla, P.; Tonellato, U. The Ligand Effect on the Hydrolytic Reactivity of Zn(II) Complexes toward Phosphate Diesters. *Inorg. Chem.* **2003**, *42* (12), 3943–3949. <https://doi.org/10.1021/ic034139x>.
- (59) Morrow, J. R.; Trogler, W. C. Hydrolysis of Phosphate Diesters with Copper(II) Catalysts. *Inorg. Chem.* **1988**, *27* (19), 3387–3394. <https://doi.org/10.1021/ic00292a025>.
- (60) Stern, M. K.; Bashkin, J. K.; Sail, E. D. Hydrolysis of RNA by Transition-Metal Complexes. *J. Am. Chem. Soc.* **1990**, *112* (13), 5357–5359.

<https://doi.org/10.1021/ja00169a057>.

- (61) Liu, S.; Hamilton, A. D. Catalysis of Phosphodiester Transesterification by Cu(II)-Terpyridine Complexes with Peripheral Pendent Base Groups: Implications for the Mechanism. *Tetrahedron Lett.* **1997**, 38 (7), 1107–1110. [https://doi.org/10.1016/S0040-4039\(96\)02519-1](https://doi.org/10.1016/S0040-4039(96)02519-1).
- (62) Kövári, E.; Krämer, R. Rapid Phosphodiester Hydrolysis by an Ammonium-Functionalized Copper(II) Complex. A Model for the Cooperativity of Metal Ions and NH-Acidic Groups in Phosphoryl Transfer Enzymes. *J. Am. Chem. Soc.* **1996**, 118 (50), 12704–12709. <https://doi.org/10.1021/ja962806y>.
- (63) Liang, G.; Corfù, N. A.; Sigel, H. Influence of Decreasing Solvent Polarity (Dioxane-Water Mixtures) on the Stability of Metal Ion Complexes Formed with Phosphate Monoesters. *Zeitschrift für Naturforsch. - Sect. B J. Chem. Sci.* **1989**, 44 (5), 538–542. <https://doi.org/10.1515/znb-1989-0506>.
- (64) R. Stan Brown, Zhong-Lin Lu, C. Tony Li, Wing Yin Tsang, David R. Edwards, Alexei A. Neverov. Dinuclear Zn(II) Catalysts as Biomimics of RNA and DNA Phosphoryl Transfer Enzymes: Changing the Medium from Water to Alcohol Provides Enzyme-like Rate Enhancements. *J. Phys. Org. Chem.* **2010**, 23 (1), 1–15. <https://doi.org/10.1002/poc.1584>.
- (65) Wall, M.; Linkletter, B.; Williams, D.; Lebus, A. M.; Hynes, R. C.; Chin, J. Rapid Hydrolysis of 2',3'-CAMP with a Cu(II) Complex: Effect of Intramolecular Hydrogen Bonding on the Basicity and Reactivity of a Metal-Bound Hydroxide. *J. Am. Chem. Soc.* **1999**, 121 (19), 4710–4711. <https://doi.org/10.1021/ja981227l>.
- (66) Liu, S.; Luo, Z.; Hamilton, A. D. Rapid and Highly Selective Cleavage of Ribonucleoside 2,3'-Cyclic Monophosphates by Dinuclear Cu^{II} Complexes. *Angew. Chemie (International Ed. English)* **1997**, 36 (23), 2678–2680. <https://doi.org/10.1002/anie.199726781>.
- (67) Yashiro, M.; Ishikubo, A.; Komiyama, M. Efficient and Unique Cooperation of

- Three Zinc(II) Ions in the Hydrolysis of Diribonucleotides by a Trinuclear Zinc(II) Complex. *Chem. Commun.* **1997**, No. 1, 83–84. <https://doi.org/10.1039/a606505h>.
- (68) Liu, S.; Hamilton, A. D. *Catalysis of Phosphodiester Transesterification by Dinuclear Cu(II) Complexes: The Role of the Second Cu(II) Ion*; 1997; Vol. 7.
- (69) Liu, S.; Hamilton, A. D. Rapid and Highly Base Selective RNA Cleavage by a Dinuclear Cu(II) Complex. *Chem. Commun.* **1999**, No. 7, 587–588. <https://doi.org/10.1039/a808195f>.
- (70) O'Brien, P. J.; Herschlag, D. Alkaline Phosphatase Revisited: Hydrolysis of Alkyl Phosphates. *Biochemistry* **2002**, 41 (9), 3207–3225. <https://doi.org/10.1021/bi012166y>.
- (71) Eiichi Kimura, Yorimitsu Kodama, T. K. and M. S. Phosphodiester Hydrolysis by a New Zinc(II) Macrocyclic Tetraamine Complex with an Alcohol Pendant: Elucidation of the Roles of Ser-102 and Zinc(II) in Alkaline Phosphatase. *J. Am. Chem. Soc.* **1995**, 117, 8304–8311.
- (72) Carla Bazzicalupi, Andrea Bencini, Emanuela Berni, Antonio Bianchi, Valentina Fedi, Vieri Fusi, Claudia Giorgi, Piero Paoletti, B. V. Carboxy and Diphosphate Ester Hydrolysis by a Dizinc Complex with a New Alcohol-Pendant Macrocyclic. *Inorg. Chem.* **1999**, 38 (18), 4115–4122. <https://doi.org/10.1021/ic9902929>.
- (73) Feng, G.; Mareque-Rivas, J. C.; Williams, N. H. Comparing a Mononuclear Zn(II) Complex with Hydrogen Bond Donors with a Dinuclear Zn(II) Complex for Catalysing Phosphate Ester Cleavage. *Chem. Commun.* **2006**, 2 (17), 1845–1847. <https://doi.org/10.1039/b514328d>.
- (74) Livieri, M.; Mancin, F.; Tonellato, U.; Chin, J. Multiple Functional Group Cooperation in Phosphate Diester Cleavage Promoted by Zn(II) Complexes. *Chem. Commun.* **2004**, No. 24, 2862–2863. <https://doi.org/10.1039/b412111b>.
- (75) Wilcox, D. E. Binuclear Metallohydrolases. *Chem. Rev.* **1996**, 96 (7), 2435–2458. <https://doi.org/10.1021/cr950043b>.

- (76) Ichikawa, K.; Tarnai, M.; Uddin, M. K.; Nakata, K.; Sato, S. Hydrolysis of Natural and Artificial Phosphoesters Using Zinc Model Compound with a Histidine-Containing Pseudopeptide. *J. Inorg. Biochem.* **2002**, *91* (3), 437–450. [https://doi.org/10.1016/S0162-0134\(02\)00452-X](https://doi.org/10.1016/S0162-0134(02)00452-X).
- (77) Alessandra Greatti, Marciela Scarpellini, Rosely A. Peralta, Annelise Casellato, Adailton J. Bortoluzzi, Fernanado R. Xavier, Rafael Jovito, Marcos Aires de Brito, Bruno Szpoganicz, Zbigniew Tomkowicz, Michal Rams, Wolfgang Haase, Ademir Neves, I. Synthesis, Structure, and Physicochemical Properties of Dinuclear Ni II Complexes as Highly Efficient Functional Models of Phosphohydrolases. *Inorg. Chem.* **2008**, *47* (3), 1107–1119. <https://doi.org/10.1021/ic702132t>.
- (78) Livieri, M.; Mancin, F.; Tonellato, U.; Chin, J. Multiple Functional Group Cooperation in Phosphate Diester Cleavage Promoted by Zn(II) Complexes. *Chem. Commun.* **2004**, No. 24, 2862–2863. <https://doi.org/10.1039/b412111b>.
- (79) Tirel, E. Y.; Bellamy, Z.; Adams, H.; Lebrun, V.; Duarte, F.; Williams, N. H. Catalytic Zinc Complexes for Phosphate Diester Hydrolysis. *Angew. Chemie - Int. Ed.* **2014**, *53* (31), 8246–8250. <https://doi.org/10.1002/anie.201400335>.
- (80) Ronald Breslow Dan Berger, D.-L. H. Bifunctional Zinc-Imidazole and Zinc-Thiophenol Catalysts. *J. Am. Chem. Soc.* **1990**, *112* (9), 3686–3687. <https://doi.org/10.1021/ja00165a079>.
- (81) Stec, B.; Hehir, M. J.; Brennan, C.; Nolte, M.; Kantrowitz, E. R. Kinetic and X-Ray Structural Studies of Three Mutant E. Coli Alkaline Phosphatases: Insights into the Catalytic Mechanism without the Nucleophile Ser102. *J. Mol. Biol.* **1998**, *277* (3), 647–662. <https://doi.org/10.1006/jmbi.1998.1635>.
- (82) Stec, B.; Holtz, K. M.; Kantrowitz, E. R. A Revised Mechanism for the Alkaline Phosphatase Reaction Involving Three Metal Ions. *J. Mol. Biol.* **2000**, *299* (5), 1303–1311. <https://doi.org/10.1006/jmbi.2000.3799>.
- (83) He, J.; Sun, J.; Mao, Z. W.; Ji, L. N.; Sun, H. Phosphodiester Hydrolysis and Specific

- DNA Binding and Cleavage Promoted by Guanidinium-Functionalized Zinc Complexes. *J. Inorg. Biochem.* **2009**, *103* (5), 851–858. <https://doi.org/10.1016/j.jinorgbio.2009.02.010>.
- (84) Young, M. J.; Wahnnon, D.; Hynes, R. C.; Chin, J. Reactivity of Copper(II) Hydroxides and Copper(H) Alkoxides for Cleaving an Activated Phosphate Diester. *J. Am. Chem. Soc.* **1995**, *117* (37), 9441–9447. <https://doi.org/10.1021/ja00142a010>.
- (85) Tirel, E. Y.; Williams, N. H. Enhancing Phosphate Diester Cleavage by a Zinc Complex through Controlling Nucleophile Coordination. *Chem. - A Eur. J.* **2015**, *21* (19), 7053–7056. <https://doi.org/10.1002/chem.201500619>.
- (86) Hunter, C. A. Quantifying Intermolecular Interactions: Guidelines for the Molecular Recognition Toolbox. *Angew. Chemie - Int. Ed.* **2004**, *43* (40), 5310–5324. <https://doi.org/10.1002/anie.200301739>.
- (87) Tirel, E. Y. Zinc Complexes for Phosphate Diester Hydrolysis, 2014. <https://doi.org/10.1002/ange.201400335>.
- (88) Gans, P.; Sabatini, A.; Vacca, A. Investigation of Equilibria in Solution. Determination of Equilibrium Constants with the HYPERQUAD Suite of Programs. *Talanta* **1996**, *43* (10), 1739–1753. [https://doi.org/10.1016/0039-9140\(96\)01958-3](https://doi.org/10.1016/0039-9140(96)01958-3).
- (89) Abdulkarim, Z. Probing the Properties of Zn Complexes for the Cleavage of Phosphate Diester and the Influence of Non-Covalent Assembly, 2015.
- (90) Yatsimirsky, A. K.; Gómez-Tagle, P.; Escalante-Tovar, S.; Ruiz-Ramírez, L. Kinetics and Mechanism of Ester Hydrolysis by Metal Complexes of 2,6-Diacetylpyridine Dioxime. *Inorganica Chim. Acta* **1998**, *273* (1–2), 167–174. [https://doi.org/10.1016/s0020-1693\(97\)05971-9](https://doi.org/10.1016/s0020-1693(97)05971-9).
- (91) Wahnnon, D.; Hynes, R. C.; Chin, J. Dramatic Ligand Effect in Copper(II) Complex Promoted Transesterification of a Phosphate Diester Daphne. **1994**, 1441–1442.
- (92) Mareque-Rivas, J. C.; Prabakaran, R.; Martín de Rosales, R. T. Relative Importance

- of Hydrogen Bonding and Coordinating Groups in Modulating the Zinc-Water Acidity. *Chem. Commun.* **2004**, 4 (1), 76–77. <https://doi.org/10.1039/b310956a>.
- (93) Livieri, M.; Mancin, F.; Saielli, G.; Chin, J.; Tonellato, U. Mimicking Enzymes: Cooperation between Organic Functional Groups and Metal Ions in the Cleavage of Phosphate Diesters. *Chem. - A Eur. J.* **2007**, 13 (8), 2246–2256. <https://doi.org/10.1002/chem.200600672>.
- (94) Bonomi, R.; Saielli, G.; Tonellato, U.; Scrimin, P.; Mancin, F. Insights on Nuclease Mechanism: The Role of Proximal Ammonium Group on Phosphate Esters Cleavage. *J. Am. Chem. Soc.* **2009**, 131 (32), 11278–11279. <https://doi.org/10.1021/ja9033236>.
- (95) R. Breslow and D. Chipman. Mixed Metal Complexes as Enzyme Models. I. Intracomplex Nucleophilic Catalysis by an Oxime Anion. *J. Am. Chem. Soc.* **1965**, 87:18 (September 20,), 4195–4196.
- (96) Lugo-González, J. C.; Gómez-Tagle, P.; Huang, X.; M. Del Campo, J.; Yatsimirsky, A. K. Substrate Specificity and Leaving Group Effect in Ester Cleavage by Metal Complexes of an Oximate Nucleophile. *Inorg. Chem.* **2017**, 56 (4), 2060–2069. <https://doi.org/10.1021/acs.inorgchem.6b02739>.
- (97) Feng, G.; Natale, D.; Prabakaran, R.; Mareque-Rivas, J. C.; Williams, N. H. Efficient Phosphodiester Binding and Cleavage by a Zn II Complex Combining Hydrogen-Bonding Interactions and Double Lewis Acid Activation. *Angew. Chemie - Int. Ed.* **2006**, 45 (42), 7056–7059. <https://doi.org/10.1002/anie.200602532>.
- (98) Bourne, N.; Williams, A. Effective Charge on Oxygen in Phosphoryl (-PO₃²⁻) Group Transfer from an Oxygen Donor. *J. Org. Chem.* **1984**, 49 (7), 1200–1204. <https://doi.org/10.1021/jo00181a011>.
- (99) Mancin, F.; Prins, L. J.; Pengo, P.; Pasquato, L.; Tecilla, P.; Scrimin, P. Hydrolytic Metallo-Nanozymes: From Micelles and Vesicles to Gold Nanoparticles. *Molecules* **2016**, 21 (8). <https://doi.org/10.3390/molecules21081014>.

- (100) F. Reis, I.; Miguez, F. B.; Vargas, C. A. A.; Menzonatto, T. G.; Silva, I. M. S.; Verano-Braga, T.; Lopes, J. F.; Brandão, T. A. S.; De Sousa, F. B. Structural and Electronic Characterization of a Photoresponsive Lanthanum(III) Complex Incorporated into Electrospun Fibers for Phosphate Ester Catalysis. *ACS Appl. Mater. Interfaces* **2020**, *12* (25), 28607–28615. <https://doi.org/10.1021/acsami.0c03571>.
- (101) Suwantong, O. Biomedical Applications of Electrospun Polycaprolactone Fiber Mats. *Polym. Adv. Technol.* **2016**, *27* (10), 1264–1273. <https://doi.org/10.1002/pat.3876>.
- (102) Krebs, J. F.; Ippolito, J. A.; Christianson, D. W.; Fierke, C. A. Structural and Functional Importance of a Conserved Hydrogen Bond Network in Human Carbonic Anhydrase II. *J. Biol. Chem.* **1993**, *268* (36), 27458–27466. [https://doi.org/10.1016/s0021-9258\(19\)74269-0](https://doi.org/10.1016/s0021-9258(19)74269-0).
- (103) Mareque-Rivas, J. C.; Torres Martín de Rosales, R.; Parsons, S. The Affinity of Phosphates to Zinc(II) Complexes Can Be Increased with Hydrogen Bond Donors. *Chem. Commun.* **2004**, *4* (5), 610–611. <https://doi.org/10.1039/b314616b>.
- (104) Dahl, E. W.; Kiernicki, J. J.; Zeller, M.; Szymczak, N. K. Hydrogen Bonds Dictate O₂ Capture and Release within a Zinc Tripod. *J. Am. Chem. Soc.* **2018**, *140* (32), 10075–10079. <https://doi.org/10.1021/jacs.8b04266>.
- (105) Dahl, E. W.; Dong, H. T.; Szymczak, N. K. Phenylamino Derivatives of Tris(2-Pyridylmethyl)Amine: Hydrogen-Bonded Peroxodicopper Complexes. *Chem. Commun.* **2018**, *54* (8), 892–895. <https://doi.org/10.1039/c7cc08619a>.
- (106) Chuang, C. L.; Dos Santos, O.; Xu, X.; Canary, J. W. Synthesis and Cyclic Voltammetry Studies of Copper Complexes of Bromo- and Alkoxyphenyl-Substituted Derivatives of Tris(2-Pyridylmethyl)Amine: Influence of Cation - Alkoxy Interactions on Copper Redox Potentials. *Inorg. Chem.* **1997**, *36* (9), 1967–1972. <https://doi.org/10.1021/ic960942y>.

- (107) Yatsimirsky. Solvent Effects and Alkali Metal Ion Catalysis in Phosphodiester Hydrolysis. *J. Org. Chem.* **2006**, *71* (26), 9713–9722. <https://doi.org/10.1021/jo061780i>.
- (108) Barbosa, J.; Barrón, D.; Bergés, R.; Sanz-Nebot, V.; Toro, I. Preferential Solvation in Acetonitrile-Water Mixtures: Relationship between Solvatochromic Parameters and PK Values of Carboxylic Acids. *J. Chem. Soc. - Faraday Trans.* **1997**, *93* (10), 1915–1920. <https://doi.org/10.1039/a606763h>.
- (109) Selmeczi, K.; Michel, C.; Milet, A.; Gautier-Luneau, I.; Philouze, C.; Pierre, J. L.; Schnieders, D.; Rompel, A.; Belle, C. Structural, Kinetic, and Theoretical Studies on Models of the Zinc-Containing Phosphodiesterase Active Center: Medium-Dependent Reaction Mechanisms. *Chem. - A Eur. J.* **2007**, *13* (32), 9093–9106. <https://doi.org/10.1002/chem.200700104>.
- (110) Sigel, H.; Martin, R. B.; Tribolet, R.; Häring, U. K.; Malini-Balakrishnan, R. An Estimation of the Equivalent Solution Dielectric Constant in the Active-Site Cavity of Metalloenzymes. Dependence of Carboxylate - Metal-Ion Complex Stabilities on the Polarity of Mixed Aqueous/Organic Solvents. *Eur. J. Biochem.* **1985**, *152* (1), 187–193. <https://doi.org/10.1111/j.1432-1033.1985.tb09180.x>.
- (111) Thordarson, P. Determining Association Constants from Titration Experiments in Supramolecular Chemistry. *Chem. Soc. Rev.* **2011**, *40* (3), 1305–1323. <https://doi.org/10.1039/c0cs00062k>.
- (112) Hansch, C.; Leo, A.; Taft, R. W. A Survey of Hammett Substituent Constants and Resonance and Field Parameters. *Chem. Rev.* **1991**, *91* (2), 165–195. <https://doi.org/10.1021/cr00002a004>.
- (113) Young, K. J.; Gill, F.; Grasby, J. A. Metal Ions Play a Passive Role in the Hairpin Ribozyme Catalysed Reaction. *Nucleic Acids Res.* **1997**, *25* (19), 3760–3766. <https://doi.org/10.1093/nar/25.19.3760>.
- (114) Steitz, T. A.; Steitz, J. A. A General Two-Metal-Ion Mechanism for Catalytic RNA.

- Proc. Natl. Acad. Sci. U. S. A.* **1993**, 90 (14), 6498–6502.
<https://doi.org/10.1073/pnas.90.14.6498>.
- (115) Young, M. J.; Chin, J. Dinuclear Copper (II) Complex That Hydrolyzes RNA. *J. Am. Chem. Soc.* **1995**, 117 (42), 10577–10578. <https://doi.org/10.1021/ja00147a022>.
- (116) Iranzo, O.; Elmer, T.; Richard, J. P.; Morrow, J. R. Cooperativity between Metal Ions in the Cleavage of Phosphate Diesters and RNA by Dinuclear Zn(II) Catalysts. *Inorg. Chem.* **2003**, 42 (24), 7737–7746. <https://doi.org/10.1021/ic030131b>.
- (117) Sträter, N.; Lipscomb, W. N. Two-Metal Ion Catalysis in Enzymatic Acyl- and Phosphoryl-Transfer Reactions. *Angew. Chemie (International Ed. English)* **1996**, 35 (18), 2024–2055. <https://doi.org/10.1002/anie.199620241>.
- (118) Iranzo, O.; Kovalevsky, A. Y.; Morrow, J. R.; Richard, J. P. Physical and Kinetic Analysis of the Cooperative Role of Metal Ions in Catalysis of Phosphodiester Cleavage by a Dinuclear Zn(II) Complex. *J. Am. Chem. Soc.* **2003**, 125 (7), 1988–1993. <https://doi.org/10.1021/ja027728v>.
- (119) O'Donoghue, A.; Pyun, S. Y.; Yang, M. Y.; Morrow, J. R.; Richard, J. P. Substrate Specificity of an Active Dinuclear Zn(II) Catalyst for Cleavage of RNA Analogues and a Dinucleoside. *J. Am. Chem. Soc.* **2006**, 128 (5), 1615–1621. <https://doi.org/10.1021/ja056167f>.
- (120) Neverov, A. A.; Lu, Z. L.; Maxwell, C. I.; Mohamed, M. F.; White, C. J.; Tsang, J. S. W.; Brown, R. S. Combination of a Dinuclear Zn²⁺ Complex and a Medium Effect Exerts a 10¹²-Fold Rate Enhancement of Cleavage of an RNA and DNA Model System. *J. Am. Chem. Soc.* **2006**, 128 (50), 16398–16405. <https://doi.org/10.1021/ja0651714>.
- (121) Mohamed, M. F.; Neverov, A. A.; Brown, R. S. Investigation of the Effect of Oxy Bridging Groups in Dinuclear Zn(II) Complexes That Catalyze the Cleavage of a Simple Phosphate Diester RNA Analogue. *Inorg. Chem.* **2009**, 48 (23), 11425–11433. <https://doi.org/10.1021/ic9015965>.

- (122) Cacciapaglia, R.; Casnati, A.; Mandolini, L.; Peracchi, A.; Reinhoudt, D. N.; Salvio, R.; Sartori, A.; Ungaro, R. Efficient and Selective Cleavage of RNA Oligonucleotides by Calix[4]Arene-Based Synthetic Metallonucleases. *J. Am. Chem. Soc.* **2007**, *129* (41), 12512–12520. <https://doi.org/10.1021/ja0737366>.
- (123) Cacciapaglia, R.; Casnati, A.; Mandolini, L.; Reinhoudt, D. N.; Salvio, R.; Sartori, A.; Ungaro, R. Catalysis of Diribonucleoside Monophosphate Cleavage by Water Soluble Copper(II) Complexes of Calix[4]Arene Based Nitrogen Ligands. *J. Am. Chem. Soc.* **2006**, *128* (37), 12322–12330. <https://doi.org/10.1021/ja0632106>.
- (124) Korhonen, H.; Mikkola, S.; Williams, N. H. The Mechanism of Cleavage and Isomerisation of RNA Promoted by an Efficient Dinuclear Zn ²⁺ Complex. *Chem. - A Eur. J.* **2012**, *18* (2), 659–670. <https://doi.org/10.1002/chem.201100721>.
- (125) Ruiz-Castillo, P.; Buchwald, S. L. Applications of Palladium-Catalyzed C-N Cross-Coupling Reactions. *Chem. Rev.* **2016**, *116* (19), 12564–12649. <https://doi.org/10.1021/acs.chemrev.6b00512>.
- (126) Ferreira, C. M. H.; Pinto, I. S. S.; Soares, E. V.; Soares, H. M. V. M. (Un)Suitability of the Use of PH Buffers in Biological, Biochemical and Environmental Studies and Their Interaction with Metal Ions-a Review. *RSC Adv.* **2015**, *5* (39), 30989–31003. <https://doi.org/10.1039/c4ra15453c>.
- (127) Yang, M. Y.; Richard, J. P.; Morrow, J. R. Substrate Specificity for Catalysis of Phosphodiester Cleavage by a Dinuclear Zn(II) Complex. *Chem. Commun.* **2003**, *3* (22), 2832–2833. <https://doi.org/10.1039/b308644e>.
- (128) Liu, C. T.; Neverov, A. A.; Brown, R. S. A Reductionist Biomimetic Model System That Demonstrates Highly Effective Zn(II)-Catalyzed Cleavage of an RNA Model. *Inorg. Chem.* **2007**, *46* (5), 1778–1788. <https://doi.org/10.1021/ic062065u>.
- (129) Shelton, V. M.; Morrow, J. R. Catalytic Transesterification and Hydrolysis of RNA by Zinc(II) Complexes. *Inorg. Chem.* **1991**, *30* (23), 4295–4299. <https://doi.org/10.1021/ic00023a003>.

- (130) McCue, K. P.; Morrow, J. R. Hydrolysis of a Model for the 5'-Cap of mRNA by Dinuclear Copper(II) and Zinc(II) Complexes. Rapid Hydrolysis by Four Copper(II) Ions. *Inorg. Chem.* **1999**, 38 (26), 6136–6142. <https://doi.org/10.1021/ic990380t>.
- (131) Domínguez, A.; Fernández, A.; González, N.; Iglesias, E.; Montenegro, L. Determination of Critical Micelle Concentration of Some Surfactants by Three Techniques *Anal.* **1997**, 74 (10), 1227–1231.
- (132) Kalyanasundaram, K.; Thomas, J. K. Environmental Effects on Vibronic Band Intensities in Pyrene Monomer Fluorescence and Their Application in Studies of Micellar Systems. *J. Am. Chem. Soc.* **1977**, 99 (7), 2039–2044. <https://doi.org/10.1021/ja00449a004>.
- (133) Heravi, M. M.; Kheilkordi, Z.; Zadsirjan, V.; Heydari, M.; Malmir, M. Buchwald-Hartwig Reaction: An Overview. *J. Organomet. Chem.* **2018**, 861, 17–104. <https://doi.org/10.1016/j.jorganchem.2018.02.023>.
- (134) Langton, M. J.; Keymeulen, F.; Ciaccia, M.; Williams, N. H.; Hunter, C. A. Controlled Membrane Translocation Provides a Mechanism for Signal Transduction and Amplification. *Nat. Chem.* **2017**, 9 (5), 426–430. <https://doi.org/10.1038/nchem.2678>.